Graduate Texts in Physics

Wokyung Sung

Statistical Physics for Biological Matter

Springer

Graduate Texts in Physics

Graduate Texts in Physics

Graduate Texts in Physics publishes core learning/teaching material for graduate- and advanced-level undergraduate courses on topics of current and emerging fields within physics, both pure and applied. These textbooks serve students at the MS- or PhD-level and their instructors as comprehensive sources of principles, definitions, derivations, experiments and applications (as relevant) for their mastery and teaching, respectively. International in scope and relevance, the textbooks correspond to course syllabi sufficiently to serve as required reading. Their didactic style, comprehensiveness and coverage of fundamental material also make them suitable as introductions or references for scientists entering, or requiring timely knowledge of, a research field.

More information about this series at http://www.springer.com/series/8431

Wokyung Sung

Statistical Physics for Biological Matter

Springer

Wokyung Sung
Department of Physics
Pohang University of Science
and Technology
Pohang, Korea (Republic of)

ISSN 1868-4513 ISSN 1868-4521 (electronic)
Graduate Texts in Physics
ISBN 978-94-024-1583-4 ISBN 978-94-024-1584-1 (eBook)
https://doi.org/10.1007/978-94-024-1584-1

Library of Congress Control Number: 2018942003

Cover Image: DNA, chromosomes and genes
Courtesy: National Human Genome Research Institute

This Springer imprint is published by the registered company Springer Nature B.V.
The registered company address is: Van Godewijckstraat 30, 3311 GX Dordrecht, The Netherlands

To my lifelong companion, Jung

Preface

This book aims to cover a broad range of topics in extended statistical physics, including statistical mechanics (equilibrium and non-equilibrium), soft condensed matter, and fluid physics, for applications to biological phenomena at both cellular and macromolecular levels. It is expected to be a graduate-level textbook, but can also be addressed to the interested senior-level undergraduates. The book is written also for those interested in research on biological systems or soft matter based on physics, particularly on statistical physics.

One of the most important directions in science nowadays is physical approach to biology. The tremendous challenges that come widely from emerging fields, such as biotechnology, biomaterials, and biomedicine, demand quantitative, physical explanations. A basic understanding of biological systems and phenomena also provides a new paradigm by which current physics can advance. In this book, we are mostly interested in biological systems at a mesoscopic or cellular level, which ranges from nanometers to micrometers in length. Such biological systems comprise cells and the constituent biopolymers, membranes, and other subcellular structures. This bio-soft condensed matter is subject to thermal fluctuations and non-equilibrium noises, and, owing to its structural flexibility and connectivity, manifests a variety of emergent, cooperative behaviors, the explanation of which calls for novel developments and applications of statistical physics.

Students and researchers alike have difficulties in applying to biological problems the knowledge and methods they learned from presently available textbooks on statistical physics. One possible reason for this is that, in biology, the systems consist of complex, soft matter, which is usually not included in traditional physics curricula. Typical statistical physics courses cover ideal gases (classical and quantum) and interacting units of simple structures. In contrast, even simple biological fluids are solutions of macromolecules, the structures of which are very complex. The goal of this book is to fill this wide gap by providing appropriate content as well as by explaining the theoretical method that typifies good modeling, namely, the method of coarse-grained descriptions that extract the most salient features emerging at mesoscopic scales. This book is, of course, in no way comprehensive in covering all the varied and important subjects of statistical physics

applicable to biology. I went to great effort to incorporate what I consider to be the essential topics, which, of course, may reflect my own personal interests and limitations. The major topics covered in this book include thermodynamics, equilibrium statistical mechanics, soft matter physics of polymers and membranes, non-equilibrium statistical physics covering stochastic processes, transport phenomena, hydrodynamics, etc. More than 100 problems are given alongside the text rather than at the end of the chapters, because they are a part of the text and the logical flow; these problems, some of which are quite challenging to solve, will help readers develop a deeper understanding of the content.

A number of good textbooks have recently been written under the titles of physical biology, biological physics, and biophysics. A number of these books give excellent guides to biological phenomena illustrated in the quantitative language of physics. In some of these books, biological systems and phenomena are first described, and then analyzed quantitatively, using thermodynamics and statistical physics. Following bio-specific topics, physics-oriented readers might struggle to build, systematically and coherently on the basics, their own understanding of nonspecific concepts and theoretical methods, which they may be able to apply to a broader class of biological problems. In this book, another approach is taken that is, nonspecific basic methods and theories with detailed derivations and then biological examples and applications are given.

The book is based on lectures I gave to graduate students at POSTECH in a course under the title of Biological Statistical Physics. It is my hope that by attempting to fill this aforementioned gap, I can, at the very least, help students and researchers appreciate and learn the immense potential of statistical physics for biology, particularly for biological systems at mesoscopic scales.

Pohang, Korea (Republic of) Wokyung Sung

Acknowledgements

I owe a great debt of thanks to a number of my teachers and colleagues that I have been influenced by and associated with throughout my scientific career: Profs. Yun Suk Koh, Koo Chul Lee, David Finkelstein, George Stell, John Dahler, Harold Friedman, Norman March, Philip Pincus, Man Won Kim, Alexander Neiman, Dmitri Kuznetsov, Tapio Ala Nissila, Michel Kosterlitz, Kimoon Kim, Byung Il Min, Jongbong Lee, Nam Ki Lee, and Jaeyoung Sung. I also wish to extend my thanks to a number of previous graduate students of mine, Pyeong Jun Park, Yong Woon Kim, Kwonmoo Lee, Jae-Hyung Jeon, Won Kyu Kim, Jae-oh Shin, and in particular Ochul Lee who helped me with formatting the manuscript and drawing the figures in the book. I would like to express my deep gratitude to Springer's Editorial Director, Dr. Liesbeth Mol, and Prof. Eugene Stanley who suggested and encouraged me to attempt this daunting task. It is with pleasure to acknowledge the support of Institute of Basic Science for Self-Assembly and Complexity.

About the Author

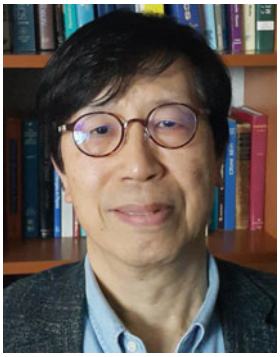

Wokyung Sung is Professor Emeritus at Pohang University of Science and Technology (POSTECH), where he taught and researched in the fields of statistical physics and biological physics for about 30 years. He obtained his Bachelor of Science at Seoul National University and Ph.D. at the State University of New York at Stony Brook. He has been working mostly on a variety of biological matter and processes at the mesoscopic level, using statistical physics of soft matter and stochastic phenomena. In particular, he pioneered the theory of polymer translocation through membranes, engendering a whole new field in biological and polymer physics. He is a member of the Journal of Biological Physics editorial board and was an editor in chief in the period 2007–2009. For his seminal contributions to science, in particular to statistical/biological physics, Prof. Sung was awarded a Medal of Science and Technology bestowed by the Korean Government in 2010. He also served as a director of Center for Theoretical Physics at POSTECH, and the Distinguished Research Fellow at Center for Self-Assembly and Complexity, Institute of Basic Science, in Pohang. Professor Sung was a visiting scientist and professor at Oxford University, the Jülich Research Center, University of Pennsylvania, and Brown University.

Contents

Symbols

$A, \mathcal{A}$	Surface area
a	Unit length, ionic radius, the unit area, attraction strength
B	Magnetic field
B_2	Second virial coefficient
b	Bond energy, unit length in a polyelectrolyte
C	Heat capacity
C, c_i	Concentration, three-dimensional concentration
D	Diffusion constant, inter-surface distance
$\mathcal{D}$	Noise strength
D_f	Fractal dimension
D_T	Thermal diffusion constant
E	Internal energy
$\boldsymbol{E}, \boldsymbol{E_{ext}}$	External electric field
$e(\boldsymbol{r})$	Local energy density
F, f	Helmholtz free energy, Helmholtz free energy density
f_i	Generalized force
$\boldsymbol{F}, f$	Force
$\mathcal{F}\{\mathcal{Q}\}$	Effective Hamiltonian or the free energy function associated with $\mathcal{Q}$
$f_R(t)$	Random force
$G, g, \mathcal{G}$	Gibbs free energy, Gibbs free energy per particle, variable Gibbs free energy
$G(\boldsymbol{r}, \boldsymbol{r}_0; N)$	Polymer Greens function
$g(\boldsymbol{r}), g(r)$	Pair distribution function, radial distribution function
H	Enthalpy
$\mathcal{H}$	Hamiltonian
$\hbar, h$	Planck constant, Undulation height
$\boldsymbol{J}, \boldsymbol{J}_n$	Flux, number flux vector
K	Kinetic energy
K_e	Entropic spring constant
K_s	Stretch modulus

K_T	Isothermal compressibility
$\boldsymbol{k}$	Wave vector
k_B	Boltzmann constant
k_e, k_q	Spring constant in the bead-spring model
$\mathcal{L}$	Langevin's function, evolution operator
$\mathcal{L}^+$	Adjoint evolution operator
$\mathcal{L}_{FP}$	Fokker–Planck operator
l	Segmental length, step length, dipole length
l_B	Bjerrum length
l_p	Persistence length
M	Magnetic moment
M, m	Mass
$\mathcal{M}$	Microstate
$N, \mathcal{N}$	Number of particles
$n, \boldsymbol{n}$	Number density, fluctuating number density
n_0	Concentration at standard state
n_∞	Concentration at the bulk
$\boldsymbol{O}(\boldsymbol{r})$	Oseen tensor
P, p	Pressure
P	Probability distribution function (PDF)
$\boldsymbol{p}$	Momentum, dipole moment
Q	Heat, charge, mesoscopic degrees of freedom
Q_N	Configuration partition function (Chap. 4)
q	Charge, coordination number, wave number, stochastic variable
$\boldsymbol{q}$	Wave vector
R	Radius
R_G	Radius of gyration
Re	Reynolds number
$\boldsymbol{r}$	Position vector, distance vector
$\boldsymbol{r}_n$	The position of nth bead
S, s	Entropy, entropy density
$S(\boldsymbol{q})$	Structure factor
$S(\omega)$	Power spectrum
$S(\boldsymbol{q}, \omega)$	Dynamic structure factor
s	Arc length
T	Absolute temperature
T_Ω	Periodicity
t	Time
$U\{\boldsymbol{r}_i\}, u(\boldsymbol{r}_i)$	External potential energy
$\mathcal{U}(q)$	Drift
$\boldsymbol{u}$	Unit tangent vector, fluid velocity
V, v	Volume, Velocity
W	Work applied to the system
$w(\mathcal{E})$	Density of states

$X_i, \mathcal{X}_i, \mathcal{X}$	Generalized displacement, macroscopic and microscopic
$Z, \mathcal{Z}$	Canonical partition function
z	Valence of ions, single-particle partition function, fugacity
α	Polarizability
β	$1/k_BT$
$\Gamma(t)$	Systems' phase space point
γ	Surface tension
$\mathcal{E}$	System energy
ε	Electric permeability, internal energy density
ε_0	Electrical permeability in vacuum
ε_w	Electrical permeability of water
ϵ	Binding energy
ζ, ζ_s	Friction coefficient, surface friction coefficient
η	Shear viscosity
Θ	Strength of thermal noise
θ	Coverage of protein (Chaps. 2, 3), polar angle (Chap. 3)
$\kappa, \varkappa$	Bending rigidity, curvature modulus
$\varkappa_G$	Gaussian modulus
$\varkappa_G$	Curvature modulus for sphere
κ_T	Heat conductivity
λ	Thermal wavelength, wave length, linear charge density
λ_D	Debye screening length
μ	Chemical potential
ξ	Correlation length
$\rho(\boldsymbol{r}), \rho_e(\boldsymbol{r})$	Mass density, charge densities
$\boldsymbol{\sigma}$	Pressure tensor or stress tensor surface force density
τ	Mean first passage time (MFPT), correlation or relaxation time
τ_R, τ_Z	Rouse time, Zimm time
τ_K	Kramers time
τ_p	Momentum relaxation time
$\Phi\{\boldsymbol{r_i}\}, \varphi(\boldsymbol{r}_{ij})$	Interaction potential energy
φ	Azimuthal angle, potential energy
ϕ_s	Surface potential
χ	Magnetic susceptibility
χ_P	Static electric susceptibility
$\chi(t)$	The dynamic response function
Ω	Grand potential (Chaps. 2, 3), solid angle (Chap. 3)
ω	Frequency

Chapter 1
Introduction: Biological Systems and Physical Approaches

—Open the door, open the door, the Flower,
Thunder and Storm be the only way,
the Flower, open the door!—

Seo Jung Ju

In January 1999, at the dawn of the new millennium, Time Magazine devoted the majority of its coverage to a special issue entitled "*The Future of Medicine.*" The cover story began as follows: "*Ring farewell to the century of physics, the one in which we split the atom and turned silicon into computing power. It's time to ring in the century of biotechnology.*" Despite the tremendous importance of life science and biotechnology nowadays as the above statements proclaim, at this stage their knowledge appears to be largely phenomenological, and thus undeniably calls for fundamental and quantitative understandings of the complex phenomena. It will be timely to ring in the century of a new physical science to meet this challenge.

1.1 Bring Physics to Life, Bring Life to Physics

Biological Physics or Biophysics is a new genre of physics which has attempted to describe and understand biology. Despite a few important achievements such as unravelling DNA's double-helical structure by James Watson and Francis Crick using X-ray diffraction, biological physics, as the fundamental and quantitative

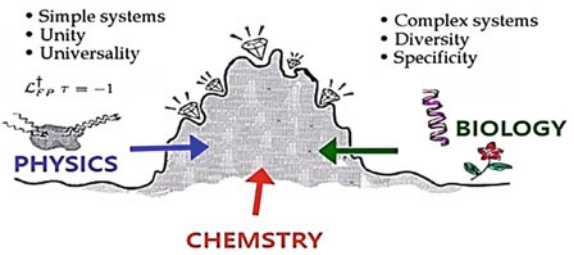

Fig. 1.1 Physics and biology. Between them lies a mountain called biological physics or physical biology. On the axis toward you is chemistry

W. Sung, *Statistical Physics for Biological Matter*, Graduate Texts in Physics,
https://doi.org/10.1007/978-94-024-1584-1_1

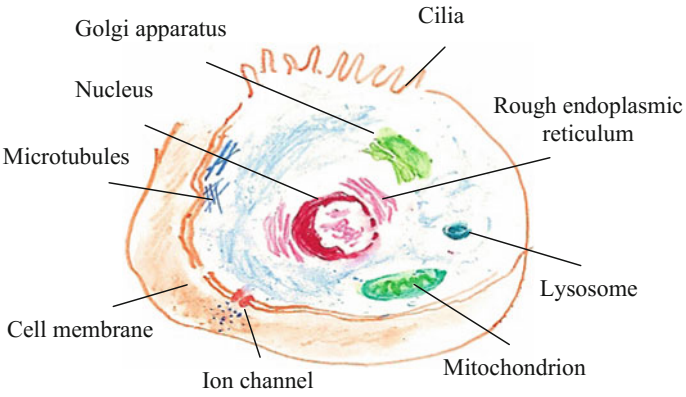

Fig. 1.2 A biological cell is the elementary factory of life, with self-organizing micro-nano scale internal structures. Several key organelles are drawn

science of biological phenomena, has had rather a slow growth and is yet in its infancy. There are dramatic differences between two sciences, physics and biology, in study methods and objects. Physics, by tradition, pursues unity and universality in underpinning principles, and quantitative descriptions for rather simple systems. Biology, in contrast, used to deal with variety and specificity, and seek qualitative descriptions for very complex systems. Physics and biology represent two opposite extremes of sciences, so presence of a seemingly-insurmountable barrier between them is not a surprise (Fig. 1.1).

From the view point of physics, biological systems have enormously complex hierarchies of structures that range from the microscopic molecular worlds to macroscopic living organisms. In this book, major emphasis is focused on the mesoscopic, or cellular level, which covers nanometer to micrometer lengths, in which cells and their constituent biopolymers, membranes, and other subcellular structures are the main components of interest (Fig. 1.2). Cells consist of nanometer and micrometer sized subcellular structures, which appear to be enormously complex, yet exhibit certain orders for biological functions, the phenomenon what we call biological self-organization. The flexible structures incessantly undergo thermal motion, and, in close cooperation with each other and the environment, play the symphony of life.

1.2 The Players of Living: Self-organizing Structures

Biopolymers are the most essential functional elements, which can be appropriately called *the threads of life*. Among them, DNA is the most important biopolymer, which stores hereditary information. The monomers of DNA, called nucleotides, form two complementary chains in double helices, encoding genetic information.

At first glance, DNA appears to be quite complex as it winds to form chromosomes, but it reveals a fascinating hierarchy of ordered structures. It is remarkable that although a cell's DNA may be as long as a few meters, it can miraculously be packed into a nucleus that is only a few micrometers in size (Fig. 1.3).

Proteins are also important biopolymers. Proteins are chains of monomers called amino acids, interconnected via a variety of interactions in water. The interactions cause proteins to fold into the native structures that have the lowest energies among a vast variety of configurations. Mother Nature accomplishes with ease the protein folding into the native structures, in which they perform biological functions. Understanding this mystery remains yet an important challenge in biological physics.

Another dramatic example of self-organization occurs at a **biological membrane**, which we may call the *interface of life* (Fig. 1.4). A lipid molecule (lipid), which is the basic constituents of the membrane, is composed of a hydrophilic head and hydrophobic tails. The lipids spontaneously self-assemble into a bilayer, forming a barrier to permeation of ions and macromolecules, thus providing the most basic function of a biological membrane. For certain functions of life like

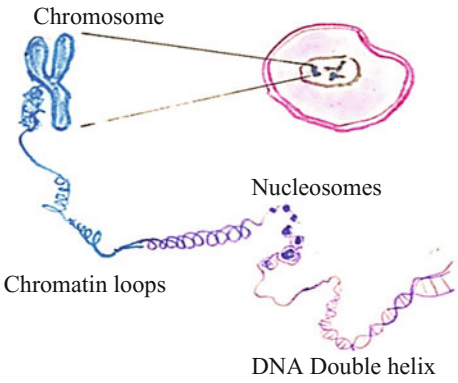

Fig. 1.3 DNA folded and packed within a nucleus in a multiscale hierarchy from double-stranded duplex to chromosome

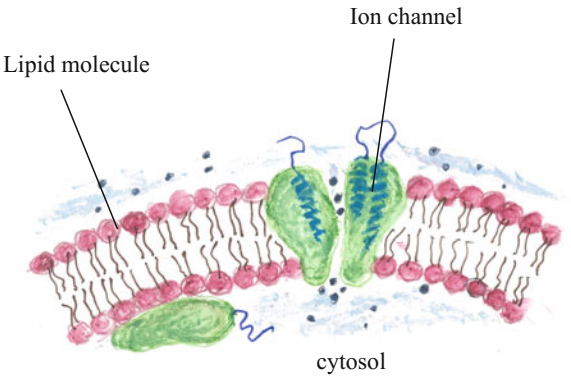

Fig. 1.4 A cross section of a cell membrane with associated ion channels and proteins

neural transmissions and sensory activities, certain specific ions must pass through the membrane. For this reason, Nature dictates some certain proteins to fold into the membrane and form a **nano-machine called an ion channel** to regulate passage of ions. The information of the channel structures is given gradually, but comprehensive physical understanding of how they work is yet to be achieved.

1.3 Basic Physical Features: Fluctuations and Soft Matter Nature

The preceding overview has implied that **the biological components self-organize themselves to function. To perform the biological self-organization, they often cross over the energy barriers that seem to be insurmountable in the view point of simple physics. To this end, there are two physical characteristics that feature in the mesoscopic biological systems introduced above. The first one is their aqueous environments and thermal fluctuations therein. The water has many outstanding properties among all liquids.** Its heat capacity is almost higher than any other common substance, meaning that it functions as a heat reservoir with negligible temperature change. The most outstanding property of water is its dielectric constant (around 80) that is much higher than those of other liquids. Because of this, water can reduce electrostatic energy of the interaction to the level of thermal energy. These unique properties of water originate microscopically from hydrogen bonding between water molecules. This bonding is also a relatively weak interaction; even though the bonding can be broken due to thermal fluctuations, it causes long-range correlation between water molecules. As a result, the liquid water manifests a quasi-critical state where it responds collectively and sensitively to external stimuli.

Another physical characteristics is the structural connectivity and flexibility the systems may have, the features that are not seen in traditional physics. Although interactions between monomers (e.g., the covalent bonding between two adjacent nucleotides in a DNA strand) can be as large as or larger than several electron volts (eV), the chain as a whole displays collective motions and excitations of energy as low as in the order of thermal energy $k_BT \sim 0.025$ eV. Such a low energy is commensurate with **weak biological interactions,** e.g., hydrophobic/hydrophilic, the Van der Waals, and the screened Coulomb interactions between two segments mediated by water. Thus, thermal agitations can easily change **conformations (shapes)** of the biological components, and at the long times when the equilibrium is reached, minimize their free energies at the temperature of the surrounding; examples include conformational transitions such as DNA/protein folding, lipid self-assembly, and membrane fusion. The **conformation** emerges as a new, primary variable, and **conformation transition** becomes the central problem for biological physics. The biological systems in mesoscale characterized by the **soft interconnectivity and weak interactions** may appropriately be called the

bio-soft condensed matter. **To this matter, a thermal fluctuation with energy of the magnitude k_BT may come as a thunderstorm; it adds to the disorder in ordinary matter but may assist biological matter to surmount the barriers for self-organization.**

The biological systems in vivo function out of equilibrium, driven by external influences. Due to the macromolecular nature and the viscous backgrounds, the dynamics of biological components at mesoscales is usually **dissipative, slow, yet stochastic**. The biological dynamics can be modelled as **generalized Brownian motion**, not only with the internal constituents fluctuating while interacting with each other, but also with external forces that can fluctuate often far from equilibrium. It was found that thermal fluctuations or internal noises do not simply add to the disorder of the system but, counter-intuitively, contribute to **the coherence and resonance to external noises**. In short, the basic physical features behind biological self-organization are thought to be thermal fluctuations and non-equilibrium stochasticity combined with soft matter flexibility and weak interactions.

1.4 About the Book

This book addresses the basic statistical physics for biological systems and phenomena at the mesoscopic level ranging from nanometer to cellular scales. Because of thermal fluctuations and stochasticity, probabilistic description is inevitable. The statistical physics description for such biological systems requires a systematic way of characterizing the complex features effectively in terms of relevant degrees of freedom, what we call "coarse graining".

The book first deals with equilibrium state of matter, starting with thermodynamics and its foundational science, statistical mechanics. To illustrate its practical utility we apply statistical ensemble methods to relatively simple but archetypal systems, in particular, two-state biological systems. We then present the application of statistical mechanics to both simple and complex fluids, the playgrounds for biological complexes. We introduce the method of coarse-grained description for the emerging degrees of freedom and the associated effective Hamiltonians. We then devote several chapters to the general physical aspects of water, weak interactions between the objects therein, and to reactions, transitions and self-assembly. The lattice and Ising models are presented to deal with a number of two-state problems such as molecular binding on substrates, and biopolymer transitions. We then describe how the responses to a stimulus and a scattering on matter are related with the internal fluctuations and their spatial correlations. In two chapters on polymers, we adapt statistical physics to mesoscopic descriptions of flexible and semiflexible polymers, their conformational/entropic properties, exclusion/collapse, confinement/stretching, and electrostatic properties, etc. The next chapter is devoted to mesoscopic description of membranes in terms of the shapes and curvatures.

The other part of the book is devoted to non-equilibrium phenomena. Dynamics of biological systems is essentially the non-equilibrium process often with their soft matter nature displayed. The basic methods include a stochastic approach in which the mesoscopic degrees of freedom undergo the generalized Brownian motions. We start with the Einstein-Smoluchowski–Langevin theories of Brownian motion, which are extended within the framework of Markov process theory; the master equation and the Fokker-Planck equation are discussed and applied to biological problems. The thermally-induced crossing over free energy or activation barriers is discussed using the rate theory and mean first passage time theory. The response of a dynamic variable to time-dependent forces or fields is introduced along with underlying time correlation function theories (Fluctuation-Dissipation Theorem). A thermal fluctuation, when optimally tuned, will be shown to induce coherence and resonance to a small external driving. Also, an emphasis is placed on the fluid backgrounds, and its own hydrodynamics and transport phenomena. The dynamics of biological soft matter such as simple polymers and membranes interacting hydrodynamically in a viscous fluid, often anomalous due to the structural connectivity, is then described.

Further Reading and References

J. Knight, Physics meets biology: Bridging the culture gap. Nature **419**, 244–246 (2002)
H. Frauenfelder, P.G. Wolynes, R.H. Austin, Biological Physics. Rev. Mod. Phys. **71**, S419–S430 (1999)
R. Phillips, S.R. Quake, The biological frontier of physics. Phys. Today **59**, 5 (2006)

Biological Physics Books (Examples)

R. Phillips, J. Kondev, J. Therio, *Physical Biology of the Cell* (Garland Science-Taylor and Francis Group, 2008)
P. Nelson, *Biological Physics* (W-H Freeman, 2007)
K. Sneppen, G. Zocchi, *Physics in Molecular Biology* (Cambridge University Press, 2006)
D. Ball, *Mechanics of the Cell* (Cambridge University Press, 2002)
M. Daune, *Molecular Biophysics* (Oxford University Press, 1999)
M.B. Jackson, *Molecular and Cellular Biophysics* (Cambridge University Press, 2006)
W. Bialek, *Biophysics: Searching for Principles* (Princeton University Press, 2012)
T.A. Waigh, *The Physics of Living Processes: A Mesoscopic Approach* (Wiley, 2014)
H. Schiessel, *Biophysics for Beginners: A Journey through the Cell Nucleus* (Pan Stanford Publishing, 2014)
D. Andelman, *Soft Condensed Matter Physics in Molecular and Cell Biology*, Ed. by W.C.K. Poon (Taylor and Francis, 2006)
J.A. Tuszynsky, M. Kurzynski, *Introduction to Molecular Biophysics* (CRS Press, 2003)

Chapter 2
Basic Concepts of Relevant Thermodynamics and Thermodynamic Variables

A macroscopic or a mesoscopic system contains many microscopic constituents, such as atoms and molecules, with *a huge number* of degrees of freedom to describe their motion. **Thermodynamics**[1] **seeks to describe properties of matter in terms of only *a few variables*, arguably being the all-around, basic area of sciences and engineering, including biology.** Thermodynamics and thermodynamic variables characterize states of matter and their transitions phenomenologically without recourse to microscopic constituents. In this chapter we summarize what we believe to be the essentials that will serve as references throughout the book. The link between this phenomenological description and microscopic mechanics is provided by statistical mechanics beginning next chapter.

When a macroscopic system is brought to equilibrium, where its bulk properties become time-independent, they can completely be described by *a few* variables descriptive of the state, called the **state variables**. For example, the macroscopic properties of an ideal gas or of an ideal solution at equilibrium can be described by the pressure or the osmotic pressure p, volume V, and absolute temperature T; e.g., for a mole of them, the equation of state is $pV = RT$, where the R is the universal gas constant. The thermodynamic state variables are either extensive or intensive. Extensive variables are proportional to the size of the system under consideration; intensive variables are independent of the system size; for example, the gas' volume V and internal energy E are extensive, whereas the pressure p and the temperature T are intensive.

Here, we briefly summarize the universal relations beginning with the first law of thermodynamics. By a universal relation we mean the relation independent of the systems' microscopic details. We introduce the basic thermodynamic potentials

[1]Contrary to what the nomenclature implies, thermo*dynamic*s mostly deals with the equilibrium state of matter at macroscale, so often is also coined as thermo*statics*. The second law of thermodynamics, however, is concerned with non-equilibrium processes approaching equilibrium, the rigorous treatment of which is treated in the area called non-equilibrium thermodynamics (S. R. de Groot and P. Mazur "Non-equilibrium Thermodynamics", 1984, Courier Corp.). In chemistry or biochemstry communities, "biological thermodynamics" include the chemical kinetics and reactions (e.g., Biological Thermodynamics, D. T. Haynes, 2008, Cambridge University Press.

W. Sung, *Statistical Physics for Biological Matter*, Graduate Texts in Physics,
https://doi.org/10.1007/978-94-024-1584-1_2

from which we can find the various thermodynamic variables. From the second law of thermodynamics, we discuss nature of the processes leading to equilibrium, which are governed by variational principles for the thermodynamic potentials relevant to ambient thermodynamic conditions.

2.1 The First Law and Thermodynamic Variables

2.1.1 Internal Energy, Heat, and Work: The First Law of Thermodynamics

Here we consider the changes of thermodynamic state variables controlled by *quasi-static processes*, which are ideally slow so as to retain the equilibrium state. **Quasi-static processes are reversible, i.e., can be undone.** First consider the net energy of the system, called the **internal energy** $\boldsymbol{E}$, which is conserved in a system that does not exchange matter or energy with the environment, called an isolated system. Because E is given *uniquely* by other state variables Y_i (the independent variables), $E = E(Y_1, Y_2, \ldots)$, the state variable E is also a **state function**, with its infinitesimal change dE being an **exact differential**:

$$dE = \sum_i \frac{\partial E}{\partial Y_i} dY_i. \tag{2.1}$$

The first law of thermodynamics is simply the statement of energy conservation involving various forms of energies. It says

$$dE = đQ + đW, \tag{2.2}$$

where $đQ$ and $đW$ are respectively the infinitesimal **heat** and the infinitesimal **work applied to the system** by certain external agents. Equation (2.2) says that its internal energy increases if it is heated and decreases if the work is done by it. Unlike the internal energy, both of the heat and work cannot be solely described by the present state variables but depend on the processes through which they are changed. As such their infinitesimal changes denoted by đ signify **inexact differentials**, which depend on the paths or histories of the processes taken. For example consider a quai-static cyclic process of a gas undergoing an expansion (process $1 \to 2$) and compression ($2 \to 1$) returning to its initial state 1 under a pressure (Fig. 2.1). The cyclic change of the work, defined by $\oint đW = -\oint pdV$, is not vanishing but given by the shaded area. In contrast, the cyclic change of the internal energy (a state variable with its differential being exact) denoted by $\oint dE = E_1 - E_1$ is zero.

In a similar manner the cyclic change of the heat is not vanishing,

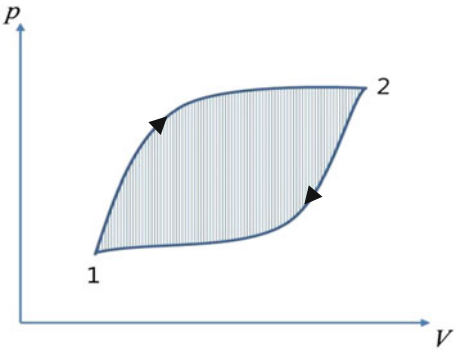

Fig. 2.1 The relation between pressure (p) and volume (V) for a cyclic process consisting of a reversible expansion ($\mathbf{1} \rightarrow \mathbf{2}$) and a reversible contraction ($\mathbf{2} \rightarrow \mathbf{1}$) on a gas. In this cylic process the system does work by the amount given by the shaded area

$$\oint đQ \neq 0. \tag{2.3}$$

However, according to Rudolf Clausius, for any cyclic change controlled to be reversible,

$$\oint \frac{đQ}{T} = 0, \tag{2.4}$$

where ***T* is a state variable called the temperature**. From the equation **an exact differential of a state function *S*, called entropy**, is defined as

$$dS = \frac{đQ}{T}. \tag{2.5}$$

Entropy, which is the central concept in thermodynamics and in various aspects of biological processes, will be discussed later repeatedly.

P2.1 *Show that, for an ideal gas or solution of one mole for which $E = 3RT/2$ and $pV = RT$ are known, (2.5) for a reversible process of changing the volume and temperature is $dS = (3R/2T)dT + (R/V)dV$, which is indeed an exact differential. The entropy change from V_1, T_1 to V_2, T_2 is $\Delta S = (3R/2)\ln(T_2/T_1) + R\ln(V_2/V_1)$. Although derived for a reversible process, because S is a state variable, this relation is independent of the thermodynamic paths taken between the initial and final states, so that ΔS it is applicable to any processes (including irreversible one) that connects the same initial and final states, 1 and 2.*

2.1.2 *Thermodynamic Potentials, Generalized Forces, and Displacements*

Now consider the work in detail; it can be generated by various agents such as external forces and fields acting on the system,

$$đW = \mu dN + \sum_i f_i dX_i. \tag{2.6}$$

The first term on the right is the **chemical work (involving the chemical potential μ)** necessary to increase the number of particles N of the system by unity. For a mixture of m component particles it can be generalized to $\sum_{k=1}^{m} \mu_k dN_k$, where k denotes the species. In the second term, **f_i is a generalized force or a field and X_i is a thermodynamic conjugate to it, called a displacement** (Table 2.1). The first three generalized forces and displacements in the table are mechanical, while the last two examples are electromagnetic. f_i are intensive *state* variables, whereas X_i are extensive *state* variables.

For illustration, consider a one-component system ($m = 1$) with one generalized force f_i and the associated displacement X_i. The most familiar case is a particle system such a gas or a colloidal solution confined within a volume by a pressure, for which $f_i = -p, X_i = V$. For a stretched chain, the tension f and the length of extension X are such a force-displacement pair (Table 2.1).

Using the relations (2.5) and (2.6) the first law of thermodynamics (2.1) can be written in terms of state variables S, N and X_i:

$$\begin{aligned} dE &= đQ + đW \\ &= TdS + \mu dN + f_i dX_i. \end{aligned} \tag{2.7}$$

Representing S as the primary variable, (2.7) can be rewritten as

$$dS = \frac{1}{T} dE - \frac{\mu}{T} dN - \frac{f_i}{T} dX_i, \tag{2.8}$$

which expresses S as a state function of independent state variables, E, N and X_i, $S = S(E, N, X_i)$. Equation (2.8) being an exact differential, the following relations are obtained:

$$\frac{1}{T} = \left(\frac{\partial S}{\partial E}\right)_{X_i, N}, \tag{2.9}$$

Table 2.1 Examples of generalized forces and the conjugate displacements

Systems	Generalized forces (intensive variables)	f_i	X_i	Generalized displacements (extensive variables)
Fluid	Pressure	$-p$	V	Volume
String	Tension	f	X	Length of extension
Surface	Surface tension	γ	A	Surface area
Magnet	Magnetic field	$-B$	M	Magnetization along the field
Dielectrics	Electric field	$-E$	P	Polarization along the field

$$\frac{\mu}{T} = -\left(\frac{\partial S}{\partial N}\right)_{E,X_i}, \tag{2.10}$$

$$\frac{f_i}{T} = -\left(\frac{\partial S}{\partial X_i}\right)_{E,N}, \tag{2.11}$$

where the subscripts in the partial differentiations indicate the variables that are held fixed. Equations (2.9)–(2.11) mean that once S is obtained as a function of independent variables E, N, and X_i, it can generate their thermodynamic conjugates T, μ, and f_i, by taking the first-order partial derivatives with respect to the independent variables. Functions obtained by taking first-order partial derivatives over thermodynamic potentials will be called the first-order functions.

Equations (2.9)–(2.11) show how the basic intensive variables are related to the entropy. Equation (2.9) is a fundamental thermodynamic relation that defines the **temperature**: the ratio of an increase of the entropy with respect to the energy increase is a positive quantity $1/T$. Equation (2.10) tells us that the **chemical potential μ** is a measure of the change of entropy when a particle is added to the system without an external work and change of internal energy. Equation (2.11) defines **the generalized force f_i that acts in the direction to decrease the entropy**, with E, N fixed. In a gas or a solution the force is the pressure p compressing the system to keep it from increasing its entropy. For a polymer string it is the tension force f to extend it (Fig. 2.2).

A thermodynamic potential is a state variable that describes the system's net energy, from which all other variables can be derived. One example is the internal energy we have considered; another one is the **Helmholtz free energy defined by $F = E - TS$**. If we consider this as the primary thermodynamic potential, (2.7) is transformed to

$$dF = d(E - TS) = -SdT + f_i dX_i + \mu dN, \tag{2.12}$$

which indicates that F is the state function that depends on the state variables T, X_i and N, i.e., $F = F(T, X_i, N)$. It can generate thermodynamic relations for the first-order variables,

$$S = -\left(\frac{\partial F}{\partial T}\right)_{X_i,N}, \tag{2.13}$$

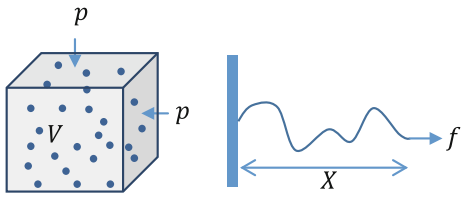

Fig. 2.2 Two kinds of forces: pressure $\boldsymbol{p}$ (force per unit area) on the gas to keep its volume as $\boldsymbol{V}$, and extensional tension $\boldsymbol{f}$ on a polymer to keep its extension as $\boldsymbol{X}$. The forces act in the directions in which to decrease the entropy

$$f_i = \left(\frac{\partial F}{\partial X_i}\right)_{T,N}, \tag{2.14}$$

$$\mu = \left(\frac{\partial F}{\partial N}\right)_{T,X_i}. \tag{2.15}$$

The internal energy is then obtained from the Helmholtz free energy:

$$E = F + TS = F - T(\partial F/\partial T)_{X_i,N} = -T^2\partial(F/T)/\partial T. \tag{2.16}$$

For systems controlled by a displacement X_i, e.g., for a fluid confined within a volume, or a string kept at a constant extension, the Helmholtz free energy is the thermodynamic potential of choice. S in this representation depends on T as well as on X_i and N, in contrast to (2.8). Since $\partial^2 F/\left(\partial x_j \partial x_k\right) = \partial^2 F/\left(\partial x_k \partial x_j\right)$, one can also obtain the **Maxwell relations** for the second order variables:

$$\frac{\partial S}{\partial X_i} = -\frac{\partial f_i}{\partial T}, \tag{2.17}$$

$$\frac{\partial f_i}{\partial N} = \frac{\partial \mu}{\partial X_i}, \tag{2.18}$$

$$\frac{\partial S}{\partial N} = -\frac{\partial \mu}{\partial T}. \tag{2.19}$$

P2.2 *Consider the* ***enthalpy*** *defined by $H = E + pV$ as a primary thermodynamic potential and obtain the thermodynamic relations for the first and second order variables.*

P2.3 *Consider that a strip of rubber is extended quasi-statically to a length X. Show how the force of extension or the tension is expressed in terms of the free energy. Find the Maxwell relations.*

Another useful representation is the one in which the Gibb's free energy $G = F - f_i X_i$ is the primary thermodynamic potential. From (2.12), its differential is given as

$$\begin{aligned} dG &= d(F - f_i X_i) \\ &= -SdT - X_i df_i + \mu dN. \end{aligned} \tag{2.20}$$

The Gibbs free energy is the thermodynamic potential that depends on three independent variables $\boldsymbol{T}, \boldsymbol{f_i}$, and $\boldsymbol{N}$, i.e., $\boldsymbol{G = G(T, f_i, N)}$. For a one-component system, because N is the only extensive variable among the three, the extensivity of G requires that

$$G(T,f_i,N) = Ng(T,f_i), \tag{2.21}$$

where $g(T,f_i)$ is the Gibbs free energy per particle. In this representation the first-order thermodynamic variables are derived as

$$S = -\left(\frac{\partial G}{\partial T}\right)_{N,f_i} \tag{2.22}$$

$$X_i = -\left(\frac{\partial G}{\partial f_i}\right)_{T,N} \tag{2.23}$$

$$\mu = \left(\frac{\partial G}{\partial N}\right)_{T,f} = g(T,f_i). \tag{2.24}$$

The chemical potential is the Gibbs free energy per particle for a one-component system, which is independent of the number of particles number, thus

$$d\mu(T,f_i) = -\frac{S}{N}dT - \frac{X_i}{N}df_i. \tag{2.25}$$

For systems controlled by the generalized force f_i, the Gibbs free energy is a convenient thermodynamic potential. Because experiments on fluids are usually performed under constant pressures, the Gibbs free energy is often chosen as the primary thermodynamic potential.

Lastly let us consider **the grand potential** as the primary thermodynamic potential, which for a one-component system is defined by

$$\Omega = F - \mu N. \tag{2.26}$$

Its differential

$$d\Omega = -SdT + f_i dX_i - Nd\mu, \tag{2.27}$$

is obtained by using (2.12), so that Ω has the independent variables T, X_i, and μ. Consequently

$$S = -\left(\frac{\partial \Omega}{\partial T}\right)_{X,\mu} \tag{2.28}$$

$$f_i = \left(\frac{\partial \Omega}{\partial X_i}\right)_{T,\mu} \tag{2.29}$$

$$N = -\left(\frac{\partial \Omega}{\partial \mu}\right)_{T,X}. \tag{2.30}$$

Noting that $G = \mu N$, i.e., $\Omega = F - G = f_i X_i$, f_i can also be obtained directly from Ω as

$$f_i = \frac{\Omega}{X_i}. \tag{2.31}$$

P2.4 *The relation $\Omega = f_i X_i$ can be generalized to the case where there are multitude of conjugate pairs. Consider a liquid droplet in a gas. In this case the grand potential is given by*

$$\Omega = -p_g V_g - p_l V_l + \gamma A$$

where p_g, V_g and p_l, V_l are the pressures and volumes of the gas and liquid phases respectively, γ is surface tension in the interfacial area A.

2.1.3 Equations of State

One of the most important tasks of equilibrium statistical mechanics is to obtain the thermodynamic potentials explicitly for specific systems as functions of their own independent variables. From this procedure the first-order variables are obtained and related to yield the equations of state.

The most well-known example is the equation of state that relates the pressure p with the volume V of a one-mole ideal gas or an ideal solution:

$$pV = RT. \tag{2.32}$$

An approximate equation of state for non-ideal fluids that includes the inter-particle interactions is **the Van der Waals equation of state**

$$\left(p + \frac{a}{V^2}\right)(V - b) = RT, \tag{2.33}$$

where a and b are the constants that parametrize inter-particle attraction and repulsion, respectively.

The equation of state that describes ideal paramagnets is Curie's law,

$$\frac{M}{B} = \frac{C}{T} \tag{2.34}$$

where B is a magnetic field along a direction, M is the magnetization induced along the direction, and C is the Curie constant which is material-specific. Due to the mutual interactions between the magnetic moments within it, a paramagnet undergoes a **phase transition**, at a temperature called the critical temperature T_c, to a ferromagnet, for which an approximate equation of state is

$$\frac{M}{B} = \frac{C}{|T - T_c|}. \tag{2.35}$$

Another example, which is of biological importance, is the equation for the force f necessary to extend a DNA fragment by an amount X:

$$f = AT\left[\frac{1}{4}\left(1 - \frac{X}{L}\right)^{-2} - \frac{1}{4} + \frac{X}{L}\right] \tag{2.36}$$

where L is a contour length and A is a constant.

P2.5 *Calculate the Helmholtz free energy of the Van-der Waals gas. What is the chemical potential? What is the isothermal compressibility?*

P2.6 *Using* (2.36),

(a) *Find the Helmholtz free energy F of the DNA as a function of X. At what value of X is the free energy minimum?*
(b) *By how much does the entropy change when the DNA is quasi-statically extended from* $X = 0$ *to* $X = L/2$ *at a fixed temperature T.*
(c) *If you increase the temperature slightly by* ΔT *with the extension force held fixed as f, how would the extension X change?*

2.1.4 Response Functions

The properties of a material can be learned by studying how it responds to small external influences. The response of the system to a variation of temperature is given by a response function called **heat capacity**

$$C = \frac{đQ}{dT} = T\frac{\partial S}{\partial T}. \tag{2.37}$$

Using (2.7) and (2.16), the heat capacity of a material with fixed N measured at fixed volume is given by

$$C_V = \left(T\frac{\partial S}{\partial T}\right)_V = \left(\frac{\partial E}{\partial T}\right)_V = -\left(T\frac{\partial^2 F}{\partial T^2}\right)_V \tag{2.38}$$

which means that the constant-volume heat capacity C_V can be obtained from either S or E. The fact that the C_V is the second-order derivative of the thermodynamic potential F implies that C_V yields higher-level information than can be afforded by the first-order variables. As we will reveal, C_V **is directly related to the intrinsic energy fluctuations of the systems, and identifies thermally-excited microscopic degrees of freedom that underlie.**

Other response functions of interest that we will study are **isothermal compressibility**

$$K_T = -\frac{1}{V}\left(\frac{\partial V}{\partial p}\right)_T \tag{2.39}$$

and **magnetic susceptibility**

$$\chi_T = \left(\frac{\partial M}{\partial B}\right)_T, \tag{2.40}$$

which are second-order thermodynamic functions related to the systems' volume and magnetization fluctuations, respectively (Chap. 9).

2.2 The Second Law and Thermodynamic Variational Principles

The state variable entropy S, first introduced by Clausius in 1850, is defined by (2.5) in terms of the heat reversibly exchanged at an absolute temperature T. However, strictly speaking, **most spontaneous processes that occur in nature are not reversible** but pass through non-equilibrium states. For example, consider a gas that undergoes free expansion. Experience tells us that the infinitesimal change of heat in the spontaneous, irreversible processes is less than that given by (2.5):

$$\delta Q \leq T\delta S, \tag{2.41}$$

where δ denotes the differential indicating an irreversible change. Therefore for an isolated system that does not exchange heat with the outside ($\delta Q = 0$),

$$\delta S \geq 0. \tag{2.42}$$

This formulates a form of the second law of thermodynamics: for an isolated system, a spontaneous process occurs in such a way that the entropy increases to

its maximum ($\delta S = 0$), which is just the equilibrium state. The entropy is identified as a measure of the system's disorder as will be shown in next chapter. This fundamental law sets the directions for natural phenomena to take, **the time arrow**, allowing us to distinguish the future from the past. This variational form of the second law for the entropy can be extended to the variational principles for other thermodynamic potentials to have approaching equilibrium (Table 2.2), as we shall see.

It is mistakenly perceived that living organisms defy the second law because they can organize themselves to increase the order, i.e., they live on negative entropy, called negentropy. Whereas the entropy maximum is referred to an isolated system at equilibrium, **the living being is an open system, which can exchange both energy and matter with its environment**. For example, the entropy of a biopolymer undergoing folding decreases, while that of the surrounding water increases in such a way that the entropy of the whole, if isolated, increases as will be shown below. Furthermore the living organisms in vivo usually function far from equilibrium. The equilibrium thermodynamics is nevertheless applied to biological systems in vitro which are either at or near the equilibrium state.

2.2.1 Approach to Equilibrium Between Two Systems

We first use the 2nd law of thermodynamics to study the approach to equilibrium between two systems at contact and the conditions of the equilibrium. Consider an isolated system composed of two subsystems A and B partitioned by a movable wall, which allows the exchange of matter as well as energy (Fig. 2.3). Suppose that each of the subsystems is at equilibrium on their own but not with respect to each other and evolve irreversibly towards the total equilibrium through the exchanges. During an infinitesimal process, the net entropy change of the isolated system is given by

$$\begin{aligned}\delta S &= \delta S_A + \delta S_B \\ &= \left(\frac{\partial S_A}{\partial E_A} + \frac{\partial S_B}{\partial E_A}\right)\delta E_A + \left(\frac{\partial S_A}{\partial V_A} + \frac{\partial S_B}{\partial V_A}\right)\delta V_A + \left(\frac{\partial S_A}{\partial N_A} + \frac{\partial S_B}{\partial N_A}\right)\delta N_A,\end{aligned} \tag{2.43}$$

where $\delta E_A, \delta V_A, \delta N_A$ are respectively the changes of the internal energy, volume, and particle number of subsystem A. Because the *net* energy, *net* volume and *net* particle number are all fixed in the isolated system, these changes are equal to $-\delta E_B, -\delta V_B, -\delta N_B$, respectively. Then, noting $(\partial S_B)/(\partial E_A) = -(\partial S_B)/(\partial E_B)$,

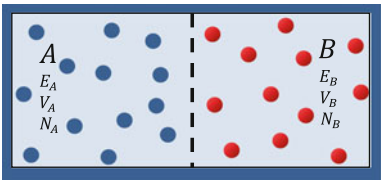

Fig. 2.3 An isolated system composed of two subsystems A and B partitioned by a movable wall. Their energies and particles can be exchanged through the wall

$(\partial S_B)/(\partial V_A) = -(\partial S_B)/(\partial V_B), (\partial S_B)/(\partial N_A) = -(\partial S_B)/(\partial N_B)$ along with the relations (2.9)–(2.11) and following the second law, the net entropy should increase until the maximum:

$$\delta S = \left(\frac{1}{T_A} - \frac{1}{T_B}\right)\delta E_A + \left(\frac{p_A}{T_A} - \frac{p_B}{T_B}\right)\delta V_A + \left(\frac{\mu_A}{T_A} - \frac{\mu_B}{T_B}\right)\delta N_A \geq 0. \tag{2.44}$$

Suppose for a moment that there is only an energy exchange, while both of each volume and particle number are fixed: $\delta V_A = \delta N_A = 0$. Then, the inequality in (2.44) means that $T_A > T_B$ leads to $\delta E_A < 0$, that is, the energy flows from A to B, i.e., form a hotter to a colder place. The entropy maximum, $\delta S = 0$, is reached when

$$T_A = T_B. \tag{2.45}$$

The equality between the temperatures is the condition for thermal equilibrium between the two subsystems in contact, which is named as the zeroth law of thermodynamics. With this thermal equilibrium established, we let the partition be movable and $p_A > p_B$ with no exchanges of the particles. Then (2.44) leads to $\delta V_A > 0$ meaning that by the pressure difference the system A expands until the pressures are equalized:

$$p_A = p_B. \tag{2.46}$$

By considering an exchange of particles, one can also show that the particles flow from the system of higher chemical potential to that of lower chemical potential, until they reach the chemical equilibrium, where

$$\mu_A = \mu_B. \tag{2.47}$$

Because $\delta E_A, \delta V_A, \delta N_A$ are independent of each other, each term in parentheses in (2.44) vanishes at the equilibrium, so the above three equations, called the condition of thermal, mechanical, and chemical equilibrium respectively, are simultaneously satisfied at the equilibrium.

2.2.2 *Variational Principles for Thermodynamic Potentials*

Now suppose that a subsystem A considered above is much smaller than B, so that the latter forms a heat bath kept at temperature T throughout (Fig. 2.4). Considering the subsystem A as our primary system (a polymer for example) to study we drop the subscript A. The infinitesimal change of total entropy δS_T of the isolated system $A + B$ is given by

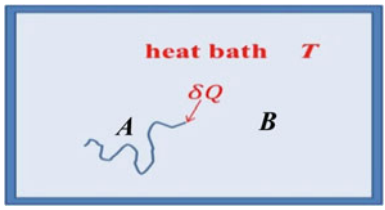

Fig. 2.4 The system A (e.g., a polymer chain) in a heat bath, which is kept at temperature T and enclosed by an isolating wall

$$\begin{aligned}\delta S_T &= \delta S + \delta S_B \\ &= \delta S - \frac{\delta Q}{T} = \delta S - \frac{\delta E - \delta W}{T} \\ &= (-\delta F + \delta W)/T.\end{aligned} \tag{2.48}$$

Here δQ is the differential heat given to system A by the bath at the fixed temperature T; by the first law $\delta Q = \delta E - \delta W$. Using the second law $\delta S_T \geq 0$, (2.48) tells us that $\delta F \leq \delta W$, i.e., δF is the minimum of the reversible work done on the system by the bath. If the system's displacement and number of particles are kept as fixed, then $\delta W = f_i \delta X_i + \mu \delta N$ is zero, and

$$\delta F \leq 0. \tag{2.49}$$

This is a famous variational principle; stating it again: **if the system at a fixed T has fixed X_i and N but is left unconstrained, its Helmholtz free energy decreases spontaneously to its minimum as the system approaches equilibrium**. For example a biopolymer, which keep its extension X as fixed and thus undergoes no work, conforms itself in a way to minimize its Helmholtz free energy.

Often the systems are under a fixed generalized force f_i, e.g., in a gas at atmospheric pressure, or a polymer chain subject to a fixed tension. In this case, $-\delta F + \delta W = -\delta(F - f_i X_i) \geq 0$, leading to

$$\delta G \leq 0, \tag{2.50}$$

i.e., **the Gibbs free energy of the system with T, kept at fixed f_i but otherwise unconstrained, decreases until it approaches the minimum, namely, the equilibrium**. The biopolymer subject to constant tension conforms itself to minimize the Gibbs free energy. A spherical vesicle blown by a pressure can have an optimal radius to minimize it (See 12.21).

Finally consider an open system in which the number of particles can vary but the displacement and chemical potential μ (not to mention the temperature) are fixed. In this case, $\delta S_T \geq 0$ with (2.48) leads to

$$\delta F - \delta W = \delta(F - \mu N) = \delta \Omega \leq 0; \tag{2.51}$$

it is the grand potential that is to be minimized. There are many situations where the numbers of systems' constituent units vary, e.g., phase transitions, reactions and self-assemblies.

Table 2.2 Constrained variables and associated thermodynamic principles

Systems	Thermodynamic variational principle
Isolated system with fixed N, E, X_i	Entropy $S \Rightarrow$ maximum
Closed system with fixed N, T, X_i	Helmholtz free energy $F \Rightarrow$ minimum
Closed system with fixed N, T, f_i	Gibbs free energy $G \Rightarrow$ minimum
Open systems with fixed μ, T, X_i	Grand potential $\Omega \Rightarrow$ minimum

Listed in Table 2.2 are the summary of the variational principles for the thermodynamic potentials to be optimized and their independent state variables conditioned to be fixed. These variational principles can be applied to any systems kept at a fixed temperature; the presence of the enclosing adiabatic wall in Fig. 2.4 is immaterial because the wall can be placed at an infinite distance away from the systems in question. As will be shown throughout this book, the variational principles will be of great importance in determining the equilibrium configurations of flexible structures at a fixed temperature, as typified by biomolecule and membrane conformations at body temperature.

Strictly speaking, these variational potentials should be distinguished from the equilibrium thermodynamic potentials (F, G, …) dealt in Sect. 2.1, which are just extrema of the variational ones. This is will be done whenever necessary hereafter, by using different scripts; e.g., $\mathcal{F}$ for F, $\mathcal{G}$ for G.

Examples:
Biopolymer Folding

A biopolymer subject to thermal agitation in an aqueous solution undergoes **folding-unfolding transitions**. For this case, the combined system of the polymer and the liquid bath can be regarded as an isolated system. According to the second law, $\delta S_T = \delta S + \delta S_B \geq 0$. Let us consider the transition from an unfolded state to a folded state at a fixed temperature. Folding means an increase of the order, which, as will be shown next chapter, signifies $\delta S < 0$, hence $\delta S_B > 0$. The entropy of the liquid bath increases, because during the folding process the water molecules unbind from the polymer and will enjoy a larger space to wander around, that is, a larger entropy. Following the thermodynamic variational principle, the free energy change of the polymer in contact with the heat bath then should satisfy $\delta F = \delta E - T\delta S \leq 0$; this equation leads to $\delta E \leq T\delta S$, and following $\delta S < 0$ as shown above, $\delta E < 0$, which implies that E decreases due to the folding of the polymer. In biological systems, conformation transitions such as this folding transition are numerous at body temperature.

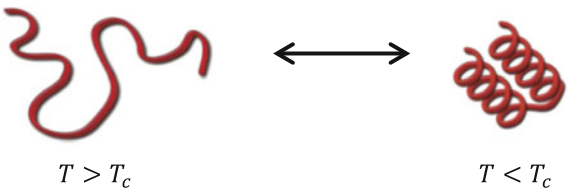

Fig. 2.5 Polymer unfolding-folding transition that occurs above and below the critical temperature T_c

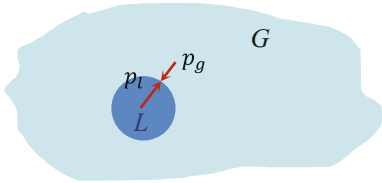

Fig. 2.6 A liquid drop (L) in a super-cooled gas (G) at a fixed temperature. Because of the interfacial tension γ, the liquid pressure $\boldsymbol{p_l}$ should be higher than the gas pressure $\boldsymbol{p_g}$

Spontaneous processes at a fixed T occur whenever the free energy of the system decreases:

$$\delta F = \delta E - T\delta S = (T_c - T)\delta S \leq 0, \tag{2.52}$$

where $T_c = (\delta E/\delta S)_{\delta F=0}$ is the critical temperature. Therefore if $T < T_c$, the transition to the ordered phase $(\delta S < 0)$ occurs, whereas if $T > T_c$, the transition to the disordered phase $(\delta S > 0)$ occurs. These are examples of a multitude of biopolymer conformational transitions, many more of which will be studied later.

Nucleation and Growth: A Liquid Drop in a Super-Cooled Gas

Nucleation is localized formation of a thermodynamic phase in a distinct phase. There are numerous examples in nature; they include ice formation, super-cooling within body fluids, self-organizing and growth process of molecular clusters, and protein aggregates. Here we include a simple case of nucleation and growth of a liquid drop in a super-cooled gas.

A gas super-cooled below its vaporization temperature is in a metastable state, giving way to a more stable equilibrium phase, that is, a liquid. In the process of condensation (phase transition of the whole system into a liquid), a droplet of liquid spontaneously nucleates and grows in the super-cooled gas. Because the gas and liquid are free to exchange the molecules and energy, both of chemical potential and temperature are equal in each phase, that is, uniform throughout the entire system. The pressure in each phase, however, cannot be same if the effects of interface are included. Because the chemical potential as well as the temperature and total volume are given as fixed, we choose, as the primary thermodynamic potential, the grand potential:

$$\Omega = -p_g V_g - p_l V_l + \gamma A, \tag{2.53}$$

where p_g, V_g and p_l, V_l are the pressures and volumes of the gas and liquid phases respectively, γ is surface tension in the interfacial area A. To minimize the surface contribution γA the liquid drop should reduce its surface area to the least possible value, and thus become spherical. The grand potential change associated with formation of a spherical drop with the varying radius r is

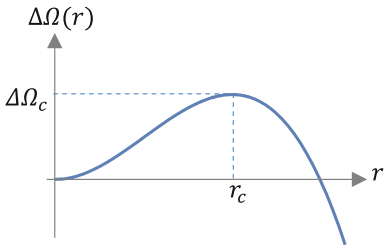

Fig. 2.7 The grand potential $\Delta\Omega(r)$ of forming a spherical droplet of radius r in a super-cooled gas

$$\Delta\Omega(r) = -\frac{4\pi r^3}{3}\Delta p + 4\pi r^2\gamma, \tag{2.54}$$

where we noted that total volume $V_g + V_l$ remains constant. With the fact that the liquid pressure is higher, $\Delta p = p_l - p_g > 0$, the profile of $\Delta\Omega(r)$ is depicted by Fig. 2.7. The mechanical equilibrium between the surface tension and volume pressure is reached when $\partial\Omega/\partial r = 0$, namely, $r = r_c$, where

$$r_c = 2\gamma/\Delta p. \tag{2.55}$$

This is called the **Young-Laplace equation**.

But the above is an unstable equilibrium condition; at the critical radius r_c the grand potential is at the maximum (Fig. 2.7); to reduce $\Delta\Omega$, the droplet will either shrink and vanish (leading to a metastable gas phase $r = 0$) or will grow to infinity (transforming the entire system into the liquid phase). For the nucleus to grow beyond r_c, the energy barrier of the amount

$$\Delta\Omega_c = \frac{16\pi\gamma^3}{3(\Delta p)^3} \tag{2.56}$$

must be overcome. Ubiquitous thermal fluctuations, however, enable the nucleus to cross over the barrier and the metastable super-cooled gas to transform to a liquid. This model of nucleation and growth can be applied to a host of the first phase transitions, e.g., condensation of vapor into liquid including cloud formation, phase separations, and crystallizations.

P2.7 *As another example consider the pore growth in a membrane. For a circular pore of radius r to form in a planar membrane, it costs a rim energy $2\pi r\lambda$, while losing the surface energy $\pi r^2\gamma$. Discuss how the pore growth and stability depend on the line and surface tensions, λ and γ.*

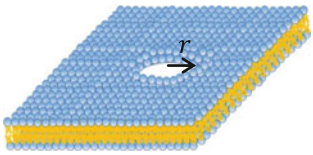

Further Reading and References

Many textbooks on thermodynamics have been written. To name a few:

A.B. Pippard, *Elements of Classical Thermodynamics* (Cambridge University Press, 1957)
H.B. Callen, *Thermodynamics and an Introduction to Thermostatistics*, 2nd edn. (Paper back) (Wiley, 1985)
E.A. Guggenheim, *Thermodynamics: An Advanced Treatment For Chemists And Physicists*, 8th edn. (North Holland, 1986)
W. Greiner, L. Neise, H. Stokër, *Thermodynamics and Statistical Mechanics* (Springer, 1995)
D. Kondepudi, I. Prigogine, *Modern Thermodynamics, From Heat Engine to Dissipative Structures* (Wiley, 1985)
D.T. Haynie, *Biological Thermodynamics* (Cambridge University Press, 2001)
G.G. Hammes, *Thermodynamics and Kinetics for Biological Sciences* (Wiley, 2000)

Many textbooks on statistical physics include chapters on thermodynamics.

Chapter 3
Basic Methods of Equilibrium Statistical Mechanics

In principle, the macroscopic (including thermodynamic) properties of matter ultimately derive from the underlying microscopic structures. Because the exact mechanics for a huge number of constituent particles is out of question, one is forced to seek statistical methods. The fundamental idea of statistical mechanics starts from the notion that an observed macroscopic property is the outcome of averaging over many underlying microscopic states. For a micro-canonical ensemble of an isolated system at equilibrium, we show how the entropy is obtained from information on the microstates, or, from the probabilities of finding the microstates. Once the entropy is given, the first order thermodynamic variables are obtained by taking derivatives of it with respect to their conjugate thermodynamic variables (as shown in Chap. 2). We then consider the microstates in canonical and grand ensembles of the system, which can exchange energy and matter with the surrounding kept at a constant temperature. From the probability of each microstate and the primary thermodynamic potentials for the ensembles, all the macroscopic properties are calculated. Statistical mechanics also allows us to obtain the information on the fluctuations of observed properties about the averages, which provides deeper understanding of the structures of matter. The standard ensemble theories of equilibrium statistical mechanics will be outlined in this chapter.

In applying such methods to biological systems we face a shift of its old paradigm (of relating the *macroscopic* properties to the *microscopic* structures). Unlike ideal and simple interacting systems covered in typical statistical mechanics text books, biological systems are too complex to be explained directly in terms of the small molecules or other atominstic structures. Nevertheless, the structures and properties can be observed on nanoscales, thanks to various single-molecule experimental methods which are now available. Certain **nanoscale subunits** or even larger units, rather than small molecules, can emerge as the basic constituents

W. Sung, *Statistical Physics for Biological Matter*, Graduate Texts in Physics,
https://doi.org/10.1007/978-94-024-1584-1_3

and properties. Throughout this chapter we demonstrate the applicability of statistical mechanics for numerous mesoscopic biological models involving these subunits.

3.1 Boltzmann's Entropy and Probability, Microcanonical Ensemble Theory for Thermodynamics

3.1.1 Microstates and Entropy

A macrostate of a macroscopic system at equilibrium is described by a few thermodynamic state variables. We consider here an isolated system with specified macrovariables, namely its internal energy E, its number of particles N, and generalized displacement X_i such as its volume (see Table 2.1 for the definitions). The number N is usually very large (for the system consisting of one mole of gas, the number of molecules N is the Avogadro number $N_A = 6.022 \times 10^{23}$), and is often taken to be infinity (thermodynamic limit) in macroscopic systems. **Many different microstates underlie a given macrostate. The set of microstates under a macrostate specified by these variables (E, N, X_i)** constitutes the *microcanonical ensemble*. For illustration, consider a one-mole classical gas that is isolated with its net energy E and enclosing volume V. Microscopic states of the classical gas are specified by the positions and momenta of all N particles. There are huge (virtually infinite) number of ways (microstates) that the particles can assume their positions and momenta without changing the values of E, N, V of the macrostate. Each of these huge number of microstates constitutes a member of the microcanonical ensemble.

Suppose that **the number of microstates** (also called the *multiplicity*) belonging to this ensemble is $W(E, N, X_i)$. Then the central postulate of statistical mechanics is that each microstate $\mathcal{M}$ within this ensemble is equally probable:

$$P\{\mathcal{M}\} = \frac{1}{W(E, N, X_i)}. \tag{3.1}$$

This **equal-a-priori probability** is the least-biased estimate under the constraints of fixed total energy. This very plausible postulate is associated with another fundamental equation that relates the macroscopic properties with the microscopic information, the so-called **Boltzmann formula for entropy**:

$$S(E, N, X_i) = k_B \ln W(E, N, X_i). \tag{3.2}$$

where $k_B = 1.38 \times 10^{-23}\text{J/K} = 1.38 \times 10^{-18}$ erg/K is **the Boltzmann constant**. Equation (3.2) is the famous equation inscribed on Boltzmann's gravestone in Vienna, (Fig. 3.1) and is regarded as the cornerstone of statistical mechanics. It proclaims that **the entropy is a measure of disorder**; $S = 0$ at the most ordered

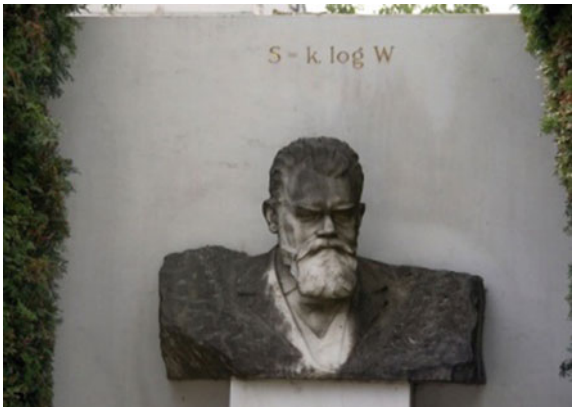

Fig. 3.1 The gravestone of Ludwig Boltzmann in Vienna where the famous formula $S = k_B \ln W$ is inscribed

state where only one microstate is accessible ($W = 1$); the irreversible approach to an entropy maximum is due to emergence of most numerous microstates, i.e., most disordered state, which is attained at equilibrium. Furthermore it tells us that once W is given in terms of the independent variables E, N and X_i, all the thermodynamic variables can be generated by $S(E, N, X_i)$ using (2.9–2.11).

For an alternative, useful expression for the entropy, imagine that M (virtually infinite) replicas exist of the system in question. Suppose that the number of replicas that are in a microstate state i is n_i. Then the number of ways to arrange n_1 systems to be in state 1 and n_2 systems to be in state 2, etc. is

$$W_M = \frac{M!}{n_1! n_2! \ldots}. \tag{3.3}$$

Consider that the values of n_i are so large that the **Stirling approximation** $\boldsymbol{\ln n! \cong n_i \ln n_i - n_i}$ is valid. Then, by noting that $\sum_i n_i = M$,

$$\ln W_M = M \ln M - M - \sum_i (n_i \ln n_i - n_i) = -\sum_i n_i \ln \frac{n_i}{M}, \tag{3.4}$$

and the entropy of the system is given by the total entropy of the M replicas divided by M:

$$S = \frac{1}{M} k_B \ln W_M = -k_B \sum_i P_i \ln P_i = -k_B \sum_{\mathcal{M}} P\{\mathcal{M}\} \ln P\{\mathcal{M}\}, \tag{3.5}$$

where $P_i = n_i/M$ is the probability of finding n_i replicas out of M. This entropy is expressed in terms of P_i, which can be interpreted as the probability $P\{\mathcal{M}\}$ for microstate $\mathcal{M}$ of a *single* replica (system). It is in the form of the information entropy, $S_I = -K \sum_i P_i \ln P_i$ introduced by Shannon, where here with $K = k_B$. In

the microcanonical ensemble of the system, in which $P\{\mathcal{M}\} = 1/W$, the entropy is indeed given by $S = k_B \ln W$. Within the **information theory**, the probability and thermodynamic entropy at equilibrium are the outcomes of maximization of the information entropy (Shannon 1948; Jaynes 1957).

P3.1 *Show that the probability distribution that maximizes the entropy* (3.5) *under a constraint* $\sum_{\mathcal{M}} P\{\mathcal{M}\} = 1$ *is the microcanonical probability* $P\{\mathcal{M}\} = 1/W$, (3.1). *Use the method of Lagrange's multiplier.*

3.1.2 Microcanonical Ensemble: Enumeration of Microstates and Thermodynamics

The designation of microstates depends on the level of the description chosen. Let us consider a system composed N interacting molecules. In the most microscopic level of the description, where the system is described quantum mechanically involving molecules and their subunits such as atoms and electrons, the microstates are the quantum states labeled by a simultaneously measurable set of quantum numbers of the system, which are virtually infinite. At the classical level of description, the microscopic states are specified by the N-particle phase space, i.e., the momenta and coordinates of all the molecules as well as their internal degrees of freedom. For both of these cases, enumeration of total number W of microstates in a microcanonical ensemble would be a formidable task.

Example: Two-State Model

In many interesting situations, however, the description of the system need not be expressed in terms of the underlying quantum states or phase space. Consider a system that has N distinguishable subunits, each of which can be in one of two states. A simple example is a linear array of N sites each of which is either in the state 1 or 0 (Fig. 3.2a). Such two-state situations occur often in mesoscopic systems that lie between microscopic and macroscopic domains. The two state model not only allows the analytical calculation; although seemingly quite simple, it can be applied to many different, interesting problems of biological significance. Of particular interest are biological systems that consist of nanoscale subunits, for example (Fig. 3.2b) the specific sites in a biopolymer where proteins can bind via selective and non-covalent interactions and (c) the base-pairs in double-stranded DNA that can close or open.

Now, let us consider as our microcanonical system an array of N such subunits (e.g., a biopolymer with N binding sites, or a N-base DNA), each of which has two states with different energies. For simplicity we neglect the interaction between subunits. Due to thermal agitations the subunits undergo incessant transitions from

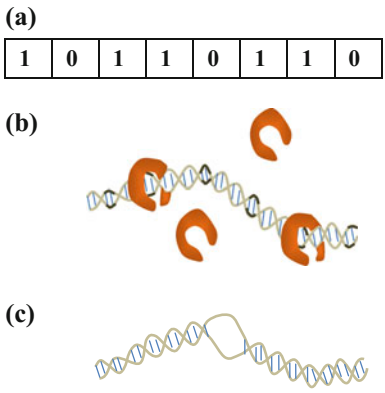

Fig. 3.2 Two state problems. **a** Linear lattice with each site that is either in the state 1 or 0. Two biological examples of two state subunits: **b** Sites in a biopolymer (double stranded DNA for this case) bound by a protein or not. The binding sites are marked dark. **c** DNA with base pairs in closed (slashed) and open (looped) states

an energy state to the other. What is the entropy of the array and what is the probability at which each state occurs in a subunit?

The $\mathcal{M}$ here are chosen to be the mesoscopic states represented by a set $\{n_i\} = (n_1, n_2 \ldots n_N)$ where n_i is the occupation number of the i-th subunit. n_i is either 0 or 1 depending on whether the subunit is unbound or bound with the energy ϵ_0 or ϵ_1, respectively. The net energy is

$$E = \sum_{i=1}^{N} \{(1 - n_i)\epsilon_0 + n_i \epsilon_1\} = N_0\epsilon_0 + N_1\epsilon_1 \tag{3.6}$$

where N_0 and $N_1 = N - N_0$ are the number of subunits belong to the energy states, ϵ_0 and ϵ_1 respectively. Because E is determined once N_0 and N_1 are given, $W(E, N)$ of the total microstates in a micro-canonical ensemble that is subject to the net energy E and total number N, is the number of ways to divide N sites into two groups, N_0 unbound sites and N_1 bound sites:

$$W = \frac{N!}{N_0!\, N_1!} \tag{3.7}$$

Following Boltzmann, the entropy on this level of description is expressed as

$$\begin{aligned} S &= k_B \ln W \\ &\approx k_B[N \ln N - N - N_0 \ln N_0 + N_0 - N_1 \ln N_1 + N_1] \\ &= -Nk_B \left[\frac{N_0}{N} \ln \frac{N_0}{N} + \frac{N_1}{N} \ln \frac{N_1}{N}\right], \end{aligned} \tag{3.8}$$

where the Stirling's formula $N! \cong N \ln N - N$ is used assuming that N_0, N_1 and N are large numbers. Note that in microcanical ensemble theory the primary thermodynamic potential S should be expressed as a function of the given independent

variables N and E; expressing N_0 and N_1 in terms of N and E, yields $N_0 = (N\epsilon_1 - E)/\Delta\epsilon$ and $N_1 = (E - N\epsilon_0)/\Delta\epsilon$, where $\Delta\epsilon = \epsilon_1 - \epsilon_0$:

$$S(E,N) = -k_B\left[\frac{N\epsilon_1 - E}{\Delta\epsilon}\ln\frac{N\epsilon_1 - E}{N\Delta\epsilon} + \frac{E - N\epsilon_0}{\Delta\epsilon}\ln\frac{E - N\epsilon_0}{N\Delta\epsilon}\right]. \tag{3.9}$$

Using (2.9), the temperature is expressed as

$$\begin{aligned}\frac{1}{T} &= \left(\frac{\partial S}{\partial E}\right)_{N,X_i} \\ &= \frac{k_B}{\Delta\epsilon}\ln\frac{N\epsilon_1 - E}{E - N\epsilon_0},\end{aligned} \tag{3.10}$$

from which we can express the internal energy E in terms of temperature T,

$$E = \frac{N\left(\epsilon_0 e^{-\beta\epsilon_0} + \epsilon_1 e^{-\beta\epsilon_1}\right)}{e^{-\beta\epsilon_0} + e^{-\beta\epsilon_1}}, \tag{3.11}$$

where $\beta = 1/(k_B T)$.

The probability that a subunit will be in the state $n = 0$ is

$$P_0 = \frac{W(N-1, E-\epsilon_0)}{W(N,E)} = \frac{(N-1)!}{(N_0-1)!N_1!}\frac{N_0!N_1!}{N!} = \frac{N_0}{N}, \tag{3.12}$$

where the equal-a priori probability $1/W(N,E)$ (3.1) of finding any one of the subunit with ϵ_0 is multiplied by $W(N-1, E-\epsilon_0)$, which is the number of ways that the remaining energy can be distributed among the other $N-1$ subunits. The result (3.12) is very obvious. In a similar way, one can find

$$P_1 = \frac{N_1}{N}. \tag{3.13}$$

Substituting the expression for E (3.11) into $N_0 = (N\epsilon_1 - E)/\Delta\epsilon$ and $N_1 = (E - N\epsilon_0)/\Delta\epsilon$ yields

$$P_n = \frac{N_n}{N} = \frac{e^{-\beta\epsilon_n}}{\sum_{n=0}^{1} e^{-\beta\epsilon_n}}, \quad n = 0, 1. \tag{3.14}$$

This is the **single-subunit Boltzmann distribution**. It signifies that the higher energy state is less probable unless excited by very high thermal energy $k_B T = \beta^{-1}$. Each probability can be rewritten explicitly as

$$P_0 = \frac{1}{1+e^{-\beta\Delta\epsilon}} \tag{3.15}$$

$$\begin{aligned} P_1 &= \frac{e^{-\beta\Delta\epsilon}}{1+e^{-\beta\Delta\epsilon}} = \frac{1}{1+e^{\beta\Delta\epsilon}} \\ &= 1 - P_0. \end{aligned} \tag{3.16}$$

The relative probability of finding state 1 relative to state 0 is $e^{-\beta\Delta\epsilon}$. If we put the unbound and bound state energies of the subunit to be 0 and $-\epsilon$, respectively, the probability of the bound state is given by

$$P_1 = \frac{1}{1+e^{-\beta\epsilon}} \equiv S(\beta\epsilon). \tag{3.17}$$

$S(\beta\epsilon)$, called the **sigmoid function** (Fig. 3.3), is typical of the transition probability in two-level systems. When $\epsilon = 0, P_0 = P_1 = 1/2$, i.e., the open and closed states are equally probable. When $\epsilon \gg k_B T$, $P_1 \approx 1$, i.e., a site or base pair tends to be mostly bound. If there were attraction between subunits, P_1 rises more sharply at a given temperature than the sigmoid. This cooperative binding will be studied in detail in Chap. 8 in the context of DNA base-pair opening or denaturation.

In terms of single subunit probability (3.14), the energy (3.11) is expressed by

$$E = N \sum_{n=0}^{1} \epsilon_n P_n, \tag{3.18}$$

meaning that the internal energy is given by the thermal average. The entropy (3.8) is expressed as

$$S = -Nk_B \sum_{n=0}^{1} P_n \ln P_n \tag{3.19}$$

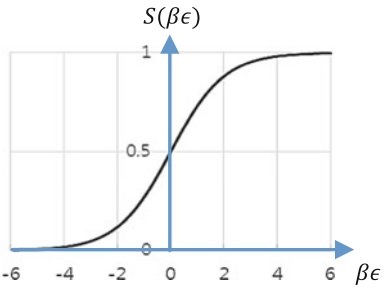

Fig. 3.3 The sigmoid function $S(\beta\epsilon)$. For low temperature ($\beta\epsilon \gg 1$), the function rises sharply at $\epsilon = 0$ and become unity for large ϵ.

For a biopolymer with N binding sites bound by $N_p(\leq N)$ proteins, the entropy is

$$S = -Nk_B[\theta \ln \theta + (1-\theta)\ln(1-\theta)] \tag{3.20}$$

where $\theta = N_p/N$ is coverage of the proteins. This is the well-known **entropy of mixing** two components. When only one state exists, $\theta = 1$ or $\theta = 0$, then the entropy of mixing is 0. When the two states are equally probable, i.e., $\theta = 1/2$, the entropy is at the maximum.

P3.2 *Show that the Helmholtz free energy is given by*

$$F = -Nk_BT \ln(e^{-\beta\epsilon_0} + e^{-\beta\epsilon_1}).$$

P3.3 *Find the chemical potential of the system.*
Solution: Because the primary thermodynamic potential is $S(E,N,X)$, the chemical potential is given by

$$\mu = -T\left(\frac{\partial S}{\partial N}\right)_{E,X}$$

as a function of E and N. If we obtain it by taking a derivative on (3.20) with respect to N, it would be wrong because the entropy is not explicitly expressed as a function of the independent variables, E and N.

The two-state model can be applied to a host of biological transitions between two states, such as coiled and helix states, B-DNA (right handed) and Z-DNA (left-handed states) in addition to the examples mentioned above. The model can be applied even to the higher levels biological phenomena such as the ion channel gating transitions from an open to a closed state, ligand binding on receptors, and much more.

Colloid Translocation

As another example of the two state transitions, consider translocation of colloidal particles from one place to the other. Consider identical colloidal particles (Fig. 3.4), initially confined within the chamber on the left, pass through a narrow pore in the partitioning membrane toward the right chamber. Suppose that the internal energy does not change during this translocation process.

The number of microstates with N_1 particles translocated to the right is given by

$$W(N-N_1, N_1) = \frac{N!}{(N-N_1)!N_1!}, \tag{3.21}$$

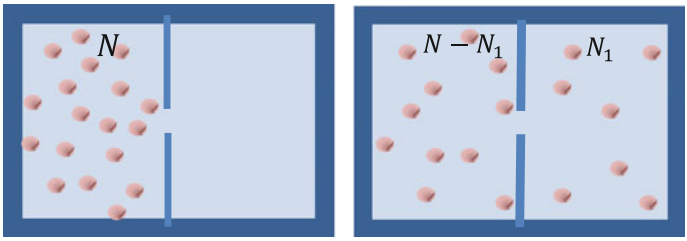

Fig. 3.4 Colloidal particles translocating from a chamber to another through a pore beween them

The probability with which N_1 particles exist in the right chamber is given by

$$P(N_1) = \frac{W(N-N_1,N_1)}{\sum_{N_1=0}^{N_1=N} W(N-N_1,N_1)} = W(N-N_1,N_1)/2^N, \tag{3.22}$$

where we use $\sum_{N_1=0}^{N_1=N} W(N-N_1,N_1) = \sum_{N_1=0}^{N_1=N} N!/((N-N_1)!N_1!) = 2^N$. $P(N_1)$ is the binomial distribution for N_1, shown by Fig. 3.5a. The average is

$$\langle N_1 \rangle = \sum_{N_1=0}^{N_1=N} N_1 P(N_1) = \frac{N}{2} \tag{3.23}$$

and the variance is

$$(N_1 - \langle N_1 \rangle)^2 = \sum_{N_1=0}^{N_1=N} (N_1 - \langle N_1 \rangle)^2 P(N_1) = \frac{N}{4}. \tag{3.24}$$

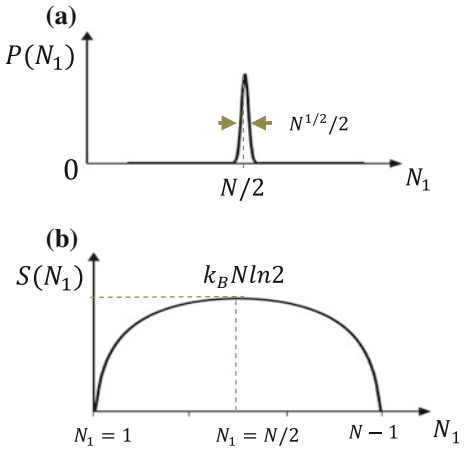

Fig. 3.5 **a** The probability distribution $P(N_1)$ of number of particles that translocate to the right side. **b** The entropy associated with translocation $S(N_1)$.

For large N, $P(N_1)$ or $W(N-N_1, N_1)$ shows a sharp peak at $N_1 = N/2$ (Fig. 3.5a) because **root mean squared (rms) deviation or standard deviation** of N_1, $\bar{\Delta}N_1 \equiv \langle (N_1 - \langle N_1 \rangle)^2 \rangle^{1/2} = N^{1/2}/2$ is much smaller than N. This means that in real situations of large N this sharply-peaked state with $N_1 = N/2$ dominates over all other possibilities, as is observed at equilibrium. Thermodynamically this is the equilibrium state where the entropy

$$S = k_B \ln W = k_B[N \ln N - (N - N_1) \ln(N - N_1) - N_1 \ln N_1] \tag{3.25}$$

has the maximum $k_B N \ln 2$. **This means that the second law of thermodynamics forbid *all* the particles initially placed on the left to translocate toward the right, even in infinitely long time.**

We have demonstrated that the basic postulates of equal-a priori probability and Boltzmann entropy lead to a clear and satisfactory construction of a statistical mechanical method for finding statistical and thermodynamic properties. The results derived above, the thermodynamics and probabilities, are obtained for the micro-canonical ensemble of isolated systems, in which the total energy and total number are regarded as fixed. Despite these constraints, these micro-canonical ensemble theory results are equal to those for the natural situations where these variables fluctuate, provided that the standard deviations or root mean squares of the fluctuations are much smaller than their averages. As we will show next, thermodynamic variables can be calculated more easily by considering ensembles in which the constraints on fixed variables (E, X_i and N) are relaxed.

3.2 Canonical Ensemble Theory

Due to the constraints of fixed total energy E and total number of particles or subunits N, the number of available microstates in a micro-canonical ensemble is difficult to calculate for the most of nontrivial systems. In what is called **a *canonical ensemble*** the constraint is relaxed by considering that the system in question is put into a heat reservoir or bath (of size much larger than the system size) at a fixed temperature, so that **the macrostate is characterized by its temperature T instead of its energy E**, and by N and X in addition. The system's energy, by exchange with the reservoir, can take any of the accessible energy values.

3.2.1 Canonical Ensemble and the Boltzmann Distribution

What is the probability that the system in the canonical ensemble will be at a certain microstate $\mathcal{M}$? To find this probability we suppose that the composite of the system and the heat bath or reservoir (B) surrounding it is an isolated system with total

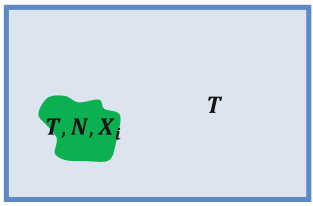

Fig. 3.6 The canonical ensemble is the collection of many microstates of a macrosystem characterized by its temperature $\boldsymbol{T}$, $\boldsymbol{N}$ and $\boldsymbol{X_i}$. To retain the temperature as fixed the system is put into a contact with a heat bath of the same temperature

energy E_T, as depicted in Figs. 2.4 and 3.6. Then the number of all the accessible microstates in the total system is

$$W_T(E_T) = \sum_{\mathcal{M}} W(\mathcal{E}_{\mathcal{M}}) W_B(E_T - \mathcal{E}_{\mathcal{M}}), \tag{3.26}$$

where $\sum_{\mathcal{M}}$ signifies the summation over all accessible microstates of the system, each having the energy $\mathcal{E}_{\mathcal{M}}$, $W(\mathcal{E}_{\mathcal{M}})$ is its number of microstates. $W_B(E_T - \mathcal{E}_{\mathcal{M}})$ is the number of the microstates of the heat bath, *given that the system has the energy* $\mathcal{E}_{\mathcal{M}}$. In the each one of the microstates counted in (3.26) is equally probable a priori by the postulate (3.1), so that the probability that the system will be in a specific state $\mathcal{M}$ $(W(\mathcal{E}_{\mathcal{M}}) = 1)$ is

$$P\{\mathcal{M}\} = \frac{W_B(E_T - \mathcal{E}_{\mathcal{M}})}{\sum_{\mathcal{M}} W_B(E_T - \mathcal{E}_{\mathcal{M}})}. \tag{3.27}$$

To go further, we note that

$$W_B(E_T - \mathcal{E}_{\mathcal{M}}) = \exp\left[\frac{1}{k_B} S_B(E_T - \mathcal{E}_{\mathcal{M}})\right] \tag{3.28}$$

and the system's energy $\mathcal{E}_{\mathcal{M}}$ is much smaller than the total energy E_T or the reservoir energy $E_T - \mathcal{E}_{\mathcal{M}}$. Consequently the exponent above is expanded as

$$\begin{aligned} \exp\left[\frac{1}{k_B} S_B(E_T - \mathcal{E}_{\mathcal{M}})\right] &\cong \exp\left[\frac{1}{k_B}\left(S_B(E_T) - \mathcal{E}_{\mathcal{M}} \frac{\partial}{\partial E_T} S_B(E_T)\right)\right] \\ &= \exp\left[\frac{1}{k_B}\left(S_B(E_T) - \frac{\mathcal{E}_{\mathcal{M}}}{T}\right)\right]. \end{aligned} \tag{3.29}$$

where the relation (2.9), $\partial S_B(E)/\partial E = 1/T$ is used. From (3.27–3.29), we find an important relation

$$P\{\mathcal{M}\} = \frac{e^{-\beta \mathcal{E}_{\mathcal{M}}}}{\sum_{\mathcal{M}} e^{-\beta \mathcal{E}_{\mathcal{M}}}}, \tag{3.30}$$

where still $\beta = 1/(k_B T)$. This relation means that the **probability of finding a system at a temperature T to be in a microstate $\mathcal{M}$ depends solely on the system's energy $\mathcal{E}_{\mathcal{M}}$ and decays exponentially with it, following the so-called Boltzmann factor $e^{-\beta \mathcal{E}_{\mathcal{M}}}$.** This canonical distribution is valid to the system in equilibrium at a fixed temperature T, *independently of its size*. It should be noted that the system need not be large enough to assure its statistical independence from the thermal bath, as wrongly claimed in some textbooks. This fundamental relation can be derived in various ways. One way is by maximizing the information entropy under constraints, as given by the following problem.

P3.4 *By maximizing the information entropy* (3.5)

$$S = -k_B \sum_{\mathcal{M}} P\{\mathcal{M}\} \ln P\{\mathcal{M}\}$$

subject to constraints $\sum_{\mathcal{M}} P\{\mathcal{M}\} = 1$ *and* $\sum_{\mathcal{M}} \mathcal{E}_{\mathcal{M}} P\{\mathcal{M}\} = E$, *find that* $P\{\mathcal{M}\}$ *is given by the canonical distribution* (3.30)*. Use the method of Lagrange's multiplier.*

$\mathcal{E}_{\mathcal{M}}$, being a fluctuating energy that depends on the microstates or degrees of freedom $\mathcal{M}$, is identified as the Hamiltonian $\mathcal{H}\{\mathcal{M}\}$. Thus, we express the probability in a more conventional form:

$$P\{\mathcal{M}\} = \frac{e^{-\beta \mathcal{H}\{\mathcal{M}\}}}{Z(T, N, X_i)}. \tag{3.31}$$

The normalization factor

$$Z(T, N, X) = \sum_{\mathcal{M}} e^{-\beta \mathcal{H}\{\mathcal{M}\}} \tag{3.32}$$

is called the **canonical partition function or partition sum.** Including the multiplicity $W(\mathcal{E}_{\mathcal{M}})$ of states that have energy $\mathcal{E}_{\mathcal{M}}$, the partition function is also given as

$$Z(T, N, X) = \sum\nolimits_{\mathcal{E}_{\mathcal{M}}} W(\mathcal{E}_{\mathcal{M}})\, e^{-\beta \mathcal{E}_{\mathcal{M}}} \tag{3.33}$$

Thus, the probability for the systems to have the energy $\mathcal{E}_{\mathcal{M}}$ is proportional to $W(\mathcal{E}_{\mathcal{M}})\, e^{-\beta \mathcal{E}_{\mathcal{M}}}$, not to the Boltzmann factor $e^{-\beta \mathcal{E}_{\mathcal{M}}}$, which refers to the probability for the system to be at a microstate $\mathcal{M}$.

Given the probability, various thermodynamic variables of the system can be obtained. First the internal energy is the average energy of the system given by

$$\begin{aligned} E = \langle \mathcal{H} \rangle &= \sum_{\mathcal{M}} \mathcal{H}\{\mathcal{M}\} \frac{e^{-\beta \mathcal{H}\{\mathcal{M}\}}}{Z} \\ &= -\frac{\partial \left(\sum_{\mathcal{M}} e^{-\beta \mathcal{H}\{\mathcal{M}\}} \right)}{Z \partial \beta} = -\frac{\partial \ln Z}{\partial \beta}. \end{aligned} \tag{3.34}$$

Using the relation $E = -T^2 \partial (F/T)/\partial T$ (2.16), we can identify the Helmholtz free energy

$$F(T, N, X) = -k_B T \ln Z. \tag{3.35}$$

In this way, by using the thermodynamic relations involving the derivatives with respect to F (2.13–2.15), the partition function can generate all the thermodynamic variables.

P3.5 *Consider a simple model where DNA unbinding of the double helix is like unzipping of a zipper; a base pair (bp) can open if all bps to its left are already open as shown in the figure below. The DNA has N bps, each of which can be in one of two states, an open state with the energy 0 and closed state with the energy* $-\epsilon$. *(a) Find the partition function. (b) Find the average number of open bps when* $\epsilon = 0.4 k_B T$.

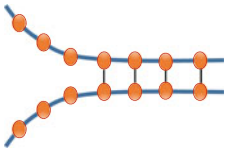

3.2.2 The Energy Fluctuations

The energy distribution of macroscopic systems in canonical ensemble is a sharp Gaussian around the average energy. To show this, consider that values of the microstate energy $\mathcal{E}$ are continuously distributed with density of states $w(\mathcal{E})$ over a range $d\mathcal{E}$, so that the partition function (3.33) can be written as

$$Z = \int d\mathcal{E}\, w(\mathcal{E}) e^{-\beta \mathcal{E}}, \tag{3.36}$$

which implies that probability distribution of the energy within the range $d\mathcal{E}$ is

$$P(\mathcal{E}) = \frac{w(\mathcal{E})e^{-\beta\mathcal{E}}}{Z} = e^{-\beta\{\mathcal{E}-T\mathcal{S}(\mathcal{E})\}}/Z = e^{-\beta\mathcal{F}(\mathcal{E})}/Z, \tag{3.37}$$

where $\mathcal{F}(\mathcal{E}) = \mathcal{E} - T\mathcal{S}(\mathcal{E}) = \mathcal{E} - k_B T \ln w(\mathcal{E})$ is the free energy given as a function of an energy $\mathcal{E}$. Because $e^{-\beta T\mathcal{S}(\mathcal{E})}$ increases and $e^{-\beta\mathcal{E}}$ decreases with $\mathcal{E}$, we expect that $P(\mathcal{E})$ is peaked at $\mathcal{E}^*$, where $\mathcal{F}(\mathcal{E})$ is minimum. Around the minimum, $\mathcal{F}(\mathcal{E})$ can be expanded:

$$\begin{aligned}\mathcal{F}(\mathcal{E}) &\cong \mathcal{E}^* - T\mathcal{S}(\mathcal{E}^*) + \frac{1}{2}T\left(\frac{\partial^2\mathcal{S}(\mathcal{E}^*)}{\partial\mathcal{E}^{*2}}\right)(\mathcal{E}-\mathcal{E}^*)^2 \\ &= \mathcal{F}(\mathcal{E}^*) - \frac{1}{2TC_V}(\mathcal{E}-\mathcal{E}^*)^2.\end{aligned} \tag{3.38}$$

In the above, we used $\partial^2\mathcal{S}(\mathcal{E}^*)/\partial\mathcal{E}^{*2} = \partial/\partial\mathcal{E}^*(1/T) = -1/(T^2C_V)$, along with $\partial\mathcal{S}(\mathcal{E}^*)/\partial\mathcal{E}^* = 1/T$ and $\partial T/(\partial\mathcal{E}^*) = 1/(\partial\mathcal{E}^*/\partial T) = 1/C_V$ (2. 38).

Finally, we obtain

$$P(\mathcal{E}) \propto e^{-\beta\mathcal{F}(\mathcal{E})} \cong \exp\left[-\frac{1}{2k_BT^2C_V}(\mathcal{E}-\mathcal{E}^*)^2\right], \tag{3.39}$$

The probability distribution for the energy $\mathcal{E}$, which is allowed to exchange with the bath at temperature T, is Gaussian with a mean $\mathcal{E}^* = \langle\mathcal{E}\rangle = E$, and a rms deviation

$$\bar{\Delta}\mathcal{E} = \langle(\mathcal{E}-\mathcal{E}^*)^2\rangle^{1/2} = T\sqrt{k_BC_V} \tag{3.40}$$

from the mean. The energy distribution $P(\mathcal{E})$ is peaked at the mean $\mathcal{E}^*$ which minimizes he free energy $\mathcal{F}(\mathcal{E})$ to $\mathcal{F}(\mathcal{E}^*) = F$. Because $\mathcal{E}^*$ and C_V are extensive quantities that increase with system size N, the relative peak width $\bar{\Delta}\mathcal{E}/\ \mathcal{E}^*$ scales as $N^{-1/2}$. Therefore, on a macroscopic scale, $P(\mathcal{E})$ is very sharp, and looks like a delta function about the mean, $P(\mathcal{E}) = \delta(\mathcal{E}-\mathcal{E}^*)$ (Fig. 3.7). For this reason, when measuring the energy $\mathcal{E}$ of a macroscopic system we observe negligible fluctuations about the mean which as the outstandingly probable outcome. Because energy fluctuation is practically absent in this case, the canonical ensemble yields the same thermodynamics that the micro-canonical one does.

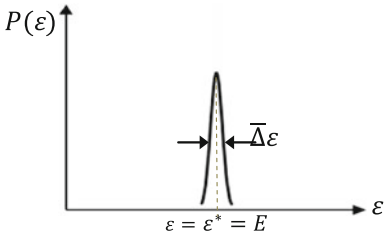

Fig. 3.7 The distribution of the energy $\mathcal{E}$ in a macroscopic system is sharply peaked around the average energy $\mathcal{E}^* = E$. Even a macroscopic system experiences the energy fluctuation $\bar{\Delta}\mathcal{E}$, although very small compared with E.

An important lesson here, however, is that, **even the macroscopic variables fluctuate, although imperceptibly**. The fluctuations are consequence of the intrinsic, universal thermal motion of microscopic constituents inherent in systems at a non-vanishing temperature. The relative effect of the fluctuations increases as the system size decreases, as dramatically visualized in Brownian motion.

The canonical ensemble results could differ significantly from the micro-canonical results as the system size gets small. Therefore, when considering mesoscopic systems of small system sizes, an appropriate type of ensembles must be chosen carefully to meet the actual situation.

Water has a distinctively high heat capacity so that its temperatures remain nearly constant. For biological systems bathed in an aqueous solvent, the canonical ensemble (including the Gibbs and grand canonical ones shown next) are a most natural choice to take.

3.2.3 *Example: Two-State Model*

As a simple example we revisit the two-state model of independent N subunits that was studied earlier in a microcanonical way. The Hamiltonian is derived from (3.6),

$$\mathcal{H}\{n_i\} = \sum_{i=1}^{N} \{(1-n_i)\epsilon_0 + n_i\epsilon_1\} \tag{3.41}$$

where n_i, the occupation number of the i-th subunit, can be either 0 or 1. The probability of the microstate, that is, the joint probability that all subunits are in the state $n_1, n_2, \ldots n_N$ simultaneously is given by

$$P\{n_i\} = \frac{\exp[-\beta\mathcal{H}\{n_i\}]}{Z} = Z^{-1} \exp\left(-\beta \sum_{i=1}^{N} (1-n_i)\epsilon_0 + n_i\epsilon_1\right), \tag{3.42}$$

where

$$\begin{aligned} Z &= \sum_{\{n_i\}} \exp[-\beta H\{n_i\}] = \sum_{n_i=0}^{1} \exp\left(-\beta \sum_{i=1}^{N} (1-n_i)\epsilon_0 + n_i\epsilon_1)\right) \\ &= \prod_{i=1}^{N} \sum_{n_i=0}^{1} \exp\{-\beta(1-n_i)\epsilon_0 + n_i\epsilon_1\} \\ &= \left(e^{-\beta\epsilon_0} + e^{-\beta\epsilon_1}\right)^N \end{aligned} \tag{3.43}$$

is the partition function. In deriving it, the two summations in the second expression above was exchangeable. The binomial expansion of (3.43) expresses the partition function as

$$Z = \sum_{N_1=0}^{N} \frac{N!}{N_0!N_1!} e^{-\beta(\epsilon_0 N_0 + \epsilon_1 N_1)} \tag{3.44}$$

where N_0, N_1 are the numbers of empty and occupied subunits respectively; $N!/(N_0!N_1!)$ represents the number of microstates for the state that has net energy $\epsilon_0 N_0 + \epsilon_1 N_1$ (3.7).

The (3.42) implies the obvious statistical independence of subunits:

$$P\{n_i\} = P_{n_1} P_{n_2} \ldots P_{n_N}, \tag{3.45}$$

where

$$P_{n_i} = \frac{e^{-\beta\{(1-n_i)\epsilon_0 + n_i\epsilon_i\}}}{\sum_{n=0}^{1} e^{-\beta\epsilon_n}}, \tag{3.46}$$

is the probability for the subunit to be in the state n_i; this is identical to (3.14).

The calculation of thermodynamic variables is straightforward. The Helmholtz free energy is

$$F = -k_B T \ln Z = -N k_B T \ln(e^{-\beta\epsilon_0} + e^{-\beta\epsilon_1}), \tag{3.47}$$

which is obtained in a more straightforward way compared with the micro-canonical theory. From the free energy, we obtain the entropy:

$$\begin{aligned} S(T,N) &= -\frac{\partial F}{\partial T} = N k_B \ln\left(e^{-\beta\epsilon_0} + e^{-\beta\epsilon_1}\right) + \frac{N(\epsilon_0 e^{-\beta\epsilon_0} + \epsilon_1 e^{-\beta\epsilon_1})}{T(e^{-\beta\epsilon_0} + e^{-\beta\epsilon_1})} \\ &= -\frac{F}{T} + \frac{E}{T} \end{aligned} \tag{3.48}$$

and the internal energy

$$E = \frac{N(\epsilon_0 e^{-\beta\epsilon_0} + \epsilon_1 e^{-\beta\epsilon_1})}{e^{-\beta\epsilon_0} + e^{-\beta\epsilon_1}}, \tag{3.49}$$

which can be also directly derived from (3.34). All of thermodynamic quantities derived coincide with those of the micro-canonical ensemble, which is no surprise because we considered the thermodynamic limit of large numbers (using the Stirling's formula) in micro-canonical calculations.

P3.6 *Referring to the problem of colloid translocation, if each particle loses energy by $\mathcal{E}$ when passing through the pore to the right, at what configuration is the probability maximum? Find the probability that N_1 particles are on the right while $N_2 = N - N_1$ particles are on the left and the associated entropy.*

As the name implies, *canonical* ensemble theory provides the most standard method by which the microstate probabilties and the thermal properties are evaluated. In later chapters, it will be used to study diverse systems ranging from small molecular fluids to polymers and membranes, and to study a multitude of phenomena such as transitions, cooperative phenomena, and self-assembly. Although versatile, the canonical ensemble condition of fixed X and N can make analytical calculations difficult in some situations. In the following we consider other ensembles where one of the two variables is free to fluctuate.

3.3 The Gibbs Canonical Ensemble

Now, **a system in contact with a thermal bath is subject to a generalized force f_i**, which is kept at constant, so that the system's Hamiltonian is modified to

$$\mathcal{H}_g\{\mathcal{M}\} = \mathcal{H}\{\mathcal{M}\} - f_i \mathcal{X}_i\{\mathcal{M}\}. \tag{3.50}$$

Here the generalized displacement $\mathcal{X}_i\{\mathcal{M}\}$, the conjugate to the force f_i, is a thermally fluctuating variable. The system is specified by the macroscopic variables (T, f_i, N) and the underlying microstates constitute the so called "Gibbs canonical ensemble".

The microstate $\mathcal{M}$ occurs with the canonical probability

$$P\{\mathcal{M}\} = \frac{e^{-\beta \mathcal{H}_g\{\mathcal{M}\}}}{Z_g(T, f_i, N)} = \frac{e^{-\beta \mathcal{H}\{\mathcal{M}\} + \beta f_i \mathcal{X}_i\{\mathcal{M}\}}}{Z_g(T, f_i, N)}, \tag{3.51}$$

where

$$Z_g(T, f_i, N) = \sum_{\mathcal{M}} e^{-\beta \mathcal{H}\{\mathcal{M}\} + \beta f_i \mathcal{X}_i\{\mathcal{M}\}} \tag{3.52}$$

is the **Gibbs partition function**. Examples are a magnet subject to a constant magnetic field, and a polymer chain subject to a constant force which is discussed below. The average displacement in this ensemble is given by

$$\begin{aligned} X_i = \langle \mathcal{X}_i\{\mathcal{M}\} \rangle &= \frac{\sum_{\mathcal{M}} \mathcal{X}_i\{\mathcal{M}\} e^{-\beta \mathcal{H}\{\mathcal{M}\} + \beta f_i \mathcal{X}_i\{\mathcal{M}\}}}{\sum_{\mathcal{M}} e^{-\beta \mathcal{H}\{\mathcal{M}\} + \beta f_i \mathcal{X}_i\{\mathcal{M}\}}} \\ &= \frac{\partial Z_g}{\beta \partial f_i} / Z_g = k_B T \frac{\partial}{\partial f_i} \ln Z_g(T, f_i, N) \end{aligned} \tag{3.53}$$

In view of the thermodynamic identity, $X_i = -\frac{\partial}{\partial f_i} G$, (2.23), the Gibbs free energy is identified as

$$G(T,f_i,N) = -k_B T \ln Z_g(T,f_i,N), \tag{3.54}$$

from which all the thermodynamic variables are generated as explained in Chap. 2.

Freely-Jointed Chain (FJC) for a Polymer Under a Tension

A simple model for a flexible polymer is the **freely-joined chain (FJC)** consisting of N segments (each with length l) which can rotate by an arbitrary angle independently of each other (Fig. 3.8). How much is the chain stretched on average by an applied tension?

Due to the thermal agitation of the heat bath, in the absence of the applied tension the freely jointed chain segments are randomly oriented, and thus the corresponding chain Hamiltonian $\mathcal{H}$ does not depend on the segment orientation, i.e., is trivial. In the presence of an applied tension $\boldsymbol{f}$ acting on an end $\boldsymbol{r}_N$, with the other end held fixed at the origin $\boldsymbol{r}_0$, the Hamiltonian is given by

$$\begin{aligned} \mathcal{H}_g\{\mathcal{M}\} &= -\boldsymbol{f}\cdot\boldsymbol{r}_N = -f\mathcal{X}_i\{\mathcal{M}\} \\ &= -\boldsymbol{f}\cdot\sum_{n=1}^{N} l\boldsymbol{u}_n = -f\sum_{n=1}^{N} l\,\cos\,\theta_n \end{aligned} \tag{3.55}$$

The microstates of the FJC here is $\mathcal{M} = (\boldsymbol{u}_1, \boldsymbol{u}_2, \ldots \boldsymbol{u}_N)$, where $\boldsymbol{u}_n$ is the unit tangent vector of the n-th segment oriented with polar angle θ_n along the axis of the applied tension. The partition function is

$$\begin{aligned} Z_g(T,f,N) &= \int d\Omega_1 \ldots \int d\Omega_N\, e^{\beta f \sum_n l\,\cos\theta_n} \\ &= \left[\int d\Omega_n\, e^{\beta f l\,\cos\theta_n}\right]^N = \left[\frac{4\pi\sinh(\beta f l)}{\beta f l}\right]^N \end{aligned} \tag{3.56}$$

Here Ω_n, is the solid angle of the n-th segment with respect to the direction of the force. $\int d\Omega_n = \int_{-1}^{1} d\cos\theta_n \int_0^{2\pi} d\varphi_n$ where φ_n is the azimuthal angle.

Using (3.53), the average value X of the end-to-end distance of the chain along the axis, $\mathcal{X} = \sum_n l\cos\theta_n$, is given by

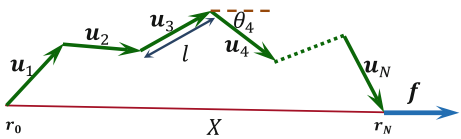

Fig. 3.8 A freely-jointed chain extended to a distance X under a tension f

$$\frac{X}{Nl} = \coth(\beta f l) - \frac{1}{\beta f l} \equiv \mathcal{L}(\beta f l), \tag{3.57}$$

where $\mathcal{L}(x)$ is the Langevin's function. Now we ask ourselves the inverse question, what is the tension f necessary to keep the end-to-end distance as X? Because X is given as fixed and f is a derived quantity, this problem in principle should be tackled by the canonical ensembe theory. However it is quite complicated to impose the constraint of fixed extension X in the analytical calculation. Because the force-extension relation for a long chain is independent of the ensemble taken, the (3.57) provides the solution, with interpretation f as the derived, average tension, which is written as the inverse of the Langevin's function

$$f = \frac{k_B T}{l} \mathcal{L}^{-1}\left(\frac{X}{Nl}\right) \tag{3.58}$$

and is depicted by Fig. 3.9.

Let us first consider the case of small force, $\beta f l \ll 1$, or $f \ll k_B T/l$. Because $\mathcal{L}(\beta f l) \cong \beta f l/3$, (3.57) leads to

$$\frac{X}{Nl} \cong \frac{f l}{3 k_B T}, \tag{3.59}$$

which one can alternatively put as $f \cong (3k_B T/Nl^2)X$, where f is the force necessary to fix the chain extension as X. This is the well-known Gaussian chain behavior (10.20) where the force is linear in the extension (the domain within the broken ellipse in Fig. 3.9). Its temperature dependence implies that it is an **entropic force**; the restoring force $-f$ is directed towards the origin $X = 0$ where the entropy is the maximum.

Next we consider the opposite extreme where $f \gg k_B T/l$. Because $\cot(\beta f l) \cong 1$, $\langle X \rangle / Nl \cong 1 - 1/(\beta f l)$ in (3.57), from which one obtains the entropic force to keep an extension X:

$$f \cong \frac{k_B T}{l}\left(1 - \frac{X}{Nl}\right)^{-1}. \tag{3.60}$$

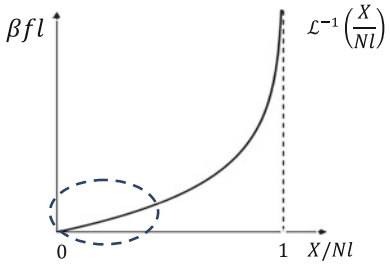

Fig. 3.9 Tension f necessary to keep the extension as X in a freely-jointed chain. The tension is entirely the entropic force

An infinite force is required to extend the chain to its full length Nl, at which the chain entropy is zero!

P3.7 *What are the Gibbs and Helmholtz free energies for the chain extended with the tension f and the distance X for the case $f \gg k_B T/l$?*
Solution: Because $f = \frac{\partial F}{\partial X}$, we integrate the (3.60) over X to find the Helmholtz free energy

$$F(X,T,N) = -Nk_BT\ \ln\{1 - X/(Nl)\},$$

where the irrelvant constant is omitted. On the other hand the Gibbs free energy is $G(f,T,N) = F(X,T,N) - fX \approx N\{-fl + k_BT\ln(fl/(k_BT))\}$ where F and X are expressed as functions of f. Alternatively G is directly obtained from the partition function expression

$$G(f,T,N) = -Nk_BT\ \ln\left\{\frac{e^{\beta fl} - e^{-\beta fl}}{\beta fl}\right\} \approx -Nk_BT\ \ln\left\{\frac{e^{\beta fl}}{\beta fl}\right\}.$$

P3.8 *A biopolymer is composed of N monomers, each of which can assume two conformational states of energy ϵ_1 and ϵ_2 and coressponding segmental extension lengths l_1 and l_2 respectively. Calculate the partition function. When a tension f is applied to the both ends, what would be the extension X?*

3.4 Grand Canonical Ensemble Theory

When a system is in contact with a thermal bath, its number of particles can fluctuate naturally as its energy does. Because the system is at equilibrium with the bath, the temperature and chemical potential of system are the same as those of the bath. The microstates of the system compatible with this macrostate of given temperature T, chemical potential μ, and displacement X, constitute the grand canonical ensemble (Fig. 3.10).

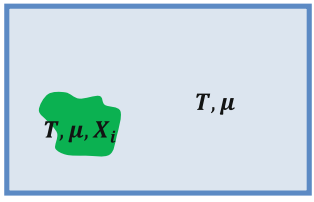

Fig. 3.10 The grand canonical ensemble of a system is characterized by its temperature $\boldsymbol{T}$, chemical potential $\boldsymbol{\mu}$ and displacement $\boldsymbol{X_i}$. To retain the temperature and chemical potential as fixed the system is put into a contact with a heat bath of the same temperature and chemical potential

3.4.1 Grand Canonical Distribution and Thermodynamics

The distribution of an underlying microstate $\mathcal{M}$ of the system with the energy $\mathcal{H}\{\mathcal{M}\}$ and particle number $\mathcal{N}$ is derived using logic similar to that for the canonical ensemble:

$$P\{\mathcal{M}\} = \frac{e^{-\beta(\mathcal{H}\{\mathcal{M}\}-\mu\mathcal{N})}}{Z_G(T,\mu,X_i)} \tag{3.61}$$

where

$$\begin{aligned} Z_G(T,\mu,X_i) &= \sum_{\mathcal{M}} e^{-\beta(\mathcal{H}\{\mathcal{M}\}-\mu\mathcal{N}\{\mathcal{M}\})} = \sum_{\mathcal{N}=0}^{\infty}\sum_{\mathcal{M}/\mathcal{N}} e^{-\beta(\mathcal{H}\{\mathcal{M}\}-\mu\mathcal{N})} \\ &= \sum_{\mathcal{N}=0}^{\infty} e^{-\beta\mu\mathcal{N}} Z_{\mathcal{N}} \end{aligned} \tag{3.62}$$

is **the grand canonical partition function**. Here $\sum_{\mathcal{M}/\mathcal{N}}$ is the summation over the microstates of the system with $\mathcal{N}$ given, of which the canonical partition function is $Z_{\mathcal{N}}$.

The average number of particles in the system is given as

$$N = \langle\mathcal{N}\rangle = \frac{\sum_{\mathcal{M}} \mathcal{N}\{\mathcal{M}\} e^{-\beta(\mathcal{H}\{\mathcal{M}\}-\mu\mathcal{N}\{\mathcal{M}\})}}{\sum_{\mathcal{M}} e^{-\beta(\mathcal{H}\{\mathcal{M}\}-\mu\mathcal{N}\{\mathcal{M}\})}} = \frac{\partial Z_G}{Z_G \partial(\beta\mu)} \tag{3.63}$$

The grand canonical ensemble theory is useful for systems in which the number of particles varies, i.e., for '**open systems**'. The fluctuation in the number of particles in the system about the mean $\langle\mathcal{N}\rangle = N$ is

$$\begin{aligned} \langle(\Delta\mathcal{N})^2\rangle &= \langle\mathcal{N}^2\rangle - \langle\mathcal{N}^2\rangle \\ &= \frac{\partial^2 Z_G}{Z_G \partial(\beta\mu)^2} - \left[\frac{\partial Z_G}{Z_G \partial(\beta\mu)}\right]^2 = \frac{\partial^2 \ln Z_G}{\partial(\beta\mu)^2} \\ &= \frac{\partial N}{\beta\partial\mu}, \end{aligned} \tag{3.64}$$

where (3.63) is used. Because $\partial N/\beta\partial\mu$ is an extensive quantity, the rms deviation $\bar{\Delta}\mathcal{N} = \langle(\Delta\mathcal{N})^2\rangle^{1/2}$ scales as $N^{1/2}$. Consider that N is very large. Then, one can show the distribution over the number of the particles is very sharp Gaussian around $\mathcal{N} = N$, which dominates the partition sum:

$$Z_G(T,\mu,X_i)=\sum_{\mathcal{N}=0}^{\infty}e^{\beta\mu\mathcal{N}}Z_{\mathcal{N}}=Ce^{\beta\mu N}Z_N, \tag{3.65}$$

where C is a constant independent of N. This domination allows the grand potential to be given by

$$\Omega(T,\mu,X_i)\equiv -k_BT\,\ln Z_G(T,\mu,X_i)=-\mu N+F \tag{3.66}$$

Starting from this thermodynamic potential, the average number, entropy, and entropic force are generated as given earlier (2.28–2.31): $S=-\partial\Omega/\partial T$, $N=-\partial\Omega/\partial\mu$, $f_i=\partial\Omega/\partial X_i=\Omega/X_i$.

The fluctuation of particle number, given by $\partial N/\partial\mu$, (3.64), can be related to mechanical susceptibility of the system, e.g., isothermal compressibility of the system. To see this, we note that, $Nd\mu=-X_idf_i$ (2.25) for an isothermal change, so

$$N\left(\frac{\partial\mu}{\partial N}\right)_{T,X_i}=-X_i\left(\frac{\partial f_i}{\partial N}\right)_{T,X_i}. \tag{3.67}$$

Consider the right hand side of the above equation for the fluid systems where $X_i=V$ and $f_i=-p$. In view of $p=p(T,n=N/V)$, $V(\partial p/\partial N)_{T,V}=-V^2/N(\partial p/\partial V)_{T,N}=1/(nK_T)$ (2.39). Therefore, (3.64) leads to the relative fluctuation for the number,

$$\left(\bar{\Delta}\mathcal{N}\right)/N=(nk_BTK_T)^{1/2}N^{-1/2}, \tag{3.68}$$

which, evidently, tells us that the isothermal compressibility K_T is always positive, and further that the relative fluctuation is negligible for a system with large N.

But **for mesoscopic systems the relative fluctuation can be quite sizable**. The relation (3.68) can be applied to, for example, a membrane in equilibrium with its lipids in a solution. If the stretching modulus K_s, (12.13), corresponding to the inverse of the mechanical susceptibility, is quite small, then the number $\mathcal{N}$ of lipids in a membrane, with its average N being not very large, can show large relative fluctuations.

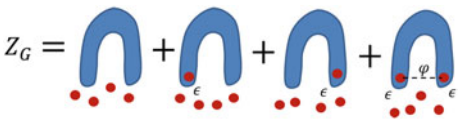

Fig. 3.11 The configurations of ligand binding on two sites of a protein that contribute to the grand canonical partition function expressed in (3.69)

3.4.2 Ligand Binding on Proteins with Interaction

As an example to show the utility of the grand canonical ensemble theory, we consider systems of molecules or ligands (such as O_2) that can bind on two identical, but distinguishable sites in a protein (e.g., myoglobin, hemoglobin) (Fig. 3.11). How does the average number of bound ligands depend on their ambient concentrations? Compared with a similar problem of two-state molecular binding treated in Sect. 3.1, there is an important difference: earlier, the system of interest was a biopolymer with fixed N binding sites, whereas the system in question here is the bound ligands, whose number $\mathcal{N}$ can vary.

In this case the grand partition function is expressed as

$$Z_G = \sum_{\mathcal{N}=0} e^{\beta\mu\mathcal{N}} Z_{\mathcal{N}} = Z_0(0,0) + zZ_1(1,0) + zZ_1(0,1) + z^2 Z_2(1,1), \tag{3.69}$$

where $Z_{m+n}(m,n)$ is the canonical partition function with m and n ligands bound on two sites, and $z = e^{\beta\mu}$ is the **fugacity** of a ligand. If the energy in the bound state is $-\epsilon(<0)$, and the interaction energy is φ, $Z_0(0,0) = 1$, $Z_1(1,0) = Z_1(0,1) = e^{\beta\epsilon}$, and $Z_2(1,1) = e^{\beta(2\epsilon-\varphi)}$, so Z_G is given as

$$Z_G = 1 + 2ze^{\beta\epsilon} + z^2 e^{\beta(2\epsilon-\varphi)}. \tag{3.70}$$

Using (3.63), **the coverage per site is**

$$\theta = \frac{1}{2}\langle\mathcal{N}\rangle = \frac{1}{2} z\frac{\partial}{\partial z}\ln Z_G = \frac{z\left\{e^{\beta\epsilon} + ze^{\beta(2\epsilon-\varphi)}\right\}}{1 + 2ze^{\beta\epsilon} + z^2 e^{\beta(2\epsilon-\varphi)}}. \tag{3.71}$$

If $\varphi = 0$ so that two sites are independent of each other, the coverage is

$$\theta = \frac{ze^{\beta\epsilon}}{1 + ze^{\beta\epsilon}} = \frac{1}{e^{-\beta(\epsilon+\mu)} + 1}. \tag{3.72}$$

To find μ, consider that at equilibrium the chemical potential of the bound particles is the same as that of the unbound particles in the bath. Because the unbound particles form an ideal gas or solution with density n, their chemical potential is given by

$$\mu = \mu_0(T) + k_B T \ln\{n/n_0(T)\}, \tag{3.73}$$

as will be shown in next chapter. $\mu_0(T)$ is the chemical potential of the gas at the standard density $n_0(T)$. Equating the chemical potentials, we obtain

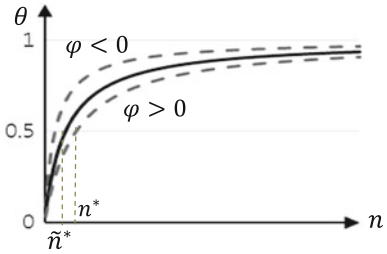

Fig. 3.12 Ligand binding isotherm. The coverage $\boldsymbol{\theta}$ increases with the ambient density $\boldsymbol{n}$ at a given temperature. The attraction ($\boldsymbol{\varphi} < 0$) between the bound particles enhances the coverage $\boldsymbol{\theta}$ over that of the Langmuir isotherm (solid curve). The repulsion ($\boldsymbol{\varphi} > 0$) lowers the coverage

$$\theta = \frac{1}{1 + \frac{n_0}{n} e^{-\beta(\epsilon + \mu_0)}} = \frac{n}{n + n^*(T)}, \tag{3.74}$$

where

$$n^*(T) = n_0(T) e^{-\beta[\epsilon + \mu_0(T)]} \tag{3.75}$$

is purely a temperature-dependent reference density. The **Langmuir isotherm** (solid curve in Fig. 3.12) shows how the coverage increases as the background density or concentration n increases at a temperature. $n^*(T)$ is the crossover concentration at which the coverage is 1/2.

If the bound particles interact, (3.71) can be written as

$$\theta = \frac{n}{n + \tilde{n}^*(T, n, \varphi)}. \tag{3.76}$$

For an attractive interaction such that $e^{-\beta\varphi} > 1$, θ is higher, and thus $\tilde{n}^*$ is less than that for the Langmuir isotherm (Fig. 3.12): **because of the attraction, binding is enhanced**. On the other hand, when the interaction is repulsive, $\varphi > 0$, the binding is reduced. These interesting effects due to the interaction are called **the cooperativity**.

P3.9 *Find the rms fluctuation in coverage. How are they affected by the interaction between the binding ligands?*

Further Reading and References

The original references for the Shannon Entropy and the Information theory are

C. Shannon, A mathematical theory of communication. Bell Syst. Tech. J. **27**, 379–423 (1948)
E.T. Jaynes, Information theory and statistical mechanics. Phys. Rev. Series II **106**(4), 620–630 (1957)

For more details on basic concepts on ensemble theories, see standard textbooks on statistical mechanics in graduate level as exemplified below.

M. Kardar, *Statistical Physics of Particles* (Cambridge University Press, 2007)
W. Greiner, L. Neise, H. Stocker, *Thermodynamics and Statistical Mechanics* (Springer, 1995)
R.K. Pathria, *Statistical Mechanics,* 2nd edn. (Butterworth-Heinemann, 1996)
M. Plischke, B. Bergersen, *Equilibrium Statistical Physics,* 2nd edn. (Prentice Hall, 1994)
K. Huang, *Statistical Mechanics*, 2nd edn. (Wiley, 1987)
D.A. McQuarrie, *Statistical Mechanics* (Universal Science Books, 2000)
L. Reichl, *A Modern Course in Statistical Physics,* 2nd edn. (Wiley-Interscience, 1998)
M. Toda, R. Kubo, N. Saito, *Statistical Physics I: Equilibrium Statistical Mechanics* (Springer, 1983)
G.F. Mazenko, *Equilibrium Statistical Mechanics* (Wiley, 2001)
G. Morandi, E. Ercolessi, F. Napoli, *Statistical Mechanics, An Intermediate Course,* 2nd edn. (World Scientific, 2001)

Chapter 4
Statistical Mechanics of Fluids and Solutions

Biological components function often in watery environments. Biological fluids are either water solvent or various aqueous solutions and suspensions of ions and macromolecules, with which virtually all chapters of this book are concerned. In this chapter we start with a review of how the canonical ensemble method of statistical mechanics can be used to derive some basic properties of simple, classical fluids that consist of small molecules. We derive the well-known thermodynamic properties of non-interacting gases either in the absence or in the presence of external forces. For dilute and non-dilute fluids, we study how the inter-particle interactions give rise to the spatial correlations in the fluids, which affects the thermodynamic behaviors.

These results, which are essential for a simple fluid for its own, can be extended to aqueous solutions of colloids and macromolecules; e.g., the results of dilute simple gas can be directly applied to dilute solutions. We outline coarse-grained descriptions in which the solutions are treated as the fluids of solutes undergoing the solvent-averaged effective interactions. As a particularly simple but useful variation we shall introduce the lattice model.

4.1 Phase-Space Description of Fluids

4.1.1 N Particle Distribution Function and Partition Function

Consider a simple fluid consisting of N identical classical particles of mass m each with no internal degrees of freedom. The fluid is confined in a rectangular volume V with sides L_x, L_y, L_z and kept at a temperature T. For a classical but microscopic description, the microstate $\mathcal{M}$ of the system is specified by a point in **$6N$ dimensional phase space** $\boldsymbol{\Gamma} = (\boldsymbol{p}_1, \boldsymbol{r}_1; \ldots \boldsymbol{p}_i, \boldsymbol{r}_i; \ldots \boldsymbol{p}_N, \boldsymbol{r}_N) \equiv \{\boldsymbol{p}_i, \boldsymbol{r}_i\}$ where $\boldsymbol{p}_i, \boldsymbol{r}_i$ are the

W. Sung, *Statistical Physics for Biological Matter*, Graduate Texts in Physics,
https://doi.org/10.1007/978-94-024-1584-1_4

three-dimensional momentum and position vectors of the i-th particles. The particles are in motion with the Hamiltonian

$$\mathcal{H}\{\boldsymbol{p}_i, \boldsymbol{r}_i\} = K\{\boldsymbol{p}_i\} + U\{\boldsymbol{r}_i\} + \Phi\{\boldsymbol{r}_i\}. \tag{4.1}$$

Here $K\{\boldsymbol{p}_i\} = \sum_{i=1}^{N} \boldsymbol{p}_i^2/(2m)$ is net kinetic energy of the system, $U\{\boldsymbol{r}_i\} = \sum_{i=1}^{N} u(\boldsymbol{r}_i)$ is the net external potential energy, where $u(\boldsymbol{r}_i)$ is one body potential energy of particle i. $\Phi\{\boldsymbol{r}_i\} = \sum_{i>j} \varphi(\boldsymbol{r}_i - \boldsymbol{r}_j)$, the net interaction potential energy, which is the sum of $N(N-1)/2$ **pairwise interaction potential energies** between particles positioned at $\boldsymbol{r}_i$ and $\boldsymbol{r}_j$, $\varphi(\boldsymbol{r}_i - \boldsymbol{r}_j) \equiv \varphi(\boldsymbol{r}_{ij})$.

The canonical microstate distribution (3.31) for this system is the N particle **phase-space distribution function:**

$$P\{\boldsymbol{p}_i, \boldsymbol{r}_i\} = \frac{1}{N!}\frac{1}{h^{3N}} e^{-\beta\mathcal{H}\{\boldsymbol{p}_i, \boldsymbol{r}_i\}}/Z_N. \tag{4.2}$$

This is the joint probability distribution with which the N particles have their all positions and momenta at $\boldsymbol{p}_1, \boldsymbol{r}_1; \ldots \boldsymbol{p}_i, \boldsymbol{r}_i; \ldots \boldsymbol{p}_N, \boldsymbol{r}_N$ simultaneously. The partition function Z_N is given as the $6N$-dimensional integral:

$$\begin{aligned} Z_N &= \frac{1}{N!}\frac{1}{h^{3N}} \int d\boldsymbol{\Gamma}\, e^{-\beta\mathcal{H}(\boldsymbol{\Gamma})} \\ &= \frac{1}{N!}\frac{1}{h^{3N}} \int \ldots \int d\boldsymbol{p}_1 d\boldsymbol{r}_1 \ldots d\boldsymbol{p}_N d\boldsymbol{r}_N\, e^{-\beta\mathcal{H}\{\boldsymbol{p}_i, \boldsymbol{r}_i\}} \end{aligned} \tag{4.3}$$

Here the Planck's constant h is introduced to enumerate the microstates in phase space. The phase space volume for a particle in three dimension is h^3 due to the underlying quantum mechanical uncertainty principle that forbids a simultaneous determination of the position and momentum of a particle; the 3-D N-particle phase space volume should be divided by h^{3N}. This kind of consideration to appropriately count the number of states depends on the level of the description that defines the states, and is not essential for thermodynamic *changes*, as we will see below. More importantly the division factor $N!$ is inserted to avoid overcounting states of the N identical particles, which are indistinguishable with respect to mutual exchanges.

A close look at the integral, whose hyper-dimensionality may seem overwhelming, allows the factorization

$$Z_N = Z_N^0 Q_N, \tag{4.4}$$

where

$$Z_N^0 = \frac{1}{N!}\frac{V^N}{h^{3N}} \int \ldots \int d\boldsymbol{p}_1 \ldots d\boldsymbol{p}_N\, e^{-\beta K\{\boldsymbol{p}_i\}} \tag{4.5}$$

is the partition function of the particles with no mutual interactions and no external fields, and

$$Q_N = \frac{1}{V^N} \int \ldots \int d\boldsymbol{r}_1 \ldots d\boldsymbol{r}_N \, e^{-\beta[U\{\boldsymbol{r}_i\} + \Phi\{\boldsymbol{r}_i\}]} \tag{4.6}$$

is the configuration partition function that includes the effects of the potential energies. Z_N^0 is readily calculated by noting the factorization:

$$Z_N^0 = \frac{1}{N!} \frac{V^N}{h^{3N}} \left[\int d\boldsymbol{p}_i \, e^{-\frac{\beta \boldsymbol{p}_i^2}{2m}} \right]^N = \frac{1}{N!} \frac{V^N}{h^{3N}} \left(\frac{2m\pi}{\beta} \right)^{3N/2}, \tag{4.7}$$

where

$$\begin{aligned} \int d\boldsymbol{p} \, e^{-\frac{\beta \boldsymbol{p}^2}{2m}} &= \int_{-\infty}^{+\infty} dp_x \, e^{-\frac{\beta \boldsymbol{p}_x{}^2}{2m}} \int_{-\infty}^{+\infty} dp_y \, e^{-\frac{\beta \boldsymbol{p}_y{}^2}{2m}} \int_{-\infty}^{+\infty} dp_z \, e^{-\frac{\beta \boldsymbol{p}_z{}^2}{2m}} \\ &= \left(\frac{2m\pi}{\beta} \right)^{3/2}, \end{aligned} \tag{4.8}$$

and $\int_{-\infty}^{+\infty} dp \, e^{-\frac{\beta \boldsymbol{p}^2}{2m}} = (2m\pi/\beta)^{1/2}$. The ideal gas partition function Z_N^0 is then written as

$$Z_N^0(T, N, V) = \frac{1}{N!} \left(\frac{V}{\lambda(T)^3} \right)^N, \tag{4.9}$$

where

$$\lambda(T) = \left(\frac{h^2}{2\pi m k_B T} \right)^{1/2} \tag{4.10}$$

is called the "**thermal wavelength**".

4.1.2 The Maxwell-Boltzmann Distribution

From this canonical distribution and partition functions given above the statistical and macroscopic properties of the classical fluids at a temperature can be found in a great variety. Let us start with the famous **Maxwell-Boltzmann distribution for the particle velocity**. The mean number of particles with the momentum between

$\boldsymbol{p}_1$ and $\boldsymbol{p}_1 + d\boldsymbol{p}_1$ and at the position between $\boldsymbol{r}_1$ and $\boldsymbol{r}_1 + d\boldsymbol{r}_1$ is given by $f(\boldsymbol{p}_1, \boldsymbol{r}_1) d\boldsymbol{p}_1 d\boldsymbol{r}_1$, where

$$\begin{aligned} f(\boldsymbol{p}_1, \boldsymbol{r}_1) &= N \int \ldots \int d\boldsymbol{p}_2 d\boldsymbol{r}_2 \ldots d\boldsymbol{p}_N d\boldsymbol{r}_N \, P\{\boldsymbol{p}_i, \boldsymbol{r}_i\} \\ &= \frac{N}{N!} \frac{1}{h^{3N} Z_N} \int \ldots \int d\boldsymbol{p}_2 \ldots d\boldsymbol{p}_N \, e^{-\beta \sum_{i=1}^{N} \boldsymbol{p}_i^2 / 2m} \int \ldots \int d\boldsymbol{r}_2 \ldots d\boldsymbol{r}_N \, e^{-\beta [U\{\boldsymbol{r}_i\} + \Phi\{\boldsymbol{r}_i\}]}. \end{aligned} \tag{4.11}$$

Here we used (4.2), and inserted N into the numerator as the number of ways to assign a particle with the subscript 1. Integrating over the momenta yields

$$f(\boldsymbol{p}_1, \boldsymbol{r}_1) = P(\boldsymbol{p}_1) n(\boldsymbol{r}_1). \tag{4.12}$$

where

$$P(\boldsymbol{p}_1) = \left(\frac{2m\pi}{\beta} \right)^{-3/2} e^{-\frac{\beta \boldsymbol{p}_1^{\,2}}{2m}}, \tag{4.13}$$

and

$$n(\boldsymbol{r}_1) = \frac{N}{V^N Q_N} \int \ldots \int d\boldsymbol{r}_2 \ldots d\boldsymbol{r}_N \, e^{-\beta [U\{\boldsymbol{r}_i\} + \Phi\{\boldsymbol{r}_i\}]}. \tag{4.14}$$

Integrating (4.12) over $\boldsymbol{r}_1$ yields

$$f(\boldsymbol{p}_1) = N P(\boldsymbol{p}_1). \tag{4.15}$$

Therefore $f(\boldsymbol{p}_1) d\boldsymbol{p}_1$ is the number of molecules that have a momentum between $\boldsymbol{p}_1$ and $\boldsymbol{p}_1 + d\boldsymbol{p}_1$, and $P(\boldsymbol{p})$ is a particle's momentum probability distribution or probability density, from which the well-known Maxwell-Boltzmann (MB) distribution of velocities can be found:

$$\Phi(\boldsymbol{v}) = m^{-3} P(\boldsymbol{p}) = \left(\frac{2\pi}{m\beta} \right)^{3/2} e^{-\frac{\beta m v^2}{2}} = \left(\frac{2\pi k_B T}{m} \right)^{3/2} e^{-\frac{m v^2}{2 k_B T}}. \tag{4.16}$$

The prefactors ensure the normalizations $\int d\boldsymbol{p} \, P(\boldsymbol{p}) = 1$ and $\int d\boldsymbol{v} \, \Phi(\boldsymbol{v}) = 1$.

The MB distribution is a Gaussian distribution in velocity (Fig. 4.1), **and applies universally to thermalized particles at equilibrium.** Because the phase space distribution (4.2) is factorized into a momentum-dependent part and a position-dependent part, the MB distribution is independent of the intermolecular interaction strength, and so may also be valid to structured molecules in a liquid phase where their center-of-mass translational degrees of freedom are decoupled with the internal degrees of freedom.

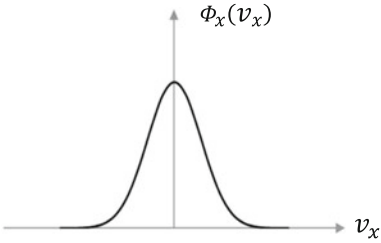

Fig. 4.1 The Maxwell-Boltzmann distribution function for x-component velocity. The most probable velocity is zero

Each component of the velocity is statistically independent of every other component:

$$\Phi(\boldsymbol{v}) = \Phi_x(v_x)\Phi_y(v_y)\Phi_z(v_z), \tag{4.17}$$

where

$$\Phi_\alpha(v_\alpha) = \left(\frac{2\pi k_B T}{m}\right)^{1/2} e^{-\frac{mv_\alpha^2}{2k_B T}}. \tag{4.18}$$

In the MB distribution, the average velocity component is zero:

$$\langle v_\alpha \rangle = \int_{-\infty}^{\infty} dv_\alpha v_\alpha \Phi_\alpha(v_\alpha) = 0, \tag{4.19}$$

so is $\langle \boldsymbol{v} \rangle$. Also

$$\langle v_\alpha^2 \rangle = \int_{-\infty}^{\infty} dv_\alpha v_\alpha^2 \Phi_\alpha(v_\alpha) = \frac{k_B T}{m}, \tag{4.20}$$

so that the average kinetic energy of a particle is

$$\frac{1}{2}m\langle v^2 \rangle = \frac{1}{2}m\left[\langle v_x^2 \rangle + \left\langle v_y^2 \right\rangle + \langle v_z^2 \rangle\right] = \frac{3}{2}k_B T. \tag{4.21}$$

It means that each of the three translational degrees of freedom has energy of $k_B T/2$, which is a special case of **the equipartition theorem** stating more generally that the energy in thermal equilibrium is shared equally among all degrees of freedom that appear quadratically in the total energy.

Although the average velocity of a particle is zero, the average speed is not. We note that the probability that the speed has the value between v and $v + dv$ is $\Phi(v)4\pi v^2 dv = D(v)dv$, which defines the **MB speed distribution** function (Fig. 4.2).

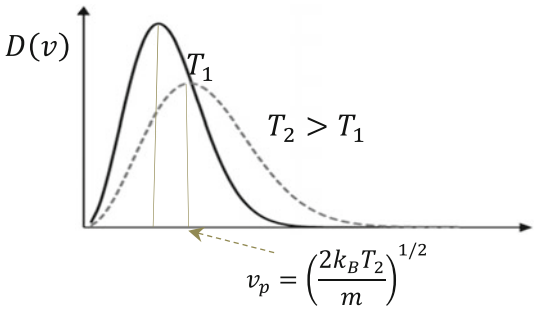

Fig. 4.2 The Maxwell Boltz mann speed distribution function curve. The most probable speed at temperature T_i is not zero but $v_p = \left(\frac{2k_BT_i}{m}\right)^{1/2}$

$$D(v) = 4\pi\left(\frac{m}{2\pi k_BT}\right)^{3/2} v^2 e^{-\frac{mv^2}{2k_BT}}. \tag{4.22}$$

The average speed is then calculated to be

$$\langle v\rangle = \int_0^\infty vD(v)dv = \left(\frac{8k_BT}{\pi m}\right)^{1/2}. \tag{4.23}$$

The most probable speed, where the probability is the maximum given by the condition $dD(v)/dv = 0$, is

$$v_p = \left(\frac{2k_BT}{m}\right)^{1/2}. \tag{4.24}$$

The peak of the speed distribution increases as the square root of temperature, and the right skew means there an appreciable fraction of molecules have speed is much higher than v_p. The water molecules that belong to the high-speed tail of the distribution can escape the surface of water; because of this removal of high-energy molecules, the average speed of the remaining molecules i.e., their energy (temperature) decreases. Thus evaporation of water alone is cooling process, which can be balanced by heat transfer from the environment to retain the water temperature. The evaporation process makes rain possible.

P4.1 *What is the probability that a nitrogen gas molecule on surface of the earth can escape the gravisphere? Assume that the temperature throughout is 300* K.

P4.2 *Suppose that water molecules escape a planar surface of a liquid water if its energy exceeds the average* $3k_BT/2$. *Calculate the cooling rate of the liquid.*

Now going back to the (4.14), $n(\boldsymbol{r})$ is recognized as the **number density or concentration** of the molecules at position $\boldsymbol{r}$. In the absence of all potential energies, external and interactional, it can be shown to be uniform, $n(\boldsymbol{r}) = N/V = n$. This also holds true for a fluid of particles that are mutually interacting with an isotropic potential $\varphi(\boldsymbol{r}) = \varphi(r)$ but in the absence of the external potential, where the fluid is translationally invariant and homogeneous. Below we consider the

alternative case, in which interaction is absent but external potentials exist to make the fluid non-uniform.

4.2 Fluids of Non-interacting Particles

4.2.1 *Thermodynamic Variables of Non-uniform Ideal Gases*

When $\Phi\{\boldsymbol{r}_i\} = 0$, the configuration partition function (4.6) reduces to

$$Q_N = q_1^N, \tag{4.25}$$

where

$$q_1 = \frac{1}{V}\int d\boldsymbol{r}\, e^{-\beta u(\boldsymbol{r})}, \tag{4.26}$$

so (4.14) becomes

$$n(\boldsymbol{r}) = ne^{-\beta u(\boldsymbol{r})}. \tag{4.27}$$

The non-uniform fluid density follows the Boltzmann distribution. For a gas under uniform gravity directed downward along the z axis, $u(z) = mgz$, we get

$$n(z) = ne^{-\beta mgz} = ne^{-z/z^*}, \tag{4.28}$$

which is none other than **the barometric formula**. It means that thermal agitation allows the gas to overcome gravitational sedimentation. It is because the characteristic altitude $z^* = k_B T/(mg)$ of the density decay increases with T and decreases with m. At $T = 300\,\mathrm{K}$, z^* of O_2 ($m = 32\ \mathrm{g/mol} = 5.32 \times 10^{-26}\ \mathrm{kg/molecule}$) is 7.95 km and the z^* of H_2 ($m = 2\ \mathrm{g/mol} = 3.32 \times 10^{-27}\ \mathrm{kg/molecule}$) is 127 km; this inverse relationship between z^* and m means that at high altitude light gases are more abundant than heavy gases. This prediction is not strictly valid because T and g vary with altitude. Also we note that the barometric formula can be applied to sedimentation of colloidal particles suspended in a solvent provided that the mass is modified in such a way to incorporate the buoyancy and hydration.

For thermodynamic properties, the partition function (4.4) is calculated easily using (4.9) and (4.25):

$$Z_N = \frac{1}{N!}\left(\frac{V}{\lambda^3}\right)^N q_1^N. \tag{4.29}$$

The Helmholtz free energy is obtained as:

$$F(T,V,N) = -k_B T \ln Z_N = -k_B TN\left[\ln\left(Vq_1/N\lambda^3\right)+1\right] \tag{4.30}$$

where Stirling's formula is used. In the absence of the external potential,

$$F(T,V,N) = -k_B TN\left[\ln\left(\frac{V}{N\lambda(T)^3}\right)+1\right]. \tag{4.31}$$

If volume V is taken to be microscopically large enough to contain many molecules but macroscopically very small so that it can be regarded as a point located at $\boldsymbol{r}$, we note that $q_1 = e^{-\beta u(\boldsymbol{r})}$. Then the local free energy density in the presence of the potential is given by

$$f(\boldsymbol{r}) = \frac{F}{V} = k_B T n(\boldsymbol{r})\{\ln\left(n(\boldsymbol{r})\lambda^3\right) - 1\} + n(\boldsymbol{r})u(\boldsymbol{r}) \tag{4.32}$$

where $n(\boldsymbol{r})$ is number density of the non-uniform fluid.

It is straightforward to obtain the first order thermodynamic variables from the free energy. First, the pressure of the gas confined in a box of the volume V is given by

$$p = -\left(\frac{\partial F}{\partial V}\right)_{T,N} = Nk_B T\left(\frac{1}{V} + \frac{\partial}{\partial V}\ln q_1\right) \tag{4.33}$$

In the absence of an external force, it is reduced to the well-known **ideal gas equation of state**

$$p = \frac{Nk_B T}{V} = nk_B T. \tag{4.34}$$

If the external potential is present, the pressure, i.e., the force per unit area on the enclosing wall, depends on its normal direction, and is therefore not isotropic.

P4.3 *For the gas under a uniform gravity along the z–axis, the pressure acting on the wall normal to z-axis is given by* $p_z = -\partial F/\left(L_x L_y \partial L_z\right)_{T,N}$. *Show that, unless* $mgL_z \ll k_B T$, *this differs from* p_x *and* p_y, *both of which are* $Nk_B T/V$.

Considering an infinitesimal volume that encloses the point $\boldsymbol{r}$, we find the **local pressure** is position-dependent but isotropic:

$$p(\boldsymbol{r}) = n(\boldsymbol{r})k_B T. \tag{4.35}$$

The entropy is given by

$$S(N,V,T) = -\frac{\partial F}{\partial T} = Nk_B\left[\ln\frac{Vq_1}{N\lambda^3} + \frac{5}{2}\right] + \frac{N\langle u\rangle}{T}, \tag{4.36}$$

where

$$\langle u \rangle = \frac{\int d\boldsymbol{r} u(\boldsymbol{r}) e^{-\beta u(\boldsymbol{r})}}{\int d\boldsymbol{r} e^{-\beta u(\boldsymbol{r})}}. \tag{4.37}$$

In the absence of the external potential, (4.36) reduces to

$$S(N,V,T) = k_B N \left[\ln \frac{V}{N\lambda^3} + \frac{5}{2} \right] = k_B N \left(\ln \frac{V}{N} + \frac{3}{2} \ln T \right) + constant. \tag{4.38}$$

The **local entropy** in the presence of the external potential is

$$s(\boldsymbol{r}) = S/V = k_B n(\boldsymbol{r}) \left[- \ln \left\{ n(\boldsymbol{r}) \lambda^3 \right\} + 5/2 \right]. \tag{4.39}$$

In addition, the internal energy is obtained as

$$E = F + TS = \frac{3}{2} N k_B T + N \langle u \rangle. \tag{4.40}$$

The internal energy E is the sum of the average translational kinetic energy $3Nk_BT/2$ and the average potential energy $N\langle u \rangle$, and can be obtained alternatively from the relation $E = -\partial \ln Z_N / \partial \beta$. Considering the enclosing volume around the point $\boldsymbol{r}$ to be small we obtain the obvious result for local energy density (energy per unit volume):

$$e(\boldsymbol{r}) = \frac{3}{2} n(\boldsymbol{r}) k_B T + n(\boldsymbol{r}) u(\boldsymbol{r}). \tag{4.41}$$

The overall chemical potential is obtained as

$$\mu = \frac{\partial F}{\partial N} = k_B T \ln \left(n\lambda^3 / q_1 \right), \tag{4.42}$$

whereas the **local chemical potential** $\mu(\boldsymbol{r})$ is

$$\mu(\boldsymbol{r}) = u(\boldsymbol{r}) + k_B T k \ln \left\{ n(\boldsymbol{r}) \lambda^3 \right\}. \tag{4.43}$$

The second term is the contribution from the entropy. The condition of equilibrium within the fluid, $\mu(\boldsymbol{r}) =$ constant, yields the earlier-obtained result $n(\boldsymbol{r}) = ne^{-\beta u(\boldsymbol{r})}$, where n is the density at which $u = 0$.

The heat capacity at fixed volume is

$$C_V = \frac{\partial E}{\partial T} = \frac{3}{2} N k_B + N \frac{\partial}{\partial T} \langle u \rangle, \tag{4.44}$$

which indicates that each particle has three translational degrees of freedom that are thermally excited.

4.2.2 A gas of Polyatomic Molecules-the Internal Degrees of Freedom

A polyatomic molecule consists of two or more nuclei and many electrons. In addition to the translational degrees of freedom of the center of the mass, the molecule has the internal degrees of freedom, arising from rotational, vibrational molecular motions, and electronic, other subatomic motions. At room temperature, $T \approx 300$ K, two rotational degrees of freedom in diatomic molecule can fully be excited, and therefore contribute k_B to heat capacity per molecule. The partition function of an ideal gas of polyatomic molecules, including **the internal degrees of the freedom**, may be written as

$$Z_N = \frac{1}{N!}\left(\frac{Vq_1}{\lambda^3} z_i(T)\right)^N, \tag{4.45}$$

where $z_i(T)$ is the partition function from the internal degrees of the freedom per molecule. In the absence of an external potential, the chemical potential is

$$\begin{aligned} \mu &= \frac{\partial F}{\partial N} = k_B T \ln\left[n\lambda^3 / z_i(T)\right] \\ &= k_B T \ln\left(n\lambda^3\right) + f_i(T), \end{aligned} \tag{4.46}$$

where $f_i = -k_B T \ln(z_i(T))$ is the free energy from the internal degrees of freedom in a single molecule.

In general, chemical potential can be written as

$$\mu = \mu_0(T) + k_B T \ln\{n/n_0(T)\}. \tag{4.47}$$

Here the subscript 0 denotes a **standard or reference state** at which the density and chemical potential are $n_0(T)$ and $\mu_0(T)$ respectively. At the standard state, the 2nd term (concentration-dependent entropy) in (4.47) vanishes, so $\mu_0(T)$ is the intrinsic free energy of a *single* polyatomic molecule that includes such an extreme as a long chain polymer. For solutes, the standard density $n_0(T)$ is usually taken to be 1 mol concentration (M), which is an Avogadro number (N_a) per 1 L (liter).

P4.4 *Consider a classical ideal gas of N diatomic molecules interacting* via *harmonic potential.* $\varphi(\boldsymbol{r}_i - \boldsymbol{r}_j) = k(\boldsymbol{r}_i - \boldsymbol{r}_j)^2/2$. *Calculate the Helmholtz free energy, entropy, and heat capacity. What is the mean square molecule diameter* $\langle(\boldsymbol{r}_i - \boldsymbol{r}_j)^2\rangle^{1/2}$?

4.3 Fluids of Interacting Particles

Now we focus on the particles that have no internal structures but have mutual interaction $\Phi\{\boldsymbol{r}_i\} = \sum_{i>j} \varphi(\boldsymbol{r}_i - \boldsymbol{r}_j)$ where the interaction potential is isotropic: $\varphi(\boldsymbol{r}_i - \boldsymbol{r}_j) = \varphi(|\boldsymbol{r}_i - \boldsymbol{r}_j|) \equiv \varphi(r_{ij})$. Considering the Hamiltonian, $\mathcal{H}\{\boldsymbol{p}_i, \boldsymbol{r}_i\} = K\{\boldsymbol{p}_i\} + \Phi\{\boldsymbol{r}_i\}$, the partition function is given by

$$\begin{aligned} Z_N &= \frac{1}{N!}\frac{1}{h^{3N}} \int \dots \int d\boldsymbol{p}_1 d\boldsymbol{r}_1 \dots d\boldsymbol{p}_N d\boldsymbol{r}_N \, e^{-\beta\left[\sum_{i=1}^{N} \frac{p_i^2}{2m} + \sum_{i>j} \varphi(\boldsymbol{r}_i - \boldsymbol{r}_j)\right]} \\ &= Z_N^0 Q_N = \frac{1}{N!}\left(\frac{V}{\lambda^3}\right)^N Q_N, \end{aligned} \tag{4.48}$$

where

$$Q_N = \frac{1}{V^N} \int \dots \int d\boldsymbol{r}_1 \dots d\boldsymbol{r}_N \, e^{-\beta \sum_{i>j} \varphi(\boldsymbol{r}_i - \boldsymbol{r}_j)} \tag{4.49}$$

is the **configurational partition function** of N interacting particles.

P4.5 *A lot of biological problems is modelled to be one-dimensional; for an example, protein or ion in motion along DNA. As a useful model* [Möbius et al, 2013]*, consider Tonks gas, which is a collection of N particles in the interval* $0 < x < L$ *mutually interacting pairwise through a hard core repulsion;* $\varphi(x) = \infty$*, for* $|x| < \sigma$ *and* $\varphi(x) = 0$*, for* $|x| > \sigma$*. Calculate the configuration partition function* Q_N*, and the one-dimensional pressure acting at an end.*

4.3.1 The Virial Expansion–Low Density Approximation

We first consider dilute fluids where the inter-particle interactions can be regarded as a perturbation. We start by rewriting Q_N as

$$Q_N = V^{-N} \int d\boldsymbol{r}_1 \dots d\boldsymbol{r}_N \prod_{i>j} (1 + f_{ij}), \tag{4.50}$$

where $f_{ij} = e^{-\beta\varphi(r_{ij})} - 1$ is a function that is appreciable only when r_{ij} is within the range of potential, which we regard as short. For dilute gases, the value of f_{ij} is small and serves as a perturbation in terms of which we perform expansion:

$$\prod_{i>j}\left(1+f_{ij}\right)=1+\sum_{i>j}f_{ij}+\sum_{i<j}\sum_{k<l}f_{ij}\,f_{kl}+\cdots \tag{4.51}$$

We consider the case of a dilute gas in which the first two terms in (4.51) are included. Then

$$\begin{aligned} Q_N &\approx \frac{1}{V^N}\int\ldots\int d\boldsymbol{r}_1\ldots d\boldsymbol{r}_N\left(1+\sum_{i>j}f_{ij}\right)\\ &= 1+\frac{1}{V^N}\int\ldots\int d\boldsymbol{r}_1\ldots d\boldsymbol{r}_N\sum_{i>j}f_{ij}\\ &= 1+\frac{N^2}{2V}\int d\boldsymbol{r}_{21}\,f_{12}, \end{aligned} \tag{4.52}$$

where we note the number of interacting pairs is $N(N-1)/2\approx N^2/2$, and

$$\int d\boldsymbol{r}_1 d\boldsymbol{r}_2 d\boldsymbol{r}_3\ldots d\boldsymbol{r}_N=\int d\boldsymbol{r}_1 d\boldsymbol{r}_{21} d\boldsymbol{r}_3\ldots d\boldsymbol{r}_N=V^{N-1}\int d\boldsymbol{r}_{21}.$$

This leads to the total partition function and free energy

$$Z_N=Z_N^0\left\{1+\frac{N^2}{2V}\int d\boldsymbol{r}_{21}\,f_{12}\right\} \tag{4.53}$$

$$\begin{aligned} F &= F^0-k_BT\,\ln\left[1+\frac{N^2}{2V}\int d\boldsymbol{r}_{21}\,f_{12}\right]\\ &\approx F^0-k_BT\frac{N^2}{2V}\int d\boldsymbol{r}_{21}\{e^{-\beta\varphi(r_{12})}-1\}\\ &= F^0+k_BT\frac{N^2}{V}B_2, \end{aligned} \tag{4.54}$$

where the superscript 0 denotes the ideal gas part and B_2 is **the second virial coefficient**:

$$\begin{aligned} B_2 &= -\frac{1}{2}\int d\boldsymbol{r}_{21}\{e^{-\beta\varphi(r_{12})}-1\}\\ &= -2\pi\int dr\,r^2\{e^{-\beta\varphi(r)}-1\}. \end{aligned} \tag{4.55}$$

The pressure is obtained by differentiating the free energy with respect to volume:

$$p=p^0+B_2\frac{N^2}{V^2}k_BT \tag{4.56}$$

This is the second order approximation of the density or virial expansion for the pressure:

$$\frac{p}{k_B T} = n + B_2 n^2 + B_3 n^3 + \cdots . \tag{4.57}$$

where B_3 is the third virial coefficient that includes three-body pairwise interactions involving $f_{ij} f_{ik} f_{jk}$. Likewise, the free energy is expanded as below:

$$F = F^0 + k_B T \frac{N^2}{V} B_2 + \frac{k_B T}{2} \frac{N^3}{V^2} B_3 + \cdots . \tag{4.58}$$

4.3.2 The Van der Waals Equation of State

We now make an approximation that is useful for non-dilute fluids and derive the van-der Waals equation by statistical mechanical methods. The intermolecular pair potential $\varphi(r)$ can in many cases be separated into two parts, a harsh, short-range (hard-core) repulsion for $r < \sigma$ and a smooth, relatively long-range attraction for $r > \sigma$, where σ is the hard-core size or the diameter of molecules. A typical example is the Lennard-Jones potential (Fig. 4.3).

$$\varphi_{LJ}(r) = 4\epsilon \left\{ \left(\frac{r}{\sigma}\right)^{-12} - \left(\frac{r}{\sigma}\right)^{-6} \right\} \tag{4.59}$$

Then the second virial coefficient (4.55) is expressed as the sum of two integrals, each representing the hard-repulsion and soft-attraction part:

$$B_2 = 2\pi \left[\int_0^{\sigma} dr\, r^2 \{1 - e^{-\beta\varphi(r)}\} + \int_{\sigma}^{\infty} dr\, r^2 \{1 - e^{-\beta\varphi(r)}\} \right]. \tag{4.60}$$

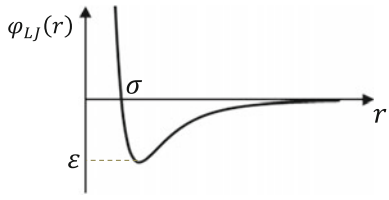

Fig. 4.3 The Lennard-Jones potential $\varphi_{LJ}(r) = 4\varepsilon\left[(\sigma/r)^{12} - (\sigma/r)^{6}\right]$

In the first integral, the exponent $e^{-\beta\varphi(r)}$ is negligible for $r<\sigma$ where the potential sharply rises to infinity, so that the integral is evaluated as $2\pi\sigma^3/3 \equiv b$. For $r > \sigma$, $\varphi(r)$ is a weak attraction effectively so that $e^{-\beta\varphi(r)} \approx 1 - \beta\varphi(r)$, yielding the second integral as $-a/(k_BT)$, where

$$a = -2\pi \int_{\sigma}^{\infty} r^2 \varphi(r) dr. \tag{4.61}$$

Then, the second virial coefficient is given as

$$B_2 = b - \frac{a}{k_BT} = b\left(1 - \frac{\Theta}{T}\right), \tag{4.62}$$

where the $\Theta = a/(k_Bb)$ is the parameter called the Boyle temperature. If $T > \Theta$, then $B_2 > 0$; the repulsion dominates the attraction overall, contributing positively to the pressure and free energy. If $T = \Theta$, then $B_2 = 0$ and the gas behaves ideally. For $T<\Theta$ and $B_2<0$, the attraction dominates the repulsion, contributing negatively to them.

Then we rewrite (4.56) as

$$\frac{p}{k_BT} = n(1+bn) - \frac{an^2}{k_BT}. \tag{4.63}$$

Although we derived (4.63) for a dilute gas, we seek a way to extend the equation to denser fluids. This we do by replacing $1+bn$ by $(1-bn)^{-1}$, which yields the same pressure at low densities but an infinite pressure as $bn = 2\pi n\sigma^3/3$ approaches to 1, characteristic of incompressible liquids. The resulting equation is the **Van der Waals' equation of state**

$$p + an^2 = \frac{nk_BT}{1-bn}. \tag{4.64}$$

Although by no means exact, this equation is valid for dense gas and even liquids, and is useful for explaining the gas-liquid phase transition. A more-justified way of deriving it without invoking the low density approximation at the outset is the mean field theory (MFT). In MFT, the interactions of all the other particles on a particle is approximated by a **one-body external potential, called a mean field**, thus reducing a many-body problem to a one-body problem. That is, a particle is thought to feel a mean (uniform) field given by the excluded volume b and the attraction of the strength $2a/V$ per pair (which is the volume average of the attractive potential). The hard-core repulsion and soft-weak attraction are the key

features that well characterize the liquid state and gas state respectively. The partition function, (4.29), then is expressed in the form

$$\begin{aligned} Z_N &= \frac{1}{N!}\left(\frac{V-Nb}{\lambda^3}\right)^N \exp\{\beta(N^2/2)(2a/V)\} \\ &= Z_N^0\left(\frac{V-Nb}{V}\right)^N \exp\left(\frac{\beta N^2 a}{V}\right). \end{aligned} \tag{4.65}$$

This equation yields all thermodynamic variables, including the Van der Waals pressure equation. The free energy, internal energy, entropy and chemical potential are obtained as

$$F = F^0 - Nk_BT\,\ln(1-nb) - \frac{N^2a}{V} \tag{4.66}$$

$$E = E^0 - \frac{N^2a}{V} \tag{4.67}$$

$$S = S^0 + Nk_B\ln(1-nb) \tag{4.68}$$

$$\mu = \mu^0 - k_BT\left\{\ln(1-nb) - \frac{nb}{1-nb}\right\} - 2na, \tag{4.69}$$

respectively. Here the quantities superscripted by 0 are those of an ideal gas.

4.3.3 *The Effects of Spatial Correlations: Pair Distribution Function*

Now we consider a non-dilute fluid that has arbitrary density. From (4.48), and (4.49), the internal energy of the system is obtained:

$$E = -\frac{\partial}{\partial\beta}\ln\,Z_N = \frac{3}{2}Nk_BT + \langle\Phi\rangle, \tag{4.70}$$

where the average interaction energy is

$$\begin{aligned}\langle \Phi \rangle &= \frac{1}{V^N Q_N} \sum_{i>j} \int \cdots \int d\boldsymbol{r}_1 \ldots d\boldsymbol{r}_N \varphi(\boldsymbol{r}_i - \boldsymbol{r}_j) e^{-\beta \Sigma_{i>j} \varphi(\boldsymbol{r}_i - \boldsymbol{r}_j)} \\ &= \frac{1}{V^N} \sum_{i>j} \iint d\boldsymbol{r}' \; d\boldsymbol{r}'' \; \varphi(\boldsymbol{r}' - \boldsymbol{r}'') \frac{1}{Q_N} \int \cdots \int d\boldsymbol{r}_1 \ldots d\boldsymbol{r}_N \delta(\boldsymbol{r}_i - \boldsymbol{r}') \delta(\boldsymbol{r}_j - \boldsymbol{r}'') e^{-\beta \Sigma_{i>j} \varphi(\boldsymbol{r}_i - \boldsymbol{r}_j)} \\ &= \frac{N(N-1)}{2V^2} \int d\boldsymbol{r}' \; d\boldsymbol{r}'' \; \varphi(\boldsymbol{r}' - \boldsymbol{r}'') g(\boldsymbol{r}' - \boldsymbol{r}'').\end{aligned} \tag{4.71}$$

Here we note

$$\left\langle \delta(\boldsymbol{r}_i - \boldsymbol{r}') \delta(\boldsymbol{r}_j - \boldsymbol{r}'') \right\rangle = \frac{1}{Q_N} \int \cdots \int d\boldsymbol{r}_1 \ldots d\boldsymbol{r}_N \delta(\boldsymbol{r}_i - \boldsymbol{r}') \delta(\boldsymbol{r}_j - \boldsymbol{r}'') e^{-\beta \Sigma_{i>j} \varphi(\boldsymbol{r}_i - \boldsymbol{r}_j)}$$

and define

$$\begin{aligned} g(\boldsymbol{r}' - \boldsymbol{r}'') &= \frac{V^2}{N(N-1)} \sum_{i>j} \left\langle \delta(\boldsymbol{r}_i - \boldsymbol{r}') \delta(\boldsymbol{r}_j - \boldsymbol{r}'') \right\rangle \\ &= \frac{1}{nN} \sum_{i>j} \left\langle \delta(\boldsymbol{r}_{ij} - (\boldsymbol{r}' - \boldsymbol{r}'')) \right\rangle. \end{aligned} \tag{4.72}$$

$g(\boldsymbol{r}' - \boldsymbol{r}'')$ is called the **pair distribution function**, and is applicable to any one of $N(N-1)/2$ pairs. This is the probability of finding a particle at a position $\boldsymbol{r}'$ given another particle placed at $\boldsymbol{r}''$, relative to that for an ideal gas; it provides a measure of the spatial correlation between a pair of particles. In the absence of an external potential this function as well as the potential is isotropic, $\varphi(\boldsymbol{r}) = \varphi(r), g(\boldsymbol{r}) = g(r)$, so we derive the energy equation

$$\begin{aligned} \frac{\langle \Phi \rangle}{N} &= \frac{N-1}{2V^2} \int d(\boldsymbol{r}' - \boldsymbol{r}'') \; d\boldsymbol{r}'' \; \varphi(\boldsymbol{r}' - \boldsymbol{r}'') g(\boldsymbol{r}' - \boldsymbol{r}'') \\ &= 2\pi n \int_0^\infty dr \; r^2 \varphi(r) g(r), \end{aligned} \tag{4.73}$$

where r is the radial distance between the pair (Fig. 4.4). The average number of particles at a distance between r and $r + dr$ from a particle put at an origin $r = 0$ is

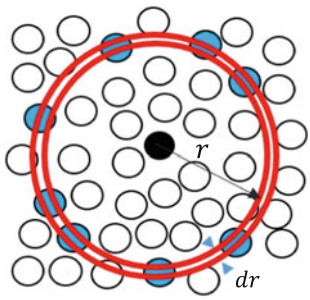

Fig. 4.4 The radial distribution function $g(r)$ *is* given in such a way that the average number of particles within a shell dr of the radius r form the central particle is $4\pi r^2 g(r) n dr$

$dN(r) = 4\pi r^2 g(r) n dr$, so $g(r)$ for this isotropic case is appropriately called the **radial distribution function**.

Next we consider the pressure. In the absence of an external potential, the pressure on the wall of the container is independent of its shape, so we will assume it is a cube of size L. The pressure is given by

$$p = k_B T \frac{\partial}{\partial V} \ln Z_N = k_B T \frac{\partial}{\partial V} \ln V^N Q_N . \tag{4.74}$$

To extract V-dependence, $V^N Q_N$ is rewritten as

$$V^N Q_N = L^{3N} \int \dots \int d\boldsymbol{r}_1^* \dots d\boldsymbol{r}_N^* \, e^{-\beta \sum_{i>j} \varphi\left(r_{ij}^* L\right)} \tag{4.75}$$

in terms of the dimensionless length, e.g, $\boldsymbol{r}_i^* = \boldsymbol{r}_i / L$, $r_{ij}^* = r_{ij}/L$, where $r_{ij} = \left|\boldsymbol{r}_i - \boldsymbol{r}_j\right|$. We take the derivative with respect to volume $V = L^3$,

$$p = k_B T \frac{\partial}{3L^2 \partial L} \ln L^{3N} Q_N, \tag{4.76}$$

which, by noting,

$$\frac{\partial}{\partial L} \ln L^{3N} Q_N = \frac{3N}{L} - \beta \sum_{i>j} \left\langle \frac{d\varphi\left(r_{ij}\right)}{dr_{ij}} \frac{r_{ij}}{L} \right\rangle , \tag{4.77}$$

is finally expressed as

$$p = n k_B T - \frac{2\pi}{3} n^2 \int_0^\infty dr r^3 \frac{d\varphi(r)}{dr} g(r), \tag{4.78}$$

which indicates the pair distribution $g(\boldsymbol{r})$, or the radial distribution $g(r)$, plays the central role in determining thermodynamic properties of simple fluids.

Furthermore, $g(\boldsymbol{r})$ (4.72) provides the most essential knowledge on the configurations of the interacting particles. When the separation r becomes much larger than the potential range, $g(r)$ approaches the ideal gas limit $g(r \to \infty) = 1$, which indicates that particles are not spatially correlated. In contrast, as a result of the hard core repulsion, $g(r \to 0) = 0$. In the low density limit of an interacting fluid, one can envision only a two particle interaction for $g(r)$, so that $g(r) = e^{-\beta\varphi(r)}$. Theoretical studies of dense fluids and liquids have centered around analytical and

computational investigations of the pair distribution function, and on developing a variety of approximation schemes.

For the Lenard-Jones potential at a liquid density, $g(r)$ shows damped oscillations around 1 (Fig. 4.5), with peaks at integer multiples of σ and troughs at half-integer multiples of σ; this feature is called the short-range order. **At a distance $r<\sigma$, $g(r)$ is zero, because the two particles cannot overlap due to harsh repulsion. At $r = \sigma_+$, a distance of close contact, $g(r)$ tends to peak; this means that two particles caged at contact is in the most probable and stable state, because surrounding particles of high density fluid constantly hitting and thereby the two particles do not have chance to be separated.** In contrast, $g(r)$ is at a minimum at $r \approx 1.5\,\sigma$, when two particles tend to be most unstable to background agitations and least likely to stay in contact. The probability increases again when $r \approx 2\,\sigma$, where two particles tends to be stable because they are separated by just distance for another particle to fit between them. The oscillation in probability persists with decaying amplitude. **$g(r)$ can be interpreted as the probability of finding another particle at a distance r from one, so we may write**

$$g(r) = e^{-\varphi_{eff}(r)/k_B T} \tag{4.79}$$

where $\varphi_{eff}(r)$ is the effective interaction potential energy between two particles. $\varphi_{eff}(r)$ is the reversible work needed to bring the two particles from the infinite distance to r. In dilute gas it is just $\varphi(r)$, the bare interaction between the two, because the presence of a third molecule is negligible. $\varphi_{eff}(r)$ is called **the potential of mean force**, which, at liquid density, oscillates between negative and positive values due to the influences of surrounding molecules, as explained above.

The pair distribution function is directly related (via Fourier transform) to the structure factor of the system. This is a central topic to study for the structure of matter in condensed phase, and can be determined experimentally using X-ray diffraction or neutron scattering. In the Chap. 9 we will study this in detail.

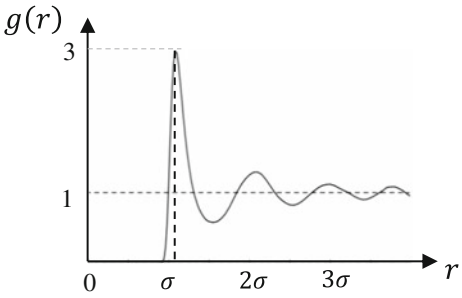

Fig. 4.5 Radial distribution function $g(r)$ of a dense Lennard-Jones fluid at $\pi n\sigma^3 \approx 0.8$ exhibits a short range order

4.4 Extension to Solutions: Coarse-Grained Descriptions

4.4.1 Solvent-Averaged Solute Particles

We have been considering a simple fluid of one–component particles moving in a *vacuum*. However, in biology we consider solute particles such as ions, and macromolecules immersed in water, which itself is a complex liquid that undergoes anisotropic molecular interactions. We remind ourselves that at equilibrium the momentum degrees of freedom of all the particles and molecules are usually separated and become irrelevant. Yet the statistical mechanics involves complex situations in which the configurations of all particles in mixtures (i.e., solutions), solute as well as solvent, must be considered, including all interactions.

A simple approach to bypass this formidable task is to **highlight the solute particles while treating the solvent as the continuous background whose degrees of freedom are averaged** (Fig. 4.6). To describe this formally, we write the total interaction energy as the sum, $\Phi_V\{\boldsymbol{r}_V\} + \Phi_U\{\boldsymbol{r}_U\} + \Phi_{VU}\{\boldsymbol{r}_V, \boldsymbol{r}_U\}$. Here Φ_V, Φ_U are the interaction energies among the solvent particles and solute particles respectively, and Φ_{VU} is the interaction energy between the solvent and solute particles with $\{\boldsymbol{r}_V\}, \{\boldsymbol{r}_U\}$ representing the solvent and solute particle positions. The configuration partition function is given by

$$Q = \iint d\{\boldsymbol{r}_V\} d\{\boldsymbol{r}_U\} \exp(-\beta[\Phi_V\{\boldsymbol{r}_V\} + \Phi_U\{\boldsymbol{r}_U\} + \Phi_{VU}\{\boldsymbol{r}_V, \boldsymbol{r}_U\}]) \tag{4.80}$$

where $d\{\boldsymbol{r}_V\} = d\boldsymbol{r}_v^1 \, d\boldsymbol{r}_v^2, \ldots, d\{\boldsymbol{r}_U\} = d\boldsymbol{r}_u^1 \, d\boldsymbol{r}_u^2 \ldots$. Then we can write

$$\begin{aligned} Q &= \int d\{\boldsymbol{r}_U\} \exp(-\beta[\Phi_U\{r\}]) \int d\{\boldsymbol{r}_V\} \exp(-\beta[\Phi_V\{\boldsymbol{r}_V\} + \Phi_{VU}\{\boldsymbol{r}_V, \boldsymbol{r}_U\}]) \\ &= \int d\{\boldsymbol{r}_U\} \exp\left(-\beta\left[\Phi_{\mathit{eff}}\{\boldsymbol{r}_U\}\right]\right) \end{aligned} \tag{4.81}$$

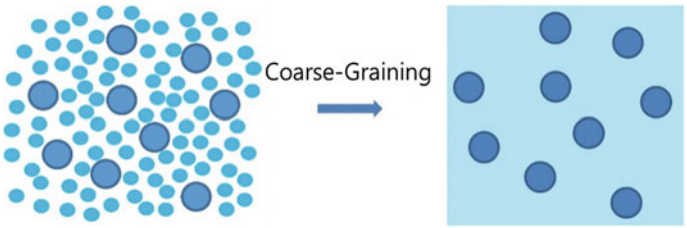

Fig. 4.6 Construction of a reduced description for a solution in terms of solutes' configurational degrees of freedom

where

$$\Phi_{eff}\{\boldsymbol{r}_U\} = \Phi_U\{\boldsymbol{r}_U\} + \Delta\Phi_U\{\boldsymbol{r}_U\} \tag{4.82}$$

with the solvent (averaged) part of the potential,

$$\Delta\Phi_U\{\boldsymbol{r}_U\} = -k_BT \ln \int d\{\boldsymbol{r}_V\} \exp(-\beta[\Phi_V\{\boldsymbol{r}_V\} + \Phi_{VU}\{\boldsymbol{r}_V, \boldsymbol{r}_U\}]). \tag{4.83}$$

In this formulation, the total partition function is integrated over the solvent degrees of freedom, with the remaining **solute particles left to interact with one another with the effective interaction $\Phi_{eff}\{\boldsymbol{r}_U\}$** (4.82), which is different from the bare interaction $\Phi_U\{\boldsymbol{r}_U\}$, by $\Delta\Phi_U\{\boldsymbol{r}_U\}$ (4.83). This solvent averaged effective potential, also called the potential of the mean force, is temperature-dependent. This **coarse-grained description** is typical in colloid science. As a simple example, the effective interaction between two ions of charges q_1 and q_2 at a distance r_{12} in water is given by the Coulomb interaction $\varphi(r_{12}) = q_1q_2/(4\pi\varepsilon_w r_{12})$, which is about 1/80 of the Coulomb interaction in vacuum, because the dielectric constant ε_w of water, a temperature-dependent quantity, is about 80 times that of the vacuum.

For N identical solute particles, the starting point for the statistical description is the partition function

$$Z_U = \frac{1}{N!v_0^N} \int \dots \int d\boldsymbol{r}_u^1 d\boldsymbol{r}_u^2 \dots \exp\left[-\beta\left(\Phi_{eff}\{\boldsymbol{r}_U\} + U\{\boldsymbol{r}_U\}\right)\right], \tag{4.84}$$

where $U\{\boldsymbol{r}_U\}$ is an effective external potential energy of the solute. The elementary volume v_0 is introduced to count the states; it is the volume allocated per particle so the entire volume V includes V/v_0 states per particle. In the absence of the potentials the partition function is

$$Z_U{}^0 = \frac{1}{N!v_0^N} \int \dots \int d\boldsymbol{r}_u^1 d\boldsymbol{r}_u^2 \cdots = \frac{1}{N!}\left(\frac{V}{v_0}\right)^N, \tag{4.85}$$

which gives the number of ways to place N identical, non-interacting particles in the volume V. The (4.85) differs from (4.9) in that $\lambda(T)^3$ is replaced by v_0. Because of this replacement, the partition function yields the thermodynamic quantities of an ideal solution that, with v_0 put to be independent of temperature, exclude contributions from the translational momentum degree of freedom, as shown below, by $E = 0$ in particular:

The Helmholtz free energy of the ideal solution:

$$F(T, V, N) = Nk_BT\left[\ln\left(\frac{Nv_0}{V}\right) - 1\right]. \tag{4.86}$$

The internal energy:

$$E = 0 \tag{4.87}$$

The osmotic pressure:

$$p = \frac{Nk_BT}{V} = nk_BT. \tag{4.88}$$

The entropy:

$$S = -Nk_B\left[\ln\left(\frac{Nv_0}{V}\right) - 1\right]. \tag{4.89}$$

The chemical potential:

$$\mu = k_BT\ \ln(nv_0). \tag{4.90}$$

In the presence of an external potential $u(\boldsymbol{r})$ per solute particle applied to the ideal solution, the intensive local thermodynamic variables are non-uniform and are given in terms of the solute concentration $n(\boldsymbol{r}) = n_0e^{-\beta u(\boldsymbol{r})}$:

The free energy density:

$$f(\boldsymbol{r}) = k_BTn(\boldsymbol{r})\{\ln(n(\boldsymbol{r})v_0) - 1\} + n(\boldsymbol{r})u(\boldsymbol{r}). \tag{4.91}$$

The local osmotic pressure:

$$p(\boldsymbol{r}) = n(\boldsymbol{r})k_BT. \tag{4.92}$$

The entropy density:

$$s(\boldsymbol{r}) = -k_Bn(\boldsymbol{r})[\ln\{n(\boldsymbol{r})v_0\} - 1]. \tag{4.93}$$

The local chemical potential:

$$\mu(\boldsymbol{r}) = u(\boldsymbol{r}) + k_BT\ \ln\{n(\boldsymbol{r})v_0\}. \tag{4.94}$$

With provisos that the effective potentials Φ_{eff} replace the bare potentials Φ, virtually all of the results obtained for interacting simple fluids are valid and usefully extended to interacting colloids, and more complex situations. For example, we will use the second virial expansion to model how polymer collapse transition depends on the solvent, in Chap. 10.

4.4.2 *Lattice model*

An analytically simple but useful variation of the coarse grained description given above is the lattice model. In the model the space continuum is discretized into $M = V/v_0$ lattice sites (Fig. 4.7). Each lattice site can be empty or occupied by a particle, so that this is a two-state model with each site characterized by occupation number $n_i = 0$ or 1. This model incorporates the excluded volume effects. Once we have M lattice sites onto which a particle can bind, we then have $M - 1$ sites for the next particle, so on. The number of ways of configuring N particles in ***M* distinct lattice sites** is $M(M-1)\ldots(M-N-1)$. With the factor $1/N!$ multiplied due to indistinguishability of N particles, the partition function is given as

$$Z_U = \frac{1}{N!} M(M-1)\ldots(M-N-1), \tag{4.95}$$

which is equal to

$$Z_U = \frac{M!}{N!\,(M-N)!}. \tag{4.96}$$

This is the same as the factor which we already considered when two state model was first introduced in chap. 3. If $N \ll M, M!/(M-N)! \approx M^N = (V/v_0)^N$ and Z_U is reduced to Z_U^0 (4.85), the partition function of non-interacting particles.

P4.6 *Show that the equation of state of the lattice gas is given as:*

$$\frac{pV}{Nk_BT} = -\frac{1}{\theta}\ln(1-\theta).$$

where $0 \leq \theta = N/M \leq 1$. *The chemical potential is given by*

$$\mu = k_BT\,\ln\left(\frac{\theta}{1-\theta}\right),$$

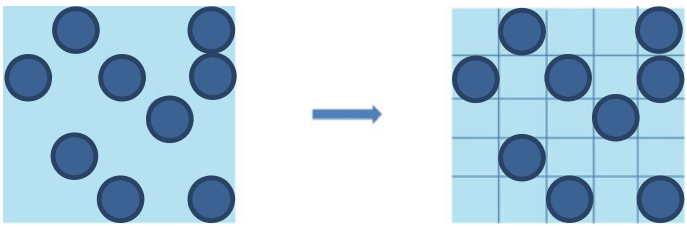

Fig. 4.7 From the solute particles moving in interactions to the lattice model, where the solute coordinates are described by the occupation number at each lattice

Both p and μ become the infinity in the limit of $\theta \to 1$ *due to the excluded volume effects and recover* $p = nk_BT, \mu = k_BT \ln(nv_0)$ *in the low concentration limit. What is the second virial coefficient?*

In addition to the excluded volume effect we can consider that a particle can bind with an energy $-\epsilon$ to a site. This leads to the famous Langmuir model of adsorption in one and two-dimensional lattices, such as protein binding on DNA and ligand binding on a surface. In this case the canonical partition function is

$$Z_U = \frac{M!}{N!\,(M-N)!} e^{\beta N\epsilon}. \tag{4.97}$$

P4.7 *Suppose that ligands (which imparts an osmotic pressure p in a solution) binds on a polymer with a binding energy* ϵ*. What is the ligand concentration on the polymer?*
(Hint: Equate $\mu = -\epsilon + k_BT \ln(\theta/(1-\theta))$ *of a bound ligand with* $\mu = k_BT \ln(pv_0/k_BT)$ *of an unbound ligand in the bulk.)*

Furthermore, the N adsorbed particles in general interact with one another with a short-range interaction potential. With the binding energy ϵ now excluded, the model can be studied to understand condensation and aggregation of particles due to mutual interactions in various dimensions. A rich variety of biologically interesting problems of adsorption, transitions, and self-assembly, will be studied using this lattice model in Chaps. 7 and 8.

Further Reading and References

J.P. Hansen, I.R. McDonald, *Theory of Simple Liquids* (Academic Press, 1986)
J.L. Barrat, J.P. Hansen, *Basic Concepts for Simple and Complex Liquids* (Cambridge University Press, 2003)
V.I. Kalikmanov, *Statistical Mechanics of Fluids, Basic Concepts and Applications* (Springer, 2001)
A.P. Hughes, U. Thiele, A.J. Archer, An introduction to inhomogeneous liquids, density functional theory, and the wetting transition. Am. J. Phys. **82**, 1119 (2014)
W. Möbius et al., Toward a unified physical model of nucleosome patterns flanking transcription start sites Proc. Natl. Acad. Sci. U.S.A. **110**(14), 5719–5724 (2013)

Chapter 5
Coarse-Grained Description: Mesoscopic States, Effective Hamiltonian and Free Energy Functions

Biological components at mesoscales, such as cells, membranes, and biopolymers are complex systems composed of many constituents of diverse kind that interact. The challenge is to use the first principles of physics to describe the phenomena that emerge in such systems as a result of these interactions and correlations, without losing salient features of the phenomena. To meet this difficult challenge, we must fundamentally shift the paradigm for physical description of complex systems, **from one of taking photos of every detail to one of drawing cartoons of relevant key features**. In this short chapter, we discuss a way to build coarse-grained descriptions of the relevant physics from fine-grained descriptions of the underlying microscopic degrees of freedom for equilibrium systems.

5.1 Mesoscopic Degrees of Freedom, Effective Hamiltonian, and Free Energy

The macroscopic behavior of an equilibrium at a fixed temperature T is determined formally by the Hamiltonian, through the relation (3.32) supplemented by (3.35):

$$e^{-\beta F} = \sum_{\mathcal{M}} e^{-\beta \mathcal{H}\{\mathcal{M}\}}, \tag{5.1}$$

where F is the Helmholtz free energy, $\sum_{\mathcal{M}}(\cdot)$ denotes the summation over all microscopic degrees of freedom represented by $\mathcal{M}$; if $\mathcal{M}$ is continuous, the summation signifies the integration, e.g. for a classical particle system the integration over the phase space spanned by all the particles. For illustrative purpose we consider a combined system (solution) of solute and solvent at T, including the solution of polymer chains where the monomers are linearly connected solute particles. The microscopic states are given by the phase space of all solute molecules and solvent molecules, and, if required, the microscopic quantum states that

W. Sung, *Statistical Physics for Biological Matter*, Graduate Texts in Physics,
https://doi.org/10.1007/978-94-024-1584-1_5

underlie the molecules. Considering the appreciable complexity seen even in the statistical mechanics of simple fluids (Chap. 4), an attempt to conduct the standard scheme using the formalism, (5.1) would be very costly. Even if we could do so the results can obscure the most salient and interesting features of the system.

We may wisely abandon the full microscopic description and choose a coarse-grained description in terms of **the relevant degrees of freedom, represented by $\boldsymbol{Q}$**, in terms of which we have

$$e^{-\beta F} = \sum_{\mathcal{Q}} e^{-\beta \mathcal{F}\{\mathcal{Q}\}}. \tag{5.2}$$

The $\mathcal{Q}'$s represent the degrees of freedom which are of primary interest for study. It can be chosen depending on the scale of the description, that is, a level of coarse graining one chooses. **$\mathcal{F}\{\boldsymbol{Q}\}$ is the effective Hamiltonian for the reduced variables $\boldsymbol{Q}$**. For solutions, $\mathcal{Q}$ can be chosen as the coordinates of the solute particle coordinates $\mathcal{Q} = \{\boldsymbol{r}_U\}$, as discussed in Chap. 4 (Fig. 4.6). For this case, **the effective Hamiltonian** $\mathcal{F}\{\mathcal{Q}\}$ is the effective interaction $\Phi_{eff}\{\mathcal{Q}\}$ between the solute particles. Formally one can identify the effective Hamiltonian by noting that

$$\sum_{\mathcal{M}} e^{-\beta \mathcal{H}\{\mathcal{M}\}} = \sum_{\mathcal{Q}} \sum_{\mathcal{M}/\mathcal{Q}} e^{-\beta \mathcal{H}\{\mathcal{M}\}} = \sum_{\mathcal{Q}} e^{-\beta \mathcal{F}\{\mathcal{Q}\}}, \tag{5.3}$$

where $\sum_{\mathcal{M}/\mathcal{Q}}(\cdot)$ is the partial sum (integration) over the microstates $\mathcal{M}$ with the mesostate $\mathcal{Q}$ fixed. From the relation (5.3) we identify

$$e^{-\beta \mathcal{F}\{\mathcal{Q}\}} = \sum_{\mathcal{M}/\mathcal{Q}} e^{-\beta \mathcal{H}\{\mathcal{M}\}}. \tag{5.4}$$

For the solutions, the partial sum means integrating (averaging) only over solvent degrees of freedom with the solute coordinates given as fixed.

In view of the similarity between (5.1) and (5.4), we call the effective Hamiltonian $\mathcal{F}\{\mathcal{Q}\}$ alternatively as **the free energy *function* of $\boldsymbol{Q}$**. Equation (5.4) implies that **$\mathcal{F}\{\boldsymbol{Q}\}$ can depend on temperature, because of the microscopic fluctuations that underlie $\boldsymbol{Q}$, unlike the microscopic Hamiltonian $\mathcal{H}\{\mathcal{M}\}$**. The probability distribution of $\mathcal{Q}$ is given by (See Eq. 5.4)

$$P(\mathcal{Q}) = \frac{e^{-\beta \mathcal{F}\{\mathcal{Q}\}}}{\sum_{\mathcal{Q}} e^{-\beta \mathcal{F}\{\mathcal{Q}\}}}. \tag{5.5}$$

The most probable value of $\mathcal{Q}$ emerges where the free energy function $\mathcal{F}(\mathcal{Q})$ is the minimum; this is the thermodynamic variational principle that we introduced in Chap. 2: In an approach to equilibrium, the degrees of freedom $\mathcal{Q}$, assisted by the fluctuations, organize themselves to achieve this most probable state. As the entropy from the thermal fluctuations become very significant in competition

with the internal energy from the interactions, this organization are realized as a host of thermal transitions, which we will study often in the first part of this book.

Denoting such most probable $\mathcal{Q}$ as $\mathcal{Q}^*$, we rewrite (5.2) as

$$e^{-\beta F} = \sum_{\mathcal{Q}} e^{-\beta \mathcal{F}\{\mathcal{Q}\}} = C e^{-\beta \mathcal{F}(\mathcal{Q}^*)}, \tag{5.6}$$

where C is a certain constant that is characteristic of the distribution width (fluctuation). Thus we find

$$F \approx \mathcal{F}(\mathcal{Q}^*) + constant. \tag{5.7}$$

The equality $F \approx \mathcal{F}(\mathcal{Q}^*)$ is called a mean field approximation because it neglects the fluctuation around the mean $\mathcal{Q}^*$. The validity of F depends on the sharpness of $P(\mathcal{Q})$.

5.2 Phenomenological Methods of Coarse-Graining

A task of modelling biological systems thus starts with identifying the primary degrees of freedom $\mathcal{Q}$ and the associated effective Hamiltonian or free energy function $\mathcal{F}(\mathcal{Q})$. For a solution of many solute particles with nontrivial interactions $\Phi_{eff}\{\mathcal{Q}\}$ (4.82), $\mathcal{Q}$ is $\{\boldsymbol{r}_U\}$, the configurations of all the solute particles. The evaluation of the free energy using (5.2) with $\mathcal{F}\{\mathcal{Q}\} = \Phi_{eff}\{\mathcal{Q}\}$, however, is very difficult analytically and quite costly numerically. As introduced earlier, a further simplification of the coarse-grained description is possible by adopting the lattice model. In the model the volume of the solution is divided into cells or sites, each of which contains a solute particle or none. As was shown in Chap. 4, the mesoscopic state is then represented by the occupation number in each site, $\mathcal{Q} = \{n_i\}(i = 1, 2\ldots)$, where n_i is either 0 or 1. With the interactions between two particles in the nearest neighborhood included as contact attraction and hard-core exclusion, the lattice model can deal with a great variety of problems with relative simplicity.

For analysis of a long-chain polymer, we may use a lattice model in which particles in the cells are interconnected (Fig. 5.1a). We may conduct further coarse-graining, and regard the polymer as a semi-flexible, curved rod, called a worm-like chain (Fig. 5.1b). Instead of a configuration of particles, $\mathcal{Q}$ is now a continuous function $\{\boldsymbol{r}(s)\}$, which represents the position of the chain along the contour distance s. In this case of a semi-flexible chain there is an orientational correlation between neighboring chain segments. If the polymer chain is very long, it can be represented as a flexible string of beads, each of which comprises sufficient

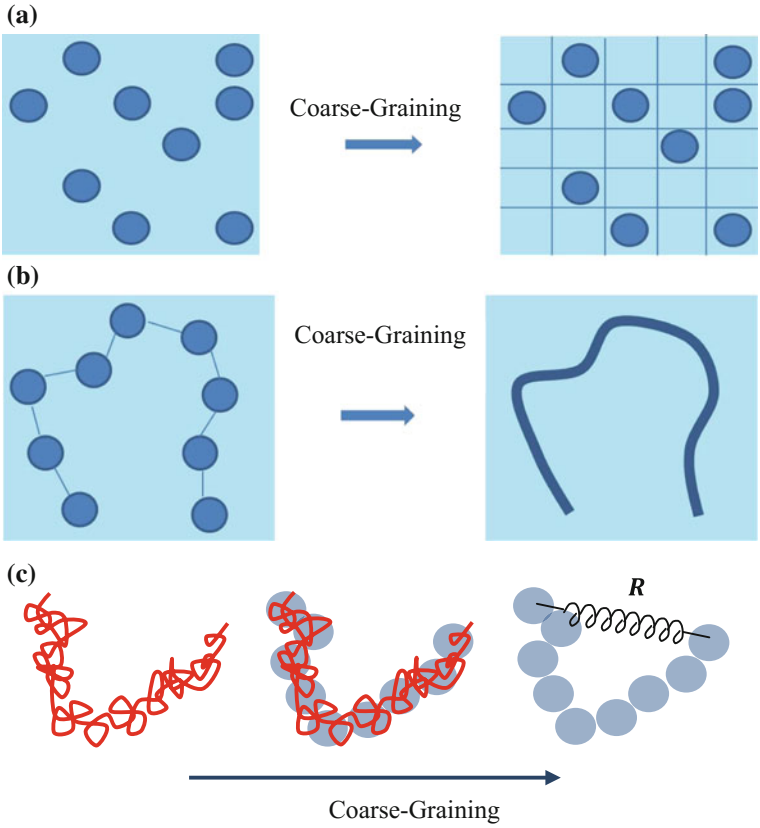

Fig. 5.1 Schematic diagrams of coarse graining for the particles in a solution, **a** coarse-graining into lattice model, **b** a polymer coarse-grained into a semi-flexible string, **c** a flexible polymer coarse-grained into the linearly connected beads and to an entropic spring extended by a distance R

number of monomers such that there is no correlation between the beads; this process gives rise to a flexible chain with a new coarse-grained continuous curve $\{\boldsymbol{r}_f(s)\}$. The relevant level of the description is often guided by measurement. An example is the end-to-end distance of the polymer to describe its conformation $\mathcal{Q} = \boldsymbol{R}$ (Fig. 5.1c).

While the primary degree of freedom $\boldsymbol{Q}$, dictated by the measurement and observation to make, can be easily identified, it is often formidable to derive $\mathcal{F}(\boldsymbol{Q})$ from (5.4), in general. In many cases $\mathcal{F}(\boldsymbol{Q})$ can be adopted directly from a macroscopic, phenomenological energy, or the probability of $\boldsymbol{Q}$. Because the end-end distance $\boldsymbol{R}$ of a long flexible chain is distributed in Gaussian, the associated free energy $\mathcal{F}(\boldsymbol{R})$ will be harmonic, as shown in Chap. 10.

The method of coarse-graining in terms of $\mathcal{Q}$ can be regarded as an art of cartoon-drawing, which captures the salient and emergent behaviors. But it is constrained to yield quantitative agreement with experimental measurements.

Despite their complex natures, **many biological phenomena can be described effectively in terms of phenomenologically observed states that emerge beyond the complexity of the underlying microstates**. In many cases of the mesocopic level biological systems we consider throughout this book, we will use this method. Two-states we introduced as biological microstates in Chap. 3 exemplify such mesoscopic states. **The definition of 'mesoscopic' depends on the perspective. If the perspective is macroscopic, then these 'meso' states are relatively microscopic. Throughout this book, thus, either one of the notations $\mathcal{M}$ and Q for the state, and, correspondingly, one of $\mathcal{H}\{\mathcal{M}\}$ and $\mathcal{F}(Q)$ for the Hamiltonian will be adopted, depending on the perspective**.

Chapter 6
Water and Biologically-Relevant Interactions

Water is abundant and ubiquitous in our body and on earth. Despite its critical importance in life, and compared with the spectacular development of modern physics, fundamental understanding of its physics is surprisingly poor. In principle statistical mechanics is expected to explain its physical properties in a quantitative detail, but is quite difficult to implement due to the relative complexity of water molecules and the non-isotropic interactions among them. The statistical mechanics study for water is rare and limited (Dill et al. 2005; Stanley et al. 2002). Instead of the statistical mechanics we give a semi-quantitative sketch of basic thermal properties of water and the hydrogen bonding that underlies the unique characteristics of water.

We also introduce the biologically relevant interactions between objects in water. They are hydrophilic and hydrophobic interactions, the electrostatic interaction among charges and dipoles, and Van der Waals interactions. In many cases, the electrostatic interactions turn out to be weak with the strength comparable to the thermal energy k_BT and much less upon thermalization, due to the screening effects of water's high dielectric constant and the ion concentration. **These weak interactions facilitate conformational changes of biological soft matter such as polymers and membranes at body temperature**.

6.1 Thermodynamic Properties of Water

Liquid water has many properties that are distinct from other liquids. One of water's most well-known anomalies is that it expands when cooled, contrary to ordinary liquids. At atmospheric pressure, when ice melts to form liquid water at 0 °C, the density increases discontinuously, and then the liquid density continues to increase until it reaches a maximum at 4 °C (Fig. 6.1a). This behavior leads to a well-known consequence that a lake freezes top-down from the surface, on which

W. Sung, *Statistical Physics for Biological Matter*, Graduate Texts in Physics,
https://doi.org/10.1007/978-94-024-1584-1_6

the ice floats, whereas the bottom of the lake remains at 4 °C. Children skate on the icy surface while fishes swim over the watery bottom.

The phase diagram (Fig. 6.1b) shows how the ice, vapor, and water liquid phases exist as functions of temperature T and pressure p. The curved solid lines indicate coexistence of the different phases at equilibrium. They meet at the triple point (about 0.01 °C and 0.008 atmospheric pressure (atm)), where the three phases coexist. The coexistence line of liquid and vapor terminates at the critical point ($T = 378$ K, $p = 218$ atm). Near this point the interfaces of coexisting liquid and vapor become unstable and fluctuate widely, showing a variety of divergent response behaviors called the critical phenomena. The critical phenomena that occur in diverse matter have been one of central problems in modern statistical physics, but are beyond the scope of this book.

In Fig. 6.1b each of phase-coexistence (solid) lines is given by the Clausius-Clapeyron equation

$$\frac{dp}{dT} = \frac{\Delta s}{\Delta v}, \tag{6.1}$$

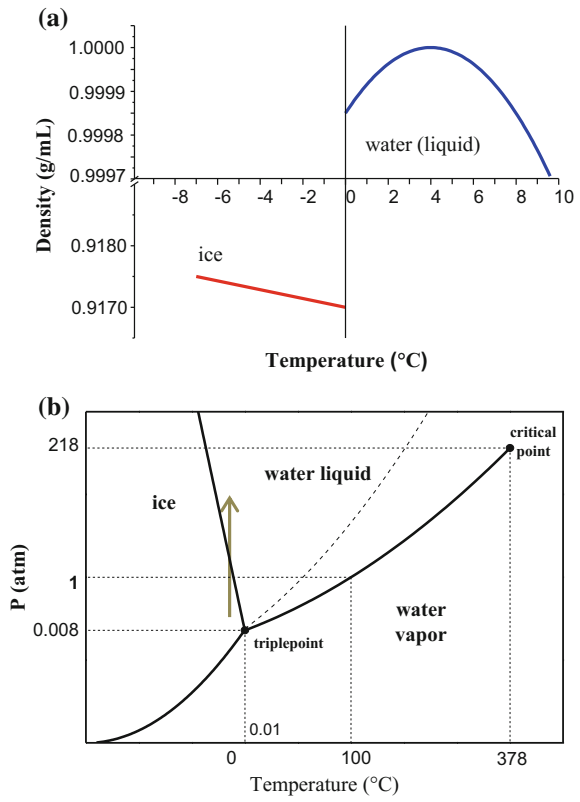

Fig. 6.1 The phase-diagrams of water. **a** The density of water increases discontinuously as it undergoes the phase transition from solid (ice) phase to liquid phase. In the liquid phase the density is maximum at 4 °C. **b** Pressure in atmospheric pressure units (atm) versus temperature in Celsius. The solid lines represent the coexistence between two different phases of water. The dashed curve is the phase coexistence between ordinary liquids and their vapors

where $\Delta s = s_\beta - s_\alpha$ and $\Delta v = v_\beta - v_\alpha$ are respectively the changes in entropy ($s = S/N$) and volume ($v = V/N = 1/n$) per particle, which occurs across the line (phase boundary) between the phases α and β. The equation is derived by imposing the chemical potential equality $\mu_\alpha = \mu_\beta$ between two phases. In the representation where T and p are the independent variables, the differential change in the chemical potential is given by $d\mu(T,p) = -sdT + vdp$, (2.25), which is balanced along the phase boundary: $-s_\alpha dT + v_\alpha dp = -s_\beta dT + v_\beta dp$. This leads to (6.1).

Across the water-ice (liquid-solid) phase boundary, the entropy change $\Delta s = s_S - s_L$ is negative because the solid is more ordered than the liquid. But the volume difference $\Delta v = v_S - v_L$ is peculiarly positive as mentioned earlier. Therefore, the slope dp/dT of the coexistence line is negative, whereas for most substances it is positive. The line also shows that, when p is increased at 1 atm and a temperature below 0 °C, as indicated by the arrow in Fig. 6.1, the ice melts (The ice, pressurized by skater blades, melts). This is why you can skate on ice, but on no other solids.

Lastly focus on the phase boundary between water and vapor. Because $v_L \ll v_G$, and the vapor pressure is given by $v_G \approx (k_B T)/p$, (6.1) can be written as

$$\frac{dp}{dT} \approx \frac{p l_{GL}}{k_B T^2}, \tag{6.2}$$

where $l_{GL} = T(s_G - s_L)$ is latent heat of vaporization per molecule. Assuming l_{GL} is nearly constant, integrating (6.2) yields the equation for the phase coexistence line

$$p \approx p_0 \exp\left\{-\frac{l_{GL}}{k_B T}\right\} = p_0 \exp\left\{-\frac{L_{GL}}{RT}\right\}, \tag{6.3}$$

where p_0 is a constant. Equation (6.3) is in quite a good agreement with the experimental data on the vapor pressure of water for a wide range of temperature away from the critical point. The fact that water's heat of vaporization ($L_{GL} = 40.7$ kJ/mole), and surface tension (~ 30 dyne/cm) as well, are distinctively high means that water is a most cohesive liquid.

Liquid water is among the liquids of highest heat capacities, having the specific heat 1cal/(g·K) at 15 °C. Perhaps the most significant of water's unusual properties is its dielectric constant $\varepsilon_w/\varepsilon_0 = 78.5$, where ε_w is the electrical permeability of water and ε_0 is that of vacuum. The water's dielectric constant is almost highest among those of all liquids; because of this, our cells live in water. The high dielectric constant weakens the Coulomb interaction between two ions in solution and charged residues in biopolymers and membranes, to the level of thermal energy $k_B T$ which, at room temperature is $\approx 1/40$ eV, or 0.6 kcal/mol $\approx$ 2.5 kJ/mol, or 4.1 pN · nm.

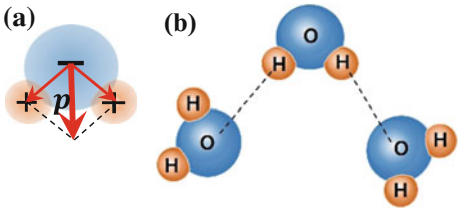

Fig. 6.2 **a** The dipole moment of a water molecule. **b** Hydrogen bonding (dashed line) between water molecules

6.2 The Interactions in Water

6.2.1 Hydrogen Bonding and Hydrophilic/Hydrophobic Interaction

The remarkable properties of water discussed above derive from its unique molecular structure, and to hydrogen bonding (HB) among water molecules. In a water molecule an oxygen atom is covalent-bonded with two hydrogen atoms by sharing electrons. But the oxygen atom has much greater affinity for electrons than the hydrogen atoms, making the molecule polar with a high dipole moment (Fig. 6.2a). HB is the electrostatic attraction between hydrogen containing polar molecules in which electropositive hydrogen in one molecule is attracted to an electronegative atom such as oxygen in another molecule nearby (Fig. 6.2b).

The HB in water has strength of a few kJ/mole, which is much weaker than covalent or ionic bonds, but much stronger than the generic (non-HB) bonds between small molecules. This is the reason why the heat of vaporization, boiling point, and surface tension are relatively high in water. Furthermore, in water, HB forms a network with large orientation fluctuations of the molecules that can be correlated over a long range. The large fluctuations and long-range correlation hint at water's high response functions (susceptibilities) such as high dielectric constant and high heat capacity, somewhat likened to the phenomena near the critical point. HBs occur in both inorganic molecules and biopolymers like DNA and proteins.

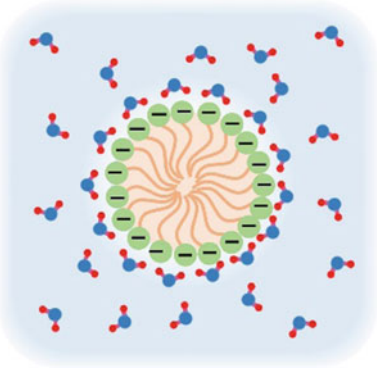

Fig. 6.3 The hydrophilic interaction. The negatively charged polar heads of lipid molecules in a micelle attracts water molecules

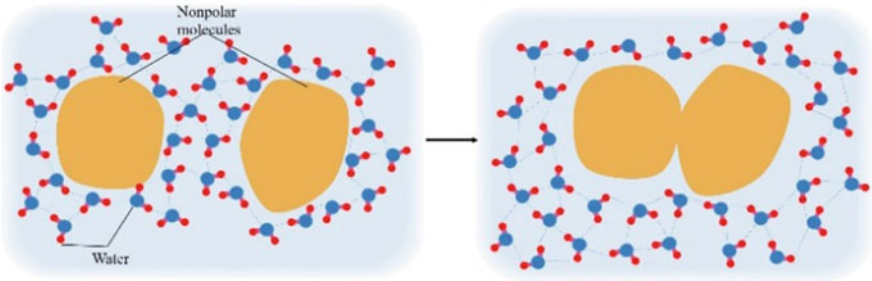

Fig. 6.4 Hydrophobic interaction. Two nonpolar objects, upon approaching to contact, liberate water molecules between them into the bulk, where they have more entropy and hydrogen bonding. Nature favors this and drives the contact, namely, hydrophobic attraction

The attractive interaction between water and other polar or charged objects is called **hydrophilic interaction**. For example, charged parts of an object are attracted to the oppositely charged parts of the water dipoles (Fig. 6.3). This is an important reason why water is such a good solvent.

Hydrophobic interaction, in contrast, is an indirect interaction between nonpolar objects in water. The association of water molecules on nonpolar objects is entropically unfavorable because of restriction of the water molecule orientation on the interface. When two nonpolar objects come in contact, there is a strong gain of entropy due to reduction of the entropically unfavorable intervening region, from which the water molecules are released; this process eventually induces aggregation of the nonpolar objects (Fig. 6.4). The phase separation of fat in water is a good example of this particular interaction. The hydrophobic interactions in part enable the folding of proteins, because it allows the protein to decrease the surface area in contact with water. It also induces phospholipids to **self-assemble into bilayer membranes**.

6.2.2 The Coulomb Interaction

The water medium affects fundamentally the interaction between two ions. Phenomenologically the interaction between two ions of charges q_1 and q_2 separated by a distance r_{12} is just the Coulomb interaction,

$$\varphi_{12} = \frac{q_1 q_2}{4\pi\varepsilon_w r_{12}}, \tag{6.4}$$

where ε_w is the electric permeability of water. As mentioned in Sect. 4.4, this effective interaction is formally obtained by integrating (averaging) over all the

degrees of freedom of the water molecules surrounding the two ions, with the distance between the two ions r_{12} given as fixed. The effect of the water medium, treated as a continuum, is incorporated by ε_w, which depends on T.

Equation (6.4) is based on a coarse continuum picture. While it neglects the microscopic details involving the water molecules at short distance, it often gives a reasonable understanding when the distance r longer than the small molecule scale. At such separation the electrostatic interaction energy can be smaller than the thermal energy. If two elementary charges e are separated by ~ 1 nm in a vacuum, they would have the Coulomb energy in the order of 1 eV, but in water its high dielectric constant $\varepsilon_w/\varepsilon_0 = 78.5$ can reduce the Coulomb energy below the thermal energy which is $\boldsymbol{k_BT \approx 1/40}$ **eV** at room temperature. A convenient scale to assess dominance of the thermal energy is

$$l_B = \frac{e^2}{4\pi\varepsilon k_B T}, \tag{6.5}$$

called the **Bjerrum length**, above which the elementary Coulomb interaction energy is less than k_BT; in water at 25 °C it is 7.1 Å.

Consider a single ion of charge q in water. Assuming that the ion is a sphere of radius a, the work necessary to charge the sphere from zero to q in water continuum is

$$\varphi_b = \int_0^q \frac{q'dq'}{4\pi\varepsilon_w a} = \frac{q^2}{8\pi\varepsilon_w a}. \tag{6.6}$$

This is called **the Born energy** of the ion in water, and is also the energy associated with the field of the ion itself, called the self-energy. **The solvation or hydration energy** of an ion in water is the reversible work necessary to bring it from vacuum to water,

$$\Delta\varphi_s = \frac{q^2}{8\pi a}\left(\frac{1}{\varepsilon_w} - \frac{1}{\varepsilon_0}\right) \approx -\frac{q^2}{8\pi\varepsilon_0 a}, \tag{6.7}$$

which is negative, and has much larger magnitude than the Born energy. This large negative energy means that ions can be easily solvated in water. Indeed, **thanks to high dielectric constant, water is a good solvent to ions and many biological components that carry charges**. Now we ask, can this ion in water move to the inside a medium, say a membrane, of the electric permeability ε_m ($\approx 2\varepsilon_0$). The process costs the energy change

$$\Delta\varphi_m = \frac{q^2}{8\pi a}\left(\frac{1}{\varepsilon_m} - \frac{1}{\varepsilon_w}\right) \approx \frac{q^2}{8\pi a \varepsilon_m} \tag{6.8}$$

because $\varepsilon_w \gg \varepsilon_m$. The above is about $28k_BT$ for $a = 0.5$ nm, so the relative probability that the ion can get into the membrane is $K = \exp[-\beta\Delta\varphi_m] \sim \mathrm{e}^{-28}$, which is virtually zero!

In the spirit of the coarse-grained description introduced in Chaps. 4 and 5, the phenomenological electrostatic energies (6.6) and (6.4) can be regarded as the free energy associated with an isolated ion and with two interacting ions in water respectively, recast as $\mathcal{F}_1 = q^2/(8\pi\varepsilon_w a)$ and $\mathcal{F}_{12}(r) = q_1 q_2/(4\pi\varepsilon_w r)$. Recall that the result of integrating over the underlying degrees of freedom of the associated water molecules is incorporated into the electrical permeability ε_w, which is a function of T. Because the two free energy expressions are both proportional to T and $1/\varepsilon_w$, the associated entropy is given by

$$S = -\frac{\partial \mathcal{F}}{\partial T} = \mathcal{F}\frac{1}{\varepsilon_w}\frac{\partial \varepsilon_w}{\partial T}. \tag{6.9}$$

From experiment we know (Israelachvili 2000)

$$\frac{T}{\varepsilon_w}\frac{\partial \varepsilon_w}{\partial T} \approx -1.36 \; at \; T = 25\ ^\circ\mathrm{C}, \tag{6.10}$$

so $S \approx -1.36\,\mathcal{F}/T$. For the Born energy, the entropy is negative, a result that can be attributed to water molecules surrounding the charge: when an ion is placed in water, the entropy of the solution decreases because charge–dipole interaction causes the water to solvate around the ion and thereby to suffer a reduction of configuration freedom compared with that without the ion. The negativity of the entropy change holds also for the Coulomb repulsion between the two charges. This may be attributed to an enhanced ordering of the water molecules solvated to the charges upon their approach, within the validity of the continuum approximation.

P6.1 *What is the internal energy change when two ions Na and Cl are brought to the NaCl radius $a = 0.28$ nm from infinity in water? For the two ions brought to the distance a, find that the internal energy changes are negative and the entropy changes are positive. Give physical reasons.*

Virtually all interactions between molecules are electrostatic in origin. A polar molecule has a net dipole moment due to permanent separation of charges of opposite sign and equal magnitude. The dipole moment is defined by $\boldsymbol{p} = q_d\boldsymbol{l}$, where $\boldsymbol{l}$ is the displacement vector pointing from the negative charge $(-q_d)$ to the positive charge (q_d). In a small molecule, typically q_d is about elementary charge e and d is 1 Å in order of magnitude. In Fig. 6.2a, the HOH bond is bent at angle 109.5° so its net dipole vector of an H_2O is obtained as an addition of two HO dipole vectors, with magnitude $p = 1.85$ D (1 D (debye) $= (1/3)10^{-29}$ C m) (Fig. 6.2a). There are a

variety of electrostatic interactions among charges, dipoles, even induced diploes in biological solutions. Below we estimate a various types of electrostatic interaction energies in water. Mostly we will consider the case of interaction distance r much longer than the Bjerrum length $l_B = 0.7$ nm where the interaction energies is much smaller than the thermal energy; this case is both analytically tractable and also consistent with the approximation of water as a dielectric continuum.

6.2.3 Ion-Dipole Interaction

Consider an ion of charge q and a molecule of permanent dipole moment $\boldsymbol{p}$ where the charges q_d and $-q_d$ are separated by distance $\boldsymbol{l}$ (Fig. 6.5). The energy of electrostatic interaction between the ion and the dipole at a distance r is

$$\begin{aligned}\varphi_{id}(r,\Omega) &= \frac{q_d q}{4\pi\varepsilon_w|\boldsymbol{r}+\boldsymbol{l}/2|} - \frac{q_d q}{4\pi\varepsilon_w|\boldsymbol{r}-\boldsymbol{l}/2|} \approx q_d\boldsymbol{l}\cdot\nabla\frac{q}{4\pi\varepsilon_w r} \\ &= -\boldsymbol{p}\cdot\boldsymbol{E} = -pE\cos\theta,\end{aligned} \tag{6.11}$$

where $E = q/(4\pi\varepsilon_w r^2)$ is the electric field from the ion, θ is the polar angle that the dipole vector $\boldsymbol{p} = q_d\boldsymbol{l}$ makes with the field direction (Fig. 6.5).

The dipole is undergoing thermal fluctuations (rotation). The induced polarization along the field observed at equilibrium is the thermal average over the orientation,

$$\begin{aligned}P_d = p\langle\cos\theta\rangle &= p\frac{\int d\Omega\cos\theta\, e^{-\beta\varphi_{id}(r,\Omega)}}{\int d\Omega\, e^{-\beta\varphi_{id}(r,\Omega)}} = p\frac{\int d\Omega\cos\theta\, e^{\beta pE\cos\theta}}{\int d\Omega\, e^{\beta pE\cos\theta}} \\ &= p\frac{\partial}{\partial(\beta pE)}\ln Z_{id} = p[\coth(\beta pE) - \frac{1}{\beta pE}] \equiv p\mathcal{L}(\beta pE),\end{aligned} \tag{6.12}$$

where $d\Omega = d(\cos\theta)d\phi$ is the solid angle element, $Z_{id} = \int d\Omega\, e^{\beta pE\cos\theta} = (4\pi\sinh\beta pE)/\beta pE$, and $\mathcal{L}(x)$ is the Langevin's function earlier seen in polymer extension problem (3.57).

Now we note that $\beta pE = pq/(4\pi\varepsilon_w r^2 k_B T) \sim l l_B/r^2$ where the l_B is about 7 Å at room temperature. If, for example, the dipole is due to a small polar molecule like a water molecule, the charge separation length l is also a length in the order of 1 Å, so, at a distance r over the nanoscale, $\beta pE(r) \ll 1$. We will consider this case throughout.

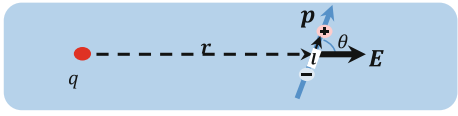

Fig. 6.5 A dipole moment $\boldsymbol{p}$ interacts with a charge q, making a polar angle θ with the direction of the electric field $\boldsymbol{E}$

Then, with $\mathcal{L}(\beta pE) \approx \beta pE/3$, (6.12) is reduced to

$$P_d = \frac{p^2 E}{3k_B T} = \alpha_d E, \tag{6.13}$$

where $\alpha_d = p^2/(3k_B T)$ is identified as the **induced polarizability** of a single dipole. This indicates that the electric susceptibility of a dielectric varies as the square of the net dipole moment. If a constituent polar molecule were independent of each other, the electric susceptibility would be given as sum of the square of its dipole moment. However, in liquid water, the electric permeability is much higher than given by this estimate, because of the long-range correlation in the HB network mentioned earlier.

The angle-averaged interaction energy between the dipole and ion with r fixed is

$$\begin{aligned} \varphi_{id}(r) &= \langle \varphi_{id}(r, \Omega) \rangle = -pE \langle \cos\theta \rangle \\ &= -\frac{(pE)^2}{3k_B T} = -\frac{p^2 q^2}{3(4\pi\varepsilon_w r^2)^2 k_B T}. \end{aligned} \tag{6.14}$$

Remarkably, $\varphi_{id}(r)$ varies as $-T^{-1}\varepsilon_w{}^{-2} r^{-4}$; compared with $\varphi_{id}(r, \Omega)$, (6.11), $\varphi_{id}(r)$ is more short-ranged, and also much weaker by the factor $\beta pE(r) \ll 1$. It can also be estimated as $\varphi_{id}(r) \sim (l l_B/r^2)^2 k_B T$.

What are the free energy and entropy changes that are induced when the dipole is brought to the ion at a distance r from infinity? In the coarse-grained description in which r is the only relevant degree of freedom, $\mathcal{Q} = r$, the degrees of freedom $\mathcal{M}$ except r are to be integrated over. The solvent degree of freedom is already incorporated partly via the temperature-dependent dielectric constant, so the remaining degree of freedom is the angle Ω over which an integration is done to yield the free energy:

$$e^{-\beta \mathcal{F}(\mathcal{Q})} = \sum_{\mathcal{M}/\mathcal{Q}} e^{-\beta \mathcal{H}(\mathcal{M})} = \int d\Omega \, e^{-\beta \varphi_{id}(r, \Omega)} = Z_{id}(r). \tag{6.15}$$

Apart from the term that is independent of r, the free energy of the ion-dipole is identified as

$$\mathcal{F}_{id}(r) = -k_B T \ln Z_{id}(r) = -k_B T \ln \frac{\sinh \beta pE(r)}{\beta pE(r)}. \tag{6.16}$$

Noting that $\beta pE(r) \ll 1$,

$$\mathcal{F}_{id}(r) = -\frac{1}{6k_B T} \left(\frac{pq}{4\pi\varepsilon_w r^2} \right)^2 = \frac{1}{2} \varphi_{id}(r). \tag{6.17}$$

The entropy is given as

$$\begin{aligned} S_{id}(r) &= -\frac{\partial \mathcal{F}_{id}(r)}{\partial T} \\ &= \frac{\mathcal{F}_{id}(r)}{T}\left(1+2\frac{T}{\varepsilon_w}\frac{\partial \varepsilon_w}{\partial T}\right) \end{aligned} \tag{6.18}$$

Using (6.10),

$$S_{id}(r) = -\frac{1.72\mathcal{F}_{id}(r)}{T}. \tag{6.19}$$

at 25 °C. Because $\mathcal{F}_{id}(r \to \infty) = 0$, and $\mathcal{F}_{id}(r) < 0$, this means that as the dipole approach the charge, the entropy increases. The first term in (6.18) is negative, due to reduction of the rotational motion of the dipole. The second term, which is positive, may arise because the water is released from the intervening region into the free space in which its entropy can increase. As the dipole approaches the charge, the net entropy thus increases $S_{id}(r) > 0$, within the validity of the approximation.

6.2.4 Dipole-Dipole Interaction (Keesom Force)

When a polar molecule with dipole moment $\boldsymbol{p}_1$ approaches to another polar molecule with dipole moment $\boldsymbol{p}_2$ (Fig. 6.6) at a distance r, the latter has a potential energy

$$\varphi_{dd} = -\boldsymbol{p}_2 \cdot \boldsymbol{E}_2, \tag{6.20}$$

where $\boldsymbol{E}_2$ is the electric field on dipole 2 emanating from the dipole 1. The electrical potential from the dipole 1 obtained by

$$\phi_2 = -\boldsymbol{p}_1 \cdot \nabla \frac{1}{4\pi\varepsilon_w r} = \frac{\boldsymbol{p}_1 \cdot \boldsymbol{r}}{4\pi\varepsilon_w r^3}, \tag{6.21}$$

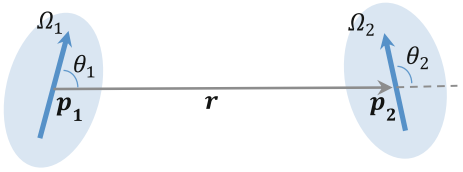

Fig. 6.6 The interaction between two dipoles $\boldsymbol{p}_1, \boldsymbol{p}_2$, separated by a distance $\boldsymbol{r}$

where the $\boldsymbol{r} = \boldsymbol{r}_2 - \boldsymbol{r}_1 = r\boldsymbol{n}$ is the radial vector pointing to the dipole 2. We then have

$$\boldsymbol{E}_2 = -\nabla\phi_2 = -\frac{1}{4\pi\varepsilon_w r^3}(\boldsymbol{p}_1 - 3\boldsymbol{p}_1 \cdot \boldsymbol{n}\boldsymbol{n}), \tag{6.22}$$

which varies as r^{-3}. Finally, (6.20) yields the interaction energy between two dipoles oriented with the solid angles Ω_1 and Ω_2:

$$\begin{aligned}\varphi_{dd}(r, \Omega_1, \Omega_2) &= -\frac{1}{4\pi\varepsilon_w r^3}[3(\boldsymbol{p}_1 \cdot \boldsymbol{n})(\boldsymbol{p}_2 \cdot \boldsymbol{n}) - \boldsymbol{p}_1 \cdot \boldsymbol{p}_2] \\ &= -\frac{p_1 p_2}{4\pi\varepsilon_w r^3}[3\cos\theta_1 \cos\theta_2 - \cos\theta_{12}].\end{aligned} \tag{6.23}$$

Here θ_1, θ_2 are the polar angles that the dipoles make with the radial vector and θ_{12} is the angle between two dipoles. This interaction energy varies as $\sim r^{-3}$.

The angle-averaged interaction energy is

$$\begin{aligned}\varphi_{dd}(r) &= \frac{\int d\Omega_1 \int d\Omega_2 \varphi_{dd}(r, \Omega_1, \Omega_2) e^{-\beta\varphi_{dd}(r,\Omega_1,\Omega_2)}}{\int d\Omega_1 \int d\Omega_2 e^{-\beta\varphi_{dd}(r,\Omega_1,\Omega_2)}} \\ &= -\frac{\partial}{\partial\beta}\ln Z_{dd}(r)\end{aligned} \tag{6.24}$$

where $Z_{dd}(r) = \int d\Omega_1 \int d\Omega_2 \exp[-\beta\varphi_{dd}(r, \Omega_1, \Omega_2)]$. $\varphi_{dd}(r, \Omega_1, \Omega_2)/(k_B T) \sim l^2 l_B / r^3$ is assumed to be much less than 1, so we have

$$Z_{dd}(r) \approx \int d\Omega_1 \int d\Omega_2 \{1 - \beta\varphi_{dd}(r, \Omega_1, \Omega_2)\} \tag{6.25}$$

and

$$\varphi_{dd}(r) \approx -\frac{2p_1^2 p_2^2}{3k_B T(4\pi\varepsilon_w r^3)^2} \sim -T^{-1}\varepsilon_w{}^{-2} \cdot r^{-6} \tag{6.26}$$

Compared with the interaction $\varphi_{dd}(r, \Omega_1, \Omega_2)$, $\varphi_{dd}(r)$ is weaker and short ranged (r^{-6}). It is estimated as $\varphi_{dd}(r) \sim (l^2 l_B / r^3)^2 k_B T$, which is smaller than ion-dipole interaction by the factor l^2/r^2.

The free energy of the two dipoles at a distance r is

$$\mathcal{F}_{dd}(r) = -k_B T \ln Z_{dd}(r) \approx -\frac{p_1^2 p_2^2}{3k_B T(4\pi\varepsilon_w r^3)^2} = \frac{1}{2}\varphi_{dd}(r). \tag{6.27}$$

Consequently,

$$S_{dd}(r) = \frac{\mathcal{F}}{T}\left(1 + 2\frac{T}{\varepsilon_w}\frac{\partial \varepsilon_w}{\partial T}\right) = -1.72\frac{\mathcal{F}_{dd}(r)}{T}, \tag{6.28}$$

which indicates that, like in ion-dipole case, the entropy of the system containing two dipoles increases as they approach each other, mostly due to the increased disorder of the water.

P6.2 *Derive the results* (6.26) *and* (6.27) *for* $\frac{\varphi_{dd}(r,\Omega_1,\Omega_2)}{k_BT} \ll 1$.

6.2.5 *Induced Dipoles and Van der Waals Attraction*

Now we consider the electrostatic interaction involving nonpolar molecules. An external field $\boldsymbol{E}(\boldsymbol{r})$ can induce a polarization even in a nonpolar molecule, $\boldsymbol{P}_{ind} = \alpha \boldsymbol{E}$, where α is the polarizability, thereby reducing the electrostatic energy. The energy change induced by the field that polarizes the molecule is

$$\begin{aligned} \varphi_n &= -\int_0^{\boldsymbol{E}} \boldsymbol{P}_{ind} \cdot d\boldsymbol{E} \\ &= -\alpha \int_0^{\boldsymbol{E}} \boldsymbol{E} \cdot d\boldsymbol{E} = -\frac{\alpha \boldsymbol{E}^2}{2}. \end{aligned} \tag{6.29}$$

This is an attractive interaction between the nonpolar molecule and the object that emanates the electric field. For example, the potential energy between the nonpolar molecule and an ion of charge q is given by

$$\varphi_{in} = -\frac{\alpha E^2}{2} = -\frac{\alpha}{2}\left(\frac{q}{4\pi\varepsilon_w r^2}\right)^2, \tag{6.30}$$

which is comparable to (6.14) of ion-dipole attraction; both are identical if α is replaced by that of a free dipole $\alpha_d = p^2/(3k_BT)$.

Consider the interaction between small nonpolar molecules 1 and 2 with their dipole moments instantaneously induced with the polarizabilities, α_1, α_2. A detailed derivation of the interaction is too complicated involving quantum fluctuations as well as thermal fluctuations to be relevant here. To find how it depends on the distance r between the two objects, we give a simple argument following (6.29). The potential energy of the polarized molecule 2 due to the field $\boldsymbol{E}_2$ emanating from molecule 1 is $\varphi_{nn} = -\alpha_2\langle E_2^2\rangle/2$, where $\boldsymbol{E}_2$ is now recognized as a fluctuating field due to an instantaneous dipole of molecule 1. In view of the fact $E_2 \sim -1/r^3$ (6.22) and the symmetry with respect to exchange between 1 and 2, we have

$$\varphi_{nn} = -\frac{C}{r^6} \tag{6.31}$$

where C is a constant proportional to $\alpha_1\alpha_2$.

P6.3 *Find the attraction energy between a dipole* $\mathbf{p}$ *and an induced dipole with polarizability* α *that are separated at a distance* r.

Interestingly the interaction potential between two dipoles, either permanent or induced, has the attractive tail r^{-6}. This universal interaction $(-r^{-6})$ is called the Van der Waals (vdW) attraction. The vdW force between the nonpolar atoms or molecules is also called the London dispersion force; it is due to electrons revolving in each atom or molecule and causing instantaneous (fluctuating) polarizations that tend to be correlated as the two approaches. **The Van der Waals attraction acts universally on all pairs of objects, microscopic or macroscopic, even if they do not carry charges or dipoles.** This fluctuation-induced attraction is an important component in a wide variety of phenomena such as adhesion, surface tension, and adsorption.

Let us consider two semi-infinite media of equal number density n of small molecules (or point sources of the interaction) separated at a distance D and find the vdW attraction between the two media. First consider the attraction potential $u(r)$ that a molecule 1 feels at a distance h vertically away from one of the surfaces (Fig. 6.7). Integrating the pair potential energy $\varphi(r) = -C/r^6$ over the volume element of a medium located at a distance $r = (x^2 + z^2)^{1/2}$ from the point 1 yields the attraction

$$\begin{aligned} u(r) &= -2\pi nC \int_h^\infty dz \int_0^\infty \frac{x dx}{(x^2+z^2)^3} \\ &= -\frac{\pi nC}{6h^3}, \end{aligned} \tag{6.32}$$

where $2\pi x dx dz$ is the volume element (ring) to be integrated over. We integrate this potential energy over the other semi-infinite medium (to which the molecule 1 belongs) to find the vdW attraction energy per unit area between the two media:

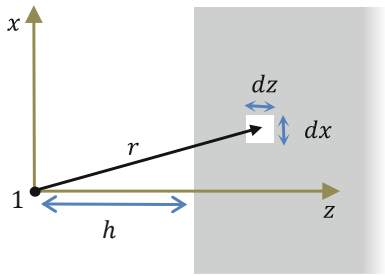

Fig. 6.7 The Van der Waals attraction between a molecule 1 and a semi-infinite medium (shaded)

$$U_{vdw} = -\frac{\pi n^2 C}{6}\int_D^\infty \frac{dh}{h^3} = -\frac{H}{12\pi D^2}, \tag{6.33}$$

where $H = \pi n^2 C$ is called the Hamaker constant and is typically in the order of 10^{-21} J $\sim k_B T$ for interactions between organic substances in water. The energy of the vdW attraction between two such macroscopic blocks with surfaces separated by 1 nm (1 μm), therefore, is about a small fraction of $k_B T$ per area 1nm^2 ($1\mu\text{m}^2$).

Via a similar calculation, one can show that the vdW interaction between two homogeneous and identical spheres of radius R separated by a much shorter closest distance D is given by

$$U_{vdw} = -\frac{HR}{12D} \tag{6.34}$$

Interestingly, the attraction is long-ranged (D^{-1}) and proportional to size of the particle (R). For two colloidal particles of $R = 0.5$ μm at a distance $D = 1$ nm, the attractive energy is in the order of $10\,k_B T$. This strength and the long range of attraction is effective enough to initiate aggregation or adhesion of the colloids. To assess the ultimate colloidal stability, however, one should consider various types of the interactions, including the repulsions.

When two atoms or monoatomic molecules merge together, a sharp, short-ranged repulsion occurs due to the Coulomb repulsion between nuclei, combined with the Pauli exclusion between electrons. The hybrid of the long-ranged Van der Waal's interaction and the short-ranged harsh repulsion is often incorporated using the Lennard Jones model,

$$\varphi_{LJ}(r) = 4\epsilon\left[(\sigma/r)^{12} - (\sigma/r)^6\right] \tag{4.59}$$

that we introduced earlier (4.59). This is a most popular model interaction that is characterized by two features, short-range repulsion and long-range attraction, and also by two parameters, hard core length σ and attraction strength ϵ; it is applicable not only to atoms and small molecules but also to colloids and coarse-grained units such as polymer beads.

6.3 Screened Coulomb Interactions and Electrical Double Layers

The presence of ions in water is critical for living. While their transport through membranes plays a key role in neuronal transmission in cell, they modulate the electrostatic interactions between charged objects in solutions. Here we study how

the ions in water screen the Coulomb interaction between charges and are distributed near a charged surface.

6.3.1 The Poisson-Boltzmann Equation

Understanding the behaviors of the ions thermally fluctuating under long-range Coulomb interactions is a many-body problem, for which rigorous use of statistical mechanics (Chap. 4) to solve it is a formidable task. Here we present a simple approximation that can capture the main physical features for the case *of dilute ionic (electrolyte) solutions*. First, the ionic solution is regarded as a continuum, so that the electric potential ϕ at a position $\boldsymbol{r}$ satisfies the basic equation in electrostatics, namely, **the Poisson equation**

$$\nabla^2\phi(\boldsymbol{r}) = -\frac{\rho_e(\boldsymbol{r})}{\varepsilon}, \tag{6.35}$$

where $\rho_e(\boldsymbol{r})$ is the charge density and ε is its electric permeability, which is nearly that of water, $\varepsilon \cong \varepsilon_w$, for the cases of dilute ionic solutions we consider throughout. We further assume that an ion at $\boldsymbol{r}$ is subject to a one-body electric potential $\phi(\boldsymbol{r})$, that is, a mean field, which effectively includes the influence of the other ions. In this mean field theory, for the ions each with charge q, the charge density in the solution is given by the Boltzmann factor

$$\rho_e(\boldsymbol{r}) = \rho_\infty \, e^{-\beta q\phi(\boldsymbol{r})}, \tag{6.36}$$

where ρ_∞ is the reference charge density at the point in the bulk where the potential is zero. Equation (6.35) then becomes a nonlinear equation for $\phi(\boldsymbol{r})$, called **the Poisson-Boltzmann (PB) equation**

$$\nabla^2\phi(\boldsymbol{r}) = -\frac{\rho_\infty}{\varepsilon} e^{-\beta q\phi(\boldsymbol{r})}. \tag{6.37}$$

As will be shown in the next section, this equation is exactly solved in one dimension, namely, for the potential and charge distribution at a vertical distance from a planar charged surface/membrane.

Within a cellular environment, the presence of electrolyte, commonly called salt, is essential. In a salt, positively-charged ions (cations) of number density $n_+(\boldsymbol{r})$ and valency z_+ coexist with negatively charged ions (anions) of density $n_-(\boldsymbol{r})$ and valency z_- in such a way to satisfy the charge neutrality at a reference point in the bulk:

$$z_+ n_{+\infty} + z_- n_{-\infty} = 0. \tag{6.38}$$

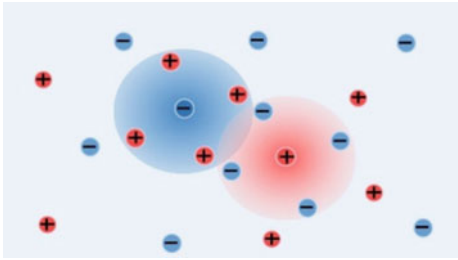

Fig. 6.8 The background ions centered around two ions screen the Coulomb interaction between them

The PB equation then takes the form

$$\nabla^2\phi = -\frac{1}{\varepsilon}\left[z_+ e n_{+\infty} e^{-\beta z_+ e\phi(\boldsymbol{r})} + z_- e n_{-\infty} e^{-\beta z_- e\phi(\boldsymbol{r})}\right]. \tag{6.39}$$

6.3.2 The Debye-Hückel Theory

Except for a few cases that we will treat later, PB equation cannot be solved analytically due to the nonlinearity of the equation. Thus, we consider the cases in which the potential is low enough that $e|\phi|/k_BT \ll 1$ ($|\phi| \ll 25$ mV at room temperature for $z_\pm = 1$). Using the approximation, $e^{-\beta z_\pm e\phi(\boldsymbol{r})} \cong 1 - \beta e z_\pm \phi(\boldsymbol{r})$, and the charge neutrality condition (6.38), we derive a linear equation for ϕ:

$$\nabla^2\phi = \kappa_D^2\phi, \tag{6.40}$$

where

$$\kappa_D^2 = \frac{e^2}{\varepsilon k_B T}\left(z_+^2 n_{+\infty} + z_-^2 n_{-\infty}\right). \tag{6.41}$$

Equation (6.40), called **the linearized Poisson-Boltzmann equation or Debye-Hückel equation**, can be solved exactly for a numerous geometrical situations. $\lambda_D = \kappa_D^{-1}$ is a characteristic length called the **Debye length**.

P6.3 *What is the charge (cations and anions) distribution of a salt at a vertical distance x from a plane with a surface charge density σ?*

Consider a sphere of radius R and charge Q immersed within the ionic solution. In this spherically symmetric situation, the Debye-Hückel equation gives the electrical potential at a radial distance r from the charged sphere:

$$\frac{1}{r}\frac{d^2}{dr^2} r\phi(r) = \kappa_D^2\phi(r). \tag{6.42}$$

The solution for $r \geq R$ that satisfies the boundary condition $\phi(r \to \infty) = 0$ is

$$\phi(r) = \phi_s \frac{R}{r} e^{-\kappa_D(r-R)}. \tag{6.43}$$

The constant $\phi_s = \phi(R)$ is the surface potential of the charged sphere; it is determined by invoking the Gauss theorem (after integrating (6.35) over volume of the sphere with radius R),

$$-\varphi'(R)4\pi R^2 = \frac{Q}{\varepsilon}, \tag{6.44}$$

from which one obtains

$$\phi_s = \frac{Q}{4\pi\varepsilon R(1+\kappa_D R)}, \tag{6.45}$$

and

$$\phi(r) = \frac{Q}{4\pi\varepsilon(1+\kappa_D R)r} e^{-\kappa_D(r-R)}. \tag{6.46}$$

For point-like ions, this equation simplifies to

$$\phi(r) = \frac{Q}{4\pi\varepsilon r} e^{-\kappa_D r}. \tag{6.47}$$

Compared with the Coulomb potential, the electrical potential from the central ion is screened appreciably beyond the Debye length $\lambda_D = \kappa_D^{-1}$. For 1:1 electrolyte ($z_+ = 1 = -z_-, n_{+\infty} = n_{-\infty} = n_\infty$), this can be written as

$$\begin{aligned} \lambda_D &= \left(\frac{\varepsilon k_B T}{2n_\infty e^2}\right)^{1/2} = \left(\frac{1}{8\pi n_\infty l_B}\right)^{1/2} \\ &\approx 0.304\, C^{-1/2}\text{nm (at 25 °C)} \end{aligned} \tag{6.48}$$

where $C = n_\infty \cdot \text{L/mol}$ is the molar concentration of the electrolyte. **The screening length λ_D for the 1:1 salt (e.g., NaCl) at 25 °C and a physiological concentration of $C = 0.1$ M is 0.96 nm.** The screening occurs because of the presence of the ions surrounding an ion located at the center. Equation (6.35) combined with (6.40) leads to

$$\rho_e(\boldsymbol{r}) = -\varepsilon\kappa_D^2\phi(\boldsymbol{r}), \tag{6.49}$$

which demonstrates that the density distribution of the background ions $|\rho_e(\boldsymbol{r})|$ is proportional to $|\phi(\boldsymbol{r})|$, and thus to $r^{-1}e^{-\kappa_D(r-a)}$, if the ions are charged spheres each with radius a. The charge within a spherical shell at r around the center ion is $|dq| = 4\pi r^2|\rho_e(r)|dr \sim re^{-\kappa_D(r-a)}dr$, so radial distribution has a peak at $r = \lambda_D$.

Thus the screening length λ_D is also called the thickness of the ion cloud around each ion.

The change of chemical potential of an ion arising from its interaction with other ions can be calculated within the Debye-Hückel theory. The chemical potential change is simply the reversible work done in charging the ions around the central ion

$$\Delta\mu = \int_0^\infty dr\ 4\pi r^2 \rho_e(r)\phi(r) = -\varepsilon\kappa_D^2 \int_0^\infty dr\ 4\pi r^2 \phi^2(r) \\ = -\frac{\kappa_D q^2}{8\pi\varepsilon}. \quad (a \to 0) \tag{6.50}$$

The result above is called the Debye-Hückel limiting law. A noteworthy feature here is that the contribution from the interaction is proportional to $C^{1/2}$ rather than to C that can be attained by the virial expansion. This behavior is attributed to the long-range nature of electrostatic interaction. Equation (6.50) is valid also for a dilute solution of finite-sized ions, where $ez\phi(\lambda_D)/(k_BT) \ll 1$, or $\lambda_D \gg l_B$.

P6.4 *Show that the contribution of ionic interactions to pressure corresponding to (6.50), is* $\Delta p = -k_BT/24{\lambda_D}^3$. *What is the contribution to entropy?*

6.3.3 Charged Surface, Counterions, and Electrical Double Layer (EDL)

When neutral polymers, membranes and colloids are dissolved in water, they can acquire charges through ionization of polar groups on their surfaces. The ions that are released in water are called counterions. These counterions are electrostatically attracted to the ionized surface, while tending to move away from the surface to the bulk of the solution to enjoy more entropy. Furthermore, the solutions generally contain anions and cations from the added salt. The balance of the electrostatic

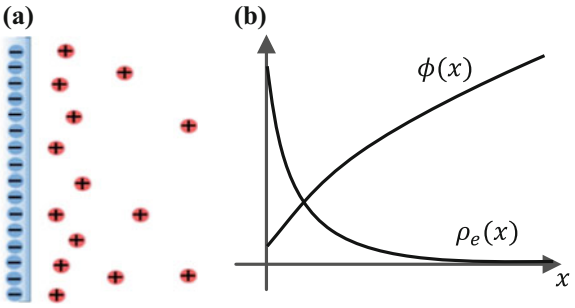

Fig. 6.9 **a** A planar surface charged negatively due to counterion release. **b** The profiles of the electrical potential $\phi(x)$ and the counterion charge density. $\rho_e(x)$

attraction and the opposing effect of entropy leads to formation of an electric double layer (EDL) on the surface, where the ions are more or less condensed.

Here we will consider an infinite charged surface located at a position $x = 0$. We want to find the an electrostatic potential $\phi(x)$ and the charge density $\rho_e(x)$ at a vertical position x in the solution (Fig. 6.9). First consider that there are no salt but only counterions each with charge q. The counterion charge density at any points x in solution is given by $\rho_e(x) = \rho_\infty e^{-\beta q\phi(x)}$, which can be found by solving the PB equation

$$\phi''(x) = -\rho_e(x)/\varepsilon = -\rho_\infty e^{-\beta q\phi(x)}/\varepsilon, \tag{6.51}$$

where $\phi''(x) = d^2\phi(x)/dx^2$. Due to net charge neutrality the surface charge density of the surface is given by

$$\sigma = -\int_0^\infty dx\rho_e(x) = \varepsilon\int_0^\infty dx\phi''(x) = \varepsilon E_s, \tag{6.52}$$

where $E_s = -\phi'(x)|_{x=0}$ is the electric field at the surface. Equation (6.52) serves as a boundary condition (BC) on the surface along with the natural BC $E = 0$ at $x = \infty$.

By multiplying (6.51) by $\phi'(x)$ we have

$$\phi'(x)\phi''(x) = \frac{1}{2}[(\phi'(x))^2]' = -(\rho_\infty/\varepsilon)\phi'(x)e^{-\beta q\phi(x)}, \tag{6.53}$$

which is integrated to

$$(\phi'(x))^2 = \frac{2\rho_\infty k_B T}{\varepsilon q}\{e^{-\beta q\phi(x)} - e^{-\beta q\phi(\infty)}\}. \tag{6.54}$$

The above equation is analytically solved for $\phi(x)$ and then for $\rho_e(x) = \rho_\infty e^{-\beta q\phi(x)}$:

$$\phi(x) = \frac{2k_B T}{q}\{\ln K(x+b)\} \tag{6.55}$$

$$\rho_e(x) = \frac{q}{2\pi l_B(x+b)^2}. \tag{6.56}$$

where $K^2 = 2\pi l_B\rho_\infty$. The potential increases logarithmically whereas the density decays algebraically as a function of x (Fig. 6.9b). The characteristic length b of the decay is determined from the BC (charge neutrality) (6.52) as

$$b = \frac{2\varepsilon k_B T}{q|\sigma|} = \frac{q}{2\pi l_B |\sigma|}. \tag{6.57}$$

This is called the Gouy-Chapman length, the thickness characteristic of the diffusive counterion layer near the surface, within which the half of the counterions reside.

Equation (6.54) can be expressed as

$$n(x) - n_\infty = \frac{\beta\varepsilon}{2} E(x)^2, \tag{6.58}$$

which gives the ionic number density $n(x)$ at any point in terms of the electric field $E(x) = -\phi'(x)$ and the reference density n_∞ at infinity where the electric field is zero. Because there are no *explicit* interionic interactions within this mean field theory for the dilute ionic solutions, the osmotic pressure is proportional to the density: the difference of osmotic pressure of the ions between a point x and in bulk is given by

$$\Delta p(x) = k_B T\{n(x) - n_\infty\} = \frac{\varepsilon}{2}(E(x))^2, \tag{6.59}$$

where the RHS is identified as electrostatic pressure, which is equal to the field energy density. The ionic charge density at the surface is given by

$$\rho_s = \rho_\infty + \frac{\beta q\varepsilon}{2} {E_s}^2 = \rho_\infty + \frac{q}{2\varepsilon k_B T}\sigma^2, \tag{6.60}$$

where (6.52) is used. The *volume* charge density surface increases parabolically with the *surface* charge density σ.

Now consider the case where the salt is added. Whereas the counterions are localized only near the surface, the salt can remain in the bulk with finite number densities for the cation and anions $n_\pm(\infty) = n_\infty$; the number and the overall effect of the counterions is negligible compared with those of the salt ions. Considering the case of 1:1 electrolyte the PB equation reads as $\phi''(x) = (2n_\infty e/\varepsilon)\sinh\{\beta e\phi(x)\}$, which is rewritten as

$$\Phi''(x) = \kappa_D^2 \sinh \Phi(x), \tag{6.61}$$

where $\Phi(x) = \beta e\phi(x)$ and κ_D is the inverse Debye length (6.48).

By multiplying (6.61) by $\Phi'(x)$ and integrating the result we find

$$(\Phi'(x))^2 = 2\kappa_D^2(\cosh\Phi - 1) = 4\kappa_D^2\left(\sinh\frac{\Phi}{2}\right)^2, \tag{6.62}$$

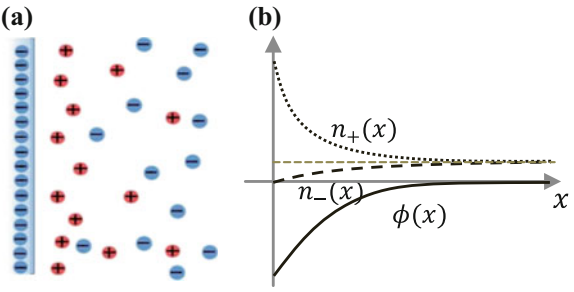

Fig. 6.10 **a** A negatively charged surface and salt ions. **b** The profiles of electrical potential and cation (n_+) and anion (n_-) number distributions

and obtain

$$\phi(x) = -\frac{2k_BT}{e}\ln\frac{1+\gamma e^{-\kappa_D x}}{1-\gamma e^{-\kappa_D x}} \tag{6.63}$$

$$n_\pm(x) = n_\infty e^{\mp\beta e\phi(x)} = n_\infty\left(\frac{1\pm\gamma e^{-\kappa_D x}}{1\mp\gamma e^{-\kappa_D x}}\right)^2 \tag{6.64}$$

where $\gamma = \tanh(e\phi_s/4k_BT)$, and $\phi_s = \phi(x=0)$ is the surface potential.

P6.5 *Show that the surface potential ϕ_s and the surface charge density σ are related by the BC (6.52), leading to $\sigma = (2\varepsilon\kappa_D k_B T)\sinh\{(e\phi_s)/(2k_BT)\}$. For low surface potential, $\sigma = \varepsilon\kappa_D\phi_s = \varepsilon\phi_s/\lambda_D$, which means that the electrical double layer behaves like a condenser of thickness λ_D.*

Figure 6.10 shows how the potential and densities vary with the distance x. In the weak coupling case $q\phi/(k_BT) \ll 1$, for which DH linearization is justified, the above results are simplified. First, $\gamma \approx e\phi_s/4k_BT$ and

$$\phi(x) \approx \phi_s e^{-\kappa_D x} = \frac{\sigma}{\varepsilon\kappa_D}e^{-\kappa_D x}. \tag{6.65}$$

Compared with the counterion case where the potential diverges in the bulk, the potential decays to zero due to the screening effect of the salt. The number density is given by

$$n_\pm(x) = n_\infty\left(1\mp\frac{e\sigma}{\varepsilon\kappa_D k_BT}e^{-\kappa_D x}\right), \tag{6.66}$$

which shows that both of the cations and anion distributions approach exponentially to their bulk values. The width of the electrical double layer is of the order of λ_D.

Equation (6.58) is valid also for the total number density $n = n_+ + n_-$. It leads to the pressure difference in the solution and number density of ions at surface.

$$\Delta p(x) = k_B T\{n(x) - 2n_\infty\} = \frac{\varepsilon}{2}(E(x))^2 \tag{6.67}$$

$$n_s = 2n_\infty + \frac{\varepsilon}{2k_B T}{E_s}^2 = 2n_\infty + \frac{1}{2\varepsilon k_B T}\sigma^2. \tag{6.68}$$

The total number density of the ions n_s induced on the surface grows parabolically with the surface electric field E_s and surface charge density σ. At sufficiently high values of σ enlarge to the n_s (6.68) can be unphysically high so as to exceed the close packing density. This is the limitation of PB equation which neglects the correlation between the ions arising from their interaction and finite sizes. What is really observed is a thin layer of the ions bound to the highly charged surface, called Stern layer; this limits the surface charge density σ to be below a critical value. In the solution beyond the Stern layer, the PB equation theory is applicable.

Further Readings and References

J. Israelachvili, *Intermolecular & Surface Forces*, 2nd edn. (Academic Press, 2000)
R.A.L. Jones, *Soft Condensed Matter* (Oxford University Press, 2002)
J. Lyklema, *Fundamentals of Interface and Colloid Science*, vol. 1 (1991)
D.F. Evans, H. Wennerström, *The Colloidal Domain*, 2nd edn. (Wiley, 1999)
K.A. Dill, T.M. Truskett, V. Vlachy, B. Hribar-Lee, Modeling water, the hydrophobic effect, and ion solvation. Annu. Rev. Biophys. Biomol. Struct. **34**, 173–199 (2005)
H.E. Stanley, M.C. Barbosa, S. Mossa, P.A. Netz, F. Sciortino, Statistical physics and liquid water at negative pressures, ed. by F.W. Starrf, M. Yamad, Physica A **315**, 281–289 (2002)

Chapter 7
Law of Chemical Forces: Transitions, Reactions, and Self-assemblies

Physical and biological components are often in a certain phases or conformations that can undergo physical transitions and chemical reactions. The simplest of the reactions or transitions is

$$A \leftrightarrow B. \tag{7.1}$$

It denotes transition between states A and B, where the bidirectional arrow $\leftrightarrow$ indicates either forward or backward direction. One class of the examples is biopolymer conformational transition that we already discussed earlier in numerous situations. 'A' and 'B' can also represent two phases of matter, such as gas and liquid. Often the biochemical systems consist of many species that can react. One simple but important chemical reaction is

$$2H_2 + O_2 \leftrightarrow 2H_2O. \tag{7.2}$$

One further example is the process of self-assembly or association, in which monomers aggregate into larger structural units, and its backward process called dissociation:

$$A_1 + \cdots + A_1 \leftrightarrow A_n, \tag{7.3}$$

where A_n is the aggregate of n units. Here we describe basic relations and conditions of the reactions and transitions at equilibrium, in particular the relations between the concentrations of the substances involved, called the law of mass action (LMA). LMA can be one of most basic laws for biological transitions involving various conformational states of biopolymers and supramolecular aggregates.

W. Sung, *Statistical Physics for Biological Matter*, Graduate Texts in Physics,
https://doi.org/10.1007/978-94-024-1584-1_7

7.1 Law of Mass Action (LMA)

7.1.1 Derivation

Here we begin with derivation of LMA using statistical mechanics. All of the processes mentioned above can be represented by the equation

$$\sum_{i=1}^{m} \nu_i B_i = 0, \tag{7.4}$$

where B_i denotes the reaction or transition unit (e.g., molecule, macromolecule, supramolecular aggregate) of the species i or the state i, and ν_i is its stoichiometric coefficient. For example, (7.2) is represented by the reaction equation

$$-2\mathrm{H}_2 - \mathrm{O}_2 + 2\mathrm{H}_2\mathrm{O} = 0, \tag{7.5}$$

where $B_1 = \mathrm{H}_2 \;\; \nu_1 = -2,\; B_2 = \mathrm{O}_2 \;\; \nu_2 = -1,\; B_3 = \mathrm{H}_2\mathrm{O} \;\; \nu_3 = 2$ respectively. The values of ν_i are negative for reactants and positive for products. The central question here is: what is the relation between the concentrations of the units involved in the reaction at equilibrium; how is it given by the thermodynamic state of each unit?

We consider a mixture of m reacting units, among which r are reactants and $m - r$ are products, at fixed temperature T and volume V. Throughout the reaction the free energy of the mixture changes by modulating the number of each unit ΔN_i:

$$\Delta F(T, V, N_1, N_2, \cdots, N_m) = \sum_{i=1}^{m} \left(\frac{\partial F}{\partial N_i}\right) \Delta N_i. \tag{7.6}$$

Because $\partial F/\partial N_i = \mu_i$ (chemical potential of the unit i), and $\Delta N_i \propto \nu_i$, the above is proportional to the free energy change of the reaction defined by

$$\Delta f = \sum_{i=1}^{m} \nu_i \mu_i. \tag{7.7}$$

At equilibrium, the free energy is minimum, $\Delta F = 0 = \Delta f$, so that we have

$$\sum_{i=1}^{m} \nu_i \mu_i = 0, \tag{7.8}$$

which we may call the law of chemical force balance at equilibrium.

First, we apply this fundamental equation to the transition $A \leftrightarrow B$, or $-A + B = 0$, where the units A and B have $\nu_A = -1, \nu_B = 1$. Then

$$-\mu_A + \mu_B = 0, \quad \text{or} \quad \mu_A = \mu_B \tag{7.9}$$

which is just the condition of chemical equilibrium that we derived earlier. One example is the transitions between two conformational states A and B of a biopolymer. Other examples include phase transition between liquid and gas; here A and B represent the liquid and gas state to which an unit (molecule) belongs. A monomer in a bound state A and unbound state B in adsorption-desorption transition is a similar example (Fig. 7.1).

To proceed further, we assume that all units involved in the reaction or transition form *ideal* gases at a fixed temperature T. The chemical potential of each species or state then is

$$\mu_i = \mu_{i0} + k_B T \ln (n_i/n_{i0}), \tag{7.10}$$

where 0 denote the standard state values (4.47). Usually in experiments the standard concentration n_{i0} for a solute is assigned to be 1 mol/L $\approx 0.6/(\text{nm})^3$. We denote the dimensionless concentration n_i/n_{i0} by C_i, and call it the molar or mole concentration (unit symbol: M), which is defined as the number of moles per liter (1 molar $= 1\ M = 1$ mol/L).

Equation (7.7) becomes

$$\Delta f = \Delta f_0 + k_B T \sum_{i=1}^{m} \nu_i \ln C_i \tag{7.11}$$

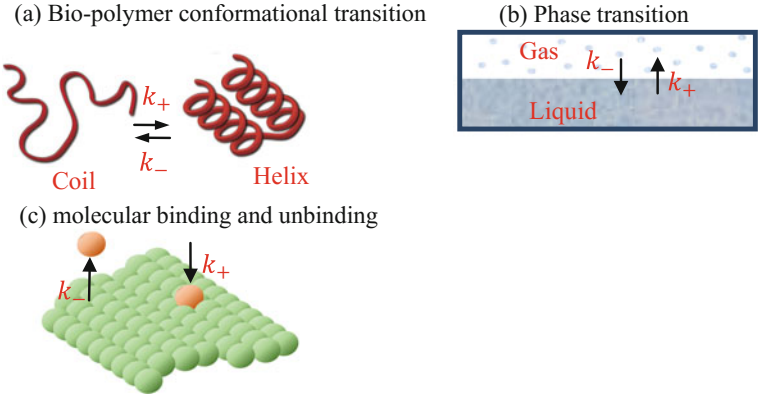

Fig. 7.1 Examples of two state transitions. **a** Coil to helix transition, **b** the gas to liquid transition of water, **c** molecular binding-unbinding transition on surface

where

$$\Delta f_0 = \sum_{i=1}^{m} \nu_i \mu_{i0} \tag{7.12}$$

is the intrinsic quantity independent of the concentrations called the standard free energy change of the reaction. Now the condition of the chemical equilibrium, $\Delta f = 0$ leads to **"the law of mass action (LMA)" for *equilibrium* concentrations**:

$$\prod_{i}^{m} C_i^{\nu_i} = \frac{C_{r+1}^{\nu_{r+1}} \ldots C_m^{\nu_m}}{C_1^{|\nu_1|} C_2^{|\nu_2|} \ldots C_r^{|\nu_r|}} = K(T). \tag{7.13}$$

Here

$$K(T) = \exp\left(-\beta \Delta f_0\right) \tag{7.14}$$

is called **the equilibrium constant**.

Equation (7.13) states the condition of chemical forces at equilibrium where $\Delta f = 0$. The constant $K(T)$ is concentration-independent but temperature-dependent. It is a measure of the reactivity. The rate $k_+ C_1^{|\nu_1|} C_2^{|\nu_2|} \ldots C_r^{|\nu_r|}$ of the forward reaction must be equal to $k_- C_{r+1}^{\nu_{r+1}} \ldots C_m^{\nu_m}$ of the backward reaction so (7.13) means that

$$K(T) = k_+ / k_-. \tag{7.15}$$

If $K(T) > 1$, then $\Delta F_0 < 0$ and $k_+ > k_-$; i.e., the standard free energy decreases and the reaction runs forward, yielding more products at the cost of the reactants. If $K(T) < 1$, the reaction will run backward. The balance between generation of reactants and products occurs only when $K(T) = 1$, i.e., $\Delta f_0 = 0$ and $k_+ = k_-$.

Using (7.14), further understanding of $K(T)$ is gained by considering the following,

$$\begin{aligned} \frac{\partial \ln K(T)}{\partial (1/T)} &= \frac{1}{k_B} \frac{\partial}{\partial \beta} (-\beta \Delta f_0) = \frac{1}{k_B} \sum \nu_i \left(\frac{\partial}{\partial \beta} \right) \ln z_i \\ &= -\frac{1}{k_B} \sum \nu_i e_i = -\Delta e_0 / k_B, \end{aligned} \tag{7.16}$$

where z_i is the partition function of *a single substance* of the species or state i, e_i is its internal energy, and Δe_0 is called the standard internal energy change of the reaction. Equation (7.16) indicates that Δe_0 is the slope of a plot of $\ln K(T)$ versus $(1/T)$ obtained experimentally (for example, Fig. 8.2). If $\Delta e_0 > 0$, via the reaction heat is absorbed, and $K(T)$ rises as the temperature increases, because (7.16) can be rewritten as $\partial \ln K(T)/\partial T = T^2 \Delta e_0 / k_B$.

7.1.2 Conformational Transitions of Biopolymers

For the conformational transition $A \leftrightarrow B$ of a biopolymer, LMA tells us that

$$\frac{C_B}{C_A} = K(T) = e^{-\frac{\Delta f_0}{k_B T}} \tag{7.17}$$

where Δf_0 is the free energy of the conformational change of *a single biopolymer*, which depends only on the temperature. This equation along with (7.16) indicates that given the equilibrium constant by the concentration ratio, the standard internal energy and free energy changes in a conformational transition can be obtained.

P7.1 *Suppose you have data for $K(T)$* (Fig. 7.2) *from a biopolymer conformational transition from a state to another from the measurements of the concentrations in the two states. From the curve, how can you find the entropy change at temperature T_1? (Answer) From the value $K(T_1)$ itself one obtain the free energy change Δf_0. From the slope of the curve at T_1 one can find Δe_0 using* (7.16)*. Using these, the entropy change Δs_0 is obtained from $\Delta f_0 = \Delta e_0 - T_1 \Delta s_0$.*

One often deals with systems that do not have a fixed volume but a fixed pressure in laboratories; for such systems, the primary thermodynamic potential is the Gibbs free energy. For this case, the theoretical development is same, with F replaced by Gibbs free energy G, and E replaced by enthalpy H. Thus, (7.14) and (7.16) are replaced by

$$K(T) = e^{-\frac{\Delta g_0}{k_B T}} \tag{7.18}$$

and the Van 't Hoff equation,

$$\frac{\partial \ln K(T)}{\partial (1/T)} = -\Delta h_0 / k_B, \tag{7.19}$$

respectively, where Δh_0 and Δg_0 respectively are the standard enthalpy and Gibbs free energy changes associated with the transition.

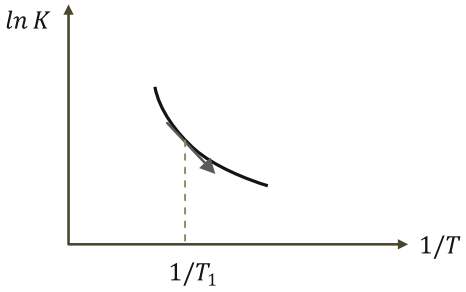

Fig. 7.2 The plot of $\ln K$ versus $1/T$. From the value of $\ln K$ and its slope the changes of free energy and internal energy (enthalpy) are deduced

7.1.3 Some Chemical Reactions

Dissociation of Diatomic Molecules

The association of diatomic molecules from atoms in a gaseous phase and the reverse dissociation process is given by the reaction equation

$$2A_1 \leftrightarrow A_2 \quad \text{or} \quad A_2 - 2A_1 = 0, \tag{7.20}$$

for which the relation for the chemical potential is

$$\mu_{A_2} - 2\mu_{A_1} = 0. \tag{7.21}$$

The LMA (7.13) tells us that the relation between the concentrations of the molecules C_{A_2} and the free atoms C_{A_1} is given by

$$\frac{C_{A_2}}{C_{A_1}^2} = K(T), \tag{7.22}$$

where $K(T)$, or the intrinsic free energy change $\Delta f_0 = \mu_{A_2}^0 - 2\mu_{A_1}^0$ can be in principle calculated from knowledge of the internal structures of the molecule and atom involved.

With the knowledge of $K(T)$ we can determine each concentration above from the given *total* concentration of the atoms C_A, using the relations:

$$C_A = C_{A_1} + 2C_{A_2} \tag{7.23}$$

Because we have two equations, the two unknown concentrations can be uniquely obtained. For the concentration of the free atoms C_{A_1}, we obtain

$$C_{A_1} = \frac{\sqrt{1 + 8KC_A} - 1}{4K} \tag{7.24}$$

Note that, when K is very small, C_{A_1} approaches C_A, meaning that most of the atoms remain inert or most molecules dissociate. When K is very large, $C_{A_1} \to \sqrt{C_A/2K}$, thus the gas is mostly diatomic.

Ionization of Water

Water has electrical conductivity, which is attributed to ionization (dissociation) of a water molecule into hydrogen ion and hydroxyl ion to a slight extent:

$$H_2O \leftrightarrow H^+ + OH^-. \tag{7.25}$$

Thermodynamically, the dissociation occurs when entropy is dominant over the binding energy. Because the water liquid is far from being an ideal gas, the LMA in the form (7.13) does not hold true; the water molar concentration C_{H_2O} should be replaced by the activity a_{H_2O}:

$$\frac{C_{H^+} C_{OH^-}}{a_{H_2O}} = K(T). \tag{7.26}$$

The activity a_{H_2O} assumes unity for pure water, which we choose as the standard state. At 25 °C, $K(T)$ is measured to be 10^{-14}, with the standard concentrations chosen as $n_{i0} = 1\,\text{mol/L}$ for H^+ and OH^-. Because the concentrations of H^+ and OH^- are very small, the water in the solution of has the activity nearly that of pure water, we have

$$C_{H^+} C_{OH^-} = K(T), \tag{7.27}$$

so that, in pure water, $C_{H^+} = C_{OH}$, and thus $C_{H^+} = 10^{-7}$, leading to

$$\text{pH} \equiv -\log_{10} C_{H^+} = 7. \tag{7.28}$$

Adding an acid to water increases the concentration of H^+ relative to OH^- so pH decreases.

ATP Hydrolysis

ATP hydrolysis is a chemical reaction by which one adenosine triphosphate (ATP) molecule reacts in water to produce an adenosine diphosphate (ADP) molecule and an inorganic phosphate (P_i):

$$\text{ATP} \leftrightarrow \text{ADP} + P_i. \tag{7.29}$$

It is an essential process by which the chemical energy stored in ATP is released to do useful work, for example, in muscles. The equilibrium constant is given by

$$K(T) = \frac{C_{ADP} C_{Pi}}{C_{ATP}} = e^{-\frac{\Delta f_0}{k_B T}}. \tag{7.30}$$

The typical value of the standard free energy change is $\Delta f_0 \approx -12 k_B T$ per molecule. *In vivo*, the free energy of the hydrolysis reaction is given by the net free energy change (7.11),

$$\Delta f\{\boldsymbol{C}_i\} = \Delta f_0 + k_B T \ln \frac{\boldsymbol{C}_{ADP}\boldsymbol{C}_{Pi}}{\boldsymbol{C}_{ATP}} \approx -20\, k_B T, \tag{7.31}$$

where $\boldsymbol{C}_i$ here are the *cellular* concentrations different from the equilibrium concentrations.

7.1.4 Protein Bindings on Substrates

Kinesin motors (K) bind to microtubules (M), for which the reaction equation and the equilibrium constant are

$$K + M \leftrightarrow KM, \tag{7.32}$$

$$\frac{C_{KM}}{C_K C_M} = K(T). \tag{7.33}$$

If the process of binding is accompanied by a mechanical force on the motor that does a work by the amount Δw, to be specific if a constant force f is applied against the binding process over a displacement l, we have

$$\frac{C_{KM}}{C_K C_M} = K(T) e^{-\frac{\Delta w}{k_B T}} = K(T) e^{-\frac{fl}{k_B T}} \tag{7.34}$$

It indicates the work can shift the equilibrium so as to induce the backward reaction.

LMA provides a simple route to finding the coverages of molecules bound on substrates. Let a protein have N binding sites to be either fully occupied (concerted binding) or empty. For the binding of N ligands on a protein P, the reaction equation is

$$P_0 + NL \leftrightarrow P_N, \tag{7.35}$$

where P_0 is a protein with empty binding sites, P_N is a protein with all N sites occupied, and L is a free ligand. The equilibrium condition for their respective concentrations is given by

$$\frac{C_N}{{C_L}^N C_0} = K(T), \tag{7.36}$$

The fraction of the bound proteins then is

$$\begin{aligned} \theta &= \frac{C_N}{C_N + C_0} \\ &= \frac{{C_L}^N}{{C_L}^N + K(T)^{-1}}, \end{aligned} \tag{7.37}$$

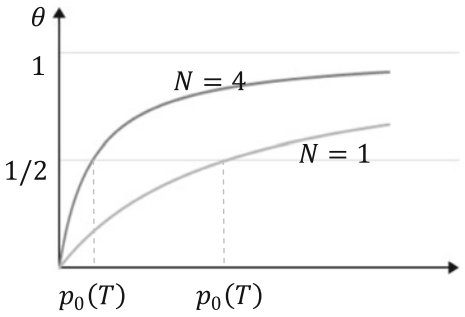

Fig. 7.3 The fraction of bound ligands θ as a function of pressure p. N is number of binding sites to be fully occupied or empty. The value of $p_0(T)$ at which the fraction is 1/2 is much smaller for $N = 4$ than for $N = 1$.

which is often referred as **the Hill equation**. Since concentration of the free ligands C_L is dilute enough to be proportional to the ambient pressure p they imparts on the substrates, we have

$$\theta = p^N / \left(p^N + {p_0}^N(T)\right), \tag{7.38}$$

where p_0 is a purely temperature-dependent quantity. The case with $N = 1$ is the Langmuir isotherm discussed earlier (3.74). As the integer number N increases, θ increases more steeply with p, which means the binding becomes more cooperative (Fig. 7.3).

7.2 Self-assembly

Self-assembly is a ubiquitous process that occurs in nature on various scales, by which objects spontaneously aggregate into more complex structures. The universe and life may have evolved through this process. Atoms interact to form molecules. Molecules bond to form crystals and supramolecular structures. In biology, self-assembly is fundamental and plentiful. Monomers aggregate linearly to form biopolymers. Two complementary single strands of DNA form a double helix. Lipid molecules spontaneously assemble to form membranes in water.

Here we are interested in how supramolecular aggregates such as one and two-dimensional polymers are formed from smaller molecules and are distributed in size (Fig. 7.4). Basically, left alone, all processes at a given temperature evolve by competition between energy and entropy to achieve the equilibrium structure in which the free energy is minimized under certain constraints. These are passive self-organization processes. We do not address here the active self-organization driven by a variety of external stimuli and noises that operate far from equilibrium as demonstrated by the growth of cytoskeletal filaments in cells.

Here we will focus on self-assembly at equilibrium. Consider the transition between n free monomers (A_1) and an aggregate composed of n monomers (A_n), called an n-mer,

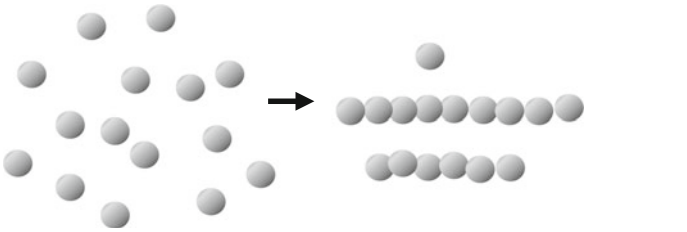

Fig. 7.4 Formation of linear aggregates from monomers

$$nA_1 \leftrightarrow A_n. \tag{7.39}$$

Assuming that the aggregates as well as the monomers are very dilute, the LMA (7.13) tells us that the relation between the mole concentrations (molarities) of n-mers C_n and the free monomers C_1 is given by

$$C_n/\left(C_1^n\right) = e^{-\beta\Delta f_{n0}} \tag{7.40}$$

where Δf_{n0} (7.12) is the standard part of free energy change (from n monomers to an n-mer) that excludes the concentration contributions. Δf_{n0} should be negative increasingly with n to induce the aggregation. Our goal here is to find the distributions of n-mers and their mean size $\langle n \rangle$ in terms of the total monomer concentration,

$$C = \sum_n nC_n, \tag{7.41}$$

which is a quantity initially controlled by experiment. The first task with which we proceed to this end is to evaluate the Δf_{n0} as a function of n.

P7.2 *Equation* (7.40) *can also be derived as follows. Consider an ideal mixture of n-mers with the free energy (which is a variant of* (4.91)*):*

$$F = \sum_{n=1} C_n\{f_{n0} + k_BT(\ln C_n - 1)\}$$

The first term is the standard (free) energy and the second is the entropy associated with the distribution of the aggregates. By minimizing the free energy by varying C_n *subject to constraint of given total monomer concentration* $C = \sum_n nC_n$*, derive*

$$C_n = C_1^n e^{-\beta(\mu_n^0 - \mu_1^0)},$$

where $\mu_n^0 = f_{n0}/n$. *The above equation is also obtained by the equilibrium condition of chemical potentials per monomer in aggregates of various sizes,* $\mu_n = \mu_{n-1} = \cdots = \mu_1$ (Israelachivili 2011) *along with the ideal gas condition,* $n\mu_n = n\mu_n^0 + k_BT \ln C_n$.

7.2.1 Linear Aggregates

First let us consider the linear aggregates where thermal undulations are neglected, e.g., stiff polymer chains such as short cytoskeletal filaments (Fig. 7.5). If each of the $n-1$ bonds of an n-mer has the bond energy b, we have

$$\Delta f_{n0} = -(n-1)b \tag{7.42}$$

relative to an unbound monomer energy. Substituting (7.42) into (7.40) yields the concentration of n-mers

$$C_n = \left[C_1 e^{\beta b}\right]^n e^{-\beta b} = [C_1/C^*]^n C^*, \tag{7.43}$$

where $C^* = e^{-\beta b}$. Equation (7.43) indicates that C_1 can increase up to C^* and no further, otherwise C_n can be large exceeding 1 molar. At concentration C^* of the unbound monomers, called the critical aggregation concentration, large aggregates can form, as we shall see shortly. Equation (7.43) can be rewritten as

$$C_n = C^* e^{-an}, \tag{7.44}$$

where

$$a = \ln (C^*/C_1) \tag{7.45}$$

is positive because C_1 is less than C^*. The probability of finding n-aggregates is given by

$$P(n) = \frac{C_n}{\sum_1^\infty C_n} = (e^a - 1)e^{-an}. \tag{7.46}$$

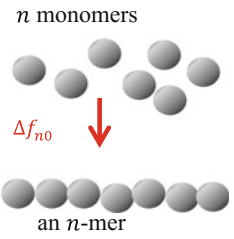

Fig. 7.5 The process of linear aggregation and the associated standard (intrinsic) free energy change Δf_{n0}

$P(n)$ is an exponentially decaying function of the aggregate size n, which is in a good agreement with the distribution of the length of actin filaments in cells (Burlacu et al. 1992). The mean aggregate size is given by

$$\langle n\rangle = \sum_1^\infty nP_n = -(e^a - 1)\frac{\partial}{\partial a}\sum_1^\infty e^{-an} = \frac{1}{1-e^{-a}}. \tag{7.47}$$

C_n and a are to be found in terms of the total monomer concentration C rather than C_1. We note from (7.43) that

$$C = \sum_{n=1}^\infty nC_n = C^* y/(1-y)^2, \tag{7.48}$$

where $y = C_1/C^*$, which is solved in terms of C and C^*:

$$\frac{C_1}{C^*} = \frac{2C/C^* + 1 - \sqrt{4C/C^* + 1}}{2C/C^*}. \tag{7.49}$$

From (7.49), we find for low concentrations, $C \ll C^*$, $C_1 \approx C(1 - 2C/C^*)$, so that $a \approx \ln(C^*/C)$ and $\langle n\rangle \approx 1 + C/C^*$. This indicates the aggregates are mostly in the monomer state $n = 1$. As C increases further, C_1 is saturated to C^*, whereas the concentration of bound monomers $C - C_1$ increases (Fig. 7.6). For high concentration $C \gg C^*$, (7.49) yields

$$C_1 \approx C^*\left[1 - \left(\frac{C^*}{C}\right)^{1/2}\right] \tag{7.50}$$

so that $a \approx (C^*/C)^{1/2} \ll 1$ and $\langle n\rangle \approx 1/a \approx (C/C^*)^{1/2} \gg 1$: the distribution tends to be broad with a large average size.

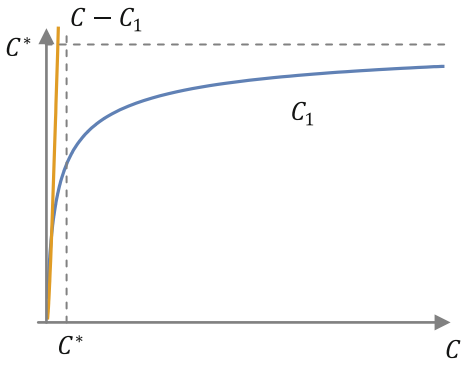

Fig. 7.6 The monomer (C_1) and aggregate concentrations ($C - C_1$) versus total concentration C. As C increase C_1 approaches C^* asymptotically whereas $C - C_1$ becomes dominant

Overall, the size distribution is the outcome of competitions between energy and entropy to minimize the net free energy. **At low concentration, $C < C^*$, many small aggregates tend to form in favor of large entropy. As C increases above C^*, fewer but larger aggregates tend to form to minimize the energy**.

P7.3 *Sketch how the internal energy and entropy change in the equilibrium mixture of the aggregates as the concentration C increases.*

P7.4 *The distribution C_n (7.44) can also be obtained considering the process where an n aggregate becomes an $n+1$-aggregate by adding a monomer $A_n + A_1 \rightarrow A_{n+1}$* (see the figure below). *The law of mass action for this association process assures the conditions for the concentrations,*

$$C_{n+1}/C_n C_1 = e^{-\beta \Delta f_0}$$

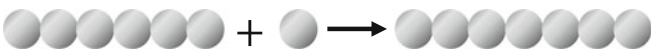

where $\Delta f_0 = (n+1)\mu_{n+1}^0 - \left(n\mu_n^0 + \mu_1^0\right)$ is the intrinsic free energy of association, which is b for the simple linear assembly. Then the solution of the equation $C_{n+1}/C_n C_1 = C^*$ where $C^* = e^{-\beta b}$, is $C_n = C^* e^{-an}$, where $a = \ln(C^*/C_1)$.

7.2.2 Two-Dimensional Disk Formation

The general principle of the chemical force balance given by (7.40) can be extended to the aggregates in various shapes by appropriately determining the key factor Δf_{n0}. Suppose that the monomers assemble to form a two dimensional disk of the n monomers bound among nearest-neighbors at a distance d (Fig. 7.7). In this case

$$\begin{aligned} \Delta f_{n0} &= -n_s b_s - n_r b_r \\ &= -n b_s + n_r \Delta b_r, \end{aligned} \tag{7.51}$$

where n_r is the numbers of the monomers on the rim, $n_s = n - n_r$ is the number of other monomers within the disc, and b_r and b_s are their respective bond energies *per monomer*. nb_s in (7.51) is the surface cohesion energy. $n_r \Delta b_r$ is the line tension (or the energy cost for forming the rim), where $\Delta b_r = b_s - b_r > 0$, because the number of neighboring monomers (coordination number) is larger within the disk than on the rim. The disk of radius R has the area $\pi R^2 = ngd^2$, where g is a geometrical factor such that gd^2 is the area per monomer; if the aggregates form hexagonally packed lattices, $g = 1$. For large enough n the number of bound monomers on the rim is $n_r = 2\pi R/d = 2(\pi g n)^{1/2}$, so

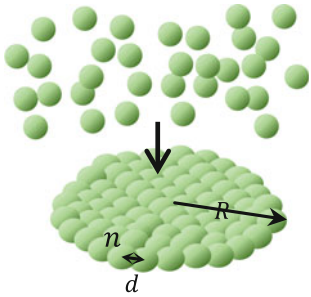

Fig. 7.7 The self-assembly of monomers into a disk

$$\Delta f_{n0} = -b_s n + 2\pi^{1/2}\Delta b_r\, n^{1/2}, \tag{7.52}$$

If $\Delta f_{n0} < 0$, i.e., for $n > n_c = 4\pi g(\Delta b_r/b_s)^2$, the aggregates form in favor of less energy. But this is balanced by the configuration entropy that tends to favor formation of many small aggregates.

We now use (7.40) and (7.52) to obtain the size distribution, for n larger than n_c:

$$C_n = e^{-an-rn^{1/2}}, \tag{7.53}$$

where $a = \ln(C^*/C_1)$, $C^* = e^{-\beta b_s}$, and $r = 2\beta(\pi g)^{1/2}\Delta b_r$. The distribution decays more steeply than exponential. Unless the rim energy is smaller than thermal energy, i.e., unless $r \ll 1$, C_n is negligibly small for all n, that is, there is no size distribution. It is because that the large rim energy cost forbids disks to form. Alternatively, the monomers can condense only into a single large aggregate, whose size N then is given by

$$C = C_1 + Ne^{-aN-rN^{1/2}} \approx Ne^{-aN-rN^{1/2}}. \tag{7.54}$$

This can be indeed realized by increasing C and also C_1 above C^*, so that $a = \ln(C^*/C_1)$ becomes negative. Furthermore, the growing two dimensional aggregates, if they are capable of bending, may undergo shape transition into hollow spheres or capsules as described next.

7.2.3 Hollow Sphere Formation

Two dimensional polymer hollow spheres or capsules of 10–100 nm sizes were recently synthesized by self-assembling pumpkin-looking molecules called cucurbiturils with linker molecules hexagonally at the periphery (Kim et al. 2010), without aid of pre-organized structures or templates. The assemblies, driven by the side-wise covalent bonding between monomers, grow in two dimension. They postulated that monomers first self-assemble to circular disks, which then

spontaneously bend due to thermal fluctuation and grows to a capsule (a hollow sphere) (Fig. 7.8).

In this system, two major kinds of energy compete with each other: cohesive energy, which tends to increase the surface area and bending energy that resists the bending. The number of monomers in the sphere is for the hexagonal assembly $n = (4\pi R^2)/d^2$, where R is the radius of the sphere and d is the distance between two adjacent monomer units in the aggregate. Compared with an unbound monomer, a bound monomer in the aggregate has lower energy $-b_s = -qb/2$ where b is the bond energy per linkage and q is the number of interacting neighbors per monomer called the coordination number. They considered an ideal case in which every monomer in the aggregate is fully bonded (hexagonally in their case) with neighboring monomers, i.e., $q = 6$. The surface cohesive energy is then given by $nb_s = 3b(4\pi R^2)/d^2 = 12\pi bR^2/d^2$. In addition, an energy $8\pi\varkappa_s$ is required to form the sphere, where $\varkappa_s$ is the curvature modulus for sphere (12.20). The total energy change for forming the sphere then is

$$\Delta f_{n0} = -nb_s + 8\pi\varkappa_s. \tag{7.55}$$

which falls below zero for the n larger than the critical values $n_c = 8\pi\varkappa_s/b_s$. The cohesive energy gain dominates over the bending energy cost, driving a hollow sphere of a radius larger than the critical value $R_c = d(2\varkappa_s/b_s)^{1/2}$ to form.

Although the energy dictates a small number of large hollow spheres to form as mentioned above, the entropy favors a large number of small spheres. To determine the optimal equilibrium size distribution of the spheres, we use (7.40) to find the concentration of n-spheres $(n > n_c)$:

$$C_n = {C_1}^n e^{\beta(-nb_s + 8\pi\varkappa_s)} = [C_1/C^*]^n e^{-8\pi\beta\varkappa_s}, \tag{7.56}$$

Let us consider the case in which C is much larger than the critical concentration $C^* = e^{-\beta b_s}$ which C_1 approaches asymptotically. The total monomer concentration is given by

$$\begin{aligned} C &= \sum_{n_c}^{\infty} nC_n \\ &= \frac{n_c y^{n_c - 1} - (n_c - 1)y^{n_c}}{(1-y)^2} e^{-8\pi\beta\varkappa_s} \approx \frac{1}{(1-y)^2} e^{-8\pi\beta\varkappa_s}, \end{aligned} \tag{7.57}$$

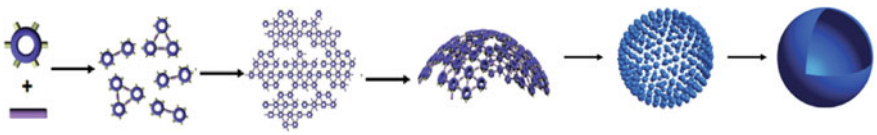

Fig. 7.8 Proposed mechanism of the polymer nanocapsule formation. Adapted with permission from Kim et al. (2007, 2010) conveyed through Copyright Clearance Center, Inc.

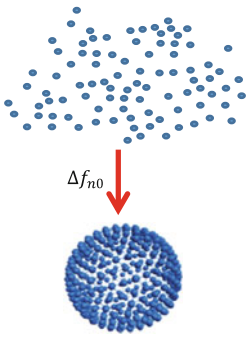

Fig. 7.9 The process of hollow sphere formation from monomers and associated standard free energy change Δf_{n0}

where $y = C_1/C^* \approx 1$. Equation (7.57) yields

$$\frac{C_1}{C^*} \approx \left[1 - \left(Ce^{-8\pi\beta\varkappa_s}\right)^{-1/2}\right], \tag{7.58}$$

which indeed is close to 1 because $8\pi\varkappa_s \gg k_BT$. From (7.56) we have

$$C_n = e^{-an-8\pi\beta\varkappa_s}, \tag{7.59}$$

where

$$a = \ln\left(C^*/C_1\right) \approx \left(Ce^{-8\pi\beta\varkappa_s}\right)^{-1/2}. \tag{7.60}$$

The distribution of the aggregate size is exponentially decaying, with the average size $n \approx 1/a \approx \left(Ce^{-8\pi\beta\varkappa_s}\right)^{1/2}$ that grows like $C^{1/2}$.

To find the radius distribution $P(R)$ of the spheres rather than the concentration C_n, we note that they are related by $P(R) \propto C_n dn/dR$, from which we obtain

$$P(R) = 2\alpha R e^{-\alpha R^2}. \tag{7.61}$$

where we note $n = 4\pi R^2/d^2$, and $\alpha = (4\pi/d^2)(Ce^{-8\pi\beta\varkappa_s})^{-1/2}$. In contrast to $P(n)$, the radius distribution function $P(R)$ is in the form of a weighted Gaussian with the average

$$\langle R\rangle = \int_0^\infty dR\, RP(R) = \frac{1}{4} dC^{1/4} \exp\frac{2\pi\varkappa_s}{k_BT} \sim C^{1/4}. \tag{7.62}$$

Equation (7.62) predicts that the average radius increases as $C^{1/4}$ and depends strongly on the curvature modulus $\varkappa_s$, which can be modulated by solvents. This result is qualitatively in good agreement with the experimental results Fig. 7.10 (Kim et al. 2010).

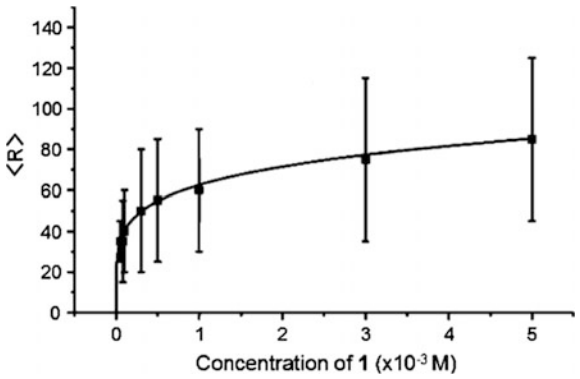

Fig. 7.10 The average size of hollow spheres as a function of the total monomer concentration C, which shows $\langle R \rangle \sim C^{\delta}$. $\delta = 2 \sim 2.5$ Adapted with permission from Kim et al. (2007, 2010) conveyed through Copyright Clearance Center, Inc.

Further Readings and References

G.G. Hammes, *Thermodynamics and Kinetics for Biological Sciences* (Wiley Interscience, 2000)
G.M. Whitesides, B. Grzybowski, Self-assembly at all scales. Science **295**, 2418 (2002)
J. Israelachvili, *Intermolecular and Surface Forces*, 3rd edn. (Academic Press, 2011)
S. Safran, *Statistical Thermodynamics of Surfaces, Interfaces, and Membranes*. Frontiers in Physics (Westview Press, 2003)
D. Kim et al., Direct synthesis of polymer nanocapsules with a noncovalently tailorable surface. Angew. Chem. Int. Ed. **46**, 3471 (2007)
D. Kim, E. Kim, J. Lee, S. Hong, W. Sung, N. Lim, C.G. Park, K. Kim, Direct synthesis of polymer nanocapsules: self-assembly of polymer hollow spheres through irreversible covalent bond formation. J. Am. Chem. Soc. **132**, 9908 (2010)

Chapter 8
The Lattice and Ising Models

As introduced in Chap. 4, the lattice model is a highly coarse-grained model of statistical mechanics for particle systems, with built-in excluded-volume interaction. The model can address the structural and thermodynamic properties on length scales much larger than molecular size. To incorporate the configurational degrees of freedom of many-particle systems, the system is decomposed into identical cells over which the particles are distributed. With the short-range interaction between the adjacent particles included, this seemingly simple model can be usefully extended to a variety of problems such as gas-to liquid transitions, molecular binding on substrates, and mixing and phase separation of binary mixtures. For the particles that are mutually interacting in two and three dimensions, we will introduce the mean field approximations. The lattice model is isomorphic to the Ising model that describes magnetism and paramagnet-to-ferromagnetic transitions. We study the exact solution for the Ising model in one dimension, which is applied to a host of biopolymer properties and the two-state transitions.

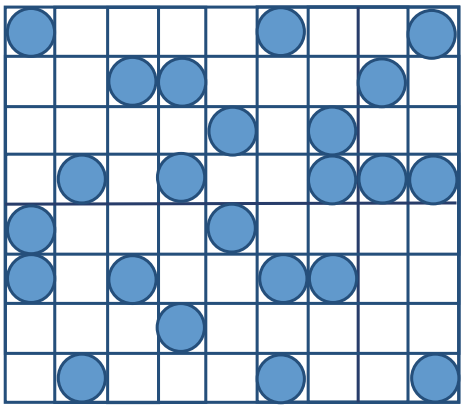

Fig. 8.1 Lattice model. The substrate or volume is decom posed into many cells, each of which either occupies a particle or not

W. Sung, *Statistical Physics for Biological Matter*, Graduate Texts in Physics,
https://doi.org/10.1007/978-94-024-1584-1_8

8.1 Adsorption and Aggregation of Molecules

Adsorption is a process by which molecules bind to a surface from the bulk. Molecular adsorption onto a finite number of binding sites is ubiquitous in nature, and is of particular interest in biology (e.g., ligand binding on receptors, protein binding on DNA). The molecules that adsorb are called **adsorbates** and the surface is called the **adsorbent or substrate**. We are interested in finding **the adsorption isotherm that relates the fraction of adsorbed molecules to the ambient pressure** arising from unabsorbed particles at a given temperature. Considering the single-layer adsorption, we will first study the Langmuir isotherm of the adsorbed molecules that are non-interacting and immobile, then investigate the effects of inter-particle interaction.

8.1.1 The Canonical Ensemble Method

We consider that each of $\boldsymbol{M}$ **distinguishable sites** can bind a molecule. Our system is $\boldsymbol{N}(\leq \boldsymbol{M})$ **identical particles** adsorbed (the adsorbate) with no mutual interactions, in the heat bath at temperature T. Our purpose here is to find the thermal behaviors of the adsorbed particles, the coverage in particular as a function of temperature and ambient pressure of the background.

Given M and N, the system's *canonical partition function* is given by

$$Z(N, M, T) = \frac{M!}{(M-N)!N!} z^N, \tag{8.1}$$

where $M!/\{(M-N)!N!\}$ is the number of ways to distribute N particles among M sites: it is the configurational partition function. z is the partition function of a single adsorbed particle; if only the adsorption on the surface with the energy $-\epsilon$ is included, $z = e^{\beta\epsilon}$. We can incorporate also the particle's internal degrees of freedom by considering that ϵ is a temperature-dependent effective binding energy. Using the Stirling's approximation, the Helmholtz free energy of the adsorbate is

$$\begin{aligned} F(N, M, T) &= -k_B T \ln Z(N, M, T) \\ &= -N\epsilon - k_B T \left\{ M \ln \frac{M}{M-N} + N \ln \frac{M-N}{N} \right\}, \end{aligned} \tag{8.2}$$

the second term of which is the mixing entropy contribution, rewritten as

$$-TS = k_B T M \{\theta \ln \theta + (1-\theta) \ln(1-\theta)\}, \tag{8.3}$$

where $\theta = N/M$ is the coverage.

The chemical potential then is given by

$$\begin{aligned}\mu &= \frac{\partial F}{\partial N} = -\epsilon + k_B T \ln\left(\frac{M}{N} - 1\right) \\ &= -\epsilon + k_B T \ln[\theta/(1-\theta)].\end{aligned} \tag{8.4}$$

Now, note that **the system is at equilibrium with the background**, which is a dilute gas or solution of unbound particles. The background chemical potential,

$$\mu = \mu_0(T) + k_B T \ln\{n/n_0(T)\} = k_B T \ln z, \tag{8.5}$$

thus, is equal to (8.4). n is the density of the unbound particles and z is its fugacity, which are related to the unbound particle pressure by $p = nk_B T = \alpha z$. A temperature-dependent constant $\alpha(T) = n_0(T) k_B T e^{-\beta\mu_0(T)}$ is available from the data at the reference state subscripted by '0'. Using the chemical potential (8.5), we rewrite the coverage in (8.4) as

$$\theta = \frac{1}{e^{-\beta(\epsilon+\mu)} + 1} = \frac{z e^{\beta\epsilon}}{1 + z e^{\beta\epsilon}} = \frac{p}{p + p_0(T)}, \tag{8.6}$$

where $p_0(T) = \alpha(T) e^{-\beta\epsilon}$ is a quantity that is a function of temperature only. This type of coverage behavior, depicted by Figs. (3.8) and (7.3), called the Langmuir adsorption isotherm, has been studied earlier. As the pressure increases indefinitely the coverage approaches unity asymptotically. The pressure at which coverage is 1/2 is $p_0(T)$, which depends on the adsorption energy and on the internal degrees of freedom of the adsorbed particles.

The contribution of the adsorbed particles to surface tension is identified as

$$\begin{aligned}\gamma &= \frac{\partial F}{\partial A} = \frac{\partial F}{a \partial M} \\ &= \frac{k_B T}{a} \ln(1-\theta)\end{aligned} \tag{8.7}$$

where $A = Ma$ is the surface area. **The surface tension acts on the surface in the direction opposite to surface (two-dimensional) pressure, which is the force per unit area to keep the surface from expanding**. In the limit of a very small coverage $\theta \ll 1$, the surface pressure is

$$-\gamma \approx \frac{k_B T}{a}\theta = \frac{N k_B T}{A}, \tag{8.8}$$

which is a two-dimensional version of the ideal gas law. As θ approaches unity, the pressure diverges to infinity due to the excluded-volume effect.

8.1.2 The Grand Canonical Ensemble Method

The adsorbate is in reality an open system that can exchange not only its energy but also the adsorbed particles with the background (Fig. 8.2). One may naturally consider the grand canonical ensemble theory in which the chemical potential is given instead of the adsorbed particle number, which can fluctuate. For a pedagogical reason, we redo the calculation of the earlier section using this theory. The grand canonical partition function of the adsorbate is

$$\begin{aligned} Z_G(\mu, M, T) &= \sum_{\mathcal{N}=0}^{M} e^{\beta \mathcal{N} \mu} Z(\mathcal{N}, M, T) \\ &= \sum_{\mathcal{N}=0}^{M} \frac{M!}{(M-\mathcal{N})!\mathcal{N}!} e^{\beta \mathcal{N}(\epsilon+\mu)}, \end{aligned} \tag{8.9}$$

where $\mathcal{N}$ is the number of the adsorbed particles. Equation (8.9) is just the binomial expansion of

$$Z(\mu, M, T) = \left(1 + e^{\beta(\epsilon+\mu)}\right)^M. \tag{8.10}$$

This could also have been obtained using the Hamiltonian $\mathcal{H} = -\sum_{i=1}^{M} \epsilon n_i$ where n_i is either 1 (the site is occupied) or 0 (the site is empty):

$$\begin{aligned} Z_G(\mu, M, T) &= \sum_{\mathcal{M}} e^{-\beta(\mathcal{H}-\mu\mathcal{N})} = \sum_{n_i=0}^{1} \exp\left(\beta \sum_{i=1}^{M} (\epsilon+\mu) n_i\right) \\ &= \prod_{i=1}^{M} \sum_{n_i=0}^{1} e^{\beta(\epsilon+\mu)n_i} = \left(1 + e^{\beta(\epsilon+\mu)}\right)^M. \end{aligned} \tag{8.11}$$

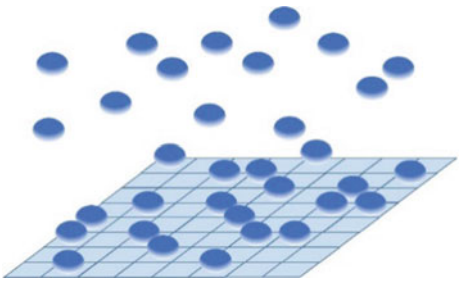

Fig. 8.2 The number of adsorbed particles $\mathcal{N}$ fluctuate in an chemical equilibrium with the background of unbound particles

The natural logarithm of the grand partition function yields its primary thermodynamic potential, that is, the grand potential:

$$\begin{aligned}\Omega(\mu, M, T) &= -k_B T \ln Z_G(\mu, M, T) \\ &= -M k_B T \ln\left(1 + e^{\beta(\epsilon+\mu)}\right).\end{aligned} \tag{8.12}$$

The average number of the adsorbed particles is

$$\begin{aligned}N &= k_B T \frac{\partial}{\partial \mu} \ln Z_G(\mu, M, T) \\ &= -\frac{\partial \Omega}{\partial \mu} = \frac{M}{e^{-\beta(\epsilon+\mu)} + 1},\end{aligned} \tag{8.13}$$

from which we obtain the expression for the coverage:

$$\theta = \frac{N}{M} = \frac{1}{e^{-\beta(\epsilon+\mu)} + 1}.$$

This result is same as that obtained from the canonical theory (8.6) but does not suffer from the approximate nature of the Stirling's formula; this result is valid for the nearly-occupied $(N \approx M)$ as well as nearly-empty $(N \sim 1)$ situations.

P8.1 *Find* $\frac{\overline{\Delta N}}{N}$ *and state the condition where this is indeed negligible.*

All of the other quantities, e.g., the chemical potential, the entropy, and the surface tension can be shown easily to be the same as given in the canonical theory of the earlier section. The grand potential can directly be obtained as

$$\begin{aligned}\Omega &= M k_B T \ln(1 - \theta) \\ &= \gamma A,\end{aligned} \tag{8.14}$$

where the second equality follows from (2.31).

8.1.3 *Effects of the Interactions*

We now include the attraction between the neighboring adsorbed particles. Using occupation number representation, the Hamiltonian is

$$\mathcal{H} = -\sum_{i=1}^{M} \epsilon n_i - \frac{1}{2} \sum_{\langle ij \rangle} b n_i n_j, \tag{8.15}$$

were $\langle ij \rangle$ denotes every pair of particles that mutually attract, and b is the strength of the bond energy. The model can be mapped into the Ising model for ferromagnetism with non-vanishing magnetic field as shown next. For the one-dimensional problem, the exact solution is well known, and will be studied next. For the present problem, which is two-dimensional, the exact solution is not available in general, so an approximation is sought.

To study the effect of the interaction within the canonical ensemble theory, we introduce the **Bragg-Williams approximation**, according to which the internal energy is first approximated by

$$\begin{aligned} E = \langle \mathcal{H} \rangle &\approx -\sum_{i=1}^{M} \epsilon\theta - \frac{1}{2}\sum_{\langle ij \rangle} b\theta^2 \\ &= -M\left(\epsilon\theta + \frac{1}{2}qb\theta^2\right), \end{aligned} \tag{8.16}$$

where q is the coordination number. For the two dimensional cubic lattice (Fig. 8.1), $q = 4$. The approximation may be naturally called the mean field approximation (MFA) in that the fluctuating variable n_i is replaced by its mean $\theta = \langle n_i \rangle = N/M$. Using the mixing entropy given by (8.3),

$$S = -k_B M\{\theta \ln\theta + (1-\theta)\ln(1-\theta)\},$$

the free energy is given by

$$\begin{aligned} F(\theta, M, T) &= E - TS \\ &= M\left[-\epsilon\theta - \frac{1}{2}qb\theta^2 + k_B T\{\theta \ln\theta + (1-\theta)\ln(1-\theta)\}\right], \end{aligned} \tag{8.17}$$

from which we can obtain the chemical potential

$$\mu = \frac{\partial F\left(\frac{N}{M}, M, T\right)}{\partial N} = \frac{\partial F(\theta, M, T)}{M\partial\theta} = -\epsilon - qb\theta + k_B T \ln(\theta/(1-\theta)), \tag{8.18}$$

leading to the coverage

$$\theta = \frac{1}{\{e^{\beta(-\epsilon - qb\theta - \mu)} + 1\}}. \tag{8.19}$$

In the absence of the bond energy b, (8.18) and (8.19) are identical to (8.4) and (8.6). The solution of (8.19) for the coverage θ in terms of T can be obtained numerically or using a graphical method.

Because **an adsorbed particle is in chemical equilibrium with an unbound particle** in the background, the fugacity $z \equiv e^{\beta\mu}$ of the absorbent is set to be identical to that of the ambient gas of unbound particles, which is $\alpha^{-1}p$ (p = ambient pressure). Then (8.19) becomes

$$\theta = \frac{p}{p + p_0(T, \theta)}, \tag{8.20}$$

where

$$p_0(T, \theta) = \alpha \exp[-\beta(\epsilon + qb\theta)] \tag{8.21}$$

is reduced by the factor $e^{-\beta qb\theta}$ from that in the Langmuir isotherm (the case with $b = 0$), and thus the adsorption is enhanced due to the mutual interaction, as will be further detailed below.

Figure 8.3 depicts the coverage θ as a function of p for various values of $q\beta b$. As $q\beta b$ increases, the adsorption isotherm deviates significantly from the Langmuir isotherm ($q\beta b = 0$). Considering for an example the case with $\beta\epsilon = 1$, the coverage rises dramatically as $q\beta b$ increases (Fig. 8.3). This is the cooperate effect of the attractive interaction on the adsorption, which we studied earlier in ligand binding (Chap. 3).

Above a certain critical value of $q\beta b$, the curve develops a wiggle (dashed line). This indicates the presences of a thermodynamically unstable region in which $\partial\theta/\partial p < 0$, i.e., the coverage decreases as ambient pressure increases. This phenomenon is an artifact of the mean field approximation that we used. What is observed in experiment is **the vertical line that bisects the wiggle**; it occurs at $q\beta b = 4.8$ in the theory, as shown in Fig. 8.3. Along the line the adsorbate undergoes **abrupt phase transition from a dispersed phase with θ_1 to a condensed phase with θ_2 at a constant pressure**.

8.1.4 Transition Between Dispersed and Condensed Phases

Now we consider the detail of the critical condition for the transition by focusing on the case with $\epsilon = 0$. For $q\beta b$ above the critical value the $\theta - p$ curve yet develops a wiggle. The critical point is the inflection point where $dp/d\theta = 0 = p(1/\theta(1-\theta) - q\beta b), d^2p/d\theta^2 = 0 = p(2\theta - 1)/[\theta(1-\theta)]^2$, i.e., *via* (8.20) and (8.21)

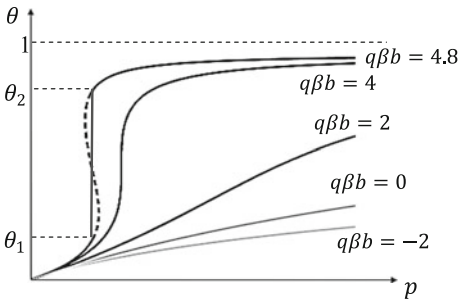

Fig. 8.3 The adsorption isotherm of particles with bond strength b and coordination number q, for the surface binding energy $\epsilon = k_B T$. θ is the coverage and p is the ambient pressure

$$\theta = 1/2; \text{ and } q\beta b = 4, \text{ leading to } p = \alpha e^{-2}. \tag{8.22}$$

At T lower than the critical temperature $T_c = qb/(4k_B)$, (or for an attraction strength qb higher than $qb_c = 4k_BT$), and simultaneously at an ambient pressure lower than $p_c = \alpha e^{-2}$, the condensation to an aggregate occurs with a discontinuous jump in the coverage θ.

P8.2 *If the molecules adsorb on surface with the binding energy ϵ, how much is the coverage affected? Consider that the b has a strength of the covalent bonding and θ is nearly 1.*

The vertical isotherm in the $\theta - p$ diagram is obtained by a semi-empirical scheme called the Maxwell construction as in the $\gamma - \theta$ phase diagram given below. The surface tension γ is obtained by

$$\begin{aligned}\gamma &= \frac{\partial F(N/M, M, T)}{a\partial M} = \frac{f(\theta, T)}{a} + M\frac{\partial f(\theta, T)}{a\partial\theta}\frac{\partial\theta}{\partial M} \\ &= \frac{1}{a}\{f(\theta, T) - \mu\theta\} \\ &= \frac{k_BT}{a}\ln(1-\theta) + \frac{q}{2a}b\theta^2,\end{aligned} \tag{8.23}$$

where $f(\theta, T) = F(\theta, M, T)/M = -qb\theta^2/2 + k_BT\{\theta \ln\theta + (1-\theta)\ \ln(1-\theta)\}$ is the Helmholtz free energy per site and the relation $\theta = N/M$ should be noted in taking the derivative with respect to M.

The value $-\gamma$ is the surface pressure, which should not be confused with the three-dimensional ambient pressure p. The value of $-\gamma$ is depicted as a function of θ at a given temperature (Fig. 8.4). For small bond strength qb, $-\gamma$ increases monotonically with θ as it does in the absence of the interaction. As the bond strength increases above the critical value $qb = 4k_BT$ already mentioned, the pressure decreases with θ due to attraction. As θ increases further to approach unity, the surface pressure $-\gamma$ rises sharply due to the excluded-volume effect. Consequently there is a portion (dashed line) where $-\partial\gamma/\partial\theta$ is negative. Since θ decreases as the pressure $(-\gamma)$ rises, this is the **thermodynamically unstable portion**. This trend is an artifact of the MFA as mentioned earlier. To remedy this, a straight line is constructed from a point 1 corresponding to the disperse phase to the point 2 corresponding to the condensed phase.

The straight line is determined as follows. Along the curve at a fixed temperature T, $d\mu = -ad\gamma/\theta$, (see (2.25) with $A/N = a/\theta, f = \gamma$), which, upon integration from point 1 to 2, becomes $\mu(2) - \mu(1)$ that is zero for the phase equilibrium. Because the integral sweeps an area along the $\gamma - \theta$ curve, the straight line should be chosen to bisect the wiggle into two **equal areas** $(\mathcal{A}_1 = \mathcal{A}_2)$; this is the **Maxwell construction** of explaining the gas-liquid phase transition from the van der Waals equation of state, which stems from the same mean-field theory. Along the straight line (i.e., at

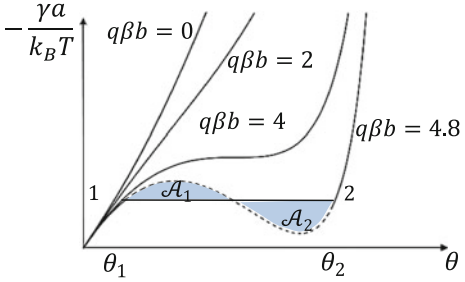

Fig. 8.4 The two dimensional pressure $-\gamma$ versus coverage θ for various bond strength b, with surface binding energy $\epsilon = 0$. The straight isotherm is the dispersed **a** and condensed phase **b** coexistence line drawn by the Maxwell construction of the equal areas $(\mathcal{A}_1 = \mathcal{A}_2)$

constant pressure), the condensed (liquid) phase (γ_2, θ_2) coexists with the dispersed (gas) phase (γ_1, θ_1) in a **phase-separated state**.

The critical condition of the transition is given by the inflection point at which $d\gamma/d\theta = -(1-\theta)^{-1} + qb\theta/a = 0$ and $d^2\gamma/\left(d\theta^2\right) = -(1-\theta)^{-2} + qb/a = 0$. These lead to just the conditions (8.22), $\theta = 1/2$ and $q\beta b = 4$. When $qb > k_B T/4$ with T fixed, (or when $T < T_c = qb/(4k_B)$ with b fixed), and when $-\gamma$ is lower than the critical pressure $-\gamma_c = qb/\{4a(\ln 2 - 1/2)\}$, the condensation can occur leading to the aggregates of much higher coverage.

P8.3 *What is the value of constant pressure p that represents the vertical line in Fig.* 8.3?

The theoretical results given here can also be applied to adsorption and condensation phenomena in one and three dimensions. The MFA, which is better in higher dimension, can be quite poor in one dimension, where no phase transition occurs at a finite temperature, contrary to the MFA prediction.

8.2 Binary Mixtures

8.2.1 Mixing and Phase Separation

The lattice model can be adapted to binary mixtures of liquids, colloids, polymers, as well as lipid mixtures in membranes and non-membrane-bound liquid drops within cells (Anthony et al. 2014). We consider an **incompressible mixture** in which every cell is occupied by a particle of either species A or species B, so that the total number of molecules $N = N_A + N_B = M$ is fixed. The occupation number n_i is 0 when the cell i is occupied by a particle of species A and is 1 when it is occupied by a particle of species B. Only particles in the nearest neighborhood interact, with bond energies $b_{AA}, b_{BB}, b_{AB} = b_{BA}$, for $A-A$, $B-B$, and $A-B$ pairs respectively. The Hamiltonian can be written as

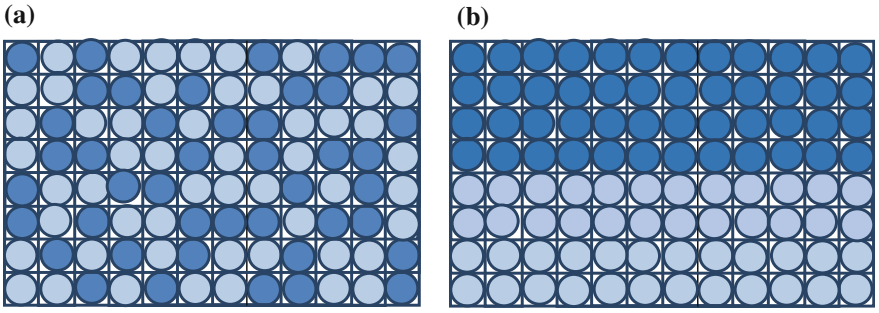

Fig. 8.5 **a** Random mixing and **b** phase separation of particles in a completely-filled lattice

$$\mathcal{H} = -\frac{1}{2}\sum_{\langle ij\rangle}[b_{AA}(1-n_i)\big(1-n_j\big) + b_{BB}n_in_j + b_{AB}(1-n_i)n_j + b_{AB}n_i\big(1-n_j\big)], \tag{8.24}$$

where the sum is over all $qN/2$ nearest neighbor pairs, and q is the coordination number. Then the Hamiltonian can be rewritten as

$$\mathcal{H} = \frac{1}{2}\sum_{\langle ij\rangle} b(1-n_i)n_j + \sum_i hn_i + C, \tag{8.25}$$

where $b = b_{AA} + b_{BB} - 2b_{AB}$, $h = q(b_{AA} - b_{BB})/2$ chosen to be negative, and C is the (trivial) constant energy that the mixture would have if the particles were identical.

We use the mean field approximation as in the earlier section. Replacing n_i in the Hamiltonian by the relative coverage of species B

$$\theta = \frac{\left\langle \sum_i^M n_i \right\rangle}{N} = \frac{N_B}{N}, \tag{8.26}$$

the internal energy then is approximated as

$$E = N\left[\frac{1}{2}qb(1-\theta)\theta + h\theta\right]. \tag{8.27}$$

Adding to this the contribution from the mixing entropy yields the Helmholtz free energy

$$\begin{aligned} F &= E - TS \\ &= N\left[\frac{qb}{2}\theta(1-\theta) + h\theta + k_BT\{\theta\ \ln\ \theta + (1-\theta)\ \ln\,(1-\theta)\}\right]. \end{aligned} \tag{8.28}$$

The entropy alone will favor mixing into one homogeneous phase, because the contribution $-TS$ of entropy to the free energy is negative. If b is negative so that the internal energy is also negative, the free energy is negative for all T and the entire composition range. This means that the system is stable as a homogeneous mixture and, for the symmetric mixture where $b_{AA} = b_{BB}$, has the minimum at $\theta = 1/2$ (Fig. 8.6a) indicative of complete miscibility.

If b is positive, the energy which now can be positive, compete with the mixing entropy. For βqb below a critical value, which is $\beta qb = 4$ in a symmetric mixture (show this), the entropy dominates the energy to retain a single minimum in the free energy landscape. At a large value of βqb above the critical value, the repulsion becomes so dominant that the free energy landscape exhibits two minima at $\theta = \theta_1$ and $\theta = \theta_2$ (Fig. 8.6b). The curve (dashed line) between these two minima are concave, signaling that the homogeneous phase mixture is unstable with respect to formation of A-rich phase with $\theta = \theta_1$ and B-rich phase with $\theta = \theta_2$. For a mixture of given qb, such **two-phase separation occurs for $T < T_c = qJ/(4k_B)$, that is, by quenching the system below the critical temperature T_c.**

The condition of the two separate phases at equilibrium is set by the equality of the chemical potential of each species, $\mu_A(\theta_1) = \mu_A(\theta_2)$, $\mu_B(\theta_1) = \mu_B(\theta_2)$. Then the tangent $\partial F/N\partial\theta = \mu$ (called the relative chemical potential), which, by noting $N_A + N_B = N$, is equal to $\partial F(N_A, N_B)/\partial N_B = \mu_B - \mu_A$, should be the same at θ_1 and θ_2, namely, the curve has a common tangent line (Fig. 8.6b), whose slope is zero for a symmetric mixture ($\mu_B = \mu_A$). The common tangent line, which indicates the lower free energy than the concave curve, represents the true free energy for $\theta_1 < \theta < \theta_2$; the free energy now is given linearly in θ,

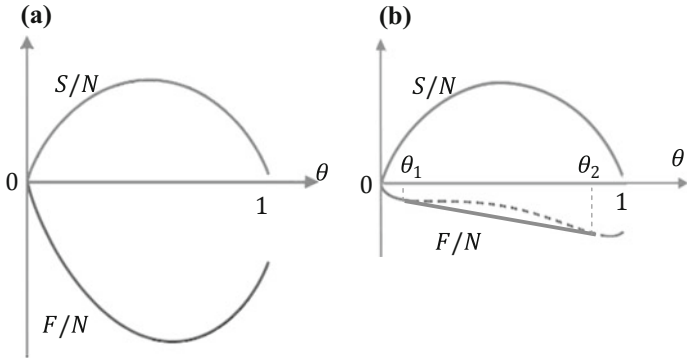

Fig. 8.6 **a** The entropy (*S/N*) and free energy (*F/N*) per particle versus the coverage θ of the B particles, for the case $b < 0$, **b** the same for $b > 0$. In this case the free energy landscape has two minima interconnected by a straight line that describes the phase-separation

$$\begin{aligned} F &= N\mu(\theta_1)\theta + F_A = N\mu(\theta_1)(\theta - 1) + F_B \\ &= (F_B - F_A)\theta + F_A, \end{aligned} \tag{8.29}$$

where F_A and F_B are the free energies of single components A and B, respectively. Evidently (8.29) is the lever rule in which **the two phases coexist in a phase-separated state** for $\theta_1 < \theta < \theta_2$ (Fig. 8.6b).

P8.4 *Explain why oil and water do not mix unless one component is dilute.*

P8.5 *Find the critical conditions for* qb *and* θ *to form the phase separation for an asymmetric mixture* $(h \neq 0)$ *at a constant temperature* T.

For $\theta < \theta_1$ or $\theta > \theta_2$, we have the relative chemical potential,

$$\mu = \frac{\partial F}{N\partial\theta} = \frac{1}{2}qb(1 - 2\theta) + h\theta + k_B T \ln\left(\frac{\theta}{1-\theta}\right),$$

from which one obtains

$$\theta = \frac{1}{1 + \exp[-\beta\{\mu - h\theta + qb(\theta - 1/2)\}]}. \tag{8.30}$$

For the symmetric $(h = 0,\ \mu = 0)$ and immiscible $(b > 0)$ cases in which component B is very dilute, $\theta \ll 1$, we have

$$\theta = e^{-qb/(2k_B T)}. \tag{8.31}$$

This is the equilibrium constant for exchanging a A molecule and a B molecule both of which are in their pure media.

8.2.2 Interfaces and Interfacial Surface Tensions

In the case where the repulsive energy between two different species predominates over the entropy of mixing, two phases well separate forming domain boundaries or interfaces as shown in Fig. 8.5b. If there are n molecules of species A and B each at the two dimensional interface, $N_A - n$ and $N_B - n$ molecules are within the three dimensional bulk phases of A and B. The interfacial surface tension, which is the free energy derivative with respect to the change of the surface area, is given as follows. Since each phase are ordered, their entropies are zero, while the internal energy is

$$E = -\frac{q}{2}\{(N_A - n)b_{AA} + (N_B - n)b_{BB}\} - n\left\{\frac{q-1}{2}(b_{AA} + b_{BB}) + b_{AB}\right\}, \quad (8.32)$$

where the first term is from the bulk and the second from the interface.

The surface tension is given by

$$\begin{aligned}\gamma &= \left(\frac{\partial F}{\partial A}\right) = \frac{\partial E}{a\partial n} \\ &= \frac{1}{a}\{(b_{AA} + b_{BB})/2 - b_{AB}\} = \frac{b}{2a},\end{aligned} \quad (8.33)$$

where $A = na$ is the total area of the interface and a is the area per site. The surface tension, which is positive for this case, describes the energy of transferring a molecule from the two bulk media into the interface. For the surface of a pure media composed of A molecules in contact with the vacuum or a gas, one may apply (8.33) to find the surface tension; with $b_{BB} = 0 = b_{AB}$, it yields

$$\gamma = b_{AA}/(2a). \quad (8.34)$$

These results can be adapted to line tension of a domain in two dimensions, with a interpreted as the size of a molecule.

8.3 1-D Ising Model and Applications

The Ising model is a remarkably simple model to describe phase transitions and cooperative phenomena, and has numerous applications. The one-dimensional Ising model, in particular, represents one of few exactly solvable models in statistical mechanics. Its partition function not only provides the exact thermodynamic and correlational behaviors in magnets but also is applicable to a multitude of linear chains in which each unit has two internal states. For this reason, we study the exact solution of the Ising model in detail.

8.3.1 Exact Solution of 1-D Ising Model

Consider a linear chain with N spins, where each site i can assume two possible states $\sigma_i = +1, -1$ for the spin up and down (Fig. 8.7). A particular configuration or microstate of the lattice is specified by the set of variables $\{\sigma_1, \sigma_2 \ldots \sigma_N\}$ for all lattice sites.

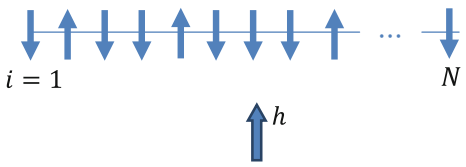

Fig. 8.7 The ising model in one-dimension N spins are subject to a magnetic field proportional to h

The Hamiltonian is

$$\mathcal{H} = -J\sum_{i=1}^{N}\sigma_i\sigma_{i+1} - h\sum_{i=1}^{N}\sigma_i. \tag{8.35}$$

where J is the nearest neighbor coupling constant and h is proportional to an external magnetic field. With the correspondence $\sigma_i = 2n_i - 1$ where $n_i = 1$ and 0 for spin up and down, and $J = b/4$, the Ising model is isomorphic to the lattice model (8.15). Consider that N is large enough to neglect the end effects so that we are free to use the periodic boundary condition, $\sigma_1 = \sigma_{N+1.}$ The Hamiltonian is rewritten as

$$\mathcal{H} = \sum_{i=1}^{N}\mathcal{H}_{i,i+1}, \tag{8.36}$$

where

$$\mathcal{H}_{i,i+1} = -J\sigma_i\sigma_{i+1} - \frac{h}{2}(\sigma_i + \sigma_{i+1}). \tag{8.37}$$

Then the partition function is given by

$$\begin{aligned} Z &= \sum_{\sigma_1=\pm1} e^{-\beta\mathcal{H}_{1,2}} \cdots \sum_{\sigma_N=\pm1} e^{-\beta\mathcal{H}_{N,N+1}} \\ &= \sum_{\{\sigma_i=\pm1\}} \langle\sigma_1|P|\sigma_2\rangle\langle\sigma_2|P|\sigma_3\rangle \ldots \langle\sigma_{N-1}|P|\sigma_N\rangle\langle\sigma_N|P|\sigma_{N+1}\rangle, \end{aligned} \tag{8.38}$$

where

$$P = \begin{pmatrix} e^{\beta(J+h)} & e^{-\beta J} \\ e^{-\beta J} & e^{\beta(J-h)} \end{pmatrix} \tag{8.39}$$

is a **transfer matrix**. The partition function is then written as

$$Z = \sum_{\sigma_1=\pm1} \langle\sigma_1|\boldsymbol{P}^N|\sigma_1\rangle = Tr\,\boldsymbol{P}^N. \tag{8.40}$$

The traced (Tr) quantities are invariant under a transformation of the basis; in the basis $\boldsymbol{P}$ is diagonal (8.40) can be expressed in terms of the two eigenvalues $\lambda_{\pm}$ of $\boldsymbol{P}$ with $\lambda_{+} > \lambda_{-}$:

$$\begin{aligned} Z &= \lambda_{+}^{N} + \lambda_{-}^{N} \\ &= \lambda_{+}^{N}\left(1 + \left(\frac{\lambda_{-}}{\lambda_{+}}\right)^{N}\right) \approx \lambda_{+}^{N}, \end{aligned} \tag{8.41}$$

where the last can be an excellent approximation provided that N is very large. The eigenvalues are obtained by the secular determinant $|\boldsymbol{P} - \lambda \boldsymbol{I}| = 0$:

$$\lambda_{\pm} = e^{\beta J}\left\{\cosh \beta h \pm \left(\sinh^2 \beta h + e^{-4\beta J}\right)^{1/2}\right\}. \tag{8.42}$$

The free energy then is

$$\begin{aligned} F &= -k_B T \ln Z \\ &= -N k_B T \ln\left[e^{\beta J}\left\{\cosh \beta h + \left(\sinh^2 \beta h + e^{-4\beta J}\right)^{1/2}\right\}\right]. \end{aligned} \tag{8.43}$$

The **average magnetization** per site is proportional to

$$\begin{aligned} m = \sigma &= -\frac{\partial F}{N \partial h} \\ &= \frac{\sinh \beta h}{\left(\sinh^2 \beta h + e^{-4\beta J}\right)^{1/2}}, \end{aligned} \tag{8.44}$$

In the absence of an external field $(h = 0)$, $m = 0$, i.e., spontaneous magnetization does not occur at any finite temperature, i.e., no ferromagnetic phase transition occurs in one dimensional spin systems. The reason is that the entropy associated with randomizing the spins dominates over the internal energy associated with aligning the spins at any temperature. This domination occurs because the number of nearest neighbors is too small to enable formation of a sufficient number of attractive pairs in one dimension. However, in higher dimensions, the number of nearest neighbor attractions is large enough to induce ferromagnetic transition. As temperature approaches zero, $\sinh \beta h \gg e^{-2\beta J}, F = -NJ$, and $m = \pm 1$; this result suggests that ferromagnetic transition to perfectly aligned spins occurs only at $T = 0$. At a finite temperature, this perfect alignment occurs only when h is very high.

Let us turn our attention to **the correlation function**

$$C(n) = \langle \sigma_1 \sigma_{n+1} \rangle - \langle \sigma_1 \rangle \langle \sigma_{n+1} \rangle. \tag{8.45}$$

When $h = 0$ this equation can be written as

$$\begin{aligned} C(n) &= \langle \sigma_1 \sigma_{n+1} \rangle \\ &= \frac{1}{Z_N(J)} \sum_{\{\sigma_i = \pm 1\}} (\sigma_1 \sigma_2)(\sigma_2 \sigma_3) \cdots (\sigma_n \sigma_{n+1}) \exp(\beta J_i \sigma_i \sigma_{i+1}) \\ &= \frac{1}{Z_N(J) \beta^n} \left[\frac{\partial^n Z_N(J_1 \cdots J_{n+1})}{\partial J_1 \cdots \partial J_{n+1}} \right]_{J_i = J}, \end{aligned} \tag{8.46}$$

where

$$Z_N(J_1 \cdots J_{n+1}) = \sum_{\{\sigma_i = \pm 1\}} \exp(\beta J_i \sigma_i \sigma_{i+1}) = 2^N \cosh \beta J_1 \cdots \cosh \beta J_N. \tag{8.47}$$

One can derive

$$\begin{aligned} C(n) &= (\tanh \beta J)^n \\ &= e^{-n/\xi}, \end{aligned} \tag{8.48}$$

where ξ is **the correlation length** given by

$$\xi = -[\ln(\tanh \beta J)]^{-1}. \tag{8.49}$$

Because $\tanh \beta J < 1$, the correlation length is positive. As T approaches zero the correlation length diverges like

$$\xi = \frac{1}{2} e^{\beta J}. \tag{8.50}$$

If $J \gg k_B T$, the orientations of the spins are correlated over a long distance.

8.3.2 DNA Melting and Bubbles

The 1-D Ising model can be applied to various problems of linear biopolymers composed of interacting subunits each with two states. One primary example is the problem of molecular binding on polymer which we discussed in an earlier section. As other prominent examples we consider two similar problems of biopolymer conformational transitions: local and global melting of double stranded DNA (Fig. 8.8a), and the helix-to-coil transition (Fig. 8.8b).

Two single strands of a DNA molecule are bound into a double-helix structure by hydrogen-bonding and stacking interactions along complementary base-pairs

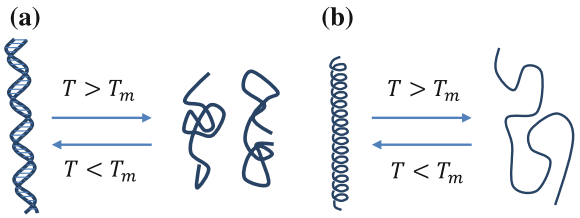

Fig. 8.8 **a** A double stranded DNA fragment can denature (melt) into two single stranded DNA fragments above a melting temperature T_m, **b** a single biopolymer helix can transform to a coil above T_m

(bp). The thermal excitation can induce **global denaturation or melting**, namely, complete separation into the two single stranded DNA, above the melting temperature (T_m) of about 350 K. This arises from **competition between entropically favorable single-strand (ss) state and energetically favorable double-strand (ds) state**. For a process to occur spontaneously the associated free energy change $\Delta F = \Delta E - T\Delta S$ should be negative. For $T > T_m$, the denaturation proceeds as the entropy gain $T\Delta S > 0$ dominates over the energy change $\Delta E > 0$, to render a decrease of the free energy. However, when $T < T_m$, ds state is retained because for the binding process the energy change $\Delta E < 0$ dominates over the entropy decrease $T\Delta S < 0$.

Even below the melting temperature, due to ubiquitous thermal fluctuation, a local opening of the duplex structure, called a **bubble**, can occur (Fig. 8.9), as a precursor to melting. But the bubbles in an unconstrained dsDNA occur rarely at body temperature $T \cong 310^{\circ}$K because **it costs the energy much higher than $k_B T$ to initiate a base pair (bp) opening.** Real DNA has heterogeneous sequences with A-T and G-C bp bounded by two and three hydrogen bonds respectively, so the bubble formation is more likely to occur in an A-T rich region.

We can adopt the Ising model to study the conditions of local and global denaturation in sequence-homogeneous DNA. Symbols $\sigma_i = +1, -1$ represent the bound and unbound bp states respectively (Fig. 8.9). To get some idea of the energy parameters involved, consider a bubble domain consisting of l open bps that starts from a junction at site $i = k$ and terminates at $i = k + l + 1$ (Fig. 8.9). Because $\sigma_i \sigma_{i+1}$ are -1 at $i = k$ and $i = k + l$, and those for the other nearest neighbors are 1, the energy required to form a bubble of size l from a completely closed duplex is

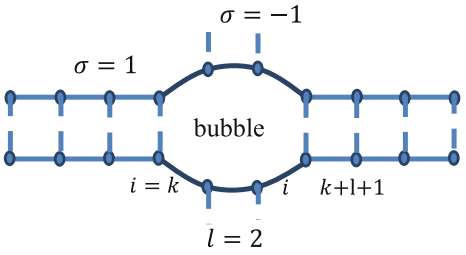

Fig. 8.9 A schematic figure of the unbound base pairs nucleated into a bubble of the size l

$$\mathcal{E}_l = 4J + l(2h) \quad \text{for } l \geq 1. \tag{8.51}$$

Here $2h$ is identified as the bp binding energy per pair, and $4J$ is the energy to initiate the bubble opening. The values of the parameters reflect the thermal undulations of the chain that are not incorporated by the two state variables and therefore depend on temperature. We take $J \sim 3k_BT, h \sim 0.2k_BT$, at $T = 310^\circ$K which we will consider from now on (Palmeri et al. 2008).

The average number of open base pairs is obtained as

$$N_o = \frac{1}{2}\sum_{i=1}^{N}(1 - \langle\sigma_i\rangle) = \frac{1}{2}N(1 - \langle\sigma\rangle), \tag{8.52}$$

where the latter equality holds for a homogeneously-sequenced DNA, the case which we will consider. Using the result for $\langle\sigma\rangle$ above we find the **fraction of open bps**:

$$\begin{aligned}\theta_o = \frac{N_o}{N} &= \frac{1}{2}\left[1 - \frac{\sinh\beta h}{\left(\sinh^2\beta h + e^{-4\beta J}\right)^{1/2}}\right] \\ &\approx e^{-4\beta J}/\left(4\sinh^2\beta h\right),\end{aligned} \tag{8.53}$$

where in the second line we use the approximation $\sinh^2\beta h \gg e^{-4\beta J}$ at $T = 310$K. Equation (8.53) shows that θ_o sensitively depends on J. For the values of the parameters mentioned above, we have

$$\theta_o \sim 4 \times 10^{-4}, \tag{8.54}$$

which is very small, meaning that the duplex structure is quite stable under physiological conditions. This stability is due to the relatively large value of the bubble initiation energy $4J$, which originates from stiff stacking interaction. If J were to be zero, θ_o would approach the simple result for the non-interacting two state model (3.15)

$$\theta_o = 1/\left(1 + e^{2\beta h}\right) \sim 1/2. \tag{8.55}$$

This means that the double strand stability is disrupted in the absence of the stacking interaction.

The average number of the bubbles N_b is given by

$$N_b = \frac{1}{2}\sum_{i=1}^{N}(1 - \langle\sigma_i\sigma_{i+1}\rangle), \tag{8.56}$$

because $\sigma_i\sigma_{i+1} = -1$ at the junctions between bound and unbound bps. By noting

$$\sum_{i=1}^{N}\langle\sigma_i\sigma_{i+1}\rangle = \frac{\partial}{\beta\partial J}\ln Z, \tag{8.57}$$

we can obtain

$$N_b = \frac{Ne^{-4\beta J}\left(\sinh^2\beta h + e^{-4\beta J}\right)^{-1/2}}{\cosh\beta h + \left(\sinh^2\beta h + e^{-4\beta J}\right)^{1/2}}. \tag{8.58}$$

Under physiological conditions, the fraction of the bubble domains is

$$\theta_b = N_b/N \approx e^{-\beta(4J+h)}/\sinh\beta h. \tag{8.59}$$

This is also a very small quantity, so only for a DNA fragment longer than $N \approx \sinh\beta h/e^{-\beta(4J+h)}$, the average number of bubbles is appreciable. If $J = 0$, then (8.58) yields

$$\theta_b = \frac{1}{2\cosh^2\beta h}. \tag{8.60}$$

P8.6 *Calculate the bp correlation function for dsDNA at body temperature* $T = 310^{\circ}K$. *Find the correlation length.*

P8.7 *Show that the probability of forming a single bubble of size n in a homogeneous DNA is much higher than that of forming two separate bubbles of the same total size, say, sizes* $n - m$ *and m for each.*

8.3.3 Zipper Model for DNA Melting and Helix-to Coil Transitions

Because the bubble initiation energy $4J$ is much larger than the base pairing energy $2h$ in dsDNA, **an open bp, once formed, persists to grow rather than multiple open bps emerge separately**. This is the cooperative effect arising from the chain connectivity. Therefore, for short DNAs, open bps tend to exist only within a bubble domain (Lee and Sung 2012). This **single-domain model, called the Zipper model**, provides a more direct way to calculate the average size of the bubble and to assess the transition to global denaturation, because we consider the bubble size l instead of $\{\sigma_1\sigma_2\cdots\sigma_N\}$, as the relevant degree of freedom. Using the effective Hamiltonian of the bubble, $\mathcal{E}_l = 4J + l(2h)$ (8.51), the partition function is given by

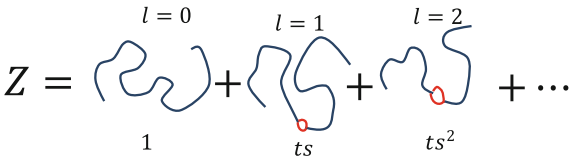

Fig. 8.10 Diagrammatic representation of the partition function for DNA denaturation with bubbles of size l

$$Z = 1 + \sum_{l=1}^{N-2} w_l e^{-\beta \mathcal{E}_l}, \tag{8.61}$$

where the first term '1' represents the case in which bubbles are absent (Fig. 8.10). The multiplicity w_l is the number of ways to place the bubble of size l within $N-2$ sites:

$$w_l = N - 1 - l. \tag{8.62}$$

Introducing parameters $s = e^{-2\beta h}$, and $t = e^{-4\beta J}$, one can find the partition function:

$$Z = 1 + \sum_{l=1}^{N-2} (N-1-l) t s^l = 1 + \frac{ts}{(s-1)^2}\left\{s^{N-1} - (N-1)s + N - 2\right\}. \tag{8.63}$$

The fraction of the open bps in a chain is given as

$$\begin{aligned} \theta_o &= \frac{\langle l \rangle}{N-2} = \frac{\sum_{l=1}^{N-2} l(N-1-l) t s^l}{(N-2)Z} = \frac{s}{(N-2)Z}\frac{\partial Z}{\partial s} \\ &= \frac{ts(s-1)^{-3}[(N-2)s^N - Ns^{N-1} + Ns - (N-2)]}{(N-2)\left\{1 + ts(s-1)^{-2}[s^{N-1} - (N-1)s + N - 2]\right\}} \end{aligned} \tag{8.64}$$

The Zipper model can be applied to a variety of two-state transitions in biopolymers when the transition factor s and the initiation factor t are available. In addition to DNA melting, **helix-coil transition**, which may be also called helix-melting, is a famous example. The α-helix is the most common secondary structure found in globular proteins, where the polypeptide is twisted by hydrogen bonds between the residues. As temperature increases, a helical structure undergoes a transition into a random coil conformation, akin to DNA melting. The conformational state of chain is described by two states for each residue, either helical state or coiled state. The free energy change associated with the helix melting is $2h$, while the energy cost to initiate a coiled residue from a helical one is $4J$.

Figure 8.11a depicts how θ_o, the fraction of the open bp or coiled residues, calculated from (8.64), varies with s for values of the parameter t. If $t = 1$, there is no nearest-neighbor coupling ($J = 0$), so θ_o increases slowly with s following $\theta_o = s/(s+1)$ as in (3.15). If $t \ll 1$, θ_o is negligibly small for $s < 1$, but rises abruptly to

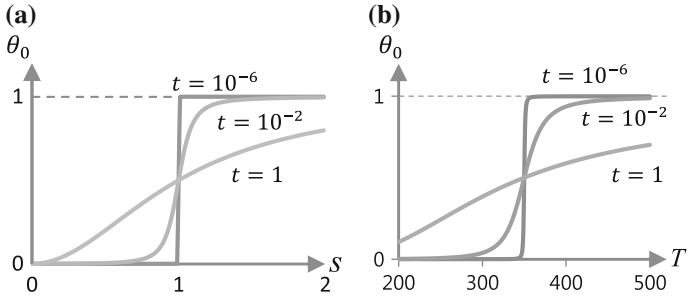

Fig. 8.11 The melting curves, the fraction of the melt regions θ_o **versus** $s = e^{-2\beta h}$ and θ_o **versus** T for various values of $t = e^{-4\beta J}$.

1/2 and eventually to 1 as s approaches 1. The figure is indistinguishable from that obtained using the exact Ising model result, the first equation in (8.53), attesting the validity of the single domain approximation. **The sharp melting transition for very small t is due to cooperative effect of the interaction with the strength $J \geq k_B T$**, but is not a phase transition, which only occurs at $T = 0$ in one-dimensional systems, as shown by the $1D$ Ising model. The inflection point $s = 1$, $\theta_o = 1/2$ is the melting point.

In order to find the melting curve θ_o directly as a function of T, we must consider the physical nature of h explicitly, its temperature dependence in particular. To do so, we exploit the fact that $2h$ is the free energy (Helmholtz or Gibbs) of breaking a bp or a helix, written as $2h = \Delta e_0 - T\Delta s_0$. The quantity has two contributions: an energetic (or enthalpic) one Δe_0, and an entropy gain Δs_0 that are associated with the unbinding of a double strand or a helix into two single-stranded chains or a coiled residue; the latter are relatively flexible, so have more entropies. At the melting point, $h = 0$, so $2h = \Delta e_0(1 - T/T_m)$ where $T_m = \Delta e_0/\Delta s_0$ is the melting temperature. With this input, we calculate (8.64) and construct the $\theta_o - T$ melting curve as Fig. 8.11b.

Furthermore, one can find

$$\frac{d \ln s}{dT} = -\frac{d\{\beta(\Delta e_0 - T\Delta s_0)\}}{dT} = \frac{\Delta e_0}{k_B T^2}, \tag{8.65}$$

which is identical to (7.16) or (7.19) with equilibrium constant $s = e^{-2\beta h}$ for the melting transition. Equation (8.65) applied at the melting point yields

$$\Delta e_0 = k_B T_m^2 \left(\frac{ds}{d\theta_o}\frac{d\theta_o}{dT}\right)_{T=T_m, s=1}. \tag{8.66}$$

Equation (8.66) tells us that the internal energy (or enthalpy) change of melting can be obtained from the slopes of the curves $d\theta_o/ds$ and $d\theta_o/dT$ at the melting point, $s = 1$ $(T = T_m)$ and $\theta_o = 1/2$.

Further Reading and References

K.A. Dill, S. Bromberg, *Molecular Driving Forces*, 2nd edn. (Garland Science, 2011)
M. Plischke, B. Bergersen, *Equilibrium Statistical Physics*, 3rd edn. (2006)
A.W. Adamson, A.P. Gast, *Physical Chemistry of Surfaces*, 6th edn. (Wiley, 1997)
A.A. Hyman, C.A. Weber, F. Jülicher, Liquid-liquid phase separation in biology. Annu. Rev. Cell Dev. Biol. **30**, 39–58 (2014)
J. Palmeri, M. Manghi, N. Destainville, Thermal denaturation of fluctuating DNA driven by bending entropy. Phys. Rev. Lett. **99**, 088103 (2007); J. Palmeri, M. Manghi, N. Destainville, Thermal denaturation of fluctuating finite DNA chains: the role of bending rigidity in bubble nucleation. Phys. Rev. E **77**, 011913 (2008)
O. Lee, W. Sung, Enhanced bubble formation in looped short double-stranded DNA. Phys. Rev. E **85**, 021902 (2012)

Chapter 9
Responses, Fluctuations, Correlations and Scatterings

The way how matter responds to an external stimulus can reflect a certain important aspect of its internal properties. In this chapter we introduce the static linear response theory that relates the response function of the matter with the underlying fluctuation and correlation of the variable conjugate to the stimulus. Also we directly relate the correlation of density fluctuation to the configurational organization (structure factor) that is probed by scattering of quanta and radiations onto the matter, giving some prevalent examples. These relations are important to unravelling the structural order and correlation in condensed and complex materials on various length scales.

9.1 Linear Responses and Fluctuations: Fluctuation-Response Theorem

The response or susceptibility functions are quantitative means of expressing the relationships between the cause and effect. Typical examples are electrical and magnetic susceptibilities, which describe the polarizations induced respectively by applied electrical and magnetic fields. Also, we already have seen an important thermodynamic response function, the heat capacity, which describes the amount of heat needed to increase the temperature of the system C_V; the heat capacity of a system at a temperature T is proportional to the mean square fluctuation or variance of the energy (3.40), rewritten as,

$$\left\langle (\Delta\mathcal{E})^2 \right\rangle = -k_B T \frac{\partial \langle \mathcal{E} \rangle}{\partial T} = k_B T^2 C_V .$$

This is a remarkable formula which shows that **the responses (e.g., heat capacity) is directly related to the fluctuations inherent in the system**. The rms fluctuation

W. Sung, *Statistical Physics for Biological Matter*, Graduate Texts in Physics,
https://doi.org/10.1007/978-94-024-1584-1_9

of the energy $\langle(\Delta\mathcal{E})^2\rangle^{1/2}$ is negligible compared the average value $\langle\mathcal{E}\rangle$ in normal macroscopic systems, but may become significant in small systems. Anomalously, at the critical point, at which the system is infinitely susceptible to an external stimulus, the rms fluctuations diverge to infinity. Here we study the relation between the fluctuations and responses with generality, which we call **the fluctuation-response theorem**.

Consider that a system with the Hamiltonian $\mathcal{H}_0\{\mathcal{M}\}$ is surrounded by a background of temperature T and perturbed by a certain external field or force f_i. The total Hamiltonian is $\mathcal{H} = \mathcal{H}_0 + \mathcal{H}'$ where the perturbation term is

$$\mathcal{H}' = -f_i\mathcal{X}_i. \tag{9.1}$$

The $\mathcal{X}_i$ is the microscopic displacement that is conjugate to f_i; its average $\langle\mathcal{X}_i\rangle$ is the macroscopic displacement X_i introduced in Chap. 2 (Table 2.1).

The average of a variable $\mathcal{X}_j$ over a canonical distribution of the perturbed system is

$$\begin{aligned}\langle\mathcal{X}_j\rangle &= \frac{\sum_{\mathcal{M}}\mathcal{X}_j e^{-\beta\mathcal{H}\{\mathcal{M}\}}}{\sum_{\mathcal{M}} e^{-\beta\mathcal{H}\{\mathcal{M}\}}} \\ &\approx \frac{\sum_{\mathcal{M}}\mathcal{X}_j e^{-\beta\mathcal{H}_0}(1+\beta f_i\mathcal{X}_i)}{\sum_{\mathcal{M}} e^{-\beta\mathcal{H}_0}(1+\beta f_i\mathcal{X}_i)}.\end{aligned} \tag{9.2}$$

Here we consider that f_i is small enough to allow the linear approximation $e^{\beta f_i\mathcal{X}_i} \approx 1+\beta f_i\mathcal{X}_i$. In terms of the average in the absence of the perturbation, $\langle\cdots\rangle_0 = \sum_{\mathcal{M}}\cdots e^{-\beta\mathcal{H}_0}/\sum_{\mathcal{M}} e^{-\beta\mathcal{H}_0}$, (9.2) can be rewritten to the linear order in the f_i:

$$\begin{aligned}\langle\mathcal{X}_j\rangle &\approx \frac{\langle\mathcal{X}_j\rangle_0 + \beta f_i\langle\mathcal{X}_j\mathcal{X}_i\rangle_0}{1+\beta f_i\langle\mathcal{X}_i\rangle_0} \\ &\approx \langle\mathcal{X}_j\rangle_0 + \beta f_i\left(\langle\mathcal{X}_j\mathcal{X}_i\rangle_0 - \langle\mathcal{X}_j\rangle_0\langle\mathcal{X}_i\rangle_0\right) \\ &= \langle\mathcal{X}_j\rangle_0 + \beta f_i\langle\Delta\mathcal{X}_j\Delta\mathcal{X}_i\rangle_0\end{aligned} \tag{9.3}$$

where $\Delta\mathcal{X}_i = \mathcal{X}_i - \langle\mathcal{X}_i\rangle_0$ and $\Delta\mathcal{X}_j = \mathcal{X}_j - \langle\mathcal{X}_j\rangle_0$ are the fluctuations about the means $\langle\mathcal{X}_i\rangle_0$ and $\langle\mathcal{X}_j\rangle_0$ respectively.

Defining the average change $\Delta X_j = \langle\Delta\mathcal{X}_j\rangle = \langle\mathcal{X}_j\rangle - \langle\mathcal{X}_j\rangle_0$ caused by f_i, (9.3) can be rewritten as

$$\langle\Delta\mathcal{X}_j\Delta\mathcal{X}_i\rangle_0 = k_B T\frac{\partial}{\partial f_i}\Delta X_j. \tag{9.4}$$

If $i = j$, then

$$\left\langle \Delta \mathcal{X}_i^2 \right\rangle_0 = k_B T \frac{\partial}{\partial f_i} \Delta X_i, \tag{9.5}$$

which states that **the intrinsic fluctuation of a system's variable can be obtained by its average response to a perturbation of the field or force that is its conjugate**.

For example, for $X_i = M$ (magnetization) and $X_i = P$ (polarization), which are conjugate to the magnetic (H) and electric (E) fields (Table 2.1), (9.5) yields

$$\left\langle (\Delta \mathcal{M})^2 \right\rangle_0 = k_B T \frac{\partial}{\partial H} \Delta M = k_B T \chi_M \tag{9.6}$$

$$\left\langle (\Delta \mathcal{P})^2 \right\rangle_0 = k_B T \frac{\partial}{\partial E} \Delta P = k_B T \chi_P, \tag{9.7}$$

where χ_M and χ_P are magnetic susceptibility and electrical susceptibility respectively. If $\mathcal{X}_i = \mathcal{V}$ (solution volume), $\mathcal{X}_i = \mathcal{X}$ (chain extension), then

$$\left\langle (\Delta \mathcal{V})^2 \right\rangle_0 = -k_B T \frac{\partial}{\partial p} \Delta V = k_B T V K_T \tag{9.8}$$

$$\left\langle (\Delta \mathcal{X})^2 \right\rangle_0 = k_B T \frac{\partial}{\partial f} \Delta X = k_B T L k_s, \tag{9.9}$$

where K_T and k_s are isothermal compressibility and stretch modulus. These susceptibilities or response functions are directly related to the internal fluctuations of the associated variables in the absence of the fields or forces.

P9.1 *We shall learn later in* Chap. 11 *the Marko-Siggia model where the force–extension* $(f - X)$ *relation of a DNA fragment of the persistent and contour lengths* l_p *and* L *is*

$$f = \frac{k_B T}{4 l_p} \left[\left(1 - \frac{X}{L} \right)^{-2} - 1 + \frac{4X}{L} \right].$$

Find the extension fluctuation $\langle (\Delta \mathcal{X})^2 \rangle_0$ *of the chain extended by a force* f_0.

Another important example is the fluctuation of particle number $\mathcal{N}$,

$$\left\langle (\Delta \mathcal{N})^2 \right\rangle_0 = k_B T \frac{\partial}{\partial \mu} \Delta N, \tag{9.10}$$

which is related to the response to chemical work $\mathcal{H}' = \mu\mathcal{N}$ done on the system. This equation is identical to (3.64); from $(\partial\mu/\partial N)_{T,N} = V/N^2K_T$ (3.67), (2.39), we have $\langle(\Delta\mathcal{N})^2\rangle_0 = k_BTnNK_T$.

Equation (9.4) relates the average response of a certain variable $\mathcal{X}_j$ with its correlation with another variable $\mathcal{X}_i$ conjugate to the external stimulus f_i. For example for a linear charged object like a DNA fragment, the correlation between extension and polarization is given by

$$\langle\Delta\mathcal{X}\Delta\mathcal{P}\rangle_0 = k_BT\frac{\partial}{\partial f}\Delta P, \tag{9.11}$$

which can be nonzero if the polarization P can change because of the applied tension f. Because $\langle\Delta\mathcal{X}\Delta\mathcal{P}\rangle_0 = \langle\Delta\mathcal{P}\Delta\mathcal{X}\rangle_0$, (9.11) can also be given by

$$\langle\Delta\mathcal{P}\Delta\mathcal{X}\rangle_0 = k_BT\frac{\partial}{\partial E}\Delta X, \tag{9.12}$$

which cannot vanish if the system's length changes (response) to an applied electric field (stimulus).

P9.2 *How is the correlation $\langle\Delta\mathcal{N}_1\Delta\mathcal{N}_2\rangle_0$ expressed in a two component mixture?*

Now consider a system that is subject to a multitude of stimuli f_μ each with a conjugate response variable x_μ, which thereby induces the perturbation

$$\mathcal{H}' = -\Sigma_\mu f_\mu x_\mu. \tag{9.13}$$

We follow the procedure in (9.3) to obtain

$$\begin{aligned}\langle x_\nu\rangle &\approx \frac{\sum_{\mathcal{M}} x_\nu e^{-\beta\mathcal{H}_0}\left(1+\beta\Sigma_\mu f_\mu x_\mu\right)}{\sum_{\mathcal{M}} e^{-\beta\mathcal{H}_0}\left(1+\beta\Sigma_\mu f_\mu x_\mu\right)}\\ &\approx \langle x_\nu\rangle_0 + \beta\Sigma_\mu f_\mu\langle\Delta x_\nu\Delta x_\mu\rangle_0,\end{aligned} \tag{9.14}$$

which leads to

$$\begin{aligned}\Delta x_\nu &= \langle x_\nu\rangle - \langle x_\nu\rangle_0 = \beta\Sigma_\mu f_\mu\langle\Delta x_\nu\Delta x_\mu\rangle_0\\ &= \Sigma_\mu\chi_{\nu\mu}f_\mu,\end{aligned} \tag{9.15}$$

where

$$\chi_{\nu\mu} = \frac{\partial}{\partial f_\mu}\Delta x_\nu = k_BT\langle\Delta x_\nu\Delta x_\mu\rangle_0 \tag{9.16}$$

is **the associated response function given in terms of the correlation function** $\langle\Delta x_\mu\Delta x_\nu\rangle_0$ in the absence of the external stimulus.

Of our interest is the case in which x and its conjugate f are continuously varying over space so that the perturbing Hamiltonian is a functional:

$$\mathcal{H}' = -\int d\boldsymbol{r}' f(\boldsymbol{r}')x(\boldsymbol{r}'). \tag{9.17}$$

Then,

$$\Delta x(\boldsymbol{r}) = \int d\boldsymbol{r}' \chi(\boldsymbol{r},\boldsymbol{r}')f(\boldsymbol{r}'), \tag{9.18}$$

with the response function given in terms of the correlation function

$$\chi(\boldsymbol{r},\boldsymbol{r}') = \frac{\partial}{\delta f(\boldsymbol{r}')}\Delta x(\boldsymbol{r}) = k_B T\langle \Delta x(\boldsymbol{r})\Delta x(\boldsymbol{r}')\rangle_0, \tag{9.19}$$

where $\partial/\delta f(\boldsymbol{r}')$ is a functional derivative which is continuum generalization of $\partial/\partial f_\mu$.

A typical example is the perturbation caused by a locally varying external potential u acting on an N-particle system:

$$\mathcal{H}' = \sum_{\alpha=1}^{N} u(\boldsymbol{r}_\alpha) = \int d\boldsymbol{r}\, u(\boldsymbol{r})\boldsymbol{n}(\boldsymbol{r}), \tag{9.20}$$

where $\boldsymbol{n}(\boldsymbol{r})$ is **microscopic local number density**:

$$\boldsymbol{n}(\boldsymbol{r}) = \sum_{\alpha=1}^{N} \delta(\boldsymbol{r} - \boldsymbol{r}_\alpha). \tag{9.21}$$

The average density change induced at $\boldsymbol{r}$ due to the external potential fields applied at another position $\boldsymbol{r}'$ is

$$\Delta n(\boldsymbol{r}) = -\int d\boldsymbol{r}' \chi_n(\boldsymbol{r},\boldsymbol{r}')u(\boldsymbol{r}'), \tag{9.22}$$

where the response function is

$$\chi_n(\boldsymbol{r},\boldsymbol{r}') = k_B T C_n(\boldsymbol{r},\boldsymbol{r}'), \tag{9.23}$$

and $C_{\boldsymbol{n}}(\boldsymbol{r},\boldsymbol{r}')$ **is the correlation function of local density fluctuations** at two different positions $\boldsymbol{r}$ and $\boldsymbol{r}'$ in the absence of the external potential:

$$C_n(\boldsymbol{r},\boldsymbol{r}') = \langle \Delta\boldsymbol{n}(\boldsymbol{r})\Delta\boldsymbol{n}(\boldsymbol{r}')\rangle_0, \tag{9.24}$$

where

$$\Delta\boldsymbol{n}(\boldsymbol{r}) = \boldsymbol{n}(\boldsymbol{r}) - n, \tag{9.25}$$

and $n = \langle \boldsymbol{n}(\boldsymbol{r})\rangle_0$ is the unperturbed, equilibrium density. The fluctuation of total number, $\mathcal{N} = \int d\boldsymbol{r}\, \boldsymbol{n}(\boldsymbol{r})$, is given by

$$\langle (\Delta\mathcal{N})^2\rangle_0 = \iint d\boldsymbol{r}d\boldsymbol{r}' \langle \Delta\boldsymbol{n}(\boldsymbol{r})\Delta\boldsymbol{n}(\boldsymbol{r}')\rangle_0. \tag{9.26}$$

To illustrate the relations among local density correlation, fluctuation of the total number of particles, and the associated susceptibility, consider a fluid near the critical point of the gas-to-liquid phase transition with the correlation function:

$$C_n(\boldsymbol{r},\boldsymbol{r}') \sim |\boldsymbol{r}-\boldsymbol{r}'|^{-(d-2+\eta)} \exp\left(-\frac{|\boldsymbol{r}-\boldsymbol{r}'|}{\xi}\right). \tag{9.27}$$

Here d is the space dimensionality, ξ is the correlation length that grows like $|T - T_c|^{-\nu}$ near T_c, η and ν are positive numbers called critical exponents. Integration over the positions $\boldsymbol{r}$ and $\boldsymbol{r}'$ (9.27) yields

$$\begin{aligned} \langle (\Delta\mathcal{N})^2\rangle_0 &\sim \iint d\boldsymbol{r}d\boldsymbol{r}' |\boldsymbol{r}-\boldsymbol{r}'|^{-(d-2+\eta)} \exp\left(-\frac{|\boldsymbol{r}-\boldsymbol{r}'|}{\xi}\right) \\ &\sim V \int ds\, s^{d-1} s^{-(d-2+\eta)} \exp(-s/\xi) \\ &\sim V\xi^{2-\eta}\left[\int dx\, x^{1-\eta}\exp(-x)\right], \end{aligned} \tag{9.28}$$

where $\iint d\boldsymbol{r}d\boldsymbol{r}' = \iint d\boldsymbol{r}d(\boldsymbol{r}'-\boldsymbol{r}) = V\int d(\boldsymbol{r}'-\boldsymbol{r})$, and the quantity in the bracket, expressed in term of a dimensionless variable $x = |\boldsymbol{r}-\boldsymbol{r}'|/\xi$, is also dimensionless. Equation (9.28) tells us that as the system approaches the critical point, the number fluctuation $\langle (\Delta\mathcal{N})^2\rangle_0$ and the related susceptibility (the compressibility K_T) diverge to infinity as $\xi^{2-\eta} \sim |T - T_c|^{-\gamma}$, where $\gamma = \nu(2-\eta)$.

If an applied field is sharply localized to a point $\boldsymbol{r}_0$, $u(\boldsymbol{r}) = U\delta(\boldsymbol{r}-\boldsymbol{r}_0)$, leading to

$$\Delta n(\boldsymbol{r}) = -\chi_n(\boldsymbol{r}-\boldsymbol{r}_0)U = -\beta U\langle \Delta\boldsymbol{n}(\boldsymbol{r})\Delta\boldsymbol{n}(\boldsymbol{r}_0)\rangle_0, \tag{9.29}$$

i.e., the local density perturbation induced at $\boldsymbol{r}$ is a measure of the density correlation propagated to the position from the source of disturbance at $\boldsymbol{r}_0$.

The linear response relations can be applied to a wider variety of variables than are listed in Table 2.1. As a biological example let us consider a planar membrane.

The membrane charge density can fluctuate due to the thermal motion of the charged lipid molecules and the background ions that can adsorb on the membrane. We perform a thought experiment in which a small potential V_m is applied to a small area a at a point $\boldsymbol{x}_0$ on the membrane. The perturbing Hamiltonian is

$$\mathcal{H}' = \sigma(\boldsymbol{x}_0) a V_m, \tag{9.30}$$

where σ is the surface charge density. Applying (9.3), the change of the average charge densities at $\boldsymbol{x}$ around $\boldsymbol{x}_0$ is

$$\Delta\langle\sigma(\boldsymbol{x})\rangle = -\beta a V_m \langle\Delta\sigma(\boldsymbol{x})\Delta\sigma(\boldsymbol{x}_0)\rangle_0, \tag{9.31}$$

that is, by measuring the average surface density at a point $\boldsymbol{x}$, one can get the information about the charge correlation function.

9.2 Scatterings, Fluctuations, and Structures of Matter

Projecting a beam of radiation on matter is another way to perturb it so that its properties can be probed. **The response of the matter is shown in the intensity of the scattered radiation into a certain angle, the measurement of which provides information on microscopic structure of the matter**. One primary type is **x-ray scattering or diffraction**, in which incident photons with angular frequency ω, wave vector k, and energy $\epsilon = \hbar\omega = \hbar ck = hc/\lambda$ scatter electrons in the matter. The typical x ray with energy $\epsilon \sim 10^4$ eV and wavelength $\lambda = 2\pi/k \sim 0.1$ nm can resolve the atominstic structure of the matter and the density fluctuations of the constituent particles.

A type which could be more relevant for biological applications is **light scattering in solutions**, which probes the length scales of 100 nm–10 μm. For the light to scatter, the particles should have the indices of diffraction distinct from that of the background fluid. What matters fundamentally is the density fluctuations of otherwise homogeneous medium.

Another type is **neutron scattering**; a neutron of mass m_n has energy $\epsilon = \hbar^2 k^2/(2m_n) = h^2/\left(2m_n\lambda^2\right)$ so a thermal neutron with the energy $\sim k_B T$ at room temperature can probe the atomistic structure at resolution $\lambda \sim 0.1$ nm. The incident neutrons have spins that can interact with the spins of the nuclei so as to probe the density fluctuations of the atoms as can other radiation sources.

The radiation can probe not only the structures of matter on various scales but also a variety of the collective motions that arise from the interactions between particles. The energies of low-lying collective excitations are in the order of or less than thermal energy $k_B T$, which is much lower than the x-ray energy. Thus the x-ray scatters the matter quasi-elastically and measures its static structure. In

contrast, the thermal neutron undergoes inelastic scattering and is useful to probe the dynamics of such excitations.

9.2.1 Scattering and Structure Factor

Consider that a plane wave or a beam of quanta that has wave vector $\boldsymbol{k}$ impinges a systems composed of particles. The particles scatter the wave, and the intensity of the scattered wave, which is spherical, is then measured at a detector located at a distance R away as a function of the scattering angle θ (Fig. 9.1). If the scattering is elastic ($k' = k$) the angle θ is related to the scattered wave vector $\boldsymbol{k}'$ by the relation

$$q = 2k \sin\frac{\theta}{2} \tag{9.32}$$

where q is the magnitude of $\boldsymbol{q} = \boldsymbol{k} - \boldsymbol{k}'$.

The amplitude of the radiation scattered by a particle positioned at $\boldsymbol{r}_\alpha$ has the phase shift $(\boldsymbol{k}' - \boldsymbol{k}) \cdot \boldsymbol{r}_\alpha = -\boldsymbol{q} \cdot \boldsymbol{r}_\alpha$ relative to the incident wave at the particle, so that the scattering amplitude from the particle is

$$A = \frac{f(\theta)}{R} e^{-i\boldsymbol{q}\cdot\boldsymbol{r}_\alpha}. \tag{9.33}$$

If the beam is scattered by N particles, the total amplitude is

$$A = \frac{f(\theta)}{R} \sum_{\alpha=1}^{N} e^{-i\boldsymbol{q}\cdot\boldsymbol{r}_\alpha} \tag{9.34}$$

The measured intensity I of the scattered beam at the detector is $\langle |A|^2 \rangle$, where $\langle \cdots \rangle$ is the thermal average or time average, so

$$I = \left(\frac{|f(\theta)|}{R} \right)^2 NS(\boldsymbol{q}), \tag{9.35}$$

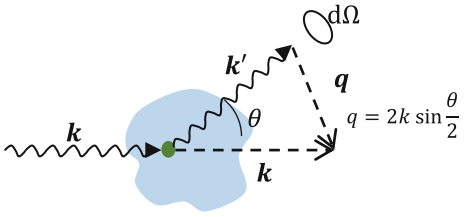

Fig. 9.1 Typical elastic scattering experiment. $\boldsymbol{k}$ and $\boldsymbol{k}'$ are incident and scattered wave vectors, $\boldsymbol{q} = \boldsymbol{k} - \boldsymbol{k}'$, and θ is the scattering polar angle

where

$$S(\boldsymbol{q}) = N^{-1}\left\langle \sum_{\alpha=1}^{N}\sum_{\alpha'=1}^{N} e^{-i\boldsymbol{q}\cdot(\boldsymbol{r}_\alpha - \boldsymbol{r}_{\alpha'})} \right\rangle. \tag{9.36}$$

$|f(\theta)|^2$ is the form factor descriptive of the particle's internal structure, which is not relevant here. What is important is the **structure factor** $S(\boldsymbol{q})$, which describes the **configurational organization of the particles**. The above relations mean that $S(\boldsymbol{q})$ can be determined by intensity of the radiation of wavelength λ scattered into a solid-angle element $d\Omega$ around the scattering angle θ, which, for elastic scattering, is related to q by (9.32). The length scale that can be probed is given by $\sim q^{-1} \sim \lambda/\sin(\theta/2)$. **The structures of matter in macromolecular scales larger than λ are usually probed by X-ray and neutron scattering at small q (i.e., small angle θ).**

9.2.2 Structure Factor and Density Fluctuation/Correlation

Introducing the Fourier transform of the microscopic number density (9.21)

$$\boldsymbol{n}(\boldsymbol{q}) = \int d\boldsymbol{r} e^{-i\boldsymbol{q}\cdot\boldsymbol{r}} \sum_{\alpha=1}^{N} \delta(\boldsymbol{r} - \boldsymbol{r}_\alpha) = \sum_{\alpha=1}^{N} e^{-i\boldsymbol{q}\cdot\boldsymbol{r}_\alpha}, \tag{9.37}$$

the structure factor (9.36) is expressed as

$$S(\boldsymbol{q}) = N^{-1}\left\langle |\boldsymbol{n}(\boldsymbol{q})|^2 \right\rangle = N^{-1}\left\langle |\Delta\boldsymbol{n}(\boldsymbol{q})|^2 \right\rangle, \quad \boldsymbol{q} \neq 0 \tag{9.38}$$

where $\Delta\boldsymbol{n}(\boldsymbol{q}) = \boldsymbol{n}(\boldsymbol{q}) - \langle \boldsymbol{n}(\boldsymbol{q})\rangle$. The second equality holds for uniform systems in which $\langle \boldsymbol{n}(\boldsymbol{r})\rangle = n$ is constant, so $\langle \boldsymbol{n}(\boldsymbol{q})\rangle = n\int d\boldsymbol{r} e^{-i\boldsymbol{q}\cdot\boldsymbol{r}} = (2\pi)^3 n\delta(\boldsymbol{q})$ is zero unless $\boldsymbol{q} = 0$. $\boldsymbol{q} = 0$ is the case of forward scattering, which will not be considered.

Equation (9.38) means that **the static structure factor is a measure of the density fluctuation in Fourier space**. Equation (9.38) can also be written as

$$\begin{aligned} S(\boldsymbol{q}) &= N^{-1}\iint d\boldsymbol{r}\, d\boldsymbol{r}' e^{-i\boldsymbol{q}\cdot(\boldsymbol{r}-\boldsymbol{r}')} \langle \Delta\boldsymbol{n}(\boldsymbol{r})\Delta\boldsymbol{n}(\boldsymbol{r}')\rangle \\ &= N^{-1}\iint d\boldsymbol{r}\, d\boldsymbol{r}' e^{-i\boldsymbol{q}\cdot(\boldsymbol{r}-\boldsymbol{r}')} C_n(\boldsymbol{r},\boldsymbol{r}') \end{aligned} \tag{9.39}$$

where $C_n(\boldsymbol{r},\boldsymbol{r}') = \langle \Delta\boldsymbol{n}(\boldsymbol{r})\Delta\boldsymbol{n}(\boldsymbol{r}')\rangle$ is the density correlation function (9.24). Uniform systems such as fluids have a number of spatial symmetries to consider for the

correlation function. The spatial homogeneity allows the systems to have the translational invariance:

$$C_n(\boldsymbol{r},\boldsymbol{r}') = C_n(\boldsymbol{r}-\boldsymbol{r}'), \tag{9.40}$$

and correspondingly

$$S(\boldsymbol{q}) = n^{-1}\int d\boldsymbol{r}\, e^{-i\boldsymbol{q}\cdot\boldsymbol{r}} C_n(\boldsymbol{r}), \tag{9.41}$$

meaning that **the structure factor is a Fourier transform of the density correlation**. Due to the isotropy, the uniform fluids have also rotational symmetry $C_n(\boldsymbol{r}-\boldsymbol{r}') = C_n(|\boldsymbol{r}-\boldsymbol{r}'|)$; $S(\boldsymbol{q}) = S(q)$.

9.2.3 Structure Factor and Pair Correlation Function

Another meaningful representation of the structure factor is obtained directly from (9.36), which can be rewritten as

$$S(\boldsymbol{q}) = N^{-1}\int d\boldsymbol{r}\, e^{-i\boldsymbol{q}\cdot\boldsymbol{r}} \left\langle \sum_{\alpha=1}^{N}\sum_{\alpha'=1}^{N} \delta(\boldsymbol{r}-\boldsymbol{r}_\alpha+\boldsymbol{r}_{\alpha'}) \right\rangle \tag{9.42}$$

$$= 1 + n\int d\boldsymbol{r}\, e^{-i\boldsymbol{q}\cdot\boldsymbol{r}} g(\boldsymbol{r}) \tag{9.43}$$

$$= 1 + n\int d\boldsymbol{r}\, e^{-i\boldsymbol{q}\cdot\boldsymbol{r}} (g(\boldsymbol{r})-1), \quad \boldsymbol{q}\neq 0 \tag{9.44}$$

where the '1' comes from the (N) contributions from $\alpha = \alpha'$ in the sum, and the second term is from the rest, involving

$$ng(\boldsymbol{r}) = N^{-1}\left\langle \sum_{\alpha}^{N}\sum_{\alpha'\neq\alpha}^{N-1} \delta(\boldsymbol{r}-\boldsymbol{r}_\alpha+\boldsymbol{r}_{\alpha'}) \right\rangle, \tag{9.45}$$

where $g(\boldsymbol{r})$ is the pair distribution function (4.72). Equation (9.44) follows because we are not considering $\boldsymbol{q} = 0$.

Integrating (9.45) yields

$$\begin{aligned} n\int d\boldsymbol{r}\, g(\boldsymbol{r}) &= N^{-1}\langle \mathcal{N}(\mathcal{N}-1)\rangle \\ &= N^{-1}\langle \Delta\mathcal{N}\rangle^2 + N - 1, \end{aligned} \tag{9.46}$$

The average is taken over the grand canonical ensemble where the particle number in the double sum in (9.45) is taken to be a fluctuating value $\mathcal{N}$, because $g(r)$ is independent of the ensemble chosen. Using (9.46) along with (3.68), (9.44) in the limit $\boldsymbol{q} \to 0$ can be written as

$$1 + n \int d\boldsymbol{r}(g(\boldsymbol{r}) - 1) = k_B T n K_T = S(\boldsymbol{q} \to 0), \tag{9.47}$$

which is called the compressibility relation. It relates the structure factor with its compressibility, which can be directly read off from the scattering data: $S(\boldsymbol{q} \to 0)$.

The configurational organization of the particles in the matter is best visualized by the pair distribution function. Positioning an arbitrary particle, called a central particle, say, α', at the origin of a reference coordinate, and noting that the system is composed of N such particles, (9.45) is recast as

$$ng(\boldsymbol{r}) = \left\langle \sum_{\alpha=1}^{N-1} \delta(\boldsymbol{r} - \boldsymbol{r}_\alpha) \right\rangle, \tag{9.48}$$

which is the density of the $N - 1$ particles at $\boldsymbol{r}$ given (conditional upon the presence of) the central particle.

For an ideal gas in which the particles do not interact, $\langle \sum_{\alpha=1}^{N-1} \delta(\boldsymbol{r} - \boldsymbol{r}_\alpha) \rangle = n$, irrespective of the particle at origin. Then,

$$g(\boldsymbol{r}) = g(r) = 1, \tag{9.49}$$

and, using (9.44),

$$S(\boldsymbol{q}) = S(q) = 1, \quad \text{for } q \neq 0 \tag{9.50}$$

meaning that the system has no structure. Now consider a crystalline solid in which the particles are placed periodically with a spacing called the lattice constant a. At $T = 0$, thermal vibration (fluctuation) is absent, so

$$g(\boldsymbol{r}) = n^{-1} \sum_{\alpha=1}^{N-1} \delta(\boldsymbol{r} - \boldsymbol{r}_\alpha) \tag{9.51}$$

$$S(\boldsymbol{q}) = N^{-1} \left| \sum_{\alpha=1}^{N} e^{-i\boldsymbol{q}\cdot\boldsymbol{r}_\alpha} \right|^2. \tag{9.52}$$

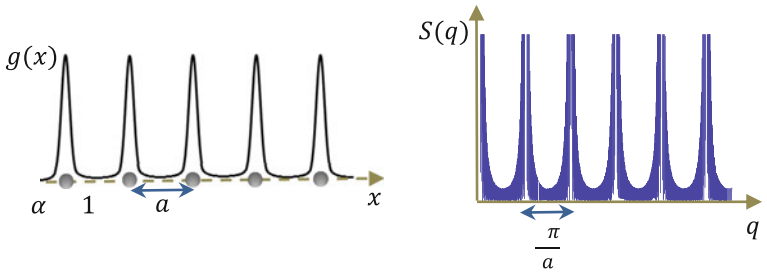

Fig. 9.2 The pair distribution function $g(x)$ and the structure factor $S(q)$ in one dimensional solid at $T = 0$ with lattice constant a. There are delta-function like peaks not only in the position space but also in the Fourier (reciprocal) space

For a 1-D crystal with lattice constant a, the static structure is calculated as

$$S(q) = N^{-1}\left|\frac{1 - e^{-iqNa}}{1 - e^{-iqa}}\right|^2 = N^{-1}\left(\frac{\sin(Nqa/2)}{\sin(qa/2)}\right)^2, \tag{9.53}$$

which shows Bragg peaks at $q = 2n\pi/a$ that sharpen as N increases (Fig. 9.2). For a real 3-D crystal at a finite temperature in which the particles undergo thermal oscillation, the sharp peaks either in $g(\boldsymbol{r})$ or $S(\boldsymbol{q})$ are broadened. At a temperature lower than the crystal's melting temperature these long-range order and structure are not disrupted.

P9.3 *As a model of a rod-like protein, consider a chain of finite N particles that are connected linearly and harmonically. Calculate the static structure factor. Assume that the particles are undergoing one-dimensional harmonic motion independently. From* $S(q \to 0)$ *find the stretch modulus.*

If a spherical virus (Fig. 9.3a) of submicron size is viewed as a condensed collection of particles (scatterers) rather than as a single composite particle, its form factor is the structural factor. Neglecting its icosahedral structure the virus can be approximated as a sphere with a uniform density n and radius R. Then we note

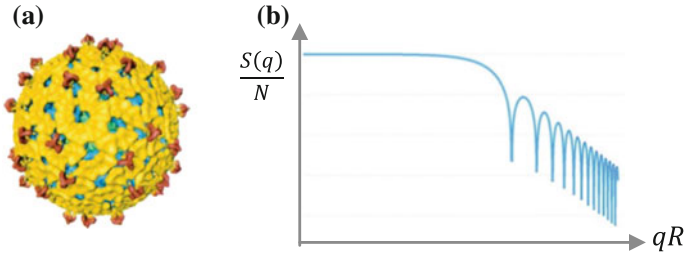

Fig. 9.3 **a** Three dimensional reconstruction of rotavirus [J. B. Pesavento et al. Prasad, Copyright (2001) National Academy of Sciences, U.S.A] and **b** the structure factor of a uniform sphere

$$n(\boldsymbol{q}) = \sum_{\alpha=1}^{N} e^{-i\boldsymbol{q}\cdot\boldsymbol{r}_\alpha} = n \int_0^R r^2 dr 2\pi \int_{-1}^{1} d\,\cos\theta\; e^{-iqr\,\cos\theta}$$
$$= 4\pi n \int_0^R dr r^2 \frac{\sin qr}{qr} = \frac{3Nj_1(qR)}{(qR)}, \tag{9.54}$$

where $j_1(x) = (\sin x - x\cos x)/x^2$ is the first-order spherical Bessel function. The structure factor (9.38) is

$$S(q) = N\left\{\frac{3j_1(qR)}{qR}\right\}^2, \tag{9.55}$$

(Figure 9.3). The radius can be estimated by the position $q \approx 4.5\,R^{-1}$ of the first minimum of $S(q)$ or the data for small q, $S(q) \approx N\left\{1 - 2(qR)^2/5\right\}^2/16$. For a spherical shell of radius R and thickness $d \ll R$ (like a vesicle), the factor can be easily calculated to be

$$S(q) = N\left\{\frac{\sin(qR)}{qR}\right\}^2, \tag{9.56}$$

which is quite distinct from (9.55). Whether the virus is hollow sphere like a vesicle or is filled with complex structure including DNA can be discerned by the scattering experiment using appropriate radiation source.

What will happen when a solid melts to a liquid? In Chap. 4, we already described the pair correlation and radial distribution functions and the short range order characteristic of liquids. Here we show the radial distribution function along

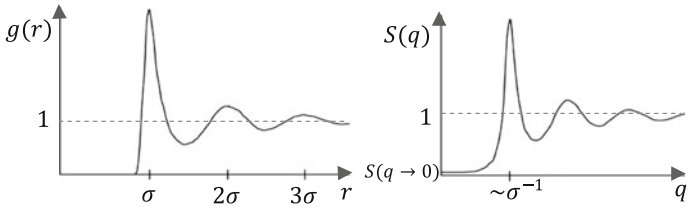

Fig. 9.4 A sketch of the radial distribution function $g(r)$ and the structure factor $S(q)$ for a simple and colloid liquid. The short-range order with a periodicity of particle diameter σ is observed both in real (r) and Fourier space (q). The small value of $S(q \to 0)$ represents the compressibility of the liquid

with the structure factor. Interestingly, the curve $S(q)$ looks apparently similar to $g(r)$ as it does for the cases of ideal gas and solid. The small value of $S(q \to 0)$ (Fig. 9.4) indicates that the liquid is nearly incompressible.

9.2.4 *Fractal Structures*

Near the critical point of gas-to-liquid phase transition, $C_n(r)$ (9.27) showed long range correlation. At the critical point, where the correlation length ξ diverges, $C_n(r) \sim r^{-\alpha}$, where $\alpha = d - 2 + \eta$, and d is space dimension. Using (9.41)

$$S(\boldsymbol{q}) \sim \int d^d r \; e^{-i\boldsymbol{q}\cdot\boldsymbol{r}} r^{-\alpha} = q^{-d+\alpha} \int d^d(qr) \; e^{-i\boldsymbol{q}\cdot\boldsymbol{r}} (qr)^{-\alpha} \sim q^{-d+\alpha}. \tag{9.57}$$

The power laws both in the correlation and the structure implies an absence of any characteristic length scales, i.e., the structure looks the same at any magnification. This **scale-invariant self-similar structure** is called fractal.

Fractals are ubiquitous in nature (in the systems at thermodynamic critical points as well as in complex systems, e.g., polymers, snowflakes, colloidal aggregates, coastlines), and also can be artificially designed. **Application of the concept of fractal nature may be valuable when measuring the properties of irregular biological structures, such as living organs** (Fig. 9.5b). Consider a fractal of size R that contains N particles or units. The structure of a random fractal is characterized by the **fractal dimension**, which is defined by the way in which N changes with R. For ordinary compact structures in *3D*, $N \sim (R/l)^3$, where l is inter-particle distance. For isotropic fractals,

$$N \sim (R/l)^{D_f}, \tag{9.58}$$

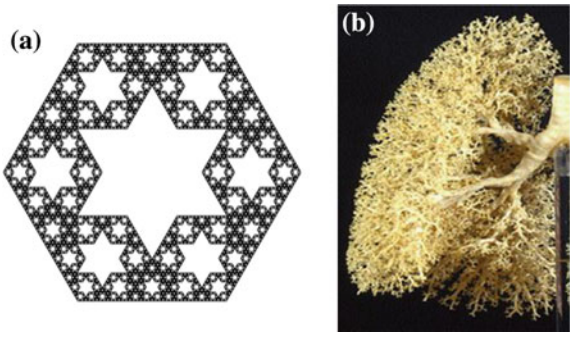

Fig. 9.5 **a** Examples of fractal structures (Digital image kindly supplied by Zachary Abel), and **b** human lung (Weibel 2009)

where D_f, called the fractal dimension, is less than 3 and can also be a non-integer number. For example, D_f of an ideal polymer chain is 2, as shown below. The fractal dimension is related to the radial distribution $g(r)$ and its Fourier transform $S(q)$ as following. Consider the number $N(r)$ of particles within a radius r ($l \ll r \ll R$) from a central particle deep within the fractal. By the definition of radial distribution function, the number of particles within a shell of thickness dr located at distance r (Fig. 4.4) is

$$dN(r) \sim g(r) r^{d-1} dr. \tag{9.59}$$

This, along with $N(r) \sim (r/l)^{D_f}$, leads to $g(r) \sim (r/l)^{-d+D_f}$, so (9.43) yields

$$S(q) \sim (ql)^{-D_f} \sim q^{-D_f}, \tag{9.60}$$

for the region of moderate q ($R^{-1} \ll q \ll l^{-1}$), in which scale-invariance is expected. The fractal dimension D_f can be read from the power law decay of the structure factor (9.57) tells us $D_f = d - \alpha = 2 - \eta$ for a fluid at the critical point. The scattering for very small q, on the other hand, senses the large lengths beyond the finite size of the system R, on which the structure factor depends. A flexible chain studied below serves as another example and allows an analytical understanding of the features mentioned above.

9.2.5 *Structure Factor of a Flexible Polymer Chain*

The polymer structure can be probed by scattering experiments, such as small angle x-ray scattering (SAXS) and small angle neutron scattering (SANS). The scattering intensity for a single chain is proportional to the structure factor $S(\boldsymbol{q}) = N^{-1}\langle \sum_{n,m}^{N} e^{-i\boldsymbol{q}\cdot\boldsymbol{r}_{nm}} \rangle$ (9.36), where N is the number of beads that compose the polymer, and $\boldsymbol{r}_{nm} = \boldsymbol{r}_n - \boldsymbol{r}_m$ is the distance between the nth and mth beads. Averaging over the orientations of the vector $\boldsymbol{r}_{nm}$ yields

$$\left\langle e^{-i\boldsymbol{q}\cdot\boldsymbol{r}_{nm}} \right\rangle = \frac{1}{4\pi} \int_0^{2\pi} d\varphi \int_{-1}^{1} d\, \cos\theta \left\langle e^{-i\cos\theta q|\boldsymbol{r}_{nm}|} \right\rangle = \left\langle \frac{\sin(q|\boldsymbol{r}_{nm}|)}{q|\boldsymbol{r}_{nm}|} \right\rangle. \tag{9.61}$$

For small q, or small scattering angle θ ($q = 2k\sin(\theta/2)$, Fig. 9.1),

$$S(\boldsymbol{q}) = N^{-1}\sum_{n,m}^{N}\left\langle \frac{\sin(q|\boldsymbol{r}_{nm}|)}{q|\boldsymbol{r}_{nm}|}\right\rangle \approx N^{-1}\sum_{n,m}^{N}\left\langle 1-\frac{1}{6}q^2|\boldsymbol{r}_{nm}|^2\right\rangle = N\left(1-\frac{1}{3}q^2R_G^2\right) \tag{9.62}$$

where the radius of gyration R_G defined by

$$R_G^2 = \frac{1}{2N^2}\sum_{n,m}^{N}\left\langle (\boldsymbol{r}_n-\boldsymbol{r}_m)^2\right\rangle = \frac{1}{N}\sum_{n=1}^{N}\left\langle (\boldsymbol{r}_n-\boldsymbol{R}_{cm})^2\right\rangle \tag{9.63}$$

represents the chain size R and $\boldsymbol{R}_{cm}$ is the center of mass position. Therefore, from the data of small q or small angle scattering, one can get information about the radius of gyration.

For a chain in which $\boldsymbol{r}_{nm}$ is distributed in Gaussian,

$$S(\boldsymbol{q}) = N^{-1}\sum_{n,m}^{N}\langle e^{-i\boldsymbol{q}\cdot\boldsymbol{r}_{nm}}\rangle = N^{-1}\sum_{n,m}^{N}\exp\left(-\tfrac{1}{2}\langle(\boldsymbol{q}\cdot\boldsymbol{r}_{nm})^2\rangle\right) = N^{-1}\sum_{n,m}^{N}\exp\left(-\tfrac{1}{6}q^2\langle\boldsymbol{r}_{nm}^2\rangle\right). \tag{9.64}$$

Considering that, in the Gaussian chain, $\langle \boldsymbol{r}_{nm}{}^2\rangle = l^2|n-m|$ (10.4), $R_G^2 = l^2N/6$, where l is the segmental length, the structure factor can be calculated as

$$S(\boldsymbol{q}) = N^{-1}\int_0^N dn\int_0^N dm\,\exp\left(-\frac{1}{6}q^2l^2|n-m|\right) = ND\left(q^2R_G^2\right), \tag{9.65}$$

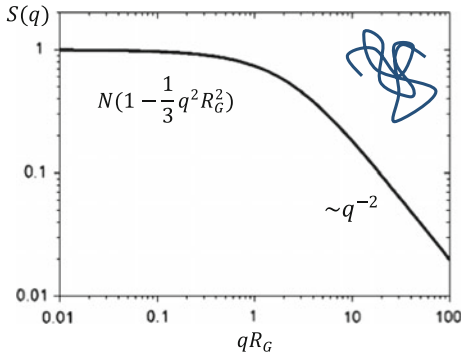

Fig. 9.6 Structure factor $S(q)$ of a Gaussian chain. From the data of low q, the radius of gyration R_G can be determined. For the relatively high q, $S(q) \sim q^{-D_f}$, where $D_f = 2$ is the fractal dimension

where

$$D(x) = \frac{2}{x^2}(e^{-x} - 1 + x), \tag{9.66}$$

called the Debye function. $S(q)$ decreases as qR_G increases (Fig. 9.6); **the scattering can determine the R_G at small q regimes and probe the scaling law at high q regimes**.

If qR is large,

$$S(\boldsymbol{q}) \to \frac{2N}{q^2 R_G^2} \sim \left(\frac{1}{ql}\right)^{-D_f} \tag{9.67}$$

with $D_f = 2$. This fractal dimension of the ideal chain is also obtained from (9.58) with $R \sim R_G \sim N^{1/2} l$. In general, as we have discussed, $S(\boldsymbol{q})$ can probe the self-similar structures; for a real polymer chain where $R \sim N^{\nu}$ (10.105), for large q $S(\boldsymbol{q}) \sim q^{-D_f}$ with $D_f = 1/\nu$.

Equation (9.64) can be approximated by the form $S(q) \approx N/\left(1 + q^2 R_G^2/2\right)$ within 15% error over the whole range of q. Its inverse Fourier transform yields

$$g(r) - 1 = \frac{R_G}{r} \exp\left(-2^{1/2} \frac{r}{R_G}\right), \tag{9.68}$$

which looks similar to that for a fluid near critical point with the correlation length $2^{-1/2} R_G$ that can be very large for a long chain.

Further Reading and References

P.M. Chaikin, T.C. Lubensky, *Principles of Condensed Matter Physics* (Cambridge University Press, 2006)

D. Andelman, *Soft Condensed Matter Physics in Molecular and Cell Biology*, ed. by W.C.K. Poon (Taylor and Francis, 2006)

I.G. Serdyuk, N.R. Zaccai, J. Zaccal, *Methods in Molecular Biophysics* (Cambridge University Press, 2007)

B.J. Berne, R. Percora, *Dynamic Light Scattering* (Wiley-Interscience Publications, 1976)

S. Havlin, S.V. Buldyrev, A.L. Goldberger, R.N. Mantegna, S.M. Ossadnik, C.-K. Peng, M. Simon, H.E. Stanley, Fractals in biology and medicine chaos. Solitons Frorrals **6**, 171–201 (1995)

R.A. Crowther, Procedures for three-dimensional reconstruction of spherical viruses by Fourier synthesis from electron micrographs. Philos. Trans. Roy. Soc. Lond. B. **261**, 221–230 (1971)

E.R. Weibel, What makes a good lung? Swiss Med. Wkly. **139**(27–28) (2009)

J.B. Pesavento, J.A. Lawton, M.K. Estes, B.V.V. Prasad, The reversible condensation and expansion of the rotavirus genome. PNAS **98**(4), 1381–1386 (2001)

Chapter 10
Mesoscopic Models of Polymers: Flexible Chains

A **polymer** is a compound macromolecule consisting of many repeating structural units (monomers). It is created through an assembly process called polymerization or polycondensation. Many materials in our environment are made of polymers; these include plastics, rubbers, woods, and papers. In particular biopolymers such as nucleic acids and proteins are primary constituents of our bodies, playing key functional roles in living.

In this and next chapters, we study linear polymers' some basic physical properties that emerge on mesoscopic length scales beyond the details of the monomer structure. The microscopic details are of course essential, in particular to chemists and biologists, but are not relevant to universal physical features that emerge in long chain polymers. One such feature is **chain flexibility**, which yields many novel features that have not been studied in earlier chapters. Here we study such aspects considering a single polymer.

In contrast to synthetic polymers such as polyethylene (Fig. 10.1a), a typical biopolymer is an enormously complex macromolecule formed by linking many monomers, which themselves are not simple, as a protein formed of amino acids and

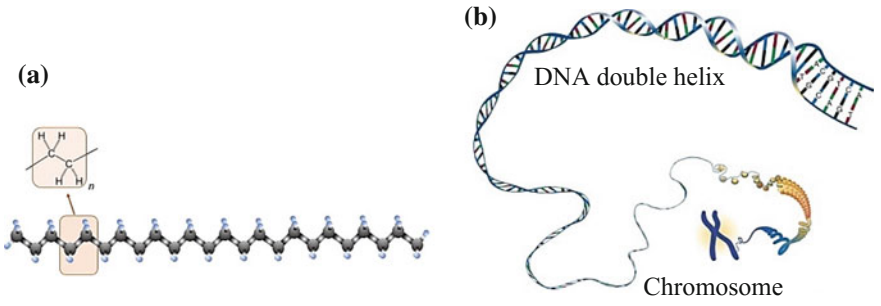

Fig. 10.1 **a** Polyethylene molecule ($CH_2 - CH_2 - CH_2 - \cdots$), **b** a double stranded DNA viewed on different length scales. *Courtesy* National Human Genome Research Institute

W. Sung, *Statistical Physics for Biological Matter*, Graduate Texts in Physics,
https://doi.org/10.1007/978-94-024-1584-1_10

DNA formed of nucleotides. Figure 10.1b sketches a fascinating hierarchy of double stranded DNA's structures folded over multi-scales from double helices to chromosomes. On the atominstic scale, the energy involved in the bonding is mostly covalent, which is in the order of eV or higher. Even though there are any monomeric internal degrees of freedom such as rotational and vibrational ones that can be thermally excited, the chain is locally very stiff. But, when viewed over long-length scales, the chain interconnectivity gives rise to chain flexibility and susceptibility to thermal fluctuations (Fig. 10.1b). **This chain flexibility, coupled with the weak interactions therein** (Chap. 6) **in aqueous environments may enable the biopolymers to undergo the essential conformational transitions at body temperature**.

For a linear polymer one can define the length l_p, called the **persistence length, above which the chain looks curved and flexible**. The chain fragment shorter than l_p may look nearly straight and rigid. The persistence length of a simple synthetic polymer, polyethylene, Fig. 10.1a, where rotational motion is the major flexibility mechanism, is about 0.4 nm. For biopolymers like polypetides or ds DNA thermal vibration is the flexibility mechanism. The single stranded (ss) DNA is a flexible chain with $l_p \sim 1$ nm compared with ds DNA in which the persistence length is about 50 nm. Below we start with the simplest case, that is, the highly flexible chain that emerges when coarse–grained over a long length scale.

10.1 Random Walk Model for a Flexible Chain

We consider a flexible polymer that has the contour length much longer than its persistence length, e.g., a 1μ long ss DNA fragment. We introduce the ideal chain model, in which the chain conformation is made by a random walk. In this model, a chain consists of a large number (N) of freely-jointed links each with length l that we studied in Chap. 3 (Fig. 10.2). This segmental length l, called the Kuhn length, is not necessarily the molecular bond length, but is introduced to represent the length over which the link orientation is uncorrelated, namely,

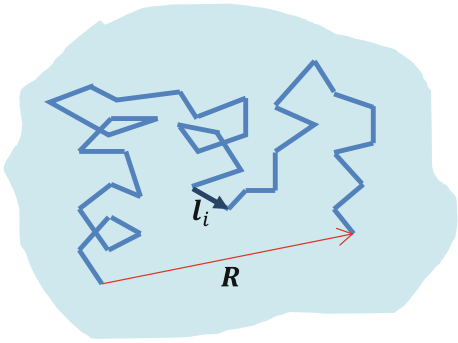

Fig. 10.2 Random walk model for polymer conformations with the end-to-end distance $\boldsymbol{R}$ and segmental displacement (link vector) $\boldsymbol{l}_i$

$$\langle \boldsymbol{l}_i \cdot \boldsymbol{l}_j \rangle = l^2 \delta_{ij}, \tag{10.1}$$

where $\boldsymbol{l}_i$ is the ith link vector. $\langle \cdots \rangle$ denotes the average over equilibrium ensemble of the chains of N links, and δ_{ij} is the Kronecker delta function, which is 1 if $i = j$, and 0 otherwise.

Let us characterize the conformational state of the chain by its end-to-end distance (EED) vector,

$$\boldsymbol{R} = \sum_{i=1}^{N} \boldsymbol{l}_i. \tag{10.2}$$

Taking the ensemble averages, we have

$$\langle \boldsymbol{R} \rangle = 0 \tag{10.3}$$

and

$$\langle \boldsymbol{R}^2 \rangle = Nl^2 \equiv R_0^2. \tag{10.4}$$

The root-mean-squared (rms) EED for the ideal chain

$$R_0 \equiv \langle \boldsymbol{R}^2 \rangle^{1/2} = N^{1/2} l \tag{10.5}$$

is a measure of the natural size of the chain.

Although seemingly very simple, (10.5) signifies quite a number of important features that characterize long chains. First the power 1/2 in $N^{1/2}$ is a universal exponent that is independent of molecular details, i.e., is valid whether the polymer is ssDNA or polyethylene. Second, R_0 is very small compared with the full length in the model, $L = Nl$; we have $R_0/L = N^{-1/2} \ll 1$, which implies that a long chain is coiled at equilibrium so as to be highly flexible to extension.

The distribution of the EED vector $\boldsymbol{R}$ can be obtained by invoking the **Central Limit Theorem (CLT)** [see for example Reif (1965)]. As explained in the box shortly, CLT states that, in the ensemble of the random walks, each of which consists of infinitely many (N) steps with the length l in **statistically independent or uncorrelated directions, the end-to end distance $\boldsymbol{R}$ is distributed in Gaussian**,

$$P(\boldsymbol{R}) = \left(\frac{3}{2\pi \langle \Delta R^2 \rangle} \right)^{3/2} \exp\left[-\frac{3\boldsymbol{R}^2}{2\langle \Delta R^2 \rangle} \right], \tag{10.6}$$

with variance,

$$\begin{aligned}\left\langle \Delta R^2 \right\rangle &= \left\langle (\boldsymbol{R} - \langle \boldsymbol{R} \rangle)^2 \right\rangle \\ &= \left\langle \boldsymbol{R}^2 \right\rangle - \langle \boldsymbol{R} \rangle^2 = Nl^2\end{aligned} \tag{10.7}$$

in a manner independent of the details of the steps. The chain that satisfies above properties are called an ideal chain or a **Gaussian chain**.

P10.1 *The radius of gyration R_G in a Gaussian chain of N Kuhn lengths is defined by*

$$R_G^2 = \frac{\left\langle \sum_{i=1}^{N} (\boldsymbol{r_i} - \boldsymbol{R}_{cm})^2 \right\rangle}{N},$$

where $\boldsymbol{r_i}$ is the position vector of the ith vertex and $\boldsymbol{R}_{cm}$ is the center of mass of the chain. Show that ${R_G}^2 = Nl^2/6$.

10.1.1 Central Limit Theorem (CLT)-Extended

Because its applicability of a broad spectrum of natural phenomena, below we give a derivation of the CLT. For generality, consider that the step or link lengths ($|\boldsymbol{l}_i|$) in the random walk are not all same. The EED probability density $P(\boldsymbol{R};N)$ is obtained by summation (integration) over all the N link vectors ($\boldsymbol{l}_1,\boldsymbol{l}_2 \ldots \boldsymbol{l}_N$) under the condition that $\boldsymbol{R} = \boldsymbol{l}_1 + \boldsymbol{l}_2 \cdots + \boldsymbol{l}_N$ is given as fixed, as implemented by a delta function below:

$$P(\boldsymbol{R};N) = \int d\boldsymbol{l}_1 \int d\boldsymbol{l}_2 \ldots \int d\boldsymbol{l}_N \, \delta(\boldsymbol{l}_1 + \boldsymbol{l}_2 \cdots + \boldsymbol{l}_N - \boldsymbol{R}) P_N(\boldsymbol{l}_1, \boldsymbol{l}_2, \ldots \boldsymbol{l}_N). \tag{10.8}$$

Here $P_N(\boldsymbol{l}_1, \boldsymbol{l}_2, \ldots \boldsymbol{l}_N)$ is the joint probability distribution of all links. We consider that every link distribution is independent of each other,

$$P_N(\boldsymbol{l}_1, \boldsymbol{l}_2, \ldots \boldsymbol{l}_N) = p_1(\boldsymbol{l}_1) \ldots p_N(\boldsymbol{l}_N) \tag{10.9}$$

Equation (10.8) is evaluated by inserting the above relation and

$$\delta(\boldsymbol{l}_1 + \boldsymbol{l}_2 \cdots + \boldsymbol{l}_N - \boldsymbol{R}) = (2\pi)^{-3} \int d\boldsymbol{k} \, e^{i\boldsymbol{k}\cdot(\boldsymbol{l}_1 + \boldsymbol{l}_2 \cdots + \boldsymbol{l}_N - \boldsymbol{R})}, \tag{10.10}$$

into the integral, which now can be expressed as

$$P(\boldsymbol{R};N) = (2\pi)^{-3} \int d\boldsymbol{k} \, e^{-i\boldsymbol{k}\cdot\boldsymbol{R}} \{p_1(\boldsymbol{k}) \ldots p_N(\boldsymbol{k})\}, \tag{10.11}$$

where

$$p_n(\boldsymbol{k}) = \int d\boldsymbol{l_n}\, p_n(\boldsymbol{l_n}) e^{i\boldsymbol{k}\cdot\boldsymbol{l_n}} = \left\langle e^{i\boldsymbol{k}\cdot\boldsymbol{l_n}} \right\rangle \tag{10.12}$$

is a Fourier transform, known as the characteristic function of $p_n(\boldsymbol{l})$.

In the integral above, $e^{i\boldsymbol{k}\cdot\boldsymbol{l_n}}$ is a function that, for large k, oscillates rapidly and gives a diminishing contribution to $p_n(\boldsymbol{k})$. For a large N, $\{p_1(\boldsymbol{k})\ldots p_N(\boldsymbol{k})\}$ decreases very rapidly to zero as k increases. Therefore, the function $\ln\{p_1(\boldsymbol{k})\ldots p_N(\boldsymbol{k})\}$, which varies more smoothly than $\{p_1(\boldsymbol{k})\ldots p_N(\boldsymbol{k})\}$, can nicely be approximated by its expansion to the second order in k,

$$\begin{aligned} \ln\{p_1(\boldsymbol{k})\ldots p_N(\boldsymbol{k})\} &\cong \sum_{n=1}^{N} \ln\left(1 + i\boldsymbol{k}\cdot\langle\boldsymbol{l_n}\rangle - \frac{1}{2}(\boldsymbol{k}\cdot\langle\boldsymbol{l_n}\rangle)^2\right) \\ &\cong \sum_{n=1}^{N}\left(i\langle\boldsymbol{l_n}\rangle\cdot\boldsymbol{k} - \frac{1}{6}\langle\Delta {l_n}^2\rangle k^2\right), \end{aligned} \tag{10.13}$$

so that $\{p_1(\boldsymbol{k})\ldots p_N(\boldsymbol{k})\} \cong \exp\left[N\left(i\langle\boldsymbol{l}\rangle\cdot\boldsymbol{k} - \frac{1}{6}\langle\Delta l^2\rangle k^2\right)\right]$, and

$$p(\boldsymbol{k}) = \exp\left[\left(i\langle\boldsymbol{l}\rangle\cdot\boldsymbol{k} - \frac{1}{6}\langle\Delta l^2\rangle k^2\right)\right], \tag{10.14}$$

where the average and variance $\langle\boldsymbol{l_n}\rangle$, $\langle\Delta l_n^2\rangle$ are taken over the single bond distribution $p_n(\boldsymbol{l})$ and $\langle\boldsymbol{l}\rangle = \sum_{n=1}^{N}\langle\boldsymbol{l_n}\rangle/N$, $\langle\Delta l^2\rangle = \sum_{n=1}^{N}\langle\Delta l_n^2\rangle/N$. In general, $\langle\boldsymbol{l_n}\rangle \neq 0$, i.e., the random walk can be biased. Inserting (10.14) into (10.11) and performing a Fourier transformation therein just yields the Gaussian probability distribution of $\boldsymbol{R}$,

$$P(\boldsymbol{R};N) = \left(\frac{3}{2\pi\langle\Delta R^2\rangle}\right)^{3/2} \exp\left[-\frac{3(\boldsymbol{R}-\langle\boldsymbol{R}\rangle)^2}{2\langle\Delta R^2\rangle}\right] \tag{10.15}$$

with the non-vanishing mean and variance:

$$\langle\boldsymbol{R}\rangle = N\langle\boldsymbol{l}\rangle = \sum_{n=1}^{N}\langle\boldsymbol{l_n}\rangle \tag{10.16}$$

$$\langle\Delta R^2\rangle = N\langle\Delta l^2\rangle = \sum_{n=1}^{N}\langle\Delta l_n^2\rangle. \tag{10.17}$$

The Gaussian distribution (10.15) is more general than previous one (10.6) in that the individual steps can have different sizes ($|\boldsymbol{l}_i| \neq |\boldsymbol{l}_j|$) and can be biased $\langle \boldsymbol{l}_i \rangle \neq 0$. **No matter what the individual step distribution $p_n(\boldsymbol{l}_n)$ may be, provided that it is statistically independent, the general Gaussian distribution is valid for large N, and exact in $N \to \infty$ limit.** This very important result is the statement of CLT.

This universality does not only concern the ideal long chain polymer properties; it also accounts for numerous phenomena in nature that involve large numbers. For example a measurement error can be regarded to be an accumulation of many statistically independent errors, so their distribution is Gaussian. Consider the variables (e.g., E, V, N) of macroscopic or mesoscopic systems. The deviations of the variables about their averages can be constructed to be the sum of many small quantities that are statistically independent. So the deviations are also distributed in Gaussian. For example, **the Gaussian distribution of these macroscopic properties about their means** could be obtained earlier (e.g., for energy (3.39)) using the ensemble theory.

10.1.2 The Entropic Chain

In light of the coarse-grained description described in Chap. 5, the relevant degree of freedom for the chain is $\mathcal{Q} = \boldsymbol{R}$, and its distribution is $P(\mathcal{Q}) \propto e^{-\beta \mathcal{F}(\mathcal{Q})}$ (5.5). Then, the (10.6) allows us to identify **the chain's effective Hamiltonian or the free energy function associated with $\boldsymbol{R}$** as

$$\mathcal{F}(\boldsymbol{R}) = \frac{3k_B T}{2Nl^2}\boldsymbol{R}^2, \tag{10.18}$$

apart from a term $\sim k_B T \ln N$, which is independent of $\boldsymbol{R}$ so is irrelevant. By virtue of the thermodynamic relations introduced in Chap. 2, the associated entropy function is

$$S(\boldsymbol{R}) = -\frac{\partial \mathcal{F}(\boldsymbol{R})}{\partial T} = -\frac{3k_B}{2Nl^2}\boldsymbol{R}^2. \tag{10.19}$$

This demonstrates that as the chain is extended (R increases) the entropy decreases. When $\boldsymbol{R} = 0$, the free energy is minimum, and the entropy is maximum; it is because the number of chain (random walk) configurations is maximal. Although (10.18) reasonably describes the entropy change associated with the extension, it neglects other contributions that are irrelevant to $\boldsymbol{R}$. To keep the EED of the chain at $\boldsymbol{R}$, a force

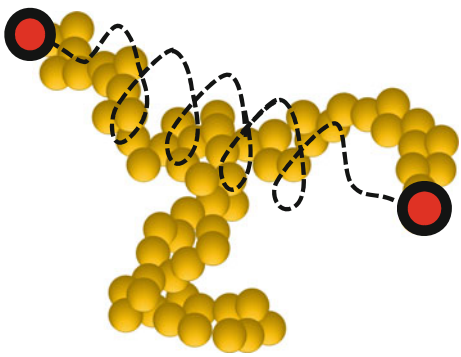

Fig. 10.3 A long flexible chain of N uncorrelated beads behaves elastically as if its two ends are connected by an spring of the (entropic) spring constant $K_e = 3k_BT/Nl^2$

$$\boldsymbol{f}(\boldsymbol{R}) = \frac{\partial \mathcal{F}(\boldsymbol{R})}{\partial \boldsymbol{R}} = K_e \boldsymbol{R}, \tag{10.20}$$

must be applied along the direction in which the entropy decreases. Here

$$K_e = \frac{3k_BT}{Nl^2}, \tag{10.21}$$

called the **entropic spring constant** (Fig. 10.3), increases with temperature but decreases with contour length. This remarkable behavior of chain entropy and flexibility is indeed the emergent behaviors of a long chain. This behavior was derived earlier using the freely-jointed chain model in Chap. 3.

The description in terms of the effective Hamiltonian or the free energy function $\mathcal{F}\{\mathcal{Q}\}$ has further conceptual and practical advantages. Consider that the chain carries positive charges Q at both ends in water. What is the entropy associated with an extension of the chain ends? We can easily accept that the free energy (10.18) is changed to

$$\mathcal{F}(\boldsymbol{R}) = \frac{3k_BT}{2Nl^2}\boldsymbol{R}^2 + \frac{Q^2}{4\pi\varepsilon_w|\boldsymbol{R}|}, \tag{10.22}$$

by assuming the charges do not induce polarization in the polymer. This yields the probability density for the EED $\boldsymbol{R}$, $P(\boldsymbol{R}) \sim e^{-\beta\mathcal{F}(\boldsymbol{R})}$. Also the entropy of the chain given $\boldsymbol{R}$ is given by

$$S(\boldsymbol{R}) = -\frac{\partial \mathcal{F}(\boldsymbol{R})}{\partial T} = -\frac{3k_B}{2Nl^2}\boldsymbol{R}^2 + \frac{Q^2}{4\pi\varepsilon_w{}^2|\boldsymbol{R}|}\left(\frac{\partial \varepsilon_w}{\partial T}\right). \tag{10.23}$$

The second term on the right denotes the contribution of the charges, which depends on the solvent through the temperature dependence of its dielectric constant ε_w; via (6.10), the contribution is $-1.36Q^2/(4\pi\varepsilon_w|\boldsymbol{R}|T)$ at $T = 25\ ^\circ\mathrm{C}$ for waterly solvents. As explained earlier, this implies that, as $|\boldsymbol{R}|$ decreases, the entropy does decrease due

enhanced alignment of the water molecules solvated to the charges. This highly nontrivial result, albeit quite approximate, is obtained by our methodology of the free energy or effective Hamiltonian function $\mathcal{F}(\boldsymbol{R})$. The evaluation of chain statistics under the Coulomb interaction or other microscopic approaches would be not be easy to accommodate the entropy contribution from the charges and the solvent background in any approximate ways.

P10.2 *What is the most probable magnitude $\overline{R}$ of the EED in the above problem? To answer this question we should note the probability density $P(R)$ of the scalar R is proportional to $R^2 e^{-\beta\mathcal{F}(\boldsymbol{R})}$. Making a second order expansion for $P(R)$ about $\overline{R}$, find the mean and variance of R.*

If the initial position of the polymer is $\boldsymbol{r}_0$, (10.6) can be rewritten as

$$G_0(\boldsymbol{r}, \boldsymbol{r}_0; N) = \left(2\pi N l^2/3\right)^{-3/2} \exp\left[-\frac{3(\boldsymbol{r}-\boldsymbol{r}_0)^2}{2Nl^2}\right]. \tag{10.24}$$

The $G_0(\boldsymbol{r}, \boldsymbol{r}_0; N)$ is the polymer Greens function that describes the probability density of finding the end point at $\boldsymbol{r}$ with its initial point located at $\boldsymbol{r}_0$, in a free space. As can be verified by direct substitution, $P(\boldsymbol{r}; N) = G_0(\boldsymbol{r}, \boldsymbol{r}_0; N)$ satisfies the diffusion-type equation in free space,

$$\frac{\partial}{\partial N} P(\boldsymbol{r}; N) = \frac{1}{6} l^2 \nabla^2 P(\boldsymbol{r}; N). \tag{10.25}$$

The $G_0(\boldsymbol{r}, \boldsymbol{r}_0; N)$ is also termed as the fundamental solution to the differential equation (10.25), in that it satisfies the initial condition $G_0(\boldsymbol{r}, \boldsymbol{r}_0; N = 0) = \delta(\boldsymbol{r} - \boldsymbol{r}_0)$. The diffusion equation is a special case of the Edwards equation for the random walk in the presence of an external influence, which will be derived next. If the initial position is not known for certainty but distributed by a PDF $P(\boldsymbol{r}_0; 0)$, the PDF for the chain end (N th vertex) to be at $\boldsymbol{r}$ can be obtained by

$$P(\boldsymbol{r}; N) = \int d\boldsymbol{r}_0 G_0(\boldsymbol{r}, \boldsymbol{r}_0; N) P(\boldsymbol{r}_0; 0). \tag{10.26}$$

This means the solution of (10.25) that meets the appropriate boundary conditions can be constructed by a linear superposition of different fundamental solutions, thanks to linearity of the equation.

Example: A Chain Anchored on Surface

Consider an ideal N-segment chain that is anchored at one end to a point on a surface (on (y, z) plane). The interaction between a segment and surface is assumed to be only a steric one, namely, segments cannot cross the surface (Fig. 10.4). What

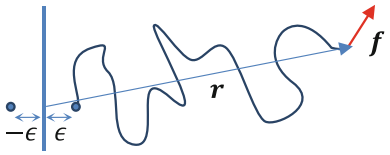

Fig. 10.4 A polymer chain anchored on surface (with $\epsilon \to 0$) is extended by a force $\boldsymbol{f}$ to the distance $\boldsymbol{r}$

are the free energy $\mathcal{F}(\boldsymbol{r})$ and the applied force $\boldsymbol{f}(\boldsymbol{r})$ that are necessary to keep the other end at the position $\boldsymbol{r} = (x, y, z)$ from the anchorage?

The presence of the impenetrable wall imposes a boundary condition (BC) on the polymer distribution function: $P(\boldsymbol{r}; n) = 0$, for any n; $0 < n \leq N$. To meet the BC we construct the solution by superposing two free-space fundamental solutions to (10.25) with a point source at $\boldsymbol{r}_0 = (\epsilon, 0, 0)$ and its mirror image at $-\boldsymbol{r}_0 = (-\epsilon, 0, 0)$, in a way akin to the image solution method in electrostatics, with ϵ taken to be infinitesimally small:

$$P(\boldsymbol{r}; n) = \left(2\pi n l^2/3\right)^{-3/2} \exp\left[-\frac{3(\boldsymbol{r}-\boldsymbol{r}_0)^2}{2nl^2}\right] - \left(2\pi n l^2/3\right)^{-3/2} \exp\left[-\frac{3(\boldsymbol{r}+\boldsymbol{r}_0)^2}{2nl^2}\right]. \tag{10.27}$$

Taking the limit $\epsilon \to 0$, we have

$$P(\boldsymbol{r}; n) = \left(2\pi n l^2/3\right)^{-3/2} \frac{6x\epsilon}{nl^2} \exp\left(-\frac{3\boldsymbol{r}^2}{2nl^2}\right). \tag{10.28}$$

Then, the **free energy of the chain with the end kept at $\boldsymbol{r}$** is

$$\begin{aligned} \mathcal{F}(\boldsymbol{r}) &= -k_B T \ln P(\boldsymbol{r}; N) \\ &= \frac{3k_B T}{2Nl^2}\boldsymbol{r}^2 - k_B T \ln x \end{aligned} \tag{10.29}$$

apart from a constant independent of the position. **The force that the chain end experiences** is

$$-\boldsymbol{f}(\boldsymbol{r}) = -\frac{\partial \mathcal{F}(\boldsymbol{r})}{\partial \boldsymbol{r}} = -\frac{3k_B T}{Nl^2}\boldsymbol{r} + \frac{k_B T}{x^2}\boldsymbol{x}, \tag{10.30}$$

which is indeed proportional to T due to the entropic nature of chain. On the right hand side, the first term is the entropic restoring force opposite to the applied force discussed before, while the latter is the entropic repulsive force due to the presence of the wall; remarkably this noncentral repulsive force tends to be infinity as x approaches 0.

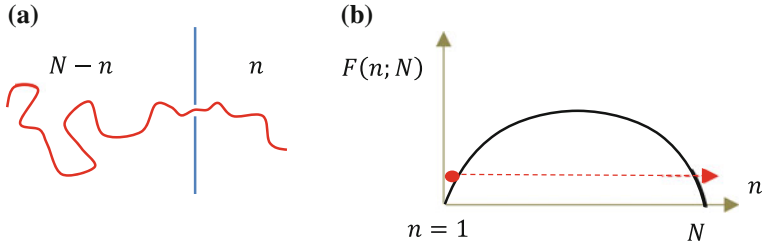

Fig. 10.5 **a** A polymer configuration under translocation through a pore and **b** the associate free energy as a function of translocated segment number n. The chain initially at the initial state $\boldsymbol{n} = 1$ can cross over the free energy barrier to arrive at the final state $\boldsymbol{n} = \boldsymbol{N}$, that is, it can translocate

The Free Energy of Polymer Translocation

Consider a flexible polymer of N-segments during translocation through a narrow pore in a membrane with n segments on the tran-side and $N - n$ on the cis-side as shown in then Fig. 10.5a. What is the free energy $\mathcal{F}(n; N)$ required to maintain the chain in this configuration, namely, the free energy of the translocation?

Focusing the chain on the trans side, we consider that n is its primary degree of freedom; integrating over all accessible configurations given n yields the chain free energy $\mathcal{F}(n)$:

$$e^{-\beta\mathcal{F}(n)} = \sum_{\boldsymbol{r}} e^{-\beta\mathcal{F}(\boldsymbol{r}/n)} = \int_{x>0} d\boldsymbol{r}\; P(\boldsymbol{r}; n), \tag{10.31}$$

where $P(\boldsymbol{r}; n)$ is given by (10.28) and the integration is performed over the position in the half space where $x > 0$. The integration yields

$$\int_o^\infty dx \left(2\pi n l^2/3\right)^{-1/2} \frac{6x\epsilon}{nl^2} \exp\left(-\frac{3x^2}{2nl^2}\right) \sim n^{-1/2} \int_0^\infty d\tilde{x}\, \tilde{x}\; e^{-3\tilde{x}^2/2} \sim n^{-1/2}, \tag{10.32}$$

where $\tilde{x} = (nl^2)^{-1/2} x$ is a dimensionless coordinate. Consequently, the free energy given by (10.31) is

$$\mathcal{F}(n) = \frac{1}{2} k_B T \ln n \tag{10.33}$$

apart from a irrelevant constant. Considering the chain in the cis side is anchored also at the origin, its free energy is obtained similarly as

$$\mathcal{F}(N-n) = \frac{1}{2} k_B T \ln(N-n). \tag{10.34}$$

Thus we can find the free energy of the whole chain in translocation:

$$\mathcal{F}(n;N) = \mathcal{F}(n) + \mathcal{F}(N-n) = \frac{1}{2} k_B T \ln n(N-n), \tag{10.35}$$

apart from the irrelevant term independent of n (Sung and Park 1996). The free energy is depicted as a function of n in Fig. 10.5b. It is in a sharp contrast to that colloidal particle translocation in Sect. 3.1; at $n = N/2$ the chain's free energy is maximum, and the entropy $S(n;N) = -\partial F(n;N)/\partial T = -F(n;N)/T$ is minimum. This difference is due to chain connectivity; if the colloidal particles were to be linearly interconnected to form a polymer, the free energy function would become drastically different. **The free energy barrier** of the height $k_B T \ln(N/2) \sim k_B T$, which the initial state $n = 1$ faces for translocation, **can be overcome by thermal agitation, leading to eventual translocation of the entire chain to the right**. In contrast, unconnected particles cannot translocate to the right entirely.

P10.3 *What is force necessary to extend the chain to initiate the translocation at the pore as shown below. Assume that the chain in the trans side is tightly extended.*

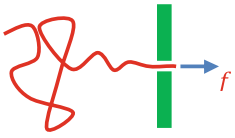

10.2 A Flexible Chain Under External Fields and Confinements

In many situations a polymer is subject to external forces, confinements, and intra-chain interactions. An important problem is to find the chain conformations and thermodynamic behaviors under such conditions. Due to the chain connectivity a polymer under such constraints manifests many interesting entropic behaviors that are not seen in ordinary particle systems.

We consider an approximation in which each segment can be treated as if it is under **an effective external potential, called the self-consistent field**, similar to the mean field in the Debye-Hückel theory. A central object to find first is the **polymer Green's function**, $G(\boldsymbol{r}, \boldsymbol{r}'; N)$, which is the probability density of finding the chain end at the distance $\boldsymbol{r}$ given the initial segment position at $\boldsymbol{r}'$. We consider the N-step random walk with each step influenced by an effective external potential energy u. Given the probability $G(\boldsymbol{r}_{N-1}, \boldsymbol{r}'; N-1)$ for the $N-1$ th step to be at $\boldsymbol{r}_{N-1}$, it can

jump to $\boldsymbol{r}$ at the N th step with the probability density $p(\boldsymbol{r}-\boldsymbol{r}_{N-1})$, satisfying the recurrence relation,

$$G(\boldsymbol{r},\boldsymbol{r}';N)=\int d\boldsymbol{r}_{N-1}\, e^{-\beta u(\boldsymbol{r})}p(\boldsymbol{r}-\boldsymbol{r}_{N-1})G(\boldsymbol{r}_{N-1},\boldsymbol{r}';N-1), \tag{10.36}$$

where the $u(\boldsymbol{r})$ is the effective potential energy at $\boldsymbol{r}$.

10.2.1 Polymer Green's Function and Edwards' Equation

There are two ways of solving (10.36). The first is to convert the equation into a differential equation called **the Edwards equation** (Edwards 1965). The other is to iterate the equation to represent the Green's function as a path integral. To derive the differential equation, we consider the case where G varies slowly over unit step distance $\boldsymbol{l}$, and so is expanded to the second order in $\boldsymbol{l}$:

$$\begin{aligned} G(\boldsymbol{r},\boldsymbol{r}';N) &\cong e^{-\beta u(\boldsymbol{r})}\int d\boldsymbol{l}\; p(\boldsymbol{l})\left[1+\boldsymbol{l}\cdot\nabla+\frac{1}{2}(\boldsymbol{l}\cdot\nabla)^2\right]G(\boldsymbol{r},\boldsymbol{r}';N-1) \\ &= e^{-\beta u(\boldsymbol{r})}\left[1+\langle\boldsymbol{l}\rangle\cdot\nabla+\frac{1}{2}(\boldsymbol{l}\cdot\nabla)^2\right]G(\boldsymbol{r},\boldsymbol{r}';N-1). \end{aligned} \tag{10.37}$$

Over a segment $p(\boldsymbol{l})$ is isotropic, $\langle\boldsymbol{l}\rangle=0$, and $\left\langle(\boldsymbol{l}\cdot\nabla)^2\right\rangle=\sum_{\alpha,\beta}\langle l_\alpha l_\beta\rangle\nabla_\alpha\nabla_\beta=(l^2/3)\sum_{\alpha,\beta}\delta_{\alpha\beta}\nabla_\alpha\nabla_\beta=l^2\nabla^2/3$, and (10.37) can be written as

$$G(\boldsymbol{r},\boldsymbol{r}';N)\cong e^{-\beta u(\boldsymbol{r})}\left[1+\frac{1}{6}l^2\nabla^2\right]G(\boldsymbol{r},\boldsymbol{r}';N-1). \tag{10.38}$$

Rewriting it as

$$\ln\left[\frac{G(\boldsymbol{r},\boldsymbol{r}';N)}{G(\boldsymbol{r},\boldsymbol{r}';N-1)}\right]\cong\ln\left[\frac{e^{-\beta u(\boldsymbol{r})}\left[1+\frac{1}{6}l^2\nabla^2\right]G(\boldsymbol{r},\boldsymbol{r}';N-1)}{G(\boldsymbol{r},\boldsymbol{r}';N-1)}\right] \tag{10.39}$$

and considering $G(\boldsymbol{r},\boldsymbol{r}';N)\cong G(\boldsymbol{r},\boldsymbol{r}';N-1)+\partial G(\boldsymbol{r},\boldsymbol{r}';N-1)/\partial N$. While keeping the leading orders, we obtain a partial differential equation,

$$-\frac{\partial}{\partial N}G(\boldsymbol{r},\boldsymbol{r}';N)=\mathcal{L}_E G(\boldsymbol{r},\boldsymbol{r}';N), \tag{10.40}$$

where

$$\mathcal{L}_E = -\frac{l^2}{6}\nabla^2 + \beta u(\boldsymbol{r}). \tag{10.41}$$

Note that, unlike treatments in some monographs [e.g., Doi and Edwards (1988)], $\beta u(\boldsymbol{r})$ is not necessarily much smaller than unity in magnitude. Equation (10.40), called the Edwards equation, is similar in structure to the Schrödinger equation, from which several well-known methods to find the solution can be borrowed. When $\beta u(\boldsymbol{r}) = 0$, the Edwards equation is reduced to the diffusion equation (10.25).

The Green's function solution of the Edwards equation (10.40), with the initial condition $G(\boldsymbol{r}, \boldsymbol{r}'; 0) = \delta(\boldsymbol{r} - \boldsymbol{r}')$, is formally written as

$$G(\boldsymbol{r}, \boldsymbol{r}'; N) = e^{-N\mathcal{L}_E} G(\boldsymbol{r}, \boldsymbol{r}'; 0) = e^{-N\mathcal{L}_E} \delta(\boldsymbol{r} - \boldsymbol{r}'). \tag{10.42}$$

Suppose that the ψ_n and ϵ_n are respectively the n-th eigenfunction and eigenvalue of the operator $\mathcal{L}_E$,

$$\mathcal{L}_E \psi_n(\boldsymbol{r}) = \epsilon_n \psi_n(\boldsymbol{r}), \tag{10.43}$$

where $\psi_n(\boldsymbol{r})$ are *real* functions that form a complete, orthonormal basis:

$$\delta_{nm} = \int \mathrm{d}\boldsymbol{r}\, \psi_n(\boldsymbol{r}) \psi_m(\boldsymbol{r}), \tag{10.44}$$

$$\delta(\boldsymbol{r} - \boldsymbol{r}') = \sum_{n=0}^{\infty} \psi_n(\boldsymbol{r}) \psi_n(\boldsymbol{r}'). \tag{10.45}$$

Using this eigen-basis, the solution (10.42) is expanded as

$$G(\boldsymbol{r}, \boldsymbol{r}'; N) = \sum_{n=0}^{\infty} e^{-N\epsilon_n} \psi_n(\boldsymbol{r}) \psi_n(\boldsymbol{r}') \tag{10.46}$$

10.2.2 The Formulation of Path-Integral and Effective Hamiltonian of a Chain

An alternative to the eigenfunction expansion for the polymer Green's function is the path integral representation. An iteration of (10.36) generates

$$
\begin{aligned}
G(\boldsymbol{r},\boldsymbol{r}';N) &= \int d\boldsymbol{r}_{N-1}\, e^{-\beta u(\boldsymbol{r})} p(\boldsymbol{r}-\boldsymbol{r}_{N-1}) \\
&\quad \int d\boldsymbol{r}_{N-2}\, e^{-\beta u(\boldsymbol{r}_{N-1})} p(\boldsymbol{r}_{N-1}-\boldsymbol{r}_{N-2}) G(\boldsymbol{r}_{N-2},\boldsymbol{r}';N-2) \\
&= \int d\boldsymbol{r}_{N-1}\, e^{-\beta u(\boldsymbol{r})} p(\boldsymbol{r}-\boldsymbol{r}_{N-1}) \int d\boldsymbol{r}_{N-2}\, e^{-\beta u(\boldsymbol{r}_{N-1})} p(\boldsymbol{r}_{N-1}-\boldsymbol{r}_{N-2}) \\
&\quad \ldots \int d\boldsymbol{r}_0\, e^{-\beta u(\boldsymbol{r}_1)} p(\boldsymbol{r}_1-\boldsymbol{r}_0) G(\boldsymbol{r}_0,\boldsymbol{r}';0),
\end{aligned}
\tag{10.47}
$$

which, with $G(\boldsymbol{r}_0,\boldsymbol{r}';0)=\delta(\boldsymbol{r}_0-\boldsymbol{r}')$, can be written as

$$
\begin{aligned}
G(\boldsymbol{r},\boldsymbol{r}';N) = \int d\boldsymbol{r}_1 \ldots \int d\boldsymbol{r}_{N-1} e^{-\beta\{u(\boldsymbol{r}')+u(\boldsymbol{r}_1)+u(\boldsymbol{r}_2)\cdots+u(\boldsymbol{r}_{N-1})+u(\boldsymbol{r})\}} \\
p(\boldsymbol{r}_1-\boldsymbol{r}')p(\boldsymbol{r}_2-\boldsymbol{r}_1)p(\boldsymbol{r}_3-\boldsymbol{r}_2)\ldots p(\boldsymbol{r}_{N-1}-\boldsymbol{r}_{N-2})p(\boldsymbol{r}-\boldsymbol{r}_{N-1}).
\end{aligned}
\tag{10.48}
$$

The segmental orientation distribution function is

$$
p(\boldsymbol{r}_n-\boldsymbol{r}_{n-1}) = \left(\frac{3}{2\pi l^2}\right)^{3/2} \exp\left[-\frac{3(\boldsymbol{r}_n-\boldsymbol{r}_{n-1})^2}{2l^2}\right] \tag{10.49}
$$

as can be obtained from the Fourier transform of $p(\boldsymbol{k}) = \exp\left(-l^2\boldsymbol{k}^2/6\right)$ (10.14). Substituting this into (10.49) yields

$$
\begin{aligned}
G(\boldsymbol{r},\boldsymbol{r}';N) = \left(\frac{3}{2\pi l^2}\right)^{\frac{3(N-1)}{2}} \int_{\boldsymbol{r}_0=\boldsymbol{r}'}^{\boldsymbol{r}_N=\boldsymbol{r}} \ldots \int d\boldsymbol{r}_1 \ldots d\boldsymbol{r}_{N-1} \\
\exp\left[-\sum_{n=1}^{N}\left\{\frac{3}{2}\frac{(\boldsymbol{r}_n-\boldsymbol{r}_{n-1})^2}{l^2}+\beta u(\boldsymbol{r}_n)\right\}\right],
\end{aligned}
\tag{10.50}
$$

where the integration is performed over all positions of vertices $\boldsymbol{r}_n$ between the initial and final points that are fixed at $\boldsymbol{r}'$ and $\boldsymbol{r}$ as indicated.

By associating the exponent in (10.50) with $\exp[-\beta\mathcal{F}\{\boldsymbol{r}_n\}]$, ***the effective Hamiltonian of the chain at the segmental level*** is identified as

$$
\mathcal{F}\{\boldsymbol{r}_n\} = \sum_{n=1}^{N}\left[\frac{3k_BT}{2l^2}(\boldsymbol{r}_n-\boldsymbol{r}_{n-1})^2+u(\boldsymbol{r}_n)\right], \tag{10.51}
$$

which implies that the each vertex is interconnected by an "entropic spring" of the constant $(3k_BT)/l^2$. Henceforth, the flexible polymer chain is regarded as a linear array of the $(N+1)$ beads interconnected by N entropic springs, which bears the name, the **bead-spring model**. In the continuum limit of a long chain in which the

link length l is infinitesimally small in such a way that Nl^2 is finite, (10.51) is written as the functional integral

$$\mathcal{F}\{\boldsymbol{r}_n\} = \int_0^N dn \left[\frac{3k_BT}{2l^2}\left(\frac{\partial \boldsymbol{r}_n}{\partial n}\right)^2 + u(\boldsymbol{r}_n)\right]. \tag{10.52}$$

With this, (10.50) is written as

$$G(\boldsymbol{r}\,\boldsymbol{r}';N) = \int_{r_0=r'}^{r_N=r} \mathcal{D}\{\boldsymbol{r_n}\}\exp[-\beta\mathcal{F}\{\boldsymbol{r_n}\}], \tag{10.53}$$

where the integration is made over all continuous paths connecting the initial and final positions $\boldsymbol{r}$ and $\boldsymbol{r}'$ (Fig. 10.6) and $\mathcal{D}\{r_n\}$ is the path differential element. This **path integral formulation** of polymer conformation is closely similar to Feynman's formulation of a quantum particle propagator [a Green's function of the Schrödinger equation (Feynman and Hibbs 1965)],

$$G(\boldsymbol{r},\boldsymbol{r}';t) = \int \mathcal{D}\{\boldsymbol{r}(t)\}\exp\left[\frac{i}{\hbar}S(t)\right], \tag{10.54}$$

where

$$S(t) = \int_0^t dt\left[\frac{1}{2}m\left(\frac{d\boldsymbol{r}}{dt}\right)^2 - V(\boldsymbol{r})\right] \tag{10.55}$$

is the classical action of a particle with mass m moving under a potential $V(\boldsymbol{r})$. In the classical limit where $\hbar \to 0$, the path in which the action $S(t)$ is minimum is the governing the Newton's equation of motion: $md^2\boldsymbol{r}/dt^2 = -\partial V(\boldsymbol{r})/\partial \boldsymbol{r}$. In a similar

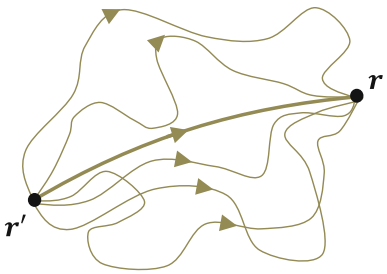

Fig. 10.6 Polymer path integral: $G(\boldsymbol{r}\boldsymbol{r}';N)$ is the sum (integral) of $\exp[-\beta\mathcal{F}\{\boldsymbol{r_n}\}]$ over all the paths connecting two points $\boldsymbol{r},\boldsymbol{r}'$ in the presence of external potential or constraints. The thick curve represents the dominant (classical) path, in which the path probability is maximum

manner in the limit where the thermal fluctuation k_BT is negligible, the dominant polymer configuration would be the trajectory given by the equation $(3/2l^2)d^2\boldsymbol{r}/dn^2 = \partial u(\boldsymbol{r})/\partial \boldsymbol{r}$. The similarity suggests that the classical chain trajectory looks identical to that of a quasi-particle of a mass $3k_BT/l^2$ moving under a potential energy $-u(\boldsymbol{r}_n)$ running in time from $n = 0$ to $n = N$.

10.2.3 The Chain Free Energy and Segmental Distribution

Once we find the polymer Green's function, we can obtain the free energy function $\mathcal{F}(\boldsymbol{r}, \boldsymbol{r}')$ with its initial and final positions as the relevant degrees of freedom $Q = (\boldsymbol{r}, \boldsymbol{r}')$ via the relation

$$e^{-\beta \mathcal{F}(\boldsymbol{r}, \boldsymbol{r}')} \propto G(\boldsymbol{r}, \boldsymbol{r}'; N). \tag{10.56}$$

The integration of (10.50) over $\boldsymbol{r}$, $\boldsymbol{r}'$ yields the partition function of the chain,

$$Z_N \propto \int d\boldsymbol{r} \int d\boldsymbol{r}' G(\boldsymbol{r}, \boldsymbol{r}'; N), \tag{10.57}$$

from which thermodynamic free energy $F(N) = -k_BT \ln Z_N$ is obtained. The proportionality in (10.57) will often be replaced by equality, without incurring any distinction in conformational and thermodynamic properties.

Because the $G(\boldsymbol{r}, \boldsymbol{r}'; N)$ is the probability density of the chain end located at the position $\boldsymbol{r}$ given the initial point at $\boldsymbol{r}'$, **the probability density of the end to be at $\boldsymbol{r}$ regardless the location of the initial point** is given by

$$\wp(\boldsymbol{r}) = \int d\boldsymbol{r}' G(\boldsymbol{r}, \boldsymbol{r}'; N) \Big/ \int d\boldsymbol{r} \int d\boldsymbol{r}' G(\boldsymbol{r}, \boldsymbol{r}'; N) \tag{10.58}$$

Now we make an approximation that is useful for a long chain, using the eigen-functions of the Edwards equation. For the case that the potential allows discrete bound states, the eigen-function expansion (10.46) **for a long chain (large N) is dominated by the ground state labeled as $n = 0$**,

$$G(\boldsymbol{r}, \boldsymbol{r}'; N) \approx e^{-N\epsilon_0} \psi_0(\boldsymbol{r}) \psi_0(\boldsymbol{r}'). \tag{10.59}$$

This feature is owing to the reality of all the variables involved in the expansion, which is not possible for the corresponding Schrödinger equation. Then, the probability density for the end segment to be at $\boldsymbol{r}$ is

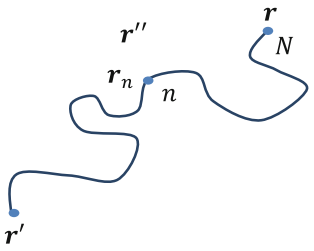

Fig. 10.7 A flexible chain. $\boldsymbol{r}'$ and $\boldsymbol{r}$ are the positions of polymer ends, $\boldsymbol{r}_n$ being that of the bead n. $\boldsymbol{r}''$ is any position in the solution

$$\wp(\boldsymbol{r}) \approx \psi_0(\boldsymbol{r}) / \int d\boldsymbol{r}\, \psi_0(\boldsymbol{r}), \tag{10.60}$$

while the free energy of the chain then is

$$F(N) = -k_B T \ln Z_N \approx N k_B T \epsilon_0, \tag{10.61}$$

apart from the term independent of N.

The Green's function also provides segmental information. Using the recurrence relation

$$G(\boldsymbol{r}, \boldsymbol{r}'; N) = \int d\boldsymbol{r}_n\, G(\boldsymbol{r}, \boldsymbol{r}_n; N-n) G(\boldsymbol{r}_n, \boldsymbol{r}'; n), \tag{10.62}$$

the average of a segmental variable $A(\boldsymbol{r}_n)$ located within the chain is given by

$$\langle A \rangle = \frac{\int d\boldsymbol{r} d\boldsymbol{r}_n d\boldsymbol{r}' G(\boldsymbol{r}, \boldsymbol{r}_n; N-n) A(\boldsymbol{r}_n) G(\boldsymbol{r}_n, \boldsymbol{r}'; n)}{\int d\boldsymbol{r} d\boldsymbol{r}' G(\boldsymbol{r}, \boldsymbol{r}'; N)}. \tag{10.63}$$

Then, the **average of the monomer concentration** at $\boldsymbol{r}''$, $\sum_{n=0}^{N} \delta(\boldsymbol{r}_n - \boldsymbol{r}'')$, is

$$c(\boldsymbol{r}'') = \frac{\sum_{n=0}^{N} \int d\boldsymbol{r} d\boldsymbol{r}' G(\boldsymbol{r}, \boldsymbol{r}''; N-n) G(\boldsymbol{r}'', \boldsymbol{r}'; n)}{\int d\boldsymbol{r} d\boldsymbol{r}' G(\boldsymbol{r}, \boldsymbol{r}'; N)} \tag{10.64}$$

The ground state dominance approximation (10.59) also allows the evaluation of the monomer concentration in a very long chain as

$$c(\boldsymbol{r}) \approx N \psi_0(\boldsymbol{r})^2 \tag{10.65}$$

Similarly, for the quantities that depend on $\boldsymbol{r}_n$ and $\boldsymbol{r}_m$, $B(\boldsymbol{r}_n, \boldsymbol{r}_m)$,

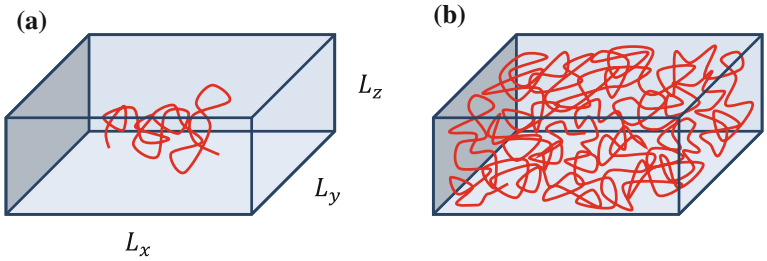

Fig. 10.8 A flexible polymer chain within a box **a** $R_0 \ll L_z$, **b** $R_0 \gg L_x$

$$\langle B \rangle = \frac{\int d\boldsymbol{r} d\boldsymbol{r}_n d\boldsymbol{r}_m d\boldsymbol{r}' G(\boldsymbol{r}, \boldsymbol{r}_n; N-n) B(\boldsymbol{r}_n, \boldsymbol{r}_m) G(\boldsymbol{r}_n, \boldsymbol{r}_m; n-m) G(\boldsymbol{r}_m, \boldsymbol{r}'; m)}{\int d\boldsymbol{r} d\boldsymbol{r}' G(\boldsymbol{r}, \boldsymbol{r}'; N)} \quad (10.66)$$

P10.4 *Using the ground state dominance, show that the mean square distance* $\langle (\boldsymbol{r}_m - \boldsymbol{r}_n)^2 \rangle$ *between two beads separated by* $(m-n) \gg 1$ *is given by*

$$\langle (\boldsymbol{r}_m - \boldsymbol{r}_n)^2 \rangle \approx \int d\boldsymbol{r}_n d\boldsymbol{r}_m \psi_0(\boldsymbol{r}_n)^2 \psi_0(\boldsymbol{r}_m)^2 (\boldsymbol{r}_m - \boldsymbol{r}_n)^2,$$

which is a constant independent of n and m. Calculate this for the chain confined within a sphere of radius R (Hahnfeldt et al. (1993)*. This is relevant to the distance between two loci within a chromosome.*

10.2.4 The Effect of Confinemening a Flexible Chain

Suppose a free chain is brought within a box (Fig 10.8). Below we study the free energy of the confinement and the pressure of the chain on the walls following Doi and Edwards (1986).

The presence of the impenetrable wall is expressed by an infinite potential, $u(\boldsymbol{r}) = \infty$, which can be implemented by the boundary condition $G(\boldsymbol{r}, \boldsymbol{r}'; N) = 0$ for $\boldsymbol{r}$ and $\boldsymbol{r}'$ on the wall, for the diffusion equation within the box:

$$\frac{\partial}{\partial N} G(\boldsymbol{r}, \boldsymbol{r}'; N) = \frac{l^2}{6} \nabla^2 G(\boldsymbol{r}, \boldsymbol{r}'; N). \quad (10.67)$$

First note that the Green's function is separable into the Cartesian components,

$$G(\boldsymbol{r}, \boldsymbol{r}'; N) = g_x(x, x'; N) g_y(y, y'; N) g_z(z, z'; N). \quad (10.68)$$

Each component, for example, the x component satisfies

$$\frac{\partial}{\partial N} g_x(x, x'; N) = \frac{l^2}{6} \frac{\partial^2}{\partial x^2} g_x(x, x'; N), \tag{10.69}$$

for which the Green's function solution is

$$g_x(x, x'; N) = \sum_{n_x=1}^{\infty} e^{-N\epsilon_{x}} \psi_{n_x}(x) \psi_{n_x}(x'). \tag{10.70}$$

The eigenfunctions and eigenvalues are

$$\psi_{n_x}(x) = \left(\frac{2}{L_x}\right)^{1/2} \sin \frac{n_x \pi x}{L_x} \tag{10.71}$$

and

$$\epsilon_{n_x} = \frac{l^2 n_x^2 \pi^2}{6 L_x} \tag{10.72}$$

respectively, where n_x is the positive integers $1, 2, 3, \ldots$.

The partition function then is $Z = Z_x Z_y Z_z$, where

$$\begin{aligned} Z_x &= \int_0^{L_x} dx \int_0^{L_x} dx' g_x(x, x'; N) \\ &= \frac{8}{\pi^2} L_x \sum_{n_x=1,3,5\ldots} \frac{1}{n_x^2} \exp\left[-\frac{\pi^2 N l^2}{6 L_x^2} n_x^2\right], \end{aligned} \tag{10.73}$$

and likewise for Z_y and Z_z with L_x replaced by L_y and L_z respectively.

Consider the case in which the size of the chain $R_0 = N^{1/2} l$ is much smaller than the smallest of L_x, L_y, L_z (Fig 10.8). Then

$$Z_x \cong \frac{8}{\pi^2} L_x \sum_{n_x=1,3,5\ldots} \frac{1}{n_x^2} = L_x \tag{10.74}$$

and thus

$$Z = L_x L_y L_z = V. \tag{10.75}$$

Understandably the true partition function should be a dimensionless quantity $Z = V/v_0$; we repeatedly ignored the elementary volume v_0, as it is irrelevant to the properties of our interest. Equation (10.75) leads to

$$F = -k_B T \ln Z = -k_B T \ln V \tag{10.76}$$

and

$$p = -\frac{\partial}{\partial V} F = \frac{k_B T}{V}. \tag{10.77}$$

The pressure is just $1/N$ times that of an ideal solution of N particles! This is the strongest effect of the chain connectivity; the chain is linearly bound hand in hand, so the center of mass position is the only translational degree of freedom free to move.

Consider the opposite limit where R_0 is larger than the largest of L_x, L_y, L_z. The ground state $n_x = 1$ dominates the sum in (10.73),

$$Z_x \cong \frac{8}{\pi^2} L_x \exp\left(-\frac{\pi R_0^2}{6L_x^2}\right), \tag{10.78}$$

so that the total partition function is

$$Z = \left(\frac{8}{\pi^2}\right)^3 V \exp\left\{-\frac{\pi R_0^2}{6}\left(\frac{1}{L_x^2} + \frac{1}{L_y^2} + \frac{1}{L_z^2}\right)\right\}, \tag{10.79}$$

leading to the free energy and the pressure on the wall normal to x axis (Fig. 10.9):

$$F = -k_B T \ln Z = k_B T \frac{\pi R_0^2}{6}\left(\frac{1}{L_x^2} + \frac{1}{L_y^2} + \frac{1}{L_z^2}\right) \tag{10.80}$$

$$p_x = -\frac{1}{L_y L_z}\frac{\partial}{\partial L_x} F = \frac{\pi R_0^2}{3L_x^2}\frac{k_B T}{V}. \tag{10.81}$$

Now the pressure is much higher than $k_B T/V$ but much smaller than $N k_B T/V$. p_x also differs from p_y and p_z, meaning that the polymer senses the anisotropy of the confining space unlike a simple fluids in the absence of an external fields. For example, when one side L_z is much smaller than the others, i.e., when **the chain is**

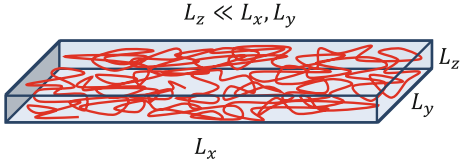

Fig. 10.9 A flexible polymer confined in a thin slab

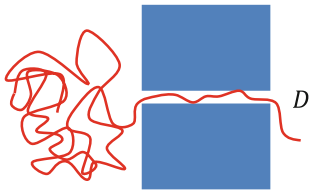

Fig. 10.10 A flexible polymer translocating through a narrow cylindrical pore

confined within a thin slab, then the free energy and pressure associated with the confinement are

$$F = k_B T \frac{\pi R_0^2}{6} \frac{1}{L_z^2} = \frac{\pi^2}{6} k_B T \left(\frac{R_0}{L_z}\right)^2 \tag{10.82}$$

$$p_z = \frac{\pi R_0^2}{3L_z^2} \frac{k_B T}{V} = \frac{N k_B T}{V} \left(\frac{\pi^2}{3} \frac{l^2}{L_z^2}\right), \tag{10.83}$$

Because L_x and L_y are much larger than L_z, p_z is much higher than p_x *or* p_y.

P10.5 *Consider a flexible chain of a Kuhn length* $l = 1$ nm *and contour length* $L = 1$ m *confined within a thin and long tube of diameter* $D = 20$ nm. *Using the Edwards' equation find the free energy needed to confine all the chain within the tube. What is the segmental distribution c(r)? Plot it.*

Many biological and biotechnological situations involve polymer translocation through narrow constrictions or pores. Consider a flexible polymer within a narrow pore of diameter D (Fig. 10.10). **The free energy required to confine the chain fragment of length $L = Nl$ into the pore** is

$$\Delta F = \alpha k_B T \frac{Ll}{D^2}, \tag{10.84}$$

where $\alpha = 0.96$ as the solution of *P10.5*. The probability of the partitioning is

$$K = e^{-\frac{\Delta F}{k_B T}} = e^{-\alpha \frac{Ll}{D^2}} = e^{-\alpha N \left(\frac{l}{D}\right)^2}, \tag{10.85}$$

which is exceedingly small if the pore diameter is much smaller than the radius of gyration.

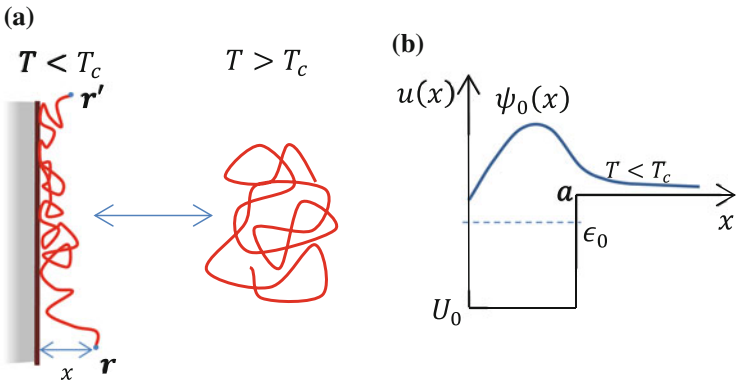

Fig. 10.11 **a** The adsorption and desorption transition of a flexible polymer, **b** The polymer wave function $\psi_0(x)$, in an adsorbed state, under the square well potential $u(x)$ per monomer

10.2.5 Polymer Binding–Unbinding (Adsorption-Desorption) Transitions

A polymer chain can bind to an attracting surface but, because of the free energy cost that the confinement incurs, it can also unbind from the surface. To study the polymer binding–unbinding transition quantitatively, consider the surface is (y, z) plane and the interaction between a polymer bead and surface given by the hard-square well potential, which is a simplest model characterized by potential depth U_0 and range a as depicted in the Fig. 10.11:

$$u(x) = \begin{cases} \infty, & x = 0 \\ U_0, & 0 < x < a \\ 0, & x > a \end{cases} \tag{10.86}$$

where x is the coordinate of the chain end vertical to the surface. Neglecting the lateral coordinates y and z, along which the chain end distribution is Gaussian, it suffice to consider the one-dimensional Edwards equation,

$$-\frac{\partial}{\partial N} G(x, x'; N) = \left[-\frac{l^2}{6} \frac{\partial^2}{\partial x^2} + \beta u(x) \right] G(x, x'; N). \tag{10.87}$$

The solution and its ground state dominance approximation is given as

$$\begin{aligned} G(x, x'; N) &= \sum_{n=0} e^{-N\epsilon_n} \psi_n(x) \psi_n(x') \\ &\approx e^{-N\epsilon_0} \psi_0(x) \psi_0(x'). \end{aligned} \tag{10.88}$$

The ground state eigenfunction $\psi_0(x)$ and eigenvalue ϵ_0 satisfy

$$\left[-\frac{l^2}{6}\frac{\partial^2}{\partial x^2}+\beta u(x)\right]\psi_0(x)=\epsilon_0\psi_0(x) \tag{10.89}$$

$\psi_0(x)$ that satisfies the BC ($\psi_0(x=0)=0, \psi_0(x\to\infty)=0$) are given by

$$\psi_0(x)=\begin{cases} A\ \sin\ kx & x\geq a \\ Be^{-\kappa x} & x<a \end{cases} \tag{10.90}$$

where

$$k=\left\{\frac{6}{l^2}(\beta U_0-|\epsilon_0|)\right\}^{1/2}, \tag{10.91}$$

and

$$\kappa=\left\{\frac{6}{l^2}|\epsilon_0|\right\}^{1/2}. \tag{10.92}$$

A bound state (adsorption) begins to exist with ϵ_0 approaching zero from negative, if $ka>\pi/2$ (Fig. 10.11b), which, can be written as

$$\left(\frac{6}{l^2}\beta U_0\right)^{1/2}a>\frac{\pi}{2} \tag{10.93}$$

or

$$T<\frac{24a^2U_0}{\pi^2l^2k_B}\equiv T_C, \tag{10.94}$$

Here T_c is the critical temperature of adsorption-desorption transition, below which polymer is adsorbed.

To see the nature of the transition in detail, we analyze the polymer free energy per segment in the bound state, which is given by ϵ_0 in units of k_BT using (10.61):

$$\frac{F}{N}=\epsilon_0k_BT=-\int_0^a dx\,U_0\psi_0^2+k_BT\int_0^\infty dx\ \psi_0\left(-l^2\frac{d^2\psi_0}{6dx^2}\right)\psi_0 \tag{10.95}$$

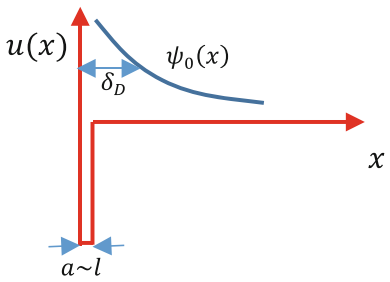

Fig. 10.12 The chain-end distribution $\psi_0(x)$ of a polymer adsorbed by a contact attraction with the short range a

The first term in the right hand side represents the energy loss per segment E/N associated with binding. The second term is the entropy cost, $-TS/N$, which is necessary to confine the chain near the surface. For $T < T_c$, the energy ($E < 0$) wins over the entropy ($S < 0$) to make the free energy negative. But as T increases to T_c and beyond, the bound state ceases to exist with the polymer wave function $\psi_0(x)$ delocalized away from the surface. The entropy gain tends to dominate the binding energy and so that polymer desorbs from the surface. The phenomenon of **polymer adsorption-desorption is genuinely a consequence of chain flexibility**. If the polymer were a rigid rod, it would remain adsorbed to an attractive surface irrespective of the temperature increases.

P10.6 *Calculate the average and variance of a monomer position in a weakly adsorbed polymer in terms of $T_c - T$, which is small. The polymer adsorption thickness is the inverse of the average vertical position, which can be regarded as the order parameter of the adsorption–desorption transition.*

In numerous situations, the attractive range a is very small, so that the Edwards equation cannot be applied to the region $0 < x < a$, over which the potential can vary rapidly (Fig. 10.12). Nevertheless the equation is applicable to the force-free region $x > a$, where

$$\psi_0(x) = Be^{-\kappa x}. \tag{10.96}$$

In this case the adsorption energy is

$$\epsilon_0 = -\frac{l^2}{6}\kappa^2, \tag{10.97}$$

where $\delta_D = \kappa^{-1}$ is called the de Gennes' (adsorption) thickness.

P10.7 *As a simple model for small polymer globule, consider the chain under a spherical point well $u(r) = a\delta(r)$ ($a < 0$). Find the polymer segmental distribution $c(r)$* (Grosberg and Khokhlov 1994).

10.3 Effects of Segmental Interactions

10.3.1 Polymer Exclusion and Condensation

The ideal chain model assumes that polymer segments can overlap, but due to the space they occupy, the real chain cannot cross itself, and thus cannot be modelled by a random walk but by a "**self-avoiding walk**". **This excluded volume effect allows the polymer coil to swell**. But if this repulsive interaction is dominated by the attractive interaction between the segments, the coiled polymer undergoes a collapse transition into a condensed state called a polymer globule. Here we characterize the EED for various conformational states and study the conditions of the transitions between them.

As a measure of the overall conformation of the polymer, which is modulated by solvent, we study how the equilibrium end-to-end length R depends on N. To this end we seek a chain's free energy function of R with N fixed. First consider an ideal chain, where there are no inter-bead interactions other than incorporated in the chain connectivity. The probability distribution function (PDF) $D(R;N)$ that the *ideal* chain's end is within dR is the EED PDF $P(\boldsymbol{R};N)$ times the volume element dV taken to be spherical shell of radius R and thickness dR:

$$\begin{aligned} D(R;N)dR &= P(\boldsymbol{R};N)dV \\ &= \left(\frac{3}{2\pi Nl^2}\right)^{3/2} \exp\left(-\frac{3R^2}{2Nl^2}\right) 4\pi R^2 dR. \end{aligned} \tag{10.98}$$

The free energy $\mathcal{F}_0(R)$ of the ideal chain associated with R is then given by,

$$\begin{aligned} \mathcal{F}_0(R) &= -k_B T \ln D(R;N) \\ &= k_B T\left(\frac{3}{2Nl^2}R^2 - 2\ln R\right), \end{aligned} \tag{10.99}$$

apart from the part independent of R. Note that $\mathcal{F}_0(R)$ is different from $\mathcal{F}(\boldsymbol{R})$, (10.18), because here we are dealing with the degree of freedom, $Q = R$, not with $Q = \boldsymbol{R}$. The most probable (free-energy minimizing) value of R is given by

$$R_p = \left(\frac{2}{3}\right)^{1/2} R_0 \sim N^{1/2}, \tag{10.100}$$

which is on par with $R_0 = N^{1/2}l$ as well as the free chain radius of gyration $R_G = (1/6)^{1/2}R_0$.

How can we incorporate the inter-bead interactions in the free energy $\mathcal{F}$ as a function of the end-to-end distance R? First note that, in view of $V \sim R^3 \sim N^{3/2}$, the concentration of the beads N/V for an ideal chain varies as $\sim N^{-1/2}$, which is very low for large N. Thus, to include the inter-bead interaction in our free energy

function, we adopt the virial expansion for the macroscopic free energy of a dilute gas (4.58). In our approach here, however, $V \sim R^3$ is not a fixed parameter as in the virial expansion but a fluctuating variable, while N is fixed. To study the departure from the ideality, it suffices to include the segmental interaction in the lowest order, $\mathcal{F}_{int}(R) = k_B T N^2 B_2(T)/V$ (4.54). B_2 is the second virial coefficient to include two-bead interactions, $B_2(T) = 1/2 \int d\boldsymbol{r}[1 - \exp\{-\beta\varphi(r)\}]$ (4.55). $\varphi(r)$ is the inter-bead potential of mean force affected by the surrounding solvent. Assuming that it consists of hard core repulsion and soft attraction, $B_2(T) = b - a/k_B T = b(1 - \Theta/T)$ (4.62), where the parameter $\Theta = a/k_B b$ is called the theta (Θ) temperature. When $T = \Theta$, we have $B_2 = 0$, called the theta condition or the theta solvent condition; to this order the effect of the repulsion cancels that of attraction and the chain becomes ideal.

If $\Theta < T$, $B_2 > 0$. The inter-bead repulsion dominates over the attraction, so a polymer segment prefers to be in contact with the solvent molecules rather than with the other segments. This is the so-called situation with a **good solvent**. In the absence of an attractive interaction, $B_2(T)$ is given by the excluded volume per monomer $b = 2\pi\sigma^3/3$ where σ is the contact diameter for two beads.

The total free energy $\mathcal{F}(R)$ in three dimension is the sum of the two contributions $\mathcal{F}_0(R)$ and $\mathcal{F}_{int}(R)$,

$$\frac{\mathcal{F}(R)}{k_B T} \sim -\ln R + \frac{R^2}{Nl^2} + \frac{N^2}{R^3} B_2. \tag{10.101}$$

In the above the exact numerical prefactor in each term is irrelevant and so omitted for the scaling analysis that we discuss below. $\mathcal{F}_{int}(R) \sim B_2 N^2/R^3$ decreases as R increases with a given N, i.e., **the excluded volume tends to swell the chain**, while elastic energy $\mathcal{F}_0(R)$ tends to shrink it. At equilibrium the chain conforms to a way that minimizes the free energy by varying R:

$$\frac{\partial}{\partial R}\mathcal{F}(R) = 0, \tag{10.102}$$

which leads to

$$-\frac{1}{R} + \frac{R}{Nl^2} - \frac{N^2}{R^4} B_2 = 0, \tag{10.103}$$

for which we examine each term for large N. $1/R$ is expected to be negligible, so the other two terms in the equation above yield the optimal radius

$$R_F \sim N^{3/5} \left(B_2 l^2\right)^{1/5}. \tag{10.104}$$

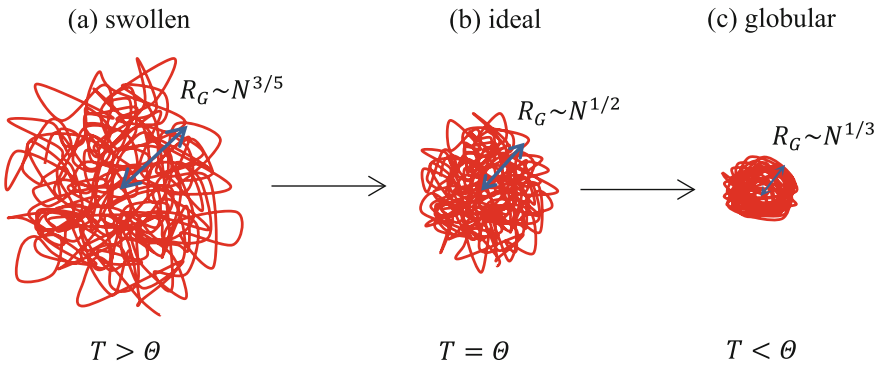

Fig. 10.13 Flexible polymer conformations and radii of gyration R_G **a** swollen state for $T > \Theta$, or in a good solvent, due to the excluded volume effect, **b** ideal chain in Θ solvent, **c** collapsed state for $T < \Theta$, or in a poor solvent, due to intere-bead attration

Indeed the scaling behavior (10.104) is correct for long chains, as one can check by inserting this into (10.103). Generalizing this argument to an arbitrary dimension d, we have

$$R_F \sim N^{\nu}, \tag{10.105}$$

where

$$\nu = \frac{3}{d+2}. \tag{10.106}$$

P10.8 *Verify* (10.106).

ν is a universal exponent, called the **Flory exponent**; it is independent of the details of the molecules that constitute the chain. In one and two dimensions we have the exponents $\nu = 1$ and $\nu = 3/4$, which are exact, whereas the exponent in three dimension $\nu = 3/5$ is very close to the exact value $\nu = 0.588$. The exponent ν larger than the ideal value $1/2$ means that at equilibrium the **chain swells beyond the idealty** (Fig. 10.13a).

If $\Theta > T$, we have $B_2 < 0$; the attraction dominates over the repulsion, which is the situation with a **poor solvent**. The minimum of free energy (10.101) is attained at $R = 0$, implying that the chain tends to collapse to a point. But in reality, the **chain will collapse to a compact structure**. Because it will be a more condensed state, the free energy model should include the three-bead interaction term in (4.58) with the third order virial coefficient B_3 which is positive (using the van der Waals equation of state for example, $B_3 = b^2$):

$$\frac{\mathcal{F}(R)}{k_B T} \sim -\ln R + \frac{R^2}{Nl^2} + \frac{N^2}{R^3} B_2 + \frac{N^3}{2R^6} B_3. \tag{10.107}$$

Considering only the last two terms, which are dominant when N is large as well as R is much smaller than $R_0 = N^{1/2}l$, we have the free energy minimum at

$$R_c \sim \left(N\frac{B_3}{|B_2|}\right)^{1/3} \sim N^{1/3}, \tag{10.108}$$

signifying an onset to transition into a compact configuration, called a globule, in which each monomer packs into the volume, $V \sim N$ (Fig. 10.13c). The coil-to-globule transitions of chain conformations following the temperature change or the solvent changes are summarized in Fig. 10.13.

The information on polymer structures, particularly **the radii of gyration and its scaling laws, can be obtained by scattering experiments**, such as small angle x-ray scattering (SAXS) and small angle neutron scattering (SANS). As studied in Chap. 9, the data of very small q or small angle scattering can provide information about the radius of gyration, which is related to the structure factor, $S(\boldsymbol{q}) \approx N\left(1 - q^2R_G^2/3\right)$ (9.62). In contrast, at a high value q, $S(\boldsymbol{q})$ probes the polymer structures within the bulk, which are self-similar; in the chain that satisfies $R_G \sim N^{\nu}$, for large q, $S(\boldsymbol{q}) \sim q^{-D_f}$ with the fractal dimension $D_f = 1/\nu$; $D_f = 2$ for ideal chain, $D_f = 5/3$, for self-avoiding chain, and $D_f = 3$ for the chain collapsed into a globule.

10.3.2 DNA Condensation in Solution in the Presence of Other Molecules

Suppose that a DNA fragment of N segments is immersed into a solution that is crowded with macromolecular solutes such as proteins (Fig. 10.14). What conformation will the fragment take? Following the argument of Sneppen and Zocchi (2005), we present a scenario that shows the DNA can collapse rather than be swollen or extended, due to excluded volume interaction between the DNA and solute.

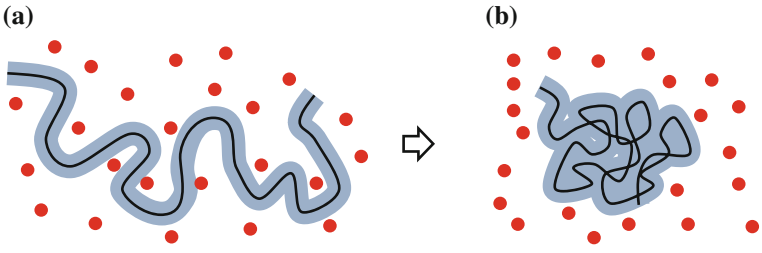

Fig. 10.14 **a** A DNA molecule with proteins excluded in the shaded area, **b** a collapsed DNA with the proteins depleted

For simplicity we consider N_U mutually non-interacting solute molecules each with radius r_U in a volume V. The partition function for the solute in the absence of the DNA is (4.85):

$$Z_U{}^0 = \frac{1}{N_U!}(V/v_0)^{N_U}. \tag{10.109}$$

Consider that a DNA fragment has N segments each with length l. We assume that the solute and DNA do not interact except via the steric effect of the excluded volume $\delta = \pi(r_{DNA} + r_U)^2 l$, per DNA segment, where r_{DNA} is cross-sectional radius. When the DNA chain does not coil but is extended, the volume available to the solutes is reduced by this interaction as $V \to V - N\delta$.

Now assume that the DNA collapses to a globule of radius R. With the solute depleted within the globule, the volume available to the solute in the solution increases. The fraction of such forbidden contacts between the solute and DNA in the globule is $\sim(N\delta/R^3)$, so the volume available to the solute particles becomes

$$V' = V - N\delta + \frac{(N\delta)^2}{R^3}. \tag{10.110}$$

Consequently, the free energy change of the solutes during transition to the collapsed state for the DNA is

$$\begin{aligned} \Delta F_U &= -N_U k_B T \ln\left(\left\{V - N\delta + \frac{(N\delta)^2}{R^3}\right\}/(V - N\delta)\right) \\ &\cong -k_B T \frac{(N\delta)^2}{R^3} n_U, \end{aligned} \tag{10.111}$$

where $n_U = N_U/V$ is the concentration of solutes and $N\delta/V \ll 1$ as well as $(N\delta)^2/VR^3 \ll 1$ are to be noted.

In addition, the free energy of the DNA increases upon collapse, due to excluded volume interaction among the segments, by the amount

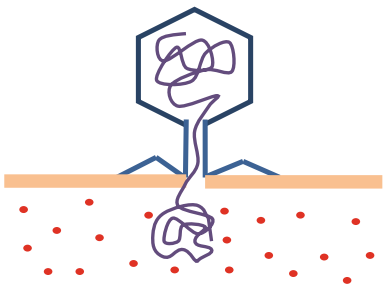

Fig. 10.15 DNA in phage extruded into a cell where DNA can collapse assisted by proteins

$$\Delta F_{DNA} \cong k_B T \frac{N^2}{R^3} B_2. \tag{10.112}$$

The net free energy change of the DNA and solutes is

$$\begin{aligned} \Delta F &= \Delta F_U + \Delta F_{DNA} \\ &\cong k_B T \frac{N^2}{R^3} B_{2eff}, \end{aligned} \tag{10.113}$$

where $B_{2eff} = b - \delta^2 n_U$ is the effective virial coefficient of the DNA. B_{2eff} can be negative, even when the solvent is good to the DNA ($B_2 = b \sim \pi r_{DNA}^2 l$ is positive). It means that, DNA can condense to a globule as argued in the earlier section, depending on the concentration of the solute. In *E. coli*, where $n_U \sim 2 \times 10^{-3}/(\text{nm})^3$, $F_{DNA} \simeq 1\,\text{nm}$, $r_U \simeq 2\,\text{nm}$, and $l \simeq 120\,\text{nm}$, the ratio $\Delta F_U / \Delta F_{DNA} \sim -\delta^2 n_U / b$ can be as large as −60 (Sneppen and Zocchi (2005)). For example, DNA from a phage can be injected into a bacterial cell that is crowded by proteins at a concentration of 20–30% (Fig. 10.15). This condensation is due to the **overriding entropy gain caused by the excluded volume that is depleted** when the phage DNA collapses into a globule upon injection (Fig. 10.15). Another possible example is the collapse of biopolymers induced by protein binding, e.g., chaperon molecule binding on protein chains. In this case the binding rather than depletion may enhance the collapse transitions.

P10.9 *If the excluded volume effect among the solute is included, how is the above result affected in the solution crowded by the solute?*

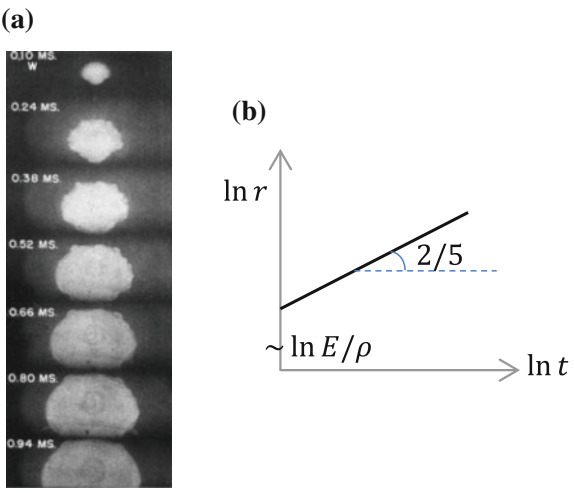

Fig. 10.16 **a** Nuclear blast expansion as time progresses and **b** the scaling relation between radius and time of the fire ball (Taylor (1950) by permission of the Royal Society)

10.4 Scaling Theory

Scaling theory is essentially a dimensional analysis, which is useful to gain insight into the complex nature of the physical behaviors that satisfy certain power laws, as in critical phenomena and polymers. For phenomena for which analytical theories and formulae are not available, scaling theory often provides an essence of the underlying physics.

Example: The First Nuclear Bomb Explosion

G. I. Taylor, a famous British theoretical physicist, was asked to find the yield (energy release) of the US' first nuclear bomb. He noted that the energy would produce a very strong shock wave that expands approximately spherically (Fig. 10.16a), and that the radius at time t would scale with the unknown energy release E and the mass density of the undisturbed air ρ (Taylor 1950):

$$\begin{aligned} r &= r(E, \rho, t) \\ &\propto E^{\alpha} \rho^{\beta} t^{\gamma} \end{aligned} \tag{10.114}$$

Using dimensional analysis with $[E] = ML^2/T^2$, $[\rho] = M/L^3$, one can easily obtain

$$r \sim \left(\frac{E}{\rho} t^2 \right)^{1/5}. \tag{10.115}$$

Analysis of a movie of the test explosion (Fig. 10.16a), confirmed that the power law $r \sim t^{2/5}$ is indeed exact. Using $r = 100\,\text{m}$ at $t = 0.016\,\text{s}$ after the explosion, and $\rho = 1.1\,\text{kg/m}^3$ at the altitude of the explosion, $E = 4 \times 10^{13}\,\text{J}$, which is about 10 kilotons of TNT within the factor of order 1.

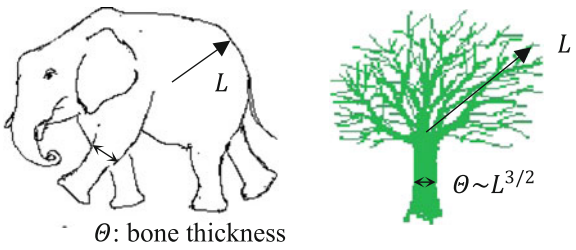

Fig. 10.17 Scaling laws for thickness Θ of animals and trees with the sizes L

On the other hand, the nuclear fallout diffuses in the manner

$$r(t) \sim (Dt)^{1/2} \sim t^{1/2} \tag{10.116}$$

where D is the diffusion constant of the fallout through the air. The time derivatives of (10.115) and (10.116), $\dot{r}_E(t) \sim t^{-3/5}$ and $\dot{r}_D(t) \sim t^{-1/2}$ respectively, reveal that the shock wave propagation is much faster than the fallout diffusion at short time.

Sizes and Speeds of Living Objects

How do the bone thickness Θ of animals scale with their sizes L? With the assumption that mass density is about the same for all animals, the weights W scale as

$$W \sim L^3 g, \tag{10.117}$$

where g is the gravitational constant. If the bone's maximum force per area to support the weight $p \sim W/\Theta^2$ is also the same, a simple substitution yields the cross section of the bone (Fig. 10.17)

$$\Theta \sim L^{3/2} g^{1/2}. \tag{10.118}$$

This simple scaling law is quite correct within mammals and vascular plants. It means that larger animals tend to be flatter (e.g. elephant and whale) and large trees tend to be thicker. It also implies that the story of Gulliver is wrong; at Brobdingnag the giants should be much stockier than Gulliver! The largest sea animal (whale) is larger than the largest land animal (elephant). Why?

Happy creatures they are, under no stress, the elephants like to move with the natural frequencies,

$$\omega \sim \left(\frac{g}{L}\right)^{1/2} \sim L^{-1/2}. \tag{10.119}$$

This leads to the motion speed

$$v \sim L\omega \sim L^{1/2}. \tag{10.120}$$

The mosquitoes on the elephants are slower than elephants, when v is measured in $\mathrm{m} \cdot \mathrm{s}^{-1}$ but move much more quickly than elephants when speed is

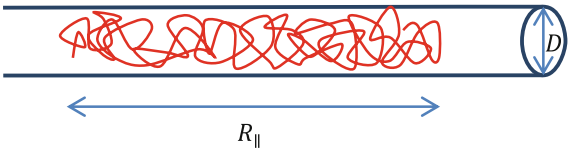

Fig. 10.18 Polymers confined within a narrow cylinder

measured in body lengths per second.

Polymer—An Entropic Animal

Without recourse to theoretical apparatus of polymer physics, one can estimate the free energy of confining a long flexible polymer within a thin tube of diameter D (de Gennes 1979). A flexible polymer is a thermally fluctuating structure with the energy scale k_BT, so considering the two length scales R_0 and D of the system, we have

$$F \sim k_BT\left(\frac{R_0}{D}\right)^m. \tag{10.121}$$

Since under strong confinement $F \sim N$ and $R_0 \sim N^{1/2}$, we identify $m = 2$ and

$$F \sim k_BT\left(\frac{R_0}{D}\right)^2 \sim D^{-2}. \tag{10.122}$$

This is comparable to the correct result, $F = 0.96\, k_BT(R_0/D)^2$, which can be obtained by solving the Edward's equation. The relation $F \sim D^{-2}$ indicates how the free energy to confine the chain within the tube increases as the tube narrows.

A real, self-avoiding chain confined in a thin tube would have a different scaling behavior. From the relation $F \sim N$, and using $R_0 \sim N^{\nu}$ (Fig. 10.18),

$$F \sim k_BT\left(\frac{R_0}{D}\right)^m \sim N \sim D^{-5/3}, \tag{10.123}$$

where $m = \nu^{-1} = 5/3$ in three dimensions. The tube length occupied by the polymer is scaled as

$$R_\parallel \sim R_0\left(\frac{R_0}{D}\right)^n, \tag{10.124}$$

which should go like $\sim N$. This relationship leads to

$$n = \nu^{-1} - 1 = 5/3 - 1 = 2/3, \tag{10.125}$$

so (10.124) can be written as $R_{\|} \sim N(1/D)^{2/3} \sim D^{-2/3}$.

Monomer concentration scales as

$$\begin{aligned} c &\sim \frac{N}{D^2 R_{\|}} \\ &\sim D^{\nu^{-1}-3} \sim D^{-4/3} \end{aligned}. \tag{10.126}$$

For ideal chain, in contrast, $\nu = 1/2$ and $c \sim D^{-1}$.

Further Reading and References

P.G. de Gennes, *Scaling Concepts in Polymer Physics* (Cornell University Press, 1979)
A.Y. Grosberg, A.R. Khokhlov, *Statistical Physics of Macromolecules* (AIP Press, New York, 1994)
M. Doi, S.F. Edwards, *Theory of Polymer Dynamics* (Clarendon Press, 1986)
K. Sneppen, G. Zocchi, *Physics in Molecular Biology* (Cambridge University Press, 2005)
F. Reif, *Fundamentals of Statistical and Thermal Physics* (McGrawHill Book Company, New York, 1965)
S.F. Edwards, The statistical mechanics of polymers with excluded volume. Proc. Phys. Soc. **85**, 163 (1965)
M. Doi, S.F. Edwards, *The Theory of Polymer Dynamics* (The Clarendon Press, Oxford University Press, New York, 1986)
R.P. Feynman, A.R. Hibbs, *Quantum Mechanics and Path Integrals*, 1st edn. (McGraw-Hill Companies, 1965)
P. Hahnfeldt et al., Polymer models for interphase chromosomes. PNAS **90**, 7854–7858 (1993)
W. Sung, P.J. Park, Polymer translocation through a pore in a membrane. Phys. Rev. Lett. **77** (4), 783 (1996)
S.G. Taylor, The formation of a blast wave by a very intense explosion. II. The atomic explosion of 1945, Proc. Roy. Soc. A, **201**, 175 (1950)

Chapter 11
Mesoscopic Models of Polymers: Semi-flexible Chains and Polyelectrolytes

Most biopolymers are semi-flexible: they can bend and undulate. Mechanically they are characterized by finite values of their persistence lengths l_p, the scales below which the chains can be regarded as straight (Fig. 11.1). For example, the persistence length of double-stranded DNA is about 50 nm, while that of actin filament is about 20 μm. For the length scale much longer than the persistence length, the chain appears to be flexible, to which the models presented earlier can be applied. This chapter covers basic mesoscopic conformations, their fluctuations, and elastic behaviors of semi-flexible chains and polyelectrolytes that are either free or subject to external forces and constraints.

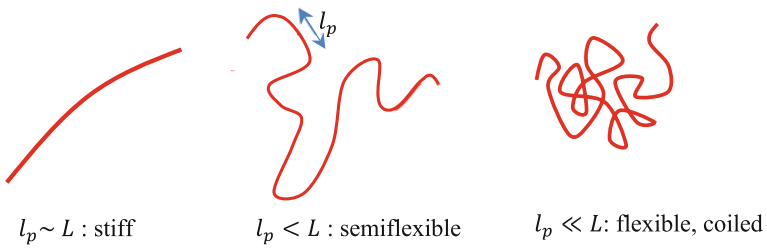

Fig. 11.1 Mesoscopic conformations of polymer chains with different persistence lengths l_p. L is the contour length

11.1 Worm-like Chain Model

We start with construction of the effective Hamiltonian for a free semi-flexible chain. As mentioned earlier, **the effective Hamiltonian can be taken from the macroscopic**, **phenomenological energy**, which, for a semi-flexible chain, is **the energy required to bend an elastic string with a locally varying curvature**:

W. Sung, *Statistical Physics for Biological Matter*, Graduate Texts in Physics,
https://doi.org/10.1007/978-94-024-1584-1_11

$$\mathcal{F} = \frac{\kappa}{2}\int_0^L ds\, C(s)^2 = \frac{\kappa}{2}\int_0^L ds \left(\frac{\partial \boldsymbol{u}(s)}{\partial s}\right)^2. \tag{11.1}$$

Here κ is an elastic constant called bending modulus (or bending rigidity) and the L is the contour length, and $C(s)$ is the curvature at an arc length s (Fig. 11.2). The curvature is given by $C(s) = 1/R(s) = |\partial \boldsymbol{u}(s)/\partial s|$, where $R(s)$ is the local radius of curvature, $\boldsymbol{u}(s)$ is the unit tangent vector given by $\boldsymbol{u}(s) = \partial \boldsymbol{r}(s)/\partial s$, where $\boldsymbol{r}(s)$ is the position vector to the arc position. By considering the local curvature to thermally fluctuate, the energy (11.1) can gain the status of an effective Hamiltonian, or a free energy function. We may say that the Hamiltonian brings the macroscopic bending energy to life with the local curvatures therein thermally fluctuating. This model is called **the worm-like chain (WLC)**. In the absence of an external potential on each segment, it stands in contrast with the flexible chain Hamiltonian (10.52),

$$\mathcal{F} = \frac{k_e}{2}\int_0^L ds \left(\frac{\partial \boldsymbol{r}(s)}{\partial s}\right)^2 = \frac{k_e}{2}\int_0^L ds (\boldsymbol{u}(s))^2, \tag{11.2}$$

which represents stretching energy with the entropic stretch modulus $k_e = 3k_BT/l^2$.

We can gain insights into segmental fluctuations and correlations by discretizing the WLC to an array of N basic links each with length a (Fig. 11.2); by considering $s = na$, where n is an integer, (11.1) can be rewritten in terms of the link tangent vectors $\boldsymbol{u}_n$:

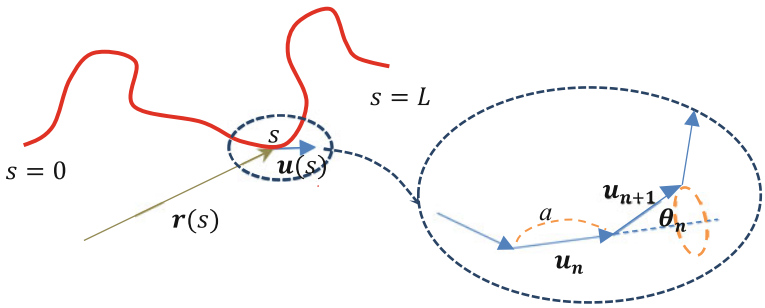

Fig. 11.2 Worm-like chain. $\boldsymbol{r}(s)$ and $\boldsymbol{u}(s)$ are the three dimensional position vector and two dimensional orientation (unit tangent vector) at the one-dimensional arc position s. The chain in the brocken ellipse is magnified into an array of unit length a jointed with a relative angle θ_n

$$\mathcal{F}\{\boldsymbol{u_n}\} = \frac{\kappa}{2a}\sum_{n=1}^{N-1}(\boldsymbol{u}_{n+1} - \boldsymbol{u}_n)^2, \tag{11.3}$$

which can be cast as

$$\begin{aligned}\mathcal{F} &= \frac{\kappa}{2a}\sum_{n=1}^{N-1}(2 - 2\boldsymbol{u}_{n+1}\cdot\boldsymbol{u}_n) \\ &= \frac{\kappa}{a}\sum_{n=1}^{N-1}(1 - \cos\theta_n),\end{aligned} \tag{11.4}$$

where θ_n is the angle which $n+1$th link makes with nth link (Fig. 11.2). Viewed over a length scale much longer than a, the chain looks continuous; in the continuum limit, $a \to 0$, $\theta_n \to 0$ with θ_n^2/a kept as finite, (11.4), and thus (11.1), is represented by:

$$\mathcal{F}\{\theta_n\} = \frac{\kappa}{2a}\sum_{n=1}^{N-1}\theta_n^2. \tag{11.5}$$

The θ_n for all n are the rotational degrees of freedom that span 2 dimension. Each n contributes to the energy via the equipartition theorem, $\kappa\langle\theta_n^2\rangle/(2a) = 2(1/2)k_BT$, so we have

$$\left\langle {\theta_n}^2 \right\rangle = \frac{2ak_BT}{\kappa}. \tag{11.6}$$

Now we focus on the nearest neighbor tangent correlation:

$$\begin{aligned}\langle\boldsymbol{u}_{n+1}\cdot\boldsymbol{u}_n\rangle &= \langle\cos\theta_n\rangle \\ &\cong 1 - \frac{1}{2}\langle\theta_n^2\rangle \\ &= 1 - \frac{a}{l_p},\end{aligned} \tag{11.7}$$

where

$$l_p = \frac{\kappa}{k_BT} \tag{11.8}$$

is defined as the **persistence length**. Extending the result to the correlation over a finite arc length $s = ma$ (where the continuum limit of large m and small a is considered), we find

$$\langle \boldsymbol{u}(s) \cdot \boldsymbol{u}(0) \rangle = \lim_{m \to \infty} \left(1 - \frac{s}{m l_p}\right)^m = e^{-s/l_p} \tag{11.9}$$

Now it is clear that the persistence length l_p is the correlation length of segmental orientation. Essentially the **WLC is the jointed chain with correlation** (compare this with the freely-jointed chain). Over an arc length s much longer than the persistence length, the orientation is not correlated. In contrast, within the length shorter than the persistence length, the chain can be viewed as straight and stiff.

Then, the end-to-end distance (EED) vector $\boldsymbol{R}$ is obtained as

$$\boldsymbol{R} = \boldsymbol{r}(L) - \boldsymbol{r}(0) = \int_0^L ds\, \boldsymbol{u}(s), \tag{11.10}$$

leading to **the mean squared EED**:

$$\begin{aligned} \langle R^2 \rangle &= \int_0^L ds \int_0^L ds' \langle \boldsymbol{u}(s) \cdot \boldsymbol{u}(s') \rangle = \int_0^L ds \int_0^L ds' e^{-|s-s'|/l_p} \\ &= 2 \int_0^L ds\, e^{-s/l_p} \int_0^s ds' e^{s'/l_p} = 2 l_p \left[L - l_p \left(1 - e^{-L/l_p} \right) \right]. \end{aligned} \tag{11.11}$$

In the above, the integration is done for the case $s > s'$, the result of which is doubled because the integral is invariant with respect to exchange $s \leftrightarrow s'$.

The mean square EED is depicted by Fig. 11.3. It shows that for a long chain or short persistence length, in which $l_p \ll L$,

$$\langle R^2 \rangle \approx 2 l_p L = l L, \tag{11.12}$$

which is the behavior of an ideal chain, (10.4), with the persistence length half of the Kuhn length, $l_p = l/2$. On the other hand, for the short chain or long persistence length, $l_p \gg L$, we find

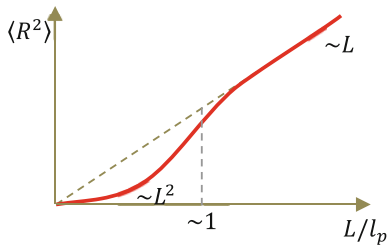

Fig. 11.3 The mean-squared end-to end distance $\langle R^2 \rangle$ of a semi-flexible chain as a function of L/l_p

$$\langle R^2 \rangle \approx L^2, \tag{11.13}$$

which is evidently the behavior of a rigid rod. The crossover between two different regions is seen at the length $L \sim l_p$ (Fig. 11.3).

P11.1 *Two double-stranded DNA fragments of $N/2$ bp length are jointed* via *a bubble of several (n) bp size in between. What is the effective persistence length and ms EED of the entire chain? How does it depend on the length N? Consider that the bubble is composed of two single stranded DNA each with the persistence length l_{ps} of ~ 1 nm. (Hint: For example, the orientation correlation between two segments composed of a ds and a ss bp is $\langle \boldsymbol{u}(0)\boldsymbol{u}(2a)\rangle = 1 - 2a/l_p = (1 - a/l_{pd})(1 - a/l_{ps})$ (11.7). Then, the effective persistence length is $l_p = 2(l_{pd}l_{ps})(l_{pd} + l_{ps})^{-1} \simeq 2l_{ps}$.*

The structure factor of the semi-flexible chain for small $\boldsymbol{q}$ is $S(q) = N(1 - q^2R_G^2/3)^{-1}$, (9.62), with the radius of gyration given by

$$\begin{aligned} R_G^2 &= \frac{1}{2N^2}\sum_{n,m}^{N}\left\langle (\boldsymbol{r}_n - \boldsymbol{r}_m)^2 \right\rangle = \frac{1}{2L^2}\int_0^L ds \int_0^L ds' \left\langle (\boldsymbol{r}(s) - \boldsymbol{r}(s'))^2 \right\rangle \\ &= \frac{1}{3}Ll_p - l_p^2 + \left(\frac{l_p}{L}\right)^2 \langle R^2 \rangle, \end{aligned} \tag{11.14}$$

where we used (11.11) and

$$\left\langle (\boldsymbol{r}(s) - \boldsymbol{r}(s')^2 \right\rangle = 2l_p\left[|\mathrm{s} - s'| - l_p\left(1 - e^{-|\mathrm{s}-s'|/l_p}\right)\right]. \tag{11.15}$$

Equation (11.14) has two limiting forms:

$$R_G^2 \approx \frac{1}{3}Ll_p, \quad l_p \ll L, \tag{11.16}$$

$$R_G^2 \approx \frac{1}{12}L^2, \quad l_p \gg L. \tag{11.17}$$

The scattering at a high momentum transfer $\boldsymbol{q}$ probes a short length scale conformation of a chain, $R_G \sim Na$; following (9.58), (9.60), the structure factor is

$$S(q) \sim q^{-1} \tag{11.18}$$

Figure 11.4 shows the dependence of the $S(q)$ on q that is obtained from small angle neuron scattering experiment. It manifests $q^{-1/\nu}$ and q^{-1} regimes, the with the crossover value q^* indicative of the persistence length $l_p \sim q^{*-1}$, which marks the transition from a flexible to a rigid chain.

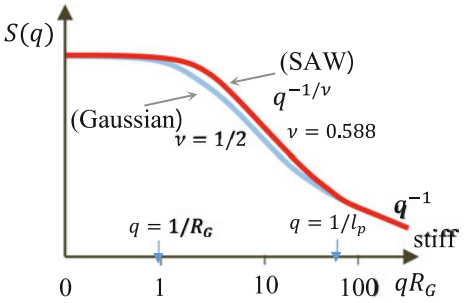

Fig. 11.4 The static structure factor $S(q)$ of a chain is characterized by two lengths, the radius of gyration R_G for low q and the persistence length l_p for large q. The crossover from the flexible chain [either Gaussian $(\nu = 1/2)$ or self-avoiding $(\nu = 0.588)$] to the rigid chain is marked by the regime $q \sim 1/l_p$

11.2 Fluctuations in Nearly Straight Semiflexible Chains and the Force-Extension Relation

11.2.1 Nearly Straight Semiflexible Chains

In this section we shall study how a nearly-straight (rod-like) semiflexible chain thermally fluctuates. Such situations include a chain fragment that is shorter than the chain's persistence length, or a chain of an arbitrary length that is stretched by a strong tension (Fig. 11.5), for which we seek the force-extension relation. Unlike the freely-jointed chain model for the flexible polymer situations (Chap. 3), the WLC calculation shown below is quite involved.

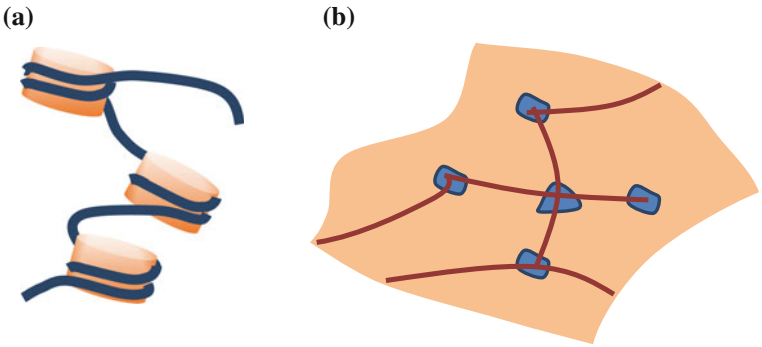

Fig. 11.5 Biological semi-flexible chains under constraints and external forces, **a** DNA constrained by histone proteins, **b** cytoskeleton on cell surface

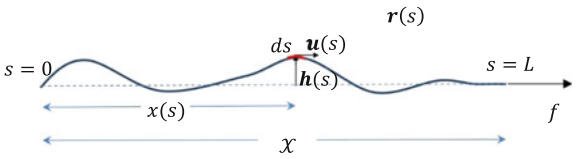

Fig. 11.6 A stretched semi-flexible chain. $\boldsymbol{h}(s)$ and $\boldsymbol{u}(s)$ are two dimensional undulation and orientation vectors at an arc length s positioned at $x(s)$ along the x axis or the direction of the tension f

We express the segmental position at an arc length s of the nearly-straight chain as

$$\boldsymbol{r}(s) = \boldsymbol{h}(s) + x(s)\hat{\boldsymbol{x}} \tag{11.19}$$

where $\hat{\boldsymbol{x}}$ is the unit vector along the tension, and $\boldsymbol{h}(s)$ is the transverse undulation vector of small magnitude that varies slowly over the distance: $|\partial \boldsymbol{h}/\partial s| \ll 1$ (Fig. 11.6). A derivative of (11.19) with respect to s is the unit tangent vector $\boldsymbol{u}(s)$, so we have $1 = (\partial \boldsymbol{h}/\partial s)^2 + (\partial x(s)/\partial s)^2$ or

$$\frac{\partial x(s)}{\partial s} = \left(1 - \left(\frac{\partial \boldsymbol{h}}{\partial s}\right)^2\right)^{1/2} \approx 1 - \frac{1}{2}\left(\frac{\partial \boldsymbol{h}}{\partial s}\right)^2. \tag{11.20}$$

The extension of the chain along the force then is

$$\mathcal{X} = \int_0^L ds \frac{\partial x(s)}{\partial s} = L - \frac{1}{2}\int_0^L ds \left(\frac{\partial \boldsymbol{h}}{\partial s}\right)^2, \tag{11.21}$$

of which the average is

$$X = L - \frac{1}{2}\int_0^L ds \left\langle \left(\frac{\partial \boldsymbol{h}}{\partial s}\right)\right\rangle^2. \tag{11.22}$$

11.2.2 The Force-Extension Relation

We want to find the transverse and longitudinal fluctuations of the chain and the relation between X and the applied tension f if present. To this end we need to first find $\langle(\partial \boldsymbol{h}/\partial s)^2\rangle$ from the effective Hamiltonian, which, for the general case with the f, reads

$$\begin{aligned}\mathcal{F} &= \frac{1}{2}\kappa \int_0^L \left(\frac{\partial^2 \boldsymbol{r}(s)}{\partial s^2}\right)^2 ds - f\mathcal{X} \\ &\approx \frac{1}{2}\int_0^L \left[\kappa\left(\frac{\partial^2 \boldsymbol{h}}{\partial s^2}\right)^2 + f\left(\frac{\partial \boldsymbol{h}}{\partial s}\right)^2\right] ds,\end{aligned} \tag{11.23}$$

the latter being in the "Gaussian level approximation" to correctly retain the second order in $\boldsymbol{h}$.

Because the functional form in real space, (11.23) is cumbersome to analyze, we introduce the Fourier transform:

$$\boldsymbol{h}(q) = \int_0^L ds\, e^{-iqs}\, \boldsymbol{h}(s) \tag{11.24}$$

$$\boldsymbol{h}(s) = \frac{1}{L}\sum_q e^{iqs}\, \boldsymbol{h}(q). \tag{11.25}$$

We adopt the conventional periodic boundary condition, $\boldsymbol{h}(s) = \boldsymbol{h}(s+L)$, which allow q to take N discrete values

$$q_n = \frac{2n\pi}{L}, \quad n = \pm 1, \pm 2 \ldots, \pm N/2, \tag{11.26}$$

where $N = L/a$ with a being the microscopic length. For a very long chain ($N \gg 1$), the choice of the boundary condition does not affect its bulk properties. However, for short chains, where the effects of the ends may not be negligible, one has to use the appropriate boundary condition that meets the actual situations.

Substituting (11.25) into (11.23), with the identity

$$\frac{1}{L}\int_0^L ds\, e^{-i(q-q')s} = \delta_{qq'} \tag{11.27}$$

we have the effective Hamiltonan in the Fourier space,

$$\mathcal{F}\{\boldsymbol{h}(q)\} = \frac{1}{2L}\sum_{\boldsymbol{q}} \left(\kappa q^4 + fq^2\right) |\boldsymbol{h}(q)|^2, \tag{11.28}$$

This is in a tractable form; due to the equipartition of energy for each mode, $\boldsymbol{h}(q)$, which is two dimensional, we have

$$\frac{1}{2L}\left(\kappa q^4 + fq^2\right)\left\langle |\boldsymbol{h}(\boldsymbol{q})|^2 \right\rangle = 2\left(\frac{1}{2}\right)k_B T, \tag{11.29}$$

leading to

$$\left\langle |\boldsymbol{h}(q)|^2 \right\rangle = \frac{2k_B TL}{\kappa q^4 + fq^2} \tag{11.30}$$

For any integrable function of s, say $\varphi(s)$, we can prove the identity (Parseval's theorem):

$$\int_0^L ds\, \varphi(s)^2 = \frac{1}{L}\sum_q |\varphi(q)|^2. \tag{11.31}$$

Thus from (11.22) we can evaluate the fluctuation of the transverse component of $\boldsymbol{u}$, $\boldsymbol{u}_\perp(s) = \partial \boldsymbol{h}/\partial s$ [whose Fourier transform is $iq\boldsymbol{h}(q)$]:

$$\begin{aligned} \left\langle {\boldsymbol{u}_\perp}^2 \right\rangle &= \frac{1}{L}\int_0^L ds \left\langle \boldsymbol{u}_\perp(s)^2 \right\rangle = 2\left(1 - \frac{X}{L}\right) \\ &= \frac{1}{L^2}\sum_q q^2 \left\langle |\boldsymbol{h}(q)|^2 \right\rangle \end{aligned} \tag{11.32}$$

Because the size of each state in q space is $2\pi/L$, for sufficiently long chains we can replace the discrete sum by the integral provided that the integrand is regular,

$$\sum_q \cdots \to \frac{L}{2\pi}\int_{-\infty}^{\infty} dq \cdots \tag{11.33}$$

so that (11.30), (11.32) leads to

$$\begin{aligned} \left\langle {\boldsymbol{u}_\perp}^2 \right\rangle &= \frac{1}{2\pi}\int_{-\infty}^{\infty} dq\, \frac{2k_B T}{\kappa q^2 + f} \\ &= k_B T (f\kappa)^{-1/2} = \left(\frac{k_B T}{f l_p}\right)^{-1/2}, \end{aligned} \tag{11.34}$$

where we used $l_p = \kappa/(k_B T)$. It shows that $\left\langle \boldsymbol{u}_\perp^2 \right\rangle$ is indeed small for the extensional force larger than $k_B T/l_p$ in consistency with our approximation of the nearly-straight conformation. Combining (11.32) and (11.34) yields

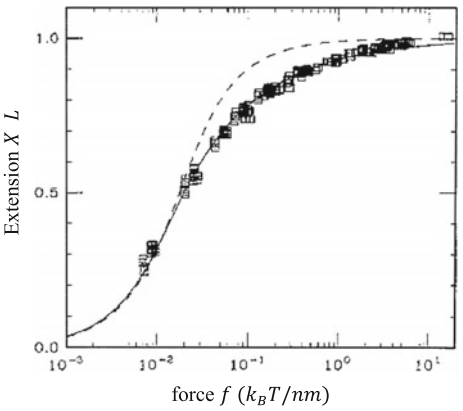

Fig. 11.7 The relative extension *X/L* versus force f for $L = 32.8$ μm. The solid line represents the theoretical results of Marko & Siggia, which fits well the experimental data. The dashed line represents the freely—jointed chain model. (Adapted with permission from Marko and Siggia (1995). Copyright 1995, American Chemical Society)

$$f = \frac{k_B T}{4 l_p} \left(1 - \frac{X}{L}\right)^{-2}. \tag{11.35}$$

This can also be interpreted as the *average* force f necessary to extend the chain to a distance X. Like those derived from Gaussian chain model or freely-jointed chain (FJC) model, the force is proportional to $k_B T$ due to entropic nature of the chain; the force required to extend the chain to its contour length L diverges to infinity, since the chain dislikes to have the minimum entropy, the behavior already observed in the FJC. For a small value of X, however, this force on the highly stretched WLC cannot recover the flexible chain result $f = 3k_B TX/(Ll) = 3k_B TX/(2Ll_p)$ (3.59), (10.20), because we assumed small thermal undulations. A formula to interpolate the highly stretched and flexible chain limits was devised by adding the last two terms below:

$$f = \frac{k_B T}{l_p} \left[\frac{1}{4}\left(1 - \frac{X}{L}\right)^{-2} + \frac{X}{L} - \frac{1}{4}\right] \tag{11.36}$$

As shown by Marko and Siggia (1995) and Bustamante et al. (1994) this formula is in an excellent agreement with the force-extension experiment on a long DNA, provided that its persistence length is $l_p \approx 50$ nm.

P11.2 *Two ends of a double-stranded DNA of the contour length* $L = 20$ nm *and persistence length* $l_p \approx 50$ nm *are attached to those of a single stranded DNA of the same contour length, as shown in the Figure. Will the fully stretched configuration shown in this figure (a) be possible? If not, why and what would be the shape at the equilibrium? Suppose that the equilibrium conformation would be in D shape where dsDNA has the shape of circular arc, while ssDNA is highly stretched, as shown in figure (b). What is the equilibrium end to end distance X? Calculate the X,*

using WLC for the dsDNA, and for the ssDNA, each with the persistence length of 50 *and* 1 nm *respectively.*

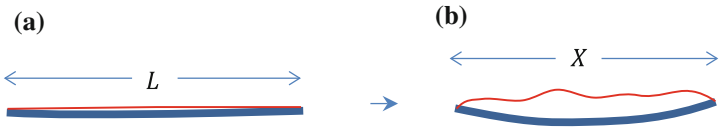

If the contour length of the DNA is 200 nm*, what will happen? Will the dsDNA still bend? How much?*

P11.3 *Find the correlation function* $\langle \boldsymbol{u}(s) \cdot \boldsymbol{u}(0) \rangle$ *for a stretched WLC by the tension* f.

11.2.3 The Intrinsic Height Undulations, Correlations, and Length Fluctuations of Short Chain Fragments

Now consider a tension-free chain fragment that is shorter than the persistence length to warrant the approximation of small undulation. From (11.30) with $f = 0$:

$$\left\langle |\boldsymbol{h}(q)|^2 \right\rangle = \frac{2k_B TL}{\kappa q^4}. \tag{11.37}$$

The transverse fluctuation defined by

$$\left\langle \boldsymbol{h}^2 \right\rangle = \frac{1}{L} \int_0^L ds \left\langle \boldsymbol{h}(s)^2 \right\rangle \tag{11.38}$$

is obtained as

$$\left\langle \boldsymbol{h}^2 \right\rangle = \frac{1}{L^2} \sum_q \left\langle |\boldsymbol{h}(q)|^2 \right\rangle = \frac{2k_B T}{L\kappa} \sum_q \frac{1}{q^4} = \frac{4}{Ll_p} \left(\frac{L}{2\pi} \right)^4 \zeta_N(4) \approx \frac{L^3}{4 \cdot 90 l_p} \tag{11.39}$$

where the numerical factor $\zeta_N(4) = \sum_1^N (1/n^4)$ converges to $\zeta_\infty(4) = \pi^4/90$ for $N > 10$. The rms transverse fluctuation grows as $L^{3/2}$. However, **for a short chain in which $L/l_p < 1$, the chain undulation is very small**, even if the chain is free. For short dsDNA fragment of $L = 20\,\text{nm}$, $l_p = 50\,\text{nm}$, $\left\langle \boldsymbol{h}^2 \right\rangle^{1/2}$ is only at sub- nanometer scale. For an actin filament of the length $L = 10\,\mu\text{m}$, $l_p = 20\,\mu\text{m}$, $\left\langle \boldsymbol{h}^2 \right\rangle^{1/2}$ is about at

nanometer scale. When a short chain or filament is bent, the thermal undulation is also expected to be negligible. This result will be utilized in next section.

P11.4 *Find the* $\langle \boldsymbol{u}_\perp{}^2 \rangle$ *and for a short, tension-free chain.*

P11.5 *For a chain with the both ends fixed, how would the above results be changed for a short chain? Show that the undulation fluctuation varies along the axis of extension as*

$$\left\langle \boldsymbol{h}(s)^2 \right\rangle = \frac{2}{3}\frac{L^3}{l_p}\left(\frac{s}{L}\right)^2\left[1-\left(\frac{s}{L}\right)\right]^2$$

The result was used to investigate the motion of a bead attached to a single microtubule in network (Caspi et al. 1998). *When averaged over the arc length, it is* $\langle \boldsymbol{h}^2 \rangle = L^3/(90 l_p)$, *which is four times larger than* (11.39). *Also it was shown that, when the both ends are fixed and stretched by a force f*

$$\left\langle \boldsymbol{h}(s)^2 \right\rangle = 2\frac{Lk_BT}{f}\left(\frac{s}{L}\right)\left[1-\left(\frac{s}{L}\right)\right]$$

(Baba et al. 2012). *This is in a good agreement with the experiment a single DNA fragment stretched by dual trap optical tweezers.*

Now we study the correlation function of the height undulations (transverse fluctuations) at two positions $C_{\boldsymbol{h}}(s,s')$; via direct Fourier transform (11.25) and (11.37), it is given by

$$C_{\boldsymbol{h}}(s,s') = \langle \boldsymbol{h}(s)\cdot\boldsymbol{h}(s')\rangle = \frac{1}{L^2}\sum_{\boldsymbol{q}}\sum_{\boldsymbol{q}'} e^{iq(s-s')}e^{-i(q'-q)s'}\langle \boldsymbol{h}(q)\cdot\boldsymbol{h}^*(q')\rangle$$

Assuming the translational invariance, $C_{\boldsymbol{h}}(s,s') = C_{\boldsymbol{h}}(s-s')$, one can show that

$$\begin{aligned} C_{\boldsymbol{h}}(s-s') &= \frac{1}{L^2}\sum_{\boldsymbol{q}} e^{iq(s-s')}\left\langle |\boldsymbol{h}(q)|^2 \right\rangle = \frac{2k_BT}{\kappa L}\sum_{q}\frac{1}{q^4}e^{iq(s-s')} \\ &= \frac{4k_BT}{\kappa L}\sum_{q_1}^{q_{N/2}} q^{-4}\cos[q(s-s')] \approx \left\{\frac{4k_BT}{\kappa L}\sum_{q_1}^{q_{N/2}} q^{-4}\right\}\cos[q_1(s-s')] \\ &= \left\langle h^2 \right\rangle \cos[q_1(s-s')] = \frac{L^3}{4\cdot 90 l_p}\cos\left[\frac{2\pi(s-s')}{L}\right], \end{aligned} \tag{11.40}$$

Here q_1 and $q_{N/2}$ are the lowest and highest wave-number cutoffs respectively, and we have used (11.39) and made a single mode (q_1) approximation owing to the rapidly decaying function q^{-4}. Equation (11.40) means that the correlation is

long-ranged over the entire chain. Related to this, we find the mean-squared displacement (MSD):

$$\begin{aligned}\left\langle (\boldsymbol{h}(s)-\boldsymbol{h}(0))^2 \right\rangle &= 2\left[\langle h^2\rangle - \langle \boldsymbol{h}(s)\cdot\boldsymbol{h}(0)\rangle\right] \\ &= \frac{4k_BT}{\kappa L}\sum_{q_1}^{q_{N/2}} q^{-4}\{1-\cos qs\} \\ &= \frac{2k_BT}{\pi\kappa}\int_{q_1}^{q_{N/2}} dq\, q^{-4}\{1-\cos qs\}.\end{aligned} \tag{11.41}$$

Consider $s \gg a$. While $\cos qs$ is nearly 1 for small q, it rapidly oscillates around 0 between $q \sim s^{-1}$ and $q = q_{N/2}$ yielding little contribution to the integral, so the MSD is approximated as:

$$\begin{aligned}\left\langle (\boldsymbol{h}(s)-\boldsymbol{h}(0))^2 \right\rangle &\approx \frac{2k_BT}{\pi\kappa}\int_{\alpha/s}^{q_{N/2}} dq\, q^{-4} \\ &= \frac{2k_BT}{3\pi\kappa}\left(\frac{s}{\alpha}\right)^3 \sim s^3/l_p,\end{aligned} \tag{11.42}$$

where $\alpha \sim 1$. This scaling behavior appears to be similar to (11.39); the MSD of WLC shows strong persistence in contrast to that of an ideal chain, which is $\sim s l_p$.

Following the transverse fluctuation, the length of the extension $\mathcal{X}$ also fluctuate around the average $\langle \mathcal{X}\rangle = X$. A straightforward way to derive this longitudinal fluctuation is to use the linear response theory, (9.9), rewritten as

$$\left\langle (\Delta\mathcal{X})^2 \right\rangle = k_BT\frac{\partial X}{\partial f}. \tag{11.43}$$

For the fluctuation of the length streched by a high force one may simply use (11.35) to obtain

$$\left\langle (\Delta\mathcal{X})^2 \right\rangle = \frac{L}{4}(k_BT/f)^{3/2} l_p{}^{-1/2}, \tag{11.44}$$

which indicates how the length does fluctuate even under such high force for a long chain. For the case where the force is not so high, (11.43) becomes via (11.32) and (11.30):

$$\left\langle (\Delta\mathcal{X})^2 \right\rangle = (k_BT)^2 \sum_q \frac{1}{(\kappa q^2 + f)^2}. \tag{11.45}$$

This is calculated for $f = 0$:

$$\left\langle (\Delta\mathcal{X})^2 \right\rangle = \frac{(k_B T)^2}{\kappa^2} \sum_q \frac{1}{q^4} = \frac{2}{l_p^2} \left(\frac{L}{2\pi} \right)^4 \zeta_N(4) = \frac{1}{8 \cdot 90} \frac{L^4}{{l_p}^2}. \tag{11.46}$$

The rms longitudinal fluctuation grows with L^2 as the chain gets long. Interestingly, however, the ratio $\langle \Delta\mathcal{X}^2 \rangle / \langle h^2 \rangle$ is $L/(2l_p)$; if the chain is stiff and short such that $L < 2l_p$, the longitudinal fluctuation is less than the transverse fluctuation.

11.2.4 The Equilibrium Shapes of Stiff Chains Under a Force

The above discussions are mostly concerned with the fluctuations. Lastly let us look at the mean configuration of the chain under a force. For the chain under the stretching at the ends, the equilibrium shape is obtained by the condition of the minimum free energy functional (11.23),

$$\delta\mathcal{F} / \delta \boldsymbol{h}(s) = 0. \tag{11.47}$$

$\delta\mathcal{F} / \delta \boldsymbol{h}(s)$ is functional derivative obtained by noting that the change $\delta\mathcal{F}$ caused by a differential change $\delta \boldsymbol{h}$ in $\boldsymbol{h}$ is written as

$$\delta\mathcal{F} = \int_0^L \left[\kappa \left(\frac{\partial^2 \boldsymbol{h}}{\partial s^2} \right) \cdot \left(\frac{\partial^2 \delta \boldsymbol{h}}{\partial s^2} \right) + f \left(\frac{\partial \boldsymbol{h}}{\partial s} \right) \cdot \left(\frac{\partial \delta \boldsymbol{h}}{\partial s} \right) \right] ds. \tag{11.48}$$

Upon integration by parts, the above becomes

$$\delta\mathcal{F} = \int_0^L \left[\kappa \{ \left(\frac{\partial^4 \boldsymbol{h}}{\partial s^4} \right) \cdot \delta \boldsymbol{h} - f \left(\frac{\partial^2 \boldsymbol{h}}{\partial s^2} \right) \cdot \delta \boldsymbol{h} \right] ds \tag{11.49}$$

Thus,

$$\delta\mathcal{F} / \delta \boldsymbol{h}(s) = \kappa \left(\frac{\partial^4 \boldsymbol{h}}{\partial s^4} \right) - f \left(\frac{\partial^2 \boldsymbol{h}}{\partial s^2} \right) = 0. \tag{11.50}$$

Taking only a single component of $\boldsymbol{h}$, we have

$$\kappa\left(\frac{\partial^2 g}{\partial s^2}\right) = fg, \tag{11.51}$$

where $g = (\partial^2 h)/(\partial s^2)$. By integration one finds

$$g = A\sinh[(f/\kappa)^{1/2}s] + B\cosh\left[(f/\kappa)^{1/2}s\right] \tag{11.52}$$

$$h(s) = a\sinh[(f/\kappa)^{1/2}s] + b\cosh\left[(f/\kappa)^{1/2}s\right] + cs + d. \tag{11.53}$$

Using the BCs at both ends the constants a, b, c, d are determined.

We can include the situation where at the ends the elastic rod is compressed longitudinally rather than stretched. For this case the above analysis is still valid if the force f is replaced by $-f$; we have

$$h(s) = a\sin\left[(f/\kappa)^{1/2}s\right] + b\cos\left[(f/\kappa)^{1/2}s\right] + cs + d. \tag{11.54}$$

Considering the ends are pinned we use the BC, $h(s=0) = h(s=L) = 0$ and $(\partial^2 h/\partial s^2)(s=0) = (\partial^2 h/\partial s^2)(s=L) = 0$. We have the trivial solution $h = 0$, or

$$h(s) = a\sin[(f/\kappa)^{1/2}s] \tag{11.55}$$

with a undetermined but under the condition,

$$(f/\kappa)^{1/2}L = n\pi, \tag{11.56}$$

where n is an integer. $h(s)$ has different modal shapes (eigen-modes) depending upon n. Thus, if the compressional force increases to the critical value corresponding to $n = 1$

$$f = \kappa(\pi/L)^2, \tag{11.57}$$

a sudden buckling occurs from the straight shape. This is called the Euler buckling instability in beam theory. Because the critical force is inversely proportional to the square of the length, relatively long chains may not be able to sustain the compression without buckling. The buckling instability may limit the lengths of the microtubules that polymerize in cells.

11.3 Polyelectrolytes

Polyelectrolytes (PE) are the polymers that carry ionizable groups, which dissociate in an aqueous solution endowing the polymers with charges. Many biological molecules are such charged polymers. For instance, polypeptides, actin filaments,

RNA and DNA molecules are polyelectrolytes. **The electrostatic interactions between charges among the PEs and ionic backgrounds fundamentally affect their conformations**.

11.3.1 Manning Condensation

The cations in the solution, due to their electrostatic attraction with PE segmental charges (which are regarded as negative here), can adsorb on the PE contour. The cations can also desorb to the bulk for entropic gain. The cation adsorption or condensation, called the **Manning condensation**, **occurs due to the attraction that wins the entropy over in minimizing the free energy of *the combined system of the PE and adsorbed cations*** (Manning 1969; Oosawa 1971).

Below we study how the condensation occurs for an infinitely long and thin but rigid PE that has charge $-e$ per segment of length b, i.e., the line charge density of the absolute magnitude $\lambda = e/b$ in a dilute 1:1 salt solution (Fig. 11.8). There are two kinds of cations. One is the counterions dissociated from the polyelectrolyte, and the other is cations of the salt. Because the counterions are much less than the salt ions, the charge neutrality within the background liquid is not violated. Assume that the $\mathcal{N}$ cations of valency z indeed condensate onto the PE per segment b and the segmental charge e is renormalized to $e_{eff} = e(1 - z\mathcal{N})$. The optimal value for $\mathcal{N}$ will be determined by the competition of energy and entropy. Because the PE is infinitely long (total segment number $M \to \infty$), the energy of electrostatic repulsion between the renormalized charges in the PE using the Debye-Hükel approximation is

$$\begin{aligned}\mathcal{E} &= \sum_{i=1}^{M}\sum_{j=i+1}^{M}\frac{e^2(1-z\mathcal{N})^2}{4\pi\varepsilon b}\frac{1}{|i-j|}e^{-\kappa_D b|i-j|} \\ &= \frac{Me^2(1-z\mathcal{N})^2}{4\pi\varepsilon b}\sum_{k=1}^{\infty}\frac{1}{k}e^{-\kappa_D bk},\end{aligned} \tag{11.58}$$

which can be summed to:

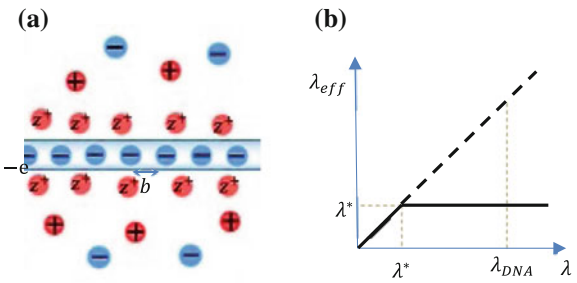

Fig. 11.8 **a** A negatively charged polyelectrolyte adsorbed by z-valent cations in 1:1 salt, **b** the effective linear charge density λ_{eff} on the polyelectrolyte versus its bare linear charge density λ. The λ^* is the critical bare density above which the Manning condensation occurs

$$\mathcal{E} = -\frac{Me^2(1-z\mathcal{N})^2}{4\pi\varepsilon b}\ln\left(1-e^{-\kappa_D b}\right). \tag{11.59}$$

The energy change due to condensation is

$$\Delta\mathcal{E} = -\frac{Me^2\left\{(1-z\mathcal{N})^2-1\right\}}{4\pi\varepsilon b}\ln(\kappa_D b), \tag{11.60}$$

because we will consider the low ionic concentration in which $\kappa_D b = b/\lambda_D \ll 1$.

During the condensation the entropy changes due to transfer of $\mathcal{N}$ cations from the bulk region where the cation concentration is n_∞ to a condensed PE segment where the concentration is $n_c = \mathcal{N}/v$. v is a certain volume allowed for a condensed cation on the PE segment that can be determined self-consistently later. Using (4.89), the condensation of the $\mathcal{N}$ cations induces a reduction of entropy:

$$T\Delta\mathcal{S} = M\mathcal{N}k_BT\ln\left(\frac{n_\infty}{n_c}\right) = -M\mathcal{N}k_BT\ln\left(\frac{\mathcal{N}}{vn_\infty}\right) \tag{11.61}$$

Then the net free energy change associated with condensation is

$$\begin{aligned}\Delta\mathcal{F} &= \Delta\mathcal{E} - T\Delta\mathcal{S}\\ &= Mk_BT\left[-\frac{l_B}{b}\left\{(1-z\mathcal{N})^2-1\right\}\ln(\kappa_D b)+\mathcal{N}\ln\frac{\mathcal{N}}{vn_\infty}\right]\end{aligned} \tag{11.62}$$

where $l_B = e^2/(4\pi\varepsilon k_BT)$ is the Bjerrum length. The condition of the free energy minimum $\partial\Delta\mathcal{F}/\partial\mathcal{N} = 0$ is

$$\frac{2zl_B}{b}(1-z\mathcal{N})\ln(\kappa_D b) + \ln\frac{\mathcal{N}}{vn_\infty} + 1 = 0, \tag{11.63}$$

which, with $\kappa_D = An_\infty^{1/2}$ (6.48), is rewritten as

$$\frac{2zl_B}{b}(1-z\mathcal{N})\ln(Ab) + \frac{zl_B}{b}(1-z\mathcal{N})\ln n_\infty + \ln\left(\frac{\mathcal{N}}{v}\right) + 1 = \ln n_\infty. \tag{11.64}$$

Since $-\ln n_\infty$ diverges to infinity as n_∞ tends to be zero, the above equality is satisfied only when $(zl_B/b)(1-z\mathcal{N})\ln n_\infty = \ln n_\infty$. It leads to the critical condition for condensation

$$1 - z\mathcal{N} = \frac{b}{zl_B}, \tag{11.65}$$

It signifies that **at equilibrium the segmental charge and charge density on the PE respectively are renormalized from the bare value e and $\lambda = e/b$ to smaller values**:

$$e_{eff} = e(1 - z\mathcal{N}) = \frac{eb}{zl_B} \tag{11.66}$$

$$\lambda_{eff} = \frac{e_{eff}}{b} = \frac{e}{zl_B} \equiv \lambda^*. \tag{11.67}$$

Of particular note is that the renormalized density (11.67) is independent of the bulk concentration of the cations and the properties of the PE. The condition for the condensation $\mathcal{N} > 0$ is satisfied by $b < zl_B$, that is, $\lambda > \lambda^*$. It can be easily met in double-stranded DNA, a highly charged PE with $b = 0.34\,\text{nm}/2 = 0.17$ nm, which is about a fourth of l_B in water at 25 °C.

The effective (renormalized) line charge density of the PE is given by Fig. 11.8b. If a PE is negatively charged with the absolute magnitude $\lambda(< \lambda^*)$, the cations tend to be in the bulk away from the PE because their entropy gain dominates over their electrostatic attraction to the contour. The linear charge density is not affected by the cations. If the PE's density is sufficiently high, $\lambda > \lambda^*$, the surrounding cations, dominated by the attraction, tend to condense to the contour, reducing the absolute magnitude of effective charge density λ_{eff} to λ^*. For dsDNA, average number of the cations adsorbed per segment b is $\mathcal{N} = (1 - b/zl_B)/z \approx 3/4$ for $z = 1$, reducing the negative charge density to one-fourth of the bare density. Equation (11.67) means that **the cation's multivalency $(z \geq 2)$ enhances the condensation**. Strictly speaking the above results are derived only for the ideal case of infinitely thin PE and infinitely dilute concentration of salt, but are fortuitously valid up to $n_\infty \sim 0.1$ mM.

P11.6 *Find the expression for v. What is the free energy change ΔF at the critical condition?*

11.3.2 The Charge Effect on Chain Persistence Length

The electrostatic interactions between charges within a polyelectrolyte are screened by counterions and also by an added salt in the solution. If the concentration of ions in the solution is low, the interaction is weakly screened and the charged polymer tends to stretch to reduce the electrostatic repulsion therein. As the concentration becomes higher, the screening also gets stronger and the chain is less stretched and more coiled, assisted by the entropic driving toward a more disordered chain conformation. Furthermore, the counterion condensation tends to neutralize the PE, making it less stiff.

The effect of the charges on the polymer flexibility or rigidity is described by the persistence length change. The enhancement of the persistence length due to the PE

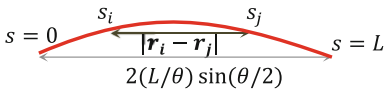

Fig. 11.9 An elastic filament of length L bent with small curvature θ/L

charges can be evaluated by supposing that the PE of length $L = Mb$ is slightly and uniformly bent to a circular arc of radius $R = L/\theta$ as shown by Fig. 11.9. Were the chain uncharged, the mechanical bending energy (11.1) is given by

$$F^0 = \frac{1}{2} k_B T l_p^0 \frac{L}{R^2} = \frac{1}{2} k_B T l_p^0 \frac{\theta^2}{L}, \tag{11.68}$$

where l_p^0 is the neutral part of the net persistence length we will evaluate.

Consider that the bent polymer is uniformly charged with linear charge density λ_{eff} in an ionic solution with the inverse Debye screening length κ_D. The Debye-Hückel theory gives the electrostatic bending energy (the electrostatic energy change due to the bending):

$$F^e = \sum_{i=1}^{N} \sum_{j=i+1}^{N} \frac{{e_{eff}}^2}{4\pi\varepsilon} \left(\frac{e^{-\kappa_D |\boldsymbol{r}_i - \boldsymbol{r}_j|}}{|\boldsymbol{r}_i - \boldsymbol{r}_j|} - \frac{e^{-\kappa_D |s_i - s_j|}}{|s_i - s_j|} \right), \tag{11.69}$$

where $|\boldsymbol{r}_i - \boldsymbol{r}_j|$ and $|s_i - s_j|$ are the straight and arc distances between two points i and j respectively (Fig. 11.9). Noting that $|\boldsymbol{r}_i - \boldsymbol{r}_j| = 2R\sin(\theta_{ij}/2) = (2L/\theta)\sin(|s_i - s_j|\theta/2L)$, we expand $(\cdots)$ in the summation to the leading order in small curvature θ/L:

$$(\cdots) \approx \frac{\theta^2}{24L^2} e^{-\kappa_D |s_i - s_j|} |s_i - s_j| (1 + \kappa_D |s_i - s_j|), \tag{11.70}$$

which is substituted into (11.69) to yield

$$\begin{aligned} F^e &= \frac{e_{eff}^2}{4\pi\varepsilon} \frac{\theta^2}{24L^2} \sum_{i=1}^{M} \sum_{j=i+1}^{M} e^{-\kappa_D |s_i - s_j|} |s_i - s_j| (1 + \kappa_D |s_i - s_j|) \\ &\approx \frac{1}{4\pi\varepsilon} \frac{\theta^2 L}{24L^2} \int_0^L ds\, {\lambda_{eff}}^2 e^{-\kappa_D s} s(1 + \kappa_D s), \end{aligned} \tag{11.71}$$

where we approximated that L is much longer than $\lambda_D = \kappa_D^{-1}$ and used the logic behind evaluating (11.58). Then

$$F^e \approx \frac{{\lambda_{eff}}^2}{4\pi\varepsilon} \frac{\theta^2 {\lambda_D}^2}{8L} \tag{11.72}$$

This F^e contributes to the total free energy of bending:

$$F = F^0 + F^e = \frac{1}{2} k_B T l_p^0 \frac{\theta^2}{L} + \frac{\lambda_{eff}^2 \lambda_D^2}{32\pi\varepsilon} \frac{\theta^2}{L} = \frac{1}{2} k_B T l_p \frac{\theta^2}{L}, \tag{11.73}$$

where the net persistence length is defined by

$$l_p = l_p^0 + l_p^e, \tag{11.74}$$

where

$$l_p^e = \frac{1}{4} l_B \left(\lambda_{eff} \lambda_D / e\right)^2 \tag{11.75}$$

is the Odijk-Skolnick-Fixman (OSF) expression for the electrostatic persistence length (Odijk 1977; Skolnick and Fixman 1977). Note that for 1:1 salt $\lambda_D = \left(\varepsilon k_B T / 2 n_0 e^2\right)^{1/2}$. Equation (11.75) then tells us how $\boldsymbol{l_p^e}$ **increases with the polyelectrolyte charge density** $(\boldsymbol{\lambda_{eff}^2})$ **but decreases with salt concentration** $(\sim n_\infty^{-1})$. On a DNA, as the result of the Manning condensation, $\lambda_{eff} = e/z l_B$, yielding

$$l_p^e = \frac{1}{4} l_B (\lambda_D / z l_B)^2. \tag{11.76}$$

Depicted in Fig. 11.10 is the dependence of DNA persistence length on monovalent salt concentration. The equation $l_p = l_p^0 + l_p^e = l_p^0 + \lambda_D^2/(4 l_B)$ (solid curve) is in an excellent agreement with the persistence length measured by pulling on single DNA molecules using optical tweezers. The persistence length approaches to bare (neutral) value $l_p^0 \approx 50\,\text{nm}$ as the salt concentration or ionic strength increases above

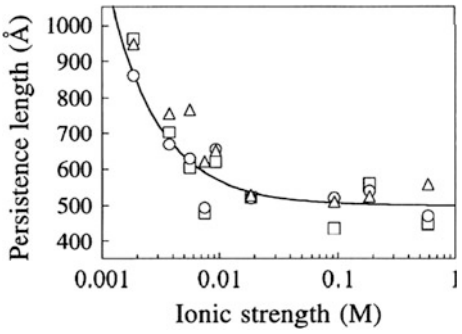

Fig. 11.10 The net persistence length $l_p = l_p^0 + l_p^e$ vs ionic (salt) concentration. Points are: □, inextensible WLC; ○, strong stretching limit; ▵, extensible WLC. Line calculated from (11.76) with $l_p^0 = 50nm$ (Baumann C G et al. PNAS, 94: 6185–6190. Copyright (1997) National Academy of Sciences, U.S.A.)

0.1 M so as to fully screen the Coulomb repulsion between segments; it increases rapidly toward OSF value as the concentration decreases below 10 mM.

11.3.3 The Effect of Charge-Density Fluctuations on Stiffness

In the above consideration, we assumed the uniformity of the effective charge density of PE. This assumption is not true in general, particularly if multivalent cations are present. Compared with monovalent cations, they tend to more strongly condense on the PE backbone, making the charge density different as well as non-uniform. For example, when divalent cations such as Ca ions adsorb on negatively charged segments of DNA, the effective charge on such a segment becomes $+e$, while that on an unabsorbed segment remains as $-e$. This temporary positioning of unlike-charges, if they are nearby, can induce the intra-DNA attraction leading to DNA collapse (Bloomfield 1997). DNA fragments in the presence of trivalent cations condense primarily into dense toroidal or spheroidal structures (Hud and Downing 2001) (Fig. 11.11a). The attraction between two DNA fragments leads to adhesion and packing within a nucleus (Ha and Liu 1997; Garcia et al. 2006). **The charge-density fluctuation-induced attraction between like-charges** has been one of topical issues in bio-soft matter research.

In order to quantify the phenomena, we add the line charge density fluctuation $\Delta\lambda(s)$ to λ_{eff}, and replace λ_{eff}^2 by $\langle\{\lambda_{eff}+\Delta\lambda(s)\}\{\lambda_{eff}+\Delta\lambda(0)\}\rangle$ within the integral (11.71):

$$F^e = \frac{1}{4\pi\varepsilon}\frac{\theta^2}{24L}\int_0^L ds\left[\lambda_{eff}^2 + \langle\Delta\lambda(s)\Delta\lambda(0)\rangle\right]e^{-\kappa_D s}s(1+\kappa_D s) \tag{11.77}$$

where we note $\langle\Delta\lambda\rangle = 0$.

According to a theoretical model that treats the charges on the PE as a one-dimensional gas interacting electrostatically, the correlation function $\langle\Delta\lambda(s)\Delta\lambda(0)\rangle$

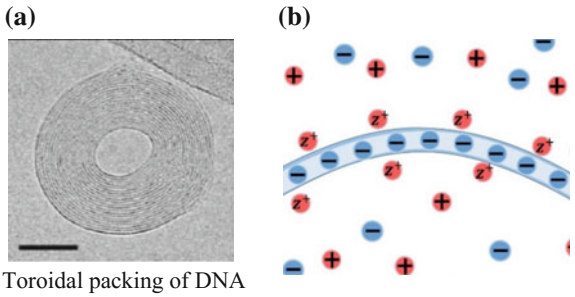

Fig. 11.11 **a** DNA collapsed into a torodial shape (Nicholas V. Hud and Kenneth H. Downing, (2001), Copyright (2001) National Academy of Sciences, U.S.A.), **b** a polyelectrolyte that bends due to the charge density fluctuations induced by multi-valent cations

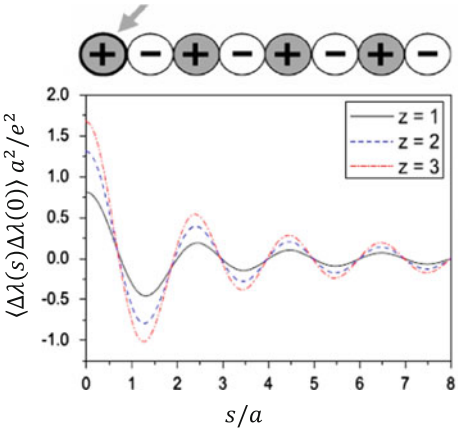

Fig. 11.12 Charge density correlation on DNA contour $\langle \Delta\lambda(s)\Delta\lambda(0)\rangle$ for different valencies (z) of cations adsorbed, according to a theoretical model. $a = 0.4$ nm is a cation's diameter. (Reprinted with permission from W. K. Kim and W. Sung, Phys. Rev. E 78, 021904 (2008). Copyright (2008) by the American Physical Society)

for a straight DNA shows an oscillatory decay with the amplitude that increases with the valency as shown in Fig. 11.12 (Kim and Sung 2008). As discussed in the linear response theory (Chap. 9), the charge density correlation function is proportional to the average charge density change induced at s in response to a charge placed at $s = 0$. Thus, the oscillation is attributable to successive coordination of charges in alternating signs in response to this central charge (marked by an arrow in Fig. 11.12); it is originated from competition between electrostatic attraction and hard-core repulsion. Overall, the contribution of this oscillation to the integral is negative, so that the fluctuation contribution reduces the free energy (11.77) below the OSF result (11.72), leading to a reduction of the persistence length. In a straight conformation of polymer, the two electrostatic contributions were found to nearly cancel so that the net persistence length is about the neutral value l_p^0, for any multivalent cations in physiological salt concentrations. In a highly bent conformation, however, the fluctuation-induced reduction can be very large, dominating the mean field enhancement, to yield a quite small persistence length (Kim and Sung 2011).

Further Reading and References

A.R. Khokhlov, A. Grosberg, V.S. Pande, *Statistical Physics of Macromolecules* (American Institute of Physics, 2002)

W.M. Gelbart, R.F. Bruinsma, P.A. Pincus, V.A. Parsegian, DNA-inspired electrostatics. Phys. Today (2000)

K. Sneppen, G. Zocchi, *Physics in Molecular Biology* (Cambridge University Press, 2006)

A.A. Kornyshev, Physics of DNA: unravelling hidden abilities encoded in the structure of 'the most important molecule'. Phys. Chem. Chem. Phys. **12**, 39 (2010)

J.F. Marko, E.D. Siggia, Stretching DNA. Macromolecules **28**, 26 (1995)

C. Bustamante et al., Entropic elasticity of lambda-phage DNA. Science **265**, 5178 (1994)

G.S. Manning, Limiting laws and counterion condensation in polyelectrolyte solutions I. Colligative properties. J. Chem. Phys. **51**, 924 (1969)

F. Oosawa, *Polyelectrolytes* (Marcel Dekker, New York, 1971)
T. Odijk, Polyelectrolytes near the rod limit. J. Polym. Sci. **15**, 477 (1977)
J. Skolnick, M. Fixman, Electrostatic persistence length of a wormlike polyelectrolyte. Macromolecules **10**, 944 (1977)
J.-L. Barrat, J.F. Joanny, *Advances in Chemical Physics: Polymeric Systems*, vol. 94 (Wiley, 2007)
R. Podgornik, V.A. Parsegian, Charge-fluctuation forces between rodlike polyelectrolytes: pairwise summability reexamined. Phys. Rev. Lett. **80**, 1560 (1998)
V.A. Bloomfield, DNA condensation by multivalent cations. Biopolymers **44**, 3, 269 (1997)
B.Y. Ha, A.J. Liu, Counterion-mediated attraction between two like-charged rods. Phys. Rev. Lett. **79**, 1289 (1997)
N.V. Hud, K.H. Downing, Cryoelectron microscopy of λ phage DNA condensates in vitreous ice: the fine structure of DNA toroids. Proc. Natl. Acad. Sci. U.S.A. **98**, 14925 (2001)
H.G. Garcia, P. Grayson, L. Han, M. Inamdar, J. Kondev, P.C. Nelson, R. Phillips, J. Widom, P.A. Wiggins, Biological consequences of tightly bent DNA: the other life of a macromolecular celebrity. Biopolymers **85**, 2 (2006)
W.K. Kim, W. Sung, Charge density coordination and dynamics in a rodlike polyelectrolyte. Phys. Rev. E **78**, 021904 (2008)
W.K. Kim, W. Sung, Charge density and bending rigidity of a rodlike polyelectrolyte: effects of multivalent counterions. Phys. Rev. E **83**, 051926 (2011)
G. Ariel, D. Andelman, Persistence length of a strongly charged rodlike polyelectrolyte in the presence of salt. Phys. Rev. E **67**, 011805 (2003)
A. Caspi et al., Semiflexible polymer network: a view from inside. Phys. Rev. Lett. **80**, 1106 (1998)
T. Baba et al., Force-fluctuation relation of a single DNA molecule. Macromolecules **45**, 2857 (2012)

Chapter 12
Membranes and Elastic Surfaces

An essential component of a cell is a biological membrane or bio-membrane; **it forms and modulates an interface of the cell and cell's various internal compartments called organelles**, **acting as a selectively permeable barrier between them**. Bio-membranes consist mostly of phospholipid (lipid) bilayers and the associated proteins. The bilayer is about 5 nm thick, being self-assembled from lipid molecules each with a hydrophilic head and hydrophobic tails. The lipids in a fluid membrane can move laterally within the bilayer, organizing themselves to adopt the phase or the shape at equilibrium, corresponding to free energy minimum. There are two kinds of membrane proteins that perform a variety of cellular functions: integral proteins (such as ion channel), all or part of which span the bilayer, and peripheral proteins, which lie outside the core of the bilayer (see Fig. 12.1).

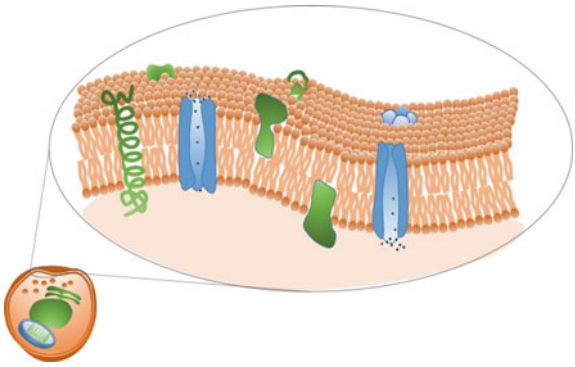

Fig. 12.1 A cell membrane and its constituents such as phospholipid molecules and membrane-bound proteins including ion channels. A phospholipid molecule is composed of a hydrophilic head and hydrophobic tails

W. Sung, *Statistical Physics for Biological Matter*, Graduate Texts in Physics,
https://doi.org/10.1007/978-94-024-1584-1_12

In this chapter we study the thermo-mechanical aspects of the membrane, with a particular focus on its mesoscopic fluctuations and conformations at equilibrium, and shape transitions. Although they are in reality very complex and heterogeneous, in this introduction, we will consider the protein-free homogeneous membranes or membrane fragments that are amenable to statistical physics analysis.

12.1 Membrane Self-assembly and Phase Transition

The membrane is composed of many species of lipids, proteins, and cholesterols, depending upon its functions. The lipid, which is the major component, has a polar head group connected with hydrophobic chain(s). When dispersed in an aqueous solution, depending on their concentrations, the **lipid molecules assemble to form monolayers called the micelles**, **and bilayers in the forms of vesicles and planar membranes**. Figure 12.2 depicts the various forms of the aggregates.

12.1.1 Self-assembly to Vesicles

Of particular interest are the bilayer membranes. The lipid chains line up side by side, with their tails clustered together within the bilayer due to their hydrophobic interactions, and with their heads interfacing with water due to hydrophilic attractions. Such **amphiphilic interactions** among lipid heads and tails are **much weaker** than the direct-attraction or covalent bond that drives formation of two dimensional structures studied in Chap. 7. Despite this difference and complex molecular architectures of the lipids, the general statistical thermodynamic theory put forward in Chap. 7 can nevertheless be applied to basic understanding of vesicle self-assembly. As we learned in Sect. 7.2, which we briefly recapitulate below, the game rule of the self-assembly is to minimize the free energy, culminating in **establishment of the chemical potential balance**, $\mu_n = \mu_1$, between a lipid bound in aggregates of n lipids (n-mers) and a lipid unbound in solution.

Closed bilayer membranes (vesicles) tend to form more easily than planar membranes, when the bending energy cost of forming a closed membrane can be

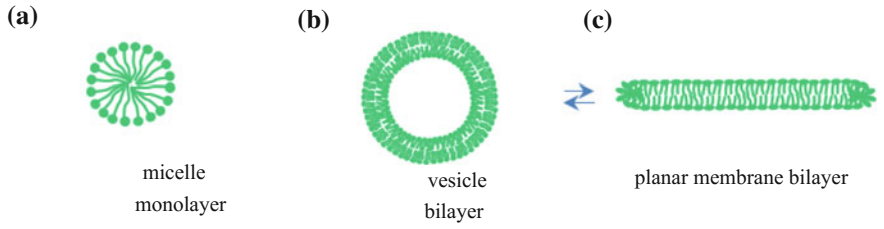

Fig. 12.2 Lipids self-assembled to a micelle (with single-tailed lipids) (**a**), a vesicle (**b**) and a planar membrane (**c**)

less than the energy cost of having the edges interfaced with the water. Let us assume that this condition is met. Subject to the rule $\mu_n = \mu_1$, the chemical potential μ_n of a lipid bound in a vesicle composed of n lipids (n: aggregation number) is given by,

$$n\mu_n = n\mu_n^0 + k_B T \ln C_n, \tag{12.1}$$

where the first term on the RHS indicates energy or enthalpy (called the standard part of the free energy) contribution and the second term is the entropy of such vesicles, which are assumed to be dilute. C_n is the molar concentration of the vesicles. The change of the energy upon assembly from n free lipid monomers to a vesicle is

$$n(\mu_n^0 - \mu_1^0) = -nb_s + 8\pi\varkappa_s \tag{12.2}$$

where $-b_s$, the cohesion energy, or the energy change per lipid upon aggregation, is negative and assumed to be independent of n. The second term on the RHS is the energy necessary to curve a planar membrane to a spherical vesicle, $\mathcal{F}_c = 8\pi\varkappa_s$, where $\varkappa_s$ is the curvature modulus of the bilayer (12.20).

The combination of the two (12.1), (12.2), along with $\mu_n = \mu_1 = \mu_1^0 + k_B T \ln C_1$, yields the concentration of the vesicles (7.56):

$$C_n = (C_1/C^*)^n e^{-8\pi\beta\varkappa_s}, \tag{12.3}$$

where $C^* = e^{-\beta b_s}$ is the critical concentration of lipids above which the aggregation is appreciable. Suppose that all the lipids are either dispersed as monomers ($n = 1$) or aggregated into the vesicles. The total lipid concentration is obtained as

$$C = \sum_n^\infty nC_n \approx \left(1 - \frac{C_1}{C^*}\right)^{-2} e^{-8\pi\beta\varkappa_s}, \tag{12.4}$$

from which we find

$$C_1 \approx C^* \left[1 - \left(Ce^{8\pi\beta\varkappa_s}\right)^{-1/2}\right] \tag{12.5}$$

and

$$C_n \approx \exp\left\{-\frac{n}{\left(Ce^{8\pi\beta\varkappa_s}\right)^{1/2}} - 8\pi\beta\varkappa_s\right\}. \tag{12.6}$$

The density of the probability that the vesicle has a radius R satisfies $P(R) \propto C_n dn/dR$. Assuming that each layer has equal number $(n/2)$ of lipids with

diameter d, $n/2 = 4\pi R^2/(gd^2)$, where g is a geometrical factor in the order of unity, the probability density is

$$P(R) = 2\chi R e^{-\chi R^2} \tag{12.7}$$

where $\chi = 8\pi/\left(gd^2\left(Ce^{8\pi\beta\varkappa_s}\right)^{1/2}\right)$. The average radius is

$$\langle R\rangle = \frac{1}{2}(\pi/\chi)^{1/2} = \frac{1}{4}(g\pi/2)^{1/2} dC^{1/4} \exp\left(\frac{2\pi\varkappa_s}{k_B T}\right) \sim C^{1/4} \tag{12.8}$$

The distribution and the average of the vesicle sizes are similar to those of the surface-attraction induced self-assembly to hollow spheres (Sect. 7.2.3); these results are independent of the effective bond energy b_s per monomer within the membranes, but sensitively depend on the curvature modulus $\varkappa_s$.

12.1.2 Phase and Shape Transitions

Another thermal phenomenon in membranes to mention is the **transitions between the liquid and solid phases**. When the temperature is lowered below the melting temperature (T_m) the liquid or fluid membrane undergoes a phase transition into a solid membrane (Fig. 12.3). Among condensed phases, the liquid phase is of pronounced relevance to biology. Due to the fluidity the proteins embedded in a membrane can attain mobility. For example, a refrigerated banana becomes dark, because its cells are dead; the membranes have undergone a phase transition from a liquid phase to a solid phase, in which proteins are immobilized.

In the later sections we will focus on liquid phase bilayer membranes and study the phenomena that occur on mesoscopic length scales much larger than a lipid molecule. We study the free energies associated with a shape, and its changes, and the local undulations due to the underlying thermal collective motions of lipid molecules. A dramatic example of the shape transitions is the fusion in which two cells or vesicles transform into one with an intermediate state, and the reverse process called cell fission (Fig. 12.4); they are critical processes in egg fertilization, signal transduction, and cell division.

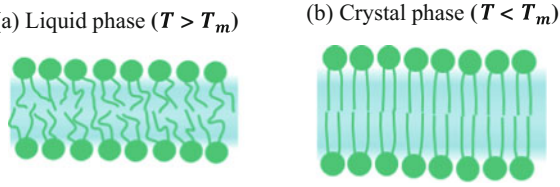

Fig. 12.3 Membrane bilayers in liquid phase (**a**) and crystal phase (**b**)

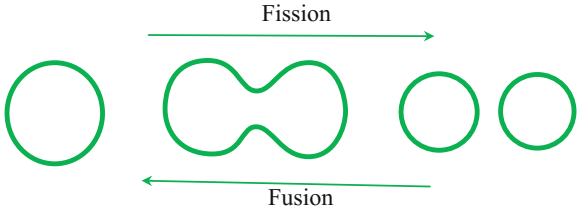

Fig. 12.4 Membrane shape changes, fission and fusion

12.2 Mesoscopic Model for Elastic Energies and Shapes

12.2.1 Elastic Deformation Energy

Over a length scale longer than the lipid length, a membrane can be regarded as a quasi-two-dimensional continuous surface immersed in the three dimensional solution. The low dimensionality and flexibility of the membrane endow it with a variety of shapes and shape transitions. To study the membrane shape and its fluctuation on a mesoscopic length scale, we consider an **effective Hamiltonian of the membrane**, which is coarse-grained beyond the molecular details, couched by the macroscopic phenomenology; the elastic energy of deformation is given by

$$\mathcal{F} = \mathcal{F}_S + \mathcal{F}_B + \mathcal{F}_G. \tag{12.9}$$

First, $\mathcal{F}_S$ is the interface energy associated with keeping the surface area A:

$$\mathcal{F}_S = \int dA\ \gamma, \tag{12.10}$$

where γ is **surface tension** defined by

$$\gamma = \frac{\partial \mathcal{F}_S}{\partial A}. \tag{12.11}$$

In a fluid membrane where the area is not constrained but varies to minimize the free energy, the surface tension is zero. This condition is valid for a free planar membrane, but not for vesicles under mechanical constraints. In real cell membranes the surface tension is far from being zero because of complex macromolecular networks associated with the surfaces.

When the membrane is stretched by an external means to increase the initial, unstressed surface area A_0 to A, the surface energy to the harmonic (2nd) order in deformation is given by

$$\mathcal{F}_S = \frac{1}{2} K_s \frac{(A - A_0)^2}{A_0}, \tag{12.12}$$

where K_s is an elastic constant called the **stretch modulus**. Equation (12.11) yields the overall surface tension,

$$\gamma = K_s \frac{A - A_0}{A_0}, \tag{12.13}$$

which is the Hooke's law for membrane stretching: the tension γ is proportional to the strain $(A - A_0)/A_0$ with the stretching modulus K_s being the constant of proportionality. The measured value of K_s is typically a few Joule/m^2, or $50-70\ k_BT/\text{nm}^2$. For unstressed fluid membranes the surface tension is vanishingly small.

The second and third terms in (12.9) are due to **curvature formation** (Helfrich 1973). In particular, the second term is the **bending energy given by mean curvature**

$$\mathcal{F}_B = \frac{1}{2}\int dA\ \varkappa(\mathcal{C}_1 + \mathcal{C}_2 - 2\mathcal{C}_0)^2, \tag{12.14}$$

where $\mathcal{C}_1$ and $\mathcal{C}_2$ are **two principal curvatures** at a point on the surface. Equation (12.14) is the two dimensional generalization of the curvature energy for the semi-flexible chain we studied in the foregoing chapter. $\varkappa$ is an elastic constant of the membrane called the **mean curvature modulus** or the **bending rigidity**. Because the lipid bilayers are molecularly thin, $\varkappa$ is quite small, typically about $10 - 100\,k_BT$ for vesicles. $\mathcal{C}_0$ is the spontaneous curvature the membrane would attain in the absence of a stress. The presence of the non-vanishing spontaneous curvature is due to asymmetry of the bilayer structures and environments.

The two principal curvatures are defined as follows. Suppose a point O of membrane is intersected by its tangent plane T (Fig. 12.5a). Let $\boldsymbol{x} = (x_1, x_2)$ be two dimensional coordinates to specify the position P of a membrane element on this plane, with the point O taken to be the origin. For small distance $|\boldsymbol{x}|$ from the origin, the height of the membrane point P relative to the tangent plane is given by

$$h(\boldsymbol{x}) = \frac{1}{2}\Sigma_{ij}\ \mathcal{C}_{ij}x_ix_j, \tag{12.15}$$

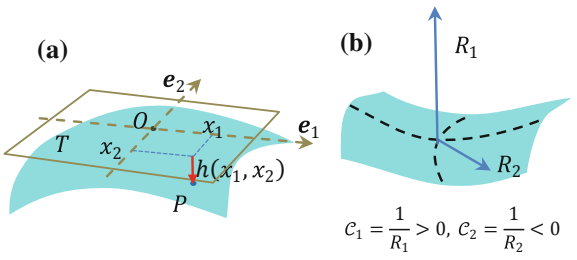

Fig. 12.5 **a** A tangent surface T to a membrane surface point $\boldsymbol{O}$. A position of a membrane point $\boldsymbol{P}$ is specified by $(x_1, x_2, h(x_1, x_2))$, **b** a surface with two curvatures of opposite signs at a saddle point

where $\mathcal{C}_{ij} = \partial^2 h(\boldsymbol{x})/\partial x_i \partial x_j$ is an element of a symmetric 2×2 curvature tensor $\boldsymbol{C}$. The $\boldsymbol{C}$ has two real eigenvalues, $\mathcal{C}_1$ and $\mathcal{C}_2$, and the associated orthonormal eigenvectors $\boldsymbol{e_1}$ and $\boldsymbol{e_2}$, so

$$h(\boldsymbol{x}) = \frac{1}{2}\mathcal{C}_1(\boldsymbol{x}\cdot\boldsymbol{e_1})^2 + \frac{1}{2}\mathcal{C}_2(\boldsymbol{x}\cdot\boldsymbol{e_2})^2. \tag{12.16}$$

The $R_1 = \mathcal{C}_1^{-1}$, $R_2 = \mathcal{C}_2^{-1}$ are the principal radii of the curvature, which can be either positive or negative. For example in Fig. 12.5b, along a principal axis $\boldsymbol{e_1}$ the surface is bent away with positive radius of curvature R_1, whereas, along the other principal axis it is bent toward the membrane with a negative radius of curvature R_2. The bending energy, which is a scalar quantity independent of the coordinate representations, is constructed from an invariant of the tensor, $Tr\,\boldsymbol{C} = \mathcal{C}_1 + \mathcal{C}_2$, as (12.14), up to the harmonic order in the bending deformation.

The last term in (12.9) is the Gaussian curvature energy:

$$\mathcal{F}_G = \varkappa_G \int dA\ \mathcal{C}_1\mathcal{C}_2, \tag{12.17}$$

where $\varkappa_G$ is the associated modulus. The energy is constructed from another scalar invariant of the tensor, $\det \boldsymbol{C} = C_1C_2 = 1/(R_1R_2)$. For closed surfaces the Gauss-Bonnet theorem (Frankel 2012) states that

$$\oint dA \frac{1}{R_1R_2} = 4\pi(1-g), \tag{12.18}$$

where g is a **topological invariant called genus number**, which is equal to the number of handles of the surface. A sphere has the genus $g = 0$, while a torus has $g = 1$, as do the surfaces of a donut and a coffee mug with a handle (Fig. 12.6b). Equation (12.18) means that, whatever the shapes, the closed surfaces with an identical genus number have the same Gaussian curvature energy. In the processes that do not change the topology (genus number) e.g., shown by Figure 12.6b, the Gaussian energy can be ignored.

As examples, consider that a rectangular membrane is rapped into a cylinder of the radius r an length L with two sides closed. In the cylinder one principal

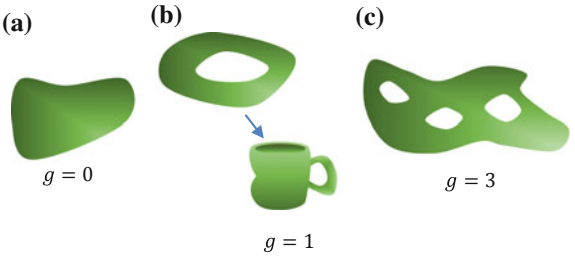

Fig. 12.6 Various shapes for closed surfaces characterized by different genus numbers g. The shape transformation **b** causes no change in the Gaussian curvature energy, because the topology (the genus number $g = 1$) is the same

curvature is nonvanishing, $\mathcal{C}_1 = 1/r$, while the other one is zero, and the spontaneous curvature $\mathcal{C}_0$ is 0. The bending energy cost is

$$\mathcal{F}_B = \frac{\varkappa}{2}\int dA(1/r)^2 = \frac{\varkappa}{2}L2\pi r(1/r)^2 = \frac{\pi\varkappa L}{r}. \tag{12.19}$$

On the other hand, the curvature energy to form a vesicle of radius R is

$$\mathcal{F}_C = \frac{\varkappa}{2}4\pi R^2\left(R^{-1}+R^{-1}\right)^2 + \varkappa_G 4\pi R^2 R^{-2} = 8\pi\varkappa + 4\pi\varkappa_G = 8\pi\varkappa_s, \tag{12.20}$$

where $\varkappa_s = \varkappa + \varkappa_G/2$ is curvature modulus for a sphere. **The curvature energies** (12.19) and (12.20) **are scale-invariant**. This implies that this size-independent energy, dominated by the size-dependent cohesion energy, can favor a large vesicle formation. A dramatic consequence of the curvature energy can be seen at a vesicle where $\mathcal{C}_0 = 0$; at a saddle point where $\mathcal{C}_1 + \mathcal{C}_2 = 0$, the local bending energy vanish and the local Gaussian curvature energy becomes negative, leading to initiation of a fission, as indicated by Fig. 12.4.

P12.1 *Calculate the curvature energy of a fluid membrane of torus shape with the major radius R and the minor radius r. Given the surface as fixed, what is the optimal R/r that minimizes the energy?*

P12.2 *Consider a long flexible polymer weakly adsorbed on a surface of a planar membrane of the bending rigidity $\varkappa$, with an adsorption thickness δ_D. The adsorbed part of the membrane attains a spontaneous curvature. Evaluate the direction and radius of the curvature.*

12.2.2 Shapes of Vesicles

With the local undulations of membranes neglected, namely, in the mean field approximation, the shapes of vesicles are determined by minimizing the free energy as functions of the shape variables, subject to physical constraints. As an example consider a spherical vesicle blown to the radius R by the pressure difference between inside and outside the vesicle, $\Delta p = p_i - p_o$ (Fig. 12.7). This is the case corresponding to the Gibb's ensemble (Sect. 3.3), in which the pressure (difference) is fixed, whereas the volume does fluctuate. In this case the Gibbs free energy

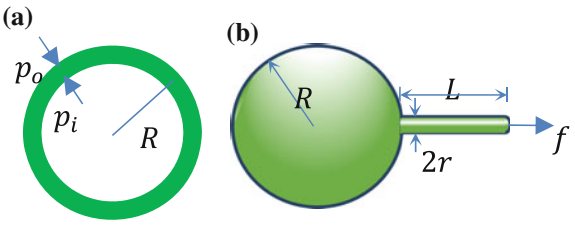

Fig. 12.7 **a** A vesicle blown by the pressure difference $\Delta p = p_i - p_o$, **b** the pressure-blown vesicles tweezed by a force f to form a tether

$$\mathcal{G} = \mathcal{F}_S + \mathcal{F}_C + (p_o - p_i)V = \frac{1}{2}K_s\frac{(A - A_0)^2}{A_0} + 8\pi\varkappa_s - V\Delta p \tag{12.21}$$

is minimized for the equilibrium shape. The condition $\partial\mathcal{G}/\partial R = 0$ with $A = 4\pi R^2$, $V = (4\pi R^3)/3$ yields

$$K_s\frac{(A - A_0)}{A_0}8\pi R = 4\pi R^2\Delta p, \tag{12.22}$$

which along with (12.13) leads to the Young-Laplace equation, $R = 2\gamma/\Delta p$. This is identical in form to (2.55), which we derived for the radius of a liquid drop in a gas. It should be noted, however, that, unlike (2.55), the equation here refers to a stable equilibrium for the shape of the vesicle, whose surface tension varies with the area increase, $\gamma = K_s(A - A_0)/A_0$.

Now we suppose that the pressure-blown vesicle is further subject to stretching force f and form a cylindrical tether ended by a hemispherical cap (Fig. 12.7b). This occurs in the situations ranging from micropipette manipulation on artificial vesicles to the formation of tubular structures induced by atomic force microscopy and optical tweezers. It is also relevant to biological processes involving membrane shape changes such as fusion, exocytosis, endocytosis, and cell division. Given the basic elastic constants, i.e., the stretching and bending moduli, $K_s, \varkappa$ of the membrane, what are the tether size and the induced surface tension?

Subject to the pressure difference between inside and outside the vesicle as well as the force on the tether, the net Gibbs free energy is

$$\mathcal{G} = \mathcal{F}_S + \mathcal{F}_C - \Delta pV - fL. \tag{12.23}$$

While the stretching energy $\mathcal{F}_S$ retains the form $K_s(A - A_0)^2/(2A_0)$ with A_0 being the unstressed area, the curvature energy $\mathcal{F}_C$ has the contributions not only from the spherical part but also from the hemispherical end cap and the cylinder:

$$\mathcal{F}_C = 8\pi\varkappa_s + 4\pi\varkappa_s + \frac{\pi\varkappa L}{r}. \tag{12.24}$$

Noting that $A = 4\pi R^2 + 2\pi rL$, $V = (4\pi R^3)/3 + \pi r^2 L$, with an assumption that tether radius r is much smaller than the tether length L and the vesicle radius R, we find the conditions for minimum $\mathcal{G}$ are given by the three equations below:

$$\frac{\partial\mathcal{G}}{\partial R} = 0 = 8\pi\gamma R - 4\pi R^2\Delta p, \tag{12.25}$$

$$\frac{\partial\mathcal{G}}{\partial r} = 0 = -\frac{\pi\varkappa L}{r^2} + 2\pi\gamma L - 2\pi rL\Delta p, \tag{12.26}$$

$$\frac{\partial \mathcal{G}}{\partial L} = 0 = \frac{\pi\varkappa}{r} + 2\pi\gamma r - \pi r^2 \Delta p - f. \tag{12.27}$$

The first equation yields $\Delta p = 2\gamma/R$, whose contributions to the second and third equations are negligibly in the order of r/R compared with other terms. Solving (12.26) for r gives

$$r = \left(\frac{\varkappa}{2\gamma}\right)^{1/2}, \tag{12.28}$$

which is substituted into (12.27) to yield:

$$\gamma = \frac{1}{2\varkappa}\left(\frac{f}{2\pi}\right)^2. \tag{12.29}$$

With the bending rigidity $\varkappa$ given as very small, the equations reveals that the induced surface tension γ can become very large for strong stretching. Substituting (12.29) back into (12.28) yields

$$r = 2\pi\varkappa/f, \tag{12.30}$$

which means that **the radius of the tether can be very small if a strong force acts on a flexible membrane with small** $\varkappa$. Using the measured forces for pulling the tethers from endoplasmic reticulum and Golgi apparatus, which are on the order of 10 pN, and $\varkappa \approx 20\, k_B T$, (12.29) and (12.30) give rough estimates of the tension and radius, $\gamma \approx 0.015$ pN/nm and $r \approx 50$ nm, which are close to experimental observations (Phillips et al. 2009).

P12.3 *Express the optimal value of L as a function of f, R and given elastic constants, assuming the deformation occurs mostly* via *tether formation. If L is very long, what factors are responsible?*
The solution: from $\gamma = K_s 2\pi r L/(4\pi R^2)$ *and using the above results,*

$$L = (R/\varkappa)^2 (f/2\pi)^3 / K_s.$$

12.3 Effects of Thermal Undulations

12.3.1 The Effective Hamiltonian of Planar Elastic Surface and Membranes

It has been well known to physiologists for more than hundred years that red **blood cells flicker**, **indicative of shape fluctuations or undulations**. The origin is the

thermal collective motion of lipid molecules. To quantify the fluctuations and their correlations, we consider a planar membrane, where a position of the membrane is specified by $\boldsymbol{r} = (\boldsymbol{x}, h(\boldsymbol{x}))$ where $\boldsymbol{x} = (x, y)$ is a two dimensional position on the reference flat surface and $h(\boldsymbol{x})$ is the height of undulation (Fig. 12.8). In this section we evaluate $\langle h^2 \rangle$, $\langle h(\boldsymbol{x}) \cdot h(0) \rangle$, $\langle (h(\boldsymbol{x}) - h(0))^2 \rangle$, and $\langle \boldsymbol{n}(\boldsymbol{x}) \cdot \boldsymbol{n}(0) \rangle$, where $\boldsymbol{n}(\boldsymbol{x})$ is a normal vector outward from the surface at $\boldsymbol{x}$. To this end, we begin with constructing the effective Hamiltonian in terms of the height undulation field $h(\boldsymbol{x})$.

Consider a stress-free, square membrane, which projects on the area $A_0 = L^2$ (Fig. 12.8). The element of the undulating surface at $\boldsymbol{r}$ is constructed by a cross product of the two surface tangent vectors along x and y axis, $\boldsymbol{u}_x = \partial \boldsymbol{r}/\partial x = (1, 0, \partial h/\partial x)$ and $\boldsymbol{u}_y = \partial \boldsymbol{r}/\partial y = (0, 1, \partial h/\partial \mathrm{y})$:

$$d\mathcal{A} = |\boldsymbol{u}_x \times \boldsymbol{u}_y| dxdy = \left[1 + \left(\frac{\partial h}{\partial x} \right)^2 + \left(\frac{\partial h}{\partial y} \right)^2 \right] dxdy$$

Due to the thermal fluctuations, the area increases to

$$\begin{aligned} \mathcal{A} &= \int_0^L dx \int_0^L dy \left[1 + \left(\frac{\partial h}{\partial x} \right)^2 + \left(\frac{\partial h}{\partial y} \right)^2 \right]^{1/2} \\ &= A_0 + \Delta\mathcal{A}. \end{aligned} \tag{12.31}$$

where

$$\Delta\mathcal{A} \approx \frac{1}{2} \int_0^L dx \int_0^L dy \left[\left(\frac{\partial h}{\partial x} \right)^2 + \left(\frac{\partial h}{\partial y} \right)^2 \right] = \frac{1}{2} \int d^2\boldsymbol{x} (\boldsymbol{\nabla}_{\boldsymbol{x}} h(\boldsymbol{x}))^2 \tag{12.32}$$

is the area increase evaluated to the harmonic order in h, where $\boldsymbol{\nabla}_{\boldsymbol{x}}$ is the two dimensional gradient. For an elastic surface with a uniform surface tension γ and no bending rigidity, the surface free energy (12.10) of deformation is

$$\mathcal{F}_S = \gamma \, \Delta\mathcal{A} = \frac{\gamma}{2} \int d^2\boldsymbol{x} (\boldsymbol{\nabla}_{\boldsymbol{x}} h(\boldsymbol{x}))^2. \tag{12.33}$$

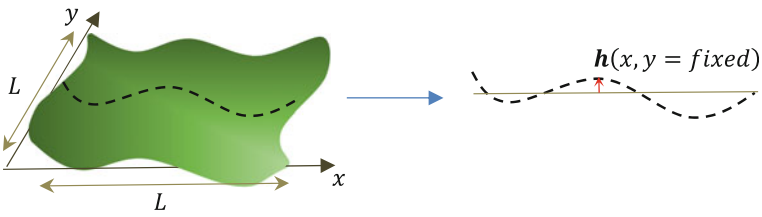

Fig. 12.8 The undulations $h(x, y)$ in a planar membrane that projects to the area $L \times L$

On the other hand, for fluid membranes in which $\gamma = 0$, we have the bending energy

$$\begin{aligned}\mathcal{F}_B &= \frac{\varkappa}{2}\int dA\ (\mathcal{C}_1 + \mathcal{C}_2)^2 \\ &\approx \frac{\varkappa}{2}\int_0^L dx \int_0^L dy \left[\frac{\partial^2 h}{\partial x^2} + \frac{\partial^2 h}{\partial y^2}\right]^2 = \frac{\varkappa}{2}\int d^2\boldsymbol{x}\left(\boldsymbol{\nabla}_{\boldsymbol{x}}^2 h(\boldsymbol{x})\right)^2,\end{aligned} \tag{12.34}$$

which is correct to the harmonic order (See Boal 2002). A cell membrane usually has a non-vanishing surface tension, so that the free energy is

$$\mathcal{F}\{h(\boldsymbol{x})\} = \frac{1}{2}\int d^2\boldsymbol{x}\left[\gamma(\boldsymbol{\nabla}_{\boldsymbol{x}} h(\boldsymbol{x}))^2 + \varkappa\left(\boldsymbol{\nabla}_{\boldsymbol{x}}^2 h(\boldsymbol{x})\right)^2\right], \tag{12.35}$$

which is expressed in terms of thermally fluctuating undulation field $h(\boldsymbol{x})$. Following our basic method of coarse-graining, $\mathcal{F}\{h(\boldsymbol{x})\}$ is the effective Hamiltonian given by

$$e^{-\beta\mathcal{F}\{h(\boldsymbol{x})\}} = \sum_{\mathcal{M}/h(\boldsymbol{x})} e^{-\beta\mathcal{H}\{\mathcal{M}\}} \tag{12.36}$$

where the summation is performed over all microscopic degrees of freedom $\mathcal{M}$, given the undulation field $h(\boldsymbol{x})$. Consequently $\mathcal{F}\{h(\boldsymbol{x})\}$ contains the temperature-dependent and entropic contributions that originate from the underlying molecular motions. The thermodynamic free energy F of the membrane then is given by the functional integral over the field $\{h(\boldsymbol{x})\}$:

$$e^{-\beta F} = \int D\{h(\boldsymbol{x})\} e^{-\beta\mathcal{F}\{h(\boldsymbol{x})\}}. \tag{12.37}$$

12.3.2 Surface Undulation Fluctuation and Correlation

To facilitate calculating the averages of the quantities associated with undulation, we deal with the Fourier transform for h:

$$h(\boldsymbol{q}) = \int d^2\boldsymbol{x}\, e^{-i\boldsymbol{q}\cdot\boldsymbol{x}} h(\boldsymbol{x}) \tag{12.38}$$

and

$$h(\boldsymbol{x}) = \frac{1}{L^2}\sum_{\boldsymbol{q}} e^{i\boldsymbol{q}\cdot\boldsymbol{x}} h(\boldsymbol{q}). \tag{12.39}$$

We use the periodic BC, so that $\boldsymbol{q} = (q_x, q_y)$ with each component respectively taking N values, $q_n = 2\pi n/L$, $n = \pm 1, \pm 2 \ldots, \pm N/2$, where $N = L/a$, a is a microscopic length which is in the order of the diameter of the lipid molecule.

The mean square of the undulation amplitude is defined as

$$\begin{aligned} \langle h^2 \rangle &\equiv \frac{1}{L^2}\int d^2\boldsymbol{x} \langle h^2(\boldsymbol{x})\rangle \\ &= \frac{1}{L^6}\int d^2\boldsymbol{x} \sum_{\boldsymbol{q}}\sum_{\boldsymbol{q}'} \langle h(\boldsymbol{q}) h^*(\boldsymbol{q}')\rangle e^{i(\boldsymbol{q}-\boldsymbol{q}')\cdot\boldsymbol{x}} \\ &= \frac{1}{L^4}\sum_{\boldsymbol{q}} \left\langle |h(\boldsymbol{q})|^2 \right\rangle, \end{aligned} \tag{12.40}$$

where we used

$$\frac{1}{L^2}\int e^{i(\boldsymbol{q}-\boldsymbol{q}')\cdot\boldsymbol{x}} d^2\boldsymbol{x} = \delta_{\boldsymbol{q}\boldsymbol{q}'}. \tag{12.41}$$

The undulation correlation function is now expressed as

$$C_h(\boldsymbol{x}, \boldsymbol{x}') = \langle h(\boldsymbol{x}) h(\boldsymbol{x}')\rangle = \frac{1}{L^4}\sum_{\boldsymbol{q}}\sum_{\boldsymbol{q}'} e^{i\boldsymbol{q}\cdot\boldsymbol{x} - i\boldsymbol{q}'\cdot\boldsymbol{x}'} \langle h(\boldsymbol{q}) h^*(\boldsymbol{q}')\rangle. \tag{12.42}$$

Assuming the translational invariance, $C_h(\boldsymbol{x}, \boldsymbol{x}') = C_h(|\boldsymbol{x} - \boldsymbol{x}'|)$, we can show

$$\begin{aligned} \langle h(\boldsymbol{q}) h^*(\boldsymbol{q}')\rangle &= \iint d^2\boldsymbol{x}\, d^2\boldsymbol{x}' \langle h(\boldsymbol{x}) h(\boldsymbol{x}')\rangle e^{-i\boldsymbol{q}\cdot\boldsymbol{x} + i\boldsymbol{q}'\cdot\boldsymbol{x}'} \\ &= \int d^2(\boldsymbol{x} - \boldsymbol{x}') C_h(|\boldsymbol{x} - \boldsymbol{x}'|) e^{-i\boldsymbol{q}\cdot(\boldsymbol{x}-\boldsymbol{x}')} \int d^2\boldsymbol{x}' e^{i(\boldsymbol{q}'-\boldsymbol{q})\cdot\boldsymbol{x}'} \\ &= \left\langle |h(\boldsymbol{q})|^2 \right\rangle \delta_{\boldsymbol{q}\boldsymbol{q}'}, \end{aligned} \tag{12.43}$$

where we used (12.41) and defined

$$\left\langle |h(\boldsymbol{q})|^2 \right\rangle = L^2 \int d^2(\boldsymbol{x} - \boldsymbol{x}') C_h(|\boldsymbol{x} - \boldsymbol{x}'|) e^{-i\boldsymbol{q}\cdot(\boldsymbol{x}-\boldsymbol{x}')}. \tag{12.44}$$

$\left\langle |h(\boldsymbol{q})|^2 \right\rangle$, called the height **undulation spectrum**, is the Fourier transform of the undulation correlation. Using (12.43), we find (12.42) is reduced to

$$\langle h(\boldsymbol{x})h(\boldsymbol{x}')\rangle = \frac{1}{L^4}\sum_{\boldsymbol{q}} e^{i\boldsymbol{q}\cdot(\boldsymbol{x}-\boldsymbol{x}')}\left\langle |h(\boldsymbol{q})|^2\right\rangle. \tag{12.45}$$

Also

$$\begin{aligned}\int d^2\boldsymbol{x}\left(\nabla_{\boldsymbol{x}}^n h(\boldsymbol{x})\right)^2 &= \frac{1}{L^4}\sum_{\boldsymbol{q}}\sum_{\boldsymbol{q}'}(\boldsymbol{q}\boldsymbol{q}')^n h(\boldsymbol{q})h^*(\boldsymbol{q}')\int e^{i(\boldsymbol{q}-\boldsymbol{q}')\cdot\boldsymbol{x}}d^2\boldsymbol{x}\\ &= \frac{1}{L^2}\sum_{\boldsymbol{q}} q^{2n}|h(\boldsymbol{q})|^2,\end{aligned} \tag{12.46}$$

which we can use for $n = 1$ to calculate the increase of the average surface area (12.32)

$$\Delta A = \langle \Delta\mathcal{A}\rangle = \frac{1}{2L^2}\sum_{\boldsymbol{q}} q^2\left\langle |h(\boldsymbol{q})|^2\right\rangle. \tag{12.47}$$

Evidently, the undulation spectrum $\left\langle |h(\boldsymbol{q})|^2\right\rangle$ is central to evaluation of the height fluctuation and the related properties in the real space. To study these properties, using the relation (12.46) we represent the effective Hamiltonian (12.35) in the Fourier space as

$$\mathcal{F} = \frac{1}{2L^2}\sum_{\boldsymbol{q}}(\gamma q^2 + \varkappa q^4)|h(\boldsymbol{q})|^2, \tag{12.48}$$

This allows us to use **the equipartition theorem per mode $\boldsymbol{q}$**,

$$\frac{1}{2L^2}\left(\gamma q^2 + \varkappa q^4\right)\left\langle |h(\boldsymbol{q})|^2\right\rangle = \frac{1}{2}\,k_B T \tag{12.49}$$

yielding an important equation

$$\left\langle |h(\boldsymbol{q})|^2\right\rangle = \frac{k_B T L^2}{\gamma q^2 + \varkappa q^4}. \tag{12.50}$$

The mean square of the undulation amplitude (12.40) is given by

$$\left\langle h^2\right\rangle = \frac{1}{L^2}\sum_{\boldsymbol{q}}\frac{k_B T}{\gamma q^2 + \varkappa q^4}, \tag{12.51}$$

which is in general difficult to evaluate in an analytical form for a square membrane. Thus, we replace it by a circular disk of the same area without changing the

physical properties. Using $\sum_{\boldsymbol{q}} = (L/2\pi)^2 \int dq\, 2\pi q$ the above sum is approximated by the integral,

$$\langle h^2 \rangle \approx \frac{k_B T}{2\pi} \int_{q_m}^{q_M} dq\, \frac{q}{\gamma q^2 + \varkappa q^4}, \tag{12.52}$$

where

$$q_m \sim \pi/L \quad \text{and} \quad q_M \sim \pi/a \tag{12.53}$$

are the lower and upper cutoffs of q that are allowed. Then, the (12.52) is integrated to:

$$\langle h^2 \rangle \approx \frac{k_B T}{4\pi\gamma} \ln\left(\frac{\gamma {q_m}^{-2} + \varkappa}{\gamma {q_M}^{-2} + \varkappa}\right), \tag{12.54}$$

which shows how a large surface tension suppresses the undulation. If $\gamma a^2 \gg \varkappa$, (12.52) is reduced to

$$\langle h^2 \rangle \sim \frac{k_B T}{2\pi\gamma} \ln\left(\frac{\alpha L}{a}\right), \tag{12.55}$$

where α is a numerical factor. The above relation is comparable to an exact numerical calculation of the sum (12.51) that is possible for the case of $\varkappa = 0$:

$$\langle h^2 \rangle = \frac{k_B T}{\gamma L^2} \left(\frac{L}{2\pi}\right)^2 4 \sum_{n_x=1}^{N/2} \sum_{n_y=1}^{N/2} \frac{1}{{n_x}^2 + {n_y}^2} \approx 0.16 \frac{k_B T}{\gamma} \ln\left(\frac{0.33L}{a}\right) \tag{12.56}$$

For a fluid membrane with negligible surface tension, $\gamma L^2 \ll \varkappa$, (12.54) is reduced to

$$\langle h^2 \rangle \sim \frac{k_B T}{4\pi^3 \varkappa} L^2. \tag{12.57}$$

An exact numerical evaluation of the sum for this case yields

$$\langle h^2 \rangle = \frac{k_B T}{\varkappa L^2} \left(\frac{L}{2\pi}\right)^4 4 \sum_{n_x=1}^{N/2} \sum_{n_y=1}^{N/2} \frac{1}{\left(n_x^2 + n_y^2\right)^2} \approx 1.9 \times 10^{-3} \frac{k_B T}{\varkappa} L^2 \tag{12.58}$$

The L^2 scaling behavior above signifies the self-similiarity: **as the fluid membrane size is doubled, so is the rms fluctuation** $\langle \boldsymbol{h^2} \rangle^{1/2}$ (Fig. 12.9).

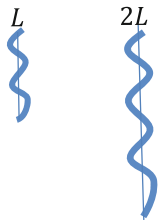

Fig. 12.9 When the membrane size is doubled, the rms fluctuation $\langle h^2 \rangle^{1/2}$ is also doubled in a fluid membrane

Because $1.9 \times 10^{-3}\ (k_B T)/\varkappa$ is exceedingly less than unity, $\langle \boldsymbol{h^2} \rangle^{1/2}$ **of a micron-sized fluid membrane is of sub-nanoscale**, and is further reduced by the presence of the surface tension.

Can a scaling argument confirm this result? Since the $\langle h^2 \rangle$ should be an outcome of thermal fluctuation it should be proportional to the thermal energy $k_B T$ balanced by the bending rigidity κ, and should depend on L. The dimensional analysis gives

$$\langle h^2 \rangle \sim \frac{k_B T}{\varkappa} L^2 \tag{12.59}$$

The surface area increase (12.47) due to the thermal undulation is similarly given by

$$\begin{aligned} \Delta A &= \frac{1}{2} \sum_{\boldsymbol{q}} q^2 \frac{k_B T}{\gamma q^2 + \varkappa q^4} \approx \frac{k_B T L^2}{4\pi} \int_{q_m}^{q_M} dq \frac{q^3}{\gamma q^2 + \varkappa q^4} \\ &= \frac{k_B T L^2}{8\pi\varkappa} \ln\left(\frac{\gamma/\varkappa + {q_M}^2}{\gamma/\varkappa + {q_m}^2} \right) \end{aligned} \tag{12.60}$$

$\Delta A / A_0$ is vanishingly small for very stiff membranes in which $\varkappa \gg k_B T$, or $\gamma a^2 \gg \varkappa$. (12.60) shows that **the thermally-induced area increase is suppressed by a large bending rigidity and surface tension**.

When the surface tension is very small ($\gamma L^2 \ll \varkappa$) we have

$$\Delta A \approx \frac{k_B T L^2}{4\pi\varkappa} \ln\left(\frac{\alpha L}{a} \right). \tag{12.61}$$

P12.4 *Find the area fluctuation* $\langle \mathcal{A}^2 \rangle - \langle \mathcal{A} \rangle^2$ *for a fluid membrane*. (*Hint*: *develop and use the linear response theory* $\langle \Delta \mathcal{A}^2 \rangle = -k_B T \left(\frac{\partial \Delta A}{\partial \gamma} \right)_{\gamma=0}$).

For the opposite case in which the bending rigidity is zero, (12.60) yields

$$\Delta A = \frac{k_B T}{2\gamma} \sum_{\boldsymbol{q}} 1 = \frac{k_B T L^2}{2\gamma a^2}, \tag{12.62}$$

where we noted that the total number of the modes is L^2/a^2.

The surface area can also increase if a high tension is applied; a membrane stretches to increase the area beyond (12.60) following (12.13):

$$\frac{\Delta A}{A_0} = \frac{k_B T}{8\pi\varkappa} \ln\left(\frac{\gamma/\varkappa + {q_M}^2}{\gamma/\varkappa + {q_m}^2}\right) + \frac{\gamma}{K_s}. \tag{12.63}$$

This relation can be applied to determine the bending and stretch moduli, $\varkappa$ and K_s, of a membrane using a vesicle stretched by a micropipette (Evans and Needham 1987).

Finally the **undulation correlation** (12.42) is given by

$$\begin{aligned} \langle h(\boldsymbol{x}) h(\boldsymbol{x}') \rangle &= \frac{1}{(2\pi)^2 L^2} \int d^2\boldsymbol{q}\, e^{i\boldsymbol{q}\cdot(\boldsymbol{x}-\boldsymbol{x}')} \langle |h(\boldsymbol{q})|^2 \rangle \\ &= \frac{1}{2\pi L^2} \int_{q_m}^{q_M} dq\, q \langle |h(\boldsymbol{q})|^2 \rangle J_0(q|\boldsymbol{x}-\boldsymbol{x}'|), \end{aligned} \tag{12.64}$$

where

$$J_0(q\rho) = \frac{1}{2\pi} \int_0^{2\pi} d\theta\, e^{-iq\rho\,\cos\theta} \tag{12.65}$$

is the zeroth order Bessel function and $\rho = |\boldsymbol{x} - \boldsymbol{x}'|$. Since $J_0(x)$ is decreasing with x and $\langle |h(q)|^2 \rangle = k_B T L^2/(\gamma q^2 + \varkappa q^4)$ takes the maximum at the lowest q, that is, q_m, (12.62) can be roughly approximated by

$$\langle h(\rho) h(0) \rangle \approx \langle h^2 \rangle J_0(q_m \rho). \tag{12.66}$$

Since $q_m \sim \pi/L$, $J_0(q_m\rho)$ remains to be non-vanishing until it decays to zero at $\rho \sim L$, so (12.64) means that **the undulation is correlated over the entire area of the membrane**. According to the linear response theory in Chap. 9, the correlation is can be seen as the bud of the membrane formed by a small force f acting at the origin; the bud height at ρ is proportional to the correlation function, i.e., it is $\beta f \langle h^2 \rangle J_0(q_m\rho)$ (Fig. 12.10).

A more detailed analysis is given to a related quantity probed by scattering: the relative height undulation at a separation $\boldsymbol{\rho}$, which is

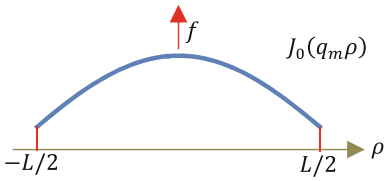

Fig. 12.10 The shape of a membrane tweezed by a small force f on the middle is proportional to $J_0(q_m\rho)$ approximately, where $q_m \sim \pi/L$

$$\begin{aligned}\left\langle (h(\boldsymbol{\rho}) - h(0))^2 \right\rangle &= 2\left[\langle h\rangle^2 - \langle (h(\boldsymbol{\rho})h(0))\rangle\right] \\ &= 2\frac{1}{2\pi L^2}\int dq\, q\left\langle |h(q)|^2\right\rangle [1 - J_0(q\rho)] \\ &= 2\frac{k_B T}{2\pi}\int_{q_m}^{q_M} dq \frac{q}{\gamma q^2 + \varkappa q^4}[1 - J_0(q\rho)].\end{aligned} \tag{12.67}$$

We consider $\rho \gg a; J_0(q\rho)$ rapidly oscillates around 0 between $q \sim \rho^{-1}$ and $q = q_M$, giving little contribution to the integral, so

$$\begin{aligned}\left\langle (h(\boldsymbol{\rho}) - h(0))^2 \right\rangle &= 2\frac{k_B T}{2\pi}\int_{\alpha'/\rho}^{q_M} dq \frac{q}{\gamma q^2 + \varkappa q^4} \\ &\approx \frac{k_B T}{2\pi\gamma}\ln\left(\frac{\gamma\rho^2/\alpha'^2 + \varkappa}{\gamma {q_M}^{-2} + \varkappa}\right),\end{aligned} \tag{12.68}$$

where α' is a constant of order unity. For fluid membranes in which γ is negligibly small,

$$\left\langle (h(\boldsymbol{\rho}) - h(0))^2 \right\rangle \sim \frac{k_B T \rho^2}{2\pi\varkappa} \sim \rho^2, \tag{12.69}$$

which shows a self-similar behavior. On the other hand, for an elastic surface in which $\varkappa = 0$,

$$\left\langle (h(\boldsymbol{\rho}) - h(0))^2 \right\rangle \approx \frac{k_B T}{\pi\gamma}\ln\left(\alpha''\frac{\rho}{a}\right) \tag{12.70}$$

where α'' is another numerical constant.

Related to the height undulation is the fluctuation of the unit vector normal to the surface, $\boldsymbol{n}(\boldsymbol{x})$. The $\boldsymbol{n}(\boldsymbol{x})$ at $\boldsymbol{r} = (x, y, h(x, y))$ is constructed by a cross product of the two surface tangent vectors along x and y axis, $\boldsymbol{u}_x = \partial\boldsymbol{r}/\partial x = (1, 0, \partial h/\partial x)$ and $u_y = (0, 1, \partial h/\partial \mathrm{y})$:

$$\boldsymbol{n}(\boldsymbol{x}) = (\boldsymbol{u}_x \times \boldsymbol{u}_y)/\left|\boldsymbol{u}_x \times \boldsymbol{u}_y\right| = [\hat{z} - \nabla_{\boldsymbol{x}} h(\boldsymbol{x})]\left[1 + (\nabla_{\boldsymbol{x}} h(\boldsymbol{x}))^2\right]^{-1/2}, \tag{12.71}$$

which, for small curvatures, is

$$\boldsymbol{n}(\boldsymbol{x}) \approx \hat{z}\left[1 - \frac{1}{2}(\nabla_{\boldsymbol{x}} h(\boldsymbol{x}))^2\right] - \nabla_{\boldsymbol{x}} h(\boldsymbol{x}). \tag{12.72}$$

The orientation correlation function (Fig. 12.11) is

$$\begin{aligned} C_{\boldsymbol{n}}(|\boldsymbol{x} - \boldsymbol{x}'|) &= \langle \boldsymbol{n}(\boldsymbol{x}) \cdot \boldsymbol{n}(\boldsymbol{x}') \rangle \\ &\approx 1 + \langle \nabla_{\boldsymbol{x}} h(\boldsymbol{x}) \cdot \nabla_{\boldsymbol{x}'} h(\boldsymbol{x}') \rangle - \frac{1}{2}\left\langle (\nabla_{\boldsymbol{x}} h(\boldsymbol{x}))^2 + (\nabla_{\boldsymbol{x}'} h(\boldsymbol{x}'))^2 \right\rangle \\ &= 1 - \frac{1}{2\pi L^2} \int_{q_m}^{q_M} dq\, q^3 \left\langle |h(q)|^2 \right\rangle [1 - J_0(q|\boldsymbol{x} - \boldsymbol{x}'|)], \end{aligned} \tag{12.73}$$

where we used (12.39) and (12.43). Consider a distance $\rho = |\boldsymbol{x} - \boldsymbol{x}'| \gg a$ in a fluid membrane. Following the procedure used in deriving (12.67),

$$C_{\boldsymbol{n}}(\rho) \approx 1 - \frac{k_B T}{2\pi\varkappa} \ln\left(\frac{\alpha'' \rho}{a}\right). \tag{12.74}$$

The persistence length L_P of the fluid membrane, over which **the orientation correlation** vanishes, $C_{\boldsymbol{n}}(L_P) = 0$, is estimated to be

$$L_P \sim a \exp\left(\frac{2\pi\varkappa}{k_B T}\right). \tag{12.75}$$

This is a macroscopic length very much larger than a unless $\varkappa \ll k_B T$. Over any distance ρ in the membrane, $C_{\boldsymbol{n}}(\rho) \approx 1$; from (12.74),

$$C_{\boldsymbol{n}}(\rho) \approx \exp\left\{ - \ln\left(\frac{\alpha'' \rho}{a}\right)^{k_B T/(2\pi\varkappa)} \right\} \sim \left(\frac{a}{\rho}\right)^{\frac{k_B T}{2\pi\varkappa}}, \tag{12.76}$$

which, for the fluid membrane with $k_B T/2\pi\varkappa \ll 1$ **decays very slowly in a power law indicative of an unusual long-range correlation**. The height undulation and the decay of the correlation may not be appreciable unless the membrane is very

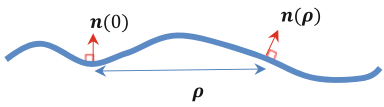

Fig. 12.11 The two orientation (normal) vectors separated by a distance ρ are strongly correlated

large. Nevertheless the emergence of intrinsic thermal fluctuations even in small membranes give rise to dramatic features essential to the living state, as exemplified below.

P12.5 *Consider an elastic surface with* $\varkappa = 0$. *Find the orientation correlation function* $C_{\boldsymbol{n}}(\rho)$.

P12.6 *A fluid membrane attached to a substrate is described by an effective Hamiltonian*

$$\mathcal{F}\{h(\boldsymbol{x})\} = \frac{1}{2}\int d^2\boldsymbol{x}\left[\varkappa\left(\boldsymbol{\nabla}_{\boldsymbol{x}}^2 h(\boldsymbol{x})\right)^2 + \omega^2 h(\boldsymbol{x})^2\right]$$

Find $\langle h^2\rangle$, $\left\langle (h(\boldsymbol{\rho}) - h(0))^2\right\rangle$, *and* $\langle \boldsymbol{n}(\boldsymbol{\rho})\cdot\boldsymbol{n}(0)\rangle$. *Discuss how they are affected by the confinement factor* ω. *Calculate the Helmhotz free energy F of the chain* (*hint*: $Z = e^{-\beta F} = \sum_{h(\boldsymbol{q})} \exp\left[-\frac{\beta}{2L^2}\sum_{\boldsymbol{q}} (\omega^2 q^2 + \varkappa q^4)|h(\boldsymbol{q})|^2\right] = \sum_{h(\boldsymbol{q})} \exp\left[-\frac{\beta}{2L^2}\sum_{\boldsymbol{q}} (\omega^2 q^2 + \varkappa q^4)|h(\boldsymbol{q})|^2\right] = \prod_{\boldsymbol{q}} \left[2\pi L^2/\left\{\beta(\omega^2 q^2 + \varkappa q^4)\right\}\right]^{1/2}$).

12.3.3 Helfrich Interaction and Unbinding Transitions

When two membranes are brought to close proximity, less space is allowed for thermal undulations to play in between, resulting in a reduction of entropy. This induces a repulsion called the **Helfrich interaction**. We use a scaling argument as below to determine the interaction as a function of the inter-membrane distance D. First, noting that the interaction is induced by thermal fluctuation and involves two length scales, $\langle h^2\rangle^{1/2}$ and D, we must have

$$U_h \sim k_B T\left[\frac{\langle h^2\rangle}{D^2}\right]^p, \tag{12.77}$$

which should scale as $\sim L^2$. Using $\langle h^2\rangle \sim (k_B T)L^2/\varkappa$, one finds $p = 1$, and

$$U_h \sim k_B T\frac{\langle h^2\rangle}{D^2} \sim \frac{(k_B T)^2 L^2}{\varkappa D^2}. \tag{12.78}$$

The equation interestingly shows that the repulsion is proportional to the factors D^{-2} and $(k_B T)^2$. Its exact expression is $U_f = 3(k_B T)^2 L^2/(\pi^2 \varkappa D^2)$ (Helfrich 1978). In addition, two membranes experience another fluctuation-induced interaction, that is, the van der Waals attraction, $U_{vdw} = -H/(12\pi D^2)$ per unit area (6.33).

If the membranes are not charged, the total free energy change is

$$F = \left\{ \frac{3(k_B T)^2}{\pi^2 \varkappa} - \frac{H}{12\pi} \right\} \frac{L^2}{D^2}. \tag{12.79}$$

The membranes of the bending rigidity $\varkappa$ bind if F is negative, i.e.,

$$T < T_c = \frac{1}{6\, k_B} (\pi H \varkappa)^{1/2}. \tag{12.80}$$

At a fixed temperature, say, the body temperature $T_b = 310\,\mathrm{K}$, the binding also occurs if

$$\varkappa > \varkappa_c = \frac{(6\, k_B T_b)^2}{\pi H} \sim 10\, k_B T_b \tag{12.81}$$

where Hamaker constant $H \sim k_B T_b$ is considered. This provides a reason why older blood cells with higher $\varkappa$ (less flexibility) tend to aggregate among themselves and adhere to vessel wall more frequently. If $T > T_c$, or $\varkappa < \varkappa_c$, the membranes unbind. This implies that **the thermal fluctuation-induced undulation**, **although very small in magnitude** (12.58), **can be an essential feature for cell stability**.

Further Reading and References

J. Israelachvili, *Intermolecular and Surface Forces*, 2nd edn. (Academic Press, 1991)

S. Safran, *Statistical Thermodynamics of Surfaces, Interfaces, and Membranes* (Frontiers in Physics) (Westview Press, 2003)

G. Cevc, D. Marsh (eds.), *Phospholipid Bilayers Physical Principles and Models* (Wiley, 1987)

R. Lipowsky, E. Sachmann, *Structure and Dynamics of Membranes. I. From Cells to Vesicles/II. Generic and Specific Interactions* (Elsevier, 1995)

R.B. Phillips, J. Kondev, J. Theriot, *Physical Biology of the Cell* (Garland Science, 2009)

D. Boal, *Mechanics of the Cell* (Cambridge University Press, 2002)

F. Jähnig, What is the surface tension of a lipid bilayer membrane? Biophys. J. **71**(3), 1348–1349 (1996)

S. Neumann, T.J. Pucadyil, S.L. Schmid, Analyzing membrane remodeling and fission using supported bilayers with excess membrane reservoir. Nat. Protoc. **8**, 213–222 (2013)

E. Evans, D. Needham, Physical properties of surfactant bilayer membranes: thermal transitions, elasticity, rigidity, cohesion, and colloidal interactions. J. Phys. Chem. **91**, 4219 (1987)

P.M. Chaikin, T.C. Lubensky, *Principles of Condensed Matter Physics* (Cambridge University Press, 2000)

W. Helfrich, Elastic properties of lipid bilayers: theory and possible experiments. Z. Naturforsch. C **28**, 693 (1973)

W. Helfrich, Steric interaction of fluid membranes in multilayer systems. Z. Naturforsch. **33a**, 305–315 (1978)

T. Frankel, *The Geometry of Physics: An Introduction*, 3rd edn. (Cambridge University Press, 2012)

Chapter 13
Brownian Motions

In previous chapters we were mostly concerned with the equilibrium state of matter. Although the equilibrium statistical physics is relevant to studying the biological structures and conformations at body temperature, the living processes operate out of equilibrium. For non-equilibrium phenomena, historically there are two pillars of statistical physics. One is **the kinetic theory of Boltzmann and Maxwell**, a ground-breaking work in non-equilibrium statistical mechanics that described the transport properties of gases on the basis of molecular motions. The other one is **the Brownian motion theory developed by Einstein, Smoluchowski and Langevin**, and others, which initiated stochastic descriptions of fluctuations in matter. If formulated on the basis of microscopic dynamics, these two approaches converge. Here we start with the stochastic approach to matter, because of our primary interest in mesoscopic level surpassing atominstic details. In this chapter and later ones we discuss the Brownian motion and extend the idea to describe the stochastic dynamics of biological systems and even other complex systems, for which the microscopic Hamiltonian cannot be defined.

In 1827, botanist Robert Brown, looking through a microscope, found that particles in pollen grains were undergoing **random and incessant motion** in water. He attributed this to the very nature of living, embodied in the old philosophy of vitalism. However, this motion, called the Brownian motion, was subsequently observed in the grains of inorganic substances. This was a great curiosity at the time, but was suspected to be an outcome of the basic constituents of matter that are susceptible to thermal agitation. In 1905, Albert Einstein published a paper that explained how the Brownian particles stochastically move surrounded by water molecules. This explanation of Brownian motion served as a confirmation that molecules and atoms actually exist, and was further verified experimentally by Jean Perrin in 1908 (Fig. 13.1).

In this chapter the Brownian motion (or diffusion equation) theories of Einstein and Smoluchowski are given with a number of biological applications. More

W. Sung, *Statistical Physics for Biological Matter*, Graduate Texts in Physics,
https://doi.org/10.1007/978-94-024-1584-1_13

Fig. 13.1 The Brownian motion is depicted in the cover page of "Atoms" (Ox Bow Press, 1923) authored by Jean Perrin, whose experiments on Brownian motion laid a foundation on atomicity of matter

general theory via the Langevin equation is then given to describe the stochastic behaviors of the Brownian motion that differ in characteristic time scales.

13.1 Brownian Motion/Diffusion Equation Theory

13.1.1 Diffusion, Smoluchowski Equation, and Einstein Relations

Understanding that the **Brownian motion is an incessant continuation of random jumps**, Einstein derived the equation for the probability density $P(\boldsymbol{r}, t)$ of a Brownian particle to be found at a position $\boldsymbol{r}$ and time t,

$$\frac{\partial P(\boldsymbol{r}, t)}{\partial t} = D\nabla^2 P(\boldsymbol{r}, t). \tag{13.1}$$

Here the D is the diffusivity or the diffusion constant given by

$$D = \frac{\langle l^2 \rangle}{6\tau}. \tag{13.2}$$

τ is the jump time, which is chosen to be macroscopically small but microscopically large enough that the motions after the time are mutually independent. In the time interval τ the particle is displaced by a distance l that is statistically distributed with

the mean-square $\langle l^2 \rangle$. The derivation of the above equations will be given in next chapter within the frame of master equation.

Equation (13.1) written for the number density or concentration of such Brownian particles $n(\boldsymbol{r}, t) = NP(\boldsymbol{r}, t)$,

$$\frac{\partial n(\boldsymbol{r}, t)}{\partial t} = D\nabla^2 n(\boldsymbol{r}, t) \tag{13.3}$$

is the well-known equation called the diffusion equation with the D same as that in (13.1) if the concentration is low enough to neglect interactions between the Brownian particles.

The diffusion equation is one of the hydrodynamic equations derived from conservation laws and constitutive relations below and in Chap. 19. The total number of the particles N being conserved, the number density, satisfies the continuity equation

$$\frac{\partial n}{\partial t} + \boldsymbol{\nabla} \cdot \boldsymbol{J_n} = 0, \tag{13.4}$$

where $\boldsymbol{J}_n$ is the number flux vector: J_{nz} is average number of particles that cross a unit area in the xy plane per unit time. Phenomenologically the flux is given by

$$\boldsymbol{J}_n = -D\boldsymbol{\nabla} n, \tag{13.5}$$

which is the Fick's law stating that the particles flow from the region of higher concentration to that of lower concentration. Substituting (13.5) into (13.4) yields the diffusion equation

$$\frac{\partial n}{\partial t} = \boldsymbol{\nabla} \cdot D\boldsymbol{\nabla} n. \tag{13.6}$$

It takes the form (13.3) for constant diffusivity, which is the case of our interest.

The solution to (13.1), given the particle's initial position at $\boldsymbol{r}_0$, is termed as the fundamental solution. In free space, it is given by

$$P(\boldsymbol{r}, t|\boldsymbol{r}_0) = \frac{1}{(4\pi Dt)^{3/2}} \exp\left[-\frac{(\boldsymbol{r} - \boldsymbol{r}_0)^2}{4Dt}\right]. \tag{13.7}$$

From this equation the mean square of the displacement (MSD) $\boldsymbol{r}(t) - \boldsymbol{r}_0$ at time t is

$$\bar{\Delta} r(t)^2 \equiv \left\langle (\boldsymbol{r}(t) - \boldsymbol{r}_0)^2 \right\rangle = \int d\boldsymbol{r} (\boldsymbol{r} - \boldsymbol{r}_0)^2 P(\boldsymbol{r}, t|\boldsymbol{r}_0) = 6Dt, \tag{13.8}$$

Or, $\bar{\Delta}r \sim t^{1/2}$. Equations (13.7) and (13.8) are universal relations that the Brownian particle has in the long times, as a consequence of the central limit theorem (CLT), which we introduced to discuss the random walk in Chap. 10. In the long times, these relations are held independently of the microscopic details, i.e., whether the diffusing particle is a large colloidal particle or a small molecule. The diffusion constant can be obtained by measuring the mean-square fluctuation by

$$D = \frac{\bar{\Delta}r(t)^2}{6t} = \frac{\bar{\Delta}x(t)^2}{2t}, \tag{13.9}$$

where $\bar{\Delta}x(t)^2$ is the mean square fluctuation of the displacement along the x-direction. This agrees with (13.2) via $\bar{\Delta}r(t)^2 = \langle l^2 \rangle t/\tau$.

The general solution for concentration or probability density, given arbitrary initial conditions, can be written as,

$$P(\boldsymbol{r}, t) = \int d\boldsymbol{r}_0 \, P(\boldsymbol{r}, t|\boldsymbol{r}_0) P(\boldsymbol{r}_0; 0) \tag{13.10}$$

$$n(\boldsymbol{r}, t) = \int d\boldsymbol{r}_0 \, P(\boldsymbol{r}, t|\boldsymbol{r}_0) n(\boldsymbol{r}_0; 0) \tag{13.11}$$

P13.1 *Initially a certain cells are localized in the region $x > 0$ within a thin tube of very long length. Find the concentration profile $n(x, t)$ at a later time.*

Now suppose there is an external force on each particle derivable from a potential, $\boldsymbol{F}(\boldsymbol{r}) = -\nabla U(\boldsymbol{r})$. Then the diffusion equation is generalized to

$$\frac{\partial n}{\partial t} = D\boldsymbol{\nabla} \cdot \{(\boldsymbol{\nabla} + \beta \boldsymbol{\nabla} U) n\}. \tag{13.12}$$

This is called the Smoluchowski Equation.

In order to derive the equation, we note that the drift velocity $\boldsymbol{V}$, which is the average velocity of a Brownian particle, is governed by the well-known phenomenological equation,

$$M\frac{d\boldsymbol{V}}{dt} = -\zeta \boldsymbol{V} + \boldsymbol{F}(\boldsymbol{r}), \tag{13.13}$$

where M, ζ are the mass and the friction coefficient of the particle. Let us first consider the case with $\boldsymbol{F} = 0$. Given the initial velocity $\boldsymbol{V}_0$, the average velocity at a later time t is given by

$$\boldsymbol{V}(t) = e^{-t/\tau_p} \boldsymbol{V}_0 \tag{13.14}$$

where

$$\tau_p \equiv M/\zeta \tag{13.15}$$

is momentum or velocity relaxation time. For $t \gg \tau_p$, $\boldsymbol{V}$ decays to zero, meaning that the initial velocity is forgotten. For a particle of molecular mass and friction, $\tau_p \leq 1$ ps. In many of the biological phenomena of our interest the friction coefficient is high enough that the relevant time scale of description is much longer than τ_p. Consequently the inertia effect (the LHS of (13.13)) is negligible, even in the presence of the force, so that the frictional force balances with the external force,

$$\boldsymbol{V} = \frac{1}{\zeta}\boldsymbol{F}(\boldsymbol{r}). \tag{13.16}$$

The particle current or flux, namely, the average number of particles flowing per unit time across unit area, is then given by

$$\boldsymbol{J}_n = -D\nabla n + n\boldsymbol{V}, \tag{13.17}$$

where the first term $-D\nabla n$ is the diffusive current that drives the particles towards the less concentrated region, while $n\boldsymbol{V}$ is the convective (drift) current that follows the driving force $\boldsymbol{F}(\boldsymbol{r})$. At equilibrium, the two terms must balance, so

$$\boldsymbol{J}_n = -D\nabla n + \frac{n}{\zeta}(-\nabla U) = 0. \tag{13.18}$$

As is dictated by equilibrium statistical mechanics, $n(\boldsymbol{r}) \propto e^{-\beta U(\boldsymbol{r})}$. This is substituted into the equation above to yield

$$D = \frac{k_B T}{\zeta}, \tag{13.19}$$

a remarkable relation between the fluctuation (D) and dissipation (ζ), which is called the Einstein relation. Then the current is rewritten as

$$\boldsymbol{J_n}(\boldsymbol{r}) = -D(\nabla n(\boldsymbol{r})) + \beta(\nabla U(\boldsymbol{r}))n(\boldsymbol{r}), \tag{13.20}$$

which can further be expressed in a convenient form for later uses:

$$\boldsymbol{J_n}(\boldsymbol{r}) = -De^{-\beta U(\boldsymbol{r})}\nabla e^{\beta U(\boldsymbol{r})}n(\boldsymbol{r}). \tag{13.21}$$

Substituting (13.20) into the continuity (13.4) yields the Smoluchowski Equation (13.12), which is valid for the times longer than τ_p. The equation can be exactly

solved for special cases of the forces such as the linear force or for many situations in steady state. This will be discussed later in depth.

Using the Stokes formula $\zeta = 6\pi\eta R$ for a spherical particle of a radius R in a fluid of viscosity η, which is obtained by hydrodynamics (19.78), one further obtains

$$D = \frac{k_B T}{6\pi\eta R}, \tag{13.22}$$

called as the **Stokes-Einstein relation**. Applying this to (13.9) yields,

$$\left(\bar{\Delta} r(t)\right)^2 = \frac{k_B T}{\pi\eta R} t. \tag{13.23}$$

This is an important relation from which Perrin estimated the Boltzmann constant k_B and the radius R of a molecule suspended in water. Historically this served as a verification of molecules and atoms, which had remained obscure by that time.

Often the diffusion can be accompanied by other processes. If particles are undergoing convection with a constant drift velocity $\boldsymbol{V}$ along x-axis the Smoluchowski equation can be written as

$$\frac{\partial n}{\partial t} + \boldsymbol{V} \cdot \boldsymbol{\nabla} n = D\boldsymbol{\nabla}^2 n.$$

If, in addition, the diffusing particles are absorbed by the solution constituents with rate α, the diffusion equation is modified to

$$\frac{\partial n}{\partial t} + \boldsymbol{V} \cdot \boldsymbol{\nabla} n = D\boldsymbol{\nabla}^2 n - \alpha n, \tag{13.24}$$

Let us solve for the fundamental solution of the above equation subject to the initial condition $n(\boldsymbol{r}, 0) = n_0 \delta(\boldsymbol{r})$. First we Fourier transform the equation (using $n(\boldsymbol{r}, t) = (2\pi)^{-3} \int d\boldsymbol{q}\, e^{i\boldsymbol{q}\cdot\mathbf{r}} n(\boldsymbol{q}, t)$ to have

$$\frac{\partial}{\partial t} n(\boldsymbol{q}, t) = \left(-V_x \cdot i q_x - D q^2 - \alpha\right) n(\boldsymbol{q}, t). \tag{13.25}$$

Using the initial condition $n(\boldsymbol{q}, t = 0) = \int d\boldsymbol{r} e^{-i\boldsymbol{q}\cdot\boldsymbol{r}} n(\boldsymbol{r}, 0) = n_0$, (13.25) is integrate to

$$n(\boldsymbol{q}, t) = n_0 e^{-t\left(V_x \cdot i q_x + D\boldsymbol{q}^2 - \alpha\right)}, \tag{13.26}$$

whose inverse Fourier transform is

$$n(\boldsymbol{r},t) = (2\pi)^{-3} n_0 e^{-\alpha t} \int dq_x e^{iq_x x - t\left(iq_x V_x + Dq_x{}^2\right)} \iint dq_y dq_y e^{i\left(q_y y + q_z z\right) - tD\left(q_y{}^2 + q_z{}^2\right)}$$
$$= \frac{n_0 e^{-\alpha t}}{(4\pi Dt)^{3/2}} \exp\left[-\frac{(x - V_x t)^2}{4Dt}\right] \exp\left[-\frac{(y^2 + z^2)}{4Dt}\right]. \tag{13.27}$$

The distribution retains the Gaussian form with its center following the convection but decays exponentially in time due to reaction. This reduces to (13.7) when $\boldsymbol{V} = 0$ and $\alpha = 0$.

P13.2 *A pollutant is uniformly distributed with a uniform surface density* σ *on a surface of sphere of radius R and then is freely released into the surrounding air with the diffusivity D at a time t = 0. Find the concentration profile of the diffusing pollutant. How would the profile be changed when the wind flows constantly to the west with a velocity u?*

13.2 Diffusive Transport in Cells

The diffusion or the Smoluchowski equation is nearly as fundamental in stochastic dynamics as the Schrödinger equation is in quantum mechanics. It can be applied to a variety of material, environmental, and biological problems. The most ubiquitous mode of transport in the world of cells is diffusion. Driven by their concentration gradients and external forces, the objects ranging from molecules to cells undergo diffusive motion, which looks locally stochastic due to thermal fluctuations. In this section we study several relatively simple but prototype biological examples.

13.2.1 Cell Capture

One particularly interesting problem is reaction or capture of certain molecules on specific sites in cells. There are plentiful examples in biology such as ligand (signaling molecules) binding on receptors, and metabolites (such as oxygen and sucrose molecules) uptake by cells. The aqueous solution is regarded as a bath so large that the bulk concentration of the molecules is not affected by the local binding on the cells. At what rate can these molecules be delivered to a cell if the transport is controlled by the diffusion?

As a simple model, consider a spherical cell of radius R immersed in an unbounded solution at a steady state in which the concentration of the molecules

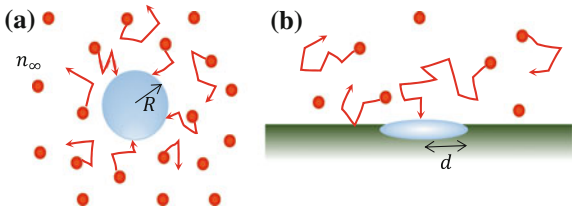

Fig. 13.2 **a** Cell capture model: whenever diffusing molecules arrive at a sphere, they are absorbed. **b** Molecules from a semi-infinite space are absorbed on a disk which is located on a nonadsorbing surface

infinitely away from the cell is maintained to be a constant, n_∞ (Fig. 13.2a). For the time being, suppose that the entire surface of the cell absorbs the molecules whenever they arrive on the surface. In a steady state of our interest, $\partial n/\partial t = 0$ and the distribution of the molecules is spherically symmetric, $n = n(r)$, so the diffusion equation is reduced to

$$D\nabla^2 n = D\frac{1}{r^2}\frac{\partial}{\partial r}\left(r^2\frac{\partial}{\partial r}n\right) = 0, \tag{13.28}$$

The equation is satisfied by $r^2\frac{\partial}{\partial r}n = A$, which is further integrated to yield

$$n(r) = -\frac{A}{r} + B. \tag{13.29}$$

The two constants A and B are determined by the two boundary conditions (BC). While the BC at $r = \infty$ is $n = n_\infty$, the BC at the cell surface $r = R$ is $n(R) = 0$, the so-called adsorbing BC: once the molecules bind on the cell they disappear. The solution that meets the BCs can be written as

$$n(r) = n_\infty\left(1 - \frac{R}{r}\right). \tag{13.30}$$

As the molecules approach the absorbing boundary, their concentration decreases until they vanish on surface. The flux of the molecules on the surface, using the Fick's law (13.5), is given by

$$J_n(R) = -D\frac{\partial}{\partial r}n|_{r=R} = -Dn_\infty/R. \tag{13.31}$$

Integrating the inward current $J_n(R)$ over the entire surface, we obtain the total number of molecules impinging on the surface per unit time, called the diffusion current,

$$I_s = |J_n(R)4\pi R^2| = 4\pi R D n_\infty. \tag{13.32}$$

The diffusion current I_s to an absorbing sphere is proportional to the concentration n_∞ as well as the diffusion constant D as one can easily expect. However, the proportionality to the radius R is not obvious. It is in fact due to the zigzag Brownian motion of the incident molecules; if the molecules were to collide with the sphere in a ballistic way the current would be proportional to the cross section πR^2. The binding (association) rate constant or the inverse diffusion resistance (R_s) is

$$k_s = \frac{I_s}{n_\infty} = 4\pi D R \equiv 1/R_s, \tag{13.33}$$

characteristic of the diffusion-limited reaction in fluid phases.

The diffusion current with the proportionality to *R* can have an important implication for the sizes of cells that nature selects. The amount of the energy that a cell needs per unit time for its survival, say, the metabolic need, is proportional to its volume. Suppose that this need is met by the metabolic intake (diffusion current):

$$4\pi D R n_\infty \geq \frac{4\pi R^3 \alpha}{3}, \tag{13.34}$$

where α is the metabolic rate constant. Then, the upper limit of the cell size is given by

$$R_M = \left(\frac{3Dn_\infty}{\alpha}\right)^{1/2} \sim D^{1/2} n_\infty^{1/2}. \tag{13.35}$$

This simple argument shows that the larger the diffusion constant and the concentration, the bigger the cell can be, following the power law. Because the diffusion constant of a molecule is $\sim 10^4$ times that in water, an aerial organism could be a one hundred times larger than its aquatic cousins (Denny 1993).

P13.3 *Calculate how the diffusion current would be changed if there is a Coulomb attraction $U(r) = -Zk_BTl_B/r$ between the cell and a ligand located at r.*

Sol. The steady state condition in spherical coordinate

$$\nabla \cdot J_n(r) = \frac{1}{r^2}\frac{\partial}{\partial r}\left(r^2 J_n(r)\right) = 0$$

leads to $4\pi r^2 J_n(r) = 4\pi R^2 J_n(R) = I$, *or* $4\pi r^2 D e^{-\beta U(r)} \frac{\partial}{\partial r} e^{\beta U(r)} n(r) = I$ (13.20), *which is integrated to*

$$I = 4\pi D n_\infty / \int_R^\infty dr r^{-2} e^{\beta U(r)} = 4\pi D R n_\infty x/(1 - e^{-x})$$

where $x = Zl_B/R$. *If* $x \gg 1$, $I \to 4\pi D Z l_B n_\infty$, *the current will be much enhanced.*

In the above, we considered the sphere as the cell's shape. Now consider a disk-shaped cell or receptor of radius a on the otherwise reflecting surface of a semi-infinite medium in which the molecules are distributed (Fig. 13.2b). One may calculate the diffusion current of the molecules whose concentration is kept as n_∞ infinitely away, following the procedure given above in cylindrical coordinate. The procedure is quite complicated (Wiegel 1991), but the result turns out to be simple:

$$I_d = 4Dan_\infty \tag{13.36}$$

The expression (13.36) is similar to (13.32) for the diffusive current to a sphere, sharing the same scaling behavior (linearity to the diffusion constant, cell size, and the concentration). The linear relation between the current and n_∞ is analogous to the Ohm's law between the electrical current and the potential difference, stemming from similarity between steady state diffusion equation and $D\nabla^2 n = 0$ and Laplace's equation for the electrostatic potential $\nabla^2\phi = 0$; given the potential difference n_∞ the resistance is $R_s = (4\pi DR)^{-1}$ for the sphere and $R_d = (4Da)^{-1}$ for the disk mentioned above.

Now we consider as a model for chemoreception, a situation where the M absorbing disks, each of radius a, are distributed over the surface of an otherwise reflecting sphere. The radius of the sphere is much larger than that of the disk, $R \gg a$, and the disks are separated by a distance much larger than a (Fig. 13.3a). Given the concentration of ligands n_∞ infinitely away, how does the rate of the capture depend on M? Having to deal with the BCs over many disks, solving the diffusion equation for the problem appears to be hopelessly complicated. Fortunately, we can find the current by appealing to the electrostatic analogy mentioned above: over the insulating surface of the sphere, there are M conducting

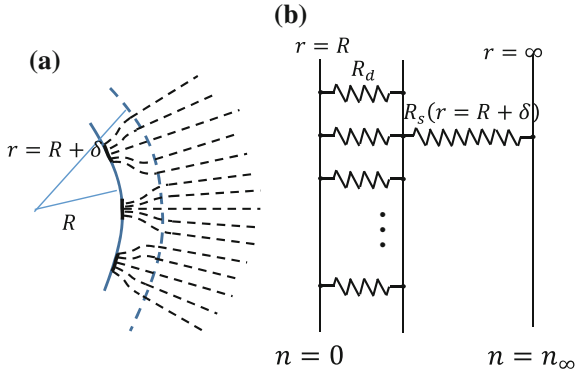

Fig. 13.3 **a** Line of diffusive flux around a sphere with absorbing disks. **b** The effective net resistance (redrawn from Berg 1983)

disks each with diffusion resistance R_d, connected together to form a single conductor (Berg and Purcell 1977; Berg 1983). Following this reference, we study the effective resistance R_c of this composite below.

Figure 13.3a is a schematic figure for the lines of flux around the surface of a sphere. At a radial distance r larger than $R+\delta$, where δ is roughly the distance between two absorbing disks, the flux is radial, but for smaller r converges on the absorbing disks. We can construct the effective circuit for the flow: on the surface of the sphere there are M resistors connected parallel without interaction among each other so that total resistance there is R_d/M, which is connected in series to the outer resistance, which is seen to be that of the absorbing sphere of the radius $R+\delta$. Thus, considering $\delta \ll R$, the composite resistance is

$$\begin{aligned} R_c &= [4\pi D(R+\delta)]^{-1} + \frac{R_d}{M} \\ &\approx (4\pi DR)^{-1} + (4MDa)^{-1} = R_s[1+\pi R/Ma]. \end{aligned} \tag{13.37}$$

The above shows that the resistance is larger than that of an adsorbing sphere by the factor $\pi R/Ma$. Thus, the diffusion current is smaller by the same factor:

$$\frac{I}{I_s} = \frac{1}{1+\pi R/Ma} \tag{13.38}$$

This result agrees with that obtained from more detailed calculations (Berg and Purcell 1977). Figure 13.4a shows the current as a function of M. When M is quite small in such a way that $\pi R/Ma \gg 1$, $I \approx (I_s Ma)/\pi R = 4MDan_\infty$ as can be expected for non-interacting disks behaving independently. But, as M increases further, the current no longer increases with M linearly because of the interference between the disks. If M is large such that $\pi R/Ma \ll 1$, the current saturates to the limit $I = I_s = 4\pi RDn_\infty$ of a completely absorbing sphere as it should be.

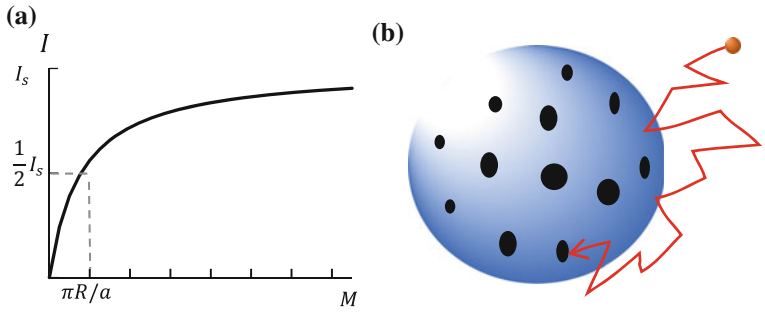

Fig. 13.4 **a** The diffusion current versus number of disks. Diffusion current becomes the half of the maximum value even with a very small fraction of the absorbing surface. **b** Receptors (absorbing disks) distributed on a non-absorbing surface of a sphere. A ligand undergoes many zig-zag motions in a solution until it is adsorbed on a disk

It is amazing how fast this saturation limit (I_s) is achieved as M increases. The number of the disks that have to exist in order to attain half of the saturation limit is $M = \pi R/a$; using $R = 10$ μm and $a = 10$ nm, gives $M \approx 3140$. With this value of M, only a minute fraction of the surface area, $M\pi a^2/(4\pi R^2) = \pi a/4R \approx 8 \times 10^{-4}$, is occupied by the receptors. This signifies **a remarkable efficiency of chemoreception**. This is again due to the zigzag motion of the impinging molecules: the molecules that are reflected from the non-absorbing area may come back due to the Brownian motion until they are absorbed on the receptors (Fig. 13.4b).

13.2.2 Ionic Diffusion Through Membrane

Ionic transport through cell membranes is a critical process occurring ubiquitously in cells, for our every thought, perception, and movement. It costs the energy much higher than thermal energy for an ion to cross the membranes (6.8), making the lipid-bilayer highly impermeable. A structure of membrane proteins called the ion channel provides a conduction pathway for specific ions to transverse the membranes. Although the structures of ion channel are so complex (Doyle et al. 1998), for simplicity, we regard the transport of an ion as one dimensional diffusion process of crossing the free energy barriers caused by the structures and interactions (Lee and Sung 2002).

We are interested in the ionic distribution and current at a steady state in the channel across a membrane in the presence of a potential as well as an imbalance of the ionic concentrations on both sides of the membrane. Suppose that ions undergo the Brownian motion along one-dimension (x-axis) subject to a potential $U(x)$ (Fig. 13.5). Its one-dimensional density $n(x)$ at steady state is described by

$$\frac{\partial}{\partial x} J(x) = 0, \tag{13.39}$$

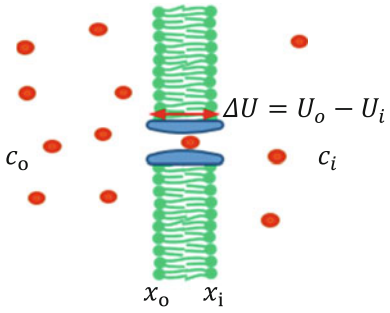

Fig. 13.5 A sketch of ionic transport through a channel in a membrane, between extracellular and intracellular sides

where the flux (13.20) and (13.21) is

$$\begin{aligned} J(x) &= -D\left[\frac{\partial}{\partial x} + \beta \frac{\partial}{\partial x} U(x)\right] n(x) \\ &= -De^{-\beta U(x)} \frac{\partial}{\partial x} e^{\beta U(x)} n(x) \end{aligned} \tag{13.40}$$

Equation (13.39) assures us that the $J(x)$ is uniform throughout, that is, a constant J. Rewriting (13.40) as $Je^{\beta U(x)} = -D\partial/\partial x e^{\beta U(x)} n(x)$, which is integrated from the outer boundary x_o to an arbitrary position x in the channel, we have

$$J \int_{x_o}^{x} dx' e^{\beta U(x')} = D\left[e^{\beta U(x_o)} n(x_o) - e^{\beta U(x)} n(x)\right]. \tag{13.41}$$

Choosing the position x to be the inner boundary x_i, the steady state current is found to be

$$J = D \frac{e^{\beta U(x_o)} n(x_o) - e^{\beta U(x_i)} n(x_i)}{\int_{x_o}^{x_i} dx' e^{\beta U(x')}} \tag{13.42}$$

If the channel is a simple non-selective pore that allows only the entry (passive channel), we impose the boundary conditions

$$n(x_o) = c_o A \tag{13.43}$$

$$n(x_i) = c_i A \tag{13.44}$$

where A is the cross sectional area of the channel assumed to be uniform, the c_o and c_i are the three dimensional (bulk) concentrations of the ions at the outer and inner boundaries (extracellular and intracellular concentrations). We rewrite (13.42) as

$$J = DA\left(e^{\beta U(x_o)} c_o - e^{\beta U(x_i)} c_i\right) / \int_{x_o}^{x_i} dx' e^{\beta U(x')}. \tag{13.45}$$

At equilibrium, $J = 0$, where we have

$$c_o / c_i = e^{\beta\{U(x_i) - U(x_o)\}} = e^{-\beta \Delta U}, \tag{13.46}$$

where $\Delta U = U(x_o) - U(x_i)$ is the potential difference across the membrane.

Consequently we have the potential difference

$$\Delta U = k_B T \ln\left(\frac{c_i}{c_0}\right), \tag{13.47}$$

which is called the Nernst potential. It tells us that the imbalance of the ionic concentration in the bathing solution at equilibrium generates a membrane potential, also called the rest potential. This means that an ion-selective membrane acts as a battery. For a typical mammalian cell at body temperature (37 °C), the extracellular and intracellular concentrations of sodium (Na^+) ions are 145 and 15 mM so that the rest potential for Na^+ is 61 mV.

On the other hand, (13.41) yields the density distribution of ions at a position inside the channel:

$$n(x) = n(x_o)e^{-\beta\{U(x)-U(x_o)\}} - \frac{J}{D}e^{-\beta U(x_o)}\int_{x_o}^{x} dx' e^{\beta U(x')} \tag{13.48}$$

At equilibrium state where $J = 0$, $n(x) = n(x_o)e^{-\beta\{U(x)-U(x_o)\}}$ as it ought to be. In the steady state, the ion population is depleted along the direction of the current J.

$U(x)$ is the effective potential experienced by an ion in the channel, which is caused by the externally imposed transmembrane potential, and the ion's interaction with the channel structure, etc. Usually the cytoplasm is charged negative relative to the outside, imparting linearly decaying electrical potential. The more critical part of the potential comes from the ion channels, whose complex structures are under intense research (Doyle et al. 1998). Because the $U(x)$ is an effective interaction the one-dimensional ion undergoes with entropic changes, it is a free energy function, previously notated by $\mathcal{F}(x)$.

Let us consider a channel that can accommodate a single ion at most, called the singly-occupied ion channel. The boundary conditions for this channel are replaced by

$$n(x_o) = c_o A P_e, \quad \text{and} \quad n(x_i) = c_i A P_e, \tag{13.49}$$

where P_e is the probability that the channel is empty:

$$P_e = 1 - \int_{x_o}^{x_i} dx\, n(x) \tag{13.50}$$

If the channel is occupied by an ion, $\int_{x_o}^{x_i} dx\, n(x) = 1$, and $P_e = 0, n(x_o) = n(x_i) = 0$, so that $J = 0$ (13.42). In general we can find that the current and concentration are

equally reduced by the factor $P_e : J = P_e J_0$ and $n(x) = P_e n_0(x)$, where $J_0, n_0(x)$ are the current and density calculated from the passive channel, (13.45) and (13.48). From (13.50), P_e then is calculated to be

$$P_e = 1/\{1 + \int_{x_o}^{x_i} dx\, n_0(x)\} \tag{13.51}$$

13.2.3 A Trapped Brownian Particle

Hitherto in this section we were considering mostly the steady state diffusive motion of Brownian particles. Below we study the time-dependent motion of a Brownian particle in one dimension confined within a trap of length L. Whenever the particle arrives on the boundary $x = 0$ or L, it is absorbed. If it is initially released at $x = x_0$, what is the probability density with which it is found at a position x within the trap at a later time? What is the average time in which it will reside within the trap? You might imagine a drunken bug within a trap.

The diffusion equation for the probability density is written as

$$\frac{\partial P(x,t)}{\partial t} = -\mathcal{L}P(x,t), \tag{13.52}$$

where $\mathcal{L} = -D\partial^2/(\partial x^2)$ is a linear operator. The solution is formally written as

$$P(x,t|x_0) = e^{-\mathcal{L}t}P(x_0,0) = e^{-\mathcal{L}t}\delta(x - x_0). \tag{13.53}$$

Consider a set of eigenfunctions ψ_n and eigenvalues λ_n:

$$\mathcal{L}\psi_n = \lambda_n \psi_n, \tag{13.54}$$

Using the completeness of the eigenfunctions, $\delta(x - x_0) = \sum_n \psi_n(x)\psi_n(x_0)$, (13.53) becomes

$$P(x,t|x_0) = \sum_n e^{-\lambda_n t}\psi_n(x)\psi_n(x_0). \tag{13.55}$$

Subject to the boundary conditions at $x = 0$ and L where $\psi_n = 0$, they are

$$\psi_n(x) = \left(\frac{2}{L}\right)^{1/2} \sin\frac{n\pi}{L}x, \quad \lambda_n = \left(\frac{n\pi}{L}\right)^2 D. \tag{13.56}$$

Then,

$$P(x,t|x_0) = \sum_{n=1}^{\infty} \left(\frac{2}{L}\right) e^{-\left(\frac{n\pi}{L}\right)^2 Dt} \sin\frac{n\pi}{L}x \sin\frac{n\pi}{L}x_0. \tag{13.57}$$

The probability density decays in time characterized by the diffusion time L^2/D, but, curious enough, oscillates sinusoidally with the position.

For the time $t \gg L^2/D$, the contribution from the lowest eigenfunction dominates in the sum:

$$P(x,t|x_0) \approx \left(\frac{2}{L}\right) e^{-\left(\frac{\pi}{L}\right)^2 Dt} \sin\frac{\pi}{L}x \sin\frac{\pi}{L}x_0. \tag{13.58}$$

The probability that it survives at long times $t \gg L^2/D$ is

$$\wp(t) = \int_0^L dx\, P(x,t|x_0) \approx \frac{4}{\pi} e^{-\left(\frac{\pi}{L}\right)^2 Dt} \sin\frac{\pi}{L}x_0. \tag{13.59}$$

Finally, the mean lifetime of the bug is

$$\tau = \int_0^\infty dt\, t\left(-\tfrac{d}{dt}\wp(t)\right) = \int_0^\infty dt\, \wp(t) = \int_0^\infty dt \int_0^L dx\, P(x,t|x_0), \tag{13.60}$$

where we note the probability that the bug survives during dt is $-d\wp(t)/dt$. Using the eigenfunction expansion (13.57),

$$\tau = \sum\nolimits_{n=odd}^{\infty} \frac{4L^2}{n^3\pi^3 D} \sin\frac{n\pi}{L}x_0, \tag{13.61}$$

which, for $x_0 = L/2$, is

$$\tau = \frac{4L^2}{\pi^3 D}\left(1 - \frac{1}{3^3} + \frac{1}{5^3} - \cdots\right) = \frac{L^2}{8D}. \tag{13.62}$$

It is insightful to draw an analogy between this problem and a flexible polymer confined within a box we studied in Chap. 10. As one can show the solution (13.57) in the limit $L \to \infty$ approaches

$$P(x,t|x_0) = \frac{1}{(4\pi Dt)^{1/2}}\left[\exp\left\{-\frac{(x-x_0)^2}{4Dt}\right\} - \exp\left\{-\frac{(x+x_0)^2}{4Dt}\right\}\right]. \tag{13.63}$$

This is none other than the image method solution that we would have if only a single wall or a boundary is present at $x = 0$. The corresponding problem of a polymer anchored on a wall was studied (10.27).

P13.4 *Suppose that a neural transmitter emitted from an axon terminal at $x = 0$ diffuses with the diffusion constant D, and drifting with constant velocity V in one dimension. When it arrives at $x = L$, the position of a receptor of a neighboring neuronal cell, it is absorbed. Considering one-dimensional diffusion model, find the probability of finding the transmitter remaining unabsorbed at a time t. Assume the boundary condition $J(x = 0) = J_0$.*

13.3 Brownian Motion/Langevin Equation Theory

The diffusion theory of Einstein and Smoluchowski we have discussed above is only applicable to long-time Brownian motion. This is evidenced by the mean square displacements of a free Brownian particle determined by scattering experiments and computer simulations as given by Fig. 13.6. Noticeably, for a time longer than the momentum relaxation time τ_p, $\bar{\Delta}r^2(t) = 6Dt$, as in the diffusion theory, but for a time shorter than that, $\bar{\Delta}r^2(t) \sim t^2$. It means there are some degrees of freedom that are missed in accounting for the short time motion. The gap is filled by the Langevin equation, which is another pillar of the Brownian motion theory.

13.3.1 The Velocity Langevin Equation

The Langevin equation is simply obtained by replacing the drift velocity V of a Brownian particle in the macroscopic deterministic equation (13.13) by a fluctuating velocity v, and adding to the right hand side a fluctuation term $f_R(t)$ called the random force. Considering $1 - D$ motion for simplicity, the Langevin equation is written as:

$$M\frac{dv}{dt} = -\zeta v + F(x) + f_R(t) \tag{13.64}$$

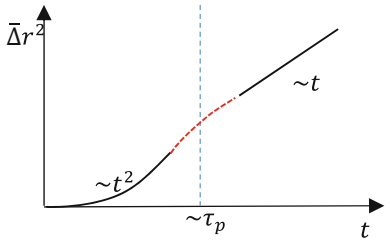

Fig. 13.6 The mean square displacement $\bar{\Delta}r^2$ of a Brownian particle in a fluid. In short times it is proportional to t^2 but at long times shows diffusive behavior $\bar{\Delta}r^2 \sim t$

The fluctuating force $f_R(t)$ is due to the collisions of surrounding fluid molecules with the Brownian particle that are not incorporated in the frictional force $-\zeta v$. Since the Brownian particle is much heavier than a fluid molecule, **the random force $f_R(t)$ is supposed to vary irregularly and rapidly** on the timescale of the velocity. $f_R(t)$ can be constructed as a sum of *many* contributions from surrounding fluid molecules at different times, each of which is *not correlated* with other on the timescale. Then the Central Limit Theorem (Chap. 10) tells us that the random force is distributed in Gaussian prescribed solely by the first two moments. The first one is the average, which, due to the randomness, vanishes:

$$\langle f_R(t) \rangle = 0. \tag{13.65}$$

The second moment is expressed as

$$\langle f_R(t) f_R(t') \rangle = 2\Theta\delta(t - t'). \tag{13.66}$$

The averages are taken over the equilibrium ensemble. On the time scale of the velocity, random force fluctuates very rapidly and does not correlate with itself at different times. This delta-function-correlated random force is called the white noise, because the Fourier transform of (13.66), which is called the power spectrum of the random force, is independent of the frequency. This **Gaussian and white noise** is called **thermal noise**; the constant Θ is the strength of the noise, which will be shown to be $\zeta k_B T$ shortly. The Langevin equation (13.64) with this non-analytic noise term is an example of the stochastic differential equation.

Let us first consider the case with $F = 0$, and study the fluctuation and correlation of the velocity. This velocity Langevin equation is formally solved as

$$v(t) = e^{-t/\tau_p} v_0 + \frac{1}{M} \int_0^t ds\, e^{-(t-s)/\tau_p} f_R(s), \tag{13.67}$$

where v_0 is the initial velocity and $\tau_p \equiv M/\zeta$ is its correlation time. Equation (13.67) can be obtained by Laplace transforming ($v[z] = \int_0^\infty dt\, e^{-zt} v(t)$) the Langevin equation, which then becomes

$$M\{zv[z] - v_{0,}\} = -\zeta v[z] + f_R[z] \tag{13.68}$$

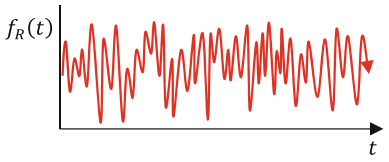

Fig. 13.7 Time series $f_R(t)$ of a random force, which varies very rapidly and erratically

or

$$v[z] = \frac{1}{zM+\zeta}(Mv_0 + f_R[z]), \tag{13.69}$$

whose inverse Laplace transform is just (13.67). Averaging all the terms over the ensemble *subject to the initial velocity* v_0 yields

$$\langle v(t)\rangle_{v_0} = e^{-t/\tau_p} v_0. \tag{13.70}$$

At a time longer than τ_p the information on the initial velocity (inertia effect) is lost.

P13.5 *Above we noted that the random force at a time t is not correlated with the velocity at an earlier time t′,* $\langle f_R(t)v(t')\rangle_{v_0} = 0$. *However, the velocity at a later time is affected by the random force at the earlier time. Calculate* $\langle v(t)f_R(t')\rangle_{v_0}$.

Now, we determine the noise strength Θ and the equilibrium time correlation function of the velocities at two times t and t' defined by

$$C_V(t,t') = \langle v(t)v(t')\rangle, \tag{13.71}$$

where the average now is taken over the equilibrium ensemble. This is evaluated as

$$\begin{aligned} C_V(t,t') = {} & \langle v_0^2\rangle e^{-(t+t')/\tau_p} \\ & + \frac{1}{M^2}\int_0^t ds \int_0^{t'} ds' e^{-((t+t'-s-s'))/\tau_p}\langle f_R(s)f_R(s')\rangle \end{aligned} \tag{13.72}$$

where $\langle f_R(t)v_0\rangle = 0$ is used. Performing the integration yields

$$C_V(t,t') = \langle v_0^2\rangle\, e^{-(t+t')/\tau_p} + \frac{\Theta\tau_p}{M^2}\left(e^{-|t-t'|/\tau_p} - e^{-(t+t')/\tau_p}\right) \tag{13.73}$$

and (13.66) is used.

We note that the equipartition relation

$$C_V(t,t) = \langle v^2(t)\rangle = \langle v_0^2\rangle = \frac{k_BT}{M} \tag{13.74}$$

should persist at any time, including $t = 0$ and ∞, due to incessancy of the Brownian motion. Thus the noise-strength should have the magnitude

$$\begin{aligned} \Theta &= M^2\tau_p^{-1}\frac{k_BT}{M} = k_BT\zeta \qquad (1-\mathrm{D}). \\ \Theta &= M^2\tau_p^{-1}\frac{3k_BT}{M} = 3k_BT\zeta \quad (3-\mathrm{D}). \end{aligned} \tag{13.75}$$

With this, the (13.73) is given by

$$C_V(t-t') = \frac{k_B T}{M} e^{-|t-t'|/\tau_p}, \tag{13.76}$$

which depends only on the time difference $t - t'$, an important property of equilibrium time correlation functions, called stationarity. The velocity correlation function decays exponentially in just the same way as the average velocity (13.70). The relation (13.66) with the Θ given by (13.75) is one of **the fluctuation and dissipation theorem**. It signifies the detailed balance between the random noise $f_R(t)$ and the dissipative force $-\zeta v$ to retain the thermal equilibrium in the long time; **if the strength of this thermal and equilibrium noise takes other values than given by (13.75), the system will not attain the stationarity and will not arrive at the equilibrium state in the long time**.

13.3.2 The Velocity and Position Distribution Functions

Since the velocity $v(t)$ is related to the Gaussian variable $f_R(s)$ linearly (13.67), it is also distributed in Gaussian. The velocity distribution function at a time t given its initial value v_0 is thus specified by the mean $e^{-t/\tau_p} v_0$ and the variance $\langle \left(v(t) - e^{-t/\tau_p} v_0\right)^2 \rangle$:

$$P(v,t|v_0) = \left[\frac{1}{2\pi \langle \left(v(t) - e^{-t/\tau_p} v_0\right)^2 \rangle}\right]^{1/2} \exp\left[-\frac{\left(v - e^{-t/\tau_p} v_0\right)^2}{2\langle \left(v(t) - e^{-t/\tau_p} v_0\right)^2 \rangle}\right]. \tag{13.77}$$

The variance is obtained as

$$\begin{aligned} \left\langle \left(v(t) - e^{-t/\tau_p} v_0\right)^2 \right\rangle &= \int_0^t ds \int_0^t ds' e^{-(2t-s-s')/\tau_p} \langle f_R(s) f_R(s') \rangle \\ &= \frac{k_B T}{M} \left(1 - e^{-2t/\tau_p}\right), \end{aligned} \tag{13.78}$$

where the relation (13.66) is used. The distribution then is explicitly given as

$$P(v,t|v_0) = \left[\frac{M}{2\pi k_B T \left(1 - e^{-2t/\tau_p}\right)}\right]^{1/2} \exp\left[-\frac{M\left(v - e^{-t/\tau_p} v_0\right)^2}{2k_B T \left(1 - e^{-2t/\tau_p}\right)}\right] \tag{13.79}$$

The distribution has correct limiting behaviors for times $t \ll \tau_p$ and $t \gg \tau_p$:

$$P(v,t|v_0) \to \delta(v-v_0) \quad (t \ll \tau_p) \tag{13.80}$$

$$P(v,t|v_0) \to \Phi(v) = \left(\frac{2\pi k_B T}{M}\right)^{-1/2} \exp\left[-\frac{Mv^2}{2k_B T}\right], \quad (t \gg \tau_p) \tag{13.81}$$

where the latter is just the Maxwell-Boltzmann distribution, representative of the equilibrium state to which the velocity reaches at the times long after τ_p.

Finally, let us return to the displacement of the Brownian particle. *Given its initial position x_0 (irrespective of the initial velocity)*, what is the probability density of the position at a later time? Because the displacement is linearly related to the velocity, $x(t) - x_0 = \int_0^t ds\, v(s)$, this is also distributed in Gaussian, given by the mean $\langle x(t)\rangle = x_0$ and the mean square of the displacement:

$$\begin{aligned}
\left\langle (x(t)-x_0)^2 \right\rangle &= \int_0^t ds \int_0^t ds' \langle v(s)v(s')\rangle \\
&= \frac{k_B T}{M} \int_0^t ds \int_0^t ds' e^{-|s-s'|/t_p} \\
&= 2\frac{k_B T}{M} \int_0^t ds\, e^{-s/t_p} \int_0^s ds' e^{s'/t_p} \\
&= \frac{2k_B T \tau_p}{M}\left[t - \tau_p\left(1 - e^{-t/t_p}\right)\right] = 2D\left[t - t_p\left(1 - e^{-t/t_p}\right)\right],
\end{aligned} \tag{13.82}$$

where we used (13.76) and the Einstein relation $D = k_B T/\zeta$. Equation (13.82) agrees with the curve in Fig. 13.6. It is easy to check that for a long time $t \gg \tau_p$, $\langle (x(t)-x_0)^2\rangle = 2Dt$, which is the result of free diffusion. On the other hand, for a short time $t \ll \tau_p$, expanding the exponential to the second order in t/τ_p,

$$\left\langle (x(t)-x_0)^2 \right\rangle = \left(\frac{k_B T}{M}\right) t^2. \tag{13.83}$$

This means that for the short time before the Brownian particle experiences collision with the background molecules, it moves ballistically with the initial velocity which has the equilibrium distribution. The position distribution for all time is given by

$$P(x;t|x_0) = \left[4\pi D\left\{t + \left(e^{-t/\tau_p} - 1\right)\tau_p\right\}\right]^{-1/2} \exp\left[-\frac{(x-x_0)^2}{4D\left\{t + \left(e^{-t/\tau_p} - 1\right)\tau_p\right\}}\right]. \tag{13.84}$$

This shows how the position distribution approaches to that of free diffusion, (13.7), as time elapses.

It is useful to observe the close similarity between Brownian particle trajectory and polymer chain configuration. Equation (13.82) is similar to the mean square end to end distance of the semiflexible chain (11.11) if one-to-one correspondences between $\boldsymbol{r}(t)$ versus $\boldsymbol{r}(s)$, $\boldsymbol{v}(t)$ versus $\boldsymbol{u}(s)$, and τ_p versus l_p are noted. Assuming they are Gaussian, the probabilities for the end to end distance and the orientation of a semi-flexible chain can respectively be given by (13.84) and (13.79).

13.3.3 A Brownian Motion Subject to a Harmonic Force

It is a challenge to analytically solve the Langevin equation with the external force in an arbitrary form. As a solvable important example, let us consider the one-dimensional case with $F = -kx$, and find $\Delta(t) = \langle x(t)^2 \rangle$ as a function of time. The Langevin equation is written as

$$Mx'' + \zeta x' + kx = f_R(t). \tag{13.85}$$

We multiply the above equation by x, and then average both sides. Noting that $\Delta' = 2\langle xx' \rangle$, $\Delta'' = 2\langle x'^2 \rangle + 2\langle xx'' \rangle = (2k_BT)/M + 2\langle xx'' \rangle$, we derive a differential equation for $\Delta(t)$:

$$\frac{1}{2}\Delta'' + \frac{1}{2}\tau_p^{-1}\Delta' + \omega^2\Delta = \frac{k_BT}{M}, \tag{13.86}$$

where $\omega^2 = k/M$.

P13.6 *Derive (13.86). Why* $\langle f_R(t)x(t) \rangle = 0$?

In a long time, the system approaches to the equilibrium, and thus (13.86) reduces to $\Delta = k_BT/(M\omega^2) = k_BT/k$, which can also be derived from the equipartition of energy for the displacement $k\langle x^2 \rangle/2 = k_BT/2$. Defining $\delta = \Delta - k_BT/k$, (13.86) becomes homogeneous,

$$\frac{1}{2}\delta'' + \frac{1}{2}\tau_p^{-1}\delta' + \omega^2\delta = 0. \tag{13.87}$$

This is identical to the equation for a damped harmonic oscillator. Assuming the solution of the form $\delta \sim e^{-\lambda t}$, we find that, by substituting it in the equation above, there are two such λ's:

$$\lambda_{\pm} = \frac{1}{2\tau_p}\left\{1 \pm \left(1 - 8\omega^2\tau_p^2\right)^{1/2}\right\}. \tag{13.88}$$

The solution that satisfies the initial conditions, $\Delta = 0, \Delta' = 0$ at $t = 0$, is

$$\Delta(t) = \frac{k_B T}{k}\left(1 - \frac{\lambda_+ e^{-\lambda_- t} - \lambda_- e^{-\lambda_+ t}}{\lambda_+ - \lambda_-}\right). \tag{13.89}$$

For the ('overdamped') case where both of $\lambda_{\pm}$ are real, Fig. 13.8 above depicts $\Delta(t)$. $\Delta(t) \sim t^2$ for short times and approaches asymptotically the equilibrium value $k_B T/k$ in the long time. Equation (13.86) illuminates **the crossovers from short to long time behaviors and the associated transition from velocity to position degree of freedom for relevant dynamics**. In a short time, $t \ll \tau_p$, (13.89) indeed recovers (13.83). Dominated by the first (inertia) term in (13.86), the particle moves as if it is free of collision (2nd term) and of the harmonic force (3rd term). As time exceeds τ_p, the inertia gives into collision with background and to thermal agitation, and it undergoes a Brownian motion, yet is little affected by the harmonic force. In a time much longer than $\tau_p^{-1}\omega^{-2} = \zeta/k$, the viscoelastic relaxation time, the particle feels bound to the harmonic potential well, dominated by the last term in LHS of (13.86). In the underdamped case when the harmonic frequency is high such that $\omega^2\tau_p^2 > 1/8, \lambda_{\pm}$ are complex and thus the intermediate time behavior of $\Delta(t)$ is oscillatory rather than monotonous.

$x(t)$ is linearly related with $f_R(t)$, so it is also Gaussian, with the distribution:

$$P(x,t) = \frac{1}{(2\pi\Delta(t))^{1/2}}\exp\left[-\frac{x^2}{2\Delta(t)}\right], \tag{13.90}$$

In the limit $t \to \infty$ it approaches

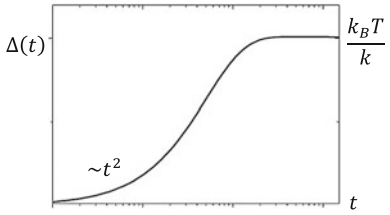

Fig. 13.8 Temporal changes in the mean-squared displacement $\Delta(t)$ of an underdamped Brownian harmonic oscillator

$$P(x) = \left(\frac{2\pi k_B T}{k}\right)^{-1/2} \exp\left[-\frac{kx^2}{2k_B T}\right], \tag{13.91}$$

which is none other than the equilibrium position distribution of a harmonic oscillator.

There are numerous situations where this damped harmonic Brownian motion is realized. Consider a closed circuit where an inductor, a resistor and a capacitor are connected in series. We learned from the first year undergraduate physics course that, with no external voltage, the current in the circuits decays to zero. However, there are persistent thermal fluctuations caused by, for example, electron collisions with the atoms in solid conductors. The equation of motion for the charge Q stored at the capacitor is given by

$$LQ'' + RQ' + Q/C = V_J(t), \tag{13.92}$$

where L, R and C are the inductance, resistance, and capacitance respectively. By analogy with the Brownian particle motion, on RHS there is **the random voltage $V_J(t)$, called the Johnson noise**, characterized by $\langle V_J(t)\rangle = 0$ and

$$\langle V_J(t)V_J(t')\rangle = 2Rk_B T\delta(t-t'). \tag{13.93}$$

Alternatively, we have an expression

$$R = \frac{1}{k_B T}\int_0^\infty dt\langle V_J(t)V_J(0)\rangle. \tag{13.94}$$

The above relations are recast to a form amenable to experiment as below. Introducing the time-Fourier transform and the inverse

$$V_J(\omega) = \int_{-\infty}^{\infty} dt\ e^{i\omega t}V_J(t). \tag{13.95}$$

$$V_J(t) = \frac{1}{2\pi}\int_{-\infty}^{\infty} d\omega\ e^{-i\omega t}V_J(\omega), \tag{13.96}$$

we have

$$\begin{aligned}\left\langle V_J(\omega)V_J^*(\omega')\right\rangle &= \int_{-\infty}^{\infty} dt \int_{-\infty}^{\infty} dt'\, e^{i(\omega t-\omega' t')}\langle V_J(t)V_J(t')\rangle \\ &= \int_{-\infty}^{\infty} dt\, e^{i(\omega-\omega')t} \int_{-\infty}^{\infty} d(t'-t)e^{-i\omega'(t'-t)}2Rk_BT\delta(t-t') \\ &= 4\pi Rk_BT\delta(\omega-\omega').\end{aligned} \tag{13.97}$$

Then V_J that is integrated over a narrow frequency band $\Delta\omega$ around ω,

$$V_\Delta(\omega) = \int_{\omega}^{\omega+\Delta\omega} d\omega_1\, V_J(\omega_1) \tag{13.98}$$

has the spectral density:

$$\begin{aligned}\langle |V_\Delta(\omega)|^2\rangle &= 4\pi Rk_BT \int_{\omega}^{\omega+\Delta\omega} d\omega_1 \int_{\omega}^{\omega+\Delta\omega} d\omega_2\delta(\omega_1-\omega_2) \\ &= 4\pi Rk_BT\Delta\omega,\end{aligned} \tag{13.99}$$

where (13.97) is used. This relation is **the Johnson-Nyquist theorem, stating that the spectral density of the Johnson noise across a resistor is proportional to the resistance and temperature**, which is in excellent agreement with the experiment. It provides an estimate of the limiting of the signal-to-noise ratio in any measurements. The relative strength of the voltage noise compared with a macroscopic voltage V is $\sim (k_BT\Delta\omega/I^2R)^{1/2}$, which tends to be imperceptibly small as the system size become macroscopic. But in mesoscopic situations, like the voltages across membranes, the Johnson noise may not be negligible. In analogy with the translational Brownian motion, we have the equipartition of the energy,

$$\frac{\langle Q^2\rangle}{2C} = \frac{1}{2}L\langle I^2\rangle = \frac{k_BT}{2}, \tag{13.100}$$

and, following the relation $V = Q/C$, the fluctuation of the voltage across the capacitor,

$$\langle V^2\rangle = \frac{k_BT}{C}. \tag{13.101}$$

P13.7 *Calculate the power spectrum of the voltage* $S_V(\omega)$ *(defined by* $S_V(\omega) = \int_{-\infty}^{\infty} dt\, e^{i\omega t} \langle V(t)V(0)\rangle$*) in RC circuits and compare it with the strength of the Jonson noise* $2Rk_BT$.

Another relevant example of the harmonic Brownian motion is an elastic rod of average length L. With the naked eye, the length of a macroscopic rod appears to be fixed, but in fact does fluctuate! You may write down the for the length X deviated from the average as

$$X'' + \gamma X' + \mu X = f_R(t), \tag{13.102}$$

where $f_R(t)$ is a Gaussian and white noise that is related to the γ, via $\langle f_R(t) f_R(t')\rangle = 2\gamma k_B T \delta(t - t')$, μ is the elastic constant proportional to the Young's modulus. The relative strength of the length fluctuation is given by $\langle X^2\rangle^{1/2} \Big/ L \sim (k_B T/\mu L^2)^{1/2}$, which is negligibly small on macroscale; as the length gets shorter, the relative fluctuation increases as typed in stretched biopolymers on nanoscale.

13.3.4 The Overdamped Langevin Equation

In many situations we deal with **the behavior of a Brownian motion at times much longer than the velocity relaxation time** τ_p, where velocity or inertia of the particle becomes irrelevant. Excellent examples are colloids and macromolecules, where τ_p can be much smaller than the relevant time scale of the motions and conformational changes. In these cases the underdamped Langevin equation (13.64) is reduced to the overdamped Langevin equation

$$\zeta \frac{dx}{dt} = F(x) + f_R(t) \tag{13.103}$$

where x may represent a position or certain conformational coordinate of interest, $f_R(t)$ is the Gaussian white noise given earlier. As will be shown later, this is the equation of motion equivalent to the Smoluchowski equation for the probability discussed earlier.

In the absence of an external force, (13.103) becomes

$$\zeta \frac{dx}{dt} = f_R(t). \tag{13.104}$$

This Langevin equation is equivalent to the diffusion equation. The stochastic dynamics of $x(t)$ is called the Wiener process. By integrating the equation above,

$$x(t) = \frac{1}{\zeta}\int_0^t f_R(t')dt' + x_0, \tag{13.105}$$

one can confirm $\langle x(t)\rangle = x_0$ and

$$\left\langle (x(t) - x_0)^2 \right\rangle = \frac{1}{\zeta^2}\int_0^t dt' \int_0^t dt'' \langle f_R(t') f_R(t'')\rangle = 2Dt, \tag{13.106}$$

which is the Einstein displacement formula in one dimension.

Consider the harmonic force $F(x) = -kx$. The overdamped Langevin equation

$$\zeta dx/dt = -kx + f_R(t) \tag{13.107}$$

looks identical in form to the velocity Langevin equation $Mdv/dt = -\zeta v + f_R(t)$ we studied; these two cases are called the Ornstein-Uhlenbeck process. By replacing v by x and the associated parameters the result (13.79) can be easily adopted to yield:

$$P(x,t|x_0) = \left[\frac{k}{2\pi(1-e^{-2t/\tau})}\right]^{1/2} \exp\left[-\frac{k\left(x - e^{-t/\tau}x_0\right)^2}{2(1-e^{-2t/\tau})}\right], \tag{13.108}$$

where $\tau = \zeta/k$ is the relaxation time.

P13.8 *Suppose that the end-to-end distance (EED) motion of a flexible polymer is given by the Langevin equation:* $\zeta\dot{\boldsymbol{R}} = -K_s\boldsymbol{R} + \boldsymbol{f}_R(t)$. *Calculate the correlation function* $\langle \boldsymbol{R}(t)\cdot\boldsymbol{R}(0)\rangle$. *If the chain is extended by a force* $F_0 \sin\omega t$, *what is the probability density that the EED will be* $\boldsymbol{R}$ *at a time t? Discuss the result both for the case* $\omega \gg K_s/\zeta$ *and* $\omega \ll K_s/\zeta$.

Further Readings and References

A. Einstein, R. Fürth, *Investigation on the Brownian Motion* (Dover Publications, New York, 1956)

J. Perrin, Mouvement brownien et réalité moléculaire. Ann. Chim. Phys. 8ième série **18**, 5–114 (1909)

P. Langevin, On the Theory of Brownian Motion. C. R. Acad. Sci. Paris **146**, 530 (1908)

M. Smoluchowski, Z. kinetischen Theorie der Brownschen Molekularbewegung und der Suspensionen. Ann. Phys. **326**, 14 (1906)

H.C. Berg, E.M. Purcell, Physics of chemoreception. Biophys. J. **20**, 193 (1977)

H.C. Berg, *Random Walks in Biology* (Princeton University Press, 1983)

F.W. Wiegel, *Physical Principles in Chemoreception* (Springer, 1991)

M. Denny, S. Gaines, *Chance in Biology* (Princeton University Press, 2000)

M. Denny, *Air and Water: The Biology and Physics of Life's Media* (Princeton University Press, 1993)

D.A. Doyle, J. Morais-Cabral, R.A. Pfuetzner, A. Kuo, J.M. Gulbis, S.L. Cohen, B.T. Chait, R. MacKinnon, The structure of the potassium channel: molecular basis of K+ conduction and selectivity. Science **280**, 5360 (1998)

K. Lee, W. Sung, A stochastic model of conductance transitions in voltage-gated ion channels. J. Biol. Phys. **28**, 279–287 (2002)

J.B. Johnson, Thermal agitation of electricity in conductors. Phys. Rev. **32**, 97 (1928); H. Nyquist, Thermal agitation of electric charge in conductors. Phys. Rev. **32**, 110 (1928)

Chapter 14
Stochastic Processes, Markov Chains and Master Equations

The last chapter dealt with several basic aspects of stochastic processes through Brownian motion, which represents the oldest and the best known physical example of the Markov processes. In this chapter, we study general concepts and theoretical frameworks of Markov processes that can extend the ideas of the foregoing chapter to a variety of physical and nonphysical phenomena. The stochastic variables, denoted by $q(t)$ below, are not limited to the position and velocity of a Brownian particle as in the last chapter; they can represent the dynamical states of more complex systems such as mesoscopic conformational states of a biological molecule. For a biological complex, the Markov processes of utmost concern are mesoscopic degrees of freedom $\mathcal{Q}(t)$ that evolve under the associated effective Hamiltonian or free energy function $\mathcal{F}\{\mathcal{Q}\}$ (Chap. 5).

In this chapter and next we study the general mathematical framework of the stochastic processes without recourse to the microscopic dynamics, while giving basic introductions of joint probabilities and time correlation functions. Two particularly well-known and useful equations for the Markov processes, the master equation and the Fokker-Planck equations are derived and solved for a wide class of examples. Their relevance and applications are discussed.

14.1 Markov Processes

14.1.1 Probability Distribution Functions (PDF)

A stochastic process means a dynamic variable, say, $q(t)$, that changes probabilistically in time. Suppose that $q(t)$ has the values $q_1, q_2, q_3 \ldots$ at times $t_1, t_2, t_3 \ldots$ (Fig. 14.1). The joint (n-time, n-point) probability distribution function (PDF), denoted by $P(q_n, t_n; q_{n-1}, t_{n-1}; \ldots; q_1, t_1)$, is the probability density that the process will have the trajectory $q_1, q_2, q_3 \ldots q_n$ in a sequence of n times, $t_1 < t_2 < \ldots < t_n$ (Fig. 14.1). Such joint PDFs were already seen when we dealt with

W. Sung, *Statistical Physics for Biological Matter*, Graduate Texts in Physics,
https://doi.org/10.1007/978-94-024-1584-1_14

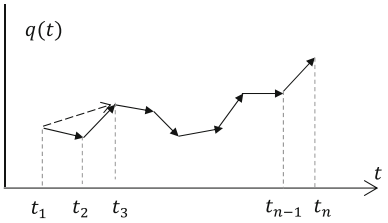

Fig. 14.1 The trajectory of a stochastic process $q(t)$ in time

fluid particles (4.2), although there different indices indicate different particles. The joint distribution has the reduction property:

$$P(q_{n-1}, t_{n-1}; \ldots; q_1, t_1) = \int dq_n \, P(q_n, t_n; q_{n-1}, t_{n-1}; \ldots; q_1, t_1), \tag{14.1}$$

which can be extended down to the one-point PDF:

$$\begin{aligned} P(q_1, t_1) &= \int dq_2 \, P(q_2, t_2; q_1, t_1) \\ &= \int dq_n dq_{n-1} \ldots dq_2 \, P(q_n, t_n; q_{n-1}, t_{n-1}; \ldots; q_1, t_1). \end{aligned} \tag{14.2}$$

Evidently, as we step down to lower point PDF, we erase the information afforded by the higher point PDF.

$P\big(q_n,t_n|q_{n-1},t_{n-1};\ldots;q_1,t_1\big)$ is the conditional probability distribution that the process will assume q_n at the time t_n, given the values $q_1, q_2, \ldots q_{n-1}$ at the earlier times $t_1, t_2, \ldots t_{n-1}$. For this we have the relation

$$P\big(q_n,t_n|q_{n-1},t_{n-1};\ldots;q_1,t_1\big) = \frac{P(q_n,t_n;q_{n-1},t_{n-1};\ldots;q_1,t_1)}{P(q_{n-1},t_{n-1};\ldots;q_1,t_1)}, \tag{14.3}$$

which is the well-known Bayes' rule. For the case of $n = 2$,

$$P\big(q_2,t_2|q_1,t_1\big) = P\big(q_2,t_2;q_1,t_1\big)/P\big(q_1,t_1\big), \tag{14.4}$$

where $P\big(q_1,t_1\big)$ and $P\big(q_2,t_2|q_1,t_1\big)$ are the PDFs (one-time PDF and the two-time transition PDF) we already saw in the last chapter.

14.1.2 Stationarity, Time Correlation, and the Wiener-Khinchin Theorem

The moments of the PDF are defined as before but are given as functions of different times, e.g., $\langle q(t)\rangle, \ldots, \langle q(t_n)\ldots q(t_2)q(t_1)\rangle$. Of particular interest is the two-time autocorrelation function (or covariance)

$$\begin{aligned} C(t_2,t_1) &= \langle q(t_2)q(t_1)\rangle \\ &= \int dq_2 dq_1\, q_2 q_1\, P\big(q_2,t_2;q_1,t_1\big). \end{aligned} \tag{14.5}$$

If the PDFs are invariant with respect to a shift by an arbitrary time s:

$$\begin{aligned} &P(q_n,t_n+s;q_{n-1},t_{n-1}+s;\ldots;q_1,t_1+s) \\ &\quad = P(q_n,t_n;q_{n-1},t_{n-1};\ldots;q_1,t_1) \end{aligned} \tag{14.6}$$

for all n, the stochastic process is called stationary. That is, **a stationary process does not depend on the origin of time**. For $n=1$, $P(q,t)=P(q)$, and the mean $\langle q(t)\rangle$ is a constant characteristic of the stationary states such as equilibrium states or steady states. For $n=2$, $P(q_2,t_2;q_1,t_1)=P(q_2,t_2-t_1;q_1,0)$, and consequently, the correlation function depends only on the time difference: $C(t_2,t_1)=C(t_2-t_1)$. The stationarity is temporal analogue of the spatial homogeneity or the translational invariance which we saw earlier for systems at equilibrium. In the Brownian motion in free space and in the absence of an external force, the velocity (the Ornstein-Uhlenbeck process) is stationary while the position (the Wiener process) is nonstationary.

Using $P(q_2,t_2;q_1,t_1)=P(q_2,t_2-t_1;q_1,0)$ for (14.4), the stationary state correlation function (14.5) is given by

$$\begin{aligned} C(t_2-t_1) &= \iint dq_2 dq_1\, q_2 q_1 P\big(q_2,t_2-t_1|q_1,0\big)P(q_1) \\ &= \int dq_1 q_1\, P(q_1) \int dq_1 q_2\, P\big(q_2,t_2-t_1|q_1,0\big). \end{aligned} \tag{14.7}$$

Here, over the ensemble compatible with the initial condition (with probability $P\big(q_2,t_2-t_1|q_1,0\big)$) we take the first average of $q_2(t)$, which is then multiplied by $q_1(0)$ and further averaged over the stationary distribution $P(q_1)$. For example, let us consider the velocity $v(t)$ of a Brownian particle prepared with the initial value v_0. The first average is $\int dv v P(v,t|v_0)=\langle v(t)\rangle_{v_0}=e^{-t/\tau_p}v_0$ (13.70), which then is multiplied by v_0 and averaged over the Maxwell-Boltzmann distribution $\Phi(v_0)$ to yield the correlation function $C(t)=\int dv_0 v_0 \Phi(v_0)e^{-t/\tau_p}v_0 = (k_BT/M)e^{-t/\tau_p}$ (13.76).

A stationary process $q(t)$ thus satisfies $C(t)=\langle q(t)q(0)\rangle=\langle q(0)q(-t)\rangle=C(-t)$, so $C(t)$ is an even function of time. The time correlation should decay to zero for an infinitely long time: $\lim_{t\to\infty}C(t)=0$. The characteristic time for the decay is called the relaxation time: for the exponentially decaying correlation function (e.g., the velocity autocorrelation function (13.76))

$$C(t) = C(0)e^{-|t|/\tau} \tag{14.8}$$

the correlation time is τ. For the case of multicomponent stationary processes, e.g., $q_A(t)$ and $q_B(t)$, for which the correlation function is

$$C_{AB}(t) = \langle q_A(t)q_B(0)\rangle, \tag{14.9}$$

we have the relation

$$C_{AB}(t) = C_{BA}(-t). \tag{14.10}$$

The averages, usually denoted by $\langle\cdots\rangle$, are taken over the ensemble of similarly prepared systems distributed by the PDF. For example, the end-to end distance (EED) $\mathcal{X}$ of a biopolymer fragment is measured. One takes the average of the EED over a large number (an ensemble) of the similar fragments, which are independent of each other but are prepared subject to a common condition. Alternatively one may also take the average only for one fragment EED over a long time T,

$$\overline{\mathcal{X}} = \left(\frac{1}{T}\right)\int_{-T/2}^{T/2} dt\ \mathcal{X}(t). \tag{14.11}$$

If the result of this time average is equal to that of the ensemble average, $\overline{\mathcal{X}} = \langle\mathcal{X}\rangle$, the system is called ergodic. The practical importance of the ergodicity is obvious. Because of the time translational invariance, stationary processes can support such ergodicity.

Consider the Fourier mode of this stationary process,

$$q(\omega) = \int_{-\infty}^{\infty} dt\, e^{i\omega t}q(t). \tag{14.12}$$

Then,

$$\begin{aligned}\langle q(\omega)q^*(\omega')\rangle &= \int_{-\infty}^{\infty} dt \int_{-\infty}^{\infty} dt' e^{i(\omega t-\omega' t')}\langle q(t)q(t')\rangle \\ &= \int_{-\infty}^{\infty} dt\, e^{i(\omega-\omega')t} \int_{-\infty}^{\infty} d(t'-t)e^{i\omega'\left(t-t'\right)}C(t-t') \\ &= 2\pi\delta(\omega-\omega')S(\omega),\end{aligned} \tag{14.13}$$

where

$$S(\omega) = \int_{-\infty}^{\infty} dt\, e^{-i\omega t}C(t), \tag{14.14}$$

and the inverse

$$C(t) = \frac{1}{2\pi} \int_{-\infty}^{\infty} d\omega\, e^{i\omega t} S(\omega) = \frac{1}{2\pi} \int_{-\infty}^{\infty} d\omega\, e^{-i\omega t} S(\omega) \tag{14.15}$$

are the Fourier transforms between the time correlation function $C(t)$, and the $S(\omega)$ called the power spectrum or spectral density of $q(t)$. The equality (14.14) holds because $C(t) = C(-t)$, which also leads to $S(\omega) = S(-\omega) = 2Re\{S(\omega)\}$. Furthermore as shown below $S(\omega)$ is positive.

How can one evaluate the power spectrum the $q(t)$ by experiment? We consider that the $q(t)$ is sampled over a long time T and approximates (14.12) by

$$q_T(\omega) = \int_{-T/2}^{T/2} dt\, e^{i\omega t} q(t). \tag{14.16}$$

Due to the stationarity, on the other hand, we have

$$\begin{aligned} \langle q(s)q(0)\rangle &= \frac{1}{T} \int_{-T/2}^{T/2} dt\ \langle q(t+s)q(t)\rangle \\ &= \left(\frac{1}{2\pi}\right)^2 \int_{-\infty}^{\infty} d\omega \int_{-\infty}^{\infty} d\omega' \langle q_T(\omega) q_T{}^*(\omega')\rangle e^{i\omega s} \frac{1}{T} \int_{-T/2}^{T/2} dt \quad e^{i(\omega-\omega')t} \\ &= \frac{1}{2\pi T} \int_{-\infty}^{\infty} d\omega\, e^{i\omega s} \left\langle |q_T(\omega)|^2 \right\rangle, \end{aligned} \tag{14.17}$$

where we used $\lim_{T\to\infty} \int_{-T/2}^{T/2} dt\, e^{i(\omega-\omega')t} = 2\pi\delta(\omega - \omega')$.

Comparison of the (14.15) with (14.17) yields

$$S(\omega) = \lim_{T\to\infty} \frac{1}{T} \left\langle |q_T(\omega)|^2 \right\rangle, \tag{14.18}$$

the so-called **the Wiener-Khinchin theorem**. **It states that, for a stationary process, the Fourier transform $S(\omega)$ of its time correlation $C(t)$ measures the intensity of fluctuations of the Fourier mode $q_T(\omega)$ taken over a long time T.** It is the temporal analogue of (9.38), which says that, for translationally invariant matter, the structure factor $S(\boldsymbol{q})$ is the Fourier transform of the spatial density correlation and its spectral density at the wave vector. We note that, if the ergodicity is further assumed, the ensemble averaging $\langle \cdots \rangle$ on RHS of (14.17) can be undone, leading to $S(\omega) = lim_{T\to\infty} |q_T(\omega)|^2/T$.

14.1.3 Markov Processes and the Chapman-Kolmogorov Equation

The Markov process is such a process that satisfies

$$P\big(q_n,t_n|q_{n-1},t_{n-1};\ldots;q_2,t_2;q_1,t_1\big)=P\big(q_n,t_n|q_{n-1},t_{n-1}\big). \tag{14.19}$$

This means that the **Markov process depends on its value only in the immediate past, but not on the values at the earlier time: it has a momentary memory**. For example, the three-time PDF $P(q_3,t_3;q_2,t_2;q_1,t_1)$, after the combined use of the above Markov definition and Bayes rule, satisfies

$$\begin{aligned} P(q_3,t_3;q_2,t_2;q_1,t_1) &\overset{Bayes}{=} P(q_3,t_3|q_2,t_2;q_1,t_1)P\big(q_2,t_2;q_1,t_1\big)\\ &\overset{Markov}{=} P\big(q_3,t_3|q_2,t_2\big)P\big(q_2,t_2;q_1,t_1\big)\\ &\overset{Bayes}{=} P\big(q_3,t_3|q_2,t_2\big)P\big(q_2,t_2|q_1,t_1\big)P\big(q_1,t_1\big), \end{aligned} \tag{14.20}$$

which can be generalized to

$$\begin{aligned} &P(q_n,t_n;q_{n-1},t_{n-1};\ldots;q_1,t_1)\\ &=P\big(q_n,t_n|q_{n-1},t_{n-1};\ldots;q_2,t_2;q_1,t_1\big)P(q_{n-1},t_{n-1};\ldots;q_2,t_2;q_1,t_1)\\ &=P(q_n,t_n|q_{n-1},t_{n-1})P(q_{n-1},t_{n-1}|q_{n-2},t_{n-2};\ldots;q_1,t_1)P\big(q_{n-2},t_{n-2};\ldots q_1,t_1\big)\\ &=P(q_n,t_n|q_{n-1},t_{n-1})P(q_{n-1},t_{n-1}|q_{n-2},t_{n-2})\ldots P(q_2,t_2|q_1,t_1)P(q_1,t_1). \end{aligned} \tag{14.21}$$

A Markov process is a chain of *elementary* Markov processes (called Markov chain) described entirely in terms of the one point PDF $P(q,t)$, and the two-time conditional PDF $P(qt|q't')$ also called a transition probability. The transition time t_i-t_{i-1} should be chosen to be sufficiently long microscopically to assure the Markov property.

In the ideal case where the all the events q_i $(i=1\ldots n)$ are statistically independent of each other, the joint PDF is factorized into the product of single time PDF:

$$P(q_n,t_n;q_{n-1},t_{n-1};\ldots;q_1,t_1)=P(q_n,t_n)P(q_{n-1},t_{n-1})\ldots P(q_1,t_1), \tag{14.22}$$

Then the conditional probability, (14.3) can be written as

$$P\big(q_n,t_n|q_{n-1},t_{n-1};\ldots;q_1,t_1\big)=P(q_n,t_n)\quad \text{for any } n\geq 2. \tag{14.23}$$

This process, called a completely random process, is a trivial case of the Markov processes.

How the transition probability is governed in any general Markovian processes is seen by (14.20) integrated over q_2: the LHS becomes $P(q_{3,}t_3;q_{1,}t_1)$, which is equal to $P(q_{3,}t_3|q_1t_1)P(q_1t_1)$, so that (14.20) is reduced to

$$P(q_3t_3|q_1t_1) = \int dq_2 P(q_3t_3|q_2t_2)P(q_2t_2|q_1t_1). \tag{14.24}$$

This relation and the identity

$$P(q_3t_3) = \int dq_1 P(q_3t_3|q_1t_1)P(q_1t_1) \tag{14.25}$$

are called the Chapman-Kolmogorov equation (CKE). The physical meaning of (14.24) is clear if one associates the processes of jump marked by the arrows as the transition probabilities (Fig. 14.1), the examples of which we already have studied in polymer path integral in Chap. 10 and the Brownian motion in the foregoing chapter.

A well-known example of the Markov processes is the Brownian motion of a particle whose mass is much heavier than that of a background fluid molecule. In the absence of an external force, its velocity change during a small time increment Δt would depend upon only its velocity at the immediate past as described by the discrete version of the Langevin equation

$$v(t+\Delta t) - v(t) = \frac{1}{M}\{-v(t)\Delta t + F_R(t)\}, \tag{14.26}$$

where $F_R(t)$ is the random force integrated over Δt. In this case the velocity is a Markov process, $q(t) = v(t)$, called the Ornstein-Uhlenbeck process. The transition probability (13.79), rewritten in the form,

$$P(q,t|q',t') = \frac{1}{2\pi(1-\gamma^2)}\exp\left[-\frac{(q-\gamma q')^2}{2(1-\gamma^2)}\right] \tag{14.27}$$

with $\gamma = e^{-|t-t'|/\tau_p}$, indeed satisfies the CKE (14.24).

The times-series of the Brownian particle positions measured over the time much longer than the velocity relaxation time $\tau_{p,}$ is also Markovian, $q(t) = x(t)$. On this coarse-gained time scale, the velocity is no longer a relevant degree of freedom as we saw in the last chapter. One can verify that the transition probably (13.7).

$$P(qt|q't') = \frac{1}{\sqrt{4\pi D(t-t')}}\exp\left[-\frac{(q-q')^2}{4D(t-t')}\right] \tag{14.28}$$

satisfies the CKE. But the position probed over the time scale shorter than τ_p would be non-Markovian since it depends on the earlier position through the velocity that has not relaxed.

P14.1 *Show that the transition probability* (13.84) *does not satisfy the CKE, meaning that* $x(t)$ *is non-Markovian.*

In the presence of an external force that depends on the position, it is clear that the velocity at a time is not Markovian, as it depends on the position which is the time integral of the velocity over earlier times. For simplicity, consider the Langevin equation for harmonic Brownian motion (13.85). The position x is also non-Markovian variable since it will depend on the earlier velocities and thus also on the earlier positions. If, however, the Langevin equation is written as the two coupled equations for x and v,

$$\frac{dx}{dt} = v, \tag{14.29}$$

$$\frac{dv}{dt} = (-\zeta v - kx + f_R)/M, \tag{14.30}$$

or, as

$$\frac{d\boldsymbol{q}}{dt} = \boldsymbol{\Lambda} \cdot \boldsymbol{q} + \boldsymbol{f_R}, \tag{14.31}$$

where $\boldsymbol{q}(t) = (x(t), v(t))^T, \boldsymbol{f_R} = (0, f_R)^T$ are the two-component variables, and

$$\boldsymbol{\Lambda} = \begin{pmatrix} 0 & 1 \\ -k/M & -\zeta/M \end{pmatrix}, \tag{14.32}$$

then, the $\boldsymbol{q}(t)$ chosen this way is Markovian, because the instantaneous (or the immediately past) value of $\boldsymbol{q}$ determines its evolution.

Whether a process is Markovian or not depends on the time scale and the choice of variable(s) for the description. The microscopic dynamics of a particle system *in phase space* (Γ) is deterministic and Markovian. As a simple case, the microscopic equation for a Brownian particle is the Newton's equation of motion under the forces acted by N fluid particles, which themselves also move following the Newton's equation. The particle motion here, as it is given by the instantaneous positions and velocities of $N + 1$ particles, is deterministic and Markovian, but is an analytically non-tractable many body problem. One naturally asks whether an effective Markov approximation can be constructed for the degrees of freedom of the Brownian particle. The Markovian motion of the Brownian particles over the long enough times we described in the last chapter serves as such an example.

In general, the many-body dynamics contracted or projected into a few degrees of freedom is naturally a non-Markovian process, described by a generalized Langevin equation involving a memory friction term. A fundamental but practical

problem in the dynamics of complex systems is how the effective Markov processes are constructed in a mesoscopic, coarse-grained level; this would be a constant concern in modeling biological dynamics.

14.2 Master Equations

14.2.1 Derivation

The master equation is essentially the CKE expressed as a differential equation of the first-order in time for the PDF of a Markov stochastic variable. To convert the integral (14.24) to a differential equation, the transition probability is expanded in a short time Δt to the first order:

$$\begin{aligned} &P(q_3, t_2 + \Delta t | q_2, t_2) \\ &\quad = \delta(q_3 - q_2)[1 - a(q_2)\Delta t] + \Delta t W(q_3|q_2) + O\Big((\Delta t)^2\Big). \end{aligned} \tag{14.33}$$

$W(q_3|q_2)$ is the rate of transition from q_2 to q_3 and $a(q_2) = \int W(q_3|q_2)dq_3$. We also used $\lim_{t' \to t} P\big(q', t' | q, t\big) = \delta(q - q')$ and $\int dq' P(q', t'|q, t) = 1$.

Substitution of (14.33) to CKE (14.24) along with the limiting procedure $\Delta t \to 0$ brings the master equation written for the transition probability $P(q, t|q_0) \equiv P\big(q, t|q_{0,} t_0 = 0\big)$:

$$\frac{\partial}{\partial t} P(q, t|q_0) = \int dq' \{W(q|q')P(q', t|q_0) - W(q'|q)P(q, t|q_0)\}. \tag{14.34}$$

The first term represents gain of the probability at q at t due to the transition into q and the second term represents the loss due to the transition out of q. The same equation is satisfied by $P(q, t)$:

$$\frac{\partial}{\partial t} P(q, t) = \int dq' \{W(q|q')P(q', t) - W(q'|q)P(q, t)\}. \tag{14.35}$$

The master equation represents the appropriate stochastic description if gain from and loss to neighboring states are specified.

If the Markov process is not continuous but assumes discrete values n, the master equation takes the form,

$$\frac{\partial}{\partial t} P(n, t|n_0) = \sum_{n'} [W_{nn'} P(n', t|n_0) - W_{n'n} P(n, t|n_0)]. \tag{14.36}$$

and

$$\frac{\partial}{\partial t}P(n,t) = \sum_{n'}[W_{nn'}P(n',t|n_0)P(n',t)) - W_{n'n}P(n,t)], \tag{14.37}$$

which we will use more often hereafter.

14.2.2 Example: Dichotomic Processes

One of the mathematically simplest master equations is for a Markov process called the **dichotomic process**, or **telegraphic process**. This process can assume two values and switches from one to the other with certain rates. As mentioned earlier, such two state situations abound in cell biology and chemical reactions. For example, an ion channel in a membrane opens and closes in a random fashion; a biopolymer undergoes transitions between two conformational states (Fig. 14.2). Denoting two states by $n = 0, 1$, the master equation for the probability reads

$$\frac{\partial}{\partial t}P(0,t) = a_1 P(1,t) - a_0 P(0,t) \tag{14.38}$$

$$\frac{\partial}{\partial t}P(1,t) = a_0 P(0,t) - a_1 P(1,t), \tag{14.39}$$

where a_0 and a_1 respectively are the transition rates from the state 0 to the state 1 and vice versa.

The equations can be solved easily for the fundamental solutions, $P(1,t|n_0)$ and $P(0,t|n_0)$ subject to the initial condition, $P(n,0|n_0) = \delta_{nn_0}$. First, from the conservation of total probability, $P(0,t) + P(1,t) = 1$, one can derive

$$P(0,t|n_0) = \frac{a_1}{a_0 + a_1} + \left(\delta_{0n_0} - \frac{a_1}{a_0 + a_1}\right)e^{-(a_0+a_1)t} \tag{14.40}$$

$$P(1,t|n_0) = \frac{a_0}{a_0 + a_1} + \left(\delta_{1n_0} - \frac{a_0}{a_0 + a_1}\right)e^{-(a_0+a_1)t}. \tag{14.41}$$

By taking the limit $t \to \infty$ in the two equations above (or by solving (14.38) and (14.39) with $\partial P(0,t)/\partial t = 0 = \partial P(1,t)/\partial t$), the stationary solutions are attained:

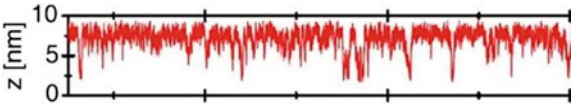

Fig. 14.2 Time-seies of RNA hairpin extension (z) showing transition between a folded state and an unfolded state (Kim et al. PNAS 2012)

$$P_s(0) = \frac{a_1}{a_0 + a_1}, \quad P_s(1) = \frac{a_0}{a_0 + a_1}. \tag{14.42}$$

The k th ($k = 1, 2\ldots$) moment at the stationary state is:

$$\langle n^k \rangle_s = \sum_{n=0,1} n^k P_s(n) = P_s(1) = \frac{a_0}{a_0 + a_1} \tag{14.43}$$

so that the variance is

$$\langle \Delta n \rangle_s^2 = \langle n^2 \rangle_s - \langle n \rangle_s^2 = a_0 a_1 / (a_0 + a_1)^2. \tag{14.44}$$

If $a_0 = a_1$, $\langle \Delta n \rangle_s^2$ amounts to 1/4.

We find the time correlation at the stationary state [the discrete version of (14.7)]:

$$\begin{aligned} \langle n(t) n(0) \rangle_s &= \sum_{n=0,1} \sum_{n_0=0,1} n\, n_0 P(n, t|n_0) P_s(n_0) = P(1, t|1) P_s(1) \\ &= \left\{ \frac{a_0}{a_0 + a_1} + \frac{a_1}{a_0 + a_1} e^{-(a_0 + a_1)t} \right\} \frac{a_0}{a_0 + a_1} \\ &= \langle n \rangle_s^2 + \langle \Delta n \rangle_s^2 \, e^{-(a_0 + a_1)t} \end{aligned} \tag{14.45}$$

or

$$\langle \Delta n(t) \Delta n(0) \rangle_s = \langle \Delta n \rangle_s^2 e^{-t/\tau}. \tag{14.46}$$

Here, $\tau = 1/(a_0 + a_1)$ is the correlation time of the dichotomic process. We can write this as $\tau^{-1} = \tau_0^{-1} + \tau_1^{-1}$ where $\tau_0 = a_0^{-1}$ and $\tau_1 = a_1^{-1}$. Although quite simple, the dichotomic process $n(t)$ can serve as a workable model for a non-equilibrium noise that, added to thermal (equilibrium) noise, drive the system away from equilibrium (as will be exemplified in Chap. 18). The dichotomic noise is a colored noise in the sense that its power spectrum is frequency-dependent. By Fourier transform, the power spectrum is given by

$$\begin{aligned} S(\omega) &= \langle \Delta n \rangle_s^2 \int_{-\infty}^{\infty} dt\, e^{i\omega t} e^{-|t|/\tau} = 2 \langle \Delta n \rangle_s^2 Re \left\{ \int_0^{\infty} dt\, e^{i\omega t} e^{-t/\tau} \right\} \\ &= 2 \langle \Delta n \rangle_s^2 \tau / \left(1 + \omega^2 \tau^2\right), \end{aligned} \tag{14.47}$$

which is in the type of the so-called Lorentzian.

P14.2 *Suppose that the current through a single ion channel is a dichotomic process undergoing close-open transitions with the rare a_0 and a_1 respectively. Only in an open state the ions can transport through a membrane with a current j. Find the total charge transported at a time t across the channel, which was initially closed.*
Sol) The charge transported is given by

$$Q(t) = j\int^t dt\ \langle n(t)\rangle = j\int^t dt\ P(1,t|0) = j\tau\tau_0^{-1}\int^t dt\ \left(1-e^{-t/\tau}\right)$$
$$= P_s(1)j\left\{t-\tau\left(1-e^{-t/\tau}\right)\right\}.$$

14.2.3 Detailed Balance

At stationary states (equilibrium or steady state), when $\frac{\partial}{\partial t}P(t)=0$, in (14.35) and (14.37), the PDF becomes $P_s(q)$ or $P_s(n)$ that is satisfied by

$$\int dq'[W(q|q')P_s(q') - W(q'|q)P_s(q)] = 0 \tag{14.48}$$

$$\sum_{n'}[W_{nn'}P_s(n') - W_{n'n}P_s(n)] = 0. \tag{14.49}$$

The stronger condition for the stationary state is **the detailed balance of the gain and the loss between two states**:

$$W(q|q')P_s(q') = W(q'|q)P_s(q) \tag{14.50}$$

$$W_{nn'}P_s(n') = W_{n'n}P_s(n). \tag{14.51}$$

For the dichotomic process (14.51) reads as $a_0\,P_s(0) = a_1P_s(1)$, which is satisfied by (14.42).

It is worth mentioning that the atomic transition described by the Schrödinger equation is also Markovian. For example, n and n' can represent quantum states, between which the rate of transition under a time dependent perturbing Hamiltonian $\mathcal{H}'$ is given by the Fermi's golden rule:

$$W_{nn'} = \frac{2\pi}{\hbar}|\langle n|\mathcal{H}'|n'\rangle|^2 w(E_{n'}), \tag{14.52}$$

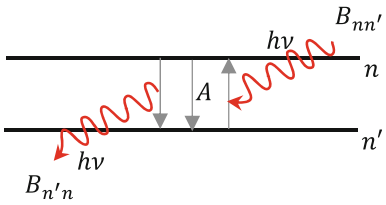

Fig. 14.3 The transition between two atomic states n and n' in the presence of thermal radiation. A is the rate of spontaneous emission of radiation, $B_{nn'}$ and $B_{n'n}$ represent transitions induced by the absorption and emission of photons

where $w(E_{n'})$ is the density of states with the energy $E_{n'}$. One interesting example of the detailed balance is shown in the transition between two atomic states induced by radiation at thermal equilibrium (Fig. 14.3). In 1917, much earlier than the development of the relevant quantum theory, using this idea Einstein found that the spontaneous emission of radiation of a frequency from an atom occurs with a rate which, is related to the rate of stimulated emission as below.

Einstein assumed that the rate of emission process due to transition from the energy level n to $n'(<n)$ is given by

$$W_{n'n} = A + B_{n'n}\rho(\nu). \tag{14.53}$$

Here, the first term is the rate of spontaneous emission, which is a constant and the second is the rate of the emission induced by the radiation at a frequency $\nu = (E_n - E_{n'})/h$ with energy density $\rho(\nu)$. On the other hand there is absorption of the radiation from n' to $n(>n')$ with the rate:

$$W_{nn'} = B_{nn'}\rho(\nu). \tag{14.54}$$

We now use the detailed balance (14.51) between the two transitions, along with the Boltzmann distribution for the energy state of the atom, $P_n^{eq} \propto w_n e^{-\beta E_n}$, where w_n is multiplicity or degeneracy. Noting that $B_{nn'}w_{n'} = B_{n'n}w_n$, one can find

$$\rho(\nu) = \frac{A/B}{e^{\beta h\nu} - 1}, \tag{14.55}$$

where $B = B_{n'n}$. The formula (14.55) is just the celebrated Planck formula for the energy density of thermal radiation, with A/B given by

$$\frac{A}{B} = \frac{8\pi h\nu^3}{c^3}. \tag{14.56}$$

In fact, the Einstein coefficients A and B for the spontaneous and induced emissions are intrinsic properties of atoms, so the relation (14.56) holds true whether the system is in thermal equilibrium or not.

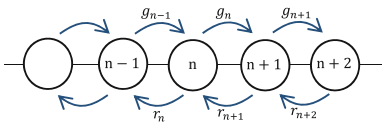

Fig. 14.4 One step Markov process in which the number n changes by unity with generation rate g_n and reduction rate r_n

14.2.4 One-Step Master Equations

One important example of Markov processes is one step processes that involve the transitions between only two adjacent states (Fig. 14.4). Here we consider discrete states, with the n indicating unbounded integers. Generalization of the results to continuum cases is straightforward. The master equation (14.37) (with simplification of the notation, $\partial P(n,t)/\partial t \equiv \dot{P}_n(t)$) is given by

$$\begin{aligned}\dot{P}_n(t) &= W_{nn+1}P_{n+1}(t) + W_{nn-1}P_{n-1}(t) - W_{n+1n}P_n(t) - W_{n-1n}P_n(t)\\ &= r_{n+1}P_{n+1} + g_{n-1}P_{n-1} - (g_n + r_n)P_n.\end{aligned} \tag{14.57}$$

Here $r_n = W_{n-1,n}$ and $g_n = W_{n+1,n}$ are respectively the rates, i.e., the probabilities per unit time, for jump processes $n \to n-1$ (reduction) and $n \to n+1$ (generation). The one-step processes abound in nature; physical processes such as the adsorption and emission of quanta we exemplified, surface growth, adsorption and desorption of molecules on substrates, and nonphysical processes such as birth and death of individuals, growth of population, etc.

Random Walk

The cases in which the reduction and generation rates r_n, g_n are constants are analytically solvable. One of the simplest is the case when $r_n = g_n = \lambda$, for which the master equation reads

$$\dot{P}_n = \lambda(P_{n+1} + P_{n-1} - 2P_n). \tag{14.58}$$

This equation, upon integration over a (short) jump time $\tau = (2\lambda)^{-1}$, transforms to a difference equation

$$P_n(t+\tau) = \frac{1}{2}P_{n+1}(t) + \frac{1}{2}P_{n-1}(t), \tag{14.59}$$

which describes the one dimensional random walk. Given the initial condition $P_n(t=0) = \delta_{n0}$, iteration of the above relation by N times, leads to

$$P_n(N\tau) = \left(\frac{1}{2}\right)^N N!\left[\left(\frac{N-n}{2}\right)!\left(\frac{N+n}{2}\right)!\right]^{-1}, \tag{14.60}$$

which is the well-known binomial distribution.

In the limit $N \to \infty$ and $n \to \infty$ with $t = N\tau$ and $x = nl$ fixed as finite, where l is the length of unit step, (14.60) becomes

$$P(x,t) = (4\pi Dt)^{-1/2}\exp\left[-\frac{x^2}{4Dt}\right], \tag{14.61}$$

and $D = l^2/2\tau$ is the diffusion constant. Alternatively, the solution (14.61) can be directly obtained from the continuum limit of (14.58), the diffusion equation, $\dot{P}_n = \lambda\left(\partial P_n^2\right)/\partial n^2$.

Poisson Process

The Poisson process is a particular case of the one-step processes (14.57), in which $r_n = 0, g_n = \lambda$; the number n increases by unity randomly with an average rate λ (Fig. 14.5). Such simple processes abound in enormous variety, ranging from photons' arrival at a retina to customers' visit at a shop. It is governed by the master equation

$$\dot{P}_n = \lambda(P_{n-1} - P_n). \tag{14.62}$$

In order to solve it, we introduce the generating function,

$$G(s,t) = \langle s^n \rangle = \sum_{n=0} s^n P_n(t), \tag{14.63}$$

in terms of which (14.62) is written as

$$\begin{aligned} \dot{G}(s,t) &= \sum_n s^n \dot{P}_n(t) = \sum_n s^n \lambda(P_{n-1} - P_n) \\ &= \lambda s \sum_n s^{n-1} P_{n-1}(t) - \lambda \sum_n s^n P_n(t) \\ &= \lambda(s-1)G(k,t), \end{aligned} \tag{14.64}$$

where we used the BC $P_{-1}(t) = 0$. Using the initial condition $P_n(0) = \delta_{n0}$, or $G(s,0) = 1$ yields

$$G(s,t) = \exp\{\lambda t(s-1)\}, \tag{14.65}$$

which is expanded in powers of s and compared with (14.63), to give the PDF:

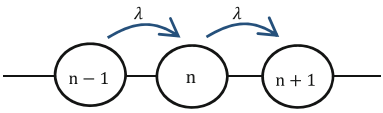

Fig. 14.5 Poisson process is a one step process in which the number only increases by unity

$$P_n(t) = \frac{e^{-\lambda t}(\lambda t)^n}{n!}. \tag{14.66}$$

This is called the Poisson distribution. Using the generating function one can easily obtain

$$\langle n(t)\rangle = \sum_{n=0}^{\infty} nP_n(t) = \frac{\partial}{\partial \mathrm{s}} G(s,t)|_{\mathrm{s}=1} = \lambda t \tag{14.67}$$

and

$$\langle n(t)(n(t)-1)\rangle = \left.\frac{\partial^2 G(s,t)}{\partial \mathrm{s}^2}\right|_{\mathrm{s}=1} = (\lambda t)^2, \tag{14.68}$$

from which the variance is given by

$$\bar{\Delta} n^2(t) = \left\langle n^2(t)\right\rangle - \langle n(t)\rangle^2 = \lambda t, \tag{14.69}$$

The interesting fact that the variance equals the mean can be a characteristic test for the distribution to be a Poissonian.

The Poisson distribution of n given its average $\langle n\rangle$ is thus expressed as

$$P_n = \frac{e^{-\langle n\rangle}}{n!}\langle n\rangle^n. \tag{14.70}$$

Figure 14.6 depicts the Poisson distribution with varying $\langle n\rangle = \lambda t$. As time goes on the probability distribution diffuses around the peak that also grows with time. The probability of $n = 0$ is simply $P_0 = e^{-\langle n\rangle} = e^{-\lambda t}$.

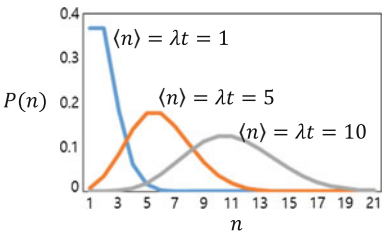

Fig. 14.6 Poisson distribution for various values of $\langle n\rangle = \lambda t$.

The Poisson distribution is applied to rare events. For instance, when the light falls on the retina of an eye, only a few of rhodopsin proteins in photoreceptor cells can absorb the photons; the absorption of each photon is a rare event with a very small probability, say, p. The probability that n photons out of N incoming photons will be absorbed is the binomial distribution,

$$P_n = \frac{N!}{(N-n)!n!} p^n (1-p)^{N-n}. \tag{14.71}$$

Considering that $n \ll N$, and $p \ll 1$, one can show that P_n reduces to the Poissonian, (14.70).

P14.3 *Verify the above statement.*

The Poisson process can be used to model a wide variety of rare random events, e.g., the sampling of bacteria in a given volume, the populations of plants and animals in a restricted space, the number of victims of specific diseases, the number of words misspelled in a text, etc.

P14.4 *Use the Poisson process to model the number of car accidents at an intersection. Given that the average accident rate is 1 per day, (a) what is the probability that no accidents occur in an hour? (b) What is the probability that two or more accidents occur in two hours*?

Linear One-Step Master Equation

The transition rates r_n, g_n can be linear functions of n in a multitude of natural processes. For example, decays and reactions, birth-death processes (in population and cell dynamics) can be modeled by $r_n = \gamma n, g_n = bn + \lambda$ where γ, b, and λ are the death, birth, and migration rates respectively. More broad classes of the linear processes are chemical and biological reactions that can be very complex involving many species of reactants and products. $P_n(t)$ for these linear cases is solvable using the generating function method.

Often it suffices to study several moments of $P_n(t)$. As the simplest case, we first consider the decay process of certain molecules, in which $g_n = 0$ and $r_n = \gamma n$. The master equation then is

$$\dot{P}_n(t) = \gamma(n+1)P_{n+1}(t) - \gamma n P_n(t). \tag{14.72}$$

We consider the average number of the molecules, that is, the first moment $\langle n(t)\rangle = \sum_{n=0}^{\infty} nP_n(t)$, which is governed by

$$\begin{aligned}\sum_{n=0}^{\infty} n\dot{P}_n &= \gamma \sum_{n=0}^{\infty} n(n+1)P_{n+1} - \gamma \sum_{n=0}^{\infty} n^2 P_n \\ &= \gamma \sum_{n=0}^{\infty} (n-1)nP_n - \gamma \sum_{n=0}^{\infty} n^2 P_n \\ &= -\gamma \sum_{n=0}^{\infty} nP_n\end{aligned} \tag{14.73}$$

so that we recover the phenomenological equation

$$\frac{d\langle n\rangle}{dt} = -\gamma\langle n\rangle \tag{14.74}$$

with the solution

$$\langle n(t)\rangle = n_0\, e^{-\gamma t}, \tag{14.75}$$

where n_0 is the initial number.

P14.5 *Find* $\bar{\Delta}n(t) = \left\{\langle n^2(t)\rangle - \langle n(t)\rangle^2\right\}^{1/2}$. *What is its maximum and at what time does it reach the maximum*?

Reactions

Consider a simple reaction where a certain collection of cells with a number n is annihilated with a rate γn and is created at a constant rate λ. The phenomenological equation for the number is obtained:

$$\frac{d\langle n(t)\rangle}{dt} = -\gamma\langle n(t)\rangle + \lambda, \tag{14.76}$$

the solution of which is

$$\langle n(t)\rangle = (n_0 - n_\infty)e^{-\gamma t} + n_\infty, \tag{14.77}$$

where $n_\infty = \lambda/\gamma$ is the number of the cells at $t = \infty$, and n_0 is the initial number.

To understand the fluctuation phenomenon that underlies this deterministic law we study the corresponding master equation ($r_n = \gamma n, g_n = \lambda$)

$$\frac{\partial}{\partial t}P_n(t) = \gamma(n+1)P_{n+1} + \lambda P_{n-1} - (\gamma n + \lambda)P_n. \tag{14.78}$$

Unlike the free diffusion and the Poisson process, for this case, the stationary solution exists, when $\gamma(n+1)P_{n+1} + \lambda P_{n-1} - (\gamma n + \lambda)P_n = 0$, or

$$(n+1)P_{n+1} - n_\infty P_n = nP_n - n_\infty P_{n-1}. \tag{14.79}$$

Since both sides of the above equation must hold for all n, they must be equal to a same constant, which can be shown to be zero to satisfy normalizability, $\sum_{n=0}^{\infty} P_n = 1$. Therefore, by iterations,

$$P_n = \frac{n_\infty}{n} P_{n-1} = \frac{n_\infty^2}{n(n-1)} P_{n-2} \cdots = \frac{n_\infty^n}{n!} P_0, \tag{14.80}$$

where $P_0 = e^{-n_\infty}$ from the normalization. The stationary solution (14.80) is then identified as the Poisson distribution with the stationary mean n_∞,

$$P_n = e^{-n_\infty} \frac{{n_\infty}^n}{n!}. \tag{14.81}$$

The equations for the moments at time t are obtained by multiplying n^l ($l =$ integer) on both sides of (14.78) and summing up over n. For $l = 1$, we recover the phenomenological (14.76). For $l = 2$,

$$\frac{d}{dt}\langle n(t)\{n(t)-1\}\rangle = 2\lambda\langle n(t)\rangle - \gamma\langle n(t)\{n(t)-1\}\rangle, \tag{14.82}$$

[Gardiner (1985)]. Via the Laplace transform we integrate the above equation for $\langle n(t)\{n(t)-1\}\rangle$ as

$$\langle n(t)\{n(t)-1\}\rangle = 2\lambda \int_0^t ds\, e^{-\gamma(t-s)}\langle n(s)\rangle + e^{-\gamma t} n_0\{n_0 - 1\} \tag{14.83}$$

and use (14.76) to find the variance:

$$\left(\bar{\Delta} n(t)\right)^2 = (n_0 e^{-\gamma t} + n_\infty)(1 - e^{-\gamma t}). \tag{14.84}$$

The fluctuation $\bar{\Delta} n(t)$ approaches $n_\infty^{1/2}$ in the long time and is not entirely negligible compared with n_∞ unless this is very large. Figure 14.7 shows a simulation of the stochastic dynamics of $n(t)$ as a function of time, which indeed confirms the analytical features studied above—steady growth of cell population with fluctuations, depending on the number of the cells, which approaches the Poission distribution.

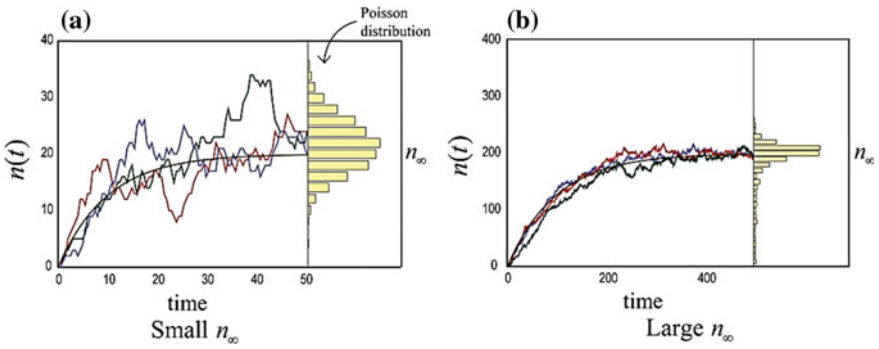

Fig. 14.7 Stochastic trajectories that underlie the phenomenological reaction equation $\langle n(t)\rangle = (1-e^{-\gamma t})n_\infty$ (14.77 with $n_0 = 0$, solid smooth line). In a long time, n approaches the stationary value n_∞, which is distributed in Poissonian. The fluctuations around the phenomenological law are larger for smaller n_∞. (Courtesy of J. Sung's lab, ChungAng University)

To solve for $P_n(t)$ we consider the generating function

$$G(s,t) = \sum_{n=0} s^n P_n(t) \tag{14.85}$$

so that

$$\frac{\partial G(s,t)}{\partial t} = \lambda(s-1)G(s,t) - \gamma(s-1)\frac{\partial G(s,t)}{\partial s}. \tag{14.86}$$

The solution to the equation given the initial condition $P_n(0) = \delta_{nn_0}$ is (Gardiner 1985)

$$G(s,t) = \exp\left[\frac{\lambda}{\gamma}(s-1)(1-e^{-\gamma t})\right][1+(s-1)e^{-\gamma t}]^{n_0}. \tag{14.87}$$

This can be expanded in power of s to give $P_n(t)$, which has a complicated expression. The stationary state for a long time can be read off (by taking $t \to \infty$ limit) from (14.87) as

$$G(s,\infty) = \exp\left[\frac{\lambda}{\gamma}(s-1)\right], \tag{14.88}$$

which tells us that the stationary solution $P_n(\infty)$ is the Poisson distribution with the mean $\langle n\rangle = \lambda/\gamma = n_\infty$. The first and second order derivatives of generating function with respect to s readily generate the first moment and variance, which we have seen above.

P14.6 *The bubbles, the locally melted domain in ds DNA, occur in the AT region of N base-pairs. The number of bubbles with n base-pairs, b_n, is governed by a master equation $\dot{b}_n = k_+ b_{n-1} - (k_+ + k_-)b_n + k_- b_{n+1}$. What are the meaning of k_+ and k_-? Solve the master equation and find the total number of the bubbles as a function of time, given an initial condition $b_n(0) = ae^{-\beta\epsilon n}$, where ϵ is the base pairing energy, and the boundary conditions are $b_0(t) = b_N(t) = 0$* [Altan-Bonnet and Libchaber (2003)].

Further Reading and References

N.G. Van Kampen, *Stochastic Processes in Physics and Chemistry*, 2nd edn. (Elsevier, North Holland, 2003)
W. Gardiner, *Handbook of Stochastic Methods*, 2nd edn. (Springer, 1985)
D.T. Gillespie, *Markov Processes* (Academic Press, 1992)
R. Kubo, M. Toda, N. Hashitsume, *Statistical Physics II*, 2nd edn. (Springer, 2003)
R. Zwanzig, *Nonequilibrium Statistical Machanics* (Oxford University Press, 2001)
G. Altan-Bonnet, A. Libchaber, Phys. Rev. Lett. **90** (2003)

Chapter 15
Theory of Markov Processes and the Fokker-Planck Equations

15.1 Fokker-Planck Equation (FPE)

The Fokker Planck equation (FPE), a special type of master equation, is a partial differential equation for time evolution of the PDF that describes Markov processes. **A FPE is obtained from a Markov process when the two lowest moments of the jump characteristic of the drift and the fluctuation are given**. The diffusion equation and the Smoluchowski equation for Brownian motion we studied fall into this category.

15.1.1 Derivation

The FPE of a certain Markov process q is in the form

$$\frac{\partial P(q,t)}{\partial t} = \left[-\frac{\partial}{\partial q}a_1(q) + \frac{\partial^2}{\partial q^2}a_2(q)\right]P(q,t). \tag{15.1}$$

To derive it with defining formulae for $a_1(q)$ and $a_2(q)$, we consider the CKE (14.25) for the process of jumping from $q-\Delta q$ at time t to q at time $t+\Delta t$:

$$\begin{aligned} P(q,t+\Delta t) &= \int d(\Delta q)P(q,t+\Delta t|q-\Delta q,t)P(q-\Delta q,t) \\ &= \int d(\Delta q)P(q+\Delta q\underline{-\Delta q},t+\Delta t|q\underline{-\Delta q},t)P\Big(q\underline{-\Delta q},t\Big). \end{aligned} \tag{15.2}$$

W. Sung, *Statistical Physics for Biological Matter*, Graduate Texts in Physics,
https://doi.org/10.1007/978-94-024-1584-1_15

The jump steps Δt, Δq are large enough microscopically to assure the Markovian approximation, yet small in the phenomenological scale of interest, so we expand the LHS in Δt and the integrand in $-\Delta q$ [underlined in (15.2)]:

$$\begin{aligned} &P(q,t)+\Delta t\frac{\partial}{\partial t}P(q,t) \\ &\quad=\int d(\Delta q)\sum_{l=0}^{\infty}\frac{1}{l!}(-\Delta q)^l\frac{\partial^l}{\partial q^l}\{P(q+\Delta q,t+\Delta t|q,t)P(q,t)\}. \end{aligned} \tag{15.3}$$

Since $\int d\{\Delta q\}P(q+\Delta q,t+\Delta t|q,t)=1$, the first leading terms in LHS and RHS cancel each other, leading to a partial differential equation

$$\frac{\partial}{\partial t}P(q,t)=\sum_{l=1}^{\infty}\frac{(-1)^l}{l!}\frac{\partial^l}{\partial q^l}[a_l(q)P(q,t)], \tag{15.4}$$

where

$$\begin{aligned} a_l(q)&=\frac{1}{\Delta t}\int d\Delta q(\Delta q)^l P(q+\Delta q,t+\Delta t|q,t) \\ &=\frac{1}{\Delta t}\langle\Delta q^l\rangle_q \end{aligned} \tag{15.5}$$

with Δt taken to be infinitesimally small. Equation (15.4) is called the Kramers-Moyal expansion. $\langle\Delta q^l\rangle_q$ is the l th order moment of the jump Δq from the given state q at time t.

Of our outmost interest is the FPE (15.1) that incorporates only two leading orders in the expansion; the first and second moments of the jump $a_1(q)=\langle\Delta q\rangle_q/\Delta t$, and $a_2(q)=\langle(\Delta q)^2\rangle_q/\Delta t$. The FPE's particular merit is that these moments can be drawn from phenomenology or experimental data, as follows.

The equation can be extended to the multidimensional or multicomponent cases, $q=\{q^i\}=(q^1,q^2,q^3,\ldots)$:

$$\frac{\partial P(\{q^i\},t)}{\partial t}=\left[-\sum_k\frac{\partial}{\partial q^k}\frac{\langle\Delta q^k\rangle_{\{q^i\}}}{\Delta t}+\frac{1}{2}\sum_k\sum_l\frac{\partial^2}{\partial q^k\partial q^l}\langle\Delta q^k\Delta q^l\rangle_{\{q^i\}}\right]P(\{q^i\},t). \tag{15.6}$$

In this case $\langle\Delta q^k\rangle_{\{q^i\}}$ and $\langle\Delta q^k\Delta q^l\rangle_{\{q^i\}}$ are the moments and correlation with $\{q^i\}$ given. For illustration two-variable Brownian motion is worked out explicitly below.

15.1.2 The FPE for Brownian Motion

We show below how the FPE is obtained by the first and second moments $a_1(q)$ and $a_2(q)$, from the Langevin equations. The primary example is the Brownian motion, where q is x, the one dimensional position of the Brownian particle. In the presence of an external force $F(x)$, the overdamped Langevin equation reads

$$\zeta \dot{x} = F(x) + f_R(t) \tag{15.7}$$

which is integrated over the time Δt:

$$\Delta x = \frac{F(x)}{\zeta}\Delta t + \frac{1}{\zeta}\int_t^{t+\Delta t} f_R(t')dt'. \tag{15.8}$$

Since $\langle f_R(t)\rangle = 0, \langle \Delta x\rangle_x = F(x)\Delta t/\zeta$, we have

$$\frac{\langle \Delta x\rangle_x}{\Delta t} = \frac{F(x)}{\zeta} = a_1(x), \tag{15.9}$$

and

$$\begin{aligned}\frac{\langle \Delta x^2\rangle_x}{\Delta t} &= \frac{(F(x)\Delta t)^2}{\zeta^2 \Delta t} + \frac{1}{\zeta^2\Delta t}\int_t^{t+\Delta t}\int_t^{t+\Delta t}\langle f_R(t')f_R(t'')\rangle dt'dt'' \\ &= O(\Delta t) + \frac{1}{\zeta^2\Delta t}\int_t^{t+\Delta t}\int_t^{t+\Delta t} 2\zeta k_B T\delta(t'-t'')dt'dt'',\end{aligned} \tag{15.10}$$

where the first term, being in the first order in Δt, is negligible, and the second, upon integration, with the Einstein relation $D = k_B T/\zeta$, yields

$$\frac{\langle \Delta x^2\rangle_x}{\Delta t} = 2D = a_2(x). \tag{15.11}$$

Substituting a_1 and a_2 into (15.1)

$$\begin{aligned}\frac{\partial P(x,t)}{\partial t} &= -\frac{\partial}{\partial x}\frac{F(x)}{\zeta}P(x,t) + \frac{\partial^2}{\partial x^2}DP(x,t) \\ &= D\frac{\partial}{\partial x}\left(\beta\frac{\partial U(x)}{\partial x} + \frac{\partial}{\partial x}\right)P(x,t),\end{aligned} \tag{15.12}$$

Then the FPE that results is just the Smoluchowski equation we studied.

Now let us study the case of two-component variable, $q = (q^1, q^2) = (x, v)$, whose Markovian equations of motion are

$$M\frac{dv}{dt} = -\zeta v + F(x) + f_R(t),$$
$$\frac{dx}{dt} = v.$$

Integrating the above equations over Δt and one finds that the first and second order moments with x, v given simultaneously are

$$\frac{\langle \Delta v \rangle_{x,v}}{\Delta t} = -\frac{\zeta}{M}v + \frac{F(x)}{M}, \tag{15.13}$$

$$\frac{\langle \Delta x \rangle_{x,v}}{\Delta t} = v, \tag{15.14}$$

$$\frac{\langle \Delta x^2 \rangle_{x,v}}{\Delta t} = v^2 \Delta t \sim O(\Delta t), \tag{15.15}$$

$$\frac{\langle \Delta x \Delta v \rangle_{x,v}}{\Delta t} = \left[-\frac{\zeta}{M}v + F(x)\right] v\Delta t \sim O(\Delta t), \tag{15.16}$$

$$\frac{\langle \Delta v^2 \rangle_{x,v}}{\Delta t} = \frac{2\zeta k_B T}{M} \tag{15.17}$$

Neglecting the terms of the linear order in Δt, $O(\Delta t)$, in the above, and substituting the results into (15.6) with two variables $q^1 = x, q^2 = v$ yields the FPE:

$$\frac{\partial P(x, v; t)}{\partial t} + v\frac{\partial P}{\partial x} + \frac{F(x)}{M}\frac{\partial P}{\partial v} = \frac{\zeta}{M}\left[\frac{\partial}{\partial v}vP + \frac{k_B T}{M}\frac{\partial^2 P}{\partial v^2}\right], \tag{15.18}$$

which is expressed in three dimension:

$$\frac{\partial P(\boldsymbol{r}, v; t)}{\partial t} + v \cdot \nabla P + \frac{\boldsymbol{F}(\boldsymbol{r})}{M} \cdot \nabla_v P = \frac{\zeta}{M}\left[\nabla_v \cdot v + \frac{k_B T}{M}\nabla_v^2\right] P. \tag{15.19}$$

This equation, first derived by Kramers, describes the evolution of the Brownian particle in its phase space.

P15.1 *Consider a two-variable Markov process written as the coupled Langevin equations*:

$$\Gamma_1 \frac{dx_1}{dt} = -k(x_1 - x_2) - \frac{\partial U(x_1)}{\partial x_1} + \xi_1(t)$$
$$\Gamma_2 \frac{dx_2}{dt} = -k(x_2 - x_1) + \xi_2(t),$$

where $\xi_i(t)$ *are Gaussian and white noises satisfying*

$$\left\langle \xi_i(t)\xi_j(0) \right\rangle = 2\Gamma_i k_B T \delta(t)\delta_{ij}.$$

Construct the corresponding Fokker-Planck equation for $P(x_1, x_2, t)$*. Find its stationary solution,* $P_s(x_2, x_1)$*, and associated probability densities,* $P_s(x_1), P_s(x_2/x_1)$*.*

15.2 The Langevin and Fokker-Planck Equations from Phenomenology and Effective Hamiltonian

The examples shown above demonstrate how one can construct the FPE for Brownian particle motion from the two lowest order moments of jump given by the Langevin equation. Then we pose a question: how can one construct the Langevin/Fokker-Planck dynamics from phenomenology and data, and the associated effective Hamiltonian or free energy?

Suppose that we have information of a certain stochastic variable $q(t)$, from which a model Langevin equation is constricted as

$$\dot{q} = \mathcal{U}(q) + R(q, t), \tag{15.20}$$

where $R(q, t)$ is an underlying noise that, first of all, satisfies $\langle R(q, t) \rangle = 0$. It also varies much faster than $q(t)$. We may approximate it as a white and Gaussian noise with the strength $\mathcal{D}(q)$:

$$\langle R(q, t)R(q, t') \rangle = 2\mathcal{D}(q)\delta(t - t'). \tag{15.21}$$

From the Langevin equatuion for $q(t)$ (15.20) with this noise, the two moments of the jump during the time Δt are given as

$$\langle \Delta q \rangle_q / \Delta t = \mathcal{U}(q), \tag{15.22}$$

$$\left\langle (\Delta q)^2 \right\rangle_q / \Delta t = 2\mathcal{D}(q). \tag{15.23}$$

For a Brownian particle with $q = x$, $\mathcal{U}(q)$ is the drift velocity, $\mathcal{D}(q)$ is the diffusivity. **$\mathcal{U}(q)$ and $\mathcal{D}(q)$ respectively characterize the external driving and the internal fluctuations, which can be derived from the phenomenology and data**. Substituting these formulae into (15.1) yields the FPE:

$$\frac{\partial P(q,t)}{\partial t} = \left[-\frac{\partial}{\partial q}\mathcal{U}(q) + \frac{\partial^2}{\partial q^2}\mathcal{D}(q) \right] P(q,t). \tag{15.24}$$

The FPE can be recast as a continuity equation,

$$\frac{\partial P(q,t)}{\partial t} + \frac{\partial J(q,t)}{\partial q} = 0, \tag{15.25}$$

where

$$J(q,t) = \mathcal{U}(q)P(q,t) - \frac{\partial}{\partial q}[\mathcal{D}(q)P(q,t)] \tag{15.26}$$

is the probability current. When J is uniform, $\partial J(q,t)/\partial q = 0$, the system attains a stationary state: equilibrium state if J is zero and steady state if it is nonzero constant. The equilibrium distribution, if it exists, is obtained by integrating (15.26) with $J = 0$ as

$$P(q) \propto \mathcal{D}^{-1}(q) \exp\left[\int^q dq' \, \frac{\mathcal{U}(q')}{\mathcal{D}(q')} \right]. \tag{15.27}$$

Thus, by finding this distribution by experimental data, one may also identify the drift $\mathcal{U}(q)$ and noise strength $\mathcal{D}(q)$. By putting the distribution to be of the Boltzmann type $P(q) \sim \exp[-\Phi(q)]$, $\Phi(q)$ is identified as

$$\Phi(q) = \ln \mathcal{D}(q) - \int^q dq' \, \frac{\mathcal{U}(q')}{\mathcal{D}(q')} \tag{15.28}$$

apart from a certain constant. $\Phi(q)$ corresponds to the dimensionless free energy of the stochastic process.

From now on we consider the case where $\mathcal{D}(q)$ is a constant $\mathcal{D}$ so that

$$-\frac{\partial \Phi(q)}{\partial q} = \frac{\mathcal{U}(q)}{\mathcal{D}}. \tag{15.29}$$

This means that the drift is driven by the gradient of a potential or free energy. For a Brownian particle with $q = x$, the Fokker-Planck equation is the Smoluchowski equation with the potential $U(x) = k_B T \Phi(q)$ and diffusivity $D = \mathcal{D}$. For the

stochastic dynamics for a degree of freedom $\mathcal{Q}$, representative of a certain mesoscopic state in a complex systems, e.g., conformation of biopolymers, $\Phi(\mathcal{Q}) = \beta\mathcal{F}(\mathcal{Q})$ where $\mathcal{F}(\mathcal{Q})$ is the free energy function or effective Hamiltonian associated with the $\mathcal{Q}$, which was discussed in Chap. 5. The Langevin equation for this case can be written as,

$$\dot{Q} = -\beta\mathcal{D}\frac{\partial}{\partial Q}\mathcal{F}(Q) + R(Q,t) \tag{15.30}$$

or

$$\zeta\dot{Q} = -\frac{\partial}{\partial Q}\mathcal{F}(Q) + f_R(Q,t), \tag{15.31}$$

where $\zeta = k_BT/\mathcal{D}$ is the effective friction coefficient, and $f_R(Q,t) = \zeta R(Q,t) = R(Q,t)/\beta\mathcal{D}$, is a Gaussian and white noise satisfying

$$\langle f_R(Q,t)f_R(Q,t')\rangle = 2k_BT\zeta\delta(t-t'). \tag{15.32}$$

P15.2 *In nature there are a number of events with the distributions following* power-laws. *Examples are distributions of income (Paretos law) and certain cell sizes, the percentage of authors publishing n papers (Lotka's law), and the frequency of the appearance of English words (Zipf's law). As a model of the power law distributions, consider a stochastic differential equation*

$$\frac{d}{dt}n(t) = -\gamma n(t) + n(t)\xi(t),$$

where $\xi(t)$ *is a white and Gaussian noise of strength* $\mathcal{D}$:

$$\langle\xi(t)\xi(0)\rangle = 2\mathcal{D}\delta(t-t').$$

Construct the FPE and find the stationary solution in which J = 0.

15.2.1 FPE from One-Step Master Equation

The master equation even with linear one step coefficients r_n and g_n are not easy to solve analytically as we have seen; furthermore they are in general nonlinear in many situations. For the case in which r_n and g_n vary slowly with n, so they can be expanded in n to the second order, we convert the master equation to a FPE. This is a great advantage because of the analytical facility of FPE, which will be further studied in next chapter. Treating n as continuous, the master equation (14.78), is rewritten as,

$$\frac{\partial}{\partial t}P(n,t) = r(n+1)P(n+1,t) + g(n-1)P(n-1,t) - (g(n)+r(n))P(n,t). \tag{15.33}$$

Expanding the function $f(n \pm 1)$ as $f(n) \pm f'(n) + \frac{1}{2}f''(n)$ the above can be written as a FPE:

$$\frac{\partial}{\partial t}P(n,t) = -\frac{\partial}{\partial n}[g(n) - r(n)]P(n,t) + \frac{1}{2}\frac{\partial}{\partial n^2}[g(n) + r(n)]P(n,t). \tag{15.34}$$

The stationary solution $P_s(n)$ satisfies $-(g-r)P_s = (\partial(g+r)P_s)/2\partial n$, which can be integrated to

$$P_s(n) = Ce^{-\Phi(n)}, \tag{15.35}$$

where

$$\Phi(n) = \ln\{g(n) + r(n)\} - 2\int^n dn' \frac{g(n') - r(n')}{g(n') + r(n')}. \tag{15.36}$$

$\Phi(n)$ can be called the free energy of the process. The phenomenological equation associated with the FPE is

$$\frac{d\langle n\rangle}{dt} = -\langle r(n)\rangle + \langle g(n)\rangle. \tag{15.37}$$

Interesting enough, the process is an overdamped dynamics under a driving force and a fluctuation given by $g(n) - r(n)$, $g(n) + r(n)$, respectively.

The stationary value of n_s is determined by the relation

$$r(n_s) = g(n_s). \tag{15.38}$$

For a small fluctuation x around the stationary value, $x = n - n_s$, (15.34) reads:

$$\frac{\partial}{\partial t}P(x,t) = \left[r'(n_s) - g'(n_s)\right]\frac{\partial}{\partial x}xP(x,t) + \frac{1}{2}\left[g(n_s) + r(n_s)\right]\frac{\partial}{\partial x^2}P(x,t). \tag{15.39}$$

Provided that $r'(n_s) - g'(n_s) > 0$, this is FPE for an overdamped harmonic Brownian motion (Ornstein-Uhlenbeck process) around a stationary state, whose solution was given in the last chapter.

P15.3 *What is the Langevin equation corresponding to* (15.39). *Explicitly find the solution and* $\left(\bar{\Delta}n(t)\right)^2$.

15.3 Solutions of Fokker-Planck Equations, Transition Probabilities and Correlation Functions

The Fokker Planck equation (FPE) is most appropriate for stochastic description for a Markov process $q(t)$, if the first and second moments $\mathcal{U}(q)$ and $\mathcal{D}(q)$ of the unit jump can be identified. As we saw, the FPE can be solved exactly for the case of linear systems, where the drift is $\mathcal{U}(q) = aq + b$ and the noise strength is constant, $\mathcal{D}(q) = \mathcal{D}$. Because of its wide applicability, in this chapter we deal with the analytical methods of solving the FPE for more general cases of the drift, focusing on the eigenfunction expansion method, and use the method to find the transition probability and time correlation functions of the process. This section is quite mathematical and formal; for impatient readers, most of the subsections except the last one can be skipped.

15.3.1 Operators Associated with FPE

The Fokker-Planck Equation (FPE) is written as for the PDF $P(q,t)$

$$\frac{\partial P(q,t)}{\partial t} = \mathcal{L}_{FP}P(q,t) = -\frac{\partial}{\partial q}J(q,t), \tag{15.40}$$

where

$$\mathcal{L}_{FP} \equiv -\frac{\partial}{\partial q}\mathcal{U}(q) + \frac{\partial^2}{\partial q^2}\mathcal{D}(q) \tag{15.41}$$

and

$$J(q,t) = \mathcal{U}(q)P(q,t) - \frac{\partial}{\partial q}\mathcal{D}(q)P(q,t) \tag{15.42}$$

are the Fokker-Planck operator and the probability current respectively. The stationary solution in which $J = 0$ is $P_{eq}(q) \sim \exp[-\Phi(q)]$. $\Phi(q)$ is given by (15.28), from which, we can derive

$$\mathcal{U}(q) = e^{\Phi}\frac{\partial}{\partial q}\{\mathcal{D}(q)e^{-\Phi}\}, \tag{15.43}$$

leading to the alternative expressions of J and $\mathcal{L}_{FP}$ in terms of Φ:

$$J(q,t) = -\mathcal{D}(q)e^{-\Phi(q)}\frac{\partial}{\partial q}e^{\Phi(q)}P(q,t), \tag{15.44}$$

$$\mathcal{L}_{FP} = \frac{\partial}{\partial q}\mathcal{D}(q)e^{-\Phi(q)}\frac{\partial}{\partial q}e^{\Phi(q)}. \tag{15.45}$$

P15.4 *Derive* (15.44) and (15.45).

The backward FP operator ${\mathcal{L}_{FP}}^{\dagger}$ is defined as below:

$$\int p_1(q)\mathcal{L}_{FP}(q)p_2(q)dq = \int \left({\mathcal{L}_{FP}}^{\dagger}p_1\right)p_2 dq \tag{15.46}$$

for two square-integrable functions $p_1(q)$ and $p_2(q)$. Then by integrating by parts, one can show:

$${\mathcal{L}_{FP}}^{\dagger} = e^{\Phi}\frac{\partial}{\partial q}\mathcal{D}(q)e^{-\Phi}\frac{\partial}{\partial q} = \mathcal{U}(q)\frac{\partial}{\partial q} + \mathcal{D}(q)\frac{\partial^2}{\partial q^2}. \tag{15.47}$$

The operator $\mathcal{L}_{FP}$ is not Hermitian (self-adjoint) due to the inequality in the relation below:

$$\int p_1(q)\mathcal{L}_{FP}p_2(q)dq = \int \left({\mathcal{L}_{FP}}^{\dagger}p_1\right)p_2 dq \neq \int p_2\mathcal{L}_{FP}p_1 dq. \tag{15.48}$$

As can be proved, the operator $\mathcal{L}_s \equiv e^{\Phi/2}\mathcal{L}_{FP}e^{-\Phi/2}$, however, is a Hermitian, and is expressed as.

$$\mathcal{L}_s = e^{\Phi(q)/2}\frac{\partial}{\partial q}\mathcal{D}(q)e^{-\Phi(q)}\frac{\partial}{\partial q}e^{\Phi(q)/2}. \tag{15.49}$$

15.3.2 Eigenfunction Method

One can mathematically transform the FPE with $\mathcal{D}(q)$ to that with constant $\mathcal{D}$ (Risken 1989). Hereafter in this section we consider the case of constant $\mathcal{D}$ without loss of generality. The FP operator and current are then written as

$$\mathcal{L}_{FP} \equiv -\frac{\partial}{\partial q}\mathcal{U}(q) + \mathcal{D}\frac{\partial^2}{\partial q^2} = \mathcal{D}\frac{\partial}{\partial q}e^{-\Phi}\frac{\partial}{\partial q}e^{\Phi}, \tag{15.50}$$

$$J(q,t) = \mathcal{U}(q)P(q,t) - \mathcal{D}\frac{\partial P(q,t)}{\partial q} = -\mathcal{D}e^{-\Phi(q)}\frac{\partial}{\partial q}e^{\Phi(q)}P(q,t), \tag{15.51}$$

where $\mathcal{U}(q) = -\mathcal{D}\partial\Phi(q)/\partial q$.

The Hermitian operator $\mathcal{L}_s$ (15.49) can be expressed as

$$\mathcal{L}_s = \mathcal{D}e^{\Phi/2}\frac{\partial}{\partial q}e^{-\Phi}\frac{\partial}{\partial q}e^{\Phi/2} = \mathcal{D}\frac{\partial^2}{\partial q^2} - V_s(q) \tag{15.52}$$

with

$$V_s(q) = \mathcal{D}\left[\frac{1}{4}\left(\frac{\partial\Phi}{\partial q}\right)^2 - \frac{1}{2}\frac{\partial^2\Phi}{\partial q^2}\right] = \mathcal{D}e^{\Phi/2}\frac{\partial^2}{\partial q^2}e^{-\Phi/2}. \tag{15.53}$$

A new function

$$\Psi(q,t) = e^{\Phi/2}P(q,t) \tag{15.54}$$

is shown to satisfy

$$\frac{\partial\Psi}{\partial t} = \mathcal{L}_s\Psi. \tag{15.55}$$

We note that $-\mathcal{L}_s$ looks like the Hamiltonian with a 'potential' $V_s(q)$ in the Schrödinger equation. In finding the solution of FPE, thus, we can exploit a variety of the familiar methods of solving the Schrödinger equation.

Let ψ_n be eigenfunctions of the $-\mathcal{L}_s$ with the eigenvalues λ_n,

$$\mathcal{L}_s\psi_n = -\lambda_n\psi_n \tag{15.56}$$

that form a complete, orthonormal basis. In order to explicitly express the eigenfunctions, we express $\mathcal{L}_s$ in an alternative form:

$$\mathcal{L}_s = -\mathcal{D}a^{\dagger}a, \tag{15.57}$$

where

$$a = e^{-\Phi/2}\frac{\partial}{\partial q}e^{\Phi/2} \tag{15.58}$$

$$a^{\dagger} = -e^{\Phi/2}\frac{\partial}{\partial q}e^{-\Phi/2} \tag{15.59}$$

are adjoints of each other. Using these operators, we can see that the eigenvalue of $\mathcal{L}_s$ is given by

$$\lambda_n = -\int \psi_n \mathcal{L}_s \psi_n dq = \mathcal{D}\int \psi_n a^{\dagger} a \psi_n dq = \mathcal{D}\int (a\psi_n)^2 dq. \tag{15.60}$$

The last equality above tells us that the λ_n can never be negative.

Now from the relation

$$\mathcal{L}_s \psi_n = e^{\Phi/2}\mathcal{L}_{FP}e^{-\Phi/2}\psi_n = -\lambda_n \psi_n, \tag{15.61}$$

the eigenfunctions φ_n of the FP operator can be identified as

$$\mathcal{L}_{FP}\varphi_n = -\lambda_n \varphi_n, \tag{15.62}$$

where

$$\varphi_n = e^{-\Phi/2}\psi_n \tag{15.63}$$

has the eigenvalue $-\lambda_n$. The eigenfunction coressponding to stationary solution of the FPE, $\mathcal{L}_{FP}\varphi_n = \dot{\varphi}_n = 0$ is that of the ground state

$$\varphi_0 = e^{-\Phi/2}\psi_0 = A^{1/2}e^{-\Phi}, \tag{15.64}$$

with zero eigenvalue, $\lambda_0 = 0$, where $A^{1/2}$ is a normalization constant. It follows that

$$\psi_0(q) = A^{1/2}e^{-\Phi/2}. \tag{15.65}$$

The above result is also obtained from (15.60).

$$a\psi_0(q) = e^{-\Phi/2}\frac{\partial}{\partial q}e^{\Phi/2}\psi_0(q) = 0, \tag{15.66}$$

The solution of the FPE with Φ can be readily given from its equivalent Schrödinger-like equation with V_s, for which the methods of the exact and approximate solutions are well established. Equation (15.64), rewritten as

$$\Phi(q) = -2\ln\,\psi_0(q) + \ln A \tag{15.67}$$

suggests that once the $\psi_0(q)$ is prescribed for the Schrödinger-like equation one can model $\Phi(q)$, with which the FPE is to be solved. For illustration, consider an infinite square-well potential Fig. 15.1 (a),

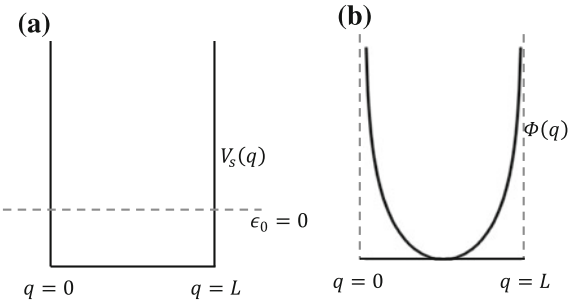

Fig. 15.1 **a** The infinite square-well potential $V_s(q)$ for the Schrödinger problem. The dashed line indicates its ground state, zero eigenvalue. **b** The corresponding potential $\Phi(q)$ for the FP problem

$$\begin{aligned} V_s(q) &= -V_0 \quad \text{for } 0<q<L, \\ &= \infty \quad \text{otherwise.} \end{aligned} \tag{15.68}$$

The eigenfunctions and eigenvalues of the Schrödinger-like equation $\mathcal{L}_s\psi_n = \{-(\mathcal{D}\partial^2)/\partial q^2 + V_s(q)\}\psi_n = \lambda_n\psi_n$ are

$$\psi_n(q) = (2/L)^{1/2}\sin\{(n+1)\pi q/L\} \tag{15.69}$$

and

$$\lambda_n = \mathcal{D}((n+1)\pi/L)^2 - V_0 = \mathcal{D}n((n+2)\pi/L)^2 \tag{15.70}$$

respectively. $V_0 = \mathcal{D}(\pi/L)^2$ is determined to render the eigenvalue $\lambda_0 = 0$.

Equation (15.67) leads to the FP potential

$$\Phi(q) = -2\ln\,\sin(\pi q/L) \tag{15.71}$$

apart from a constant. This nonharmonic potential, depicted by Fig. 15.1b, provides an exactly solvable monostable, nonlinear (force) model for the FPE. The eigen-functions and eigenvalues of the FP operator then are

$$\varphi_n(q) = e^{-\Phi/2}\psi_n = (2/L)^{1/2}\sin(\pi q/L)\,\sin\{(n+1)\pi q/L\}. \tag{15.72}$$

The ground state eigen-function

$$\varphi_0(q) = (2/L)^{1/2}\sin^2(\pi q/L) \tag{15.73}$$

yields the stationary distribution $P_{eq}(q) \sim e^{-\Phi(q)} \sim \psi_0^2(q)$ that the Brownian particle will attain in the potential $\Phi(q)$ (Fig. 15.1b).

In Chap. 10, we already have encountered the Schrödinger-like equation, called the Edwards equation, for the spatial distribution of the terminal (Nth) segment in a flexible polymer. The analogy described above tells us that as the N elapses, the

segment of a long polymer-chain confined within an infinite square-well is distributed as if it is a Brownian particle running in time N under $\Phi(q)$.

P15.5 *Find the eigenfunctions and eigenvalues of FPE for* $n = 0$ *and* 1 *for a Brownian paricle harmonically bound with* $\Phi = \frac{1}{2}\Omega q^2$.

15.3.3 The Transition Probability

The key information of the Markov process lies in the transition probabilty, which is the fundamental solution to FPE with $P(q, 0|q_0) = \delta(q - q_0)$. It is obtained by integrating the Eq. (15.40):

$$P(q, t|q_0) = e^{t\mathcal{L}_{FP}} P(q, 0|q_0) = e^{t\mathcal{L}_{FP}} \delta(q - q_0). \tag{15.74}$$

With the delta-function expanded in eigenfunctions of $\mathcal{L}_{FP}$, we have:

$$\begin{aligned} \delta(q - q_0) &= \sum_n \psi_n(q)\psi_n(q_0) \\ &= \exp\left[\frac{1}{2}\{\Phi(q) + \Phi(q_0)\}\right] \sum_n \varphi_n(q)\varphi_n(q_0) \\ &= e^{\Phi(q)} \sum_n \varphi_n(q)\varphi_n(q_0) \\ &= e^{\Phi(q_0)} \sum_n \varphi_n(q)\varphi_n(q_0), \end{aligned} \tag{15.75}$$

where the relation (15.63) is used. Then (15.74) is expressed as

$$\begin{aligned} P(q, t|q_0) &= e^{\Phi(q_0)} \sum_n e^{t\mathcal{L}_{FP}(q)} \varphi_n(q)\varphi_n(q_0) = e^{\Phi(q_0)} \sum_n e^{-\lambda_n t} \varphi_n(q)\varphi_n(q_0) \\ &= \exp\left[\frac{1}{2}\{\Phi(q_0) - \Phi(q)\}\right] \sum_n e^{-\lambda_n t} \psi_n(q)\psi_n(q_0) \\ &= \sum_n \psi_0(q)\psi_n(q) \frac{\psi_n(q_0)}{\psi_0(q_0)} e^{-\lambda_n t}. \end{aligned} \tag{15.76}$$

Equation (15.76) evidently shows that as time goes on, all the excited states ($n \geq 1$) that encompass the initial states decay, giving way to the ground state with zero eigenvalue, which survives to bring the system eventually to the equilibrium sate:

$$P(q,t|q_0) \to \psi_0^2(q) = Ae^{-\Phi(q)} = P_{eq}(q). \tag{15.77}$$

If the stationary state does not exist, the ground state would have a nonzero eigenvalue, the probability will decay to zero in a long time. Whether the state remains to be stationary or not depends on the BC imposed in addition to the natural BC allowed by $\Phi(q)$. This will be discussed later.

15.3.4 Time-Correlation Function

We study the stationary time correlation function formally defined by (14.7) rewritten as

$$\langle q(t)q(0)\rangle_s = \int dq \int dq_0 \; qq_0 \; P(qt|q_0)P_s(q_0), \tag{15.78}$$

where $P_s(q)$ is the stationary state distribution, which, for equilibrium, is $P_{eq}(q) = \psi_0(q)^2$. Substituting this and (15.76) to the above, we find that

$$\begin{aligned} \langle q(t)q(0)\rangle_{eq} &= \sum_{n=0} e^{-\lambda_n t}\left[\int dqq\psi_0(q)\psi_n(q)\right]^2 \\ &= \sum_{n=0} e^{-\lambda_n t}\langle 0|q|n\rangle^2, \end{aligned} \tag{15.79}$$

where we introduced the bracket notation, $\langle m|q|n\rangle \equiv \int dq\psi_m(q)q\psi_n(q)$. In order to appreciate the meaning of above, we first consider the short and long time limits:

(i) $t \to 0$

$$\begin{aligned} \langle q(0)q(0)\rangle_{eq} &= \sum_n \langle 0|q|n\rangle\langle n|q|0\rangle \\ &= \langle 0|q^2|0\rangle = \langle q^2\rangle_{eq}, \end{aligned} \tag{15.80}$$

where the completeness of the eigen-basis $\sum_n |n\rangle\langle n| = 1$ is used.

(ii) $t \to \infty$

$$\langle q(\infty)q(0)\rangle_{eq} = \langle 0|q|0\rangle^2 = \langle q\rangle_{eq}^2. \tag{15.81}$$

Then, the time correlation function is finally expressed as

$$\begin{aligned}\langle \Delta q(t)\Delta q(0)\rangle_{eq} &= \langle q(t)q(0)\rangle_{eq} - \langle q\rangle_{eq}^2 \\ &= \sum_{n=1} e^{-\lambda_n t}\langle 0|q|n\rangle^2 \\ &= e^{-\lambda_1 t}\langle 0|q|1\rangle^2 + e^{-\lambda_2 t}\langle 0|q|2\rangle^2 + \cdots,\end{aligned} \tag{15.82}$$

which shows how the correlation decays to zero from the maximum (static) value at $t = 0$.

P15.6 *Calculate the correlation function* (15.79) *including first two terms above For* $\Phi = \frac{1}{2}\Omega q^2$. *Compare this in a long time with the exact result shown earlier.*

15.3.5 The Boundary Conditions

Because the FPE is a second order partial differential equation, its solutions requires two boundary conditions (BC). In most of cases, there are two types, absorbing BC, $P(q_A, t) = 0$ and reflecting BC, $J(q_R, t) = 0$. At the absorbing boundary $q = q_A$ the probability is annihilated, whereas at the reflecting boundary $q = q_R$ the probability is conserved.

For an example of the foregoing formulation along with boundary conditions, consider a B motion in a semi-harmonic potential $U = \frac{1}{2}kx^2$ with an infinite wall at $x = 0$ (Fig. 15.2a). The FPE is

$$\begin{aligned}\frac{\partial P(x,t)}{\partial t} &= \mathcal{L}_{FP}P(x,t) \\ &= \mathcal{D}\frac{\partial}{\partial x}\left(\beta\frac{\partial U}{\partial x} + \frac{\partial}{\partial x}\right)P(x,t) \\ &= \mathcal{D}\frac{\partial}{\partial x}\left(\beta kx + \frac{\partial}{\partial x}\right)P(x,t).\end{aligned} \tag{15.83}$$

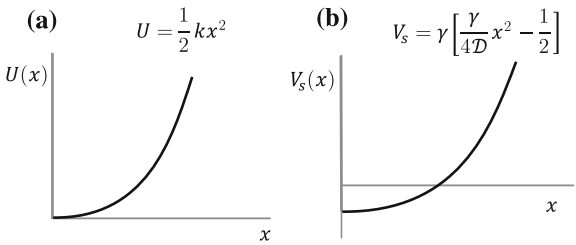

Fig. 15.2 **a** The potential $U(x)$ for a FP problem. **b** The potential $V_s(x)$ for the related Schrödinger problem

The associated Schrödinger-type equation is

$$\frac{\partial}{\partial t}\Psi(x,t) = \mathcal{L}_s\Psi(x,t) = \left[-\mathcal{D}\frac{\partial}{\partial x^2} + V_s(x)\right]\Psi(x,t) \tag{15.84}$$

with

$$\begin{aligned} V_s(x) &= \mathcal{D}\left[\frac{1}{4}\left(\frac{\partial(\beta U)}{\partial x}\right)^2 - \frac{1}{2}\frac{\partial^2\beta U}{\partial x^2}\right] \\ &= \mathcal{D}\left[\frac{1}{4}\beta^2k^2x^2 - \frac{1}{2}\beta k\right] \\ &= \gamma\left[\frac{\gamma}{4\mathcal{D}}x^2 - \frac{1}{2}\right], \end{aligned} \tag{15.85}$$

where $\gamma = \mathcal{D}\beta k$. The transformed potential V_s is also harmonic (Fig. 15.2b), so that the eigenfunctions of the Schrödinger-type equation are identified as

$$\psi_0(\xi) = \left(\frac{\gamma}{2\pi\mathcal{D}}\right)^{1/4} e^{-\xi^2/2} \tag{15.86}$$

$$\psi_n(\xi) = \left(\frac{\gamma}{2\pi\mathcal{D}}\right)^{1/4} \frac{1}{\sqrt{2^n n!}} H_n(\xi) e^{-\xi^2/2}, \tag{15.87}$$

where $H_n(\xi)$ is the Hermite polynomial with argument $\xi = (\gamma/2\mathcal{D})^{1/2}q$.

Now we note the presence of reflecting BC at $x = \infty, J = -(\beta kx + \partial/\partial x)$ $P(x,t) = -(\beta kx + \partial/\partial x)\exp(-\beta U(x)/2)\Psi(x,t) = 0$, which is given by the system. The other BC is the imposed one at $x = 0$. If the imposed BC is reflecting one, $\partial P(x,t)/\partial x$ or $\partial \Psi(x,t)/\partial x$ are zero at $x = 0$, so that only even integers n (symmetric eigenfunctions) including $n = 0$ are included in the transition probability and time correlation. In the long times $n = 0$ state with zero eigenvalue persists giving stationary distribution $P_{eq}(x) = \psi_0(x)^2$. If the absorbing boundary condition, $P(x,t) = 0$ or $\Psi(x,t) = e^{\beta kx^2/4}P(x,t) = 0$ at $x = 0$ is adopted, only odd integers n (antisymmetric eigenfunction) are allowed, so the probability that the B particle survives in the well decays zero at long times.

P15.7 *Find the transition probability $P(qt|q_0)$ of a Brownian particle moving under the semi-harmonic potential above.*

15.3.6 The Symmetric Double Well Model

The Kramers-type, symmetric and bistable model (Fig. 15.3) for $\Phi(q)$ in the FP operator (15.45) is a typical model to describe two-state transitions represented by

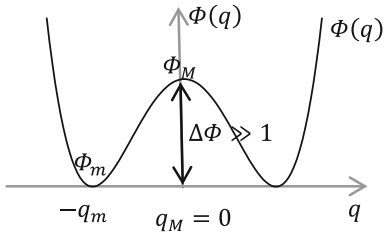

Fig. 15.3 Double well potential for the FP problem. The q_m and q_M are the values of q where the potential is at minimum (Φ_m) and maximum (Φ_m). The barrier height $\Delta\Phi$ is much larger than 1

two minima and an activation barrier between them, as will be studied closely in next chapter. Induced by a noise, the dynamical state $q(t)$ can hop from one well to the other. We will consider the case of a constant $\mathcal{D}(q) = \mathcal{D}$. The correlation function $\langle \Delta q(t) \Delta q(0) \rangle$, (15.82), is dominated by the eigenstate $\varphi_1(q)$ with the smallest nonzeo eigenvalue λ_1 of the FP operator. In the following, we evaluate the eigenvalue and then the correlation function.

The eigenvalue equation

$$\mathcal{L}_{FP}\varphi_1 = \mathcal{D}\frac{\partial}{\partial q}e^{-\Phi}\frac{\partial}{\partial q}e^{\Phi}\varphi_1 = -\lambda_1\varphi_1 \tag{15.88}$$

is equal to $-\partial J/\partial q$, where J, the current associated with the state φ_1, is obtained as

$$J(q) = -\mathcal{D}e^{-\Phi(q)}\frac{\partial}{\partial q}e^{\Phi(q)}\varphi_1(q) = \int_{-\infty}^{q} dq'\lambda_1\varphi_1(q'), \tag{15.89}$$

using the reflecting BC $J(-\infty) = 0$. Rearranging the above as

$$\frac{\partial}{\partial q}e^{\Phi(q)}\varphi_1(q) = -\frac{\lambda_1}{\mathcal{D}}e^{\Phi(q)}\int_{-\infty}^{q} dq'\varphi_1(q'), \tag{15.90}$$

which is further integrated from $-\infty$ to q to give

$$\begin{aligned}\varphi_1(q) = e^{-\Phi(q)}\Big[&e^{\Phi(-\infty)}\varphi_1(-\infty) \\ &-\frac{\lambda_1}{\mathcal{D}}\int_{-\infty}^{q} dq''e^{\Phi(q'')}\int_{-\infty}^{q''} dq'\varphi_1(q')\Big].\end{aligned} \tag{15.91}$$

We consider the case with $\lambda_1/D \ll 1$, which is consistent with the case of a high activation barrier we will study. Thus we can use the zeroth order approximation to (15.91)

$$\varphi_1(q) \sim e^{-\Phi(q)}e^{\Phi(-\infty)}\varphi_1(-\infty) \tag{15.92}$$

to find its first order approximation by substituting it into the second term in (15.91):

$$\varphi_1(q) \approx e^{-\Phi(q)} e^{\Phi(-\infty)} \varphi_1(-\infty) \left[1 - \frac{\lambda_1}{\mathcal{D}} \int_{-\infty}^{q} dq'' e^{\Phi(q'')} \int_{-\infty}^{q''} dq' e^{-\Phi(q')} \right]. \quad (15.93)$$

Due to the symmetry of the potential, the first excited state $\varphi_1(q)$ is an odd function of q : $\varphi_1(q = 0) = 0$. Henceforth we have

$$\lambda_1 \approx \mathcal{D} \left[\int_{-\infty}^{0} dq'' e^{\Phi(q'')} \int_{-\infty}^{q''} dq' e^{-\Phi(q')} \right]^{-1}. \quad (15.94)$$

Both of the eigenfunction and eigenvalue are expressed by the integrals above, which in general are hard to calculate in useful analytical forms. For the barrier height $\Delta\Phi = \Phi_M - \Phi_m$ much larger than unity, one can evaluate the integrals in (15.94) analytically, by expanding each integrand about its peak, which is very sharp: for the left integrand, by expanding Φ about its central maximum point $(0, \Phi_M)$, $\Phi(q'') = \Phi_M - \Omega_M^2 q''^2/2 + \cdots$, and for the right integrand about the left minimum point $(-q_m, \Phi_m)$, $\Phi(q') = \Phi_m + \Omega_m^2 (q' + q_m)^2/2 + \cdots$. For the right integral we can make an approximation,

$$\begin{aligned} \int_{-\infty}^{q''} dq' e^{-\Phi(q')} &\cong \int_{-\infty}^{q''} dq' \exp[-\Phi_m] \exp\left[-\frac{1}{2} \Omega_m^2 (q' + q_m)^2 \right] \\ &\cong \exp[-\Phi_m] \int_{-\infty}^{\infty} dq \ \exp\left[-\frac{1}{2} \Omega_m^2 q^2 \right] = \exp[-\Phi_m] \left(\frac{2\pi}{\Omega_m^2} \right)^{1/2}. \end{aligned} \quad (15.95)$$

The left integral then is

$$\begin{aligned} \int_{-\infty}^{0} dq'' e^{\Phi(q'')} &\cong \int_{-\infty}^{0} dq'' \exp[\Phi_M] \exp\left[-\frac{1}{2} \Omega_M^2 q''^2 \right] \\ &= \frac{1}{2} \exp[\Phi_M] \left(\frac{2\pi}{\Omega_M^2} \right)^{1/2} \end{aligned} \quad (15.96)$$

Then (15.94) yields the eigenvalue

$$\lambda_1 \approx \frac{\mathcal{D}}{\pi} \Omega_M \Omega_m e^{-\Delta\Phi}, \quad (15.97)$$

which is consistent with our initial assumption of small $\lambda_1/\mathcal{D}$. We shall see in next chapter that λ_1 is twice the mean rate of the dynamical state crossing over the barrier. For a Brownian particle subject to a friction ζ and energy barrier ΔU, we have

$$\lambda_1 \approx \frac{1}{\pi\zeta}\omega_m\omega_M\, e^{-\frac{\Delta U}{k_B T}} \tag{15.98}$$

where ω_m, ω_M are the curvature parameters of the potential at the minimum and maximum, $\omega_m^2 = U''(x_m)$, $\omega_M^2 = U''(x_M)$.

The time correlation function (15.82) is then given by

$$\langle \Delta q(t)\Delta q(0)\rangle \approx \langle 1|q|0\rangle^2 e^{-\lambda_1 t}. \tag{15.99}$$

As one may check, the next eigenstate φ_2 is widely separated from φ_1 with its eigenvalue $\lambda_2 \gg \lambda_1 \approx 0$, so its contribution to the correlation function is negligible over the correlation time λ_1^{-1}, which is the longest time scale. A better alternative to the above approximation is

$$\langle \Delta q(t)\Delta q(0)\rangle \approx \left\langle (\Delta q)^2 \right\rangle e^{-\lambda_1 t}, \tag{15.100}$$

which is exact at $t = 0$. The above expression, typical of two state transitions, is similar to the correlation function of the dichotomic process (14.46), but here the information on the relaxation time is given by the activation barrier (15.97).

P15.8 *For the bistable potential in FPE shown in the figure below, calculate λ_1 by solving the corresponding Schrödinger equation. Use the variational method.*

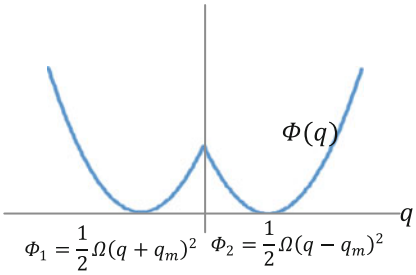

Further Reading and References

N.G. Van Kampen, *Stochastic Processes in Physics and Chemistry*, 2nd edn. (Elsevier, North Holland, 2003)

C.W. Gardiner, *Handbook of Stochastic Methods for Physics, Chemistry and the Natural Sciences*, 2nd edn. (Springer, 1985)

H. Risken, *The Fokker-Planck Equation: Methods of Solution and Applications*, 2nd edn. (Springer, Berlin, Heidelberg, New York, 1989)
W. Ebeling, I.M. Sokolov, *Statistical Thermodynamics and Stochastic Theory of Nonequilibrium Systems* (World Scientific Publishing Co. Pte. Ltd., 1992)
D.T. Gillespie, *Markov Processes: An Introduction for Physical Scientists* (Academic Press, San Diego, 1992)
R. Kubo, M. Toda, N. Hashitsume, *Statistical Physics II, Nonequilibrium Statistical Mechanics*, 2nd edn. (Springer, Berlin, Heidelberg, 1991)
R. Zwanzig, *Nonequilibrium Statistical Machanics* (Oxford University Press, Oxford, 2001)

Chapter 16
The Mean-First Passage Times and Barrier Crossing Rates

16.1 First Passage Time and Applications

The first passage time (FPT) is the duration that a stochastic variable takes to approach a given threshold for the first time: for example, the duration for a random walker shown in Fig. 16.1a to reach the cliff for the first time. The first passage time problem is important in an enormous variety of situations, to name a few, transport, reaction and targeting processes. In particular, it is of paramount importance in chemistry and biology where the rates of chemical reactions or conformational transitions are basic.

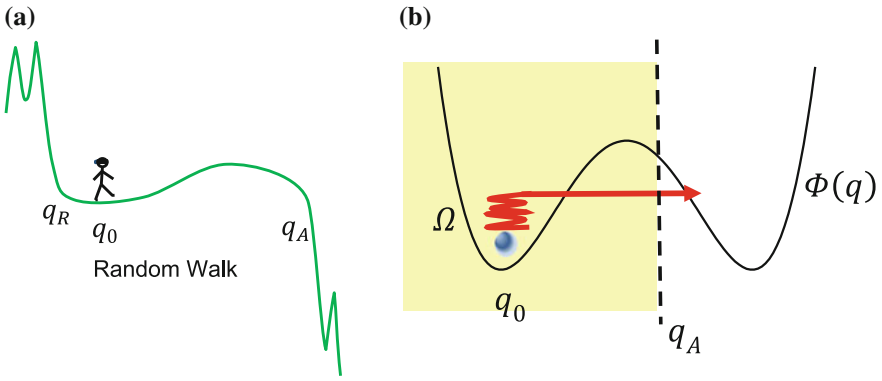

Fig. 16.1 **a** Random walk in the region Ω between a reflecting (q_R) and a absorbing (q_A) boundary, **b** a noise-induced escape of a dynamical state from the region Ω. q_0 is the initial state

W. Sung, *Statistical Physics for Biological Matter*, Graduate Texts in Physics,
https://doi.org/10.1007/978-94-024-1584-1_16

16.1.1 The Distribution and Mean of Passage Time

Suppose that a certain stochastic variable q, given its initial value $q_{0,}$ evolves in time, governed by the equation, $\partial P(q,t|q_0)/\partial t = \mathcal{L}(q)P(q,t|q_0)$ where $\mathcal{L}$ is the evolution operator for the probability. We consider that whenever a stochastic trajectory $q(t)$ crosses the threshold q_A, it is removed, which is implemented by imposing an absorbing BC, $P(q_{A,},t) = 0$. To find the mean first passage time (MFPT), we first seek the probability that the random walker survives at a time t, in a region Ω bounded by the absorbing boundary q_A:

$$\wp(t,q_0) = \int_{\Omega} dq\, P(q,t|q_0). \tag{16.1}$$

Note that $-\{\partial\wp(t,q_0)/\partial t\}dt = \wp(t,q_0) - \wp(t+dt,q_0)$ is the probability that the random walker survives during dt (the probability of the initial point q_0 that has not escaped the region before the time t but has escaped during the time interval dt). Consequently

$$W(t,q_0) = -\frac{d}{dt}\wp(t,q_0) \tag{16.2}$$

is **the FPT distribution or density**. Then **the MFPT of the process given the initial value q_0** is

$$\tau(q_0) = \int_0^{\infty} dt\, t\left(-\frac{d\wp(t,q_0)}{dt}\right) = \int_0^{\infty} \wp(t,q_0)dt, \tag{16.3}$$

where an integration is performed by parts assuming $\wp(t,q_0)$ tends to be zero faster than t^{-1} as t goes to infinity. Such fast decay can be attained due to the absorbing BC $P(q_{A,},t) = 0$ on a boundary of the region Ω. Then, (16.3) is given by:

$$\tau(q_0) = \int_0^{\infty} dt \int_{\Omega} dq\, P(q,t|q_0). \tag{16.4}$$

P16.1 *Consider that a ligand diffuses in a half space $x > 0$ until it is absorbed on the (y,z) plane located at $x = 0$. Find the lifetime distribution of the ligand initially positioned at x_0.*

P16.2 *Find the distribution and mean of the transition time from state 0 to 1 in the dichotomic process given by* (14.38), (14.39).
(Sol) By considering the absorbing boundary at $n = 1, P(1,t) = 0$, (14.38) *becomes $\partial P(0,t)/\partial t = -a_0 P(0,t)$, the solution of which with the initial condition $P(0,0) = 1$ is $P(0,t|0) = e^{-a_0 t}$, which is $\wp(t,0)$, the mean survival probability. The FPT distribution is $-(d\wp(t,0))/dt = a_0 e^{-a_0 t}$ and MFPT is $\tau(0) = \int_0^{\infty} \wp(t,0)dt = a_0^{-1} = \tau_0$. Because the transition occurs instantaneously the MFT is the mean residence time in the state 0.*

In case the transition probability $P(q,t|q_0)$ is not obtainable, we can have more direct access to MFPT. We first rewrite (16.4) as

$$\tau(q_0) = \int_0^\infty dt \int_\Omega dq\, e^{t\mathcal{L}(q)}\delta(q-q_0), \tag{16.5}$$

On both sides of the above, we apply the operator $\mathcal{L}^+$, the adjoint of $\mathcal{L}$, and perform transposition and integration in the RHS:

$$\begin{aligned}\mathcal{L}^+(q_0)\tau(q_0) &= \int_0^\infty dt \int_\Omega dq\, e^{t\mathcal{L}(q)}\mathcal{L}^+(q_0)\delta(q-q_0)\\ &= \int_0^\infty dt \int_\Omega dq\, \mathcal{L}(q)e^{t\mathcal{L}(q)}\delta(q-q_0) = \int_0^\infty dt \int_\Omega dq\, \frac{\partial P(qt;q_0)}{\partial t}\\ &= \int_\Omega dq[P(q,\infty|q_0) - \delta(q-q_0)]\end{aligned} \tag{16.6}$$

Because $P(q,\infty|q_0) = 0$, the above equation leads to a differential equation for the MFPT $\tau(q_0)$:

$$\mathcal{L}^+(q_0)\tau(q_0) = -1. \tag{16.7}$$

The above formula tells us that the MFPT is given directly from the knowledge of the operator $\mathcal{L}^+$. This can be applied to any Markov processes with an absorbing boundary, including the cases with the discrete master equations for which $\mathcal{L}^+$ are appropriately given (Reichl 2016). Below we will treat the Fokker-Planck dynamics with the evolution operator, $\mathcal{L} = \mathcal{L}_{FP}$ with its adjoint $\mathcal{L}_{FP}^+$, so that (16.7) is written as either

$$e^{\Phi(q_0)}\frac{\partial}{\partial q_0}\mathcal{D}(q_0)e^{-\Phi(q_0)}\frac{\partial}{\partial q_0}\tau(q_0) = -1 \tag{16.8}$$

or

$$\left[\mathcal{U}(q_0)\frac{\partial}{\partial q_0} + \mathcal{D}(q_0)\frac{\partial^2}{\partial q_0^2}\right]\tau(q_0) = -1. \tag{16.9}$$

In solving the second order differential equation as above, we need two kinds of boundary conditions for $\tau(q)$. One is the absorbing BC where $\tau(q_A) = 0$, as well as $P(q_A) = 0$: the random walker (Fig. 16.1a) on the cliff ($q = q_A$) falls down immediately. The other is the reflecting BC $\partial\tau(q)/\partial q = 0$, at a reflecting wall $q = q_R$ where the MFPT is maximal: the walker on reflecting wall has the longest time to reach the cliff.

The simplest example is one-dimensional diffusion with a constant $\mathcal{D}$ without drift ($\mathcal{U} = 0$), bounded by an absorbing wall $q_A = L$ and a reflecting wall at $q_R = 0$. (16.9) is reduced to

$$\mathcal{D}\frac{\partial^2}{\partial q^2}\tau(q) = -1, \tag{16.10}$$

which is integrated subject to the two BCs:

$$\mathcal{D}\frac{\partial \tau(q)}{\partial q} = -\int_0^q dq' = -q \tag{16.11}$$

$$\tau(q) = -\frac{1}{\mathcal{D}}\int_L^q dq'' q'' = \frac{1}{2\mathcal{D}}\left(L^2 - q^2\right). \tag{16.12}$$

The random walker, initially at $q = 0$ and $L/2$ respectively, falls to the cliff located at $q = L$ during the time $L^2/2\mathcal{D}$ and $3L^2/8\mathcal{D}$ respectively in average. If two absorbing BC at $q = 0, q = L$ are present, we have

$$\tau(q) = -\frac{1}{2\mathcal{D}}q(q - L) \tag{16.13}$$

and $\tau(L/2) = L^2/(8\mathcal{D})$. This is exactly same as what we previously obtained from eigenfunction expansion solution of the diffusion equation with two absorbing BC, (13.62). Replacing the reflecting boundary by an absorbing boundary reduces the life time by the factor of 3.

Let us study the case with a non-vanishing potential with an absorbing and a reflecting BC by solving the equation:

$$e^{\Phi}\frac{\partial}{\partial q}\mathcal{D}(q)e^{-\Phi}\frac{\partial}{\partial q}\tau(q_0) = -1. \tag{16.14}$$

By integrating the above, we obtain

$$\mathcal{D}(q)e^{-\Phi}\frac{\partial}{\partial q}\tau(q) = -\int_{q_R}^q dq' e^{-\Phi(q')}, \tag{16.15}$$

where we used the reflecting BC, $\partial\tau(q)/\partial q|_{q=q_R} = 0$. Another integration with the absorbing BC $\tau(q_A) = 0$ gives

$$\tau(q) = \int_q^{q_A} dq'' \frac{1}{\mathcal{D}(q'')}e^{\Phi(q'')}\int_{q_R}^{q''} dq' e^{-\Phi(q')} \tag{16.16}$$

As a simplest example, let us consider the case in which the random walker moves under a constant drift $\mathcal{U}$ and a constant noise-strength $\mathcal{D}$, so that $\Phi(q) = -\mathcal{U}q/\mathcal{D}$ (15.29). How long does it take the walker to transverse from $q = 0$ to $q = L$? By considering $q_R = 0$ and $q_A = L$, (16.16) can readily be integrated:

$$\begin{aligned}\tau(0) &= \frac{1}{\mathcal{D}} \int_0^L dq'' \, e^{-\mathcal{U}q''/\mathcal{D}} \int_0^{q''} dq' \, e^{\mathcal{U}q'/\mathcal{D}} \\ &= \frac{L}{\mathcal{U}} \left[1 + \frac{\mathcal{D}}{\mathcal{U}L} \left(e^{-\frac{\mathcal{U}L}{\mathcal{D}}} - 1 \right) \right].\end{aligned} \tag{16.17}$$

When the noise effect is insignificant such that $\mathcal{U}L/\mathcal{D} \gg 1$, we recover $\tau = L/\mathcal{U}$. If the force is weak or noise effect is strong so that $\mathcal{U}L/\mathcal{D} \ll 1$, we obtain the result for the free diffusion $\tau = L^2/2\mathcal{D}$. Consider that an ion crosses a membrane of the thickness L under a constant force F. Noting the correspondence $\mathcal{D} = D$ (diffusivity), $\mathcal{U} = DF/(k_BT) = F/\zeta$ (drift velocity), the mean crossing time is given by

$$\tau = \frac{L}{D} \frac{k_BT}{F} \left[1 + \frac{k_BT}{FL} \left(e^{-\frac{FL}{k_BT}} - 1 \right) \right] \tag{16.18}$$

P16.3 *In the last chapter, we considered a stochastic differential equation*

$$\frac{d}{dt} n(t) = -\gamma n(t) + n(t)\xi(t),$$

where $\xi(t)$ is a white and Gaussian noise of strength $\mathcal{D}$:

$$\langle \xi(t)\xi(0) \rangle = 2\mathcal{D}\delta(t - t').$$

Find the mean first passage time for the n to grow from $n = 1$ to N and to the average value at the stationary state.

P16.4 *A double strand DNA is duplex of two single stranded DNA bonded by a binding energy $\epsilon = 0.3\ k_BT$ per base pair (bp) at a room temperature. A tension of $f = 10$ pN is applied vertically on two single strands at an end to unbind them, with the other end held permanently bound. From the time it takes to completely separate DNA of 100 bp = 34 nm length, find the time that two ss to freely reassemble to ds. (Hint: use the freely jointed chain model for the ss fully stretched by the force and ss coiled force-free. The dynamical variable is the number of bp unbound by the force. The force to tear the ds per bp is $0.3\ k_BT/0.34$ nm.)*

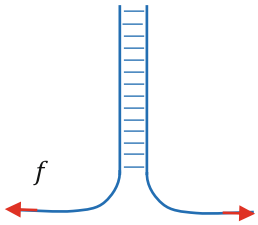

16.1.2 Example: Polymer Translocation

A polymer translocating through a membrane can be considered as a diffusion crossing over the free energy barrier affected by transmembrane biases and chain conformations (Fig. 16.2a). For a flexible chain we describe a theoretical work of Sung and Park (1996). The relevant degree of freedom that describes the translocation dynamics is $\mathcal{Q} = n$, the number of segments translocated to the trans side (Fig. 16.2). As we studied in Chap. 10, the free energy function for ideal chain associated with n is entirely given by the entropy, $\mathcal{F}(n) = \frac{1}{2} k_B T \ln[n(N-n)]$ (10.35) (Fig. 16.2b), where N is total segment number. We consider the translocation dynamics over time longer than the chain relaxation time, where the chain is in a quasi-equilibrium state. The Langevin equation for the n is given by

$$\zeta(n)\dot{n}l = -\frac{\partial}{l\partial n}\mathcal{F}(n) + f_R(n,t), \tag{16.19}$$

where $\zeta(n)$ is the friction coefficient of the translocating chain, l is the segmental length and $f_R(n,t)$ is the thermal noise. The FPE for the PDF $P(n,t)$ can be constructed as

$$\frac{\partial P(n,t)}{\partial t} = \mathcal{L}_{FP} P(n,t), \tag{16.20}$$

where

$$\mathcal{L}_{FP} = \frac{\partial}{l\partial n} D(n) e^{-\beta\mathcal{F}(n)} \frac{\partial}{l\partial n} e^{\beta\mathcal{F}(n)} \tag{16.21}$$

with $D(n) = k_B T/\zeta(n)$, the diffusivity of the translocating chain.

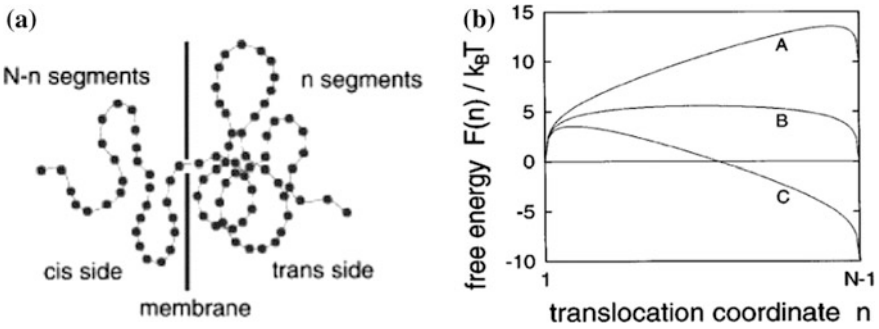

Fig. 16.2 **a** A flexible polymer translocation through a thin membrane from the cis-side to the trans-side, **b** the free energy with the n segments translocated on trans-side. ($N = 1026$, A: $\beta\Delta\mu = 10/N$, B: $\beta\Delta\mu = 0$, C: $\beta\Delta\mu = -10/N$) Reprinted from Sung and Park (1996). Copyright (1996) by the American Physical Society

The mean time for the translocation is MFPT (16.16), with choice of the reflecting BC at $n = 0$ and the absorbing BC at $n = N$. At these values of n the free energy $\mathcal{F}(n)$ shows singularity, a feature we should avoid; we do this by adopting the reflecting BC at $n = 1$ and at $n = N - 1$, which is valid for a long chain. The MFPT is

$$\tau = l^2 \int_0^{N-1} \frac{1}{D(n)} dn \, e^{\beta \mathcal{F}(n)} \int_1^n dn' e^{-\beta \mathcal{F}(n')}, \tag{16.22}$$

which, for constant diffusivity $D(n) = D$, is

$$\begin{aligned} \tau &= \frac{l^2}{D} \int_0^{N-1} dn \int_1^n dn' \left[\frac{n(N-n)}{n'(N-n')} \right]^{1/2} \\ &= \frac{\pi^2}{8} \frac{L^2}{2D} = \frac{\pi^2}{8} \tau_0, \end{aligned} \tag{16.23}$$

where $L = Nl$ is total contour length. The entropy caused by polymer fluctuation retards the translocation by the factor $\pi^2/8$ compared with $\tau_0 = L^2/2D$ that a rigid rod would have in translocation.

In fact, within cells the translocating chain is driven by a variety of biases caused by the transmembrane potential, and other environmental changes. If we include this effect via a chemical potential change $\Delta\mu$ per translocating segment, the free energy of translocation is changed to

$$\mathcal{F}(n) = \frac{1}{2} k_B T \ln[n(N-n)] + n\Delta\mu,$$

or

$$\mathcal{F}(n)/(k_B T) = \ln[x(1-x)] + x\mu^*, \tag{16.24}$$

where $x = n/N$, and $\mu^* = N\Delta\mu/(k_B T)$ are the dimensionless variables. The MFPT is calculated as a function of μ^*, and is expressed for two limiting cases:

$$\begin{aligned} \frac{\tau}{\tau_0} &= 2(-\mu^*)^{-1} \quad \text{for } \mu^* \ll -1, \\ &= 2\mu^{*-2} e^{\mu^*} \quad \text{for } \mu^* \gg 1. \end{aligned} \tag{16.25}$$

A modulation of μ^* by one, which corresponds to a very small chemical potential bias $\Delta\mu = (k_B T)/N$ for a long chain, can change appreciably the free energy landscape (Fig. 16.2b). Consequently a minute fluctuation of the chemical potential bias changes the translocation dramatically (16.25)! This remarkable cooperative behavior is **an emergent behavior of the chain arising from chain connectivity**.

16.2 The Kramers Escape Problem

The Kramers escape problem is to find the MFPT of a dynamical state q to cross or escape a region by surmounting a certain barrier. A typical 'potential' or a free energy function, to which the dynamical state is subject, is bi-stable, as shown in Figs. 16.1b and 15.3. This problem is of direct relevance to multitude of dynamic transitions between two states. One particular problem is the rate of diffusion limited chemical reaction where q is the reactions coordinate.

We calculate the mean time in which a dynamical state (e.g., a Brownian particle position) initially at q_0 existing somewhere in a well crosses over the barrier and arrive at a target in other well. To this end, an absorbing boundary is placed at the target point q_A somewhere after the barrier top (Fig. 16.1b), and the reflecting BC at $q = -\infty$. From (16.16)

$$\tau(q_0) = \mathcal{D}^{-1} \int_{q_0}^{q_A} dq'' e^{\Phi(q'')} \int_{-\infty}^{q''} dq' e^{-\Phi(q')}. \tag{16.26}$$

We consider that the dimensionless barrier $\Delta\Phi = \Phi_M - \Phi_m$ is much higher than unity (Fig. 15.3), and evaluate each integrand by quadratic expansion about the sharp maximum, as in (15.95), (15.96). The q'' that dominates first integrand is near zero (the barrier top) but can be replaced by positive infinity for the second integral, while q_0 and q_A are negative and positive respectively taken to be $-\infty$ and ∞, yielding the approximation for (16.26) as

$$\tau_K = \frac{1}{\mathcal{D}} \frac{2\pi}{\Omega_M \Omega_m} e^{\Delta\Phi} = \frac{2}{\lambda_1}, \tag{16.27}$$

where λ_1 is the first nonvanishing eigenvalue of the FP operator for the bistable potential, (15.97). This mean crossing or escaping time is called the Kramers time. For the case of a Brownian particle crossing over a potential energy barrier ΔU much higher than $k_B T$, the Kramers time is

$$\tau_K = \frac{2\pi\zeta}{\omega_M \omega_m} e^{\Delta U / k_B T}, \tag{16.28}$$

where ω_M, ω_m are the curvature parameters of the $U(x)$, $\sqrt{U''(x)}$ at the maximum and minimum of the potential.

16.2.1 Rate Theory: Flux-Over Population Method

Finding the MPFT being often problematic in some cases, much easier and more direct way is to find crossing rate via the flux over population method. As shown by Reimann et al. (1999), the rate calculated this way is equal to the inverse of the Kramers time. In this method, we visualize a steady state where particles are constantly injected into the region at the reflecting boundary with a uniform current J and are annihilated at the absorbing boundary. The rate of crossing the barrier is obtained by

$$R = \frac{J}{\wp_s}, \tag{16.29}$$

where $\wp_s$ is the probability of the particle residing within the region:

$$\wp_s = \int_{\Omega} dq\, P(q). \tag{16.30}$$

We revisit the simplest problem of one–dimensional free diffusion between a reflecting wall at $x = 0$, and an absorbing wall at $x = L$. Although the real situation may be unsteady, to use the flux-over-population method, we imagine as if that particles are constantly injected at $x = 0$ to induce a steady current J. The solution of $D\partial^2 P/\partial x^2 = 0$, is $P = ax + b$ yielding $J = -D\partial P/\partial x = -Da$. The solution subject to the absorbing BC at $x = L$ is $P(x) = -J(x - L)/D$. Because pre-transitional probability is $\wp_s = \int_0^L dx\, P(x) = (JL^2)/2D$, the rate is $J/\wp_s = 2D/L^2$, which is the inverse of the MFPT, $\tau_0 = L^2/2D$.

For the case with a potential, we start with the equation for a constant flux, (15.44)

$$J = -\mathcal{D}(q)e^{-\Phi}\frac{\partial}{\partial q}\left(e^{\Phi}P\right),$$

which is integrated to:

$$J\int_{q_A}^{q} dq' e^{\Phi(q')}/\mathcal{D}(q') = -\left[e^{\Phi(q)}P(q) - e^{\Phi(q_A)}P(q_A)\right]. \tag{16.31}$$

Since $P(q_A)$ is zero, we find

$$P(q)/J = -e^{-\Phi(q)}\int_{q_A}^{q} dq' e^{\Phi(q')}/\mathcal{D}(q'), \tag{16.32}$$

which is integrated over the region Ω:

$$\frac{\wp_s}{J} = \int_{q_R=-\infty}^{q_A} e^{-\Phi(q)} dq \int_{q}^{q_A} dq' e^{\Phi(q')} \, / \mathcal{D}(q'). \tag{16.33}$$

We consider a constant $\mathcal{D}$ and the bistable potential with a high barrier in the integrands (Figs. 15.3 and 16.1b). Because the value of q that dominates the first integrand is $-q_m$, a point where the potential is minimum, using the same logic as before, (16.33) is found to be equal to the Kramers time, which is the inverse of the Kramers rate:

$$R_K = \frac{J}{\wp_s} = \frac{\mathcal{D}}{2\pi} \Omega_M \Omega_m e^{-\Delta\Phi}. \tag{16.34}$$

For a Brownian particle subject to a friction ζ and potential energy barrier ΔU,

$$R_K = \frac{\omega_m \omega_M}{2\pi\zeta} e^{-\Delta U/(k_B T)}. \tag{16.35}$$

The proportionality of the rate to the Boltzmann factor $\exp[-\Delta U/(k_B T)]$ is called the Arrhenius law. ΔU is called the activation energy. For a dynamical state $Q(t)$ evolving under a bistable free energy landscape $\mathcal{F}(Q)$, the Kramers rate is given by (16.35) with ΔU replaced by $\Delta\mathcal{F}$, the free energy barrier that can depend on temperature, making the rate be non-Arrhenius. The Kramers rate problem for a variety of the reaction coordinates Q is widely applicable to transitions and reactions between two states, some of which we discussed earlier.

16.2.2 The Kramers Problem for Polymer

The dynamics of polymer crossing barriers is a basic problem in soft matter; it is also important in various biological applications such as polymer transport across membranes and within channels, DNA gel electrophoresis, etc. We consider that each segment of the polymer is subject to a piece-wise harmonic potential $U(x)$ (Fig. 16.3) such that the distance between well bottom and barrier top is larger than the polymer's radius of gyration. How can the Kramers rate (16.35) for a Brownian particle be extended to the linear chain of N beads each with the same friction coefficient γ?

First suppose that a flexible polymer crosses the barrier in globular conformation. For the globule, we can adopt the single particle rate (16.35) with rescaling $U(x) \to NU(x)$ and thus $\omega_m \to N^{1/2}\omega_m$, $\omega_M \to N^{1/2}\omega_M$, as well as $\gamma \to N\gamma$ neglecting the hydrodynamic interactions between the beads, and find the crossing rate:

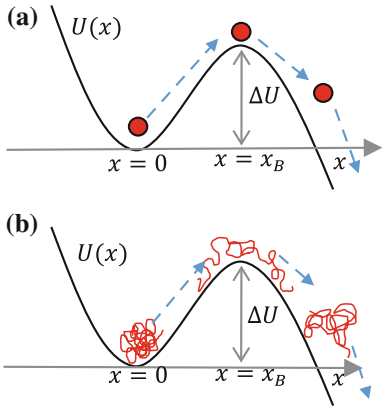

Fig. 16.3 The Kramer's problem of crossing over a piecewise harmonic potential **a** the case where the polymer is in the globular state. **b** the case is polymer is unfolded into a flexible linear chain

$$R_0 = \frac{\omega_m \omega_M}{2\pi\gamma} e^{-\beta N \Delta U}. \tag{16.36}$$

Compared with the single bead case, the prefactor $(\omega_m \omega_M)/2\pi\gamma$ remains unchanged whereas the activation energy is multiplied by N times: the crossing rate of the polymer in globular state is vanishingly small.

Now consider that the polymer in crossing the barrier is unfolded into a flexible chain. With the reaction coordinate chosen to be the center of mass (CM) of the chain, X, we then expect the rate to be modified to

$$R = \frac{\omega_m \omega_M}{2\pi\gamma} e^{-\beta \Delta \mathcal{F}} = \frac{\omega_m \omega_M}{2\pi\gamma} e^{-\beta (N\Delta U + \Delta \mathcal{F}')}. \tag{16.37}$$

Here $\Delta \mathcal{F} = N\Delta U + \Delta \mathcal{F}'$ is the free energy barrier for the chain to surmount, $\Delta \mathcal{F}' = \mathcal{F}_M - \mathcal{F}_m$, where $\mathcal{F}_M, \mathcal{F}_m$ are the polymer conformational free energies with its CM fixed at the barrier top and well bottom, respectively. The free energy barrier $\Delta \mathcal{F}$ is much less than $N\Delta U$, due to the polymer flexibility, as will be shown below. Equation (16.37) was derived on the basis of multidimensional barrier crossing theory applied to N beads interconnected by harmonic springs (Park and Sung 1999). The detailed derivation and expressions for $\mathcal{F}_M$ and $\mathcal{F}_m$ are quite involved, so here we present simple scaling theory arguments for long chains.

With the center of mass positioned at the well bottom, the flexible chain experiences confinement within the harmonic well, costing the conformational free energy, which is the sum of harmonic energy and the confinement-induced entropic contribution (10.122):

$$\mathcal{F}_m \sim \frac{1}{2} N \omega_m^2 \xi^2 + \left(\frac{R_G}{\xi}\right)^2 k_B T. \tag{16.38}$$

Here ξ is a length of the chain confined within the well $\xi^2 = \sum_{n=1}^{N} \langle x_n^2 \rangle / N$, where x_n is the position of nth bead from measured from the well bottom, and $R_G \sim N^{1/2} l$ is the radius of gyration in free space. When $\xi \sim \left(k_B T l^2 / \omega_m^2\right)^{1/4}$, the free energy function (16.38) takes the minimum

$$\mathcal{F}_m \sim N \omega_m l (k_B T)^{1/2}, \tag{16.39}$$

which increases with ω_m as well as with N.

When crossing the barrier top, the chain, if it is very long, can stretch rather than coil, because by stretching the chain can reduce the energy dramatically as shown below. This phenomenon is a kind of the coil-stretch transitions which usually are hydrodynamically induced (De Gennes 1974). The conformational free energy $\mathcal{F}_M$ then is given by

$$\mathcal{F}_M \sim -\frac{1}{2} N \omega_M^2 \xi^2. \tag{16.40}$$

Because the chain is stretched $\xi \sim Nl$, we have $\mathcal{F}_M \sim -N^3 \omega_M^2 l^2$; for long chain (large N) threading over a narrow barrier (large ω_M), the free energy is drastically reduced.

The net free energy barrier is given by

$$\Delta \mathcal{F} = N \left\{ \Delta U - \delta \omega_m l (k_B T)^{1/2} \right\} - \alpha N^3 \omega_M^2 l^2, \tag{16.41}$$

where α and δ are numerical factors. It tells us that the confinement within the well bottom and stretching at the barrier top reduce the free energy barrier far below $N\Delta U$. Consequently, (16.37) means that the crossing rate of a flexible chain can be much higher than that of a globule, R_0, due to chain flexibility that allows such conformational adaptability to an external force. The stretched conformation in particular can enhance the rate as the chain gets longer than a critical value.

The free energy $\mathcal{F}(X)$ of the chain with CM positioned at X, which also piece-wise harmonic, can be emulated by the entropy of a particle within channel of undulating cross section $A(X)$ in accordance with the relation

$$\mathcal{F}(X) = -k_B T \ln \left[A(X) / A_0 \right], \tag{16.42}$$

or $A(X) = A_0 \exp[-\mathcal{F}(X)/k_B T]$, where A_0 is the cross section at the point where $\mathcal{F}(X) = 0$. Indeed the counterintuitive phenomenon predicted by (16.41) was observed in DNA fragments that flow through fabricated micro and nano-sized channels (Han et al. 1999); longer fragments were found to escape faster, by stretching, the narrow constriction corresponding to the free energy barrier top. Furthermore, the idea in this connection can leads to a novel means of

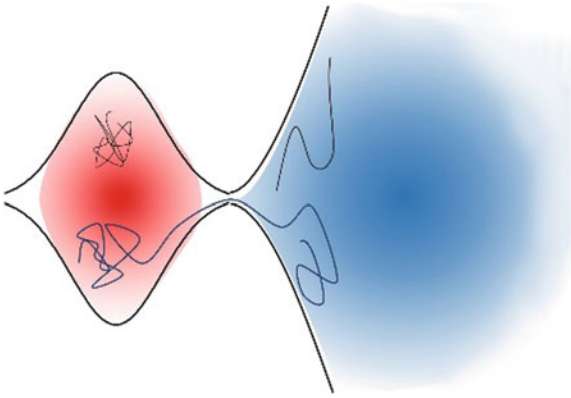

Fig. 16.4 The flexible polymers are confined within a well. Only the long chains can cross the narrow constriction toward to the open space of high entropy

separating a long DNA fragment from short fragments using the channel shown as Fig. 16.4. The long DNA will escape the well of battling confinement, preferring to pass through a narrow constriction and advance to uncontested entropy space. A short chain cannot.

Further Reading and References

L.E. Reichl, *A Modern Course in Statistical Physics* (Wiley-VCH Verlag GmbH, 2016)

N.G. Van Kampen, *Stochastic Processes in Physics & Chemistry* (Elsevier B.V.)

H. Risken, *The Fokker-Planck Equation*, vol. 18. (Springer Series in Synergetics), pp. 63–95

S. Redner, *A Guide to First-Passage Processes* (Cambridge University Press, 2001)

P. Hänggi, P. Talkner, M. Borkovec, Reaction-rate theory: fifty years after Kramers. Rev. Mod. Phys. **62**, 251 (1990)

W. Sung, P.J. Park, Polymer translocation through a pore in a membrane. Phys. Rev. Lett. **77** (4), 783 (1996)

I. Goychuk, P. Hänggi, Ion channel gating: a first-passage time analysis of the Kramers type. PNAS USA **99**(6), 3552–3556 (2002)

T. Chou, M.R. D'Orsogna, *First Passage Problems in Biology* (World Scientific, 2014)

H.-X. Zhou, Rate theories for biologists—ResearchGate. Q. Rev. Biophys. **43**(2), 219–293 (2010)

P. Reimann, G.J. Schmid, P. Hänggi, Universal equivalence of mean first-passage time and Kramers rate. Phys. Rev. E **60**(1), R1–R4 (1999)

P.G. De Gennes, Coil-stretch transition of dilute flexible polymers under ultrahigh velocity gradients. J. Chem. Phys. **60**, 5030 (1974)

J. Han, S.W. Turner, H.G. Craighead, Entropic trapping and escape of long DNA molecules at submicron size constriction. Phys. Rev. Lett. **83**, 1688 (1999)

Chapter 17
Dynamic Linear Responses and Time Correlation Functions

Although seemingly stationary, matter in equilibrium spontaneously fluctuates due to microscopic degrees of freedom thermally excited therein. Even the macroscopic properties, for example, the length of a rod or the polarization of a dielectric fluctuate, although imperceptibly; on a finer time scales the time series of these properties looks stochastic, with the variances reflecting the intrinsic response of the matter to a small external influence, as we studied in Chap. 9. Although apparently random, the time-series signals at different times are correlated at a close look. In this chapter we will find that **the time correlation is directly related to the response of the system to a time-dependent perturbation, namely, the fluctuation-dissipation theorem**. In particular, how the time correlation decays is same as how the non-equilibrium state relaxes after removal of the perturbation. From the knowledge of the time correlations, a variety of the associated dynamic response functions and transport coefficients can be obtained.

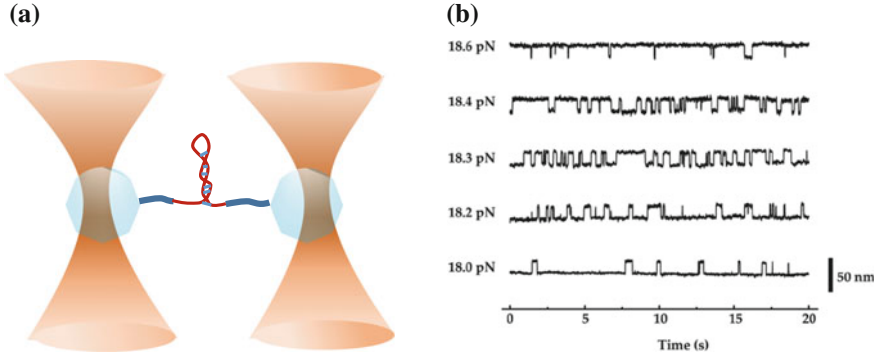

Fig. 17.1 **a** An RNA hairpin under a stretching force provided by an optical tweezer, **b** the time series of end-to-end distance of the RNA hairpin for various stretching forces (Republished from Stephenson et al. (2014), PCCP; permission conveyed through Copyright Clearance Center, Inc.)

W. Sung, *Statistical Physics for Biological Matter*, Graduate Texts in Physics,
https://doi.org/10.1007/978-94-024-1584-1_17

In earlier chapters, we learned that these fluctuations become relatively larger for smaller systems as manifested in the Brownian motion. As an example for nanometer-sized systems, an RNA hairpin extended by an optical tweezer (Fig. 17.1) depicts temporal fluctuation (time-series signal) in extension of the RNA depending on the stretching force. A fundamental question is: what can we learn from the signal and its temporal correlation, for a small system in particular? **What does a signal pattern imply with regards to the living nature of the biopolymers if it is in active state?**

17.1 Time-Dependent Linear Response Theory

17.1.1 Macroscopic Consideration

In Chap. 9, we studied the static linear response theory, in which the change of a systems' variable ΔX_i caused by a small static force or field f_i conjugate to the variable is given by its fluctuation $\langle(\Delta\mathcal{X}_i)^2\rangle_0$. For example, the change in average extension of an elastic rod ΔX in response to a small applied tension f is given by $\Delta X = \chi_s f$, where a constant χ_s is the static response function given by the fluctuation of the microscopic extension $\mathcal{X}$ at equilibrium in the absence of the force, $\chi_s = \beta\langle(\Delta\mathcal{X})^2\rangle_0$. The response function here is called stretch modulus.

Here we generalize the theory for the time-dependent situations questioning: how will the elastic rod extend dynamically in response to a small force acting on the system $f(t)$, which has an arbitrary time dependence? A naïve generalization may suggest $\Delta X(t) = \chi f(t)$, or $\Delta X(t) = \chi(t)f(t)$, either of which is wrong! Considering the linearity with respect to $f(t)$, we can deduce that the true relation is

$$\Delta X(t) = \int_{-\infty}^{t} \chi(t,t')f(t')dt'. \tag{17.1}$$

$\chi(t,t')$ is a **time-dependent dynamic response function** which is an intrinsic property of the system at the unperturbed state. Because the property is invariant with respect to time-translation, χ only depends on the difference $t - t'$ connecting the response $\Delta X(t)$ and the cause $f(t')$: $\chi(t,t') = \chi(t-t')$. Equation (17.1) signifies that system's response to the force in general is delayed. Only in the limit $\chi(t-t') \to \chi_s\delta(t-t')$, the response is instantaneous, $\Delta X(t) = \chi_s f(t)$. Second,

$\chi(t-t')$ is non-vanishing only when $t > t'$, dictated by the principle of causality that the effect follows the cause. Thus (17.1) can be replaced by

$$\Delta X(t) = \int_{-\infty}^{\infty} \chi(t-t') f(t') dt'. \tag{17.2}$$

The linear response $\Delta X(t)$ to an oscillatory force $f(t') = a\cos\Omega t' = Re\left[ae^{-i\Omega t'}\right]$ reads

$$\begin{aligned} \Delta X(t) &= \int_{-\infty}^{t} dt' \chi(t-t') Re\left[ae^{-i\Omega t'}\right] \\ &= Re\left[\int_{-\infty}^{t} dt' \chi(t-t') ae^{i\Omega(t-t')} e^{-i\Omega t}\right] \\ &= Re\left[\int_{0}^{\infty} ds \chi(s) ae^{i\Omega s} e^{-i\Omega t}\right] = Re\left[\chi(\Omega) e^{-i\Omega t}\right], \end{aligned} \tag{17.3}$$

where

$$\chi(\Omega) = \int_{0}^{\infty} dt\, e^{i\Omega t} \chi(t) = \int_{-\infty}^{\infty} dt\, e^{i\Omega t} \chi(t), \tag{17.4}$$

is a time-Fourier transform of $\chi(t)$, which vanishes for $t < 0$.

Writing $\chi(\Omega) = \chi'(\Omega) + i\chi''(\Omega)$ and $e^{-i\Omega t} = \cos(\Omega t) - i\sin(\Omega t)$, the response is obtained as

$$\begin{aligned} \Delta X(t) &= a\{\chi'(\Omega)\cos(\Omega t) + \chi''(\Omega)\sin(\Omega t)\} \\ &= |\chi(\Omega)| a\cos(\Omega t - \phi) \end{aligned} \tag{17.5}$$

with the response amplitude

$$|\chi(\Omega)| = \left[\chi'(\Omega)^2 + \chi''(\Omega)^2\right]^{1/2} \tag{17.6}$$

and the phase delay

$$\phi = \tan^{-1}(\chi''/\chi') \tag{17.7}$$

with respect to the input force. Remarkably the response generally is not in phase with the driving force. While the real part of $\chi(\Omega)$, $\chi'(\Omega)$ represents the response in phase, the imaginary part, $\chi''(\Omega)$ represents the response out of phase (by $\pi/2$) with

respect to the driving force; this is due to the dissipation inherent in the elastic rod, as we shall see shortly. The convolution integral (17.2) means that the response function and the applied force are related through their Fourier transforms:

$$\Delta X(\omega) = \chi(\omega) f(\omega). \tag{17.8}$$

To show that χ'' is a measure of the energy dissipation as mentioned, we consider the rate of work done on the system by the oscillatory force $f(t) = a\cos(\Omega t)$:

$$\begin{aligned} \dot{W} &= f(t)\frac{d}{dt}\Delta X(t) \\ &= a\,\cos\,\Omega t \cdot a\Omega\{-\chi'(\Omega)\sin(\Omega t) + \chi''(\Omega)\cos(\Omega t)\}. \end{aligned} \tag{17.9}$$

where we used (17.5). The rate of work done averaged over a period of oscillation $T_\Omega = 2\pi/\Omega$ is

$$\bar{\dot{W}} = \frac{1}{T_\Omega}\int_0^{T_\Omega} dt\ \dot{W} = \frac{1}{2}a^2\Omega\,\chi''(\Omega). \tag{17.10}$$

The above relation means that, unless the driving frequency Ω is vanishing, the work done on the system is absorbed (dissipated) to the system as heat, by the amount proportional to $\chi''(\Omega)$. It is to be contrasted with undamped systems on which the work done by an oscillatory force over a cycle is zero.

P17.1 *For an elastic rod under an oscillatory force, whose length is governed by the equation, $X'' + \gamma X' + \mu X = A\cos\Omega t$, calculate the power amplification factor $|\chi(\Omega)|^2$, the phase delay ϕ of the response to the oscillating force, and the energy dissipation incurred per cycle.*

The dynamic response function $\chi(t)$ is an intrinsic material property, which will be revealed by a small $f(t)$, regardless the way how it is applied. Thus we consider as a simple case a stepwise unloading: $f(t) = f$ for $t < 0$, $f(t) = 0$ for $t > 0$ (Fig. 17.2), that is, an equilibrium state is maintained under a constant force from

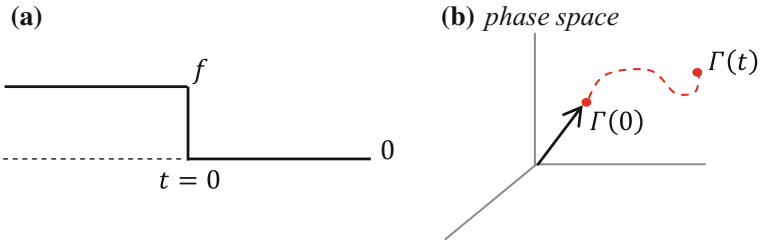

Fig. 17.2 **a** A step-wise unloading of a constant force f on the system at $t = 0$. **b** following this unloading, the phase space state of the many body system evolves from $\Gamma(0)$ to $\Gamma(t)$

the distant past until $t = 0$, after which a non-equilibrium situation is caused by turning it off. Following (17.2), the change in the length of a rod X in response to the tension $f(t)$ is:

$$\Delta X(t) = f \int_{-\infty}^{0} \chi(t - t')dt' = -f \int_{\infty}^{t} \chi(s)ds, \tag{17.11}$$

from which, one can obtain

$$\chi(t) = -\frac{1}{f}\frac{d}{dt}\Delta X(t). \tag{17.12}$$

Once $\Delta X(t)$ is obtained, e.g., measured experimentally, the response function $\chi(t)$ is determined following the equation above; if, after the force f is unloaded, the extension is observed to decays as following,

$$\Delta X(t) = Cfe^{-t/\tau}, \tag{17.13}$$

the response function is obtained as $\chi(t) = (C/\tau)e^{-t/\tau}$, yielding the extension (17.1)

$$\Delta X(t) = \frac{C}{\tau} \int_{-\infty}^{t} dt' e^{-(t-t')/\tau} f(t'). \tag{17.14}$$

The above equation is now valid for any arbitrary form of the time-dependent force $f(t)$. If a constant force is applied up to the time t, the above is reduced to the static relation $\Delta X(t) = Cf$ so that C is identified as the inverse of the stretch modulus. Under an impulse applied at $t = 0$, that is, if $f(t') = F\delta(t')$, we have $\Delta X(t) = (CF/\tau)\exp(-t/\tau)$.

P17.2 *Find how the extension depends on an oscillatory loading for this rod.*

17.1.2 Statistical Mechanics of Dynamic Response Function

Now let us obtain $\chi(t)$ using statistical mechanics based on the microscopic view, for a stepwise unloading of f_i, which is not limited to the tension but can include a variety of forces and fields. Conjugate to f_i is the system variable $\mathcal{X}_i$, whose average can not only be the macroscopic displacement X_i introduced in (Table 2.1) but also be mesoscopic variables, e.g., the displacement of a Brownian particle.

We consider that from the distant past our system, viewed as a classical many-body system, is brought to an equilibrium state under a constant force f_i until

$t = 0$, after which the force is turned off. At $t = 0$ (initially), the system's Hamiltonian is

$$\mathcal{H}(\Gamma(0)) = \mathcal{H}_0(\Gamma(0)) - f_i \mathcal{X}_i(\Gamma(0)), \tag{17.15}$$

where $\Gamma(0)$ is the systems' many-particle phase space point descriptive of the initial state and evolves to $\Gamma(t)$ at a later time t (Fig. 17.2b). The macroscopic displacement $X_j(t)$ at t is the average of the corresponding microscopic variable of the system $\mathcal{X}_j(t) = \mathcal{X}_j(\Gamma(t))$ over all microstates initially prepared with the distribution $e^{-\beta\mathcal{H}(\Gamma(0))} / \sum_{\mathcal{M}} e^{-\beta\mathcal{H}(\Gamma(0))}$:

$$X_j(t) = \langle \mathcal{X}_j(t) \rangle = \frac{\int d\Gamma(0) \{ \mathcal{X}_j(\Gamma(t)) e^{-\beta\mathcal{H}(\Gamma(0))} \}}{\int d\Gamma(0) e^{-\beta\mathcal{H}(\Gamma(0))}}. \tag{17.16}$$

Because $\mathcal{H}' = -f_i \mathcal{X}_i$ is a perturbation, $e^{-\beta\mathcal{H}(\Gamma(0))} \approx e^{-\beta\mathcal{H}_0}(1 + \beta f_i \mathcal{X}_i(0))$, and

$$\begin{aligned} \langle \mathcal{X}_j(t) \rangle &\approx \frac{\int d\Gamma(0) \{ \mathcal{X}_j(\Gamma(t)) e^{-\beta\mathcal{H}_0} (1 + \beta f_i \mathcal{X}_i(0)) \}}{\int d\Gamma(0) e^{-\beta\mathcal{H}_0} (1 + \beta f_i \mathcal{X}_i(0))} \\ &= \frac{\langle \mathcal{X}_j(t) \rangle_0 + \beta f_i \langle \mathcal{X}_j(t) \mathcal{X}_i(0) \rangle_0}{1 + \beta f_i \langle \mathcal{X}_i(0) \rangle_0} \end{aligned} \tag{17.17}$$

where $\langle \cdots \rangle_0$ is the average over the equilibrium ensemble *in the absence of the force* with the distribution $e^{-\beta\mathcal{H}_0} / \int d\Gamma(0) e^{-\beta\mathcal{H}_0(\Gamma(0))}$. Because, for time $t > 0$, the perturbation is turned off and the time evolution is generated by $\mathcal{H}_0$, $\langle \mathcal{X}_j(t) \rangle_0 \equiv \langle \mathcal{X}_j(\Gamma(t)) \rangle_0$ is equal to $\langle \mathcal{X}_j(0) \rangle_0 \equiv \langle \mathcal{X}_j \rangle_0$, which is time-independent. If we retain in (17.17) the term linear in f_i, which is small, we arrive at an important result:

$$\begin{aligned} \Delta X_j(t) &\equiv \langle \mathcal{X}_j(t) \rangle - \langle \mathcal{X}_j \rangle_0 \\ &= \beta f_i \langle \Delta\mathcal{X}_j(t) \Delta\mathcal{X}_i(0) \rangle_0 = \beta f_i C_{ji}(t). \end{aligned} \tag{17.18}$$

This is the dynamic generalization of its static counterpart, (9.3).

For quantum systems, where the two terms on RHS of (17.15) do not generally commute; $\exp(-\beta\mathcal{H}) = \exp(-\beta\mathcal{H}_0) + (f_i/\beta) \int_0^\beta d\lambda e^{\lambda\mathcal{H}_0} \mathcal{X}_i(0) e^{-\lambda\mathcal{H}}$, and following a similar procedure, the time correlation function $C_{ji}(t)$ is replaced by the Kubo's canonical correlation $C_{ji}^c(t)$ (Kubo et al.)

$$C_{ji}^c(t) = \frac{1}{\beta} \int_0^\beta d\lambda \langle e^{\lambda\mathcal{H}_0} \Delta\mathcal{X}_i(0) e^{-\lambda\mathcal{H}_0} \Delta\mathcal{X}_j(t) \rangle_0. \tag{17.19}$$

We shall be interested in the systems where the quantum coherence is negligible. In most of mesoscopic biological systems such effect is usually expected to be absent.

Equation (17.18) is also applicable to a coarse grained-level description such as FP dynamics (15.24) involving a relevant dynamical variable $q(t)$. If the system approaches a stationary state with a distribution $e^{-\Phi(q)}$ under a noise of constant strength $\mathcal{D}$, the release of small drift $\mathcal{U}$ at $t = 0$ gives rise to the response

$$\langle \Delta q(t) \rangle = (\mathcal{U}/\mathcal{D}) \langle \Delta q(t) \Delta q(0) \rangle_0. \tag{17.20}$$

Returning to (17.18) for the case $i = j$, we have

$$\Delta X_i(t) = \beta f \langle \Delta \mathcal{X}_i(t) \Delta \mathcal{X}_i(0) \rangle_0 = \beta f C_i(t) \tag{17.21}$$

This relation proves the famous **Onsager's regression theorem**, which says **"The regression of microscopic thermal fluctuations at equilibrium follows the macroscopic law of relaxation of small non-equilibrium disturbances"** (Onsager 1931). The idea is illustrated by the Fig. 17.3, in which the solid line depicts how a variable, e.g., the length of a rod, $\mathcal{X}(t)$, first extended by a small force and then released, subsequently decays (regresses) in time. The average of the decay (marked by the dashed line) at a time t, $\Delta X(t) \equiv \langle \Delta \mathcal{X}(t) \rangle$, is proportional to the stationary time correlation function of the length in the absence of the force over the time interval t, which is measured after a long time when the system reached the equilibrium (dotted line). If an experiment yields the average decay as $\Delta X(t) \sim e^{-t/\tau}$, then we can find the correlation function $\langle \Delta \mathcal{X}(t) \Delta \mathcal{X}(0) \rangle_0 = \langle (\Delta \mathcal{X})^2 \rangle_0 e^{-t/\tau}$. This Onsager theorem is an immensely powerful relation with wide applications; it tells us that once we know the phenomenological law of relaxation of a certain variable we can infer the time correlation of its intrinsic fluctuation.

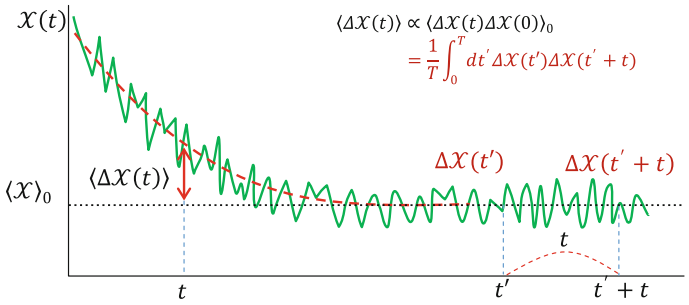

Fig. 17.3 The (fluctuating) length $\mathcal{X}(t)$ of a rod, first extended by a small force and then released, decays in time. In the time-dependence, the average decay follows that of the length time-correlation function $\langle \Delta \mathcal{X}(t) \Delta \mathcal{X}(0) \rangle_0$ measured at the stationary states reached after a long time, in the absence of the force. The correlation function for an ergodic system is equal to the time average $\frac{1}{T} \int_0^T dt' \Delta \mathcal{X}(t') \Delta \mathcal{X}(t'+t)$ taken over a long time T at the stationary state

17.1.3 Fluctuation-Dissipation Theorem

Combining (17.21) with (17.12), we find the dynamic response function is given by the relation

$$\chi_i(t) = -\beta \frac{d}{dt} C_i(t), \tag{17.22}$$

called the **fluctuation-dissipation theorem (FDT)**, which is valid ***independently of the form of the external force*** $\boldsymbol{f_i(t)}$. The relation has its generalized form,

$$\chi_{ji}(t) = -\beta \frac{d}{dt} C_{ji}(t). \tag{17.23}$$

FDT contrasts with the static linear response theory result, $\chi_{ji} = \beta \langle \Delta \mathcal{X}_j \Delta \mathcal{X}_i \rangle_0$ (9.4): while from the correlation of a time series signal at equal time one measures the static susceptibility of the system, **from the correlation at different time one can find systems' dissipative dynamic response to a time-dependent small disturbance**. It is worth mentioning that for nonphysical complex systems with the primary variable q_j and the noise strength $\mathcal{D}$ other than temperature, (17.22) is replaced by

$$\chi_{ji}(t) = -\mathcal{D}^{-1} \frac{d}{dt} \big\langle \Delta q_j(t) \Delta q_i(0) \big\rangle_0. \tag{17.24}$$

The linear response relation can be written as

$$\Delta X_j(t) = \int_{-\infty}^{t} \chi_{ji}(t-t') f(t') dt' = \int_{-\infty}^{\infty} \chi_{ji}(t-t') f_i(t') dt', \tag{17.25}$$

where the causality, $\chi_{ji}(t-t') = 0$ for $t - t' < 0$, is noted. The Fourier transform is

$$\Delta X_j(\omega) = \chi_{ji}(\omega) f_i(\omega), \tag{17.26}$$

where

$$\chi_{ji}(\omega) = \int_{-\infty}^{\infty} dt\, e^{i\omega t} \chi_{ji}(t) = \int_{0}^{\infty} dt\, e^{i\omega t} \chi_{ji}(t). \tag{17.27}$$

Let focus on the case $j = i$. From a Fourier transform of (17.22), the imaginary part of $\chi_i(\omega)$, $\chi_i''(\omega)$, can be found as

$$\begin{aligned}\chi_i''(\omega) &= -\beta \int_0^\infty dt\, \sin(\omega t) \frac{d}{dt} C_i(t) \\ &= \beta\omega \int_0^\infty dt\, \cos(\omega t) C_i(t),\end{aligned} \tag{17.28}$$

where the integration is done by parts with the time boundary condition, $\sin(\omega t) C_i(t) = 0$ at $t = 0$ and ∞. Using the symmetry $C_i(-t) = C_i(t)$, the equation is rewritten as

$$\begin{aligned}\chi_i''(\omega) &= \frac{\beta\omega}{2} \int_{-\infty}^\infty dt\, e^{i\omega t} C_i(t) \\ &= \frac{\beta\omega}{2} S_i(\omega),\end{aligned} \tag{17.29}$$

which is the Fourier transformed version of FDT. $S_i(\omega)$ is the power spectrum of $\Delta\mathcal{X}_i(t)$ in the absence of the perturbation that can be given by the Wiener-Khinchine theorem (14.18), rewritten as

$$S_i(\omega) = \lim_{T\to\infty} \frac{1}{T} \left\langle |\Delta\mathcal{X}_i(\omega)|^2 \right\rangle_0, \tag{17.30}$$

Along with this, the relation (17.29), indeed tells us that, the $\chi_i''(\omega)$, a measures of the systems' energy dissipation and the phase-delay with respect to the force $f_i(\omega)$, as shown by (17.10) and (17.7), are positive. **$\chi_i''(\omega)$ is directly related with the power spectrum that is a measure of the system's intrinsic fluctuations.**

The biological and glassy systems are observed out of equilibrium, due to chemical activity and very slow relaxation respectively. Thus, for the fluctuations at a quasi-stationary states or a steady state in such systems, FDT is violated. Nevertheless, assuming such a state is distributed by the canonical distribution with an effective temperature T_{eff} that can be different from that of the environment T, we can rewrite (17.29) as

$$k_B T_{eff} = \frac{\omega}{2} S_i(\omega)/\chi_i''(\omega). \tag{17.31}$$

If the steady state is maintained by an active mechanism that consumes the energy, the T_{eff} is smaller than T. By measuring the power spectrum and the dynamic response of hair bundle cells to an oscillating force, Martin et al. (2001) showed how the effective temperature of the systems depart from the ambient one depending on the frequency.

17.2 Applications of the Fluctuation–Dissipation Theorem

The FDT relates the systems' dynamic responses with the underlying fluctuations, and further allows **the response functions and the transport coefficients to be calculated in terms of the associated time correlation functions**. Here we give a several examples.

17.2.1 Dielectric Response

We consider a system consisting of permanent dipole moments, e.g., water, subject to an electric field $\boldsymbol{E}(t)$. The perturbing Hamiltonian is given by

$$\mathcal{H}' = -\boldsymbol{E}(t) \cdot \boldsymbol{\mathcal{P}} = -E(t)\mathcal{P} \tag{17.32}$$

where $\boldsymbol{\mathcal{P}} = \sum_{i=1}^{N} \boldsymbol{p}_i$, $\boldsymbol{p}_i$ being a dipole moment of a molecule i, $\mathcal{P}$ is total diopole moment along the direction of the field. The polarization defined by $P(t) = \langle \mathcal{P}(t) \rangle$ under the field satisfies the linear response relation

$$P(t) = \int_{-\infty}^{t} dt' \chi_P(t - t') E(t') = \int_{-\infty}^{\infty} dt' \chi_P(t - t') E(t') \tag{17.33}$$

and its Fourier transform

$$P(\omega) = \chi_P(\omega) E(\omega), \tag{17.34}$$

where

$$\chi_P(t) = -\beta \frac{d}{dt} \langle \Delta\mathcal{P}(t) \Delta\mathcal{P}(0) \rangle_0 \tag{17.35}$$

$$\chi_P(\omega) = \int_0^{\infty} dt\, e^{i\omega t} \chi_P(t). \tag{17.36}$$

are respectively the dielectric dynamic response functions in real and Fourier spaces.

As an example, we adopt the Debye model, according to which the dipole correlation function decays with a single relaxation time τ:

$$\begin{aligned}\langle \Delta\mathcal{P}(t)\Delta\mathcal{P}(0)\rangle_0 &= \left\langle (\Delta\mathcal{P})^2 \right\rangle_0 e^{-t/\tau} \\ &= k_B T \chi_P \, e^{-t/\tau}\end{aligned} \tag{17.37}$$

where χ_P is static electric susceptibility (9.7) that can be identified as $\chi_P(\omega \to 0)$, from (17.36) and (17.35). From (17.35), we obtain the dielectric response function

$$\chi_P(t) = k_B T \chi_P \tau^{-1} \, e^{-t/\tau} \tag{17.38}$$

and the frequency dependent electric subsceptibility

$$\chi_P(\omega) = \chi_P/(1 - i\omega\tau). \tag{17.39}$$

Because the frequency-dependent elecric permeability is given by

$$\varepsilon(\omega) = \varepsilon_0 + \chi_P(\omega) = \varepsilon'(\omega) + i\varepsilon''(\omega), \tag{17.40}$$

we have its real and imaginary parts:

$$\varepsilon'(\omega) = \varepsilon_0 + \chi_P / \left[1 + (\omega\tau)^2\right] \tag{17.41}$$

$$\varepsilon''(\omega) = \chi_P \omega\tau / \left[1 + (\omega\tau)^2\right], \tag{17.42}$$

the frequency dependencies of which are shown in the Fig. 17.4. Here $\varepsilon'(\omega \to 0)$ represents the static electric permeability, $\varepsilon = \varepsilon_0 + \chi_P$.

On the other hand, as ω increases to infinity, ε' approaches to ε_0, meaning that the dipoles respond to the high-frequency elecric-field oscillation as if it is in vacuum. The $\varepsilon''(\omega)$, representative of the system's energy dissipation into heat, is vanishing in both the high and low frequency limits but becomes the maximum at a frequency comparable to τ^{-1}, a kind of resonance between external driving and internal relaxation. This explains the physics behind the microwave heating.

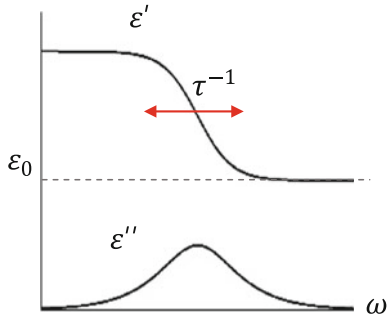

Fig. 17.4 The dielectric responses (real (ε') and imaginary (ε'') parts of the dielectric permeability) are characterized by the relaxation time τ of each dipole

17.2.2 Electrical Conduction

Consider N mobile particles in a volume V each with a charge e under a weak electric field $E(t)$ along z-direction. The field induces an electrical current. The perturbing Hamiltonian is same as (17.32) where $\mathcal{P}$ is the total dipole moment induced along the z-axis, now expressed as $\mathcal{P} = \sum_{i=1}^{N} ez_i$.

The microscopic expression for electrical current is

$$\mathcal{J}(t) = \frac{1}{V}\sum_{i=1}^{N} e\frac{d}{dt}z_i = \frac{1}{V}\frac{d}{dt}\mathcal{P}. \tag{17.43}$$

From (17.25) the current is given by

$$J(t) = \langle \mathcal{J}(t)\rangle = \int_{-\infty}^{t} dt'\chi_J(t-t')E(t') = \int_{-\infty}^{\infty} dt'\chi_J(t-t')E(t'), \tag{17.44}$$

Considering the correspondence: $\mathcal{J}(t) = \mathcal{X}_i(t)$ and $\mathcal{P} = \mathcal{X}_j$, (17.18) and (17.22) tell us that the response function is

$$\begin{aligned}\chi_J(t) &= -\frac{\beta}{V}\frac{d}{dt}\left\langle \frac{d}{dt}\Delta\mathcal{P}(t)\Delta\mathcal{P}(0)\right\rangle_0 = -\frac{\beta}{V}\frac{d}{dt}\left\langle \left[\frac{d}{dt}\Delta\mathcal{P}(t)\right]_{t=0}\Delta\mathcal{P}(-t)\right\rangle_0 \\ &= \frac{\beta}{V}\left\langle \left[\frac{d}{dt}\Delta\mathcal{P}(t)\right]_{t=0}\frac{d}{dt}\Delta\mathcal{P}(t)\right\rangle_0 = \beta V\langle \mathcal{J}(t)\mathcal{J}(0)\rangle_0.\end{aligned} \tag{17.45}$$

where the time-translational invariance $\langle \mathcal{X}_j(t)\mathcal{X}_i(0)\rangle_0 = \langle \mathcal{X}_i(0)\mathcal{X}_j(-t)\rangle_0$ is used.

The Fourier transform of (17.44) is

$$J(\omega) = \sigma(\omega)E(\omega), \tag{17.46}$$

where

$$\begin{aligned}\sigma(\omega) &= \int_{-\infty}^{\infty} dt\, e^{i\omega t}\chi_J(t) = \int_{0}^{\infty} dt\, e^{i\omega t}\chi_J(t) \\ &= \beta V\int_{0}^{\infty} dt\, e^{i\omega t}\langle \mathcal{J}(t)\mathcal{J}(0)\rangle_0\end{aligned} \tag{17.47}$$

is the frequency-dependent conductivity. It should be noted that the causality condition $\chi_J(t) = 0$ for $t<0$ is used in (17.44) and (17.47). Equation (17.47) is called **the Kubo formula for the electrical conductivity**.

Suppose that the electrical field is turned on to a constant magnitude stepwise at $t = 0$ as shown in the Fig. 17.5. Then, (17.44) yields the steady state current reached at $t \to \infty$ as

$$\begin{aligned} J &= \lim_{t\to\infty}\left[\int_0^t dt'\chi_J(t-t')\right]E \\ &= \int_0^\infty dt\ \chi_J(t)E \\ &= \sigma(\omega\to 0)E. \end{aligned} \tag{17.48}$$

Hence the steady state conductivity is given by

$$\sigma = \sigma(\omega\to 0) = \beta V\int_0^\infty dt\langle\mathcal{J}(t)\mathcal{J}(0)\rangle_0. \tag{17.49}$$

For an example let us consider N particles of charge e (electrons in crystal lattices, ions or colloids in fluids), which are dilute enough to neglect the mutual interactions. Also suppose that the current correlation function decays with a relaxation time τ,

$$\langle\mathcal{J}(t)\mathcal{J}(0)\rangle_0 = \frac{N}{V^2}\langle v^2\rangle_0\ e^{-t/\tau} = \frac{Nk_BT}{V^2M}\ e^{-t/\tau}. \tag{17.50}$$

For Brownian particles with $\tau = \tau_p$ (13.15) leads to:

$$\sigma = \frac{ne^2\tau}{M}, \tag{17.51}$$

where $n = N/V$. This is the well-known Drude formula for electrical conductivity. There are many elementary ways to derive this equation, but the linear response theory provides a systematic means to improve and generalize it.

With the correlation function (17.50) the frequency-dependent conductivity is obtained as

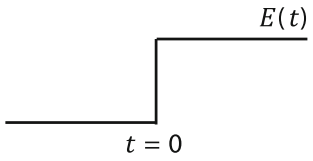

Fig. 17.5 A step-wise switching of a constant electric field at $t = 0$

$$\sigma(\omega) = \frac{ne^2\tau}{M(1 - i\omega\tau)} = \frac{\sigma}{(1 - i\omega\tau)}. \tag{17.52}$$

The real part of $\sigma(\omega)$ is

$$\sigma'(\omega) = \sigma / \left(1 + (\omega\tau)^2\right) \tag{17.53}$$

which represents the conductor's in-phase response to an oscillating elecric field. As the frequency increases it decreases due to the failure of the charges to respond in the dissipative media. Also the magnitude of the frequency dependent conductivity decreases following:

$$|\sigma(\omega)| = \frac{\sigma}{\left(1 + (\omega\tau)^2\right)^{1/2}} \tag{17.54}$$

P17.3 *Consider a stepwise force (constant for $t > 0$, and 0 otherwise) is applied to a particle in a fluid. Develop the linear response theory and derive that the diffusivity is given by the integral of the autocorrelation function of the particle's velocity:*

$$D = \int_0^\infty dt \langle v(t)v(0)\rangle_0$$

This is the fundamental Green-Kubo relation for self-diffusion.

17.2.3 FDT Under Spatially Continuous External Fields

We can generalize FDT to a case with multiple pairs of external forces and their conjugate system variables:

$$\mathcal{H}'(t) = -\sum_i \mathcal{X}_i f_i(t) \tag{17.55}$$

for which we have the response

$$\Delta X_j(t) = \sum_i \int_{-\infty}^{t} dt' \chi_{ji}(t - t') f_i(t'), \tag{17.56}$$

where $\chi_{ji}(t)$ is given by (17.23). A similar situation occurs by a spatially varying force or field $f(\boldsymbol{r},t)$ coupled to the density $x(\boldsymbol{r})$ of the property $\mathcal{X}$, which gives rise to the perturbing Hamiltonian

$$\mathcal{H}' = -\int d\boldsymbol{r}\, x(\boldsymbol{r})\, f(\boldsymbol{r},t). \tag{17.57}$$

The average change at a later time t of $x(\boldsymbol{r})$ which is the conjugate to the field is

$$\Delta x(\boldsymbol{r},t) = \int_{-\infty}^{t} dt' \int d\boldsymbol{r}'\ \chi(\boldsymbol{r}-\boldsymbol{r}', t-t') f(\boldsymbol{r}',t'), \tag{17.58}$$

involving the response function:

$$\chi(\boldsymbol{r}-\boldsymbol{r}', t-t') = -\beta \frac{d}{dt} \left\langle \Delta x(\boldsymbol{r},t) \Delta x(\boldsymbol{r}',t') \right\rangle_0. \tag{17.59}$$

The spatial Fourier transforms of above two equations are

$$\Delta x(\boldsymbol{q},t) = \int_{-\infty}^{t} dt' \chi(\boldsymbol{q}, t-t')\, f(\boldsymbol{q},t') = \int_{-\infty}^{\infty} dt' \chi(\boldsymbol{q}, t-t')\, f(\boldsymbol{q},t'), \tag{17.60}$$

and

$$\chi(\boldsymbol{q},t) = \int d\boldsymbol{r}\ e^{-i\boldsymbol{q}\cdot\boldsymbol{r}} \chi(\boldsymbol{r},t). \tag{17.61}$$

Upon a further Fourier transform in time,

$$\Delta x(\boldsymbol{q},\omega) = \chi(\boldsymbol{q},\omega)\, f(\boldsymbol{q},\omega) \tag{17.62}$$

where

$$\begin{aligned} \chi(\boldsymbol{q},\omega) &= \int_{-\infty}^{\infty} dt \int d\boldsymbol{r}\ e^{-i(\boldsymbol{q}\cdot\boldsymbol{r}-\omega t)} \chi(\boldsymbol{r},t) \\ &= \int_{0}^{\infty} dt \int d\boldsymbol{r}\ e^{-i(\boldsymbol{q}\cdot\boldsymbol{r}-\omega t)} \chi(\boldsymbol{r},t), \end{aligned} \tag{17.63}$$

which defines the Fourier transform of the dynamic response function. Familiar examples for the $\mathcal{X} - f$ conjugate pairs are local polarization density-electric field and local magnetization density-magnetic field.

P17.5 *Discuss a Gedanken experiment to learn how the charge density correlation* $\langle \Delta\sigma(\boldsymbol{r},t)\Delta\sigma(\boldsymbol{r}',0)\rangle_0$ *in a membrane can be determined.*

P17.6 *How can the undulation time correlation* $\langle h(\boldsymbol{r},t)h(\boldsymbol{r}',0)\rangle_0$ *in a stretched DNA and a planar membrane be obtained?*

17.2.4 Density Fluctuations and Dynamic Structure Factor

An important example of the FDT in a continuous system concerns the density fluctuations. Driven by an external potential field on each particle, $u(\boldsymbol{r},t)$, which varies spatially and temporally, the system has the perturbed Hamiltonian

$$\mathcal{H}' = \int \boldsymbol{n}(\boldsymbol{r})u(\boldsymbol{r},t)d\boldsymbol{r}, \tag{17.64}$$

where $\boldsymbol{n}(\boldsymbol{r}) = \sum_{\alpha=1}^{N} \delta(\boldsymbol{r}-\boldsymbol{r}_\alpha)$ is the microscopic number density. The potential applied at a position and time, $\boldsymbol{r}', t'$, disturbs the density distribution at other point and time $\boldsymbol{r}, t$ by

$$\Delta n(\boldsymbol{r},t) = -\int_{-\infty}^{t} dt' \int d\boldsymbol{r}'\chi_n(\boldsymbol{r}-\boldsymbol{r}',t-t')u(\boldsymbol{r}',t'), \tag{17.65}$$

which is expressed in the Fourier space:

$$\Delta n(\boldsymbol{q},\omega) = -\chi_n(\boldsymbol{q},\omega)u(\boldsymbol{q},\omega), \tag{17.66}$$

where the associated dynamic response function and susceptibility are:

$$\chi_n(\boldsymbol{r}-\boldsymbol{r}',t-t') = -\beta\frac{d}{dt}\langle \Delta\boldsymbol{n}(\boldsymbol{r},t)\Delta\boldsymbol{n}(\boldsymbol{r}',t')\rangle_0 \tag{17.67}$$

$$\chi_n(\boldsymbol{q},\omega) = \int_0^\infty dt \int d\boldsymbol{r}\, e^{-i(\boldsymbol{q}\cdot\boldsymbol{r}-\omega t)}\chi_n(\boldsymbol{r},t). \tag{17.68}$$

Like (17.29), the imaginary part of $\chi_n(\boldsymbol{q},\omega)$ is

$$\chi_n''(\boldsymbol{q},\omega) = \frac{\beta\omega}{2}C_n(\boldsymbol{q},\omega), \tag{17.69}$$

where

$$C_n(\boldsymbol{q},\omega) = \int_{-\infty}^{\infty} dt \int d\boldsymbol{r}\, e^{-i(\boldsymbol{q}\cdot\boldsymbol{r}-\omega t)} C_n(\boldsymbol{r},t) \tag{17.70}$$

is the Fourier transform of the density spatiotemporal correlation function

$$C_n(\boldsymbol{r}-\boldsymbol{r}',t) = \langle \Delta\boldsymbol{n}(\boldsymbol{r},\boldsymbol{t})\Delta\boldsymbol{n}(\boldsymbol{r}',)\rangle_0, \tag{17.71}$$

in the absence of the external field. Equation (17.69) means that the intrinsic density fluctuation at a Fourier mode $\boldsymbol{q},\omega$ is directly related to the energy dissipation induced by an oscillating external field at the mode. Equation (17.70) is rewritten as

$$C_n(\boldsymbol{q},\omega) = \int_{-\infty}^{\infty} dt\, e^{i\omega t} C_n(\boldsymbol{q},t) \tag{17.72}$$

where

$$\begin{aligned} C_n(\boldsymbol{q},t) &= \langle \Delta\boldsymbol{n}(\boldsymbol{q},t)\Delta\boldsymbol{n}(-\boldsymbol{q},0)\rangle_0 \\ &= \left\langle \sum_{\alpha=1}^{N}\sum_{\alpha'=1}^{N} e^{-i\boldsymbol{q}\cdot[\boldsymbol{r}_\alpha(t)-\boldsymbol{r}_{\alpha'}(0)]} \right\rangle_0 . \end{aligned} \tag{17.73}$$

Furthermore the density fluctuation is related to the dynamic structure factor $S(\boldsymbol{q},\omega)$ by

$$\begin{aligned} S(\boldsymbol{q},\omega) &= \frac{1}{2\pi N}\int_{-\infty}^{\infty} dt\, e^{i\omega t} C_n(\boldsymbol{q},t) \\ &= \frac{1}{2\pi N} C_n(\boldsymbol{q},\omega). \end{aligned} \tag{17.74}$$

The dynamic structure factor $S(\boldsymbol{q},\omega)$ is obtainable from the inelastic scattering experiments where $\boldsymbol{q},\omega$ are momentum and energy transferred to the matter by an incident radiation or a stream of quanta. It also probes the energy absorption in the system when driven by an oscillation at the wave vector $\boldsymbol{q}$ and frequency ω (17.69). Thus, a certain mode of the dispersion relation $\omega = \omega_c(\boldsymbol{q})$ that makes a peak in $S(\boldsymbol{q},\omega)$ signifies a collective mode of excitation in the system (Fig. 17.6). The dynamic structure factor is related to the static structure factor $S(\boldsymbol{q})$, (9.36), or $S(\boldsymbol{q}) = C(\boldsymbol{q},0)/N$, by

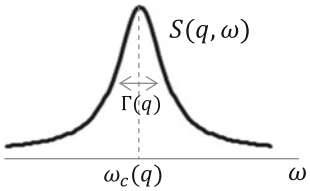

Fig. 17.6 A peak frequency $\omega_c(\boldsymbol{q})$ of a certain dynamic structure factor $S(\boldsymbol{q},\omega)$ signifies a collective mode, whereas the peak breadth $\Gamma(\boldsymbol{q})$ is a measure of dissipation associated with the mode. In self-diffusion, such a mode is density mode with $\omega_c(\boldsymbol{q}) = 0$ and $\Gamma(\boldsymbol{q}) = Dq^2$ (17.78)

$$\int_{-\infty}^{\infty} d\omega\, S(\boldsymbol{q},\omega) = S(\boldsymbol{q}) \tag{17.75}$$

$S(\boldsymbol{q},\omega)$ also contains the information on the transport properties of the systems at various length and time scales. To study diffusivity, we note that the correlation of density fluctuations at equilibrium is governed by the diffusion equation via the Onsager' regression theorem: from the Fourier transform of the diffusion equation in space, $\partial n(\boldsymbol{q},t)/\partial t = -Dq^2 n(\boldsymbol{q},t)$, we can write

$$\frac{\partial}{\partial t} C_n(\boldsymbol{q},t) = -Dq^2 C_n(\boldsymbol{q},t), \tag{17.76}$$

which is integrated to

$$C_n(\boldsymbol{q},t) = e^{-|t|Dq^2} C_n(\boldsymbol{q},0). \tag{17.77}$$

Using the relation (17.74) we find

$$\begin{aligned} S(\boldsymbol{q},\omega) &= \frac{1}{2\pi N} \int_{-\infty}^{\infty} dt\, e^{i\omega t}\; e^{-Dq^2|t|} C_n(\boldsymbol{q}, t=0) \\ &= \frac{1}{\pi} \frac{Dq^2}{\omega^2 + (Dq^2)^2} S(\boldsymbol{q}), \end{aligned} \tag{17.78}$$

$S(\boldsymbol{q},\omega)$ has a Lorenzian peak at the collective (hydrodynamic density) mode at $\omega_c(\boldsymbol{q}) = 0$ with the dispersion $\Gamma(\boldsymbol{q}) = Dq^2$. For an infinitely dilute concentration of the particles, $S(\boldsymbol{q}) = 1$, and $C_n(\boldsymbol{q},t)$ and the associated D are called the Van-Hove

correlation function and self-diffusion constant. The diffusion constant can be extracted from the dynamic structure factor determined by inelastic scattering measurement using (17.78) rewritten as the relation

$$D = \lim_{\omega \to 0} \lim_{q \to 0} \frac{\omega^2}{q^2} \pi S(\boldsymbol{q}, \omega). \tag{17.79}$$

The two limits of small q and ω means the large length and the long time scales over which the hydrodynamic transport coefficients, the self-diffusivity in this case, are defined.

Over small length and shorter time scales one can define the wavenumber and frequency-dependent diffusivity $D(\boldsymbol{q}, \omega)$ that extends the ordinary self-diffusion constant to microscopic scales; (17.78) can be rewritten as

$$S(\boldsymbol{q}, \omega) = \frac{1}{\pi} \frac{D(\boldsymbol{q}, \omega) q^2}{\omega^2 + [D(\boldsymbol{q}, \omega) q^2]^2}. \tag{17.80}$$

From this formula, one can set up the generalized diffusion equation involving a diffusivity which is nonlocal in space and non-Markovian in time; first, the number density flux is generalized to

$$\boldsymbol{J}(\boldsymbol{x}, t) = - \int_{-\infty}^{\infty} dt' \int d\boldsymbol{r}' D(\boldsymbol{r} - \boldsymbol{r}', t - t') \nabla_{\boldsymbol{r}'} n(\boldsymbol{r}', t'). \tag{17.81}$$

And then from the continuity equation $\frac{\partial}{\partial t} n(\boldsymbol{r}, t) = -\nabla \cdot \boldsymbol{J}(\boldsymbol{r}, t)$, we obtain the diffusion equation in a general form

$$\frac{\partial}{\partial t} n(\boldsymbol{r}, t) = \int_{-\infty}^{\infty} dt' \int d\boldsymbol{r}' \nabla_{\boldsymbol{r}} \cdot D(\boldsymbol{r} - \boldsymbol{r}', t - t') \nabla_{\boldsymbol{r}'} n(\boldsymbol{r}', t'). \tag{17.82}$$

For concentrated particles, or systems with complex internal structures with nontrivial $S(\boldsymbol{q})$ such as a polymer, one may still use (17.78). The concentration-dependent hydrodynamic diffusivity D, called the collective diffusivity, and its generalization $D(\boldsymbol{q}, \omega)$, can be obtained from the scattering data via

$$S(\boldsymbol{q}, \omega) = \frac{1}{\pi} \frac{D(\boldsymbol{q}, \omega) q^2}{\omega^2 + [D(\boldsymbol{q}, \omega) q^2]^2} S(\boldsymbol{q}). \tag{17.83}$$

Further Reading and References

L. Onsager, Reciprocal relations in irreversible processes. I. Phys. Rev. **37**, 405 (1931); L. Onsager, Reciprocal relations in irreversible processes. II. Phys. Rev. **38**, 2265 (1931)

R. Kubo, M. Toda, N. Hashitsume, *Statistical Physics II: Nonequilibrium Statistical Mechanics*. Series in Solid-State Sciences (Springer, Berlin, 1998)

P. Martin, A.J. Hudspeth, F. Jülicher, Comparison of a hair bundle's spontaneous oscillations with its response to mechanical stimulation reveals the underlying active process. Proc. Natl. Acad. Sci. **98**(25) (2001)

W. Stephenson et al., Combining temperature and force to study folding of an RNA hairpin. Phys. Chem. Chem. Phys. R. Soc. Chem. **16**, 906 (2014)

Chapter 18
Noise-Induced Resonances: Stochastic Resonance, Resonant Activation, and Stochastic Ratchets

Our world is replete with noises. In common sense a noise is a nuisance that blocks coherence; you feel annoyed with ambient sound noises when listening to music. In this chapter we will study **a counter-intuitive phenomenon, called stochastic resonance (SR), where a periodically modulated perturbation or signal too weak to be detected can be enhanced by adding the random noise to a nonlinear system** (Fig. 18.1). The noise with an optimal strength can be instrumental rather than harmful in driving synchrony and resonance. There exists another noise-induced phenomenon, **the resonant activation (RA), where the rate of the noise-induced transition is maximized by a modulation of an external signal at an optimal rate**.

Biological systems in cellular level live on a variety of noises, the ambient temperature in particular. Due to their flexibility manifested on mesoscopic scale, some biological complexes may utilize the ambient noises for their biological transitions and functions. As we have seen in Chap. 16, thermal fluctuations in such soft-condensed matter facilitate the barrier crossing seemingly difficult to surmount, typically assisted by conformational transitions. Added to this phenomenon, the SR and RA can provide essential physical mechanisms for inducing coherence and order in noisy and dissipative environments out of equilibrium.

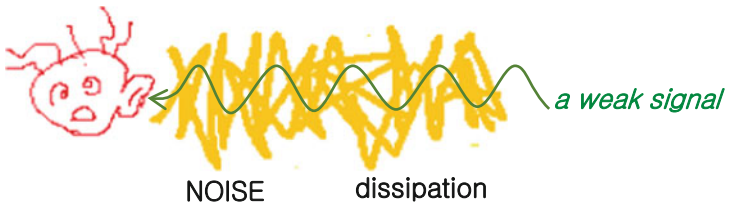

Fig. 18.1 A cartoon describing the phenomenon of stochastic resonance. A weak signal can be enhanced in a dissipative media by an ambient noise at the optimal strength

W. Sung, *Statistical Physics for Biological Matter*, Graduate Texts in Physics,
https://doi.org/10.1007/978-94-024-1584-1_18

18.1 Stochastic Resonance

18.1.1 Theory

There are many review articles on SR; to name one, (Gammaitoni et al. 1998). As a generic example of the dynamics that shows SR, consider a Markov process $q(t)$ of crossing over a barrier is governed by the Langevin equation,

$$\dot{q} = \mathcal{U}(q) + R(t). \tag{18.1}$$

Here $R(t)$ is the Gaussian and white noise that satisfies $\langle R(t)R(t')\rangle = 2\mathcal{D}\delta(t-t')$, $\mathcal{U}(q) = -\mathcal{D}\partial\Phi(q)/\partial q$ (15.29) is the driving force under a double well potential $\Phi(q)$. A concrete example of q is the position of a Brownian particle thermally hopping in a double-well potential $U(q) = k_BT\Phi(q)$, satisfying the Langevin equation, $\zeta\dot{q} = -\partial U(q)/\partial q + f_R(t)$, where $\langle f_R(t)f_R(t')\rangle = 2\zeta k_BT\delta(t)$, $\zeta = k_BT/\mathcal{D}$ is the friction coefficient of the particle.

Let us consider the case of high barrier $\Delta\Phi \gg 1$, or $\Delta U \gg k_BT$ for the Brownian particle. As we studied earlier, the mean time to cross the barrier is the Kramers time $\tau_K = 2\pi e^{A\Phi}/(\mathcal{D}\Omega_M\Omega_m)$ where the Ω_M, Ω_m are the curvatures of the potential, $\Phi''(q)$, at the barrier top and the well bottom (Chap. 16). The dynamical state or Brownian particle infrequently and randomly crosses the barrier, with the stochastic trajectory schematically shown in Fig. 18.2a.

To emphasize the role of the noise we make all variables be dimensionless with $\mathcal{U}(q) = q - q^3$ so that $\Phi(q) = \mathcal{D}(-q^2/2 + q^4/4)$. Then,

$$\tau_K(\mathcal{D}) = \sqrt{2}\pi \exp\left[\frac{1}{4\mathcal{D}}\right]. \tag{18.2}$$

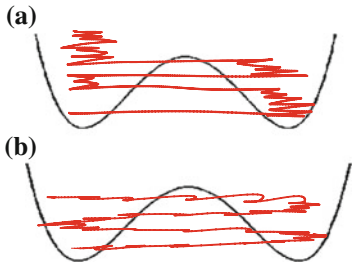

Fig. 18.2 Schematic trajectories of a Brownian particle hopping under a double well potential: **a** For the case without an external force the hopping is random, **b** but the hopping becomes coherent to the oscillating force when the SR condition is met

The τ_K depends strongly on the noise strength $\mathcal{D}$; for a Brownian particle with $\zeta = 1$, the noise is the thermal noise of strength $\mathcal{D} = k_B T$, whose variation will affect the τ_K in a very nonlinear way.

Now suppose that the state or particle is driven by an oscillating force $f(t) = a\cos\Omega t$, with the amplitude a which is too small to roll the particle from a well to the other:

$$\dot{q} = q - q^3 + a\cos\Omega t + R(t). \tag{18.3}$$

If the noise strength $\mathcal{D}$ is vanishingly small, the particle hops very rarely and mostly remains in the wells, independently of the oscillation force. If, on the other hand, the noise strength is very high, it will cross the barrier very frequently and randomly, little influenced by the oscillation force. In both limits, the particle is incoherent to the external driving. However, with the noise tuned to such an optimal strength $\mathcal{D}_R$ that the periods of thermal jumps matches with that of the oscillation, i.e.,

$$2\tau_k(\mathcal{D}_R) = \frac{2\pi}{\Omega}, \tag{18.4}$$

we can expect that **there will be the maximum coherence, that is, the maximal cooperation between the noise and external driving for the barrier crossing**. This noise-assisted phenomenon is called as stochastic resonance (SR). The optimal strength of the noise is given by

$$\mathcal{D}_R = 1/\left[4\ln\left(\frac{1}{\sqrt{2}\Omega}\right)\right]. \tag{18.5}$$

Figure 18.2b schematically depicts the hopping and its trajectory coherent to the external oscillation at this optimal condition.

The idea of SR was first introduced by Benzi et al. (1982) to account for the periodic occurrence of ice age. The data of the continental ice volume variation over 10^6 years shows that the glaciation sequence has an average periodicity of about 10^5 years. On the other hand, it is known that there is a very small change in eccentricity of the earth orbital that has about the same periodicity. An intriguing question is how this small orbital perturbation can cause such a global climate change. Benzi and others modeled the global climate as the stochastic variable $q(t)$ that varies under a double well potential with the two minima representing the ice and normal ages. The effect caused by the earth orbital eccentricity is given by a small periodic force. Then what is the noise? On the long time over the period, daily weather fluctuations can be treated as a random noise. If the noise strength is tuned to an optimal value (by whom?), the hopping between the ice age to normal age, otherwise random, can be made synchronous to the orbital modulation, according to the argument of Benzi and others.

Because the external driving is a perturbation, we can quantify the response of the system following the linear response theory we studied in Chap. 17. Due to the perturbation in the Hamiltonian

$$\mathcal{H}' = -q\,f(t) = -qa\cos(\Omega t) \tag{18.6}$$

the average deviation of $q(t)$ from the mean, which otherwise is zero in this bistable potential, emerges as

$$\langle \Delta q(t) \rangle = \int_0^t dt' \chi_q(t-t')\, f(t') = a \int_0^t dt'\ \chi_q(t-t') \cos(\Omega t'). \tag{18.7}$$

The dynamic response function $\chi_q(t)$ is given by the fluctuation-dissipation theorem (FDT) (17.24):

$$\chi_q(t) = -\frac{1}{\mathcal{D}} \frac{d}{dt} \langle \Delta q(t) \Delta q(0) \rangle_0 \tag{18.8}$$

in terms of the time correlation function in the absence of the driving. The time correlation function is given by (15.100),

$$\langle \Delta q(t) \Delta q(0) \rangle_0 \approx \left\langle \Delta q^2 \right\rangle_0 e^{-\lambda_1 t} \approx \left\langle \Delta q^2 \right\rangle_0 e^{-2t/\tau_K} \tag{18.9}$$

Here $\lambda_1 \approx 2/\tau_K \approx \left(\sqrt{2/\pi}\right) \exp[-1/4\mathcal{D}]$ (15.97) is the lowest nonvanishing eigenvalue of the FP operator corresponding to the Langevin equation (18.1) in the absence of the external force. The approximation (15.100) is valid over the long time to cross the high barrier, and is exact at $t = 0$.

Using the (18.8), (18.9), and FDT (17.24) we can calculate the frequency-dependent response function as

$$\begin{aligned} \chi_q(\Omega) &= \int_0^\infty dt\, e^{i\Omega t} \chi_q(t) = \frac{2\left\langle \Delta q^2 \right\rangle_0}{\tau_K \mathcal{D}} \int_0^\infty dt\, e^{i\Omega t} e^{-2t/\tau_K} \\ &= \frac{\left\langle \Delta q^2 \right\rangle_0}{\mathcal{D}} \frac{1 + i\Omega\tau_K/2}{1 + (\Omega\tau_K/2)^2}. \end{aligned} \tag{18.10}$$

In terms of this, the displacement is given as

$$\langle \Delta q(t) \rangle = \left|\chi_q(\Omega)\right| a \cos(\Omega t - \phi), \tag{18.11}$$

where $\left|\chi_q(\Omega)\right| = \langle \Delta q^2 \rangle_0 / [\mathcal{D}\{1 + (\Omega\tau_K/2)^2\}^{1/2}]$ is the absolute amplitude of the response. $\left|\chi_q(\Omega)\right|$ depends on Ω as well as $\mathcal{D}$ in a nontrivial way. For a small $\mathcal{D}$, the amplitude goes like $\left|\chi_q(\Omega)\right| \sim 1/(\mathcal{D}\tau_K) \sim \mathcal{D}^{-1} \exp[-1/4\mathcal{D}]$, which tends to vanish

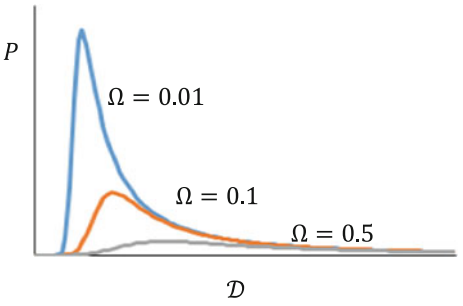

Fig. 18.3 The power amplification factor $P = \left|\chi_q(\Omega)\right|^2$ has a stochastic resonance peak at an optimal value of the noise-strength $\mathcal{D}$. The peak position and height depend on the frequency Ω

in the $\mathcal{D} \to 0$ limit. In the limit of a large $\mathcal{D}$, $\left|\chi_q(\Omega)\right| \sim \mathcal{D}^{-1} \to 0$. For a finite level of the $\mathcal{D}$ where $\tau_K \sim \Omega^{-1}$, which is consistent with the condition (18.4), $\left|\chi_q(\Omega)\right|$ can be the maximum. Figure 18.3 shows how **the power amplification** defined by

$$P = \left|\chi_q(\Omega)\right|^2 = \frac{\langle \Delta q^2 \rangle_0^2}{\mathcal{D}^2 \left\{1 + \left(\frac{\Omega \tau_K}{2}\right)^2\right\}} \tag{18.12}$$

peaks at an optimal value of the noise strength for various values of Ω.

The power amplification $\left|\chi_q(\Omega)\right|^2$ is one of the most common quantifier of SR. Not only it is a direct measure of the coherent response, it is also related with $q's$ power spectrum $S_f(\omega) = \int_{-\infty}^{\infty} dt\, e^{i\omega t} \langle q(t) q(0) \rangle$ in *the presence of the external force*. Experimentally $S_f(\omega)$ has a predominant peak at $\omega = \Omega$, as the signature of the bona-fide resonance, and the secondary peak at $\omega = 3\Omega$, which is generated by the system nonlinearity (Fig. 18.4). Analytically, because the force is a perturbation, $q(t)$ is can be separated into noisy background and periodic components so that the power spectrum is given by (Jung and Hänggi 1989)

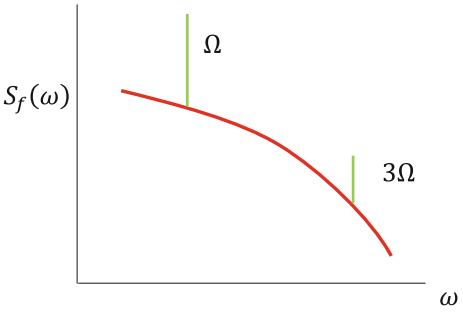

Fig. 18.4 The power spectrum $S_f(\omega)$ of the process in the presence of an oscillatory force with the frequency Ω

$$S_f(\omega) \approx \frac{1}{2}\pi a^2 \left|\chi_q(\Omega)\right|^2 \{\delta(\omega-\Omega)+\delta(\omega+\Omega)\} + S(\omega). \tag{18.13}$$

$\left|\chi_q(\Omega)\right|^2$ is proportional to the height of the primary delta peak at $\omega = \Omega$, which is superimposed on the force-free power spectrum of the noisy background $S(\omega)$. $S(\omega)$, the Fourier transform of (18.9), decays with the frequency as a Lorentzian, $S(\omega) = \langle \Delta q^2 \rangle_0 \tau_K / [1 + (\omega \tau_K/2)^2]$.

Another signature of SR is the signal-to-noise-ratio (SNR) defined and given by

$$\begin{aligned} SNR &= \lim_{\Delta\omega \to 0} \int_{\Omega-\Delta\omega}^{\Omega+\Delta\omega} d\omega \, S_f(\omega)/S(\Omega) \\ &= \pi a^2 \left\langle \Delta q^2 \right\rangle_0 R_K(\mathcal{D})/\{2\mathcal{D}^2\} \end{aligned} \tag{18.14}$$

where $R_K = \tau_K^{-1}$ is the Kramers rate. The SNR also exhibits a peak at an optimal noise strength; it is adopted as another measure of SR in some experiments (Wiesenfeld and Moss 1995).

The SR can be applied to detect the weak signals in a noisy environment in a wide variety of the situations in nature and technologies, such as signal processing, nonlinear optics, solid state devices, including biological systems such as sensory neurons, depending on the nature of the noises. In particular in the biological systems on mesoscales are susceptible to the ubiquitous thermal fluctuations, which can use the SR to modulate biological conformational transitions, as exemplified below.

P18.1 *A dynamical state of a biopolymer undergoes transition between two states 1 and 2, with rates given by* $R_{1\to 2} = Ce^{-\Delta f_{12}/k_BT}$ *and* $R_{2\to 1} = Ce^{-\Delta f_{21}/k_BT}$, *where* Δf_{ij} *is the free energy barrier for the transitions. Suppose that* $\Delta f_{12} = \Delta e - T\Delta s$, $\Delta f_{21} = \Delta e$ *where* $\Delta e > 0$ *and* Δs *is the internal energy and entropy changes that are independent of temperature T. Apply a weak oscillating force of the frequency* ω *that couples with the reaction coordinate. If the force induces a stochastic resonance, what is the optimal value for the noise strength* k_BT*? How does it depend on the entropy changes* Δs*?*

18.1.2 Biological Examples

Ion Channel

An ion channel is a protein nano-machine that regulates the ionic transport through a membrane, thus plays a fundamental role in transmitting electric signals in nerve cells. A channel can open and close in response to an external stimuli; the

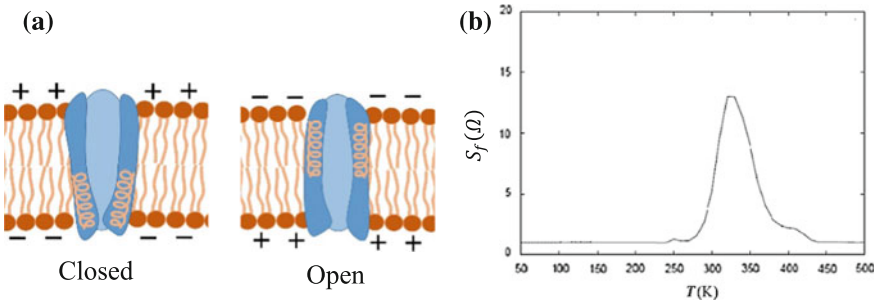

Fig. 18.5 **a** A schematic picture of a voltage-gated ion channel. With a membrane potential applied the gating charge (positively charged helix) shifts to the extra-cellular side inducing the channel to open. **b** The peak in the power spectrum $S_f(\Omega)$ for the gating charge flow emerges around 320 K in a guinea pig ileal muscle channel. Adapted from Parc et al. (2009)

voltage-gated ion channel undergoes conformational transitions between a closed state and open state depending on the membrane potential (Fig. 18.5a).

The dynamics of ion channel transitions and the associated transmembrane ion transport is an enormously complicated problem requiring multiscale descriptions. In a most coarse-grained description of voltage-gated channels, the single, relevant degree of freedom $q(t)$ can be chosen as the position of the gating charge, representive of positively charged helices within the channel, which is believed to be the major component of voltage sensor. An increase of membrane potential makes this gating charge move toward the extracellular side, triggering a conformational transition to the open, conductive state. In this coarse-grained picture, the gating charge can be considered to be a Brownian particle hopping between two conformational states.

In the presence of a noisy macromolecular and fluid environment, the center-of-mass position q of the gating charge is subject to its complex free energy landscape, with the free energy parameters such as activation barrier sensitively depending on *temperature*. For a guinea pig ileal muscle channel for which data on the parameters as well as the rates are available, a double well free energy model for the two state transitions was constructed (Parc et al. 2009). An important feature here is that the transition rates are not Arrhenius-like because of the temperature-dependent activation barrier. With a weak, oscillating voltage added to a constant potential across the membrane, a simulation of the gating charge displacement showed its power spectrum $S_f(\omega)$ indeed manifested the SR peak at the driving frequency $\omega = \Omega$. The peak height $S_f(\Omega)$ is maximum at an optimal noise strength, which is found to be just the body temperature $T_{SR} = 320\,\mathrm{K}$ of the guinea pig (Fig. 18.5b)! **The ion channel, owing to the flexible structures, opens and closes in a maximum coherence with the oscillating membrane potential at the body temperature. This suggests that the body temperature is not accidental but, possibly, an outcome of nature's selection to make it a good noise essential for living.**

Biopolymers Under Tension

RNA molecules are biopolymers that carry and relocate hereditary information of vital importance. The RNA folds into unique three dimensional conformation called tertiary structure, by sequential binding of an essential secondary structure, named as RNA hairpin.

The single-molecule experiments showed how the RNA hairpins subject to a stretching force provided by optical tweezers undergo conformational changes from folded to unfolded states (Fig. 18.6). A Brownian dynamic simulation of the folding-unfolding trajectories of a model 22-nucleotide P5GA RNA hairpin under a constant force f indicates that the free energy as a function of the extension z is bistable (Fig. 18.6b). The mean folding and unfolding times are the Kramers times

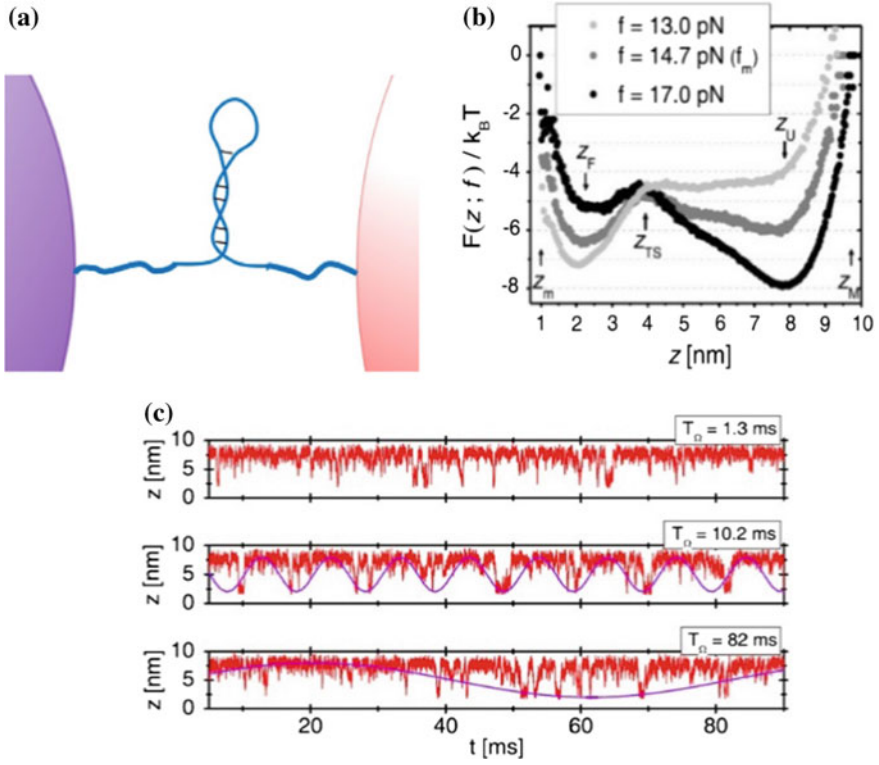

Fig. 18.6 **a** P5GA RNA hairpin under a stretching force exerted by an optical tweezer. **b** A Brownian dynamic simulation on a model 22-nucleotide P5GA RNA hairpin shows that, depending on the force f, the free energy of the extension is bistable with two conformational states, a folded state at the extension z_F, and a unfolded state at z_U and the transition state (barrier top) at z_{TS}. **c** The time trajectories of the extension under a time dependent tension $f + \delta f \cos \Omega t$ with $f = 17$ pN, $\delta f = 1.4$ pN from a Brownian dynamic simulation. The transition from the unfolded state to the folded state synchronizes to the periodic driving of the resonant period 10.2 ms, while it is incoherent to the oscillations with smaller and higher periods. Adapted from Kim et al. (2012)

for crossing the free energy barrier from right to left and vice versa, which for the case $f = 17$ pN are $\tau_F(f) = 10.3$ ms and $\tau_U(f) = 0.5$ ms, respectively.

With a small oscillatory force $\delta f \cos\Omega t$ with $\delta f = 1.4$ pN plus the constant force $f = 17$ pN applied on each segment of the RNA hairpin, the SR of the folding-unfolding dynamics was studied (Kim et al. 2012). The simulations show that although the probability of being in the folded state at a large force such as $f = 17$ pN is as low as $\approx 5\%$, folding transitions occur in coherence to the oscillation if its period $T_\Omega \equiv 2\pi/\Omega$ is tuned to be the optimal value $\simeq 10.2$ ms (Fig. 18.5c). Remarkably this T_Ω is approximately the sum of the mean folding and unfolding transition times in the absence of oscillatory driving,

$$T_\Omega = \tau_F(f) + \tau_U(f) \approx 10.8 \text{ ms}, \tag{18.15}$$

which is the matching SR condition for asymmetric bi-stable potential that generalizes (18.4).

Added to the thermal fluctuation, there are plenty of athermal, nonequilibrium noises in vivo biological systems. The phenomenon of SR means that biopolymers can filter their intrinsic resonance frequencies from the spectrum of external signals and non-equilibrium fluctuations. The particular frequency mode out of the nonequilibrium noises, although weak, may synchronize (SR) the transition dynamics of biopolymers, which can be important to biological functions.

The linear response theory allows us to determine the change of the extension of a polymer in response to an additional time-dependent force from time correlation of the extension. If it decays exponentially with a single relaxation time τ,

$$\langle \Delta\mathcal{X}(t)\Delta\mathcal{X}(0)\rangle_0 = \left\langle (\Delta\mathcal{X})^2 \right\rangle_0 e^{-t/\tau}, \tag{18.16}$$

we then have

$$P = |\chi(\Omega)|^2 = \frac{\left\langle (\Delta\mathcal{X})^2 \right\rangle_0}{(k_B T)^2} \frac{1}{1 + (\tau\Omega)^2}. \tag{18.17}$$

Indeed the power amplification P is maximum at an optimal temperature T_{SR} if τ in this model has a certain temperature dependence. It was shown that the extension of a stretched worm-like chain in water can show such behavior (Kim and Sung 2012).

18.2 Resonant Activation (RA) and Stochastic Ratchet

The free energy function to which a dynamical state is subject may fluctuate and be modulated in time, away from equilibrium in biological environments, due to reactivity and external noises. **The mean first passage time (MFPT) required to cross over the fluctuating barrier may exhibit a minimum when the**

characteristic time of the fluctuation is optimized. This is another kind of noise-induced resonance phenomenon called the **resonant activation** we will sudy here.

18.2.1 Model

As a simple analytical model, Doering and Gadoua (1992) considered the piece-wise linear potential $V(q)$, which flips randomly between two configurations $V_+(q)$ and $V_-(q)$ with maxima E_+ and E_- respectively (Fig. 18.7) as a dichotomic process. If the flipping rates between two potential are γ, the master equation for $P_\pm(t)$, the probability that the state to be at the potential $V_\pm$ at time t is

$$\frac{\partial}{\partial t}P_+(t) = -\gamma P_+(t) + \gamma P_-(t) \tag{18.18}$$

$$\frac{\partial}{\partial t}P_-(t) = -\gamma P_-(t) + \gamma P_+(t) \tag{18.19}$$

which is similar to the (14.38), (14.39) we studied. The densities of the joint probability $P_\pm(q,t)$ that the dynamical state assumes q and each configuration $V_\pm$ satisfies the coupled Fokker-Planck equations:

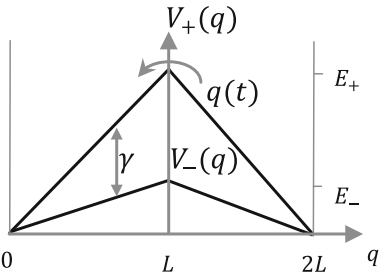

Fig. 18.7 A fluctuating potential $V_\pm(q)$ for the problem. The barrier height of the triangular potential fluctuates between E_+ and E_- at rate γ.

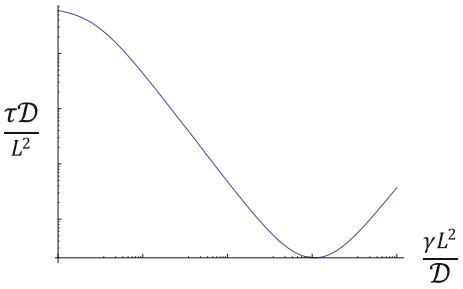

Fig. 18.8 The mean-first passage time τ versus the flipping rate γ of the dichotomic noise. Adapted from Doering and Gadoua (1992) with permission. Copyright (1992) by the American Physical Society

$$\frac{\partial}{\partial t}P_+(q,t) = [-\gamma + \mathcal{L}_+]P_+(q,t) + \gamma P_-(q,t) \tag{18.20}$$

$$\frac{\partial}{\partial t}P_-(q,t) = \gamma P_+(q,t) + [-\gamma + \mathcal{L}_-]P_-(q,t), \tag{18.21}$$

where $\mathcal{L}_\pm = \partial/\partial q\{-\mathcal{U}_\pm + \mathcal{D}\partial/\partial q\}$ is the FP operator with $\mathcal{U}\pm = -E_\pm/L$, the constant drift toward each configuration.

We consider the first passage problem, where the state variable, initially at $q = 0$ (the bottom of the left well, Fig. 18.7) crosses over the fluctuating barrier. The initial condition is $P_\pm(q,0) = \delta(q)/2$ while we assign the absorbing boundary conditions at the barrier top, $P_\pm(q = L, t) = 0$, as well as the reflecting one $(\mathcal{U}_\pm - \mathcal{D}\partial/\partial q)P_\pm(q = 0, t) = 0$ on the left wall. From (16.4), the MFPT is given by

$$\tau = \int_0^\infty dt \int_0^L dq\{P_+(q,t) + P_-(q,t)\}. \tag{18.22}$$

For the case where the barrier height fluctuates between E_+ and E_- (with the choice of $E_+ = -E_- = E$), an analytical but complicated expression for τ were obtained resulting in Fig. 18.8 (Doering and Gaduoa 2002). To highlight physics that underlies the result, we summarize two limiting situations. For $\gamma \ll \mathcal{D}/L^2$, that is, for the barrier flipping much slower than the diffusion over the length time L, the MFPT approaches the average of the MFPTs for each potential configurations:

$$\tau = \frac{1}{2}\{\tau(E) + \tau(-E)\} \tag{18.23}$$

where

$$\tau(E) = \frac{L^2}{E}\left[\frac{\mathcal{D}}{E}\left(e^{E/\mathcal{D}} - 1\right) - 1\right] \tag{18.24}$$

is MFPT for traversing the length L under the potential $V_+(q)$ (that is, under a constant backward bias $\mathcal{U} = -E/L$, (16.17)). Due to the exponential factor $\tau(E)$ dominates the average (18.23) and is much longer than that in the absence of the flipping potential, that is, the free diffusion time, $\tau(0) = L^2/2\mathcal{D}$. In the other limit when the flipping is much faster than the diffusion, $\gamma \gg (\mathcal{D}/L^2)$, the q feels the average potential $\bar{E} = (E_+ + E_-)/2$, which is zero, so that

$$\tau = \frac{L^2}{\bar{E}}\left[\frac{\mathcal{D}}{\bar{E}}\left(e^{\bar{E}/\mathcal{D}} - 1\right) - 1\right] = \tau(0), \tag{18.25}$$

the time for free diffusion. At intermediate flipping rates, however, the MFPT is less than either of these two limits, taking a minimum τ_R at an optimal rates which is comparable to the inverse of the diffusion time in the absence of the flipping potential (Fig. 18.8). This optimal condition much resembles the matching condition of SR.

Example: Rigid Polymer Translocation Under a Fluctuating Environment

A simple variant of the above analysis can be applied to biological problems. The cellular environments fluctuate ceaselessly not only thermally but also by a non equilibrium means, e.g., via the chemical reactions and external noises. We consider the translocation of a stiff chain (such as a double stranded DNA fragment shorter than its persistence length (50 nm) of N segments each of length l (Fig. 18.9a). Because of the chain stiffness, the translocation is not affected by the chain entropy but by the chemical potential difference $\Delta\mu$ per segment across the membrane. As a simple model of the thermal noise added to $\Delta\mu$, we consider the

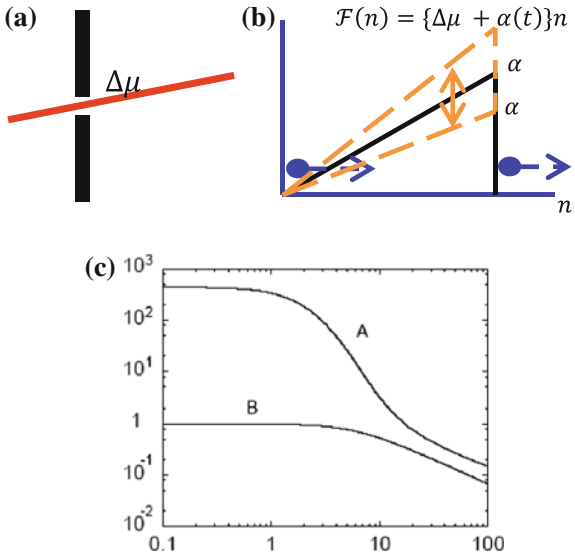

Fig. 18.9 **a** A rigid polymer translocating through a pore in a membrane, which is depicted as crossing the barrier of **b** the fluctuating free energy $\mathcal{F}(n)$. **c** Resonant (minimal) translocation time τ_R in units of $\tau_0 \equiv L^2/(2D)$ versus chemical potential fluctuation amplitude $|\alpha|/(k_BT/N)$. ($\langle\Delta\mu\rangle/(k_BT/N) = 10$ (A), ($\langle\Delta\mu\rangle/(k_BT/N) = 0$ (B). For large fluctuation amplitude, τ_R is determined mainly by $|\alpha|/(k_BT/N)$. Small nonequilibrium noise enhance translocation rate. Republished from Park and Sung (1998); permission conveyed through Copyright Clearance Center, Inc.

dichotomic process $\alpha(t)$ that flips between two levels, $\pm\alpha$ with a rate γ (Fig. 18.9b). Then, the stochastic equation for $n(t)$, the number of segments in the trans-side is

$$\zeta l\dot{n} = -\frac{\partial}{l\partial n}\mathcal{F}(n) + f_R(n,t) = -\{\Delta\mu + \alpha(t)\}/l + f_R(n,t) \tag{18.26}$$

where $f_R(n,t)$ is the usual thermal noise, and $\mathcal{F}(n) = \{\Delta\mu + \alpha(t)\}n$ is the fluctuating free energy shown Fig. 18.8b.

The FPE for $P_\pm(n,t)$ that the chain is in the state $\pm\alpha$ with the number of translocated segment n satisfies (18.20) and (18.21) with the operator $\mathcal{L}_\pm = \partial/l\partial n\{-\mathcal{U} \pm + D\partial/l\partial n\}$. Here $\mathcal{U}\pm = -\beta D(\Delta\mu \pm \alpha)/l$ and $D = k_BT/\zeta$ are respectively the drift velocity and the diffusivity of the chain. With an adsorbing BC at $n = N$ and a reflecting BC at $n = 0$ as well as the initial condition, $P_\pm(n,0) = \delta(n)/2$, the MFPT, namely, translocation time was obtained as a function of the flipping rate γ and amplitude α (Park and Sung 1998). It is shown that the MFPT indeed exhibit its minimum τ_R at the optimal flipping rate $\gamma \sim D/L^2$.

In Fig. 18.9c, the resultant minimum translocation time τ_R is depicted as a function of the amplitude α of the dichotomic noise for given values of $\Delta\mu$. First consider $\Delta\mu = 0$, the case of no bias. The dichotomic noise can reduce the translocation time to one-tenth of the free diffusion time $\tau_0 = L^2/2\mathcal{D}$, if α exceeds 100 k_BT/N, which is a small fraction of k_BT/N for a long chain. **More surprising is that even for the case of the backward bias the translocation time can be reduced below the free diffusion time for large *N*.**

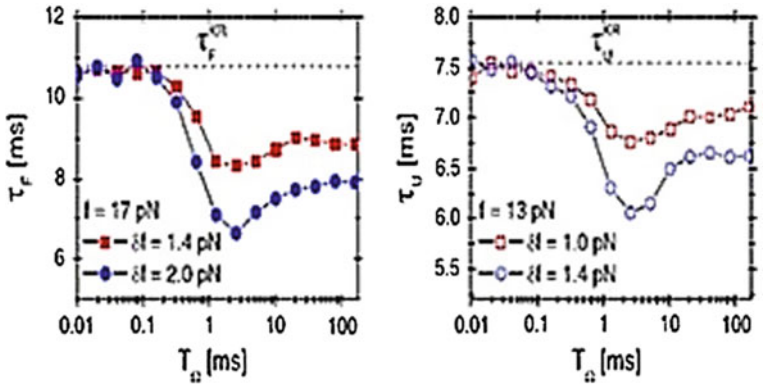

Fig. 18.10 Resonant activation (RA) in folding and unfolding transition of an RNA hairpin under the small oscillating tension *δfcosΩt added to the constant tension f*. The folding and unfolding times τ_F, τ_U become minima when the periods of the oscillation Ω are optimal. Adapted from Kim et al. (2012)

Stretched RNA Hairpin

An oscillatory tension added on the stretched RNA hairpin can also modulate the free energy of extension (Fig. 18.6b). Figure 18.10 shows that at optimal periods of oscillation both the folding and unfolding times can be be minima, which deepens as the amplitude of the oscillation increase. The optimal periods are comparable to the period of oscillation within the wells of the free energy landscape (Fig. 18.6b), so are much shorter than that required for the SR (18.15).

18.3 Stochastic Ratchets

The possibility of extracting an usable work from fluctuations has been a long-standing problem of immense interest. In the presence of the (equilibrium) thermal fluctuations alone which satisfies the FDT, $\langle f_R(t) f_R(t') \rangle = 2\zeta k_B T \delta(t)$, a Brownian particle approaches to the equilibrium, and thus does not perform net motion in an unbiased potential. **The directed motion, however, can occur in locally asymmetric potential called 'ratchet' subject to athermal noises that drives the system out of equilibrium** (Astumian and Hänggi 2002). Furthermore, the resonant activation under the fluctuating potentials can be utilized to enhance the directed motion in an optimal way.

We consider the one-dimensional overdamped Brownian motion under the ratchet potential $U(x)$, which is a periodic, but locally piece-wise linear and asymmetric (Fig. 18.11). A dichotomic noise switches the potential between $U(x)$ and zero with the rate γ. Then the joint probability in the flashing potential is given by the FPE, (18.20) and (18.21) with the drift is given by $\mathcal{U}_+ = \beta D U'(x)$ and $\mathcal{U}_- = 0$.

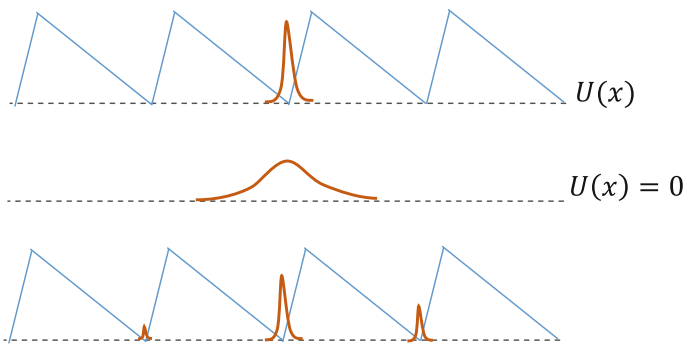

Fig. 18.11 The ratchet potential that flips between 0 to $U(x)$. Due to the asymmetry, the flipping noise drives the Brownian particle to move right

The net current of the Brownian particle is

$$J(x,t) = -D\left[\beta U'(x)P_+(x,t) + \frac{\partial}{\partial x}\{P_+(x,t) + P_-(x,t)\}\right]. \tag{18.27}$$

In the absence of the flipping, despite the asymmetry of the ratchet potential, the J becomes zero in the stationary state, at which the probability density approaches $P(x) = P_+(x) \sim e^{-\beta U(x)}$. The question is: does the flipping induce a net current? If it does, in what direction?

If the flipping is very slow, the net current is zero, because it is the average of the current generated in each configuration. For the fast flipping, it, resulting from the average potential, is also zero. But at an optimal flipping time that is comparable to the diffusion time, the net current can be induced. This can be explained as follows. In the presence of the ratchet potential, the particle will likely to be at a potential minimum. When the potential is turned off the particle begins to freely diffuse. After the potential is switched on again, it will have more chance to be near the next well located at the right hand side, than to be near the well at the left (Fig. 18.11). This way being repeated, the particle tends to move to the right systematically. Also it was shown that **the flipping noise can drive the particle on the ratchet potential to move uphill against constant applied force** (Astumian and Bier 1994).

This means that the system is capable of extracting energy from the fluctuations to use for work. The idea of this noise-assisted phenomenon has been applied to biomolecular motors, such as protein motors along microtubules, where the fluctuation is brought about by the chemical reactions involved. In this way, the stochastic ratchet idea explains how the molecular motors are capable of converting chemical energy into mechanical motion and force.

Further Reading and References

R. Benzi, G. Parisi, A. Sutera, A. Vulpiani, Stochastic resonance in climatic change. Tellus **34**(1), (1982)

L. Gammaitoni, P. Hänggi, P. Jung, F. Marchesoni, Stochastic resonance. Rev. Mod. Phys. **70**(1), (1998)

A. Bulsara, L. Gammaitoni, Tuning into noise. Phys. Today **49**(3), 39–45 (1996)

P. Jung, P. Hänggi, Stochastic nonlinear dynamics modulated by external periodic forces. Europhys. Lett. **8**(6), 505–510 (1989)

K. Wiesenfeld, F. Moss, Stochastic resonance and the benefits of noise: from ice ages to crayfish and SQUIDs. Nature **373**(6509), 33–36 (1995)

Y.W. Parc, D.S. Koh, W. Sung, Stochastic resonance in an ion channel following the non-Arrhenius gating rate. Eur. Phys. J. B **69**, 127 (2009)

W.K. Kim, C. Hyeon, W. Sung, Weak temporal signals can synchronize and accelerate the transition dynamics of biopolymers under tension. Proc. Natl. Acad. Sci. U.S.A. **109**(36), 14410–14415 (2012)

W.K. Kim, W. Sung, How a single stretched polymer responds coherently to a minute oscillation in fluctuating environments: an entropic stochastic resonance. J. Chem. Phys. **137**, 074903 (2012)
P.J. Park, W. Sung, A Stochastic model of polymer translocation dynamics through biomembranes. Int. J. Bifurcat. Chaos **8**, 927 (1998)
C.R. Doering, J.C. Gadoua, Resonant activation over a fluctuating barrier. Phys. Rev. Lett. **69**, 2318 (1992)
R.D. Astumian, P. Hänggi, Brownian motors. Phys. Today **55**(11), 33 (2002)
R.D. Astumian, M. Bier, Fluctuation driven ratchets: molecular motors. Phys. Rev. Lett. **72**, 1766 (1994)
A.B. Kolomeisky, *Motor Proteins and Molecular Motors* (CRC Press, 2015)

Chapter 19
Transport Phenomena and Fluid Dynamics

Most systems in nature are dynamic, that is, change in time. **In non-equilibrium processes there are flows (transports) of mass, momentum and energy, from one place to the other.** If a system is near equilibrium the transports occur in such ways that the distributions of the mass, momentum, and energy, which are non-uniform and time dependent, are relaxed to the equilibrium, where there are no flows. One example is the diffusion of particles from a crowded region to a less one. The equilibrium state represents a stationary state. The other stationary state is the non-equilibrium, steady state where there are constant flows driven by external means. For example, a rod whose ends are maintained at two different temperatures is in a steady state with a constant heat flow from a high temperature end to a lower one. The temperature gradient in the rod is the driving force for the heat flow.

Biological complexes are bathed in aqueous environments. Over the scales much longer than the mean free length between collisions of the solvent molecules, the solvents can be treated as continuous fluids. The complex fluids such as solutions of biopolymers and cells probed over a certain long length scale can also be treated as continua. For these cases **the hydrodynamic description of transport in terms of densities of fluids' conserved quantities—the mass, momentum, and energy—is very useful**. The governing dynamics for these hydrodynamic variables, which is also called hydrodynamics or fluid mechanics, is widely applicable to the problems, not only in basic sciences but also in engineering disciplines. For biological organisms in particular, fluid motion is something with which they must contend: a factor to which their design reflects adaptation (Vogel 1984). In this chapter we study basic principles and apply them to some important fluid flows which allow analytical treatments.

W. Sung, *Statistical Physics for Biological Matter*, Graduate Texts in Physics,
https://doi.org/10.1007/978-94-024-1584-1_19

19.1 Hydrodynamic Transport Equations

Total mass, momentum, and energy of an isolated fluid system are conserved. The densities of such conserved quantities are called hydrodynamic variables or hydrodynamic fields, collectively denoted by $\hbar(\boldsymbol{r},t)$ The temporal change of a conserved quantity within a fixed volume V, $\int_V dV\,\hbar(\boldsymbol{r},t)$, is given by

$$\frac{d}{dt}\int dV\hbar(\boldsymbol{r},\boldsymbol{t}) = -\int_A d\boldsymbol{A}\cdot\boldsymbol{J}_\hbar(\boldsymbol{r},t), \tag{19.1}$$

where the right hand side is the total amount of the quantity that flows per unit time across the surface A enclosing the volume V, as shown in Fig. 19.1. Here $J_\hbar$ is the flow per unit area (flux) at a point $\boldsymbol{r}$ and a time t. Note that $d\boldsymbol{A}$ is the surface area element vector in the outward normal direction so that the negative sign in (19.1) indicates that the outflow across the area decreases the quantity in the volume. By the divergence theorem we have

$$\int_A d\boldsymbol{A}\cdot\boldsymbol{J}_\hbar(\boldsymbol{r},t) = \int_V dV\ \nabla\cdot\boldsymbol{J}_\hbar(\boldsymbol{r},t). \tag{19.2}$$

Because (19.2) must be satisfied for an arbitrary small volume V, the combination of (19.1) and (19.2) yields

$$\frac{\partial}{\partial t}\hbar(\boldsymbol{r},t)+\nabla\cdot\boldsymbol{J}_\hbar(\boldsymbol{r},t)=0, \tag{19.3}$$

which is the continuity equation for the hydrodynamic density $\hbar(\boldsymbol{r},t)$ for all points in the fluid. Here $\boldsymbol{J}_\hbar$ is the associated current (flux) at a point $\boldsymbol{r}$ and at a time t. In the Fourier space (19.3) is transformed to

$$\frac{\partial}{\partial t}\hbar(\boldsymbol{q},t)+i\boldsymbol{q}\cdot\boldsymbol{J}_\hbar(\boldsymbol{q},t)=0, \tag{19.4}$$

where $\hbar(\boldsymbol{q},t)=\int d\boldsymbol{r}\,e^{-i\boldsymbol{q}\cdot\boldsymbol{r}}\hbar(\boldsymbol{r},t)$. Equation (19.4) assures that $\partial\hbar(\boldsymbol{q},t)/\partial t\cong 0$ for the description over a large wavelength (small q); that the hydrodynamic fields vary slowly over long length scales and thus remain relevant variables of the fluids for mesoscopic descriptions.

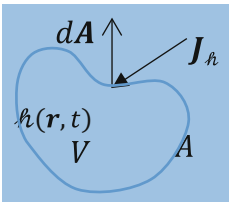

Fig. 19.1 The hydrodynamic quantities flow ($J_\hbar$) through a surface A of a fixed volume V

19.1.1 Mass Transport and the Diffusion Equation

When the $\mathscr{k}$ is mass density denoted by ρ, it satisfies the continuity equation,

$$\frac{\partial \rho(\boldsymbol{r},t)}{\partial t} + \nabla \cdot \boldsymbol{J}_{\rho}(\boldsymbol{r},t) = 0 \tag{19.5}$$

$\boldsymbol{J}_{\rho}(\boldsymbol{r},t) = \rho(\boldsymbol{r},t)\boldsymbol{u}(\boldsymbol{r},t)$ is the mass density flux, where $\boldsymbol{u}(\boldsymbol{r},t)$ is the local fluid velocity. We can rewrite (19.5) as

$$\frac{D\rho}{Dt} = -\rho \nabla \cdot \boldsymbol{u}, \tag{19.6}$$

where

$$\frac{D\rho}{Dt} = \lim_{\Delta t \to 0} \rho(\boldsymbol{r} + \Delta \boldsymbol{r}, t + \Delta t)/\Delta t \equiv \frac{\partial \rho}{\partial t} + \boldsymbol{u} \cdot \nabla \rho \tag{19.7}$$

is the convective time derivative (taken at a fluid point $\boldsymbol{r}(t)$ that flows with the velocity $\boldsymbol{u}$). Equation (19.6) tells us that, if

$$\nabla \cdot \boldsymbol{u} = 0, \tag{19.8}$$

then, $D\rho/Dt = 0$, that is, the fluid density is constant throughout the flow. It follows that for incompressible flow the continuity equation is equivalent to (19.8).

Now consider that the fluid is a mixture of species k with no chemical reaction. Because the mass of each species is conserved, the equation

$$\frac{\partial \rho_k(\boldsymbol{r},t)}{\partial t} + \nabla \cdot \rho_k(\boldsymbol{r},t)\boldsymbol{u_k}(\boldsymbol{r},t) = 0 \tag{19.9}$$

is satisfied. Furthermore (19.5) should hold for the mixture mass density

$$\rho(\boldsymbol{r},t) = \sum_k \rho_k(\boldsymbol{r},t) \tag{19.10}$$

and the mixture velocity

$$\boldsymbol{u}(\boldsymbol{r},t) = \frac{\sum_k \rho_k(\boldsymbol{r},t)\boldsymbol{u_k}(\boldsymbol{r},t)}{\rho(\boldsymbol{r},t)}. \tag{19.11}$$

Defining the mass density flux for each species as

$$\boldsymbol{J}_{\rho_k}(\boldsymbol{r},t) = \rho_k(\boldsymbol{r},t)[\boldsymbol{u_k}(\boldsymbol{r},t) - \boldsymbol{u}(\boldsymbol{r},t)], \tag{19.12}$$

we have the equation

$$\frac{\partial \rho_k(\boldsymbol{r},t)}{\partial t} = -\nabla \cdot \boldsymbol{J}_{\rho_k}(\boldsymbol{r},t) - \nabla \cdot \{\rho_k(\boldsymbol{r},t)\boldsymbol{u}(\boldsymbol{r},t)\}, \tag{19.13}$$

or

$$\frac{D\rho_k}{Dt} = \left(\frac{\partial}{\partial t} + \boldsymbol{u} \cdot \nabla\right)\rho_k = -\nabla \cdot \boldsymbol{J}_{\rho_k} - \rho_k \nabla \cdot \boldsymbol{u}. \tag{19.14}$$

Suppose that there is no convection (the fluid as a whole is stationary, $\boldsymbol{u} = 0$). The flux of each species is proportional to the gradient of the species density; the particles flow from the region of higher concentration to that of lower concentration, as stated by the so-called Fick's law:

$$\boldsymbol{J}_{\rho_k}(\boldsymbol{r},t) = -D_k \nabla \rho_k(\boldsymbol{r},t), \tag{19.15}$$

where D_k is the diffusion coefficient of the species k. The linear relation above, called as the constitutive relation of diffusion, is substituted into (19.13) to yield the diffusion equation

$$\frac{\partial \rho_k(\boldsymbol{r},t)}{\partial t} = D_k \nabla^2 \rho_k(\boldsymbol{r},t). \tag{19.16}$$

In Chap. 14, we studied the various aspects and applications of the diffusion of Brownian particles with and without an external force or a flow. The Brownian particles constitute the first species of a binary mixture with the second species representing the background, the host fluid. For an infinitely dilute concentration of Brownian particles the $\boldsymbol{u}$ in (19.11) is solely given by the background fluid. For an incompressible flow, (19.14) yields

$$\frac{D\rho_k(\boldsymbol{r},t)}{Dt} = D_k \nabla^2 \rho_k(\boldsymbol{r},t), \tag{19.17}$$

which depicts the particle diffusion relative to convection.

19.1.2 Momentum Transport and the Navier-Stokes Equation

Another hydrodynamic density of interest is the momentum density of fluid, $\rho\boldsymbol{u}$. It is a vector quantity, which is the same as $\boldsymbol{J}_\rho$, the flux of the scalar mass density. In the presence of an external force, the momentum within a fixed volume V changes following the equation

$$\frac{d}{dt}\int_V dV\rho\boldsymbol{u} = -\int_A d\boldsymbol{A}\cdot\boldsymbol{J}_{\rho\boldsymbol{u}} + \int_V dV\boldsymbol{f}, \tag{19.18}$$

where the $\boldsymbol{J}_{\rho\boldsymbol{u}}(\boldsymbol{r},t)$ **is the momentum density flux tensor** and $\boldsymbol{f}(\boldsymbol{r},t)$ **is the external force density, i.e., the local force acting on unit fluid volume**. The i-th component of the above equation reads:

$$\frac{d}{dt}\int_V dV\rho u_i = -\sum_j \int_A dA_j \left(J_{\rho\boldsymbol{u}}\right)_{ji} + \int_V dV f_i \tag{19.19}$$

The first term on the right-hand side (RHS) represents the i-th component momentum flow across the surface A enclosing the volume; the tensor element $\left(J_{\rho\boldsymbol{u}}\right)_{ji}$ denotes the i-th component momentum transferred per unit time and per unit area along the j axis. The equation for the local momentum density then is

$$\frac{\partial}{\partial t}(\rho\boldsymbol{u}) + \nabla\cdot\boldsymbol{J}_{\rho\boldsymbol{u}} = \boldsymbol{f}. \tag{19.20}$$

One part of $\left(J_{\rho\boldsymbol{u}}\right)_{ji}$ is the convective momentum flux $(\rho u_i)u_j$. Another is given by pressure p acting isotropically on the fluid, contributing to the RHS of (19.19):

$$\left(-\int_A d\boldsymbol{A}\, p\right)_i = -\int_A dA_i\, p = -\sum_j \int_A dA_j\, p\delta_{ij}. \tag{19.21}$$

These two contributions constitute the momentum flux tensor of an *inviscid* or ideal fluid:

$$\boldsymbol{J}_{\rho\boldsymbol{u}} = \rho\boldsymbol{u}\boldsymbol{u} + p\boldsymbol{I}, \tag{19.22}$$

where $\boldsymbol{I}$ is the unit tensor with the element δ_{ij}. Substituting the above equation into (19.18), and using the divergence theorem, we obtain

$$\frac{\partial}{\partial t}(\rho\boldsymbol{u}) + \nabla\cdot\rho\boldsymbol{u}\boldsymbol{u} = -\nabla p + \boldsymbol{f}. \tag{19.23}$$

Via (19.5), (19.23) can be transformed to a more familiar form:

$$\rho\frac{D\boldsymbol{u}}{Dt} \equiv \rho\left(\frac{\partial}{\partial t} + \boldsymbol{u}\cdot\nabla\right)\boldsymbol{u} = -\nabla p + \boldsymbol{f}, \tag{19.24}$$

Equation (19.24) is an extension of the Newton's equation of motion to an ideal fluid under convection: the LHS is the acceleration of the fluid element in convection, which is driven by the pressure and the external force (RHS).

P19.1 *Show that the pressure of a stationary ideal gas satisfying $p_0 = \rho k_B T/m$ at x under a uniform gravity g along the x-axis is given by*

$$p(x) = p_0 \exp(-mgx/(k_B T)).$$

P19.2 *Show that in a stationary flow of inviscid fluid under gravity along x axis, the quantity $\rho u^2/2 + p + \rho gx$ is constant (Bernoulli's law). As the consequence of the law, the pressure of the fluid acting on a narrower constriction through which it flows is smaller (the figure below). If we apply this result to a blood flow, flow speed can be so high in the narrow constriction that the artery may collapse causing a transient blockage of the flow.*

But *real* fluids are viscous. The equation of motion for such fluids is called the Navier-Stokes equation, (19.33, 19.34), the derivation of which is given below. In a *real* fluid, there is another mechanism of momentum transport due to the viscosity. For illustration, consider a steady shear flow along z-axis,

$$\boldsymbol{u} = u_z(x)\hat{z} \tag{19.25}$$

where u_z increases with x (Fig. 19.2). Imagine a plane defined by $x = x_0$ in the fluid. Due to the shear, phenomenologically, the fluid above the plane exerts a force on the fluid below the plane to the positive z direction. That is, **in a shear flow the momentum flows from the fluid region of higher velocity to that of the lower velocity**. For small values of the shear, the force acting on the area dA_x of the plane is given by

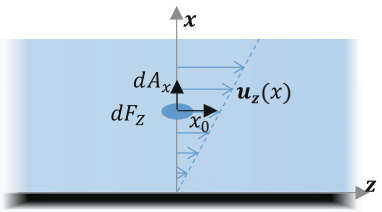

Fig. 19.2 The fluid $(x > x_0)$ with a higher velocity exerts a force in the positive z direction on the fluid $(x < x_0)$ with a lower velocity

$$dF_z = \eta \frac{\partial u_z}{\partial x} dA_x, \tag{19.26}$$

where the proportionality constant η is a transport coefficient of the fluid called shear viscosity, or simply viscosity. In view of the relation (19.19) this force can be written in terms of the momentum flux $(\boldsymbol{J}_{\rho \boldsymbol{u}})_{zx}$ over the surface element directed outward from the fluid below, $dF_z = -(\boldsymbol{J}_{\rho \boldsymbol{u}})_{zx} dA_x$, which, upon comparison with (19.26), leads to

$$\left(\boldsymbol{J}_{\rho \boldsymbol{u}}\right)_{xz} = -\eta \frac{\partial u_z}{\partial x}. \tag{19.27}$$

This is called the Newton's law of viscous flow.

In general the momentum flux is expressed as

$$\boldsymbol{J}_{\rho \boldsymbol{u}} = \rho \boldsymbol{u}\boldsymbol{u} + \boldsymbol{\sigma}. \tag{19.28}$$

$\boldsymbol{\sigma}$ is pressure tensor or stress tensor in the fluid; it consists of the isotropic pressure term $p\boldsymbol{I}$ and a deviatoric term $\boldsymbol{\sigma}'$ due to the velocity gradient, taken to be usually a second order symmetric tensor (Landau and Lifshitz 1975; Batchelor 2000):

$$\sigma_{ij} = p\delta_{ij} + \sigma'_{ij} = p\delta_{ij} - 2\eta \dot{\gamma}_{ij} - \eta_B \nabla \cdot \boldsymbol{u}\delta_{ij}. \tag{19.29}$$

Here

$$\dot{\gamma}_{ij} = [\dot{\boldsymbol{\gamma}}]_{ij} = \frac{1}{2}\left(\frac{\partial u_i}{\partial r_j} + \frac{\partial u_j}{\partial r_i}\right) - \frac{1}{3}\nabla \cdot \boldsymbol{u}\delta_{ij} \tag{19.30}$$

is the traceless part that pertains to pure shear without changing the volume of a fluid element. In the simple shear flow geometry considered above (Fig. 19.2), the second term of the last equality in (19.29) is reduced to $-2\eta\dot{\gamma}_{ij} = -\eta \partial u_z / \partial x$, which is the force on the fluid per unit area resisting the shear. The last term is the force per unit area resisting volumetric change induced by the flow, involving the bulk viscosity η_B.

Substitution of (19.28) into (19.20) yields

$$\frac{\partial}{\partial t}(\rho \boldsymbol{u}) + \nabla \cdot \rho \boldsymbol{u}\boldsymbol{u} = -\nabla \cdot \boldsymbol{\sigma} + \boldsymbol{f} \tag{19.31}$$

or a more familiar form:

$$\rho \frac{D\boldsymbol{u}}{Dt} \equiv \rho \left(\frac{\partial}{\partial t} + \boldsymbol{u} \cdot \nabla \right) \boldsymbol{u} = -\nabla \cdot \boldsymbol{\sigma} + \boldsymbol{f} \tag{19.32}$$

where (19.5) is used. This is the Newton's equation of motion for a viscous fluid per unit volume.

We will consider the situations where the external force is absent, unless otherwise specified. The stress force on the flowing fluid per unit volume is $-\nabla \cdot \boldsymbol{\sigma}$. Thus the force acting on a particle following the flow is $-\int_V dV \nabla \cdot \boldsymbol{\sigma} = -\oint d\boldsymbol{A} \cdot \boldsymbol{\sigma} = -\oint dA\, \boldsymbol{n} \cdot \boldsymbol{\sigma}$, where V and A are the volume and surface area of the particle.

P19.3 *What is the buoyance force on a spherical particle of a mass M and radius R which undergoes sedimentation under a gravity g?*

Equation (19.32) is written explicitly as

$$\rho \left(\frac{\partial}{\partial t} + \boldsymbol{u} \cdot \nabla \right) \boldsymbol{u} = -\nabla p + \eta \nabla^2 \boldsymbol{u} + \left(\eta_B + \frac{1}{3} \eta \right) \nabla \nabla \cdot \boldsymbol{u}, \tag{19.33}$$

For many practical purposes, we will be interested in incompressible flows where $\nabla \cdot \boldsymbol{u} = 0$, which simplifies the above equation to the form called the Navier-Stokes equation:

$$\rho \left(\frac{\partial}{\partial t} + \boldsymbol{u} \cdot \nabla \right) \boldsymbol{u} = -\nabla p + \eta \nabla^2 \boldsymbol{u}. \tag{19.34}$$

The (19.33) and (19.34) are to be solved subject to boundary conditions for various flow situations in the next section.

19.1.3 Energy Transport and the Heat Conduction

Finally we consider the hydrodynamic description of the energy transport. In the absence of an external force, the energy density can be written as $e = \rho u^2/2 + \varepsilon$, where ε is the internal energy density. The net energy of the fluid within a volume V varies in time:

$$\frac{d}{dt} \int_V dV\, e(\boldsymbol{r}, t) = -\int_A d\boldsymbol{A} \cdot \boldsymbol{u}\, e - \int_A d\boldsymbol{A} \cdot \boldsymbol{\sigma} \cdot \boldsymbol{u} - \int_A d\boldsymbol{A} \cdot \boldsymbol{J}_q. \tag{19.35}$$

The first term on the RHS is energy flow by mass convection. The second term is the rate of work done on the fluid by the stress acting on the surface (recall that $-d\boldsymbol{A} \cdot \boldsymbol{\sigma}$ is the force on an area dA). The last term is the energy flow by heat

conduction, where $\boldsymbol{J}_q$ is the heat flux vector. The spatiotemporal change of energy density $e(\boldsymbol{r},t)$ satisfies

$$\partial e(\boldsymbol{r},t)/\partial t + \nabla \cdot \boldsymbol{J}_e(\boldsymbol{r},t) = 0, \tag{19.36}$$

where $\boldsymbol{J}_e$ is the energy density flux given by

$$\boldsymbol{J}_e = e\boldsymbol{u} + \boldsymbol{\sigma} \cdot \boldsymbol{u} + \boldsymbol{J}_q. \tag{19.37}$$

Without derivation we show that the energy density equation is transformed to the equation for the local temperature $T(\boldsymbol{r},t)$:

$$\rho c_p \left(\frac{\partial}{\partial t} + \boldsymbol{u} \cdot \nabla \right) T = -\nabla \cdot \boldsymbol{J}_q - \boldsymbol{\sigma}' \cdot \nabla \boldsymbol{u}. \tag{19.38}$$

Here $c_p(\boldsymbol{r},t)$ is the local heat capacity per unit mass at a constant pressure. The first term on RHS is the heat flow that will be discussed below. The second terms is the viscous energy dissipation on the flowing fluid; $-\boldsymbol{\sigma}' \cdot \nabla \boldsymbol{u} = 2\eta \dot{\boldsymbol{\gamma}} \cdot \dot{\boldsymbol{\gamma}} + \eta_B (\nabla \cdot \boldsymbol{u})^2$ is positive, giving rise to a temperature increase.

P19.4 *Find the energy dissipation per volume for a steady state elongational flow of water,* $\boldsymbol{u} = \dot{\varepsilon}\left\{z\hat{z} - \frac{1}{2}x\hat{x} - \frac{1}{2}y\hat{y}\right\}$. *Write down the equation for the temperature distribution.*

The constitutive relation for the heat flux is the Fourier law,

$$\boldsymbol{J_q} = -\kappa_T \nabla T \tag{19.39}$$

descriptive of heat flows from a hot place to a cold one. The transport coefficient κ_T is called the heat conductivity. Considering a simple case in which there is no convection, (19.38) becomes remarkably simple:

$$\rho c_p \frac{\partial T}{\partial t} = \kappa_T \nabla^2 T. \tag{19.40}$$

This equation can be rewritten as

$$\frac{\partial T}{\partial t} = D_T \nabla^2 T, \tag{19.41}$$

where $D_T = \kappa_T / (\rho c_p)$ is called the thermal diffusion constant. The equation can be analytically solved for the temperature distribution given the initial and boundary conditions.

P19.5 *Consider the propagation of a temperature wave to the ground (the semi-infinite medium* $(x > 0)$ *driven by its surface* $(x = 0)$ *temperature kept as* $T(x = 0) = T_0 \cos\omega t$. *Find that the temperature distribution in the ground is given by* $T(x,t) = T_0 \exp(-x/\delta)\cos(\omega t - x/\delta)$ *where* $\delta = \sqrt{2D_T/\omega}$. *With the thermal*

diffusivity of the ground in the order of $10^2 \mathrm{m}^2\mathrm{s}^{-1}$, *what is the value of* δ *for the annual variation of the temperature* $\omega = 2\pi/year$*?*

19.1.4 Boltzmann Equation Explains Transport Equations and Time-Irreversibility

Solutions to the transport equations above can be used to describe a variety of hydrodynamic phenomena such as diffusion, laminar flow, and heat transport. Fundamentally, these macroscopic transport equations are derived from a microscopic kinetic equations, e.g., the Boltzmann equation for the case of dilute gas. The Boltzmann equation is an equation for evolution of the probability density of a particle at velocity $\boldsymbol{v}$ and position $\boldsymbol{r}$, which reads

$$\frac{\partial f(\boldsymbol{r}\boldsymbol{v}, t)}{\partial t} + \boldsymbol{v} \cdot \nabla f(\boldsymbol{r}\boldsymbol{v}, t) = J(ff). \tag{19.42}$$

Here $J(ff)$ denotes the so-called collision integral that describes the temporal change of the probability density caused by two-particle collisions. The hydrodynamic densities, which are proportional to the velocity moments of $f(\boldsymbol{r}v, t)$, e.g., $\rho\boldsymbol{u} = m \int d\boldsymbol{v}\, \boldsymbol{v} f(\boldsymbol{r}\boldsymbol{v}, t)$, are shown to satisfy the continuity equations. It took a long time before Chapmann and Enskog formulated the Boltzmann equation's particular solutions to derive the hydrodynamic transport equations along with the transport coefficients therein in terms of molecular parameters and collision mechanics of two interacting particles. The derivations of Boltzmann equation and the transport phenomena of gases therefrom mark an important page in history of non-equilibrium statistical mechanics.

One important feature of the transport phenomena is the time irreversibility. Consider that the particles initially confined in a volume freely diffuse to a region of lower particle density. The process is irreversible; in the lifetime of universe, the particle will never get back into the initial volume, by the second law of thermodynamics. The irreversibility can be seen from the diffusion equation for the density, $\partial n(r, t)/\partial t = D\nabla^2 n(r, t)$, which is not invariant with respect to the time reversal operation, $t \to -t$, but becomes $-\partial n(r, -t)/\partial t = D\nabla^2 n(r, -t)$. Because of the impossibility of this equation, the time reversed motion is not natural. There is only one direction, time arrow, from the past to the future. But look at the more fundamental, microscopic equation of the motion for the constituent particles, that is, the Newton's equation, $m d\boldsymbol{v}_i/dt = \boldsymbol{F}\{r_j\}$ for all particles labeled as i. This equation is invariant with respect to time reversal upon which $\boldsymbol{v}_i \to -\boldsymbol{v}_i$. Indeed a "time-backward" trajectory cannot be distinguished from a "time-forward" trajectory; the particles move just as well "backwards" as they do "forwards". This is fundamentally at odds with the natural phenomena we observe macroscopically! The problem is called the time irreversibility paradox.

Using (19.42), Boltzmann showed that the entropy defined by

$$S(t) = -k_B \iint d\boldsymbol{r}d\boldsymbol{v}\, f \ln f, \tag{19.43}$$

can only increase to the maximum at equilibrium, where function f becomes the Maxwell-Boltzmann distribution. This irreversibility is due to the coarse-grained description of the fluids in terms of one-particle PDF f and to an important assumption, called the ansatz of molecular chaos, that the two molecules about to collide are statistically independent. Immediately after the collision, however, the two molecules are dynamically correlated (in positions and velocities). In this way the time arrow is introduced. The coarse-grained description using the Boltzmann equation and the ansatz of molecular chaos imbedded therein are indeed valid for low density gas transport phenomena; after many collisions with other molecules, these two molecules will no longer be correlated when they are about to recollide. This explanation of the time irreversibility paradox caused a lot of controversies historically and in larger and fundamental scopes yet remains a debated issue (Lebowitz 1993).

We will not dwell on the kinetic theory further, however, because we are more concerned with simple liquids and complex fluids described on the scales much longer than the microscopic time and length between molecular collisions. For most of the situations we are dealing with, the continuum hydrodynamic description with given transport coefficients is most practical.

19.2 Dynamics of Viscous Flow

Here we focus on the momentum flow of a viscous fluid, which comprises the most of the area of fluid dynamics. Fluid dynamics covers enormous variety of flow problems, ranging from the global weather predictions to microscale flows within human body. Due to the nonlinear term $\boldsymbol{u} \cdot \nabla \boldsymbol{u}$, the equation of the fluid velocity $\boldsymbol{u}$, even the Navier-Stokes equation (19.34) for an incompressible flow, in general, is notoriously difficult to solve analytically. Below we start with a number of exactly solvable cases, which are nontrivial and relevant.

19.2.1 A Simple Shear and Planar Flow

Consider a fluid between two large plates, each with an area A, separated by a distance D. The upper plate is in steady motion at a constant velocity V, while the other is at rest (Fig. 19.3). The fluid undergoes a shear flow (called the Couette

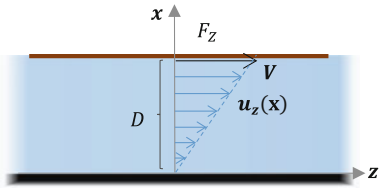

Fig. 19.3 The Couette flow bounded by a stationary surface at $x = 0$ and moving plate at $x = D$

flow) along z-axis on a (y, z) plane, $\boldsymbol{u} = u_z(x)\hat{\boldsymbol{z}}$, causing the stress $\sigma_{xz} = -\eta \partial u_z/\partial x$. The above relations reduce (19.33) to a remarkably simple form

$$\rho \frac{\partial}{\partial t} u_z(x,t) = -\frac{\partial p}{\partial z} + \eta \frac{\partial^2 u_z}{\partial x^2}. \tag{19.44}$$

Furthermore, in the Couette flow situation, the pressure is uniform along z-direction, so

$$\rho \frac{\partial u_z}{\partial t} = \eta \frac{\partial^2 u_z}{\partial x^2}. \tag{19.45}$$

The velocity u_z satisfies the diffusion equation, akin to the equation which we already studied for the mass and heat diffusions.

P19.6 *Consider an unbounded fluid above a plane at $x = 0$ that moves in the z-direction with a time dependent velocity $V(t) = V_0 \cos \omega t$. Show that the fluid velocity for $x > 0$ is given by*

$$u_z(t) = V_0 \cos\left\{\omega t - \left(\frac{\omega\rho}{2\eta}\right)^{1/2} x\right\} \exp\left\{-\left(\frac{\omega\rho}{2\eta}\right)^{1/2} x\right\}.$$

In a steady state (19.45) is

$$\eta \frac{\partial^2 u_z}{\partial x^2} = 0. \tag{19.46}$$

This equation is to be solved subject to two BC, usually the no slip BC, according to which the fluid velocity on a surface is same as that of the surface: $u_z = V$ at $x = D$ and $u_z = 0$ at $x = 0$. Thus we find the solution

$$u_z = \frac{V}{D} x, \tag{19.47}$$

which shows that the fluid velocity is sheared at a uniform rate V/D along the z-direction.

The force that the fluid acts on the upper plate is given by

$$-\int d\boldsymbol{A} \cdot \boldsymbol{\sigma} = -(-A_x)\sigma_{xz}\hat{\boldsymbol{z}} = -\frac{A}{D}\eta V \hat{\boldsymbol{z}} = -F_z \hat{\boldsymbol{z}}. \tag{19.48}$$

It should be noted that the area vector is outward from the plate, $\boldsymbol{A} = -A_x \hat{\boldsymbol{x}}$. This force is in the opposite direction to the velocity V and to the force F_z (19.26) applied by the plate to keep it moving with the velocity. On the other hand, the force by the fluid at the bottom is

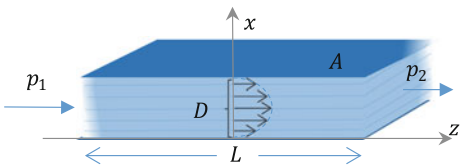

Fig. 19.4 A pressure-driven ($p_1 > p_2$) flow between two stationary plates

$$-\int d\boldsymbol{A}\cdot\boldsymbol{\sigma} = -A_x\sigma_{xz}\hat{\boldsymbol{z}} = \frac{A}{D}\eta V\hat{\boldsymbol{z}}. \tag{19.49}$$

Pressure-driven planar flow

Suppose that a steady flow between two stationary plates positioned at $x = 0$ and $x = D$ is driven by a constant pressure gradient (the pressure difference $\Delta p = p_1 - p_2$ over a long length L: $-\partial p/\partial z = (p_1 - p_2)/L = \Delta p/L$ (Fig. 19.4). From (19.44) we have

$$\eta\frac{\partial^2 u_z}{\partial x^2} = -\frac{\Delta p}{L}. \tag{19.50}$$

With use of the BC $u_z = 0$ on the surfaces, an integration of the above equation yields the velocity profile

$$u_z = -\frac{1}{2\eta}\frac{\Delta p}{L}x(x - D). \tag{19.51}$$

The total viscous force on the two plates by the fluid is given by

$$\begin{aligned} -\int \boldsymbol{\sigma}\cdot d\boldsymbol{A} &= \eta\left\{\frac{\partial u_z}{\partial x}|_{x=D}(-A) + \frac{\partial u_z}{\partial x}|_{x=0}A\right\}\hat{\boldsymbol{z}} \\ &= \frac{\Delta p}{L}DA\hat{\boldsymbol{z}} = a\Delta p\,\hat{\boldsymbol{z}}, \end{aligned} \tag{19.52}$$

where $a = DA/L$ is the cross section. The above equation represents the pressure force by the fluid; this is opposite in direction to the viscous force *acting on* the fluid.

19.2.2 The Poiseuille Flow

The flow of the fluid within a narrow cylindrical channel (tube) of radius R (Fig. 19.5) is driven by a pressure gradient $\partial p/\partial z = -\Delta p/L$ along the z axis. Equation (19.33) for the steady state in cylindrical (r, z) coordinate is given by

$$\frac{\eta}{r}\frac{\partial}{\partial r}\left(r\frac{\partial u_z(r)}{\partial r}\right) = -\frac{\Delta p}{L}. \tag{19.53}$$

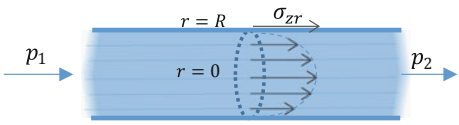

Fig. 19.5 A pressure-driven ($p_1 > p_2$), steady state flow through a circular channel

Multiplying the above by r and integrating it over r, we have the equation

$$\frac{\partial u_z(r)}{\partial r} = -\frac{\Delta p}{2\eta L}\left(r + \frac{c}{r}\right), \tag{19.54}$$

where the constant c vanishs to assure a finite value for $\partial u_z(r)/\partial r$ at $r = 0$. We note that the equation for the shear stress is

$$\sigma_{zr} = -\eta \partial u_z(r)/\partial r = \Delta p r/(2L), \tag{19.55}$$

Integrating (19.54) subject to the no-slip BC, $u_z(r = R) = 0$, leads to the parabolic velocity profile

$$u_z(r) = -\frac{\Delta p}{4\eta L}\left(r^2 - R^2\right). \tag{19.56}$$

Using this, one can obtain the volume flow per unit time (volumetric flow rate) per length along the flow:

$$Q = \int_0^R dr 2\pi r u_z(r) = \frac{\pi \Delta p}{8\eta L} R^4, \tag{19.57}$$

This is the famous formula called the Hagen-Poiseuille's law. **It shows the dominant influence (R^4 dependence) of vessel radius on flow and therefore serves as an important concept to understand how physiological changes in blood vessel radius affect blood pressure and flow.** The formula is the basis of capillary viscometer, which measures the effective viscosity η by measuring the volume flow.

Finally the viscous force that the fluid acts on the surface is

$$-\int \boldsymbol{\sigma} \cdot d\boldsymbol{A} = 2\pi RL\sigma_{zr}\hat{\boldsymbol{z}} = \pi R^2 \Delta p \hat{\boldsymbol{z}}\,, \tag{19.58}$$

which is equal to the pressure force.

P19.7 *Consider a steady state fluid flow through a cylindrical channel of radius R driven by a pressure gradient over a length L, $(p_1 - p_2)/L$. The boundary condition on the wall is given in such a way that the wall stress is balanced by a*

frictional force, $-\sigma_{zr} = \zeta_s u$ (the Navier BC). Find the fluid velocity u as a function of radial distance r. Calculate the volumetric flow rate in terms of the surface friction parameter ζ_s.

Blood Flow Through a Vessel: The Fahraeus–Lindqvist Effect

Blood is a suspension of mostly red blood cells (RBC) in a fluid called the plasma. RBC constitute 40–45% volume of a normal human blood, while the plasma, consisting mostly of water, has the viscosity of about 1.2 centi-Poise (cP) at 37 °C (1 P = 1 g/cm · s). Assuming the blood suspension to be a homogeneous fluid, the Poiseuille's law can be applied to define its effective viscosity, called the apparent viscosity. The apparent viscosity η of the blood in the tube with a diameter of about 500 μm or larger is then measured to be 3–4 cP. **As the diameter becomes smaller than 300 m, the apparent viscosity does not remain a constant, but decreases down until about 10 m** (Fig. 19.6)! This counter-intuitive phenomenon is known as the Fahraeus–Lindqvist (FL) effect (1931) (Fig. 19.7).

Related to this effect, it is known that the blood flowing through a narrow vessel tends to separate into two regions; the RBC tend to be concentrated toward the tube axis while the plasma tends to stay near the tube wall. As an attempt to explain the FL effect quantitatively, consider a simple, two-fluid model: the cell-rich fluid region constitutes the inner cylinder of radius $a(= R - \delta)$ and viscosity $\eta_C(> \eta_P)$, while the plasma is in concentric rim of outer radius of R and has the viscosity η_P.

From (19.54), the shear stress within the two regions,

$$-\eta_C \frac{\partial u_z(r)}{\partial r} = \frac{\Delta p}{2L} r, \quad \text{for} \quad 0 < r < a, \tag{19.59}$$

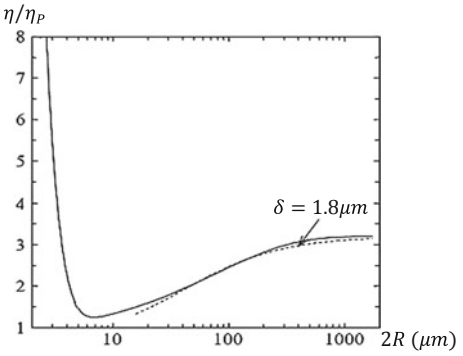

Fig. 19.6 The Fahreus-Linquivist effect. The relative viscosity η/η_P of the blood suspension (with RBC volume fraction 0.45) (solid line) decreases with diameter $2R$. The dotted line indicates the two-fluid model result with $\delta = 1.8$ μm. Adapted from Sugihara-Seki and Fu (2005); permission conveyed through Copyright Clearance Center, Inc.

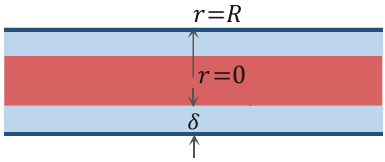

Fig. 19.7 Two-fluid model for blood flow within a narrow vessel. The core region is populated mostly by the red blood cells, while the rim region is filled with the plasma

$$-\eta_P \frac{\partial u_z(r)}{\partial r} = \frac{\Delta p}{2L}\left(r + \frac{c}{r}\right), \quad \text{for} \quad a < r < R, \tag{19.60}$$

are equal to each other at $r = a$. This continuity leads to $c = 0$. Integrating the equations with the no slip BC $u_z(R) = 0$, we have

$$u_z(r) = -\frac{\Delta p}{4\eta_c L}\left(r^2 + A\right), \quad \text{for} \quad 0 < r < a, \tag{19.61}$$

$$u_z(r) = -\frac{\Delta p}{4\eta_P L}\left(r^2 - R^2\right), \quad \text{for} \quad a < r < R, \tag{19.62}$$

which are also to be matched at $r = a$, giving

$$u_z(r) = -\frac{\Delta p}{4L}\left(\frac{r^2 - a^2}{\eta_C} + \frac{a^2 - R^2}{\eta_P}\right) \tag{19.63}$$

for $0 < r < a$. The volumetric flow rate is

$$\begin{aligned} Q &= -\frac{\Delta p}{4L}\left\{2\pi \int_0^a dr r\left(\frac{r^2 - a^2}{\eta_C} + \frac{a^2 - R^2}{\eta_P}\right) + 2\pi \int_a^R dr\, r\, \frac{\left(r^2 - R^2\right)}{\eta_P}\right\} \\ &= \frac{\pi \Delta p}{8\eta_C L}\left\{a^4 + 2\frac{\eta_C}{\eta_P} a^2\left(R^2 - a^2\right)\right\} + \frac{\pi \Delta P}{8\eta_P L}\left(R^2 - a^2\right)^2 \\ &= \frac{\pi \Delta p}{8\eta_C L} R^4 \left\{\alpha + \lambda^4 (1 - \alpha)\right\} = Q_C\, F(\lambda, \alpha) \end{aligned} \tag{19.64}$$

where

$$Q_C = \frac{\pi \Delta p}{8\eta_C L} R^4, \quad \alpha = \frac{\eta_C}{\eta_P}, \quad \lambda = \frac{a}{R}, \quad F(\lambda, \alpha) = \alpha + \lambda^4 (1 - \alpha). \tag{19.65}$$

(19.64) is set to be $\pi\Delta P R^4/8\eta L$, which allows us to identify the apparent viscosity:

$$\eta = \frac{\eta_C}{F(\lambda,\,\alpha)} = \eta_C\left[1+\left(\frac{\eta_C}{\eta_P}-1\right)\left(1-\left(1-\frac{\delta}{R}\right)^4\right)\right]^{-1}, \tag{19.66}$$

where $\delta = R - a = R(1-\lambda)$ is the cell-free layer thickness. It is shown that, by putting δ to be 1.8 μm independently of R, and $\eta_C = 3.2$ cP, the apparent viscosity η is less than η_C and decreases with R in a reasonable agreement with experiment (Sugihara-Seki and Fu 2005), (Fig. 19.6). For $R \gg \delta$, $F(\lambda,\alpha) \approx 1 + 4\delta(\eta_C/\eta_P - 1)/R$, so that

$$\eta \approx \eta_C\left\{1 - 4\frac{\delta}{R}\left(\frac{\eta_C}{\eta_P}-1\right)\right\}, \tag{19.67}$$

On the other hand the energy dissipation per length is given by

$$\begin{aligned}\dot{E} &= 2\pi\int_0^a drr\eta_C\left(\frac{\partial u_z(r)}{\partial r}\right)^2 + 2\pi\int_a^R drr\eta_P\left(\frac{\partial u_z(r)}{\partial r}\right)^2 \\ &= \frac{\pi}{8}\left(\frac{\Delta p}{L}\right)^2\left[\frac{a^4}{\eta_C}+\frac{R^4-a^4}{\eta_P}\right].\end{aligned} \tag{19.68}$$

P19.8 *Imagine that the blood flows through a tube whose diameter decreases steadily and infinitesimally along the flow. Suppose that the volumetric flow within the cell-rich region remains constant along the flow. Using the two-fluid model find whether an optimal thickness δ for the cell-free region can make the energy dissipation minimum $\dot{E}$ in the blood flow.*

19.2.3 The Low Reynolds Number Approximation and the Stokes Flow

In the Navier-Stokes equation, there are two competing terms, the nonlinear inertia term $\rho\boldsymbol{u}\cdot\nabla\boldsymbol{u}$ and the viscous dissipation term $\eta\nabla^2\boldsymbol{u}$. The ratio of the inertia term to the viscous term is called the Reynolds number: $Re = |\rho\boldsymbol{u}\cdot\nabla\boldsymbol{u}|/|\eta\nabla^2\boldsymbol{u}| \approx \rho UR/\eta$, where U and R are characteristic velocity and characteristic length of the flow. If Re is above a certain critical value so that the nonlinear inertia term is important, the flow tends to be unpredictable, called turbulent. The turbulence is important in many practical problems such as large scale weather predictions and airplane designs, but its fundamental understanding has remained a long standing problem in physics.

If the *Re* is lower than 1 so that the viscous term dominates over the nonlinear term, the flow tends to be laminar. The laminar flow is mathematically more tractable. Furthermore for the flows of biological organisms or complexes (of small R) in overdamping and viscous fluids (of high η), the laminar or low Reynolds number flows will be relevant. For example a bacterium of 1 μm diameter that swims in water with a velocity of 2 μm per second has the $Re \approx 10^{-5}$. In this case the Navier-Stokes equation is simplified to equations for flow velocity

$$\nabla \cdot \boldsymbol{u} = 0 \tag{19.69}$$

and

$$\rho \frac{\partial}{\partial t}\boldsymbol{u} = -\nabla \cdot \boldsymbol{\sigma} = -\nabla p + \eta \nabla^2 \boldsymbol{u}, \tag{19.70}$$

In the steady state the above becomes the Stokes equation

$$\nabla \cdot \boldsymbol{\sigma} = \nabla p - \eta \nabla^2 \boldsymbol{u} = 0, \tag{19.71}$$

which we study below.

We consider **the problem of Stokes flow caused by a moving sphere in an otherwise quiescent fluid**. The velocity $\boldsymbol{V}$ of the sphere is small enough to assure low Reynolds number flow (Fig. 19.8). We will calculate the velocity profile of the fluid at a radial position $\boldsymbol{r}$ around the sphere of radius R, and then obtain the force on the sphere. First, applying a divergence on (19.71) and using the incompressibility condition, $\nabla \cdot \boldsymbol{u} = 0$, we have the Laplace equation

$$\nabla^2 p = 0. \tag{19.72}$$

The disturbances should be expressed to be linear in their source, i.e., the velocity $\boldsymbol{V}$; the solution of $p(\boldsymbol{r})$ that satisfies the Laplace equation is (similar to the electrical potential due to the dipole $\boldsymbol{V}$),

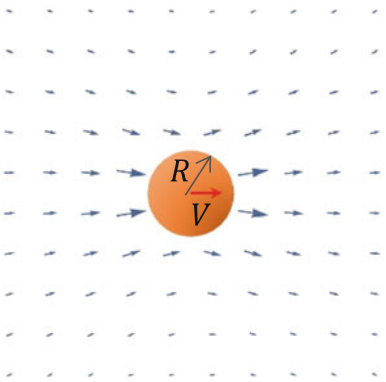

Fig. 19.8 The streamline (velocity) of the Stokes flow around a moving sphere with a velocity V

$$p(\boldsymbol{r}) = p_0 + C\boldsymbol{V}\cdot\nabla\left(\frac{1}{r}\right) = p_0 - C\frac{\boldsymbol{V}\cdot\boldsymbol{n}}{r^2}, \tag{19.73}$$

where p_0 is the static pressure of the unperturbed fluid, and $\boldsymbol{n}$ is unit radial vector: $\boldsymbol{r} = r\boldsymbol{n}$. The fluid velocity at $\boldsymbol{r}$ linear in $\boldsymbol{V}$ can be constructed in terms of these two vectors as

$$\boldsymbol{u}(\boldsymbol{r}) = f(r)\boldsymbol{V} + g(r)(\boldsymbol{n}\cdot\boldsymbol{V})\boldsymbol{n}. \tag{19.74}$$

The constant C and the radial functions, $f(r)$, $g(r)$, are to be obtained by substituting the equations into (19.71) and $\nabla\cdot\boldsymbol{u} = 0$. After a quite lengthy calculation (Landau and Lifshitz 1975) the solutions compatible with no slip BC at $r = R$ and another BC $\boldsymbol{u} = 0$ as $r \to \infty$ are

$$C = -3\eta R/2 \tag{19.75}$$

$$f(r) = \frac{3}{4}\left(\frac{R}{r}\right) + \frac{1}{4}\left(\frac{R}{r}\right)^3 \tag{19.76}$$

$$g(r) = \frac{3}{4}\left\{\left(\frac{R}{r}\right) - \left(\frac{R}{r}\right)^3\right\}. \tag{19.77}$$

Using the solutions above we can calculate the force that the fluid acts on the sphere (called the hydrodynamic friction or drag):

$$\begin{aligned}\boldsymbol{F} &= -\int d\boldsymbol{A}\cdot\boldsymbol{\sigma} = -\int dA\,\boldsymbol{n}\cdot\boldsymbol{\sigma}\\ &= -6\pi\eta R\boldsymbol{V},\end{aligned} \tag{19.78}$$

where we identify **the translational (Stokes) friction coefficient**

$$\zeta = 6\pi\eta R. \tag{19.79}$$

Remarkably this is proportional to the radius R, rather than R^2 that can be expected from binary collisions of molecules. Microscopically (19.79) is due to repeated, correlated collisions of fluid molecules on the sphere; a similar mechanism was already noted in the result (13.32).

Similarly, one can calculate the frictional torque that acts tangentially on a sphere rotating with an angular velocity $\boldsymbol{\Omega}$:

$$\boldsymbol{T} = -\int dA\, R\boldsymbol{n} \times (\boldsymbol{n} \cdot \boldsymbol{\sigma}) = -\zeta_R \boldsymbol{\Omega}, \tag{19.80}$$

where

$$\zeta_R = 8\pi\eta R^3 \tag{19.81}$$

is the rotational friction coefficient.

Suppose that a particle is placed in the fluid having a velocity field $\boldsymbol{u}_0(\boldsymbol{r})$ initially, then the force and torque on the sphere moving with the velocity $\boldsymbol{V}$ are given by the Faxen's law:

$$\boldsymbol{F} = -6\pi\eta R\{\boldsymbol{V} - [\boldsymbol{u}_0]_0\} + \pi\eta R^3 [\nabla^2 \boldsymbol{u}_0]_0, \tag{19.82}$$

$$\boldsymbol{T} = -8\pi\eta R^3 \left\{\boldsymbol{\Omega} - \frac{1}{2}[\nabla \times \boldsymbol{u}_0]_0\right\}, \tag{19.83}$$

where the subscripts 0 after the brackets […] denote the evaluation at the center of the sphere (Happel and Brenner 1991).

P19.9 *Evaluate the force and torque on a sphere moving with a velocity* $\boldsymbol{V}$ *in an elongational flow* $\boldsymbol{u}_0 = \dot{\varepsilon}\{z\hat{z} - \frac{1}{2}x\hat{x} - \frac{1}{2}y\hat{y}\}$.

19.2.4 Generalized Boundary Conditions

The no-slip boundary condition that a fluid meets on a solid surface is one of the central tenets of the macroscopic hydrodynamics. **Due, however, to the breakdown of continuum description near the surface, this boundary condition can be incorrect depending on the interface properties.**

The generalized boundary condition is a way to incorporate the interface effects within the hydrodynamic description. The condition is obtained by considering a thin microscopic boundary layer of thickness a near the surface; within the layer the momentum flux of the fluid onto the surface is evaluated microscopically, and beyond the boundary the flux is identified as the hydrodynamic stress. By virtue of

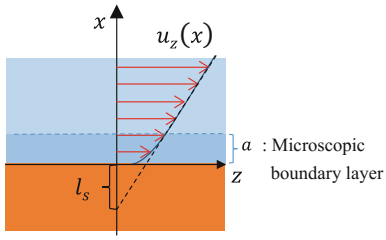

Fig. 19.9 Within the microscopic boundary layer, hydrodynamic description using no-slip boundary condition breaks down. In general, slippage of fluid velocity on the surface occurs with a finite slip length l_s.

its continuity across the boundary, these two expressions of momentum flux are matched on the boundary $x = a$: in a simple shear flow (Fig. 19.9), the microscopic frictional force of the fluid moving with velocity u_z on surface is equalized to the hydrodynamic wall stress at $x = a$, which reads

$$\begin{aligned} \zeta_s u_z &= -\sigma_{xz} \\ &= \eta \frac{\partial u_z}{\partial x}. \end{aligned} \tag{19.84}$$

This is called the Navier boundary condition. The length defined by

$$l_s = \left| u_z / \frac{\partial u_z}{\partial x} \right|_{x=a} = \eta / \zeta_s \tag{19.85}$$

is the slip length, which is given geometrically by extrapolating the slope $\partial u_z / \partial x$ at $x = a$ below the $z = 0$ plane. As depicted in Fig. 19.9, this is a measure of the slippage of the flow on the surface.

The simple relation (19.85) has two important consequences: if the surface friction coefficient ζ_s is so high that the slip length vanishes, no slip BC applies. This justifies the no-slip BC for usual cases of simple-fluid flow over rough surfaces.

If, on the other hand, the flowing liquid's viscosity η is very high or ζ_s is comparatively small, then the liquid slips on the surface. These two results are highly reasonable and experimentally confirmed. As an example of the latter, a melt of entangled long chain polymers of the contour length L, whose viscosity is very high, scaling as $\eta \sim L^{3.4}$, indeed shows a macroscopically large slippage even though the flow is linear (de Gennes 1971; Sung 1995). It is an open problem to find appropriate BCs for biological surfaces, which are elastic and thermally fluctuating; to find the surface friction in terms of elastic properties of the surface and interaction between the fluid and the surface.

P19.10 *For translational motion of a small macromolecule in a liquid, one may use the Navier BC that reads*

$$\zeta_s u_t = -(\boldsymbol{n} \cdot \boldsymbol{\sigma})_t,$$

with the subscript t denoting the tangential component, and

$$(\boldsymbol{u})_n = (\boldsymbol{V})_n,$$

which is kinematic condition for the fluid velocity in the direction normal to the surface if the particle moves with velocity $\boldsymbol{V}$*. Calculate the friction coefficient of the translating sphere of radius R and show that it approaches the result* $\zeta = 4\pi\eta R$ of complete *slip when* ζ_s *is zero. (Answer:* $\zeta = 6\pi\eta R(\zeta_s R + 2\eta)/(\zeta_s R + 3\eta)$*)*

If we consider the cases with small disturbances (perturbations) about the equilibrium, the nonlinear hydrodynamic equation can be linearized so as to be readily solvable analytically even in the cases of time-dependent and compressible flows. Upon linearization, $\boldsymbol{u} \cdot \nabla \boldsymbol{u} = 0$, the steady state equation for the fluid velocity is the same as the incompressible, infinitely low *Re* or Stokes flow case we studied above.

19.2.5 Electro-osmosis

The electro-osmosis is an electrically driven flow of an ionic liquid relative to a charged surface. The ions attracted near the surface undergo migration towards the oppositely charged electrode, dragging the viscous, charge-neutral solvent with them. The electro-osmosis has been used in a variety of applications such as dewatering of soils and porous media, and, is relevant to transport in cells because of their ubiquitous electrical environments.

To explain such electro-kinetic effects that couple the charge degree of freedom to the fluid motion, we consider a steady state flow over a stationary, planar charged surface, driven not by a pressure but by an uniform external electric field $\boldsymbol{E_{ext}}$ (Fig. 19.10a):

$$\eta \nabla^2 \boldsymbol{u} = -\boldsymbol{f}(\boldsymbol{r}) = -\rho_e(\boldsymbol{r}) \boldsymbol{E_{ext}}, \tag{19.86}$$

where $\rho_e(\boldsymbol{r})$ is the charge density in the solution. Via the Poisson equation the charge density is given by the electric potential $\phi(\boldsymbol{r})$ so that

$$\eta \nabla^2 \boldsymbol{u} = \varepsilon \boldsymbol{E_{ext}} \nabla^2 \phi(\boldsymbol{r}) \tag{19.87}$$

In the Couette flow geometry (Fig. 19.3), this equation reads

$$\eta \frac{d^2 u_z(x)}{dx^2} = \varepsilon E_{ext} \frac{d^2 \phi(x)}{dx^2}, \tag{19.88}$$

which is integrated to

$$\eta \frac{du_z(x)}{dx} = \varepsilon E_{ext} \frac{d\phi(x)}{dx} \tag{19.89}$$

where we used the BC, $du_z(x)/dx = 0$ as well as $d\phi(x)/dx = 0$ at $x = \infty$. Further integration yields

$$u_z(x) = \frac{\varepsilon E_{ext}}{\eta} \{\phi(x) - \phi_s\} = \frac{\varepsilon E_{ext}}{\eta} \phi(x) + U, \tag{19.90}$$

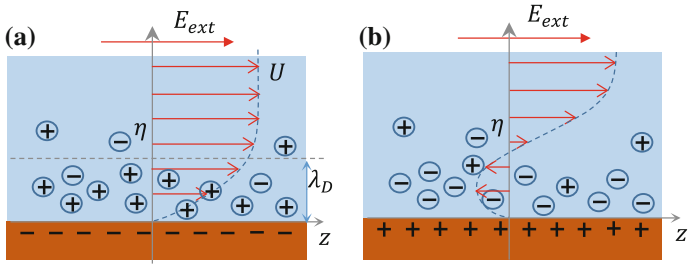

Fig. 19.10 **a** The flow of an ionic fluid over a charged surface. A charge-neutral ionic fluid (including water) is drifted by the external electric field. **b** The ionic fluid driven by the electric field and pressure within a charged circular channel

which, on the surface, meets the BC, $\phi = \phi_s$ (the surface potential) and $u_z = 0$ to yield the equation

$$U = -\frac{\varepsilon E_{ext}\phi_s}{\eta}. \tag{19.91}$$

This formula, called the Helmholtz-Smoluchowski relation, denotes the asymptotic velocity that the fluid would have at the bulk, $u(x \to \infty)$, in the usual situations where $\phi(x \to \infty)$ vanishes. The formula means that **the external electric field, via interaction with the ions in the electrical double layer (EDL), induces a flow U of the bulk fluid**, which is a neutral solvent or an electrolyte solution. If the surface charge or the surface potential is negative, the positively charged ions in the EDL will drag the solution towards the direction of the external electric field with the velocity (19.90) as sketched in Fig. 19.10a. According to the Debye-Hückel theory, $\phi(x) = \phi_s \exp(-x/\lambda_D)$, which is appreciable for x smaller than the Debye length λ_D. At physiological conditions where λ_D is only in the order of nanometers, the fluid velocity (19.90) abruptly drops to zero, that is, appears to slip at the edge of the EDL. This analysis is also applicable to flow through channels.

If a constant pressure gradient is additionally present in the fluid, we will have

$$\eta\nabla^2\boldsymbol{u} = \nabla p + \varepsilon\boldsymbol{E_{ext}}\nabla^2\phi. \tag{19.92}$$

For the case of a cylindrical channel of radius R with a pressure drop Δp over length L (19.56) along the flow, one can show that the velocity at the radial position $r = R - x$ from the central axis is

$$u(r) = \frac{\varepsilon E_{ext}}{\eta}\{\phi(R-r) - \phi_s\} - \frac{\Delta p}{4\eta L}\left(r^2 - R^2\right). \tag{19.93}$$

The flow induced by the electro-osmosis can compete with the flow induced by the pressure gradient depending on the sign of ϕ_s or the direction of field. Figure 19.10b

depicts the case where ϕ_s is positive, and the field and pressure drop are in the same direction. With the EDL contribution neglected, the volumetric flow induced by the field is $-\pi R^2 \varepsilon E_{ext} \phi_s / \eta$. On the other hand the rate of the pressure-driven flow through the channel is proportional to R^4, as we have studied. This suggests that for small R the flow rate by the electro-osmosis can dominate the flow rate by the pressure. It implies the electro-osmosis can be very effective in pumping water out of the porous media with a small average size of pores.

P19.11 *An electrolyte solution flows through a cylindrical channel of the surface potential ϕ_s driven by the pressure gradient. Show that the electrical current of the solution with the Debye length much shorter than the radius is given by*

$$I = \frac{\pi \varepsilon \Delta p R^2 \phi_s}{\eta L}.$$

This formula can be used to determine the surface potential ϕ_s from the measured values of the current.

19.2.6 Electrophoresis of Charged Particles

Electrophoresis is the migration of charged particles in fluid, driven by an external electric field. These particles can be micro-organisms, cells, colloids, and biopolymers. Electrophoresis is used widely for analysis and separation of these charged objects in biomedical technology and environmental research. Also the measurement of the electrophoretic velocity gives information on the electric double layers surrounding the particles.

Consider first a charged but non-conducting sphere of charge Q and radius R in a neutral fluid. Driven by a uniform external electric field E_{ext} the sphere moves with a steady velocity V (Fig. 19.11), which is given by the balance between electrical force QE_{ext} and the frictional force $6\pi\eta RV$:

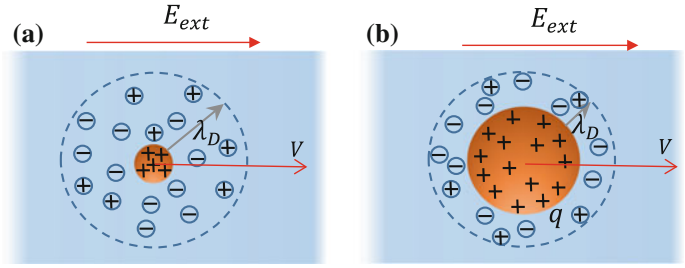

Fig. 19.11 Electrophoresis is the motion of charge sphere in an ionic fluid driven by an external electric field. **a** the case where $R/\lambda_D \ll 1$, **b** $R/\lambda_D \gg 1$

$$V = \frac{QE_{ext}}{6\pi\eta R}. \tag{19.94}$$

This simple formula tells how the charge particles can be separated by their charges and sizes. In terms of the surface potential, $\phi_s = Q/(4\pi\varepsilon R)$, which usually is measured rather than Q, the electrophoretic velocity is given by

$$V = \frac{2\phi_s\varepsilon}{3\eta}E_{ext}. \tag{19.95}$$

We consider that the particle is in an ionic solution. For the simplifying situation $R/\lambda_D \ll 1$, the case with low ionic concentrations or small particles, we can use the Debye-Hückel theory, $\phi_s = Q/\{4\pi\varepsilon R(1+R/\lambda_D)\}$ (6.45), to extend the above result.

Now consider the ionic solution where R/λ_D is not negligible (Fig. 19.11b). Difficulties lie in calculating the effects of the background ions that will influence the local fields and interact with the particle. Here we give a simple derivation for the limiting situation in which $R/\lambda_D \gg 1$. Because the particle is very large for a given λ_D, its surface can be viewed locally as planar. Furthermore, the electric field is parallel to the surface of the sphere because the sphere is non-conducting ($\boldsymbol{n}\cdot\boldsymbol{J}_e = 0$, where $\boldsymbol{J}_e = \sigma_e\boldsymbol{E}_{ext}$ and σ_e is the electrical conductivity). The situation is similar to the electro-osmosis along the planar charged surface we studied; here the surface is moving with the velocity V driven by the field. Thus, we adapt (19.90) in the form

$$u_z(r) = \frac{\varepsilon E_{ext}}{\eta}\phi(r) \tag{19.96}$$

so as to meet the BC that both u_z and $\phi(r)$ vanish when r, the radial position from the center of the sphere, goes to infinity. On the surface $r = R$, $\phi = \phi_s$ and $u_z = V$ (no-slip BC) should be met, so we have

$$V = \frac{\phi_s\varepsilon}{\eta}E_{ext}. \tag{19.97}$$

This result is independent of the particle's shape provided that λ_D is much shorter than the characteristic dimension of the particle. Noting that ϕ_s for this case of $R/\lambda_D \gg 1$ is $Q\lambda_D/(4\pi\varepsilon R^2)$ according to DH theory (6.45), the electrophoretic velocity can be expressed as

$$V = \frac{\lambda_D}{4\pi R^2\eta}QE_{ext} \tag{19.98}$$

Compared with (19.94) for the particle of the same R and Q, (19.98) is smaller by the factor $3\lambda_D/(2R)$, meaning that the ionic cloud within the EDL retards the electrophoresis.

19.2.7 Hydrodynamic Interaction

A force applied at a point in a fluid will disturb the flow field around it. Suppose that there is an object in the fluid. The force acting on a point on the surface of the object creates a disturbance on any points in the fluid, including the other points on the surface. This effect of the fluid medium is called the hydrodynamic interaction, which we derive below for the case of steady Stokes' flow.

In the presence of a force density $\boldsymbol{f}(\boldsymbol{r})$, the Stokes equation becomes

$$\nabla p = \eta \nabla^2 \boldsymbol{u} + \boldsymbol{f}(\boldsymbol{r}). \tag{19.99}$$

To relate $\boldsymbol{u}(\boldsymbol{r})$ with $\boldsymbol{f}(\boldsymbol{r}')$, we take the Fourier transform on the above equation to obtain the equation:

$$i\boldsymbol{k}p(\boldsymbol{k}) = -\eta k^2 \boldsymbol{u}(\boldsymbol{k}) + \boldsymbol{f}(\boldsymbol{k}). \tag{19.100}$$

A scalar product of the equation above with $i\boldsymbol{k}$ leads to

$$p(\boldsymbol{k}) = -\frac{i\boldsymbol{k}}{k^2} \cdot \boldsymbol{f}(\boldsymbol{k}), \tag{19.101}$$

where we used $i\boldsymbol{k} \cdot \boldsymbol{u}(\boldsymbol{k}) = 0$, the Fourier transform of $\nabla \cdot \boldsymbol{u}(\boldsymbol{r}) = 0$. Substituting (19.101) back to the (19.100) produces

$$u(\boldsymbol{k}) = \frac{1}{\eta k^2} \left(1 - \frac{\boldsymbol{k}\boldsymbol{k}}{k^2}\right) \cdot \boldsymbol{f}(\boldsymbol{k}). \tag{19.102}$$

It remains an exercise to inverse-Fourier transform the above and derive the equation:

$$\boldsymbol{u}(\boldsymbol{r}) = \int d\boldsymbol{r}' \, \boldsymbol{O}(\boldsymbol{r} - \boldsymbol{r}') \cdot \boldsymbol{f}(\boldsymbol{r}'), \tag{19.103}$$

where

$$\boldsymbol{O}(\boldsymbol{r}) = \frac{1}{8\pi\eta r} \left(\boldsymbol{I} + \frac{\boldsymbol{r}\boldsymbol{r}}{r^2}\right) \tag{19.104}$$

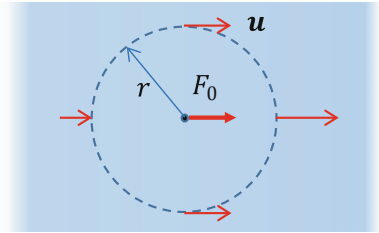

Fig. 19.12 The fluid velocities (thick arrows) at a distance r from the origin on which the force $\boldsymbol{F}_0$ acts

is the so-called Oseen tensor descriptive of the hydrodynamic interaction operating over long-range ($\sim 1/r$). On the other hand an inverse transform of (19.101) gives the pressure disturbance:

$$p(\boldsymbol{r}) - p_0 = \int d\boldsymbol{r}' \, \boldsymbol{P}(\boldsymbol{r} - \boldsymbol{r}') \cdot \boldsymbol{f}(\boldsymbol{r}'), \tag{19.105}$$

where

$$\boldsymbol{P}(\boldsymbol{r}) = \frac{\boldsymbol{r}}{4\pi r^3}. \tag{19.106}$$

Consider that there is a point force $\boldsymbol{F}_0$ at $\boldsymbol{r}' = 0, \boldsymbol{f}(\boldsymbol{r}') = \boldsymbol{F}_0 \delta(\boldsymbol{r}')$. It gives rise to a velocity disturbance at an otherwise quiescent point $\boldsymbol{r}$:

$$\boldsymbol{u}(\boldsymbol{r}) = \frac{1}{8\pi\eta r}[\boldsymbol{F}_0 + \hat{\boldsymbol{r}}(\hat{\boldsymbol{r}} \cdot \boldsymbol{F}_0)], \tag{19.107}$$

which is not in radial direction (Fig. 19.12). If a point-like particle is located at $\boldsymbol{r}$, it will experience a force proportional to its velocity which is equal to the above equation. This indicates the hydrodynamic interaction between the two fluid points. If you swim near the bottom of a swimming pool, you feel a repulsive force which tends to push you upward. This is the hydrodynamic interaction between your body and the bottom wall. In a polymer chain within a fluid, **a motion of one segment will interact with that of another, giving rise to a distinctive collective behavior**, which we will study in the next chapter.

The pressure is also perturbed by the point source (19.105):

$$p(\boldsymbol{r}) = p_0 + \frac{1}{4\pi r^2}(\hat{\boldsymbol{r}} \cdot \boldsymbol{F}_0). \tag{19.108}$$

With substitution of the dragging force $\boldsymbol{F}_0 = 6\pi\eta R\boldsymbol{V}$, with R being very small one can confirm that (19.108) and (19.107) agree with those of Stokes flow, (19.73) and (19.74).

P19.12 *Suppose that a small sphere of a charge Q translates in an electrolyte of the Debye length λ_D. Assuming the Debye-Hückel theory, calculate the effect of the charge on the fluid velocity. Hint*:

$$\boldsymbol{u_e}(\boldsymbol{r}) = \int d\boldsymbol{r}'\boldsymbol{O}(\boldsymbol{r}-\boldsymbol{r}')\cdot\rho_e(\boldsymbol{r}')\boldsymbol{E}(\boldsymbol{r}') = \int d\boldsymbol{r}'\boldsymbol{O}(\boldsymbol{r}-\boldsymbol{r}')\cdot\varepsilon\kappa_D^2\phi(\boldsymbol{r}')\nabla_{\boldsymbol{r}'}\phi(\boldsymbol{r}')$$

Further Reading and References

B.B. Bird, W.E. Stewart, E.N. Lightfoot, *Transport Phenomena*, 2nd edn. (Wiley, 2007)
S. Vogel, *Life in Moving Fluids: The Physical Biology of Flow* (Princeton University Press, 1984)
A.L. Fetter, J.D. Walecka, *Theoretical Mechanics of Particles and Continua* (McGraw-Hill Book Co., 1980)
L.D. Landau, E.M. Lifshitz, *Fluid Mechanics* (Pergamon Press, 1975)
G.K. Batchelor, *An Introduction to Fluid Dynamics* (Cambridge University Press, 2000)
J.L. Lebowitz, Boltzmann's Entropy and Time's Arrow. Phys. Today **46**(9), 32 (1993)
H. Bruus, *Theoretical Microfluidics* (Oxford University Press, 2008)
R.F. Probstein, H. Brenner, *Physicochemical Hydrodynamics* (Elsevier Inc., 1989)
J. Happel, H. Brenner, *Low Reynolds Number Hydrodynamics* (Kluwer, Dordrecht, 1991)
R. Fahraeus, T. Lindqvist, The viscosity of the blood in narrow capillary tubes. Am. J. Physiol. **96**, 562–568 (1931)
M. Sugihara-Sekia, B.M. Fu, Blood flow and permeability in microvessels. Fluid Dyn. Res. **37**, 82–132 (2005)
P.G. de Gennes, Reptation of a polymer chain in the presence of fixed obstacles. J. Chem. Phys. **55**, 572 (1971)
W. Sung, Slippage of linear flows of entangled polymers on surfaces. Phys. Rev. E **51**, 6 (1995)

Chapter 20
Dynamics of Polymers and Membranes in Fluids

The dynamics of biological soft-condensed matter (bio-soft matter), such as biopolymers membranes and cells, has at mesoscale several features which are not seen in ordinary matter consisting of particles. One is the soft matter structural connectivity; although the strengths of its atominstic interactions are in the order of eV or higher, interconnected as a whole it can undergo collective motions with the energies in the order of or less than thermal energy. **Despite the short-range interconnectivity (among near neighbors), the bio-soft matter at room temperature can be correlated over long distances** as we have studied in Chaps. 10–12. Also we studied in Chaps. 16 and 18 that it can move cooperatively in thermally fluctuating backgrounds and susceptibly in response to external fields. The biological complexes live usually in viscous, aqueous environments; the background fluids impart dissipation, but mediate hydrodynamic interactions (HI) between segments in the complexes. **In contrast to the structural connectivity, HI is long ranged, adding the unique cooperativity to dynamical behaviors**.

In this chapter we study the interplay of the structural connectivity and hydrodynamic interaction in soft matter dynamics. The basic method for the dynamics is a stochastic approach in which each internal constituent (mesoscopic subunit) undergoes Brownian motions while interacting with one another and with the fluid environment. As standard models that allow analytical understandings, we consider flexible chains, then semi-flexible nearly-straight polymers, and planar membranes. The nonspecific physical features that are obtained from the relatively simple systems can give valuable insights into the dynamics of more complex biological soft matter under flows and constraints.

W. Sung, *Statistical Physics for Biological Matter*, Graduate Texts in Physics,
https://doi.org/10.1007/978-94-024-1584-1_20

In Chap. 5, we discussed **the coarse-grained description of complex systems' static properties in terms of the relevant degrees of freedom Q. The effective Hamiltonian or the free energy $\mathcal{F}(Q)$ associated with Q describes its equilibrium distribution $P(Q) \sim \exp[-\beta \mathcal{F}(Q)]$**. In later chapters we studied the Markovian dynamics for a number of systems including polymers in several situations. The Markovian equation of motion for Q is the Langevin equation,

$$\zeta \dot{Q} = -\frac{\partial \mathcal{F}(Q)}{\partial Q} + \xi(t), \tag{20.1}$$

where $\xi(t)$, representative of microscopic degrees of freedom that underlies Q, is the Gaussian and white noise that satisfies $\langle \xi(t)\xi(0)\rangle = 2\mathcal{D}\delta(t)$, with the noise strength given as $\mathcal{D} = \zeta k_B T$. This thermal noise is essential in driving the system, under the system force $-\partial \mathcal{F}(Q)/\partial Q$ in balance with the damping force $\zeta \dot{Q}$, to reach the stationary state $P(Q) \sim e^{-\beta \mathcal{F}(Q)}$ in the long times. The next task is to solve and/or simulate the Langevin equation or its equivalent Fokker-Planck equation for evaluating the dynamic averages and correlations.

20.1 Dynamics of Flexible Polymers

In this chapter we first consider the dynamics of flexible polymer chains (e.g., a single-stranded DNA fragment) in a viscous fluid. At the highest level of coarse-graining, Q is adopted as $\boldsymbol{R}$, the end-to-end distance (EED) of the chain. The equilibrium probability density of the EED, if the chain consists of many (N) statistically independent segments of length l, is given as a Gaussian distribution by the virtue of the central limit theorem as we studied earlier in Chap. 10:

$$P(\boldsymbol{R}) \sim e^{-3\boldsymbol{R}^2/2\langle \boldsymbol{R}^2\rangle} \tag{20.2}$$

with the variance of $\boldsymbol{R}$ given by

$$\langle \boldsymbol{R}\rangle^2 = Nl^2. \tag{20.3}$$

Consequently, we obtain $\mathcal{F}(\boldsymbol{R}) = K_e \boldsymbol{R}^2/2$ where $K_e = 3k_B T/(Nl^2) \equiv k_e/N$. $\mathcal{F}(\boldsymbol{R})$ takes the minimum at $\boldsymbol{R} = 0$, meaning that the coiled conformation is the equilibrium state.

The Langevin equation (20.1) for $Q = \boldsymbol{R}$ is

$$\zeta \dot{\boldsymbol{R}} = -K_e \boldsymbol{R} + \boldsymbol{\xi}(t), \tag{20.4}$$

where ζ is the effective friction coefficient of the whole chain. From the equation, we can obtain the EED time correlation function

$$\langle \boldsymbol{R}(t) \cdot \boldsymbol{R}(0) \rangle = \langle \boldsymbol{R}^2 \rangle e^{-t/\tau} = Nl^2 e^{-t/\tau}. \tag{20.5}$$

The correlation or relaxation time τ is given by

$$\tau = \frac{\zeta}{K_e} = \frac{Nl^2\zeta}{3k_BT}. \tag{20.6}$$

If we neglect the hydrodynamic interactions between the chain segments, the friction coefficient is given by $\zeta \sim N\gamma$, where γ is the friction coefficient per segment. Then the correlation time scales as $\sim N^2$, which expresses how the chain relaxes slowly as the contour length $L = Nl$ increases. If the hydrodynamic interactions are included, the friction coefficient of the polymer coil can be regarded as that of a cohesive sphere of radius $\sim R_0 = \langle R^2 \rangle^{1/2} \sim N$ in a fluid of viscosity η: $\zeta \sim \eta R_0 \sim N^{1/2}$. This yields $\tau \sim N^{3/2}$, suggesting that the cooperativity induced by the hydrodynamic interactions enhances the diffusivity $D = k_BT/\zeta$ as well as the relaxation by the factor $N^{1/2}$. Along with $\langle R^2 \rangle = Nl^2$, the simple model captures this scaling behaviors that emerge in long chains independently of microscopic details.

20.1.1 The Rouse Model

Now consider the description of a free flexible chain at segment level based on the bead-spring (the Gaussian chain) model, where the free energy is given by (10.51) with the vanishing potential ($u = 0$).

$$\mathcal{F}\{\boldsymbol{r}_n\} = \frac{1}{2}\sum_{n=1}^{N} k_e(\boldsymbol{r}_n - \boldsymbol{r}_{n-1})^2, \tag{20.7}$$

where each bead positioned at $\boldsymbol{r}_n$ ($n = 1, 2, \ldots, N+1$) is linearly interconnected by a spring of the spring constant, $k_e = 3k_BT/l^2$ (Fig. 20.1). We extend the general equation (20.1) to the set of bead coordinates, $\boldsymbol{Q} = \{\boldsymbol{r}_n\}$ to obtain

$$\gamma \dot{\boldsymbol{r}}_n = -\frac{\partial \mathcal{F}\{\boldsymbol{r}_n\}}{\partial \boldsymbol{r}_n} + \boldsymbol{\xi}_n(t), \tag{20.8}$$

or

$$\gamma \dot{\boldsymbol{r}}_n = -k_e(\boldsymbol{r}_n - \boldsymbol{r}_{n+1} + \boldsymbol{r}_n - \boldsymbol{r}_{n-1}) + \boldsymbol{\xi}_n(t). \tag{20.9}$$

This is called the Rouse model: the beads are interconnected harmonically and dissipate with the friction coefficient γ per each but with no mutual hydrodynamic

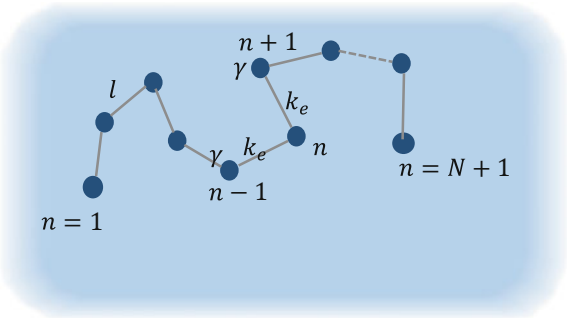

Fig. 20.1 The Rouse model for flexible polymer dynamics: the $N + 1$ beads are interconnected via the N springs (k_e) and are damped in a fluid with a friction γ per bead

interaction; each bead undergoes the Brownian motion under a Gaussian and white noise that allows the system to arrive at equilibrium,

$$\langle \xi_{n\alpha}(t) \rangle = 0, \tag{20.10}$$

$$\langle \xi_{n\alpha}(t) \xi_{m\beta}(t') \rangle = 2\gamma k_B T \delta_{nm} \delta_{\alpha\beta} \delta(t - t'), \tag{20.11}$$

where α, β label the Cartesian components.

We now solve (20.9) for a number of dynamical properties such as the time correlation of EED, dynamics of a segment probed by its mean square displacement, and dynamic structure of the polymer, etc. As was done before for a long chain, n is taken to be continuous so that (20.9) is rewritten as

$$\begin{aligned} \gamma \frac{\partial \boldsymbol{r}(n,t)}{\partial t} &= -k_e \left(-\frac{\partial \boldsymbol{r}(n+1,t)}{\partial n} + \frac{\partial \boldsymbol{r}(n,t)}{\partial n} \right) + \boldsymbol{\xi_n}(t) \\ &= k_e \frac{\partial^2 \boldsymbol{r}(n,t)}{\partial n^2} + \boldsymbol{\xi_n}(t), \end{aligned} \tag{20.12}$$

so that we have

$$\frac{\partial \boldsymbol{r}(s,t)}{\partial t} = \frac{3k_B T}{\gamma} \frac{\partial^2 \boldsymbol{r}(s,t)}{\partial s^2} + \frac{\boldsymbol{\xi}(s,t)}{\gamma}, \quad 0 \le s \le L, \tag{20.13}$$

$$\langle \xi_\alpha(s,t) \xi_\beta(s',t') \rangle = 2\gamma k_B T l \delta(s - s') \delta_{\alpha\beta} \delta(t - t'), \tag{20.14}$$

in terms of the one dimensional position along the contour of the chain, $s = nl$. The boundary conditions at the two ends are obtained as follows. For both ends, the equations of motion are

$$\gamma \dot{\boldsymbol{r}}_1 = -k_e(\boldsymbol{r}_1 - \boldsymbol{r}_2) + \boldsymbol{\xi}_1(t) \tag{20.15}$$

$$\gamma \dot{\boldsymbol{r}}_{N+1} = -k_e(\boldsymbol{r}_{N+1} - \boldsymbol{r}_N) + \boldsymbol{\xi}_{N+1}(t). \tag{20.16}$$

These equations satisfy the general form (20.9), if there are two hypothetical beads $\boldsymbol{r}_0$ and $\boldsymbol{r}_{N+2}$ defined as $\boldsymbol{r}_0 = \boldsymbol{r}_1$, and $\boldsymbol{r}_{N+2} = \boldsymbol{r}_{N+1}$. These relations lead to the boundary conditions for (20.13) at both ends:

$$\frac{\partial \boldsymbol{r}(s,t)}{\partial s} = 0. \tag{20.17}$$

In solving (20.13) or the equations for $N+1$ coupled damped oscillators (20.9), it is desirable to find the normal modes, each capable of independent motion. In mechanics, the linearly coupled harmonic oscillators give rise to the normal modes, called the sound modes, which can propagate. Similarly, for the polymer we have the normal modes, called the Rouse modes. Unlike the usual sound modes the Rouse modes are overdamped, but support certain collective dynamic features of the linear chains, which we will study below. We introduce the normal modes

$$\boldsymbol{r}_q(t) = \int_0^L ds\, \cos(qs)\, \boldsymbol{r}(s,t) \tag{20.18}$$

with q taking $N+1$ discrete values, $q_n = n\pi/L$, $(n = 0, 1, 2 \ldots N)$. A chain segment position is represented as

$$\boldsymbol{r}(s,t) = \boldsymbol{r}_c(t) + 2\sum_{q>0} \boldsymbol{r}_q(t)\cos(qs), \tag{20.19}$$

which satisfies the end boundary conditions (20.17). Here $\boldsymbol{r}_c(t)$ represents the $q = 0$ mode

$$\boldsymbol{r}_c(t) = \boldsymbol{r}_{q=0}(t) = \frac{1}{L}\int_0^L ds\, \boldsymbol{r}(s,t), \tag{20.20}$$

which is the center of mass (CM) position of the chain. We have the similar expressions for the random forces following transformation

$$\boldsymbol{\xi}_q(t) = \frac{1}{L}\int_0^L ds\, \cos(qs)\boldsymbol{\xi}(s,t) \tag{20.21}$$

where $\boldsymbol{\xi}_q(t)$ then satisfies

$$\left\langle \xi_{q\alpha}(t)\xi_{q'\beta}(t')\right\rangle = 2\zeta_q k_B T \delta_{qq'}\delta_{\alpha\beta}\delta(t-t'), \tag{20.22}$$

Substitution of the above expressions into (20.13) yields the equations for the center of mass and the N Rouse modes

$$N\gamma \frac{d}{dt}\boldsymbol{r}_c(t) = \boldsymbol{\xi}_c(t), \tag{20.23}$$

$$\zeta_q \frac{d}{dt}\boldsymbol{r}_q(t) = -k_q \boldsymbol{r}_q(t) + \boldsymbol{\xi}_q(t), \tag{20.24}$$

where

$$k_q = 6k_B TLq^2/l, \tag{20.25}$$

$$\zeta_q = 2N\gamma, \text{ for } q = n\pi/L, \quad (n = 1, 2 \ldots N). \tag{20.26}$$

Equation (20.23) tells us that the center of mass undergoes a free diffusion with a diffusivity D_c related by the total friction $N\gamma$ via

$$D_c = k_B T/(N\gamma). \tag{20.27}$$

The N independent equations (20.24) of Brownian harmonic oscillators (Rouse modes) belong to Ornstein-Uhlenbeck processes, whose time correlation function is

$$\left\langle \boldsymbol{r}_{q\alpha}(t)\boldsymbol{r}_{q'\beta}(0)\right\rangle = \frac{k_B T\delta_{qq'}\delta_{\alpha\beta}}{k_q} e^{-t/\tau_q} \tag{20.28}$$

where

$$\tau_q = \zeta_q/k_q = \gamma/\left(3k_B Tq^2\right). \tag{20.29}$$

The dynamic correlation of the Rouse mode decays with the relaxation time τ_q which is longer for a larger wave-length (smaller q) undulation.

In terms of the Rouse modes the EED vector is given by

$$\begin{aligned} \boldsymbol{R}(t) &= \boldsymbol{r}(L,t) - \boldsymbol{r}(0,t) \\ &= 2\sum_{q>0} \boldsymbol{r}_q(t)(\cos(qL) - 1) = -4\sum_{q'} \boldsymbol{r}_{q'}(t), \end{aligned} \tag{20.30}$$

where the last sum is over all the modes $q' = (\pi/L)\, n'$ with n' being odd integers. The time-correlation function of the EED, using (20.28), is

$$\begin{aligned} \langle \boldsymbol{R}(t)\cdot\boldsymbol{R}(0)\rangle &= 16\sum_{q'} \left\langle \boldsymbol{r}_{q'}(t)\cdot\boldsymbol{r}_{q'}(0)\right\rangle \\ &= 16\sum_{q'} \frac{3k_B T}{k_{q'}} e^{-t/\tau(q')} = Nl^2 \sum_{n'=odd} \frac{8}{n'^2\pi^2} e^{-n'^2 t/\tau_R}. \end{aligned} \tag{20.31}$$

Here τ_R is the slowest relaxation time corresponding to the largest wave-length (smallest $q, q_1 = \pi/L$), called the Rouse time:

$$\tau_R = \tau_{q_1} = \frac{\gamma L^2}{3\pi^2 k_B T}. \tag{20.32}$$

At $t = 0$, (20.31) becomes $\langle \boldsymbol{R}^2 \rangle = Nl^2$ via $\sum_{n'=odd} 1/n'^2 = \pi^2/8$. Because of the term $1/n'^2$ in the summation in (20.31), the first Rouse mode ($n' = 1$ or $q' = \pi/L$) dominates the sum, yielding an approximation that is constrained to be exact at $t = 0$:

$$\langle \boldsymbol{R}(t) \cdot \boldsymbol{R}(0) \rangle \approx \left\{ Nl^2 \sum_{n'=odd} \frac{8}{n'^2 \pi^2} \right\} e^{-t/\tau_R} = \langle \boldsymbol{R}^2 \rangle e^{-t/\tau_R}. \tag{20.33}$$

The Rouse time τ_R is proportional to L^2, as the combined result of high viscosity ($\zeta_{q_1} \sim L$) and high elasticity ($k_{q_1} \sim L^{-1}$) for a long chain. We may rewrite $\tau_R \sim N\gamma R_0^2/(k_B T) \sim R_0^2/D_c$; the Rouse time is the rotational relaxation time of the chain or is about the duration for the chain CM to diffuse over the EED distance.

The length scaling behaviors of this Rouse model for the diffusion constant and the relaxation time, $D_c \sim N^{-1}$ and $\tau_R \sim N^2$, do not agree with experimental results; for dilute polymer solutions at theta (Θ) conditions in which the chain is ideal, $D_c \sim N^{-1/2}$, and $\tau \sim N^{3/2}$. The disagreement is originated from the neglect of hydrodynamic interaction (HI), with which we will deal next. Nevertheless the Rouse model is valid for the concentrated polymer solutions and melts where the HI is sufficiently screened.

Often the polymer is immersed in a flowing solvent. For this case the Langevin equation (20.13) should be replaced by

$$\frac{\partial \boldsymbol{r}(s,t)}{\partial t} = \boldsymbol{u}_0(s,t) + \frac{3k_B T}{\gamma} \frac{\partial^2 \boldsymbol{r}(s,t)}{\partial s^2} + \frac{\boldsymbol{\xi}(s,t)}{\gamma} \tag{20.34}$$

where the first term on RHS is the flow velocity that the fluid would have at the arc position s in the absence of the polymer, while the second is the perturbation on the velocity caused by the chain force on the segment at s.

P20.1 *A flexible polymer is anchored on planar surface at one end is subject to a Couette flow with a shear rate $\dot{\gamma}$, as shown in the figure below. Study the conformation of the chain in a steady state by finding (i) the mean square of EED $\langle \boldsymbol{R}^2 \rangle$, where the average is taken over the steady state. (ii) Find $\langle \boldsymbol{r}(s,t) \rangle$.*

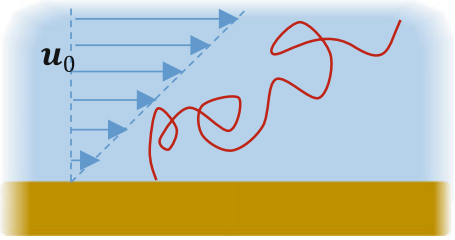

20.1.2 The Zimm Model

The Rouse model assumes that the solvent is independent of polymer motion; in reality the solvent is perturbed by the motion of the segments, which in turn affects frictional forces on them. Thus (20.8) must be replaced by

$$\gamma(\dot{\boldsymbol{r}}_n - \boldsymbol{u}_n) = -\frac{\partial \mathcal{F}\{\boldsymbol{r}_n\}}{\partial \boldsymbol{r}_n} + \boldsymbol{\xi}_n(t), \tag{20.35}$$

where $\boldsymbol{u}_n$ is velocity that the solvent has at the bead n as a result of polymer motion. Notice that the $\boldsymbol{u}_n$ is caused by the hydrodynamic interaction from the other beads; using the Stokes equation for a steady fluid, we have

$$\boldsymbol{u}_n = \sum_{m \neq n} \boldsymbol{\Lambda}_{nm} \cdot \left\{ -\frac{\partial \mathcal{F}\{\boldsymbol{r}_m\}}{\partial \boldsymbol{r}_m} + \boldsymbol{\xi}_m(t) \right\}. \tag{20.36}$$

Here $\boldsymbol{\Lambda}_{nm}$ for $n \neq m$ represents the Oseen tensor (19.104):

$$\boldsymbol{\Lambda}_{nm} = \boldsymbol{O}_{nm}(\boldsymbol{r}_{nm}) = \frac{1}{8\pi\eta|\boldsymbol{r}_{nm}|}(I + \widehat{\boldsymbol{r}}_{nm}\widehat{\boldsymbol{r}}_{nm}) \tag{20.37}$$

where $\boldsymbol{r}_{nm} = \boldsymbol{r}_n - \boldsymbol{r}_m = |\boldsymbol{r}_{nm}|\widehat{\boldsymbol{r}}_{nm}$. Consequently (20.35) can be written as

$$\dot{\boldsymbol{r}}_n = \sum_{m=1}^{N+1} \boldsymbol{\Lambda}_{nm} \cdot \left\{ -\frac{\partial \mathcal{F}\{\boldsymbol{r}_m\}}{\partial \boldsymbol{r}_m} + \boldsymbol{\xi}_m(t) \right\} \tag{20.38}$$

if we include the self-term

$$\boldsymbol{\Lambda}_{nm} = \frac{\boldsymbol{I}}{\gamma}\delta_{nm}, \tag{20.39}$$

for n, which alone leads to the Rouse model. This self-term for a bead $\boldsymbol{I}/\gamma$ is far less than the mobility it would receive from the neighboring beads via the hydrodynamic interactions, which are $1/r$ long-ranged. Thus, we may neglect the self-term hereafter and study the Zimm model that includes the hydrodynamic interaction.

In the continuum limit we have the equation

$$\frac{\partial}{\partial t}\boldsymbol{r}(s,t) = \int ds' \boldsymbol{\Lambda}(\boldsymbol{r}(s) - \boldsymbol{r}(s')) \cdot \left\{ -\frac{\delta \mathcal{F}}{\delta \boldsymbol{r}(s')} + \boldsymbol{\xi}(s',t) \right\}, \tag{20.40}$$

and, using the bead-spring model,

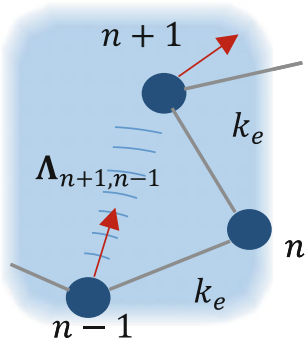

Fig. 20.2 The Zimm model: a bead-spring model with hydrodynamic interaction between beads

$$\frac{\partial}{\partial t}\boldsymbol{r}(s,t) = \int ds' [\boldsymbol{\Lambda}\{\boldsymbol{r}(s) - \boldsymbol{r}(s')\}] \cdot \left\{ 3k_B T \frac{\partial^2 \boldsymbol{r}(s',t)}{\partial s'^2} + \boldsymbol{\xi}(s',t) \right\}. \tag{20.41}$$

The above equation shows that the dynamics of a chain segment is complicated, due to its hydrodynamic coupling to all of the other segments in a nonlinear way. To linearize and solve the equation, Zimm introduced the pre-averaging approximation for $\boldsymbol{\Lambda}(\boldsymbol{r}(s) - \boldsymbol{r}(s'))$ to replace it by

$$\langle \boldsymbol{\Lambda}(\boldsymbol{r}(s) - \boldsymbol{r}(s')) \rangle = \left\langle \frac{1}{8\pi\eta |\boldsymbol{r}_{ss'}|} (\boldsymbol{I} + \widehat{\boldsymbol{r}}_{ss'} \widehat{\boldsymbol{r}}_{ss'}) \right\rangle. \tag{20.42}$$

where $\boldsymbol{r}_{ss'} = \boldsymbol{r}(s) - \boldsymbol{r}(s')$ and $\widehat{\boldsymbol{r}}_{ss'}$ is its unit vector. The averaging is done over the Gaussian distribution for the EED, $\boldsymbol{r}_{ss'}$, which is isotropic over the orientation, $\widehat{\boldsymbol{r}}_{ss'}$, so that

$$\begin{aligned} \langle \boldsymbol{\Lambda}(\boldsymbol{r}(s) - \boldsymbol{r}(s')) \rangle &= \left\langle \frac{1}{8\pi\eta |\boldsymbol{r}_{ss'}|} \right\rangle (\boldsymbol{I} + \langle \widehat{\boldsymbol{r}}_{ss'} \widehat{\boldsymbol{r}}_{ss'} \rangle) \\ &= \left\langle \frac{1}{8\pi\eta |\boldsymbol{r}_{ss'}|} \right\rangle \left(\boldsymbol{I} + \frac{1}{3}\boldsymbol{I} \right) = \frac{1}{6\pi\eta} \left\langle \frac{1}{|\boldsymbol{r}_{ss'}|} \right\rangle \boldsymbol{I} = \Lambda_Z(s - s')\boldsymbol{I}. \end{aligned} \tag{20.43}$$

where

$$\Lambda_Z(s - s') = \frac{1}{\pi\eta} \left(\frac{1}{6\pi |s - s'| l} \right)^{1/2}. \tag{20.44}$$

P20.2 *Prove the above relations.*

Intuitively we can expect that the preaveraging approximation is quite reasonable for a coiled chain conformation that is random enough to be indistinguishable from the average conformation.

Via the approximation (20.44), (20.41) becomes linear in $\boldsymbol{r}$:

$$\frac{\partial}{\partial t}\boldsymbol{r}(s,t) = \int ds' \Lambda_Z(s-s')\left\{3k_BT\frac{\partial^2 \boldsymbol{r}(s',t)}{\partial s'^2} + \boldsymbol{\xi}(s',t)\right\} \tag{20.45}$$

To analyze the equation, we consider the cosine transform (20.18), which is written as

$$\frac{\partial}{\partial t}\boldsymbol{r}_q(t) = \sum_{q'} \Lambda_{Zq,q'}\left\{-k_{q'}\boldsymbol{r}_{q'}(t) + \boldsymbol{\xi}_{q'}(t)\right\}, \tag{20.46}$$

where

$$\Lambda_{Zq,q'} = \frac{1}{L^2}\int_0^L ds \int_0^L ds' \cos(qs)\cos(q's')\Lambda_Z(s-s') \tag{20.47}$$

for all modes $(q, q' = n\pi/L, n = 0\ldots N)$. A calculation (see Doi and Edwards 1988) shows that $\Lambda_{Zq,q'}$ is nearly diagonal:

$$\Lambda_{Zq,q'} \approx \Lambda_Z(q)\delta_{q,q'}. \tag{20.48}$$

Then the equation for the center of mass is

$$\frac{\partial}{\partial t}\boldsymbol{r}_c(t) = \Lambda_Z(q=0)\boldsymbol{\xi}_c(t) \tag{20.49}$$

where

$$\Lambda_Z(q=0) = \frac{1}{L^2}\int_0^L ds \int_0^L ds' \Lambda_Z(s-s') = \frac{8}{3\eta}\left(\frac{1}{6\pi^3 Ll}\right)^{1/2} \tag{20.50}$$

is the translational mobility of the whole chain. This indicate the CM diffusion constant is

$$D_c = \frac{8k_BT}{3\eta}\left(\frac{1}{6\pi^3 Ll}\right)^{1/2} = \frac{8}{3\pi^{1/2}}\frac{k_BT}{6\pi\eta R_g} \sim N^{-1/2}, \tag{20.51}$$

where the radius of gyration $R_g = (1/6)^{1/2} N^{1/2} l$ is comparable to the hydrodynamic radius of the chain $3\pi^{1/2} R_g/8$.

The dynamics of N Rouse normal modes, $\boldsymbol{r}_q(q = \pi/L, 2\pi/L, \ldots N\pi/L = \pi/l)$, then follows the N independent equations:

$$\frac{\partial}{\partial t}\boldsymbol{r}_q(t) = \Lambda_Z(q)\{-k_q \boldsymbol{r}_q(t) + \boldsymbol{\xi}_q(t)\}, \tag{20.52}$$

where $\Lambda_Z(q)$ is approximated by

$$\Lambda_Z(q) \approx \frac{1}{2\pi(3ql)^{1/2}\eta L} \tag{20.53}$$

(Doi and Edwards 1988). From (20.52), we find

$$\langle \boldsymbol{r}_q(t) \cdot \boldsymbol{r}_q(0) \rangle = \frac{3k_B T}{k_q} e^{-t/\tau(q)}, \tag{20.54}$$

with the relaxation time given by

$$\tau_q = 1/(\Lambda_Z(q)k_q) = \tau_Z(qL/\pi)^{-3/2} = \tau_Z n^{-3/2}. \tag{20.55}$$

where we used $k_q = (6k_B T L q^2)/l$ (20.25). The τ_Z is the longest relaxation time

$$\tau_Z = \tau_{q_1} = \frac{\eta(N^{1/2}l)^3}{(3\pi)^{1/2}k_B T} \sim \frac{\eta R_g^3}{k_B T} \sim N^{3/2}. \tag{20.56}$$

These scaling behaviors of the CM diffusion and the relaxation time are in agreement with experiments for the flexible chain under theta conditions. A hand-waving argument for the behavior is given as follows. **The coil of the hydrodynamically interacting segments can be regarded as a cohesive sphere of the hydrodynamic radius $\sim \boldsymbol{R_g}$ moving in a fluid of the viscosity $\boldsymbol{\eta}$; it has the friction coefficient $\sim \boldsymbol{\eta R_g} \sim \boldsymbol{N^{1/2}} \sim \boldsymbol{D_c^{-1}}$, and the rotational friction coefficient $\sim \boldsymbol{\eta R_g^3}$.** Thus τ_Z is the rotational relaxation time, or, rewritten as $\tau_Z \sim R_0^2/D_c \sim N^{3/2}$, is about the time for the sphere to diffuse over the distance R_0. Comparing with the Rouse model results, one may say that the hydrodynamic interaction (cooperativity) speeds up the chain dynamics. All of the scaling behaviors with and without hydrodynamic interaction are identical to the corresponding results from the more coarse-grained description (20.6) introduced at the outset in this section.

P20.3 *Use the scaling argument above to show that the CM diffusion constant and EED relaxation time for the chain in good solvents with $R_g \sim N^{\nu}$ are given by*

$$D_c \sim N^{-\nu} \quad \textit{and} \quad \tau_Z \sim N^{3\nu}$$

P20.4 *Write down the equation of motion for a flexible chain with an end pulled by a force. Discuss how the chain conforms to this force.*

P20.5 *Consider a dimer or dumbel model, in which two beads are coupled by a spring and hydrodynamic interaction. Write down the equation of motion in a simple shear flow for a Brownian dynamic simulation.*

Segmental Dynamics

Now turn our attention to local dynamics of the chain. We consider the mean squared displacement (MSD) of a segment at s, $\overline{\Delta}_{\boldsymbol{r}}^2(s,t) = \langle(\boldsymbol{r}(s,t) - \boldsymbol{r}(s,0)^2\rangle$. Using (20.19), and noting that the correlations between different modes vanish, we have

$$\begin{aligned}\overline{\Delta}_{\boldsymbol{r}}^2(s,t) &= \left\langle \left[\{\boldsymbol{r}_0(t) - \boldsymbol{r}_0(0)\} + 2\sum_{q>0} \{\boldsymbol{r}_q(t) - \boldsymbol{r}_q(0)\} \cos(qs) \right]^2 \right\rangle \\ &= 6D_c t + 24 \sum_{q>0} \frac{k_B T}{k_q} \cos^2(qs) \left(1 - e^{-t/\tau_q}\right).\end{aligned} \tag{20.57}$$

The first term is the global, long-time CM diffusion contribution; the second is the local contribution from the Rouse modes. We are interested in the average over s

$$\overline{\Delta}_{\boldsymbol{r}}^2(t) = \frac{1}{L}\int_0^L ds \overline{\Delta}_{\boldsymbol{r}}^2(s,t), \tag{20.58}$$

which then is written as

$$\overline{\Delta}_{\boldsymbol{r}}^2(t) = 6D_c t + 12 \sum_q \frac{k_B T}{k_q} \left(1 - e^{-t/\tau_q}\right). \tag{20.59}$$

In a time much shorter than the shortest relaxation time $\tau_{q_N} \sim \eta l^3/(k_B T)$ we, by putting $e^{-t/\tau_q} \approx 1 - t/\tau_q$, have

$$\begin{aligned}\overline{\Delta}_{\boldsymbol{r}}^2(t) &= 6D_c t + 12k_B T t \sum_q \frac{1}{k_q \tau_q} \\ &= 6t\left[D_c + 2k_B T \sum_q \Lambda_z(q)\right] = 6Dt,\end{aligned} \tag{20.60}$$

where we note

$$\begin{aligned}2k_B T \sum_q \Lambda_z(q) &= \frac{k_B T}{\pi(3l)^{1/2}\eta L}\left(\frac{L}{\pi}\right)^{1/2} \sum_{n=1}^{N} n^{-1/2} \\ &\cong \frac{k_B T}{\pi(3l)^{1/2}\eta L}\left(\frac{L}{\pi}\right)^{1/2} \int_1^N dn\, n^{-1/2} \\ &\cong 2(3\pi)^{-1/2} k_B T/\pi\eta l \gg D_c.\end{aligned} \tag{20.61}$$

Equation (20.61) means that a segment moves with diffusivity $D \sim k_B T/\eta l$, which is much larger than CM diffusivity D_c (20.51). The diffusivity D is what one can expect for the free diffusion of a single monomer of the size $\sim l$ in the fluid. Each monomer moves as if it is not connected by neighbors.

The second term of (20.59) can be replaced by the integral:

$$\begin{aligned}12\sum_q \frac{k_B T}{k_q}\left(1 - e^{-t/\tau_q}\right) &\cong \frac{2Ll}{\pi^2}\int_1^N dn \frac{1}{n^2}\left[1 - \exp\left(-n^{3/2}t/\tau_Z\right)\right] \\ &= \frac{2Ll}{\pi^2}\left(\frac{t}{\tau_Z}\right)^{2/3} \int_{t/\tau_Z}^{N^{3/2}t/\tau_Z} dx\, x^{-2/3} \mathrm{e}^{-x},\end{aligned} \tag{20.62}$$

where $x = n^{3/2}t/\tau_Z$, and the integration is done by part. If we consider the time window, $t/\tau_Z \ll 1$, $N^{3/2}t/\tau_Z \gg 1$, that is, $\tau_Z/N^{3/2} \ll t \ll \tau_Z$ or $\eta l^3/(k_B T) \ll t \ll \eta R_0^3/(k_B T)$, the integral becomes definite:

$$\frac{2Ll}{\pi^2}\left(\frac{t}{\tau_Z}\right)^{2/3} \int_0^\infty dx\, x^{-2/3}\mathrm{e}^{-x} = \frac{2Ll}{\pi^2}\Gamma(1/3)\left(\frac{t}{\tau_Z}\right)^{2/3}, \tag{20.63}$$

where $\Gamma(1/3) = \int_0^\infty dx\, x^{-2/3}\mathrm{e}^{-x} = 2.68$. Equation (20.63) dominates over $D_c t$, so (20.60) becomes

$$\overline{\Delta}_{\boldsymbol{r}}^2(t) = 0.54Nl^2\left(\frac{t}{\tau_Z}\right)^{2/3} \sim N^0 t^{2/3}. \tag{20.64}$$

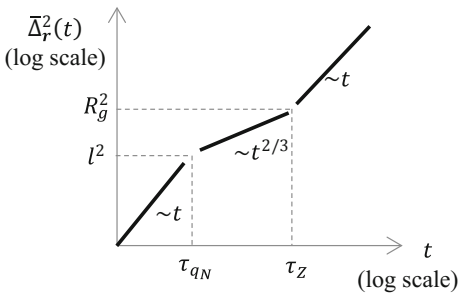

Fig. 20.3 The growth of the mean squared displacement of a segment on various time windows

Therefore, in the intermediate times, two anomalous behaviors emerge: the MSD is independent of N, while it shows a subdiffusive behavior $\overline{\Delta}_r^2(t) \sim t^{\alpha}$ with $\alpha = 2/3$, which is less than 1 expected for normal diffusion. Both of these two features are the signature of connectivity and caging of the chain that a segment strongly experiences before the chain relaxes to equilibrium.

At a long time $t \gg \tau_Z$, the exponential term in (20.59) decays to zero, yielding, by virtue of $\sum_{n=1} n^{-2} = \pi^2/6$,

$$\overline{\Delta}_r^2(t) = 6D_c t + Nl^2/3 \approx 6D_c t, \tag{20.65}$$

that is, the segment freely diffuses together with the whole chain, escaping from its local cage. Figure 20.3 depicts how the MSD grows in time, over three distinctive regions

20.2 Dynamics of a Semiflexible Chain

Many biopolymers are semi-flexible and, within cells, are confined under various kinds of forces or constraints. In Chap. 11, we studied the conformation of such semi-flexible polymers modelled by worm-like chains (WLC). Now we consider the dynamical aspect of the chain and ask important questions: **how does the chain relax; how does the chain dynamically respond to a time-dependent tension f pulling along the longitudinal direction?** We consider a nearly-straight chain that can look like a rod yet remain flexible so as to have thermal undulations. Such a situation occurs when its contour length L is shorter than the persistent length or a longer chain is stretched nearly to the full contour length by the tension. We represent the position vector of a segment at an arc length s in a cylindrical coordinates $\boldsymbol{r}(s,t) = (\boldsymbol{h}(s,t), x(s,t))$, where $\boldsymbol{h}(s,t)$ is the two-dimensional transverse undulation, while $x(s,t)$ is the arc position projected along the longitudinal direction (Fig. 20.4).

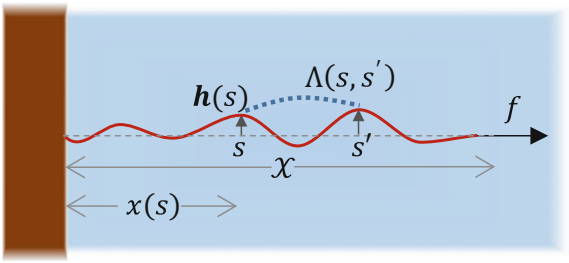

Fig. 20.4 A nearly straight semiflexible chain either with a stretching force f. Two segment at s and s' with the undulations $\boldsymbol{h}(s)$ and $\boldsymbol{h}(s')$ transmit hydrodynamic interaction $\Lambda(s, s')$

20.2.1 Transverse Dynamics

The effective Hamiltonian can also be expressed as $\mathcal{F} = -\int ds\boldsymbol{\lambda}(s) \cdot \boldsymbol{h}(s)$, where the *transverse force induced* on the segment s is obtained by (11.50):

$$\boldsymbol{\lambda}(s) = -\frac{\delta \mathcal{F}}{\delta \boldsymbol{h}(s)} = f\left(\frac{\partial^2 \boldsymbol{h}}{\partial s^2}\right) - \kappa\left(\frac{\partial^4 \boldsymbol{h}}{\partial s^4}\right). \tag{20.66}$$

Via the hydrodynamic interaction, this force at a segment s' affects the fluid velocity at another segment at s (Fig. 20.4), which is same as the average undulation velocity therein, $\partial \boldsymbol{h}(s,t)/\partial t$, by the boundary condition. Thus we have

$$\frac{\partial \boldsymbol{h}(s,t)}{\partial t} = \int ds' \boldsymbol{\Lambda}(s - s') \cdot \boldsymbol{\lambda}(s', t) + \boldsymbol{\xi}_{\boldsymbol{h}}(t). \tag{20.67}$$

where $\boldsymbol{\xi}_{\boldsymbol{h}}(t)$ is the appropriate Gaussian white noise. For a nearly straight chain, we restrict the above equation to be linear in $\boldsymbol{h}$, and the Oseen tensor $\boldsymbol{\Lambda}(s - s')$ can be simplified to:

$$\boldsymbol{\Lambda}(s - s') = \frac{1}{8\pi\eta|s - s'|}(I + \hat{\boldsymbol{x}}\hat{\boldsymbol{x}}). \tag{20.68}$$

Because $\boldsymbol{\lambda}$ is vertical to $\hat{\boldsymbol{x}}$, (20.67) is expressed as

$$\begin{aligned} \frac{\partial \boldsymbol{h}(s,t)}{\partial t} &= -\frac{1}{8\pi\eta}\int ds' \frac{1}{|s - s'|}\frac{\delta \mathcal{F}}{\delta \boldsymbol{h}(s', t)} + \boldsymbol{\xi}_{\boldsymbol{h}}(t) \\ &= \frac{1}{8\pi\eta}\int ds' \frac{1}{|s - s'|}\left\{f\left(\frac{\partial^2 \boldsymbol{h}}{\partial s'^2}\right) - \kappa\left(\frac{\partial^4 \boldsymbol{h}}{\partial s'^4}\right)\right\} + \boldsymbol{\xi}_{\boldsymbol{h}}(t). \end{aligned} \tag{20.69}$$

To facilitate solving for $\boldsymbol{h}(s,t)$ we apply the one-dimensional Fourier transform

$$\boldsymbol{h}(q,t) = \int_0^L ds\, e^{-iq\cdot s}\boldsymbol{h}(s,t) \tag{20.70}$$

and obtain the equation of motion:

$$\begin{aligned}\frac{\partial \boldsymbol{h}(q,t)}{\partial t} &= -\Lambda_h(q)\left\{fq^2+\kappa q^4\right\}\boldsymbol{h}(q,t)+\boldsymbol{\xi}_{\boldsymbol{h}}(q,t)\\ &= -\tau_T(q)^{-1}\boldsymbol{h}(q,t)+\boldsymbol{\xi}_{\boldsymbol{h}}(q,t),\end{aligned} \tag{20.71}$$

where

$$\tau_T(q) = \frac{1}{(\kappa q^4+fq^2)\Lambda_h(q)}. \tag{20.72}$$

In the above

$$\begin{aligned}\Lambda_h(q) &= \frac{1}{8\pi\eta}\int_{-L}^{L} du\ \frac{e^{-iqu}}{|u|} = \frac{1}{8\pi\eta}\left\{\int_a^L du\ \frac{e^{-iqu}}{u} - \int_{-L}^{-a} du\ \frac{e^{-iqu}}{u}\right\}\\ &= \frac{1}{4\pi\eta}\int_a^L du\ \frac{\cos qu}{u},\end{aligned} \tag{20.73}$$

where a is the smallest of the separations $|u| = |s - s'|$ between two segments at s and s'; a naturally is in the order of the monomer size. Because $L \gg a$, the above integral is approximated as

$$\begin{aligned}\Lambda_h(q) &\approx \frac{1}{4\pi\eta}\int_0^\infty du\frac{\cos qu}{(u^2+a^2)^{1/2}} = \frac{1}{4\pi\eta}K_0(qa)\\ &\approx \frac{1}{4\pi\eta}\ln\left(\frac{1}{qa}\right), \quad \text{for } \ qa \ll 1,\end{aligned} \tag{20.74}$$

where $K_0(x)$ is the zeroth order modified Bessel function of the second kind.

Now consider the case with $f = 0$. Because the chain is treated as nearly straight, we are dealing with a semi-flexible rod-like chain with the persistence length longer than L, such as a relatively short actin filament fragment. From (20.71), we find the correlation function:

$$\langle \boldsymbol{h}(q,t)\cdot\boldsymbol{h}(-q,0)\rangle = \left\langle |\boldsymbol{h}(\boldsymbol{q})|^2\right\rangle e^{-t/\tau_T(q)} = \frac{2k_BTL}{\kappa q^4}e^{-t/\tau_T(q)}, \tag{20.75}$$

where we used the result of (11.30). $\tau_T(q)$ is the relaxation time for transverse undulation:

$$\tau_T(q) = \frac{1}{\kappa q^4 \Lambda_h(q)}. \tag{20.76}$$

Using the inverse Fourier transform $\boldsymbol{h}(s) = (1/L)\sum_q e^{iqs}\boldsymbol{h}(q)$, and the extension of the relation (11.40), (20.75) yields

$$\langle \boldsymbol{h}(s,t)\cdot\boldsymbol{h}(s',0)\rangle = \frac{2k_BT}{\kappa L}\sum_q \frac{1}{q^4}\; e^{iq(s-s')-t/\tau_T(q)} \tag{20.77}$$

where q takes N discrete values $q_n = 2\pi n/L, (n = \pm 1, \pm 2\ldots, \pm N/2)$ to implement the periodic boundary condition (Chap. 11). Because of the term q^{-4} in the sum, we recognize that the sum is dominated by the smallest of q, $q_1 = 2\pi/L$, allowing an approximation:

$$\begin{aligned}\langle \boldsymbol{h}(s,t)\cdot\boldsymbol{h}(s',0)\rangle &\approx \left[\frac{4k_BT}{\kappa L}\sum_{q_1}^{q_{N/2}}\frac{1}{q^4}\right]\cos[q_1(s-s')]e^{-t/\tau_T(q_1)} \\ &= \left\langle h^2\right\rangle \cos[q_1(s-s')]e^{-t/\tau_T(q_1)},\end{aligned} \tag{20.78}$$

where $\left\langle h^2\right\rangle = (2k_BT/\kappa L)\sum q^{-4} = L^3/\left(4\cdot 90 l_p\right)$ (11.39). $\tau_T(q_1)$ is the primary transverse relaxation time associated with the longest-wave-length mode $q_1 = 2\pi/L$:

$$\tau_T(q_1) = \frac{\eta L^4}{4\pi^3\kappa\,\ln\left(\dfrac{L}{2\pi a}\right)}, \tag{20.79}$$

where we used (20.74) and (20.76). Equation (20.78) indicates an unusual dependence on the length, $\tau_T \sim L^4/\ln(L/2\pi a)$, meaning that the correlation (20.78) is not only long-ranged over the entire chain but also decays very slowly in time as the chain becomes longer. It should be also noted that an increase of the chain rigidity κ reduces the transverse fluctuation as well as speeds up the transvers relaxation dynamics.

P20.6 *Suppose a small transverse impulse λ is applied at the middle of the chain, $s = L/2$, and then released. What is the average shape $\bar{h}(s,t)$ of the chain after wards?*

Although the above analysis describes the overall slow decay dynamics of a semi-flexible chain, depending on the time windows we observe the different temporal behaviors of the segmental displacement. We first consider the auto-correlation,

$$\langle \boldsymbol{h}(s,t)\cdot\boldsymbol{h}(s,0)\rangle = \frac{2k_BT}{\kappa L}\sum_q \frac{1}{q^4} e^{-t/\tau_T(q)} \tag{20.80}$$

and the mean square displacement

$$\overline{\Delta}_{\boldsymbol{h}}^2(t) = \langle [\boldsymbol{h}(s,t)-\boldsymbol{h}(s,0)]^2\rangle \tag{20.81}$$

of the points on the chain. Using (20.80) it can be expressed as

$$\begin{aligned}\overline{\Delta}_{\boldsymbol{h}}^2(t) &= 2\left[\langle h^2\rangle - \langle(\boldsymbol{h}(s,t)\cdot\boldsymbol{h}(s,0))\rangle\right] \\ &= \frac{4k_BT}{\kappa L}\sum_q \frac{1}{q^4}\left\{1-e^{-t/\tau_T(q)}\right\}.\end{aligned} \tag{20.82}$$

For short times $t \ll \tau_T\left(q_{N/2}\right) \sim \eta a^4/\kappa$, we can put $e^{-t/\tau_T(q)} \approx 1 - t/\tau_T(q)$, so that we have

$$\overline{\Delta}_{\boldsymbol{h}}^2(t) \approx \frac{4k_BTt}{L}\sum_q \Lambda_h(q) \approx \frac{k_BTt}{\pi^2\eta}\int_{q_1}^{q_{N/2}} dq\, K_0(qa) = \frac{\alpha k_BTt}{\pi^2\eta a} \tag{20.83}$$

where (20.74, 20.76) are used and $\alpha = \int_{2\pi a/L}^{\pi} dx\, K_0(x)$ is a numerical factor in the order of unity. Equation (20.83) means that, at a time too short for a segment to escape the cage made by the neighboring segments, it undergoes a free diffusion with the hydrodynamic friction $\sim\eta a$. In long times, $t \gg \tau_T(q_1)$ in which $e^{-t/\tau_T(q_1)} \ll 1$, the second term in the sum (20.82) vanishes, leading to $\overline{\Delta}_{\boldsymbol{h}}^2(t) \to 2\langle h^2\rangle$, which means that the segment is caged within the polymer chain.

To study the dynamics in the intermediate times, we express the sum (20.82) by the integral:

$$\overline{\Delta}_{\boldsymbol{h}}^2(t) = \frac{4k_BT}{\pi\kappa}\int_{q_1}^{q_{N/2}} dq\,\frac{1}{q^4}\left\{1-e^{-\kappa q^4\Lambda_h(q)t}\right\} \tag{20.84}$$

At intermediate times, $\tau_T\left(q_{N/2}\right) \ll t \ll \tau_T(q_1)$, (20.84) becomes the definite integral:

$$\overline{\Delta}_{\boldsymbol{h}}^2(t) = \frac{4k_BT}{\pi\kappa}\int_0^{\infty} dq\,\frac{1}{q^4}\left\{1-e^{-\kappa q^4\Lambda_h(q)t}\right\}. \tag{20.85}$$

Even with the approximation (20.74) for the hydrodynamic interaction term $\Lambda_h(q)$, the above integral is difficult to evaluate analytically. Because the integral will be

dominated by the contribution from the smallest q region we make an approximation for (20.74):

$$\Lambda_h(q) \approx \Lambda_h(q_1) = \frac{1}{4\pi\eta}\ln\left(\frac{L}{2\pi a}\right). \tag{20.86}$$

$\Lambda_h(q_1)$ is same as the inverse of hydrodynamic friction per unit length of a rigid rod of length L moving in the transverse direction, so here the HI is effectively incorporated by this approximation.

P20.7 *Show from* (20.69) *that for a rigid rod under a uniform transverse force the frictional coefficient is approximately* $\Lambda_h^{-1}(q_1)L$. *With the friction per segment* $\Lambda_h^{-1}(q_1)$ *the Langevin equation*

$$\Lambda_h^{-1}(q_1)\frac{\partial \boldsymbol{h}(s,t)}{\partial t} = -\kappa\left(\frac{\partial^4 \boldsymbol{h}}{\partial s'^4}\right) + \boldsymbol{\xi_h}(t)$$

yields the primary transverse relaxation time that agrees with (20.79) (MacKintosh 2006).

Then (20.85) can be evaluated:

$$\begin{aligned}\overline{\Delta}_{\boldsymbol{h}}^2(t) &= \frac{4k_BT}{\pi\kappa}\int_0^\infty dq\,\frac{1}{q^4}\left\{1 - e^{-\kappa q^4\Lambda_h(q_1)t}\right\} \\ &= \frac{16k_BT\kappa\Lambda_h(q_1)t}{3\pi\kappa}\int_0^\infty dq\, e^{-\kappa q^4\Lambda_h(q_1)t}\end{aligned} \tag{20.87}$$

where the first integration is done by part to yield the second. It is further calculated:

$$\begin{aligned}\overline{\Delta}_{\boldsymbol{h}}^2(t) &= \frac{4k_BT}{3\pi\kappa}\{\kappa\Lambda_h(q_1)t\}^{3/4}\int_0^\infty dx x^{-3/4}e^{-x} \\ &= \frac{4k_BT}{3\pi\kappa}\left\{\frac{\kappa\,\ln(L/2\pi a)t}{4\pi\eta}\right\}^{3/4}\Gamma(1/4) \sim \frac{k_BT}{\kappa^{1/4}\eta^{3/4}}t^{3/4},\end{aligned} \tag{20.88}$$

where $x = \kappa\Lambda_h(q_1)q^4t$, $\Gamma(1/4) = \int_0^\infty dx\, x^{-3/4}e^{-x} = 3.62$. The above shows **a very complex anomalous, sub-diffusive behavior in distinction to the one we saw in flexible polymers**. A similar result was also obtained by Granek (1997) and the key $t^{3/4}$ scaling behavior was observed in an experiment (Caspi et al. 2000).

Of particular importance is the dynamic structure factor (Farge and Maggs 1993)

$$S(q,t) = \frac{1}{N}\left\langle \sum_{n=1}^{N}\sum_{m=1}^{N} e^{-iq|\boldsymbol{h}_n(t)-\boldsymbol{h}_m(0)|} \right\rangle \sim \int ds\, \exp\left\{ -\frac{q^2}{2}\left\langle [\boldsymbol{h}(s,t)-\boldsymbol{h}(0,0)]^2 \right\rangle \right\}, \tag{20.89}$$

where the summation made over all the scattering molecules in the chain, is replaced by the integral over the contour and the Gaussian nature of segmental undulation, (9.64), is used. The sub-diffusive behavior (20.88) gives rise to the stretched exponential for the dynamic structure factor $S(q,t) \sim \exp[-(\Gamma_q t)^{3/4}]$ with a relaxation rate $\Gamma_q \sim ((k_B T)/\kappa)^{1/3}(k_B T)/(\eta q^{8/3})$. This was observed in dynamic light scattering experiments (Schmidt et al. (1989) and, in real space, by optical video-microscopy (Piekenbrock and Sackmann 1992).

20.2.2 Chain Longitudinal Dynamics and Response to a Small Oscillatory Tension

Now we turn our attention to dynamics of the longitudinal length $\mathcal{X}(t)$ by starting with its equilibrium time correlation function $\langle \Delta\mathcal{X}(t)\Delta\mathcal{X}(0)\rangle_0$. To this end, it is more straightforward to use the linear response theory in which the time correlation is directly related by the response $\langle \Delta\mathcal{X}(t)\rangle$ to a small time-dependent tension as was done for the static case in Chap. 11. We consider that the time-dependent tension, $\delta f(t)$, is applied at an chain end additionally beginning from $t = 0$.

The mean equilibrium end-to-end distance, $X = \langle \mathcal{X}\rangle$ was given by (11.32) in terms of the transverse undulation. The corresponding quantity at a time t, $\langle \mathcal{X}(t)\rangle$, is given by

$$\frac{\langle \mathcal{X}(t)\rangle}{L} = 1 - \frac{1}{2L^2}\sum_q q^2 \langle \boldsymbol{h}(q,t)\cdot\boldsymbol{h}(-q,t)\rangle. \tag{20.90}$$

Solving the Langevin equation (20.71) for $\boldsymbol{h}(q,t)$ with $f = f_0 + \delta f(t)$ to the linear order in $\delta f(t)$, we can obtain

$$\langle \boldsymbol{h}(q,t)\cdot\boldsymbol{h}(-q,t)\rangle = \langle \boldsymbol{h}(q,t)\cdot\boldsymbol{h}(-q,t)\rangle_0 - \int_0^t dt' m(q,t-t')\delta f(t'), \tag{20.91}$$

where

$$m(q,t-t') = \frac{4k_BTL\Lambda_h(q)}{(\kappa q^2+f_0)} e^{-\frac{t-t'}{\tau_L(q)}}. \tag{20.92}$$

Here we define the longitudinal relaxation time by

$$\tau_L(q) = \frac{\tau_T(q)}{2} = \frac{1}{2}\left(\kappa q^4 + f_0 q^2\right)\Lambda_h(q). \tag{20.93}$$

$\langle \ldots \rangle_0$ denotes the average over the initial ensemble at equilibrium in the absence of $\delta f(t)$; from (11.30), $\langle \boldsymbol{h}(q,t)\cdot\boldsymbol{h}(-q,t)\rangle_0 = 2k_BTL/(\kappa q^4 + f_0 q^2)$.

The evaluation of the relation (20.90) for the constant force $f = f_0$ yielded the equilibrium force-extension relation (11.35), $\langle \mathcal{X}\rangle_0/L = 1 - k_BT(4\kappa f_0)^{-1/2}$. In terms of $\delta f(t)$, we can find its effect using (20.90):

$$\begin{aligned} \langle \Delta\mathcal{X}(t)\rangle &\equiv \langle \mathcal{X}(t)\rangle - \langle \mathcal{X}\rangle_0 \\ &= \int_0^t dt' \chi(t-t')\delta f(t'), \end{aligned} \tag{20.94}$$

where

$$\begin{aligned} \chi(t-t') &= \frac{1}{2L^2}\sum_q q^2 m(q,t-t') \\ &= \frac{1}{2L^2}\sum_q q^2 \frac{4k_BTL\Lambda_h(q)}{(\kappa q^2+f_0)} e^{-\frac{t-t'}{\tau_L(q)}} \end{aligned} \tag{20.95}$$

Equation (20.94) represents the chain extension change in linear response to time-dependent tension of general forms in a viscous fluid under hydrodynamic interaction (HI). These equations were used in relaxation dynamics of the chain extension under a time-dependent drag exerted by a large bead connected with a chain to an anchor (Raviv et al. 2004) and also in viscoelastic dynamics under oscillatory force without HI (Hiraiwa and Ohta 2009).

We note that (20.94) can come from the fluctuation-dissipation theorem (FDT) (Chap. 17), according to which the dynamic response function $\chi(t-t')$ is given by

$$\chi(t) = -\frac{1}{k_BT}\frac{d}{dt}\langle \Delta\mathcal{X}(t)\Delta\mathcal{X}(0)\rangle_0 \tag{20.96}$$

Integrating the above relation with (20.95) in time, we obtain the time correlation function

$$\begin{aligned}\langle \Delta\mathcal{X}(t)\Delta\mathcal{X}(0)\rangle_0 &= -k_BT\int_0^t dt'\chi(t-t') + \left\langle (\Delta\mathcal{X})^2\right\rangle_0 \\ &= (k_BT)^2\sum_q \frac{1}{(\kappa q^2+f_0)^2}e^{-t/\tau_L(q)}\end{aligned} \tag{20.97}$$

which at $t = 0$ is reduced to equilibrium fluctuation, (11.45),

$$\left\langle (\Delta\mathcal{X})^2\right\rangle_0 = (k_BT)^2\sum_q \frac{1}{(\kappa q^2+f_0)^2}. \tag{20.98}$$

Now we analyze the time correlation in detail for short semi-flexible chains in the absence of constant force $f_0 = 0$. In this case one can readily calculate:

$$\begin{aligned}\langle \Delta\mathcal{X}(t)\Delta\mathcal{X}(0)\rangle_0 &= \frac{(k_BT)^2}{\kappa^2}\sum_q \frac{1}{q^4}e^{-t/\tau_L(q)} \\ &\approx \left\langle (\Delta\mathcal{X})^2\right\rangle_0 e^{-t/\tau_L(q_1)} = \left\langle (\Delta\mathcal{X})^2\right\rangle_0 e^{-2t/\tau_T(q_1)},\end{aligned} \tag{20.99}$$

where $\langle(\Delta\mathcal{X})^2\rangle = (k_BT/\kappa)^2\sum_q q^{-4} = L^4/(8\cdot 90)l_p^2$ as given by (11.46). The approximation in (20.99) is again caused by the term $1/q^4$ in the sum, which is dominated by the contribution from longest wave length mode. **Like the transvers relaxation the longitudinal relaxation becomes also very slow as the chain length increase, but with the relaxation time halved.**

P20.8 *One might think that there is a strong correlation between the longitudinal and transverse fluctuation because the contour length L is fixed. Find the correlation functions, $\langle h(t)\Delta\mathcal{X}(0)\rangle_0$ and $\langle h(t)\Delta\mathcal{X}(t)\rangle$, where $h(t)$ is the undulation magnitude averaged over the length.*

Now we look at the longitudinal MSD,

$$\begin{aligned}\overline{\Delta}_X^2(t) &= \left\langle [\mathcal{X}(t)-\mathcal{X}(0)]^2\right\rangle_0 = \left\langle [\Delta\mathcal{X}(t)-\Delta\mathcal{X}(0)]^2\right\rangle_0 \\ &= 2\left[\left\langle (\Delta\mathcal{X})^2\right\rangle_0 - \langle\Delta\mathcal{X}(t)\Delta\mathcal{X}(0)\rangle_0\right],\end{aligned} \tag{20.100}$$

which can be expressed as

$$\overline{\Delta}_X^2(t) = \frac{2(k_BT)^2}{\kappa^2}\sum_q \frac{1}{q^4}\left[1-e^{-t/\tau_L(q)}\right]. \tag{20.101}$$

We note that the sum over q is the same as that in (20.82) with the relaxation time halved, meaning that longitudinal fluctuation dynamics (the short-time free

diffusion, the intermediate-time anomalous diffusion and the terminal caging) is correspondingly similar to the longitudinal one.

Now how would the chain respond to the small periodic force? The response function (20.95) has the integral difficult to evaluate in a single form. We consider the single relaxation time approximation for the correlation function (20.99), and use the FDT (20.96) to determine the response function as

$$\chi(t) \approx \frac{\langle|\Delta\mathcal{X}|^2\rangle}{k_BT}\frac{1}{\tau_L(q_1)}e^{-\frac{t}{\tau_L}(q_1)}, \tag{20.102}$$

where the primary longitudinal relaxation time is

$$\tau_L(q_1) = \frac{1}{2}\tau_T(q_1) = \frac{\eta L^4}{8\pi^3\kappa\,\ln(L/2\pi a)} = \frac{k_BT\eta L^4}{8\pi^3 l_p\ln(L/2\pi a)}. \tag{20.103}$$

Let us consider that the chain is stretched periodically in time:

$$\delta f(t) = f_m\sin(\Omega t). \tag{20.104}$$

As we learned in Chap. 17, the average chain length also oscillates in time but with a phase delay φ:

$$\langle\Delta\mathcal{X}(t)\rangle = |\chi(\Omega)|f_m\sin(\Omega t-\varphi). \tag{20.105}$$

The measure of the coherence is given by the power amplification factor

$$P = |\chi(\Omega)|^2 = \left(\frac{\langle|\Delta\mathcal{X}|^2\rangle_0}{k_BT}\right)^2\frac{1}{1+\{\Omega\tau_L(q_1)\}^2}. \tag{20.106}$$

With all the chain contour length, the persistence length, and the viscosity fixed as constants independent of temperature, the power amplification factor P decreases with temperature.

We can extend the analysis to the case where the chain is pre-stretched by the force f_0. Because $\langle|h(\boldsymbol{q})|^2\rangle = 2k_BTL/(\kappa q^4+f_0q^2)$, the predominance of the longest wave-length mode is less than that without the force, in which $\langle|h(\boldsymbol{q})|^2\rangle = 2k_BTL/(\kappa q^4)$; nevertheless, the longest wave-length mode would give a good estimate, as a numerical computation showed. In this case of $f_0 \neq 0$, the power amplification factor (20.106) shows a maximum at an optimal noise–strength, namely, the stochastic resonance (SR); in addition it showed a maximum at an optimal chain length (Kim and Sung 2012). As linearly interconnected systems they

are, polymers show unusual cooperative dynamics in response to external stimuli. **The SR for such systems in overdamping fluids is of entropic nature, which shows the maximal coherence to an oscillatory force, not only at optimal noise-strengths, but also at the optimal chain lengths and chain flexibility.** This entropic SR suggests important possibilities for controlling the dynamics of single biopolymer transitions utilizing their flexibility.

20.3 Dynamics of Membrane Undulation

In Chap. 12, we dealt with equilibrium, conformational behaviors of membranes including the undulation correlation. In the study of the dynamical aspect, such as the undulation time-correlation, we should note that **the surface is hydrodynamically coupled with the background fluid** (Fig. 20.5). In a neutral fluid, the density of an external force $\boldsymbol{f}(\boldsymbol{r})$ is localized on the undulating surface:

$$\boldsymbol{f}(\boldsymbol{r}) = \delta(z - h(\boldsymbol{x}))\sigma(\boldsymbol{r}) \approx \delta(z)\widehat{\boldsymbol{z}}\sigma(\boldsymbol{x}), \tag{20.107}$$

where we assume the undulation height, $h(\boldsymbol{x})$, is very small. The $\sigma(\boldsymbol{x}) = \widehat{\boldsymbol{z}}\sigma(\boldsymbol{x})$ is the surface force density normal to the two dimensional plane, $\boldsymbol{x} = (x, y)$. From the effective Hamiltonian of the planar membrane with surface tension γ and bending rigidity $\varkappa$, (12.35), the surface force density can be derived as

$$\sigma(\boldsymbol{x}) = -\frac{\delta \mathcal{F}}{\delta h(\boldsymbol{x})} = \gamma \nabla_{\boldsymbol{x}}^2 h(\boldsymbol{x}) - \varkappa \nabla_{\boldsymbol{x}}^4 h(\boldsymbol{x}), \tag{20.108}$$

which is two dimensional analogue of (20.66). Note the difference between the undulation-induced surface force $\sigma(\boldsymbol{x})$ and the surface tension γ.

For impermeable membranes, we have the surface boundary condition that $\partial h(\boldsymbol{x}, t)/\partial t$ is equal to the fluid velocity along the normal direction,

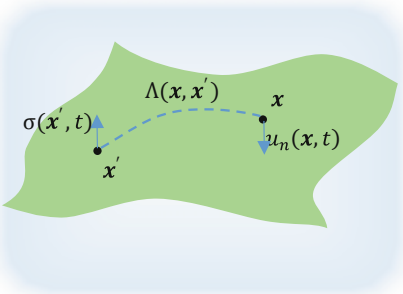

Fig. 20.5 A planar membrane in a fluid: The force $\sigma(\boldsymbol{x}')$ acting on a point $\boldsymbol{x}'$ of the membrane imparts the hydrodynamic interaction $\Lambda(\boldsymbol{x} - \boldsymbol{x}')$ onto another point $\boldsymbol{x}$, whereby the undulation is perturbed

$u_n(\boldsymbol{x},t)=\hat{\boldsymbol{z}}\cdot\boldsymbol{u}(\boldsymbol{x},z=0,t)$, which is in turn coupled to the surface force via hydrodynamic interaction:

$$\begin{aligned}\frac{\partial h(\boldsymbol{x},t)}{\partial t}&=u_n(\boldsymbol{x},t)\\&=\int d^2\boldsymbol{x}'\,\widehat{z}\cdot\frac{1}{8\pi\eta|\boldsymbol{x}-\boldsymbol{x}'|}\left(\boldsymbol{I}+\frac{(\boldsymbol{x}-\boldsymbol{x}')(\boldsymbol{x}-\boldsymbol{x}')}{|\boldsymbol{x}-\boldsymbol{x}'|^2}\right)\cdot\widehat{z}'\sigma(\boldsymbol{x}')\\&=\int d^2\boldsymbol{x}'\,\Lambda(\boldsymbol{x}-\boldsymbol{x}')\sigma(\boldsymbol{x}'),\end{aligned}\tag{20.109}$$

where

$$\Lambda(\boldsymbol{x}-\boldsymbol{x}')=\frac{1}{8\pi\eta|\boldsymbol{x}-\boldsymbol{x}'|}.\tag{20.110}$$

Consequently, we have a closed, linear stochastic equation of motion

$$\begin{aligned}\frac{\partial h(\boldsymbol{x},t)}{\partial t}&=\int d^2\boldsymbol{x}'\Lambda(\boldsymbol{x}-\boldsymbol{x}')\sigma(\boldsymbol{x}')+\xi_h(\boldsymbol{x},t)\\&=\frac{1}{8\pi\eta}\int d^2\boldsymbol{x}'\,\frac{1}{|\boldsymbol{x}-\boldsymbol{x}'|}\left\{\gamma\nabla^2_{\boldsymbol{x}'}h(\boldsymbol{x}')-\varkappa\nabla^4_{\boldsymbol{x}'}h(\boldsymbol{x}')\right\}+\xi_h(\boldsymbol{x},t),\end{aligned}\tag{20.111}$$

where we add the Gaussian and white noise $\xi_h(\boldsymbol{x},t)$ to endow otherwise deterministic equation with the thermal fluctuation. With this noise the equation assures the proper approach to equilibrium.

The equation, being an integro-differential equation involving the two dimensional Laplacian and higher order gradients, appears to be formidable to solve. To evaluate time correlation function $\langle h(\boldsymbol{x},t)h(\boldsymbol{x}',0)\rangle$ and the related functions, it is convenient to deal with the Fourier-transform of the Eq. (20.111). First we note

$$\sigma(\boldsymbol{q})=-\left(\gamma q^2+\varkappa q^4\right)h(\boldsymbol{q}).\tag{20.112}$$

On the other hand, the Fourier transform of the hydrodynamic interaction is

$$\begin{aligned}\int d^2\boldsymbol{x}\;e^{-i\boldsymbol{q}\cdot\boldsymbol{x}}\frac{1}{8\pi\eta|\boldsymbol{x}|}&=\int_0^\infty d|\boldsymbol{x}||\boldsymbol{x}|\frac{1}{8\pi\eta|\boldsymbol{x}|}\int_0^{2\pi}d\varphi\;e^{-iq|\boldsymbol{x}|\cos\varphi}\\&=\frac{2\pi}{8\pi\eta}\int_0^\infty d|\boldsymbol{x}|J_0(q|\boldsymbol{x}|)=\frac{1}{4\eta q},\end{aligned}\tag{20.113}$$

where $J_0(y)=(1/2\pi)\int_0^{2\pi}d\varphi\,e^{-iy\cos\varphi}$ and $\int_0^\infty dy\,J_0(y)=1$ are used. With the above, (20.111) is transformed to a readily solvable equation in the Fourier space!:

$$\frac{\partial h(\boldsymbol{q},t)}{\partial t} = -\frac{(\varkappa q^4 + \gamma q^2)}{4\eta q} h(\boldsymbol{q},t) + \xi_h(\boldsymbol{q},t) \tag{20.114}$$

or

$$\frac{\partial h(\boldsymbol{q},t)}{\partial t} = -\frac{1}{\tau_m(q)} h(\boldsymbol{q},t) + \xi_h(\boldsymbol{q},t). \tag{20.115}$$

The relaxation time

$$\tau_m(q) = \frac{4\eta}{\varkappa q^3 + \gamma q} \tag{20.116}$$

is the wave-number dependent. Hereafter we will only consider the case of the fluid membranes (surface tension $\gamma = 0$), $\tau_m(q) = 4\eta/(\varkappa q^3)$. The q^{-3}-dependence is owing to the hydrodynamic interaction, combined with the structural characteristics of fluid membranes, i.e., the long-range spatial correlation we noted in Chap. 12.

From (20.115), the undulation time correlation is obtained:

$$\langle h(\boldsymbol{q},t)h(-\boldsymbol{q},0)\rangle = \left\langle |h(\boldsymbol{q})|^2 \right\rangle e^{-t/\tau_m(q)} = \frac{k_B T L^2}{\varkappa q^4} \exp\left(-\varkappa q^3 t/4\eta\right) \tag{20.117}$$

Following (12.64), the undulation correlation in real space and time is given by

$$\begin{aligned}\langle h(\boldsymbol{x},t)h(\boldsymbol{x}',0)\rangle &= \frac{k_B T}{\varkappa L^2} \sum_{\boldsymbol{q}} \frac{1}{q^4} \exp\left(i\boldsymbol{q}\cdot(\boldsymbol{x}-\boldsymbol{x}') - \kappa q^3 t/4\eta\right) \\ &= \frac{1}{2\pi} \frac{k_B T}{\varkappa} \int_{q_m}^{q_M} dq\, q \frac{1}{q^4} J_0(q|\boldsymbol{x}-\boldsymbol{x}'|) \exp\left(-\varkappa q^3 t/4\eta\right) \\ &\approx h^2 J_0(q_m|x-x'|) \exp\left(-\frac{\varkappa}{4\eta} q_m^3 t\right).\end{aligned} \tag{20.118}$$

where $q_m \sim \pi/L$ and $q_M \sim \pi/a$, a being in the order of diameter of a lipid molecule. As discussed before, the sum in the above, rapidly decreasing with q, is dominated (approximated) by the contribution from the smallest wave-number mode $q_m \sim \pi/L$. This approximation is qualitatively in good agreement with the numerical calculations. Equation (20.118) means that **the correlation is not only long-ranged over the entire membrane but also decays with the relaxation time $\sim \eta L^3/\varkappa$, which can be very long for a large membrane**.

We now consider the MSD, $\overline{\Delta}_h^2(t) = \langle (h(\boldsymbol{x},t) - h(\boldsymbol{x},0))^2 \rangle$ of a point at $\boldsymbol{x}$ on surface. Using the first equality of (20.117) it can be expressed as

$$\begin{aligned}\overline{\Delta}_h^2(t) &= 2\Big[\langle h\rangle^2 - \langle (h(\boldsymbol{x},t)h(\boldsymbol{x},0))\rangle\Big] \\ &= \frac{2k_BT}{\varkappa L^2}\sum_{\boldsymbol{q}}\frac{1}{q^4}\big[1-e^{-t/\tau_m(q)}\big] \\ &= \frac{k_BT}{\pi\varkappa}\int_{q_m}^{q_M} dq\, q^{-3}\Big[1-\mathrm{e}^{-\varkappa q^3 t/4\eta}\Big].\end{aligned} \tag{20.119}$$

At short times when $t/\tau_m(q_M) = \varkappa {q_M}^3 t/4\eta \ll 1$, or $t \ll \eta a^3/\varkappa$, we can put $e^{-t/\tau_m(q)} \approx 1 - t/\tau_m(q)$, leading to

$$\overline{\Delta}_h^2(t) = \frac{k_BTt}{4\pi\eta}\int_{q_m}^{q_M} dq \sim \frac{k_BTt}{4\eta a}. \tag{20.120}$$

This indicates that the short time dynamics of undulation is none other than the free diffusion of each lipids with an effective hydrodynamic radius in the order of a.

The integral (20.119) can be expressed in the form

$$\overline{\Delta}_h^2(t) = \frac{k_BT}{3\pi\varkappa}\left(\frac{\varkappa t}{4\eta}\right)^{2/3}\int_{t/\tau_m(q_m)}^{t/\tau_m(q_M)} dx\, x^{-5/3}[1-\mathrm{e}^{-x}], \tag{20.121}$$

where $x = t/\tau_m(q) = \varkappa q^3 t/4\eta$. At intermediate times, $\tau_m(q_M)) \ll t \ll \tau_m(q_m)$ or $\eta a^3/\varkappa \ll t \ll \eta L^3/\varkappa$, the integral becomes definite:

$$\overline{\Delta}_h^2(t) = \frac{k_BT}{3\pi\varkappa}\left(\frac{\varkappa t}{4\eta}\right)^{2/3}\int_0^{\infty} dx\, x^{-5/3}[1-\mathrm{e}^{-x}], \tag{20.122}$$

which, by integration by part, becomes

$$\overline{\Delta}_h^2(t) = \frac{k_BT}{2\pi\varkappa}\left(\frac{\varkappa t}{4\eta}\right)^{2/3}\int_0^{\infty} dx\, x^{-2/3}\mathrm{e}^{-x} = \frac{k_BT}{2\pi\varkappa}\left(\frac{\varkappa t}{4\eta}\right)^{2/3}\Gamma(5/3). \tag{20.123}$$

The mean-square undulation

$$\overline{\Delta}_h^2(t) = 0.45\frac{k_BT}{\pi\varkappa}\left(\frac{\varkappa t}{4\eta}\right)^{2/3} \sim k_BTt/\left\{\eta\left(\frac{\varkappa t}{\eta}\right)^{1/3}\right\}. \tag{20.124}$$

grows in time with the power $2/3$, which is less than 1. One may say that in this anomalous dynamics of sub-diffusion, the hydrodynamic radius grows in time

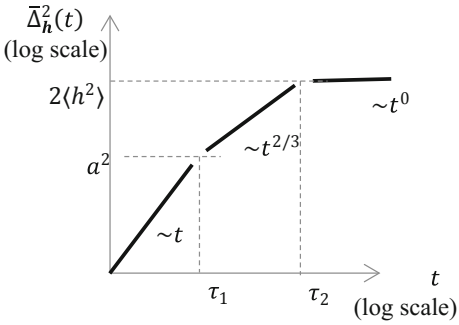

Fig. 20.6 The growth dynamics of membrane undulation in various temporal stages

$a(t) \sim (\varkappa t/\eta)^{1/3}$. For a neutral membrane, the above result is confirmed experimentally (Kimura et al. 1999).

At long times, $\varkappa q_m^3 t/4\eta \gg 1$, or $t \gg \eta L^3/\varkappa$, the membrane's undulation correlation in the integral in (20.119) vanishes, leading to

$$\overline{\Delta}_h^2(t) \to 2\langle h^2\rangle \tag{20.125}$$

This means that **the sub-diffusive behavior of the height displacement paves the way to caging of all the lipids within a membrane**. The temporal behavior of $\Delta_h(t)$ is plotted in Fig. 20.6, where the crossovers to different power law regimes occurs at characteristic times, $\tau_1 = \eta a^3/\varkappa$ and $\tau_2, = \eta L^3/\varkappa$.

P20.9 *Find the temporal behaviors of* $\overline{\Delta}_h^2(t)$ *of an elastic surface in which* $\kappa = 0$. *We first have* $\langle h(q,t)h(-q,0)\rangle = \left\langle |h(q)|^2 \right\rangle e^{-t/\tau_m(q)} = \frac{k_B T}{\gamma q^2} \exp\left(-\frac{\gamma q t}{4\eta}\right)$, *from which*

$$\langle h(\boldsymbol{x},t)h(\boldsymbol{x},0)\rangle = \frac{1}{2\pi}\int_{q_m}^{q_M} dq \frac{k_B T}{\gamma q} \exp\left(-\frac{\gamma q t}{4\eta}\right)$$

20.4 A Unified View

The diverse results for dynamics of polymer chains and fluid membranes under no tension studied in this chapter are summarized below. The dynamics of a single Brownian particle is generalized to that of a local segment in soft matter, e.g., polymers and membranes, which are the network structures in one and two dimensions $(d = 1, 2)$. **Two distinctive features emerge: short range structural connectivity within the system and long-range hydrodynamic interaction via**

Table 20.1 The dynamics of soft matter systems

Systems	Flexible polymers ($d = 1$)		Nearly straight semiflexible polymers ($d = 1$, $f = 0$)	Planar fluid membranes ($d = 2$, $\gamma = 0$)
	Rouse model	Zimm model		
Segmental displacement $\mathcal{Q}(\boldsymbol{x})$ $\mathcal{Q}(\boldsymbol{q})$	$\boldsymbol{r}(s)$ $\boldsymbol{r}_q$	$\boldsymbol{r}(s)$ $\boldsymbol{r}_q$	$\boldsymbol{h}(s)$ $\boldsymbol{h}(q)$	$h(\boldsymbol{x})$ $h(\boldsymbol{q})$
Generalized spring constant $K(q) \sim q^{\alpha}$	$k_q \sim k_e q^2$	$k_q \sim k_e q^2$	κq^4	$\varkappa q^4$
Hydrodynamic interaction $\Lambda(q) \sim q^{-\beta}$	$1/\gamma$	$1/\left(\eta q^{1/2}\right)$	$\Lambda(q) \approx \Lambda(q_1) \sim \ln(L/2\pi a)/\eta$	$1/\eta q$
Primary relaxation time $\tau_1 \sim L^{\alpha-\beta}$	$\sim L^2$	$\sim L^{3/2}$	$\sim L^4/\ln(L/2\pi a)$	$\sim L^3$
Mean-squared displacement $\overline{\Delta}^2_{\mathcal{Q}}(t) \sim t^{1-(d-\beta)/(\alpha-\beta)}$	$\sim t^{1/2}$	$\sim t^{2/3}$	$\sim t^{3/4}$	$\sim t^{2/3}$

the fluid environment. Presented below is a unifying picture of their effects on the relaxation times and the segmental dynamics.

We denote the displacement $\mathcal{Q}(\boldsymbol{x}, t)$ of a segment at $\boldsymbol{x}$: to be specific, the three and two dimensional displacements, $\boldsymbol{r}(s, t)$, and $\boldsymbol{h}(s, t)$, at one dimensional arc position s for polymers, and the transverse displacement $h(\boldsymbol{x}, t)$ at the two dimensional position $\boldsymbol{x}$ for a planar fluid membrane (Table 20.1). A segmental displacement evolves following the Langevin equation written as

$$\frac{\partial \mathcal{Q}(\boldsymbol{x}, t)}{\partial t} = -\int d\boldsymbol{x}' \boldsymbol{\Lambda}(\boldsymbol{x} - \boldsymbol{x}') \cdot \frac{\delta \mathcal{F}}{\delta \mathcal{Q}(\boldsymbol{x}', t)} + \boldsymbol{\xi}_{\mathcal{Q}}(\boldsymbol{x}, t). \tag{20.126}$$

where, in addition to the thermal noise, $\boldsymbol{\xi}_{\mathcal{Q}}$, the two aforementioned physical features are apparent: the hydrodynamic interaction $\boldsymbol{\Lambda}$, and network force on the segment $-\delta\mathcal{F}/\delta\mathcal{Q}$. In the Fourier space, the Langevin equation is written as

$$\begin{aligned} \frac{\partial \mathcal{Q}(\boldsymbol{q}, t)}{\partial t} &= -\Lambda(\boldsymbol{q}) \frac{\delta \mathcal{F}}{\delta \mathcal{Q}(\boldsymbol{q}, t)} + \boldsymbol{\xi}_{\mathcal{Q}}(\boldsymbol{q}, t) \\ &= -\Lambda(\boldsymbol{q}) K(\boldsymbol{q}) \mathcal{Q}(\boldsymbol{q}, t) + \boldsymbol{\xi}_{\mathcal{Q}}(\boldsymbol{q}, t). \end{aligned} \tag{20.127}$$

The $K(\boldsymbol{q})$ is the 'generalized spring constant' that features in the effective Hamiltonian written in the Fourier space as $\mathcal{F} = (1/2) \sum_{\boldsymbol{q}} K(\boldsymbol{q}) |\mathcal{Q}(\boldsymbol{q})|^2$.

The equipartition of each $\boldsymbol{q}$ mode to the energy yields $\langle|\mathcal{Q}(\boldsymbol{q})|^2\rangle \sim (k_BT)/K(\boldsymbol{q})$. Equation (20.127) can be rewritten in the form

$$\frac{\partial \mathcal{Q}(\boldsymbol{q},t)}{\partial t} = -\tau(\boldsymbol{q})^{-1}\mathcal{Q}(\boldsymbol{q},t) + \boldsymbol{\xi}_{\mathcal{Q}}(\boldsymbol{q},t), \tag{20.128}$$

where

$$\tau(\boldsymbol{q}) = 1/[\Lambda(\boldsymbol{q})K(\boldsymbol{q})] \tag{20.129}$$

is the characteristic time of the $\boldsymbol{q}$ undulation mode. We consider the case of polymers and membranes under no tensions, where both $\Lambda(\boldsymbol{q})$ and $K(\boldsymbol{q})$ obey power laws (Table 20.1),

$$K(\boldsymbol{q}) \sim q^{\alpha}, \quad \Lambda(\boldsymbol{q}) \sim q^{-\beta}. \tag{20.130}$$

The α is positive and β is either positive with HI or zero with no HI (Table 20.1), so that

$$\tau(\boldsymbol{q}) \sim q^{\beta-\alpha}. \tag{20.131}$$

Because the most dominant mode in the spectrum $\langle|\mathcal{Q}(\boldsymbol{q})|^2\rangle \sim 1/K(\boldsymbol{q}) \sim q^{-\alpha}$ is due from the smallest q or the longest wave length mode, $q_1 \sim L^{-1}$, the primary relaxation time goes like

$$\tau_1 = \tau(q_1) \sim L^{\alpha-\beta}. \tag{20.132}$$

This relation indicates the roles of the HI and the network interconnectivity in making the dynamics slow as the system size L is enlarged. For a flexible chain under no HI (the Rouse model), $\alpha = 2, \beta = 0$, and we have $\tau_1 \sim L^2$. For the Zimm model, $\alpha = 2$ and $\beta = 1/2$, we have $\tau_1 \sim L^{3/2}$. For a planar membrane, $\alpha = 4$, $\beta = 1$, so that $\tau_1 \sim L^3$. If α is larger, the chain connectivity is longer-ranged, so the relaxation time becomes longer. The longer-ranged HI (larger β) gives rise to the stronger dynamic cooperativity that results in the faster relaxation.

The mean square displacement of a segment is expressed as

$$\begin{aligned}\overline{\Delta}^2_{\mathcal{Q}}(t) &= \left\langle (\mathcal{Q}(\boldsymbol{x},t) - \mathcal{Q}(\boldsymbol{x},0))^2 \right\rangle = 2\left[\langle \mathcal{Q}^2(\boldsymbol{x})\rangle - \langle(\mathcal{Q}(\boldsymbol{x},t)\mathcal{Q}(\boldsymbol{x},0))\rangle\right] \\ &\sim k_BT \sum_{\boldsymbol{q}} \tfrac{1}{K(\boldsymbol{q})}\left[1 - e^{-t/\tau(\boldsymbol{q})}\right].\end{aligned} \tag{20.133}$$

Consider the intermediate time much longer than the smallest relaxation time but much shorter than the longest relaxation time (the primary relaxation time τ_1). Then (20.133) can be represented by the integral:

$$\sim k_B T \int_0^\infty dq \frac{q^{d-1}}{K(q)} \left[1 - e^{-t/\tau(q)}\right] \sim \int_0^\infty dq\, q^{d-1-\alpha} \left[1 - e^{-t/\tau(q)}\right], \tag{20.134}$$

where d is the dimensionality of the system. Integrating the last above by part yields

$$\begin{aligned} \overline{\Delta}_{\mathcal{Q}}^2(t) &\sim t \int_0^\infty dq\, q^{d-\beta-1} e^{-t/\tau(q)} \sim t^{1-(d-\beta)/(\alpha-\beta)} \int_0^\infty dx\, x^{d-\beta-1} e^{-x} \\ &\sim t^{1-(d-\beta)/(\alpha-\beta)}. \end{aligned} \tag{20.135}$$

The above power law, which indeed agrees with those we obtained for each cases (Table 20.1), shows how the chain connectivity and hydrodynamic interaction interplay in the anomalous diffusions in soft matter; (20.135) expresses how **a smaller β (weaker HI) and a higher α (longer ranged connectivity) promote the stronger sub-diffusive behaviors**.

Further Reading and References

M. Doi, S.F. Edwards, *Polymer Dynamics* (Oxford University Press, 1988)

A. Caspi, R. Granek, M. Elbaum, Enhanced diffusion in active intracellular transport. Phys. Rev. Lett. **85**, 5655 (2000)

C.F. Schmidt, M. Barmann, G. Isenberg, E. Sackmann, Chain dynamics, mesh size, and diffusive transport in networks of polymerized actin: a quasielastic light scattering and microfluorescence study. Macromolecules **22**, 3638 (1989)

Th. Piekenbrock, E. Sackmann, Quasielastic light scattering study of thermal excitations of F-actin solutions and of growth kinetics of actin filaments. Biopolymers **32**, 1471 (1992)

F. Amblard, A.C. Maggs, B. Yurke, A.N. Pargellis, S. Leibler, Subdiffusion and anomalous local viscoelasticity in actin networks. Phys. Rev. Lett. **77**, 4470 (1996)

F.C. MacKintosh, Elasticity and dynamics of cytoskeletal filaments and their networks, in *Soft Condensed Matter Physics in Molecular and Cell Biology*, ed. by W.C.K. Poon, D. Andelman (CRC Press, 2006), p. 140

R. Granek, From semi-flexible polymers to membranes: anomalous diffusion and reputation. Jounal de Physique II **7**(12), 1761–1788 (1997)

E. Farge, A.C. Maggs, Dynamic scattering from semiflexible polymers. Macromolecules **26**, 5041 (1993)

Y.B. Raviv, W.Z. Zhao, C.H. Wiggins, R. Granek, Relaxation dynamics of semiflexible polymers. Phys. Rev. Lett. **92**, 098101 (2004)

W.K. Kim, W. Sung, How a single stretched polymer responds coherently to a minute oscillation in fluctuating environments: an entropic stochastic resonance. J Chem. Phys. **137**, 074903 (2012)

W. Sung, E. Choi, Y.W. Kim, Static and dynamic correlations in a charged membrane. Phys. Rev. E **74**, 031907 (2006)

Chapter 21
Epilogue

...For one Chrysanthemum to bloom
the Thunder so must have cried again
within the dark cloud ....
Seo Jung-Ju

"Surmounting the Insurmountable"

A cell is a playground for various extraordinary events what we may call biological self-organizations. The basic components, say, biopolymers, membranes, ion-channels, and even their aqueous environments have very complex structures and yet show unusual cooperative behaviors, which go beyond the scope of traditional physics. It is grossly hopeless to solve microscopic equations of motion for the enormous number of atoms and molecules that constitute the biological matter, and even to treat them collectively using the traditional statistical mechanics. The standard analytical methods of statistical mechanics have been implemented mostly for simple systems such as ideal gases and magnets, and simple interacting units. How can we cope with the biological

W. Sung, *Statistical Physics for Biological Matter*, Graduate Texts in Physics,
https://doi.org/10.1007/978-94-024-1584-1_21

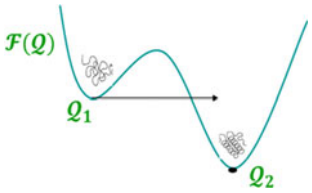

Fig. 21.1 A free energy function $\mathcal{F}\{\mathcal{Q}\}$ of a coarse-grained variable $\mathcal{Q}$, e.g., a collective variable descriptive of conformation of a polymer. In this case, a conformational transition occurs from a higher free energy state $\mathcal{Q}_1$ to a lower sate $\mathcal{Q}_2$, by crossing over the barrier in between

complexity and address the self-organizations in the language of physics without losing the quantitative explanations and predictions? This has been our primary quest. Following is a brief and partial overview of the statistical physics basis that has been laid out in this book.

For biological matter we expanded and even revised the basic premises and methods of standard statistical physics and related areas. The first one is concept of the microstates of a system that entered in the Boltzmann's entropy formula. The microstates need not necessarily be quantum states as often claimed wrongly; for even simple biological matter, it would be impossible and hopeless to enumerate all the quantum states underlying the system! We began with a proclamation that designation of the microstates should depend on the level of a description chosen.

As an example, consider a mesoscopic level conformations of a linear biopolymer such as a DNA fragment, or a protein molecule in a solution at temperature T. The relevant "microstates" are the fewer degrees of freedom $\mathcal{Q}$ that emerge beyond atominstic degrees of freedom. For a biopolymer, as examples of $\mathcal{Q}$, we chose a collective coordinate (such as the end-to-end distance) and local coordinates (such as the two state variables for subunits describing the binding).

Then we proceeded to construct, in terms of $\mathcal{Q}$, the coarse-grained, effective Hamiltonian, $\mathcal{F}\{\mathcal{Q}\}$, from which the probability distribution of the state $\mathcal{Q}$ as well as the biopolymer's equilibrium properties could be obtained. On the other hand, the effective Hamiltonian $\mathcal{F}\{\mathcal{Q}\}$ can be viewed as the $\mathcal{Q}$'s free energy function that depends on temperature, due to the microscopic fluctuations underlying $\mathcal{Q}$. In an approach to equilibrium, the degrees of freedom $\mathcal{Q}$, assisted by the fluctuations, organize themselves so as to minimize the free energy function at the equilibrium state $\bar{\mathcal{Q}}$. The free energy necessarily has two components, the internal energy from the interactions between the subunits, and the entropy from the fluctuations which become very significant due to soft matter flexibility. Via competition between these two components, this self-organization are realized as a host of thermal transitions, e.g., binding-unbinding transitions, biopolymer folding, collapses and denaturation, etc. This methodology was extended to other systems as diverse as fluids, self-assembling structures, as well as biological soft matter. These equilibrium phenomena and properties were covered in Part I.

For the coarse-grained dynamics of the relevant degrees of freedom $\mathcal{Q}$, a natural choice is the Markovian stochastic equations, e.g., the Langevin-like equations with noises (thermal fluctuation as a special case) or the equivalent Fokker-Planck/master equations. We then studied how a thermal fluctuation drives a diffusion,

transition and activates crossing the free energy barrier that may exist. The biological dynamics at mesoscale, due to the overdamping solution background, is dissipative, and slow. However, we saw a most striking phenomenon that, the noise, when tuned at an optimal strength, can induce the maximal coherence and resonance of the transitions and barrier crossing dynamics of the system, to an external time-dependent signal albeit very week. The dissipative fluid background in cell is not merely a passive medium but an active structure that signals a non-equilibrium noise therein to resonate with the system's transition dynamics. This phenomenon of stochastic resonance and related resonant activation can be nonspecific physical paradigms pointing to the critical role of the thermal fluctuations and external noises: these often-neglected degrees of freedom, which may not be seen phenomenologically, play such magic! (Part II).

After all, two eminent features boost these kinds of unique interplay between the systems and the backgrounds. One is the background water's many outstandingly high susceptibilities, in particular, the high dielectric constant that facilitates various transitions of the system by reducing the electrostatic interaction energies therein to the level of thermal energy or below. If the systems are the soft matter such as polymers and membranes, another key feature is their structural connectivity and flexibility, which gives rise to cooperativity and low energy excitations. In parallel with the weak interactions mentioned above, under the fluctuating aqueous environments, the biological soft matter can undergo whatever transitions and surmount the seemingly unsurmountable barriers at body temperature. The thermal noises may come as random thunderstorms to the soft matter, but, at optimal conditions, may lend a helping hand with accomplishing the biological self-organizations!

As a way to bypass the virtually impossible task of deriving mesoscopic descriptions for a biological complex from underlying microscopics, the well-known classical phenomenology can fortuitously be used with an input of the fluctuations. For example, the effective Hamiltonian of a DNA fragment is the classical elastic energy of bending with the curvature promoted to be fluctuating degrees of freedom (Chap. 11). Another example is the Langevin equation, which is obtained by adding noises to macroscopic equations of motion (Chaps. 13 and 15). If we allow their charge densities to fluctuate and correlate, two objects with *equal* net charges can attract, rather than repel, to minimize the free energy (Coulomb interaction). This explains how the charge fluctuations induce DNA collapse (Chap. 11) and membrane adhesion. Classical phenomenology such as elasticity, mechanics, electricity, and hydrodynamics can thereby be revived to adapt to some biological phenomena by endowing the variables with stochasticity. It is akin to how the quantum fluctuation phenomena can be realized by replacing classical variables by operators.

Additional Topics

Throughout this book we have studied the selected themes of statistical mechanics, soft-matter physics, and related areas that I believe to form a coherent basis for applications to a variety of biological phenomena mostly on mesoscales. It is rather a kind of extended statistical physics book than of biological physics or biophysics book. As such, there can be many important biophysics topics that were not addressed, particularly on molecular scales and system levels. Also, the theoretical methods and biological examples that are covered may be relatively simple. To cope with the higher complexity, the basic physical premises need to be further revised and expanded (for example the concepts of spatial homogeneity and temporal stationarity may not be valid for crowded cell environments). I hope this project will nevertheless give an example of the first step toward the challenging and time-consuming endeavor to build up paradigms of a new fusion science by surmounting barriers between biological and physical sciences.

Within biological statistical physics there are a number of topics that I initially intended to cover: non-Markovian and anomalous dynamics, molecular motors, and the applications of stochastic thermodynamics and fluctuation theorem in their infancy. To date, the present version is the best I could try with limited time. To incorporate these topics with coherence and harmony in the future edition remains a challenge.

Index

W. Sung, *Statistical Physics for Biological Matter*, Graduate Texts in Physics,
https://doi.org/10.1007/978-94-024-1584-1